OCS Study
BOEM 2021-014

Modeling At-Sea Density of Marine Birds to Support Renewable Energy Planning on the Pacific Outer Continental Shelf of the Contiguous United States

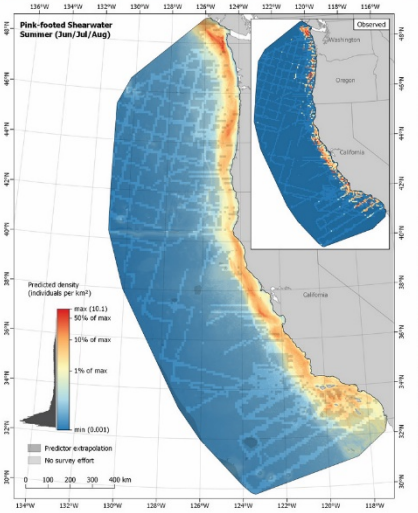

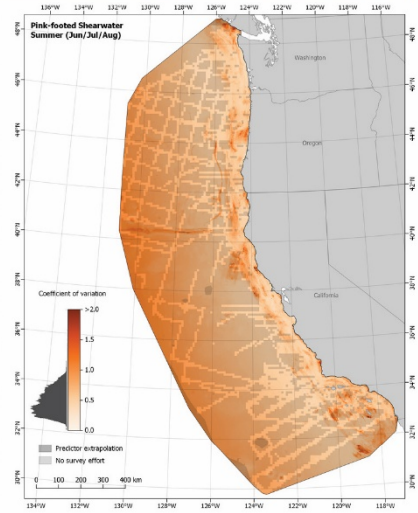

US Department of the Interior
Bureau of Ocean Energy Management
Pacific OCS Region

BOEM
Bureau of Ocean Energy Management

OCS Study
BOEM 2021-014

Modeling At-Sea Density of Marine Birds to Support Renewable Energy Planning on the Pacific Outer Continental Shelf of the Contiguous United States

August 2021

Authors:
Jeffery B. Leirness[1,2], Josh Adams[3], Lisa T. Ballance[4], Michael Coyne[1,2], Jonathan J. Felis[3], Trevor Joyce[5], David M. Pereksta[6], Arliss J. Winship[1,2], Christopher F. G. Jeffrey[1,2], David Ainley[7], Donald Croll[8], Joseph Evenson[9], Jaime Jahncke[10], William McIver[11], Peter I. Miller[12], Scott Pearson[9], Craig Strong[13], William Sydeman[14], Jeannette E. Waddell[15], Jeannette E. Zamon[16], John Christensen[2]

[1] CSS, Inc., Fairfax, VA, USA
[2] National Oceanic and Atmospheric Administration (NOAA) National Centers for Coastal Ocean Science, Silver Spring, MD, USA
[3] US Geological Survey, Western Ecological Research Center, Santa Cruz, CA, USA
[4] Oregon State University, Hatfield Marine Science Center, Marine Mammal Institute, Newport, OR, USA
[5] NOAA Fisheries, Southwest Fisheries Science Center, La Jolla, CA, USA
[6] Bureau of Ocean Energy Management, Pacific Outer Continental Shelf Region, Camarillo, CA, USA
[7] H. T. Harvey & Associates, Los Gatos, CA, USA
[8] University of California, Center for Ocean Health, Santa Cruz, CA, USA
[9] Washington Department of Fish and Wildlife, Olympia, WA, USA
[10] Point Blue Conservation Science, Petaluma, CA, USA
[11] United States Fish and Wildlife Service, Arcata Fish and Wildlife Office, Arcata, CA, USA
[12] Plymouth Marine Laboratory, PML Applications Ltd, Plymouth, UK
[13] Crescent Coastal Research, Crescent City, CA, USA
[14] Farallon Institute for Advanced Ecosystem Research, Petaluma, CA, USA
[15] NOAA Office of National Marine Sanctuaries, Olympic Coast National Marine Sanctuary, Port Angeles, WA, USA
[16] NOAA Fisheries, Northwest Fisheries Science Center, Point Adams Research Station, Hammond, OR, USA

Prepared under NCCOS IAA MOA-2015-038-9096, USGS BOEM IAA M15PG00009, and NCCOS BOEM IAA M15PG00010
By

US Department of Commerce
National Oceanic and Atmospheric Administration
National Ocean Service
National Centers for Coastal Ocean Science
Marine Spatial Ecology Division
1305 East-West Hwy, SSMC-4, N/SCI-1
Silver Spring, MD 20910

US Department of the Interior
US Geological Survey
Western Ecological Research Center
3020 State University Dr
Sacramento, CA 95819

US Department of the Interior
Bureau of Ocean Energy Management
Pacific OCS Region

BOEM
Bureau of Ocean Energy Management

DISCLAIMER

This study was funded, in part, by the US Department of the Interior, Bureau of Ocean Energy Management (BOEM), Environmental Studies Program, Washington, DC, through Interagency Agreement Number M15PG00009 with the US Geological Survey, Western Ecological Research Center and Interagency Agreement Number M15PG00010 with the National Oceanic and Atmospheric Administration, National Ocean Service, National Centers for Coastal Ocean Science. This report has been technically reviewed by BOEM, and it has been approved for publication. The views and conclusions contained in this document are those of the authors and should not be interpreted as representing the opinions or policies of BOEM, nor does mention of trade names or commercial products constitute endorsement or recommendation for use. This product has been peer reviewed and approved for publication consistent with US Geological Survey Fundamental Science Practices (https://pubs.usgs.gov/circ/1367/).

REPORT AVAILABILITY

To download a PDF file of this report, go to the US Department of the Interior, Bureau of Ocean Energy Management Data and Information Systems webpage (http://www.boem.gov/Environmental-Studies-EnvData/), click on the link for the Environmental Studies Program Information System (ESPIS), and search on 2021-014.

CITATION

Leirness JB, Adams J, Ballance LT, Coyne M, Felis JJ, Joyce T, Pereksta DM, Winship AJ, Jeffrey CFG, Ainley D, Croll D, Evenson J, Jahncke J, McIver W, Miller PI, Pearson S, Strong C, Sydeman W, Waddell JE, Zamon JE, Christensen J. 2021. Modeling at-sea density of marine birds to support renewable energy planning on the Pacific Outer Continental Shelf of the contiguous United States. Camarillo (CA): US Department of the Interior, Bureau of Ocean Energy Management. OCS Study BOEM 2021-014. 385 p.

ABOUT THE COVER

Cover photos of Pink-footed Shearwaters (*Ardenna creatopus*) courtesy of David Pereksta.

ACKNOWLEDGMENTS

We are grateful to the many scientists, seabird observers, and ship and flight crews who contributed data to this effort. We thank Matthew Poti and Laurie Bauer for providing bathymetric predictor data, Robert Rankin for initial development of the modeling framework and computer code, and Zhifa Liu for execution of the models on high performance computing systems. Sarah Hile, Jacob Howell, Charles Menza, and Martin Renner reviewed an earlier version of this report and provided helpful comments and suggestions. Jeffery Leirness, Michael Coyne, Arliss Winship, and Christopher Jeffrey were supported under NOAA Contract Numbers EA133C14NC1384 and EA133C14BA0062 with CSS, Inc.

The Applied California Current Ecosystem Studies (ACCESS, www.accessoceans.org) is funded in part by foundation and individual donor contributions to Point Blue Conservation Science. ACCESS is a partnership between Point Blue Conservation Science, Cordell Bank National Marine Sanctuary and Greater Farallones National Marine Sanctuary.

We dedicate this report to the memory of our friend and colleague Brian Kinlan.

Contents

List of Figures

List of Tables

List of Abbreviations and Acronyms

ACCESS	Applied California Current Ecosystem Studies
AE	absolute residual error
AUC	area under the receiver operating characteristic curve
AVISO	Archiving, Validation and Interpretation of Satellite Oceanographic data
BOEM	Bureau of Ocean Energy Management
CalCOFI	California Cooperative Oceanic Fisheries Investigations
CalCurCEAS	California Current Cetacean and Ecosystem Assessment Survey
CDFW	California Department of Fish and Wildlife
CMEMS	Copernicus Marine Environment Monitoring Service
CRM	Coastal Relief Model
CSCAPE	Collaborative Survey of Cetacean Abundance and the Pelagic Ecosystem
CV	coefficient of variation
EPOCS	Equatorial Pacific Ocean Climate Studies
F/V	fishing vessel
GEBCO	General Bathymetric Chart of the Oceans
GSHHG	Global Self-consistent, Hierarchical, High-resolution Geography Database
HYCOM	HYbrid Coordinate Ocean Model
JSOES	Juvenile Salmon Ocean Ecosystem Survey
MEI	multivariate El Niño-Southern Oscillation index
MGET	Marine Geospatial Ecology Tools
MMS	Minerals Management Service
MODIS	Moderate Resolution Imaging Spectroradiometer
NASA	National Aeronautics and Space Administration
NMS	National Marine Sanctuary
NOAA	National Oceanic and Atmospheric Administration
NPGO	North Pacific Gyre Oscillation
OCS	Outer Continental Shelf
ORCAWALE	Oregon, California and Washington Line-transect Expedition
OSU	Oregon State University
Pa	pascal
PaCSEA	Pacific Continental Shelf Environmental Assessment
PDE	percentage of deviance explained
PDO	Pacific Decadal Oscillation
PODS	Pacific Orca Distribution Survey
psu	practical salinity unit
RMSE	root mean square error
R/V	research vessel
SIO	Scripps Institution of Oceanography
sr	steradian
UCSC	University of California, Santa Cruz
USGS	US Geological Survey
USFS	US Forest Service
VIIRS	Visible Infrared Imaging Radiometer Suite

WDFW	Washington Department of Fish and Wildlife
ZINB	zero-inflated negative binomial
ZIP	zero-inflated Poisson

1 Introduction

Under the Energy Policy Act of 2005, the Bureau of Ocean Energy Management (BOEM) has responsibilities for evaluating and mitigating negative impacts of offshore renewable energy activities on human, coastal, and marine communities. Furthermore, BOEM requires up-to-date information to address potential impacts when developing environmental impact statements and assessments under the National Environmental Policy Act regulations. Along the Pacific coast of the contiguous U.S., the states of California, Oregon, and Washington are also evaluating siting alternatives for developing offshore energy projects within their state waters and adjacent Outer Continental Shelf (OCS) regions (Porter and Phillips 2016).

Marine birds (i.e., birds that predominantly feed in marine waters and are well adapted to the marine environment [Furness and Monaghan 1987]) can be adversely affected by offshore wind energy infrastructure. For example, birds can collide directly with the rotors of wind turbines or experience displacement from migration routes or foraging and resting habitats. Therefore, an understanding of marine bird spatial distribution and density becomes important when considering development of offshore renewable energy resources in an environmentally sound manner. Moreover, experience from onshore wind energy development, offshore development in Europe, and recent developments on the Atlantic coast of the U.S. indicates that strategic siting of offshore energy infrastructure away from areas of concentrated bird activity may eliminate many potential bird-turbine conflicts (de Lucas et al. 2007).

An important prerequisite for minimizing impacts of offshore wind energy development is knowledge of marine bird spatial distributions at sea. Presently, there are extensive marine bird survey datasets that provide density estimates along survey transects on the Pacific OCS of the contiguous U.S. (e.g., NCCOS 2003; Ford et al. 2004; Rintoul et al. 2006; Mason et al. 2007, NCCOS 2007). However, species-specific estimates of location and density from these datasets are only relevant to the locations where marine bird surveys occurred. In general, the observed distributions of marine birds at sea likely result from interactions among behaviors (e.g., foraging) and the environment (e.g., prey distribution) (Ainley et al. 2005; Ballance et al. 2006; Yen et al. 2006, Ainley et al. 2009). Atmospheric and oceanographic features and processes operating across a range of spatial and temporal scales can influence the environmental conditions and prey availability experienced by marine birds, and thus ultimately influence their at-sea distributions (Oedekoven et al. 2001; Ballance et al. 2006; Ainley et al. 2009; Renner et al. 2013; Goyert et al. 2016; Suryan et al. 2016). Consequently, distributions based on observations can be extrapolated to areas between survey transects or non-surveyed areas by using models to relate marine bird observations with environmental and oceanographic covariates to predict their distribution and density in non-surveyed areas. Under certain assumptions, high-resolution maps of predicted density created from these model outputs can be used to assess risk for marine birds and guide strategic siting of renewable energy projects that minimize negative environmental impacts of offshore wind energy development.

With the exceptions of Nur et al. (2011) and Dick (2016), previous marine bird spatial modeling efforts on the Pacific OCS of the contiguous U.S. were relatively limited in geographic scope (e.g., Clarke et al. 2003; McGowan et al. 2013; Manugian et al. 2015; Raphael et al. 2015; Studwell et al. 2017). Both Nur et al. (2011) and Dick (2016) provided spatially explicit assessments of multispecies abundance covering much of the Pacific OCS of the contiguous U.S. However, spatially explicit estimates were not provided for individual species. In addition, spatially explicit measures of model uncertainty were not provided, limiting the applicability of these studies for risk assessment or spatial planning processes. The National Oceanic and Atmospheric Administration (NOAA) National Centers for Coastal Ocean Science (NCCOS) has successfully developed high-resolution (1.2–3 km) model-based estimates of marine bird distributions and associated maps of uncertainty for multiple geographic regions (e.g., Menza et al. 2016; Winship et al. 2016; Winship et al. 2018). Similar high-resolution spatial models of marine bird distributions for the Pacific OCS of the contiguous U.S. will provide critical information for renewable

energy siting and allow BOEM to evaluate potential environmental effects of management actions and apply project decision criteria with respect to marine birds throughout the region in a manner that is consistent with other regional evaluations of renewable energy siting.

This report describes the at-sea spatial distributions of marine birds in Pacific OCS waters off the contiguous U.S. (**Figure 1.1**) to inform marine spatial planning in the region. The goal was to estimate long-term average spatial distributions for marine bird species using all available science-quality transect survey data and numerous bathymetric, oceanographic, and atmospheric predictor variables. We developed seasonal habitat-based spatial models of the at-sea distribution for 33 individual species and 13 taxonomic groups of marine birds throughout the study region. A statistical modeling framework was used to estimate numerical relationships between bird sighting data (i.e., standardized counts) and a range of temporal (e.g., Pacific Decadal Oscillation [PDO] index), spatially static (e.g., depth), and spatially dynamic (e.g., sea surface chlorophyll-a concentration) environmental variables. The estimated relationships were then used to predict spatially explicit long-term average density (individuals per km^2) throughout the study area for each species/group in each of four seasons. Bird sighting data came from multiple scientific survey programs and consisted of at-sea counts of birds collected between 1980 and 2017 using boat-based and fixed-wing aerial transect survey methods. Spatial environmental variables were derived from remote sensing satellite data and an ocean dynamics model.

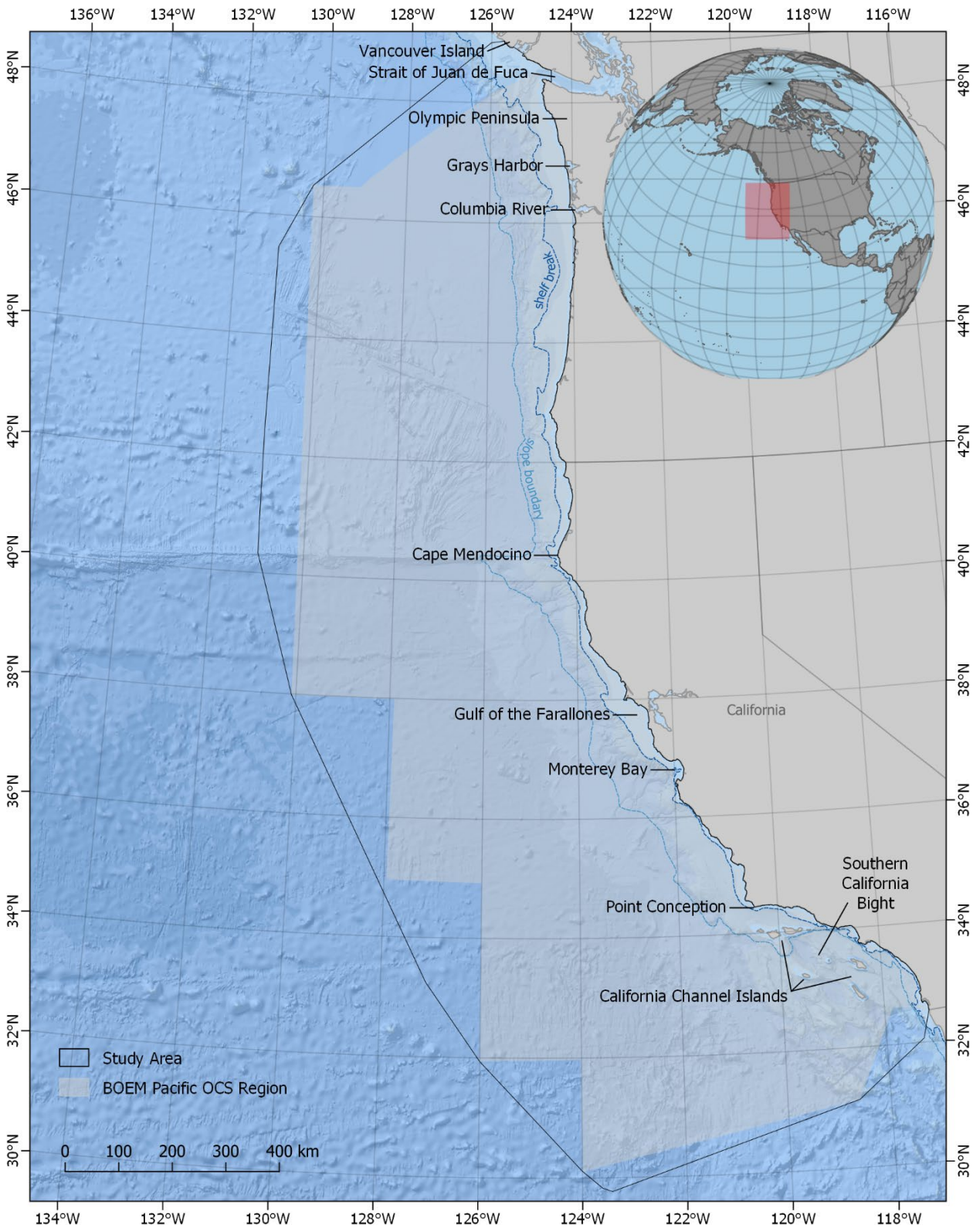

Figure 1.1. Map of the study area showing BOEM's Pacific OCS Region

2 Methods

2.1 Overview

A statistical modeling framework was used to relate bird sighting data from historical surveys to a range of temporal and spatial environmental predictor variables. The estimated relationships between the counts of birds and the predictor variables, after accounting for survey effort, were then used to predict spatially explicit long-term average density throughout the entire study area of roughly 1.2 million km^2. Separate models were developed for each combination of species and season with sufficient data. Seasons encompassed four major transitions in environmental conditions in the study region: spring (March 1 to May 31), summer (June 1 to August 31), fall (September 1 to November 30), and winter (December 1 to February 29).

2.2 Survey Data

Twenty-one survey datasets were combined for analyses (**Table 2.1 and Appendix A**). Data included visual at-sea counts of birds collected between 1980 and 2017 from fixed-wing aerial and boat-based survey platforms. All surveys except the Northwest Forest Plan Marbled Murrelet Monitoring Program Zone 2 used strip transect survey methods (Tasker et al. 1984) with variable strip width to accommodate different species, observation conditions, number of observers, and survey-specific protocols (**Appendix A**). Data from the Northwest Forest Plan Marbled Murrelet Monitoring Program Zone 2 were collected using line transect survey methods (Burnham et al. 1980). Line transect data were truncated to a strip width of 300 m (i.e., observations beyond 150 m on either side of the survey vessel were excluded), assuming constant detectability within the strip, so that survey effort could be quantified consistently among all datasets. Aerial surveys were conducted using strip widths of 50–150 m and a target elevation of 61 m. Boat-based surveys used strip widths of 100–600 m with observation height varying according to vessel size and survey-specific protocols. Bird observations were recorded to the lowest taxonomic level possible.

Where possible, transect data were divided into spatially-discrete segments with a target length of 4 km. The distance traveled along each segment was calculated using the boat/plane location data assuming travel between recorded locations followed a line of constant bearing and speed. Species-specific bird counts were summed within each segment and geographically referenced using the geographic midpoint of each segment. Data from eight survey programs were obtained pre-segmented and could not be further divided (**Table 2.1**). Pre-segmented data longer than 16 km were excluded from analyses to limit the geographic error in bird sightings assigned to each segment midpoint. Segments shorter than 500 m were excluded because of a greater probability of extreme values in observed density (i.e., birds per area surveyed), especially when large flocks were encountered.

A total of 108,169 km^2 of survey segments were used for analyses with more survey effort during spring, summer, and fall than during winter (**Table 2.1**). Survey effort was variable both interannually and spatially (**Figures 2.1 and 2.2**). Boat-based surveys accounted for nearly 86% of the overall survey effort and 98% of survey effort beyond 100 km from shore.

2.3 Species Modeled

To the extent possible, species-specific models were developed. However, identification uncertainty for some species, mainly from visual aircraft-based surveys, may have increased the probability of species misidentification and also resulted in a greater proportion of observations not identified to species (see **Table 2.2**). Therefore, for some species, species-specific observations (e.g., Surf Scoter [*Melanitta*

perspicillata]) were combined with species-nonspecific observations (e.g., unidentified scoter) to create broad taxonomic groups prior to modeling. Thirteen taxonomic groups were identified (**Table 2.2**). In these cases, taxonomic group models were developed in place of individual species-level models. However, individual species models were developed *in addition* to taxonomic group models for Pomarine Jaeger (*Stercorarius pomarinus*), Red-throated Loon (*Gavia stellata*)[1], and Common Loon (*Gavia immer*)[1]. Individual cormorant species models were developed for spring and summer seasons, when breeding plumage allowed species to be more easily distinguished. All cormorant observations were combined into a single taxonomic group for fall and winter season models.

For each season, all species/groups with at least 100 segments with sightings were modeled. By these criteria, 46 species/groups and 135 species/group-season combinations were modeled based on sightings of 1,952,696 individual birds (**Table 2.3**). These species/groups comprised 12 avian families. The five species/group-season combinations with the greatest numbers of segments with sightings were Western/Glaucous-winged Gull (*Larus occidentalis*/*glaucescens*) in spring (9,204), Short-tailed/Sooty/Flesh-footed Shearwater (*Ardenna tenuirostris*/*grisea*/*carneipes*) in spring (8,406) and summer (7,850), Common Murre (*Uria aalge*) in spring (7,078), and Western/Glaucous-winged Gull in fall (5,475).

2.4 Predictor Variables

A wide range of predictor variables were used to model variation in the number of birds observed and to predict the spatial distributions of birds throughout the study area (**Tables 2.4, 2.5, 2.6, and Appendix B**). Predictor variables fell into one of six categories: survey, temporal, geographic, bathymetric, oceanographic, and atmospheric.

Survey predictor variables (**Table 2.4**) were selected to account for variation in counts arising from heterogeneity in the type of survey platform, characteristics of the survey platform (e.g., observation height), observer identity and expertise, and sighting conditions. These factors influence the probability that individual birds will be detected (Heinänen et al. 2017) and correctly identified to the species level. Of these factors, only the type of survey platform (aerial or boat) was consistently available for all datasets, and thus directly usable as a predictor variable. We attempted to account for the effects of the remaining factors through two random-effect predictor variables representing survey identity, or ID, and transect ID, respectively. Survey ID was defined as the combination of survey name (see **Table 2.1**) and year of data collection. Transect ID was defined as the combination of survey name and date of data collection.

Temporal predictor variables (**Table 2.4**) were selected to account for variation in counts through time. Day of the year was used to account for changes in the numbers of birds in the study area through time within a season (i.e., resulting from migratory movements in and out of the study area). Year was included to account for interannual changes in the number of birds in the study area (i.e., resulting from changes in population abundance or distributional shifts). Effects of day of the year and year were modeled as smooth continuous changes through time. Three climate indices, multivariate El Niño-Southern Oscillation index (MEI), North Pacific Gyre Oscillation (NPGO; Di Lorenzo et al. 2008) index,

[1] Previous studies suggest loon species may be particularly vulnerable to displacement impacts from offshore wind energy development (Furness et al. 2013; Bradbury et al. 2014; Kelsey et al. 2018; Heinänen et al. 2020). Therefore, individual species models were developed for Red-throated Loon and Common Loon. Because Arctic/Pacific Loons (*Gavia artica/pacifica*) accounted for the majority of all loon observations in every season, and especially in spring, summer, and fall (see **Table 2.2**), model outputs for the Loon spp. taxonomic group largely represent Arctic/Pacific Loon.

and PDO index, were also included as temporal predictor variables to account for interannual and intraseasonal variation in counts arising from linkages among the environment, abundance, and distribution. Because linkages among climate indices and marine birds are likely indirect, there may be a delay in the effects on upper trophic levels (e.g., marine birds). Therefore, two values for each climate index were included as predictor variables: the value for the month and year of a given survey segment and the value for the same month one year previous to account for possible lagged effects.

Geographic predictor variables (**Table 2.5**) were selected to account for variation in counts arising from spatial location. Projected longitude and latitude were included as predictor variables and their effects were modeled two ways. The first longitude-latitude predictor term allowed for smooth changes in numbers across the study area arising from spatial factors not captured by the other predictor variables. The second longitude-latitude predictor term was formulated using radial basis functions with the intent of capturing some of the spatial autocorrelation in the data after accounting for the effects of other predictor variables. Distance to nearest land and nearest submarine canyon, as defined by Harris et al. (2014), were also included as geographic predictor variables.

Bathymetric predictor variables (**Table 2.5**) were selected to account for variation in counts arising from the direct and indirect effects of bathymetry on bird distributions. Fifty-three high-resolution multibeam bathymetry datasets (**Appendix C**) were merged into a single gridded depth dataset with a spatial resolution of 100 m. Supplemental depth values from the NOAA Coastal Relief Models (CRMs; NOAA NGDC 2003a, 2003b, 2012) and the General Bathymetric Chart of the Oceans (GEBCO) 2014 grid (Weatherall et al. 2015) were used where no multibeam data existed. Additional bathymetric variables were derived from depth including slope, slope of slope, and planform and profile curvature. Variables derived from depth were calculated at both 10-km and 20-km scales by first "smoothing" the 100-m resolution depth grid using a Gaussian filter with kernel size equal to these scales (i.e., 10 or 20 km) and then performing the relevant calculations using the coarsened depth grid.

Oceanographic and atmospheric predictor variables (**Table 2.6**) were selected to account for variation in counts arising from the direct and indirect effects of the physical state and dynamics of the ocean and air above the ocean as well as biological productivity. Twenty-five oceanographic and atmospheric predictor variables were developed from a range of data sources (**Table 2.6**). Remote sensing data were used to quantify chlorophyll-a concentration, turbidity, sea surface height, temperature, Ekman driven upwelling, and wind stress. Additional variables were derived from the remotely sensed variables including chlorophyll-a front strength and temperature front strength (Cayula and Cornillon 1992; Miller 2009; Miller et al. 2015), frequencies of cyclonic and anticyclonic eddy ring structure[2], temperature anomaly frequency[3], and wind stress divergence. Estimates from the HYbrid Coordinate Ocean Model (HYCOM; HYCOM Consortium 2018), a global data-assimilating ocean dynamics model, were used to characterize water currents, salinity, and mixed layer depth[4].

All of the oceanographic and atmospheric variables that we considered were dynamic. We rendered appropriate temporally-composited data for these predictor variables to characterize long-term spatial patterns in average values and variability. Data time series ranging in duration from 9 to 35 years were used. To characterize average values, monthly mean climatologies among years were developed and then

---

[2] Presence/absence of eddy ring structures were identified using Marine Geospatial Ecology Tools version 0.8a64: Find Okubo-Weiss Eddies in AVISO DUACS 2014 SSH Product tool (Roberts et al. 2010) in ArcGIS version 10.4.1 (ESRI 2016).

[3] Temperature anomaly frequency was defined as the proportion of days where the single-day sea surface temperature was greater than the monthly climatological mean temperature by more than 1ºC.

[4] Mixed layer depth was defined as the depth at which temperature differed from the surface by ≥0.5ºC.

averaged to create seasonal climatologies to match our four predefined seasons (spring, summer, fall, and winter). To characterize variability, standard deviations were calculated from the native temporal resolution of the corresponding predictor variables.

Geographic, bathymetric, oceanographic, and atmospheric predictor variables were spatially explicit. Each resulting variable was projected onto a standard study grid with a spatial resolution of 2 km and an oblique Mercator projected coordinate system (origin: 39ºN 125ºW; azimuth: 75º; scale: 0.9996; geodetic datum: WGS84). When the native spatial resolution of a predictor variable was finer than that of the study grid, predictor values were averaged within study grid cells. When the native spatial resolution of a predictor variable was equal to or coarser than that of the study grid, bilinear interpolation was used to derive predictor values at the center of study grid cells. Each survey segment was matched to the predictor variable values from the study grid cell that contained the midpoint of that segment.

Some spatially explicit predictor variables were highly correlated (**Figures 2.3 and 2.4**). Predictor variables were chosen to avoid absolute Spearman correlations (r_s) greater than 0.9, although each season except spring had at least one pairwise absolute correlation greater than 0.9: distance to land and depth (summer, fall, winter), distance to land and chlorophyll-a (summer), depth and chlorophyll-a (summer), and current speed and salinity (winter). Because of the high correlations between some predictor variables, inferences regarding relative variable importance should be made with caution. The accuracy of predictions should be less affected by collinearity among predictor variables.

2.5 Statistical Modeling Framework

A boosted generalized additive modeling framework (Bühlmann and Hothorn 2007; Hofner et al. 2014) was used to estimate relationships between the number of birds observed and the predictor variables. Those relationships were then used to predict the estimated density of each species/group throughout the study area in each season. Our main objective was to provide accurate predictions so we chose a modeling framework that allowed for flexible relationships and multiple interactions between predictor variables while accounting for sampling heterogeneity between and within datasets.

2.5.1 Likelihoods and Model Components

The number of individuals of a given species/group counted per segment was modeled using zero-inflated Poisson (ZIP; **Equation 2.1**) and zero-inflated negative binomial (ZINB; **Equation 2.2**) likelihoods to account for the overdispersed nature of the count data. Each component (i.e., parameter) of the likelihood was modeled as a separate function of the predictor variables (Schmid et al. 2010; Mayr et al. 2012). For the ZIP likelihood, the two model components were the probability of an "extra" zero (p) and the mean of the Poisson distribution (μ). The same components were modeled for the ZINB likelihood (with μ being the mean of the negative binomial distribution) in addition to the dispersion parameter of the negative binomial distribution (θ). The probability of an extra zero (p) was modeled on the logit scale while the mean of the Poisson/negative binomial distribution (μ) and the dispersion parameter of the negative binomial distribution (θ) were modeled on the log scale. In **Equations 2.1 and 2.2**, y_i represents the total count for segment i, $\boldsymbol{y}$ is the vector of counts for all segments, n is the total number of segments, $I_{y_i=0}$ and $I_{y_i>0}$ are indicators of whether y_i is equal to or greater than zero, respectively (i.e., $I = 1$ when the condition is true and $I = 0$ when the condition is false), and $\Gamma()$ denotes the gamma function, $\Gamma(\alpha) = \int_0^\infty t^{\alpha-1}e^{-t}dt$.

$$L(p, \mu; \boldsymbol{y}) = \prod_{i=1}^{n} [p + (1-p)e^{-\mu}]^{I_{y_i=0}} \left[(1-p)\frac{\mu^{y_i}e^{-\mu}}{y_i!}\right]^{I_{y_i>0}} \quad (2.1)$$

$$L(p,\mu,\theta;\boldsymbol{y}) = \prod_{i=1}^{n}\left[p + (1-p)\left(\frac{\theta}{\theta+\mu}\right)^{\theta}\right]^{I_{y_i=0}}\left[(1-p)\frac{\Gamma(y_i+\theta)}{y_i!\,\Gamma(\theta)}\left(\frac{\theta}{\theta+\mu}\right)^{\theta}\left(\frac{\mu}{\theta+\mu}\right)^{y_i}\right]^{I_{y_i>0}} \quad (2.2)$$

2.5.2 Effort Offset

To account for variation in the lengths and widths of survey segments, an effort offset was included in the model. Specifically, the area surveyed per segment was used as an effort offset in the μ model component, enforcing a proportional relationship between the area surveyed and the expected number of individuals counted on a segment conditional on that segment not being an "extra" zero count. Model predictions correspond to estimated counts per km^2 of survey effort.

2.5.3 Base-learners

Within the boosting framework, each model component was modeled as a function of an ensemble of "base-learners." Each base-learner represented a specific functional relationship between a model component and one or more predictor variables. We utilized a suite of base-learners each representing different predictor variables, and different sets of base-learners were employed for different model components (**Table 2.7**).

All spatially explicit predictor variables except projected longitude and latitude were included together in a single tree base-learner. The trees for that learner had a maximum depth of 5, which allowed for interacting effects among the spatially explicit predictor variables. Projected longitude and latitude appeared in two base learners, and those variables always entered the model as a pair. The remaining survey and temporal predictor variables entered the model individually, either through their own base-learners or in the case of climate indices one at a time through a tree base-learner with a maximum depth of 1. Because our goal was to estimate long-term average patterns of density, our model structure did not allow for interactions between temporal and spatial predictor variables.

2.5.4 Stochastic Gradient Boosting

Stochastic gradient boosting was used to fit models whereby a sub-sample of the data (80% during tuning, see **Section 2.5.6**, or 67% otherwise) was fitted in each boosting iteration (Friedman 2002). Rather than re-sampling the data for each boosting iteration, a set of 25 or 50 random sub-samples was created before boosting, and one sub-sample was randomly drawn from this set for each boosting iteration. Mean square error was used to select the base-learner that gave the best fit to the gradient in each boosting iteration.

2.5.5 Boosting Offsets

Model component estimates were initialized ("offset" in boosting terminology) by fitting an intercepts-only ZIP or ZINB model with an effort offset to the data (Zeileis et al. 2008; Hofner et al. 2014; Jackman 2015). The estimated intercepts for each component of that model were used as the boosting offsets.

2.5.6 Tuning of Learning Rate and Number of Boosting Iterations

A stratified (by transect ID) 5-fold cross-validation approach was used to determine the number of boosting iterations (M) and component-wise learning rates that resulted in the best predictive performance. Three different learning rates were considered for each model component: 0.001, 0.01, and 0.1. For each unique combination of component-wise learning rates and cross-validation fold the model was fit to the in-bag data (i.e., 80% of the data), and M at which the negative log-likelihood of the out-of-bag data (i.e., 20% of the data) was minimized was determined. This cross-validation was repeated four times. For each combination of component-wise learning rates the optimal M and their corresponding

performance were averaged among cross-validation folds and replicates. Finally, the combination of component-wise learning rates with the best average performance and its corresponding average optimal M were identified. The maximum M allowed was 20,000, so models with M near 20,000 should be interpreted with caution as their performance may have improved with additional boosting iterations.

2.5.7 Model Performance and Selection

Both a ZIP and ZINB model were fitted for each species/group-season combination. The performance of the two models was evaluated from a suite of six performance metrics. The first performance metric was percentage of deviance explained (PDE), which is a measure of the percentage of variation in the data explained by the fitted model beyond the amount of variation explained by a simpler model without predictor variables. PDE indicates overall model fit and is somewhat analogous to the R^2 metric for a linear regression. The second performance metric was the area under the receiver operating characteristic curve (AUC), which indicates how well a model predicts binary data. We calculated AUC by converting the count data to presence/absence data. The AUC metric indicates how well the models predicted the observed presence of a species/group, but not necessarily how well the models predicted the count of a species. The third performance metric was the Gaussian rank correlation coefficient (r_G) (Boudt et al. 2012; Bodenhofer et al. 2013) between the observed and predicted data. This metric indicates how well the model predictions for each segment correlate with the number of individuals counted. The fourth and fifth performance metrics were the median absolute residual error (AE) and mean AE, expressed as a proportion of the mean observed value (i.e., mean count). The last performance metric was root mean square error (RMSE), the square root of the average squared residual error.

It is important to recognize that the model performance metrics mainly reflect the statistical fit of the models to the data. They reflect only the data that were analyzed, and they do not reflect the quality of model predictions away from the data. For example, the survey data did not cover the full extent of the study area, so some model predictions are essentially interpolations/extrapolations from data in other parts of the study area. The accuracy of those predictions is not necessarily reflected by the model performance metrics. Nevertheless, the performance metrics give an indication of how accurately a model was able to predict the observed data, and higher performance provides a measure of increased confidence in the modeled distributions, especially within the temporal and spatial coverage of the observed data.

The values of each of these performance metrics were ranked[5] for the two models applied to each species/group-season combination, and the model with the lowest sum of ranks for these performance metrics was chosen as the final selected model. In the case of a tie, the model with the greatest PDE was selected.

2.5.8 Spatial Prediction

The final selected model of each species/group and season was used to predict density throughout the study area. It is important to recognize that the model predictions do not represent absolute density. Furthermore, the predicted densities for each species/group and season are not directly comparable among species/groups and seasons. During visual surveys, individual birds may be missed either because they are below the surface of the water (availability bias) or simply because observers failed to notice them (perception bias) (Barlow 2015). The failure to count some individuals biases estimates of density downward relative to absolute density. Animal movement can also bias estimates of density. For example, birds may be attracted or repelled by ships, small boats, and planes biasing estimates upward or downward, respectively. Flying birds can also bias estimates, with the direction of the bias depending on

[5] Lower rank value corresponded to better performance.

the speed and direction of the animals' movement relative to those of the survey platform (Spear et al. 1992). Furthermore, non-randomized survey data can result in biased estimates of abundance and density in species distribution models (Conn et al. 2017). Therefore, our model predictions should only be interpreted as indices of absolute density, proportional to the expected number of individuals per km^2, but not representative of the actual number of individuals per km^2.

The predicted density in a given grid cell corresponds to predictions for a segment whose mid-point falls within that grid cell. Spatially explicit predicted values were calculated for each cell of the study grid from the values of the spatially explicit predictor variables for that cell. Temporal predictor variables (i.e., year, day of year, climate indices) were set to their mean values in each season. The predictions integrated the zero-inflated and Poisson/negative binomial components of the likelihood.

2.5.9 Variable Importance

We calculated the relative importance of each predictor variable in the final selected models by summing the decrease in the negative log-likelihood in each boosting iteration attributable to that predictor variable. Thus, variable importance reflects the frequency with which a given predictor variable occurred in the selected base-learners across boosting iterations and that variable's ability to explain variation in the data when it was selected. When multiple predictor variables occurred in the selected base-learner for a given boosting iteration, the decrease in the negative log-likelihood was divided evenly among those predictor variables. Relative variable importance was re-scaled so that it summed to 1 across predictor variables.

2.5.10 Uncertainty

Uncertainty in model predictions was estimated using a non-parametric bootstrapping framework. For each bootstrap iteration, the set of unique transect IDs was resampled with replacement, and the data for each transect ID were assigned weights proportional to the frequency of that ID in the sample. These weights were then applied when fitting the model during that bootstrap iteration. Predictor variables that were not included in the final selected model were excluded from the bootstrap analysis. Two hundred bootstrap iterations were conducted producing a sample of predictions from which we calculated means, standard deviations (as an estimate for standard error), coefficients of variation, 5%, 25%, 50%, 75%, and 95% quantiles, and 50% and 90% confidence interval widths to characterize uncertainty in the predictions. The 50% and 90% confidence intervals were defined as the intervals between the 25% and 75% quantiles and between the 5% and 95% quantiles, respectively.

As with the model performance metrics, the estimated uncertainty in the model predictions is conditional on the model and the data. It does not capture all of the uncertainty associated with our model predictions. Nevertheless, the estimated uncertainty is an important indication of the precision of the model predictions, and it should be an integral consideration when using the model predictions.

The median value (i.e., 50% quantile) of the bootstrapped predictions was generally better (e.g., smoother density gradients and fewer artifacts) than both the mean of the bootstrapped predictions and the non-bootstrapped predictions, so we chose the median of the bootstrapped predictions as the best representation of the predicted spatial distributions of density.

2.5.11 Implementation

The analysis was conducted with R version 3.6.0 64-bit (R Core Team 2019) running under CentOS Linux 7 using custom scripts that relied on multiple R packages, including **boot** version 1.3-17 (Davison and Hinkley 1997; Canty and Ripley 2015), **DBI** version 0.3.1 (R Special Interest Group on Databases 2014), **fields** version 8.2-1 (Nychka et al. 2015), **gsubfn** version 0.6-6 (Grothendieck 2014a), **lattice** version 0.20-31 (Sarkar 2008), **maps** version 3.3.0 (Becker et al. 2018), **maptools** version 0.8-36 (Bivand and Lewin-Koh 2015), **MASS** version 7.3-42 (Venables and Ripley 2002), **Matrix** version 1.2-17 (Bates

and Maechler 2019), **mboost** version 2.4-2 (Bühlmann and Hothorn 2007; Hothorn et al. 2010; Hothorn et al. 2015), **mgcv** version 1.8-28 (Wood 2011, 2017), **modeltools** version 0.2-21 (Hothorn et al. 2013), **mvtnorm** version 1.0-2 (Genz and Bretz 2009; Genz et al. 2014), **nlme** version 3.1-139 (Pinheiro et al. 2019), **party** version 1.0-21 (Hothorn et al. 2006), **pROC** version 1.8 (Robin et al. 2011), **proto** version 0.3-10 (Kates and Petzoldt 2012), **pscl** version 1.4.9 (Jackman 2015), **raster** version 2.4-15 (Hijmans 2015), **reshape** version 0.8.5 (Wickham 2007), **rgdal** version 1.0-4 (Bivand et al. 2015), **rgeos** version 0.3-11 (Bivand and Rundel 2015), **rococo** version 1.1.2 (Bodenhofer and Klawonn 2008; Bodenhofer et al. 2013), **RSQLite** version 1.0.0 (Wickham et al. 2014), **sandwich** version 2.3-3 (Zeileis 2004, 2006), **sp** version 1.1-1 (Pebesma and Bivand 2005; Bivand et al. 2013), **spam** version 1.3-0 (Furrer and Sain 2010; Gerber and Furrer 2015), **sqldf** version 0.4-10 (Grothendieck 2014b), **stabs** version 0.5-1 (Hofner and Hothorn 2015; Hofner et al. 2015), **strucchange** version 1.5-1 (Zeileis et al. 2002), **VGAM** version 0.9-8 (Yee 2015), and **zoo** version 1.8-6 (Zeileis and Grothendieck 2005).

2.6 Map Display

Spatial predictions within the study area are displayed as a pair of maps for each species/group and season (**Figure 2.5**). The first map for each species/group and season displays the predicted density (median value of bootstrapped predictions), and the second map displays the coefficient of variation (CV) of predicted density, both at a 2-km spatial resolution. The first map also contains an inset map of observed density: the total count divided by the total area surveyed at a 10-km spatial resolution.

Color ramps are employed to visualize spatial variation in values throughout the study area. For predicted density, the colors range from blue (lower density) to red (higher density), and for the CV the colors range from light orange (lower CV, more precise) to dark orange (higher CV, less precise). For each predicted density map, the color gradient was based on predicted density values on the natural logarithmic scale.

A histogram is included next to the color bar in each map to show the relative frequency of each color represented within the study area. This can be useful when attempting to link the color shown at a specific location on the map to its corresponding predicted density value listed to the right of the color bar.

Both maps also display two semi-transparent overlays indicating areas with spatial extrapolations. The lighter gray overlay (labeled, “No survey effort”) indicates areas without survey effort at a 10-km spatial resolution. The darker gray overlay (labeled, “Predictor extrapolation”) indicates areas where the values of one or more spatial predictor variables were beyond the range of values used in fitting the model. Only the spatial predictor variable values at grid cell locations with survey effort were used to fit the models; therefore, predictions based on values beyond these ranges are considered extrapolations. Spatial extrapolations should be interpreted with caution.

Maps were created using QGIS version 3.10.9 (QGIS.org 2020).

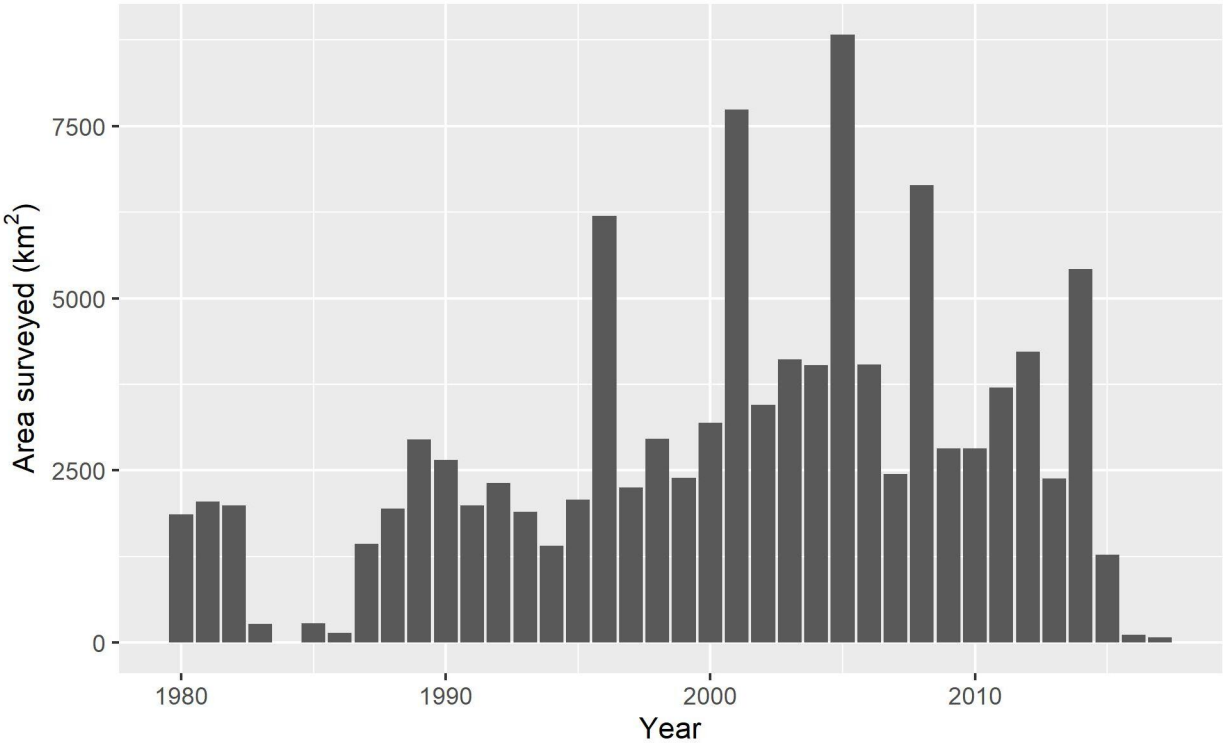

Figure 2.1. Total area surveyed each year

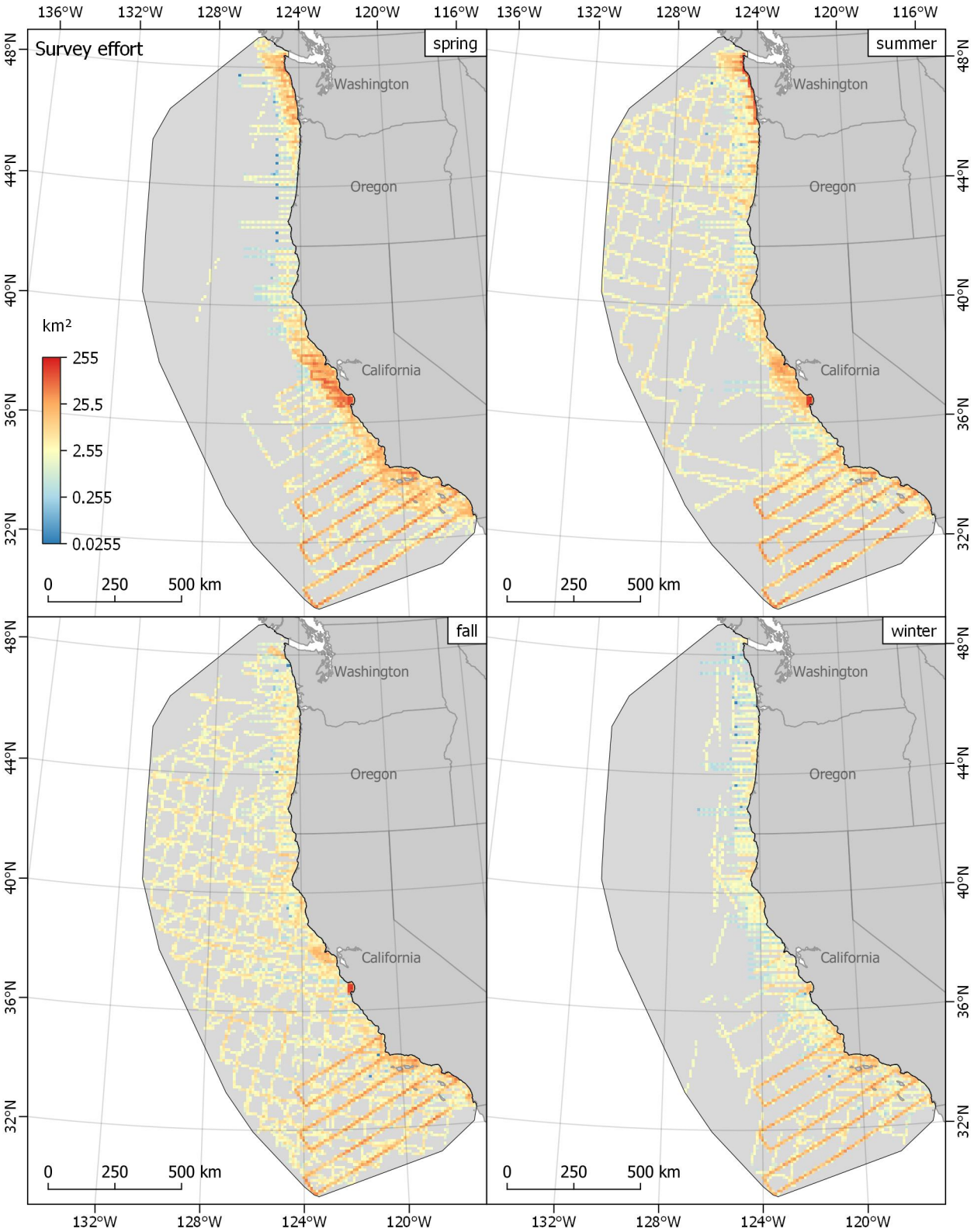

Figure 2.2. Total area surveyed each season within the study area
Area surveyed is summarized into 10 x 10 km grid cells and does not necessarily represent unique area surveyed; some surveys covered similar areas over multiple days, months, or years. Color gradient is linear on the natural logarithmic scale. White areas represent no survey effort.

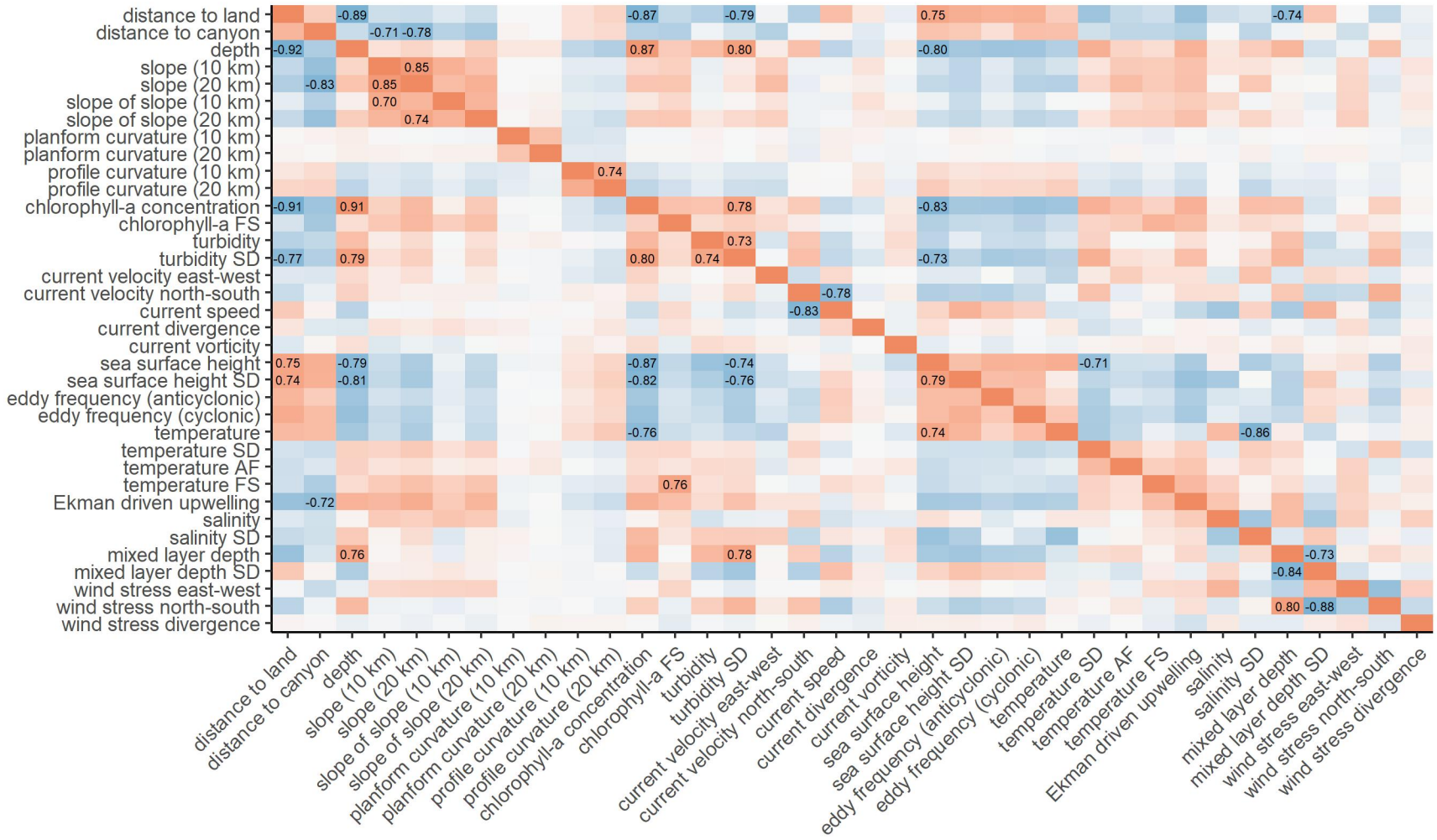

Figure 2.3. Spearman correlation matrix for spatial predictor variables used in spring (above diagonal) and summer (below diagonal) models

Positive correlations are shown in red, negative correlations in blue, with the strength increasing relative to the shading. Correlation coefficients are only displayed for values greater than 0.7 or less than -0.7.

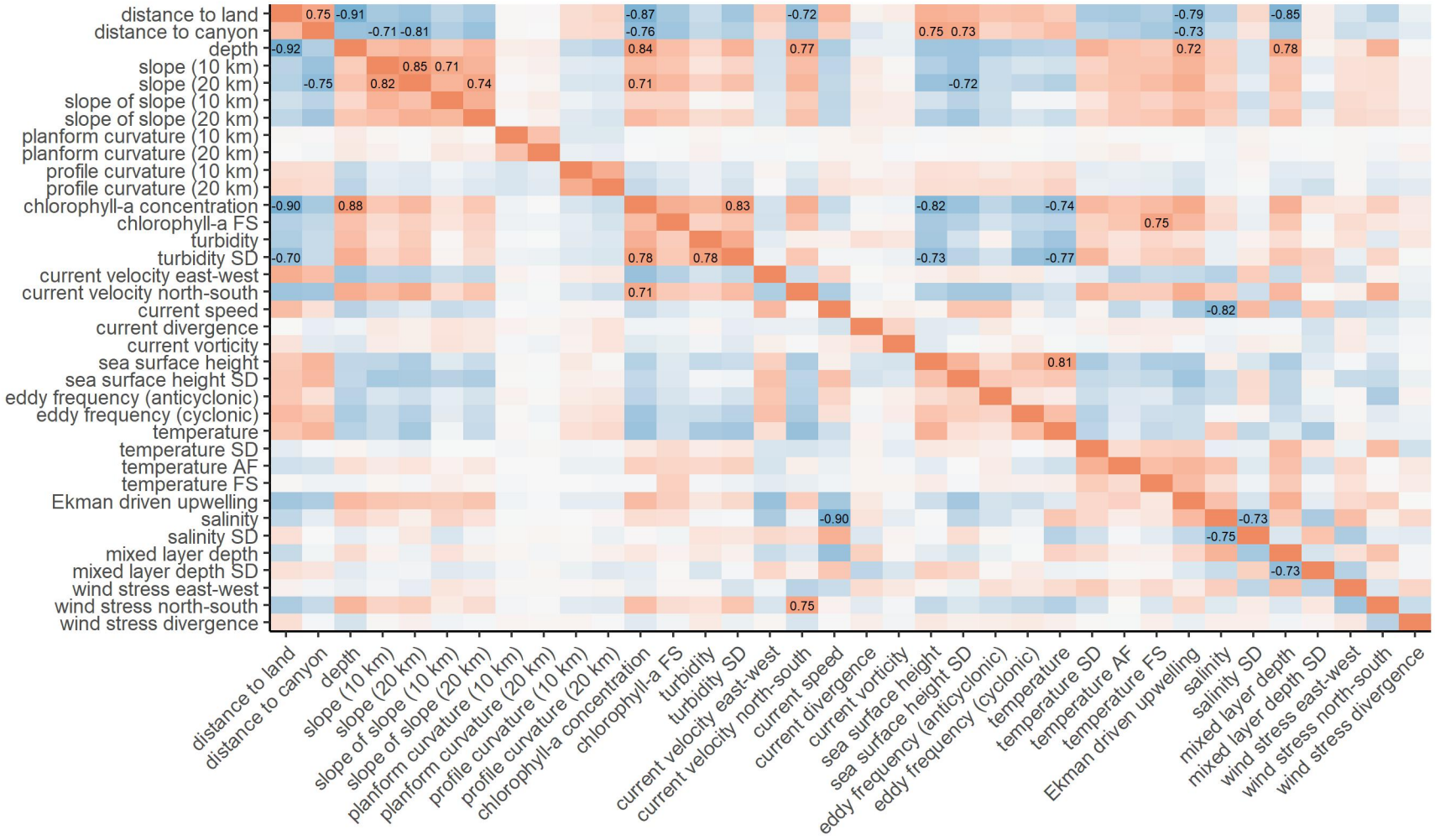

Figure 2.4. Spearman correlation matrix for spatial predictor variables used in fall (above diagonal) and winter (below diagonal) models
Positive correlations are shown in red, negative correlations in blue, with the strength increasing relative to the shading. Correlation coefficients are only displayed for values greater than 0.7 or less than -0.7.

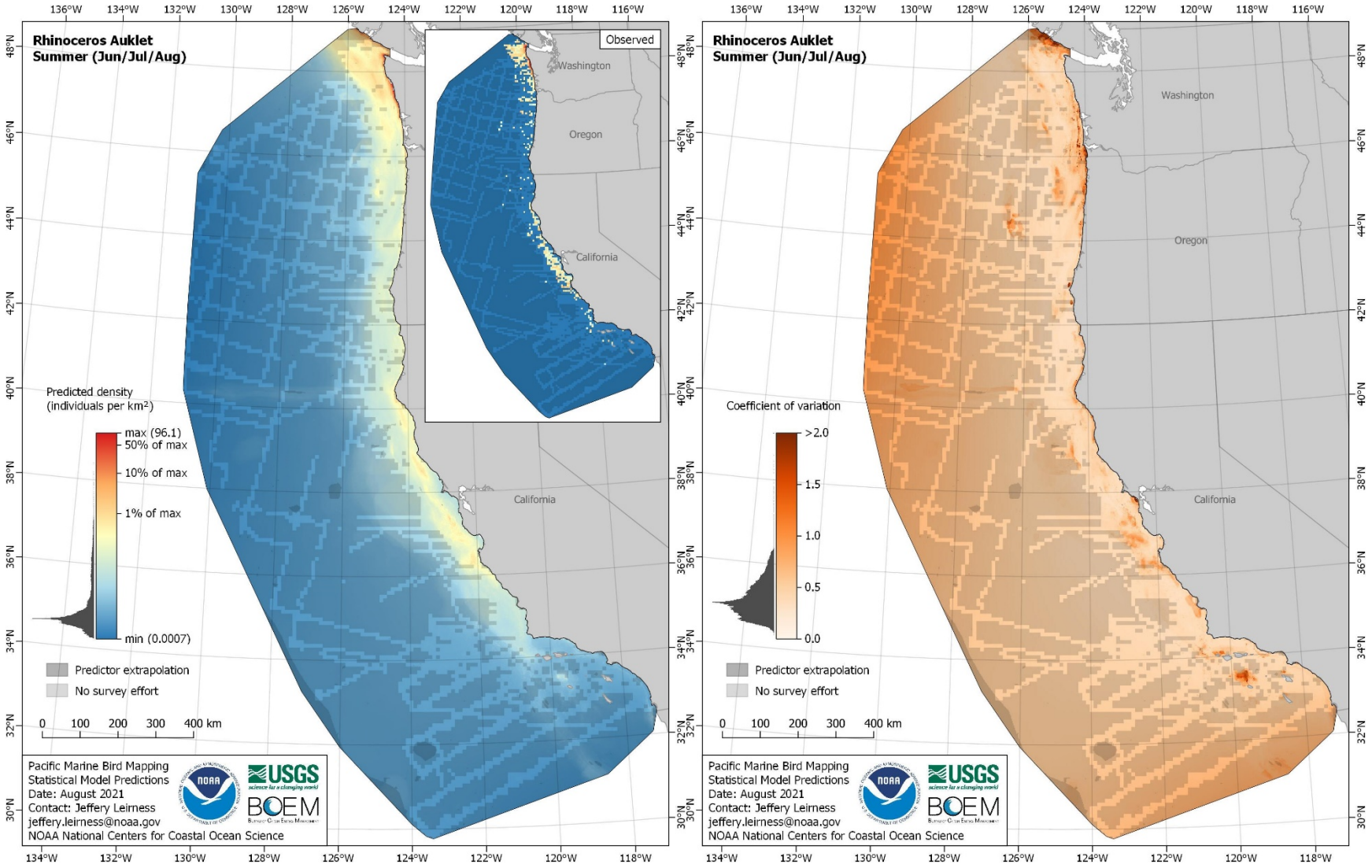

Figure 2.5. Example maps of predicted density (left panel) and coefficient of variation (right panel) for one species (Rhinoceros Auklet [*Cerorhinca monocerata*]) and season (summer)

Table 2.1. At-sea survey data used for analyses

		Year		Area Surveyed (km^2)				
Survey Name	**Platform**	**Start**	**End**	**Spring**	**Summer**	**Fall**	**Winter**	**Total**
Applied California Current Ecosystem Studies (ACCESS)	boat	2010	2015	172	679	480	0	1,331
California Cooperative Oceanic Fisheries Investigations (CalCOFI)[a]	boat	1987	2015	14,595	13,953	10,205	9,358	48,111
California Current Cetacean and Ecosystem Assessment Survey (CalCurCEAS)	boat	2014	2014	0	907	2,275	231	3,414
California Seabird Ecology Study (CDAS dataset code: SBECOL)[a]	aerial	1985	1985	200	0	0	0	200
Collaborative Survey of Cetacean Abundance and the Pelagic Ecosystem (CSCAPE)	boat	2005	2005	0	2,176	2,702	166	5,044
Equatorial Pacific Ocean Climate Studies (EPOCS)[a]	boat	1980	1995	350	109	258	681	1,397
Juvenile Salmon Ocean Ecosystem Survey (JSOES)	boat	2005	2017	396	836	0	0	1,232
Marine Mammal and Seabird Surveys of Central and Northern California (CDAS dataset codes: CLALL1 and CLALL2)[a]	aerial	1980	1983	1,560	1,475	1,459	1,571	6,065
Northwest Forest Plan Marbled Murrelet Monitoring Program Zone 2	boat	2000	2013	903	3,396	0	0	4,299
Northwest Forest Plan Marbled Murrelet Monitoring Program Zones 3-5[a,b]	boat	2000	2017	245	1,516	0	0	1,761
Olympic Coast NMS Seabird and Marine Mammal Surveys	boat	2002	2004	240	207	0	0	447
Olympic Coast NMS Pelagic Seabird Surveys	boat	2006	2016	331	86	177	0	595
Oregon and Washington Marine Mammal and Seabird Surveys (CDAS dataset code: OWPELB)[a]	aerial	1989	1990	659	621	473	152	1,904
Oregon, California, and Washington Line-transect Expedition (ORCAWALE)	boat	1996	2008	0	3,505	8,363	267	12,134
Pacific Coast Winter Sea Duck Survey	aerial	2011	2011	45	0	0	61	106
Pacific Continental Shelf Environmental Assessment (PaCSEA)	aerial	2011	2012	45	992	963	804	2,804
Pacific Orca Distribution Survey (PODS)	boat	2006	2012	1,018	0	0	46	1,064
Pelagic Juvenile Rockfish Recruitment and Ecosystem Assessment Survey[a]	boat	1996	2015	7,924	1,791	0	0	9,715
Santa Barbara Channel Surveys (CDAS dataset code: MMSSBC)[a]	aerial	1995	1997	132	110	85	117	444
Southern California Bight Surveys	aerial	1999	2002	1,218	27	1,234	1,234	3,712
Wind to Whales	boat	1997	2007	365	1,009	951	68	2,393
Total		**1980**	**2017**	**30,396**	**33,394**	**29,624**	**14,755**	**108,169**

[a] contained pre-segmented data
[b] only used in Marbled Murrelet models

Table 2.2. Species composition of taxonomic group models

For each taxonomic group, the total number of birds observed in each season are shown in *italics*. Non-italicized values represent the percentage of group-level observations contributed by each group member (e.g., total number of Surf Scoters observed in spring divided by total number of scoters observed in spring).

		Number of Birds Observed / Percent Contributions			
Group / Member Common Name	**Scientific Name**	**Spring**	**Summer**	**Fall**	**Winter**
Scoter spp.		*22,003*	*31,481*	*5,159*	*6,573*
Surf Scoter	*Melanitta perspicillata*	28.9%	31.9%	63.5%	70.9%
White-winged Scoter	*Melanitta deglandi*	53.8%	49.4%	3.1%	3.7%
Black Scoter	*Melanitta americana*	0.4%	0.1%	2.0%	1.0%
Unidentified scoter		16.9%	18.6%	31.3%	24.4%
Western/Clark's Grebe		*1,865*	*669*	*1,867*	*6,688*
Western Grebe	*Aechmophorus occidentalis*	99.6%	99.4%	95.3%	99.8%
Clark's Grebe	*Aechmophorus clarkii*	0.4%	0.6%	0.0%	0.2%
Unidentified Western/Clark's Grebe		0.0%	0.0%	4.7%	0.0%
Phalarope spp.		*124,955*	*29,755*	*40,928*	*5,802*
Wilson's Phalarope	*Phalaropus tricolor*	0.0%	0.0%	0.0%	0.0%
Red-necked Phalarope	*Phalaropus lobatus*	41.7%	36.3%	9.5%	3.1%
Red Phalarope	*Phalaropus fulicarius*	17.4%	13.2%	19.9%	36.5%
Unidentified phalarope		40.9%	50.4%	70.6%	60.4%
Parasitic/Long-tailed Jaeger		*155*	*461*	*1,171*	*55*
Parasitic Jaeger	*Stercorarius parasiticus*	78.7%	24.5%	33.0%	83.6%
Long-tailed Jaeger	*Stercorarius longicaudus*	21.3%	75.5%	65.8%	16.4%
Unidentified Parasitic/Long-tailed Jaeger		0.0%	0.0%	1.3%	0.0%
Jaeger spp.		*867*	*671*	*2,474*	*501*
Pomarine Jaeger	*Stercorarius pomarinus*	74.7%	24.4%	44.7%	78.4%
Parasitic Jaeger	*Stercorarius parasiticus*	14.1%	16.8%	15.6%	9.2%
Long-tailed Jaeger	*Stercorarius longicaudus*	3.8%	51.9%	31.1%	1.8%
Unidentified Parasitic/Long-tailed Jaeger		0.0%	0.0%	0.6%	0.0%
Unidentified jaeger		7.4%	6.9%	8.0%	10.6%

		Number of Birds Observed / Percent Contributions			
Group / Member Common Name	**Scientific Name**	**Spring**	**Summer**	**Fall**	**Winter**
Scripps's/Guadalupe/Craveri's Murrelet		*402*	*145*	*151*	*64*
Scripps's/Guadalupe Murrelet	*Synthliboramphus scrippsi/hypoleucus*	57.0%	33.1%	60.9%	26.6%
Craveri's Murrelet	*Synthliboramphus craveri*	0.7%	22.1%	13.9%	39.1%
Unidentified Scripps's/Guadalupe/Craveri's Murrelet		42.3%	44.8%	25.2%	34.4%
Western/Glaucous-winged Gull		*32,518*	*19,463*	*27,276*	*16,461*
Western Gull	*Larus occidentalis*	90.2%	78.5%	94.1%	91.8%
Glaucous-winged Gull	*Larus glaucescens*	2.0%	2.5%	4.9%	7.8%
Western x Glaucous-winged Gull hybrid		7.8%	19.0%	1.0%	0.5%
Herring/Iceland Gull		*1,061*	*369*	*3,753*	*4,919*
Herring Gull	*Larus argentatus*	97.1%	100.0%	99.5%	98.6%
Iceland Gull	*Larus glaucoides*	2.9%	0.0%	0.5%	1.4%
Common/Arctic Tern		*263*	*1,252*	*2,016*	*6*
Common Tern	*Sterna hirundo*	31.2%	4.6%	6.2%	16.7%
Arctic Tern	*Sterna paradisaea*	46.4%	95.3%	76.3%	0.0%
Unidentified Common/Arctic Tern		22.4%	0.1%	17.6%	83.3%
Royal/Elegant Tern		*811*	*1,043*	*500*	*109*
Royal Tern	*Thalasseus maximus*	14.3%	4.2%	6.8%	38.5%
Elegant Tern	*Thalasseus elegans*	60.4%	95.8%	57.0%	2.8%
Unidentified Royal/Elegant Tern		25.3%	0.0%	36.2%	58.7%
Loon spp.		*9,870*	*4,039*	*3,531*	*2,218*
Red-throated Loon	*Gavia stellata*	4.9%	11.7%	4.4%	6.6%
Arctic/Pacific Loon	*Gavia artica/pacifica*	69.6%	61.2%	81.2%	50.5%
Common Loon	*Gavia immer*	10.4%	11.6%	3.4%	4.5%
Yellow-billed Loon	*Gavia adamsii*	0.0%	0.0%	0.0%	0.0%
Unidentified loon		15.1%	15.5%	11.0%	38.4%
Short-tailed/Sooty/Flesh-footed Shearwater		*201,074*	*368,019*	*35,809*	*457*
Short-tailed Shearwater	*Ardenna tenuirostris*	0.1%	0.0%	2.3%	10.9%

		Number of Birds Observed / Percent Contributions			
Group / Member Common Name	**Scientific Name**	**Spring**	**Summer**	**Fall**	**Winter**
Sooty Shearwater	*Ardenna grisea*	97.3%	97.8%	97.1%	65.2%
Flesh-footed Shearwater	*Ardenna carneipes*	0.0%	0.0%	0.1%	6.3%
Unidentified Short-tailed/Sooty Shearwater		2.6%	2.2%	0.6%	17.5%
Cormorant spp.		*14,245*	*41,906*	*4,080*	*2,943*
Brandt's Cormorant	*Phalacrocorax penicillatus*	37.7%	12.7%	64.8%	39.0%
Pelagic Cormorant	*Phalacrocorax pelagicus*	39.0%	42.2%	2.8%	4.2%
Double-crested Cormorant	*Phalacrocorax auritus*	7.8%	28.5%	2.7%	9.7%
Unidentified cormorant		15.4%	16.7%	29.8%	47.2%

Table 2.3. Modeled individual species and taxonomic groups
Only combinations with ≥100 segments with sightings are shown.

			Number of Segments with Sightings					Number of Birds Observed				
Common Name	**Scientific Name**	**Family**	**Spring**	**Summer**	**Fall**	**Winter**	**Total**	**Spring**	**Summer**	**Fall**	**Winter**	**Total**
Scoter spp.	*Melanitta spp.*	Anatidae	690	1,107	151	380	2,328	22,003	31,481	5,159	6,573	65,216
Western/Clark's Grebe	*Aechmophorus occidentalis/clarkii*	Podicipedidae	215		169	310	694	1,865		1,867	6,688	10,420
Phalarope spp.	*Phalaropus spp.*	Scolopacidae	4,790	2,285	3,284	1,437	11,796	124,955	29,755	40,928	5,802	201,440
South Polar Skua	*Stercorarius maccormicki*	Stercorariidae			117		117			131		131
Pomarine Jaeger	*Stercorarius pomarinus*	Stercorariidae	472	134	853	303	1,762	648	164	1,106	393	2,311
Parasitic/Long-tailed Jaeger	*Stercorarius parasiticus/longicaudus*	Stercorariidae	136	301	678		1,115	155	461	1,171		1,787
Jaeger spp.	*Stercorarius pomarinus/parasiticus/ longicaudus*	Stercorariidae	649	468	1,641	394	3,152	867	671	2,474	501	4,513
Common Murre	*Uria aalge*	Alcidae	5,275	7,078	2,740	1,826	16,919	111,905	267,961	37,381	27,680	444,927
Pigeon Guillemot	*Cepphus columba*	Alcidae	455	1,108			1,563	1,835	5,251			7,086
Marbled Murrelet	*Brachyramphus marmoratus*	Alcidae	461	2,351			2,812	2,741	18,514			21,255
Scripps's/Guadalupe/ Craveri's Murrelet	*Synthliboramphus scrippsi/hypoleucus/craveri*	Alcidae	151				151	402				402
Ancient Murrelet	*Synthliboramphus antiquus*	Alcidae	214				214	1,098				1,098
Cassin's Auklet	*Ptychoramphus aleuticus*	Alcidae	2,827	2,095	1,995	2,697	9,614	20,282	19,694	13,763	14,216	67,955
Rhinoceros Auklet	*Cerorhinca monocerata*	Alcidae	2,701	2,850	1,261	1,526	8,338	15,649	65,822	3,888	7,475	92,834
Tufted Puffin	*Fratercula cirrhata*	Alcidae	290	1,042			1,332	1,397	8,240			9,637
Black-legged Kittiwake	*Rissa tridactyla*	Laridae	1,040		187	1,802	3,029	5,510		370	4,688	10,568
Sabine's Gull	*Xema sabini*	Laridae	605	170	334		1,109	2,691	422	1,509		4,622
Bonaparte's Gull	*Chroicocephalus philadelphia*	Laridae	549		397	192	1,138	3,915		3,151	2,632	9,698
Heermann's Gull	*Larus heermanni*	Laridae		626	686	368	1,680		1,372	2,239	1,170	4,781
California Gull	*Larus californicus*	Laridae	2,319	728	3,152	2,315	8,514	8,089	2,007	19,968	22,025	52,089

			Number of Segments with Sightings					Number of Birds Observed				
Common Name	**Scientific Name**	**Family**	**Spring**	**Summer**	**Fall**	**Winter**	**Total**	**Spring**	**Summer**	**Fall**	**Winter**	**Total**
Herring/Iceland Gull	*Larus argentatus/glaucoides*	Laridae	590	191	1,103	1,296	3,180	1,061	369	3,753	4,919	10,102
Western/Glaucous-winged Gull	*Larus occidentalis/glaucescens*	Laridae	9,204	5,298	5,475	3,354	23,331	32,518	19,463	27,276	16,461	95,718
Caspian Tern	*Hydroprogne caspia*	Laridae	104	584			688	490	4,564			5,054
Common/Arctic Tern	*Sterna hirundo/paradisaea*	Laridae	110	282	477		869	263	1,252	2,016		3,531
Royal/Elegant Tern	*Thalasseus maximus/elegans*	Laridae	173	308	140		621	811	1,043	500		2,354
Red-throated Loon	*Gavia stellata*	Gaviidae	183	166			349	479	473			952
Common Loon	*Gavia immer*	Gaviidae	391	250			641	1,027	468			1,495
Loon spp.	*Gavia spp.*	Gaviidae	1,871	1,104	550	633	4,158	9,870	4,039	3,531	2,218	19,658
Laysan Albatross	*Phoebastria immutabilis*	Diomedeidae	155			200	355	163			261	424
Black-footed Albatross	*Phoebastria nigripes*	Diomedeidae	3,158	2,016	1,125	311	6,610	6,179	3,886	1,836	406	12,307
Fork-tailed Storm-Petrel	*Hydrobates furcatus*	Hydrobatidae	501	762	385	145	1,793	1,265	4,932	2,406	250	8,853
Leach's Storm-Petrel	*Hydrobates leucorhous*	Hydrobatidae	1,491	4,221	3,337	979	10,028	3,438	9,986	8,350	1,904	23,678
Ashy Storm-Petrel	*Hydrobates homochroa*	Hydrobatidae	181	156	246		583	606	2,108	1,348		4,062
Black Storm-Petrel	*Hydrobates melania*	Hydrobatidae	185	348	116		649	514	1,445	324		2,283
Northern Fulmar	*Fulmarus glacialis*	Procellariidae	2,011	1,000	2,330	1,813	7,154	3,800	4,674	7,795	4,016	20,285
Murphy's Petrel	*Pterodroma ultima*	Procellariidae	150				150	193				193
Cook's Petrel	*Pterodroma cookii*	Procellariidae	457	631	144		1,232	987	1,569	214		2,770
Buller's Shearwater	*Ardenna bulleri*	Procellariidae		421	527		948		1,314	1,460		2,774
Pink-footed Shearwater	*Ardenna creatopus*	Procellariidae	2,367	2,389	1,595		6,351	6,828	14,409	8,087		29,324
Short-tailed/Sooty/Flesh-footed Shearwater	*Ardenna tenuirostris/grisea/carneipes*	Procellariidae	8,406	7,850	3,223	278	19,757	201,074	368,019	35,809	457	605,359
Black-vented Shearwater	*Puffinus opisthomelas*	Procellariidae	165		584	243	992	1,013		10,132	3,699	14,844
Brandt's Cormorant	*Phalacrocorax penicillatus*	Phalacrocoracidae	1,027	871			1,898	5,373	5,315			10,688

			Number of Segments with Sightings					Number of Birds Observed				
Common Name	**Scientific Name**	**Family**	**Spring**	**Summer**	**Fall**	**Winter**	**Total**	**Spring**	**Summer**	**Fall**	**Winter**	**Total**
Pelagic Cormorant	*Phalacrocorax pelagicus*	Phalacrocoracidae	560	1,511			2,071	5,558	17,686			23,244
Double-crested Cormorant	*Phalacrocorax auritus*	Phalacrocoracidae	270	647			917	1,116	11,923			13,039
Cormorant spp.	*Phalacrocorax spp.*	Phalacrocoracidae			944	760	1,704			4,080	2,943	7,023
Brown Pelican	*Pelecanus occidentalis*	Pelecanidae	771	1,196	1,094	520	3,581	2,976	9,853	5,521	1,562	19,912
Total								**613,609**	**940,605**	**259,543**	**138,939**	**1,952,696**

Table 2.4. Survey and temporal predictor variables

Predictor Variable	Description	Source
survey platform	platform used for data collection (i.e., aerial or boat)	survey data
survey ID	combination of survey name and year	survey data
transect ID	combination of survey name and date	survey data
Year	year of data collection	survey data
day of year	calculated from date of data collection; represented as number of days after December 31 within a given year (e.g., a value of 1 represents January 1 regardless of year)	survey data
MEI	monthly multivariate El Niño-Southern Oscillation index	NOAA Physical Sciences Laboratory (https://psl.noaa.gov/data/correlation/meiv2.data)
NPGO index	monthly North Pacific Gyre Oscillation index	http://www.o3d.org/npgo/npgo.php (Di Lorenzo et al. 2008)
PDO index	monthly Pacific Decadal Oscillation index	NOAA Physical Sciences Laboratory (https://psl.noaa.gov/data/correlation/pdo.data)

Table 2.5. Geographic and bathymetric predictor variables

Predictor Variable	Description	Units	Source
projected longitude	representation of longitude corresponding to grid cell midpoint in custom oblique Mercator projected space (i.e., x-coordinate of grid cell)	m	derived from study grid
projected latitude	representation of latitude corresponding to grid cell midpoint in custom oblique Mercator projected space (i.e., y-coordinate of grid cell)	m	derived from study grid
distance to land	distance to nearest land	km	derived from full resolution GSHHG coastline data version 2.3.6 (https://www.ngdc.noaa.gov/mgg/shorelines; Wessel and Smith 1996)
distance to canyon	distance to nearest seafloor canyon	km	derived from Global Seafloor Geomorphology 'Canyons' data (http://www.bluehabitats.org; Harris et al. 2014)
depth	seafloor depth derived from a synthesis of bathymetry datasets	m	multibeam bathymetry (**Appendix C**), NOAA CRM – Southern California Version 2, NOAA CRM Vol. 7 – Central Pacific, NOAA CRM Vol. 8 – Northwest Pacific, GEBCO_2014 grid version 20150318
slope[a]	steepness of the seafloor, calculated as the magnitude of the maximum gradient in depth from a 3 x 3 pixel array	degrees	derived from depth
slope of slope[a]	rate of change in slope of the seafloor, calculated as the magnitude of the maximum gradient in slope from a 3 x 3 pixel array	degrees of degrees	derived from depth
planform curvature[a]	curvature of the seafloor along the line of intersection between the depth surface and the horizontal plane; indicates whether seafloor is convex (>0), concave (<0), or flat (0)	radians / 100 m	derived from depth
profile curvature[a]	curvature of the seafloor along the line of intersection between the depth surface and the plane formed by the direction of slope and the z-axis; indicates whether the seafloor is convex (<0), concave (>0), or flat (0)	radians / 100 m	derived from depth

[a] calculated at 10- and 20-km scales

Table 2.6. Oceanographic and atmospheric predictor variables

Predictor Variable	Description	Statistics[a]	Units	Native Spatial Resolution	Source
chlorophyll-a concentration	concentration of chlorophyll-a at the ocean surface	mean	mg / m^3	4 x 4 km	NASA OceanColor Aqua and Terra MODIS and VIIRS (1997-2017)
chlorophyll-a front strength	gradient magnitude of fronts derived from chlorophyll-a concentration at the ocean surface from a 32 x 32 pixel array	mean	log(mg / m^3) / km	1 x 1 km	derived from NOAA CoastWatch (dataset: erdMEchla1day; 2002-2013)
turbidity	ocean surface reflectance at 447 nm	mean, standard deviation	1 / sr	4 x 4 km	NASA OceanColor Aqua and Terra MODIS (2000-2017)
current velocity (east-west)	east-west component (u) of current speed at the ocean surface	mean	m / s	8 x 8 km	HYCOM Global Reanalysis GLBu0.08 (1992-2012)
current velocity (north-south)	north-south component (v) of current speed at the ocean surface	mean	m / s	8 x 8 km	HYCOM Global Reanalysis GLBu0.08 (1992-2012)
current speed	current speed at the ocean surface	mean	m / s	8 x 8 km	derived from HYCOM Global Reanalysis GLBu0.08 (1992-2012)
current divergence	current divergence at the ocean surface	mean	unitless	8 x 8 km	derived from HYCOM Global Reanalysis GLBu0.08 (1992-2012)
current vorticity	current vorticity at the ocean surface	mean	unitless	8 x 8 km	derived from HYCOM Global Reanalysis GLBu0.08 (1992-2012)
sea surface height	height of the ocean surface relative to the geoid	mean, standard deviation	m	25 x 25 km	CMEMS (dataset: SEALEVEL_GLO_PHY_L4_REP_OBSERVATIONS_008_047; 1993-2017)
eddy frequency (anticyclonic)	proportion of days with anticyclonic eddy ring presence	mean	unitless	25 x 25 km	derived from AVISO (1994-2015)
eddy frequency (cyclonic)	proportion of days with cyclonic eddy ring presence	mean	unitless	25 x 25 km	derived from AVISO (1994-2015)
temperature	water temperature at the ocean surface	mean, standard deviation	ºC	5 x 5 km	CMEMS (dataset: SST_GLO_SST_L4_REP_OBSERVATIONS_010_024; 1981-2016)
temperature anomaly frequency	proportion of days where daily ocean surface temperature was more than 1ºC greater than the monthly climatological mean ocean surface temperature	mean	unitless	1 x 1 km	derived from CMEMS (dataset: SST_GLO_SST_L4_REP_OBSERVATIONS_010_024; 1981-2016)
temperature front strength	gradient magnitude of fronts derived from water temperature at the ocean surface from a 32 x 32 pixel array	mean	ºC / km	1 x 1 km	derived from NOAA CoastWatch (dataset: erdMEssta1day; 2003-2012)

Predictor Variable	Description	Statistics[a]	Units	Native Spatial Resolution	Source
Ekman driven upwelling	upwelling driven by Ekman transport (wind driven surface currents)	mean	m / s	13 x 13 km	NOAA CoastWatch (dataset: erdQSstress1day; 1999-2009)
salinity	salinity at the ocean surface	mean, standard deviation	psu	8 x 8 km	HYCOM Global Reanalysis GLBu0.08 (1992-2012)
mixed layer depth	depth at which temperature differed from the surface by ≥0.5ºC	mean, standard deviation	m	8 x 8 km	derived from HYCOM Global Reanalysis GLBu0.08 (1992-2012)
wind stress (east-west)	zonal east-west component (u) of wind shear stress on the ocean surface	mean	Pa	13 x 13 km	NOAA CoastWatch (dataset: erdQSstress1day; 1999-2009)
wind stress (north-south)	meridional north-south component (v) of wind shear stress on the ocean surface	mean	Pa	13 x 13 km	NOAA CoastWatch (dataset: erdQSstress1day; 1999-2009)
wind stress divergence	wind shear stress divergence on the ocean surface	mean	1 / s	13 x 13 km	derived from NOAA CoastWatch (dataset: erdQSstress1day; 1999-2009)

[a] calculated as seasonal climatologies

Table 2.7. Base-learners used in the boosted generalized additive modeling framework

Name	Description	Predictor Variables	Model Component
bols	linear	intercept	p, μ, θ
bols	linear (fixed effect)	survey platform	p, μ, θ
brandom	random effect	survey ID	θ
brandom	random effect	transect ID	p, μ
bbs	penalized regression spline[a]	year	p, μ
bbs	penalized regression spline[a]	day of year	p, μ
bspatial	penalized tensor product[a]	projected longitude, projected latitude	p, μ
brad	penalized radial basis[b]	projected longitude, projected latitude	p, μ
btree	tree[c]	all climate indices	p, μ
btree	tree[d]	distance land, distance to canyon, and all bathymetric, oceanographic, and atmospheric variables	p, μ

[a] p-spline basis
[b] matérn correlation function
[c] maximum depth = 1
[d] maximum depth = 5

3 Results

3.1 Model Selection and Performance

The final selected model (i.e., ZIP or ZINB) varied among species/groups and seasons (**Appendix D**). ZINB models were selected more frequently than ZIP models (102 versus 33 models). Models with different likelihoods (i.e., ZIP or ZINB) were often selected for different seasons for the same species/group.

The statistical performance of the final selected models was variable among species/groups and seasons (**Appendix D**). Over half of the models had $M \geq 19{,}000$, close or equal to the maximum of 20,000 (see **Section 2.5.6**). PDE ranged from 2% to 77%. AUC ranged from 0.777 to 0.996. r_G ranged from 0.06 to 0.68. The median AE and mean AE ranged from 0.1% to 85.0% and 71% to 207% of the mean count, respectively. RMSE ranged from 0.1 to 169.4.

Performance metrics were often correlated with each other, usually in the expected direction, although the correlations were often weak ($|r_s| < 0.5$). PDE was strongly correlated with AUC ($r_s = 0.84$), median AE ($r_s = -0.88$), and mean AE ($r_s = -0.71$). AUC was strongly correlated with median AE ($r_s = -0.76$). r_G was strongly correlated with mean AE ($r_s = -0.73$) and RMSE ($r_s = -0.67$). Median AE was strongly correlated with mean AE ($r_s = 0.75$). Unexpectedly, RMSE was positively correlated with PDE ($r_s = 0.42$) and negatively correlated with both median AE ($r_s = -0.51$) and mean AE ($r_s = -0.59$).

The five best performing models, determined by summing the ranks of the individual performance metrics, were Pelagic Cormorant (*Phalacrocorax pelagicus*), Pigeon Guillemot (*Cepphus columba*), and Marbled Murrelet (*Brachyramphus marmoratus*) in summer, Marbled Murrelet in spring, and Loon spp. (*Gavia* spp.) in summer – all highly coastal species. The models with the worst performance were (in order of decreasing performance) Pomarine Jaeger in summer, Ashy Storm-Petrel (*Hydrobates homochroa*) in spring, Phalarope spp. (*Phalaropus* spp.) in fall, Common/Arctic Tern (*Sterna hirundo*/*paradisaea*) in spring, and Ashy Storm-Petrel in summer. Some models had a mix of high and low performance metric rankings. For example, Pelagic Cormorant in summer had the second highest PDE and AUC values, a high r_G value, the sixth lowest median AE, the lowest mean AE, yet a moderately high (86th lowest) RMSE. Pomarine Jaeger in summer had poorly ranked PDE (134th), AUC (118th), r_G (133rd), median AE (129th), and mean AE (134th), yet it ranked 4th in RMSE. It is possible that low species prevalence in the data contributed to the poor performance of some models. For example, Pomarine Jaeger in summer had the fifth lowest number of segments with sightings, the fourth lowest number of individuals counted, and the fourth lowest count per segment when sighted (**Table 2.3**). Common/Arctic Tern in spring had the second lowest number of segments with sightings.

3.2 Predicted Spatial Distributions

3.2.1 Spatial and Seasonal Patterns

Given the large number of species/groups modeled, the spatial distributions of predicted density varied widely (**Appendix E**). Broad patterns in predicted density generally aligned with observed densities and usually were consistent with known patterns in distributions of these marine bird species. Predicted distributions of Scoter spp. (*Melanitta* spp.), Western/Clark's Grebe (*Aechmophorus occidentalis*/*clarkii*), Common Murre, Pigeon Guillemot, Marbled Murrelet, Caspian Tern (*Hydroprogne caspia*), Royal/Elegant Tern (*Thalasseus maximus*/*elegans*), Loon spp., Black-vented Shearwater (*Puffinus opisthomelas*), cormorants, and Brown Pelican (*Pelecanus occidentalis*) were mostly coastal with highest predicted densities near shore. Auklets, Tufted Puffin (*Fratercula cirrhata*), Black-legged Kittiwake

(*Rissa tridactyla*), gulls, Black-footed Albatross (*Phoebastria nigripes*), Fork-tailed Storm-Petrel (*Hydrobates furcatus*), Ashy Storm-Petrel, Black Storm-Petrel (*Hydrobates melania*), Northern Fulmar (*Fulmarus glacialis*), Pink-footed Shearwater (*Ardenna creatopus*), and Short-tailed/Sooty/Flesh-footed Shearwater had highest predicted densities along the edge of the continental shelf in spring, summer, and fall, with predicted distributions expanding offshore during the winter season. South Polar Skua (*Stercorarius maccormicki*) and jaegers (*Stercorarius pomarinus*/*parasiticus*/*longicaudus*) also had predicted distributions concentrated over shelf/slope waters, except Parasitic/Long-tailed Jaeger (*Stercorarius parasiticus*/*longicaudus*) and the Jaeger spp. taxonomic group during summer and fall, where distributions expanded farther offshore. Predicted distributions of Laysan Albatross (*Phoebastria immutabilis*), Leach's Storm-Petrel (*Hydrobates leucorhous*), Murphy's Petrel (*Pterodroma ultima*), and Cook's Petrel (*Pterodroma cookii*) were generally far offshore, beyond the continental slope. Areas of highest predicted density for Common/Arctic Tern and Buller's Shearwater (*Ardenna bulleri*) were a mixture of continental shelf/slope waters and waters farther offshore.

The predicted distributions for some species/groups within the study area were relatively restricted in area, at least seasonally. For example, the highest density areas for Parasitic/Long-tailed Jaeger in spring were predicted along the continental slope offshore of north-central California. Scripps's/Guadalupe/Craveri's Murrelet (*Synthliboramphus scrippsi/hypoleucus*/*craveri*) during spring had the highest predicted densities near the California Channel Islands. Several breeding alcid species had relatively high predicted densities directly offshore of the Olympic Peninsula in Washington including Ancient Murrelet (*Synthliboramphus antiquus*) in spring, Rhinoceros Auklet (*Cerorhinca monocerata*) in spring and summer, and Tufted Puffin in spring and summer. Predictions of high density for Royal/Elegant Tern in spring, Black Storm-Petrel in spring and summer, and Black-vented Shearwater were mostly confined to the Southern California Bight. The highest predicted densities for Pelagic Cormorant during the spring and summer breeding seasons were confined to coastal Washington. Most other predicted distributions were less restricted in area, but highest predicted densities were usually still confined to specific regions within the study area. Predicted distributions for some species/groups were concentrated in the northern part of the study area (e.g., loons in summer and Fork-tailed Storm-Petrel). Other species/groups had more southerly predicted distributions, either coastal (e.g., Brown Pelican in winter) or offshore (e.g., Ashy Storm-Petrel in spring and Cook's Petrel in summer). Several species/groups showed relatively high predicted densities near the Columbia River mouth, especially during spring and summer (e.g., Caspian Tern, Short-tailed/Sooty/Flesh-footed Shearwater, Double-crested Cormorant [*Phalacrocorax auritus*], and Brown Pelican).

The predicted spatial distributions for many species/groups changed seasonally, reflecting seasonal movements and migrations. As mentioned above, the seasonal distributions of alcids that breed in the study area were more concentrated nearshore around the colonies during summer transitioning to more widely dispersed offshore distributions during winter. For some species/groups, predictions of relatively high densities extended to areas farther north during the summer and/or farther south during the winter (e.g., Bonaparte's Gull [*Chroicocephalus philadelphia*], California Gull [*Larus californicus*], and Brown Pelican). Migrations among species that mostly leave the study area altogether were reflected by the absence of models for these species/groups during certain seasons (e.g., Western/Clark's Grebe, Black-legged Kittiwake, Bonaparte's Gull, Laysan Albatross, and Black-vented Shearwater during summer, and Sabine's Gull [*Xema sabini*], terns, storm-petrels, petrels, and most shearwaters during winter).

Within taxonomic group models, the individual species proportions were unequal and variable among seasons (**Table 2.2**); therefore, resulting predicted spatial distributions comprise different species compositions during the different seasons. For example, Parasitic Jaegers accounted for the majority of all Parasitic/Long-tailed Jaeger observations during the winter and spring seasons. The proportions reversed during summer and fall when Long-tailed Jaegers accounted for the majority of observations. Because of this, predicted densities for the Parasitic/Long-tailed Jaeger taxonomic group largely represent Parasitic

Jaeger during the winter and spring seasons, whereas during summer and fall, Long-tailed Jaeger abundance disproportionately was responsible for the predicted distribution of this group. This was similar for all taxonomic group models except Western/Clark's Grebe and Herring/Iceland Gull (*Larus argentatus*/*glaucoides*), where individual species proportions remained consistent among seasons with Western Grebe and Herring Gull comprising the vast majority of observations for the two groups.

3.2.2 Uncertainty

The estimated uncertainty in the model predictions generally was high. The minimum CV for predictions in individual spatial grid cells ranged from 0.02 to 1.05 across all models, and the maximum CV ranged from 1.53 to 14.14. Thus, all models had at least some predictions with CVs exceeding 1 indicating that the bootstrap standard deviation was greater than the mean. CVs were influenced by variable amounts of survey effort (resulting in small sample sizes among less-common species), species-specific aggregation, extrapolation based on predictor variable values that were outside the range of values observed during survey efforts, and unmodeled variation in the spatial distributions of birds (e.g., changes in spatial distributions over time). It is difficult to quantify the contribution of each of these unknown sources of variability to the CV for any particular prediction. The spatial patterns in the estimated CV of predictions varied widely among species/groups and seasons (**Appendix E**). In some cases the CV was lower in areas with higher predicted density (e.g., Rhinoceros Auklet in spring), but in others, the CV was higher in areas with higher predicted density (e.g., Black Storm-Petrel in fall). Higher CVs sometimes reflected an absence of survey effort in areas with relatively low predicted density (Jaeger spp. in spring, offshore of Washington and northern Oregon) or relatively high predicted density (Cassin's Auklet [*Ptychoramphus aleuticus*] in fall, off the coast of Vancouver Island). Many of the questionable predictions (see **Section 3.2.3**) were associated with relatively high CVs (e.g., Marbled Murrelet and Tufted Puffin offshore in spring). The spatial patterns in the estimated CV often reflected the influence of particular predictor variables, even when that influence was not as apparent in predicted density itself (e.g., Cook's Petrel in fall, anticyclonic eddy frequency and slope of slope at 10-km scale). The estimated standard errors and confidence interval widths for predicted density were highly correlated with the predicted density values, usually resulting in similar spatial patterns. As indicated by the magnitude of the CVs, the values of the standard errors and confidence interval widths generally were large relative to the corresponding predicted densities.

3.2.3 Questionable Predictions

Predicted densities for some species/groups in some areas were questionable, especially in areas with little or no survey effort. Predictions for these areas were often associated with higher CVs. For example, there was much less survey effort beyond the shelf break than near the coast and over the shelf, especially during winter and spring (**Figure 2.2**). Although predicted densities for some species/groups were relatively high far offshore, some were plausible but others were questionable. For example, some coastal species had relatively moderate predicted densities extending farther offshore during spring than were realistic (e.g., Scoter spp., Pigeon Guillemot, Common Loon). Even for species that are generally found far from shore, areas with relatively moderate to high predicted densities offshore may be larger than are realistic given the limited survey coverage there (e.g., Phalarope spp., Pomarine Jaeger, Black-legged Kittiwake, Laysan Albatross, Fork-tailed Storm-Petrel, Leach's Storm-Petrel, Northern Fulmar, Murphy's Petrel, and Cook's Petrel). Additionally, some species/groups (e.g., Black Storm-Petrel, Black-vented Shearwater, and Brown Pelican during winter) had relatively moderate to high predicted densities near Vancouver Island and the Strait of Juan de Fuca in an area without survey effort; these patterns are questionable given our understanding of these species' historic seasonal ranges based on their presence in these comprehensive survey datasets (see **Section 2.2**).

Predicted spatial distributions sometimes exhibited patterning or extremely localized areas with relatively high predicted densities that seem unrealistic. Unrealistic patterning often reflected disproportional

influence of individual predictor variables on model predictions, especially in areas with little or no survey effort, and was often associated with higher CVs. For example, several winter and spring models exhibited a vertical band of relatively moderate to high predicted densities along the western edge of the study area. This band resulted from extrapolating the estimated relationship between projected longitude and the bird sighting data to areas outside the range of values observed in the survey data. The predicted distribution of Red-throated Loon in spring exhibited an obvious effect of turbidity standard deviation that resulted in unrealistic patches with higher predicted densities near the northwestern edge of the study area. The distribution of Laysan Albatross in spring exhibited circular patterning of relatively moderate to high predicted densities that corresponded with areas of relatively high frequency of cyclonic eddy formations. Some predictions were clearly extrapolations of the relationship between bathymetric predictor variables and bird counts to areas without survey effort (e.g., Pomarine Jaeger in winter, Marbled Murrelet in spring, Sabine's Gull in spring and summer, Common/Arctic Tern in spring, Laysan Albatross in winter, Leach's Storm-Petrel in spring, Ashy Storm-Petrel in fall). It is likely that the discrete nature of these distribution patterns is unrealistic.

The highest predicted densities were sometimes limited to one or a few small areas indicating localized long-term aggregations that likely also are unrealistic. These predictions were sometimes associated with higher CVs, but not always. Some example species/groups and seasons exhibiting this behavior were Phalarope spp. in spring, Parasitic/Long-tailed Jaeger in spring, Jaeger spp. in fall, Common/Arctic Tern in spring, summer, and fall, and Cook's Petrel in fall. It is difficult to ascribe these highly-localized distribution patterns to a specific cause, but in at least some cases they may partially reflect large temporal and spatial aggregations of birds, possibly during migration, that coincided with survey effort rather than realistic average long-term spatial patterns. It is unlikely that these are persistent areas with higher absolute densities than adjacent areas. Although our spatial predictive modeling framework accounted for effort and attempted to account for the aggregated nature of bird distributions and sightings, small sample size combined with extreme aggregations can unduly influence model predictions.

3.3 Predictor Variable Relative Importance

The modeling framework used in this study was designed to provide accurate predictions. It was not designed to identify which environmental predictors were most ecologically relevant for determining the distribution of marine birds. Ecological inferences from the variable importance results should be made with caution. Nevertheless, these results may indicate interesting hypotheses for future research. Also, as discussed in **Section 3.2.3** extrapolations of the predicted relationships between observed bird count and predictor variables to areas with little or no survey effort were often questionable or unrealistic.

The most important predictor variables varied among species/groups and seasons (**Appendix F**); however, some consistent patterns emerged. Averaged among all species/groups and seasons, day of year, distance to land, depth, chlorophyll-a concentration, current speed and mean temperature were the most important predictor variables for both the p and μ model components. Mean salinity and mean mixed layer depth were also important for the p model component, but transect ID and year were important for the μ component only. In addition to the predictor variables mentioned above, turbidity standard deviation and mean mixed layer depth were important in the spring season models when averaged among all species/groups. For summer models, salinity (both mean and standard deviation), mean turbidity, and to a lesser extent chlorophyll-a front strength (mainly for the p model component) and current vorticity (mainly for the p model component) were also important. In fall, current velocity in the east-west direction and mean sea surface height were also important. Slope (20-km scale) and mean sea surface height were important, mainly for the p model component, for winter season models averaged among all species/groups.

Transect ID was an especially important predictor in the μ model component and its importance indicates substantial variation in the count data that was not explained by the temporal and spatial predictor variables. Year was one of the top four most important predictor variables on average for the μ model component in all seasons, reflecting the interannual variability in seasonal abundance within the study area. Day of year was the first or second most important predictor on average for the μ model component in spring (first), summer (first), and fall (second) models likely reflecting the movement of migratory species in and out of the study area during transitions between summer and winter. Distance to land was often an important predictor for coastal species but was also often important for species with more offshore distributions (e.g., Fork-tailed Storm-Petrel). Averaged among all species/groups, mean chlorophyll-a concentration was the most important predictor for the p model component in all seasons, underscoring the importance of this variable in predicting spatial distribution patterns, especially for coastal and continental shelf species. Mean temperature was a relatively important predictor for most models, reflecting its ability to capture broad latitudinal and California Current-related patterns in distribution.

In general, the climate index predictor variables were relatively unimportant. They were more important in the winter and spring than in the summer and fall models. The NPGO index was the most important of the three indices on average, although the MEI and the PDO index were important in some models.

4 Discussion

4.1 Interpretation of Maps

This report presents maps of the seasonal spatial distributions of predicted density for 33 marine bird species and 13 taxonomic groups observed during surveys in Pacific OCS waters off the contiguous U.S. (**Appendix E**) that can be used to inform marine spatial planning in the region. The maps of predicted density are accompanied by corresponding maps of the estimated CV of model predictions. It is important that these uncertainty maps are considered alongside the predicted density maps. In many cases the CVs are relatively large indicating substantial statistical uncertainty and variability associated with the corresponding predictions, and those predictions should be interpreted cautiously. Although model predictions are at 2-km resolution, interpretation of the maps presented to inform spatial planning is more reliable at scales of 10–100 km. The maps of predicted density are also accompanied by inset maps of observed density. These inset maps indicate where species/groups were seen during a given season by the surveys analyzed herein, and this information should also be considered when interpreting model predictions.

The maps represent model-derived spatial predictions of long-term average density. They do not provide predictions of the actual number of individuals of a given species or taxonomic group that would be expected in a given area; they only indicate where a given species/group may be more or less abundant. Also, the maps do not provide predictions of density at a specific time; they only indicate seasonal distributions averaged across the timeframe of the survey dataset (1980–2017). The spatial distributions of marine birds often change during the course of a season and from year to year in response to fluctuations in environmental conditions, prey distributions, and fisheries, so it is likely that the spatial distributions of many if not all of the modeled species/groups have changed over time. Furthermore, predictions of long-term average density do not necessarily highlight areas including movement corridors that are consistently used by a large number of birds but only for a short period during the year (e.g., hours or days).

The maps represent predicted density throughout the study area only. The study area excluded nearshore waters within 50 m of the shoreline and coastal sounds and bays (e.g., Salish Sea, Grays Harbor, Willapa

Bay, mouth of the Columbia River, San Francisco Bay) that are used by multiple marine bird species, sometimes with large numbers of birds occurring in these areas at certain times of year (e.g., scoters, grebes, alcids, loons). More generally, areas with relatively high known densities occur adjacent to the study area for some species, and these areas are not represented on the maps. Thus, the areas with the highest predicted densities are not necessarily the areas of greatest absolute density for a species were its entire range to be considered. Depending on data availability, habitat-based predictive modeling could be extended to nearshore waters and coastal sounds and bays, but such modeling would entail additional considerations. For example, relationships between bird count and environmental predictors may be different in these areas than in more offshore areas. Another consideration would be an appropriate spatial modeling technique for complex coastlines (Scott-Hayward et al. 2014).

4.2 Species Identification

A fundamental assumption of the analysis presented here is that all species, when present, were recorded. This assumption may not have been met on all surveys. A related issue is the identification of observed birds to the species level. From some survey platforms, some birds might have been less likely to be identified to species. Our decision to combine certain species into taxonomic groups prior to modeling should limit the effect of potential biases in species identification by including birds not identified to the species level (see **Section 2.3**); however, inference is then restricted to the group of species as a whole. For individual species models, birds that were not identified to species were not included in the analysis.

Our statistical modeling framework allowed for differences in the expected count of a given species between survey platforms and among transects, so theoretically the models could account for some differences arising from failure to record or identify species. However, if a geographic area was covered by a limited number of surveys or a single platform, then it would have been difficult or impossible for the model to determine whether differences in counts in that area were because of fewer birds in that area or because of differences in species recording and identification in that area. Alternative modeling techniques in combination with appropriate survey data may provide some ability to make individual species inferences from sightings of unidentified species (e.g., Johnston et al. 2015).

4.3 Data Limitations and Information Gaps

The maps presented here represent model predictions that ultimately rely on the survey data that the models were fit to. The distribution of survey effort was uneven throughout the study area and through time (**Figures 2.1 and 2.2**), so some regions and years were better sampled than others. For example, there were fewer data offshore than nearshore, especially in the northern extent of the study area. Model predictions in areas with no survey effort are indicated by light gray semi-transparent overlays on the maps. Predictions in these areas should be interpreted with caution. Additional field surveys in under-sampled areas would help to improve future model predictions. In order for future survey data to be amenable for similar analysis, surveys should adhere to standardized survey protocols for marine birds at sea and document key information related to survey effort (e.g., complete spatial descriptions of transects, duration of observation, strip width, etc.).

Future habitat-based predictive modeling could also benefit from data on additional environmental predictor variables. Most of the environmental predictors used in this study would be indirect drivers of marine bird distributions. The fact that transect ID was a relatively important predictor in several models (especially in the μ model component) indicates considerable variation in the count data that were not explained by the suite of environmental predictor variables used in these analyses (see **Section 3.3 and Appendix F**). Data on variables that birds are responding to more directly (e.g., zooplankton or fish availability) could improve model predictions, particularly in areas with little or no survey effort.

Unfortunately, comprehensive estimates of seasonal prey densities across the entire study area were not available for this study. For species that breed in close proximity to the study area, data on colony location and size, both current and historic, could also improve model predictions and may be valuable for future spatial modeling efforts in the region.

4.4 Combining Seasonal Maps

The seasonal maps presented in **Appendix E** represent periods of 3 months of the year for individual species and certain taxonomic groups. For some applications it may be of interest to consider an annual average distribution for individual species/group or a seasonal/annual average distribution among species. Such combining of seasonal maps should be done cautiously while acknowledging important assumptions.

To derive an annual map for a single species or modeled taxonomic group, we suggest averaging the seasonal predicted grids for that species/group assuming zero predicted density for seasons that were not modeled. Ideally for bootstrapped predictions, a bootstrapped sample of annual predicted grids would be derived first and then desired quantities calculated from that sample (e.g., median, quantiles, etc.). The averaging of seasonal grids entails several important assumptions. First, species are often present in the study area at low density during seasons that were not modeled, so the assumption of zero density during those seasons is an approximation. Second, the predictions in each seasonal grid correspond to the average year of the survey data (see **Section 2.5.8**), which varied among seasons (spring: 2000, summer: 2001, fall: 1999, winter: 1998). Thus, the seasonal maps represent predictions for different years, so any interannual variation in density will influence predictions averaged among seasons. Third, as discussed previously the predictions do not explicitly account for several potential biases (e.g., detectability; see **Section 2.5.8**). Any interseasonal variation in these biases will influence predictions averaged among seasons. **Figure 4.1** shows annual maps for an example species, Rhinoceros Auklet. By averaging the seasonal predicted grids, the annual map most reflects the seasons with the highest predicted density values, in this case spring and summer.

To derive multi-species maps, we suggest first normalizing the predicted grids for individual species/groups and then averaging grids among species. Predicted density values are not comparable among species/groups (see **Section 2.5.8**), so it would be inappropriate to directly average predicted grids among species. Normalization scales each grid the same, which makes averaging of grids among species more appropriate. Predicted grids can be normalized by dividing the predicted density value for each grid cell by the sum of predicted density values in all grid cells. If the grid dimensions are identical among species/groups, as they are here, dividing by the mean predicted density value will achieve an equivalent normalization. Averaged normalized predicted values do not have a straightforward interpretation, so as with all predictions of density presented in this report it is the relative differences in predictions across space that are relevant, not the actual numbers themselves. It is important to note that because of normalization each species will essentially contribute equally to the average grid. Such equal weighting for all species may be desirable in some applications, but in others it may be desirable to weight species differently, for example by their population abundance or species-specific vulnerability (see Adams et al. 2017 and Kelsey et al. 2018). The results presented here could theoretically be used to derive weighted averages, but such an approach would require supplementary information to inform the weighting (e.g., independent estimates of population abundance).

4.5 Conclusion

The maps presented in this report can be used to inform planning for ocean activities such as offshore wind energy development. The maps identify areas where the densities of marine bird species are likely to

be relatively higher or lower on a seasonal basis. This information can contribute to assessments of relative risk exposure aimed at minimizing the impacts of activities on marine birds (Winiarski et al. 2014; Fifield et al. 2017). As discussed in **Section 4.3**, the survey data analyzed here had some limitations. Any full assessments of risk exposure in specific areas at specific times should augment the information provided here with more targeted analyses and potentially additional survey (or tracking) data to inform those analyses, especially when there are few existing data. Nevertheless, our maps provide a starting point for assessing relative risks associated with exposure, which when combined with information about other aspects of vulnerability (e.g., flight height, avoidance/attraction, demographic impacts), can inform assessments of overall risk for marine birds in Pacific OCS waters off the contiguous U.S. (Garthe and Hüppop 2004; Robinson Willmott et al. 2013; Bailey et al. 2014; Bradbury et al. 2014; Adams et al. 2017; Kelsey et al. 2018).

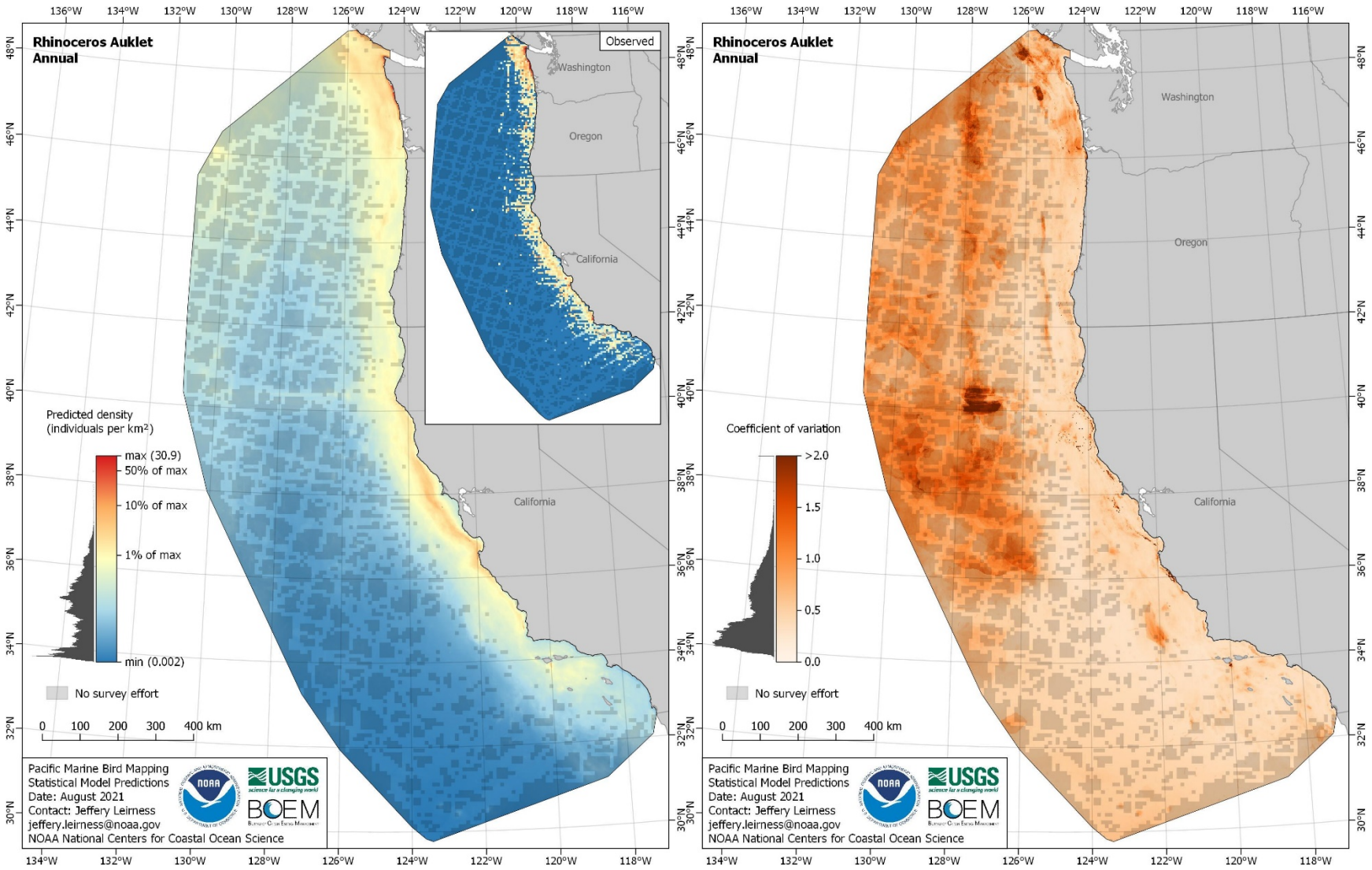

Figure 4.1. Example annual maps of predicted density (left panel) and coefficient of variation (right panel) for one species (Rhinoceros Auklet [*Cerorhinca monocerata*])

5 References

Adams J, Felis JJ, Mason JW, Takekawa JY. 2014. Pacific Continental Shelf Environmental Assessment (PaCSEA): aerial seabird and marine mammal surveys off northern California, Oregon, and Washington, 2011-2012. Camarillo (CA): US Department of the Interior, Bureau of Ocean Energy Management, Pacific OCS Region. OCS Study BOEM 2014-003.

Adams J, Felis JJ, Mason JW, Takekawa JY. 2016. Pacific Continental Shelf Environmental Assessment (PaCSEA) GIS resource database: aerial seabird and marine mammal surveys off northern California, Oregon, and Washington, 2011-2012. US Geological Survey data release.

Adams J, Kelsey EC, Felis JJ, Pereksta DM. 2017. Collision and displacement vulnerability among marine birds of the California Current System associated with offshore wind energy infrastructure (ver. 1.1, July 2017). U.S. Geological Survey Open-File Report 2016-1154. 116 p.

Ainley DG, Spear LB, Tynan CT, Barth JA, Pierce SD, Ford RG, Cowles TJ. 2005. Physical and biological variables affecting seabird distributions during the upwelling season of the northern California Current. Deep-Sea Research Part II: Topical Studies in Oceanography. 52:123-143.

Ainley DG, Dugger KD, Ford RG, Pierce SD, Reese DC, Brodeur RD, Tynan CT, Barth JA. 2009. Association of predators and prey at frontal features in the California Current: competition, facilitation, and co-occurrence. Marine Ecology Progress Series. 389:271-294.

Ainley DG, Hyrenbach KD. 2010. Top-down and bottom-up factors affecting seabird population trends in the California current system (1985-2006). Progress in Oceanography. 84(3):242-254.

Appler J, Barlow J, Rankin S. 2004. Marine mammal data collected during the Oregon, California and Washington Line-transect Expedition (ORCAWALE) conducted aboard the NOAA ships *McArthur* and *David Starr Jordan*, July - December 2001. US Department of Commerce, National Oceanic and Atmospheric Administration, National Marine Fisheries Service, Southwest Fisheries Science Center. NOAA Technical Memorandum NMFS SWFSC 359.

Bailey H, Brookes KL, Thompson PM. 2014. Assessing environmental impacts of offshore wind farms: lessons learned and recommendations for the future. Aquatic Biosystems. 10(8).

Ballance LT, Pitman RL, Fiedler PC. 2006. Oceanographic influences on seabirds and cetaceans of the eastern tropical Pacific: a review. Progress in Oceanography. 69:360-390.

Barlow J. 2015. Inferring trackline detection probabilities, g(0), for cetaceans from apparent densities in different survey conditions. Marine Mammal Science. 31(3): 923-943.

Bates D, Maechler M. 2019. Matrix: sparse and dense matrix classes and methods. R package version 1.2-17.

Becker RA, Wilks AR, Brownrigg R, Minka TA, Deckmyn A. 2018. maps: draw geographical maps. R package version 3.3.0.

Bivand RS, Pebesma E, Gómez-Rubio V. 2013. Applied spatial data analysis with R. 2nd ed. New York (NY): Springer.

Bivand R, Keitt T, Rowlingson B. 2015. rgdal: bindings for the 'Geospatial' Data Abstraction Library. R package version 1.0-4.

Bivand R, Lewin-Koh N. 2015. maptools: tools for reading and handling spatial objects. R package version 0.8-36.

Bivand R, Rundel C. 2015. rgeos: interface to Geometry Engine - Open Source ('GEOS'). R package version 0.3-11.

Bodenhofer U, Klawonn F. 2008. Robust rank correlation coefficients on the basis of fuzzy orderings: initial steps. Mathware and Soft Computing. 15(1):5-20.

Bodenhofer U, Krone M, Klawonn F, 2013. Testing noisy numerical data for monotonic association. Information Sciences. 245:21-37.

Boudt K, Cornelissen J, Croux C. 2012. The Gaussian rank correlation estimator: robustness properties. Statistics and Computing. 22(2):471-483.

Bradbury G, Trinder M, Furness B, Banks AN, Caldow RWG, Hume D. 2014. Mapping seabird sensitivity to offshore wind farms. PLoS ONE. 9(9):e106366.

Briggs KT, Tyler WB, Lewis DB, Dettmann KF. 1983. Seabirds of central and northern California, 1980-1983: status, abundance, and distribution. Part of Investigator's Final Report, Marine Mammal and Seabird Study, Central and Northern California, Contract No. 14-12-0001-29090. Prepared by Center for Marine Sciences, University of California, Santa Cruz, for the Pacific OCS Region, Minerals Management Service. OCS Study MMS 84-0043. 246 p.

Briggs KT, Ainley DG, Carlson DR, Lewis DB, Tyler WB, Spear LB, Ferris LA. 1987a. Final Report: California Seabird Ecology Study. Prepared by the Institute of Marine Sciences, University of California, Santa Cruz, for the Pacific OCS Region, Minerals Management Service, Contract No. 14-12-001-30183. 153 p.

Briggs KT, Tyler WMB, Lewis DB, Carlson DR. 1987b. Bird communities at sea off California: 1975 to 1983. Studies in Avian Biology No. 11.

Briggs KT, Varoujean DH, Williams WW, Ford RG, Bonnell ML, Casey JL. 1991. Seabirds of the Oregon and Washington OCS, 1989-1990. Final Report prepared by Ebasco Environmental, Bellevue, WA, and Ecological Consulting, Inc., Portland, OR, for the Minerals Management Service, Pacific OCS Region. OCS Study MMS 91-0093. 164 p.

Bühlmann P, Hothorn T. 2007. Boosting algorithms: regularization, prediction and model fitting. Statistical Science. 22(4):477-505.

Burnham KP, Anderson DR, Laake JL. 1980. Estimation of density from line transect sampling of biological populations. Wildlife Monographs. 72.

Calambokidis J, Steiger GH, Ellifrit DK, Troutman BL, Bowlby CE. 2004. Distribution and abundance of humpback whales (*Megaptera novaeangliae*) and other marine mammals off the northern Washington coast. Fishery Bulletin. 102(4):563-580.

Canty A, Ripley B. 2015. boot: bootstrap R (S-Plus) functions. R package version 1.3-17.

Cayula JF, Cornillon P. 1992. Edge detection algorithm for SST images. Journal of Atmospheric and Oceanic Technology. 9(1):67-80.

[CDAS] Computer Database Analysis System 3.1. 2009. Marine birds and mammals at sea. Washington, Oregon, California 1975-2008. Prepared for California Department of Fish and Game Office of Spill Prevention and Response. Data CD and Display Software.

Clarke ED, Spear LB, Mccracken ML, Marques FFC, Borchers DL, Buckland ST, Ainley DG. 2003. Validating the use of generalized additive models and at-sea surveys to estimate size and temporal trends of seabird populations. Journal of Applied Ecology. 40(2):278-292.

Conn PB, Thorson JT, Johnson DS. 2017. Confronting preferential sampling when analysing population distributions: diagnosis and model-based triage. Methods in Ecology and Evolution. 8(11):1535-1546.

Davison AC, Hinkley DV. 1997. Bootstrap methods and their applications. Cambridge (United Kingdom): Cambridge University Press.

de Lucas M, Janss GFE, Ferrer M. 2007. Birds and wind farms: risk assessment and mitigation. Madrid (Spain): Quercus.

Di Lorenzo E, Schneider N, Cobb KM, Franks PJS, Chhak K, Miller AJ, McWilliams JC, Bograd SJ, Arango H, Curchitser E, et al. 2008. North Pacific Gyre Oscillation links ocean climate and ecosystem change. Geophysical Research Letters. 35(8).

Dick DM. 2016. Spatio-temporal analysis and modeling in the marine environment: humpback whale genetic variability and seabird distributions in the northeastern Pacific Ocean [dissertation]. [Corvallis (OR)]: Oregon State University.

Energy Policy Act of 2005, Pub. L. No. 109-58, 119 Stat. 594 (2005).

ESRI. 2016. ArcGIS Desktop: Release 10.4.1. Redlands (CA): Environmental Systems Research Institute.

Evenson J, Cyra T, Murphie B, Kraege D. 2011. Summary of the winter 2011 sea duck aerial surveys of the Pacific coast of Oregon and Washington. Washington Department of Fish and Wildlife. Unpublished report.

Falxa GA, Raphael MG, tech. coords. 2016. Northwest Forest Plan—the first 20 years (1994–2013): status and trend of marbled murrelet populations and nesting habitat. Portland (OR): U.S. Department of Agriculture, Forest Service, Pacific Northwest Research Station. General Technical Report PNW-GTR-933. 132 p.

Fifield DA, Hedd A, Avery-Gomm S, Robertson GJ, Gjerdrum C, McFarlane Tranquilla L. 2017. Employing predictive spatial models to inform conservation planning for seabirds in the Labrador Sea. Frontiers in Marine Science. 4(149).

Ford RG, Ainley DG, Casey JL, Keiper CA, Spear LB, Ballance LT. 2004. The biogeographic patterns of seabirds in the central portion of the California Current. Marine Ornithology. 32:77-96.

Forney KA. 2007. Preliminary estimates of cetacean abundance along the U.S. West Coast and within four National Marine Sanctuaries during 2005. US Department of Commerce, National Oceanic and Atmospheric Administration, National Marine Fisheries Service, Southwest Fisheries Science Center. NOAA Technical Memorandum NMFS SWFSC 406.

Friedman JH. 2002. Stochastic gradient boosting. Computational Statistics & Data Analysis. 38(4):367-378.

Furness RW, Monaghan P. 1987. Seabird ecology. Boston (MA): Springer.

Furness RW, Wade HM, Masden EA. 2013. Assessing vulnerability of marine bird populations to offshore wind farms. Journal of Environmental Management. 119:56-66.

Furrer R, Sain SS. 2010. spam: a sparse matrix R package with emphasis on MCMC methods for Gaussian Markov random fields. Journal of Statistical Software. 36(10).

Garthe S, Hüppop O. 2004. Scaling possible adverse effects of marine wind farms on seabirds: developing and applying a vulnerability index. Journal of Applied Ecology. 41:724-734.

Genz A, Bretz F. 2009. Computation of multivariate normal and *t* probabilities. Lecture notes in statistics, vol. 195. Heidelberg (Germany): Springer-Verlag.

Genz A, Bretz F, Miwa T, Mi X, Leisch F, Scheipl F, Hothorn T. 2014. mvtnorm: multivariate normal and t distributions. R package version 1.0-2.

Gerber F, Furrer R. 2015. Pitfalls in the implementation of Bayesian hierarchical modeling of areal count data: an illustration using BYM and Leroux models. Journal of Statistical Software, Code Snippets. 63(1).

Goyert HF, Gardner B, Sollmann R, Veit RR, Gilbert AT, Connelly EE, Williams KA. 2016. Predicting the offshore distribution and abundance of marine birds with a hierarchical community distance sampling model. Ecological Applications. 26(6):1797-1815.

Grothendieck G. 2014a. gsubfn: utilities for strings and function arguments. R package version 0.6-6.

Grothendieck G. 2014b. sqldf: perform SQL selects on R data frames. R package version 0.4-10.

Hanson MB, Noren DP, Norris TF, Emmons CA, Holt MM, Phillips E, Zamon J, Menkel J. 2010. Pacific Orca Distribution Survey (PODS) conducted aboard the NOAA ship *McArthur II* in March-April 2009. (STATE DEPT. CRUISE NO: 2009-002). Seattle (WA): NOAA Northwest Fisheries Science Center. Unpublished report.

Harris P, Macmillan-Lawler M, Rupp J, Baker E. 2014. Geomorphology of the oceans. Marine Geology. 352:4-24.

Heinänen S, Žydelis R, Dorsch M, Nehls G, Skov H. 2017. High-resolution sea duck distribution modeling: Relating aerial and ship survey data to food resources, anthropogenic pressures, and topographic variables. The Condor. 119(2):175-190.

Heinänen S, Žydelis R, Kleinschmidt B, Dorsch M, Burger C, Morkūnas J, Quillfeldt P, Nehls G. 2020. Satellite telemetry and digital aerial surveys show strong displacement of red-throated divers (*Gavia stellata*) from offshore wind farms. Marine Environmental Research. 160:104989.

Hijmans RJ. 2015. raster: geographic data analysis and modeling. R package version 2.4-15.

Hofner B, Mayr A, Robinzonov N, Schmid M. 2014. Model-based boosting in R: a hands-on tutorial using the R package mboost. Computational Statistics. 29(1):3-35.

Hofner B, Boccuto L, Göker M. 2015. Controlling false discoveries in high-dimensional situations: boosting with stability selection. BMC Bioinformatics. 16:144.

Hofner B, Hothorn T. 2015. stabs: stability selection with error control. R package version 0.5-1.

Hothorn T, Hornik K, Zeileis A. 2006. Unbiased recursive partitioning: a conditional inference framework. Journal of Computational and Graphical Statistics. 15(3):651-674.

Hothorn T, Büehlmann P, Kneib T, Schmid M, Hofner B. 2010. Model-based boosting 2.0. Journal of Machine Learning Research. 11:2109-2113.

Hothorn T, Leisch F, Zeileis A. 2013. modeltools: tools and classes for statistical models. R package version 0.2-21.

Hothorn T, Büehlmann P, Kneib T, Schmid M, Hofner B. 2015. mboost: model-based boosting. R package version 2.4-2.

HYCOM Consortium. 2018. HYCOM + NCODA Global 1/12° Reanalysis. Available from: https://www.hycom.org/dataserver/gofs-3pt0/reanalysis.

Hyrenbach KD, Veit RR. 2003. Ocean warming and seabird communities of the southern California Current System (1987-98): response at multiple temporal scales. Deep-Sea Research Part II: Topical Studies in Oceanography. 50(14):2537-2565.

Jackman S. 2015. pscl: classes and methods for R developed in the Political Science Computational Laboratory, Stanford University. Stanford (CA): Department of Political Science, Stanford University.

Johnston A, Thaxter CB, Austin GE, Cook AS, Humphreys EM, Still DA, Mackay A, Irvine R, Webb A, Burton NH. 2015. Modelling the abundance and distribution of marine birds accounting for uncertain species identification. Journal of Applied Ecology. 52:150-160.

Kates L, Petzoldt T. 2012. proto: prototype object-based programming. R package version 0.3-10.

Kelsey EC, Felis JJ, Czapanskiy M, Pereksta DM, Adams J. 2018. Collision and displacement vulnerability to offshore wind energy infrastructure among marine birds of the Pacific Outer Continental Shelf. Journal of Environmental Management. 227:229-247.

Lopez J, Bowlby E, Wright N, Brenkman K. 2011. Seabird density in the Olympic Coast National Marine Sanctuary, 1995-2007. Olympic Coast National Marine Sanctuary. Unpublished report.

Manugian S, Elliott ML, Bradley R, Howar J, Karnovsky N, Saenz B, Studwell A, Warzybok P, Nur N, Jahncke J. 2015. Spatial distribution and temporal patterns of Cassin's Auklet foraging and their euphausiid prey in a variable ocean environment. PLoS ONE. 10(12):e0144232.

Mason JW, McChesney GJ, McIver WR, Carter HR, Takekawa JY, Golightly RT, Ackerman JT, Orthmeyer DL, Perry WM, Yee JL, et al. 2007. At-sea distribution and abundance of seabirds off southern California: a 20-year comparison. Studies in Avian Biology No. 33.

Mayr A, Fenske N, Hofner B, Kneib T, Schmid M. 2012. Generalized additive models for location, scale and shape for high dimensional data—a flexible approach based on boosting. Applied Statistics. 61(3):403-427.

McGowan J, Hines E, Elliott M, Howar J, Dransfield A, Nur N, Jahncke J. 2013. Using seabird habitat modeling to inform marine spatial planning in Central California's National Marine Sanctuaries. PLoS ONE. 8(8):e71406.

McIver W, Baldwin J, Lance MM, Pearson SF, Strong C, Johnson N, Lynch D, Raphael MG, Young R, Lorenz T, et al. 2019. Marbled murrelet effectiveness monitoring, Northwest Forest Plan: 2018 summary report. Northwest Forest Plan Interagency Regional Monitoring Program. 22 p.

Menza C, Leirness J, White T, Winship A, Kinlan B, Kracker L, Zamon JE, Ballance L, Becker E, Forney KA et al. 2016. Predictive mapping of seabirds, pinnipeds and cetaceans off the Pacific coast of Washington. Silver Spring (MD): NOAA Technical Memorandum NOS NCCOS 210. 96 p.

Miller P. 2009. Composite front maps for improved visibility of dynamic sea-surface features on cloudy SeaWiFS and AVHRR data. Journal of Marine Systems. 78(3):327-336.

Miller PI, Scales KL, Ingram SN, Southall EJ, Sims DW. 2015. Basking sharks and oceanographic fronts: quantifying associations in the north-east Atlantic. Functional Ecology. 29(8):1099-1109.

[NCCOS] National Centers for Coastal Ocean Science. 2003. A biogeographic assessment off North/Central California: to support the joint management plan review for Cordell Bank, Gulf of the Farallones, and Monterey Bay National Marine Sanctuaries: phase I – marine fishes, birds and mammals. Silver Spring (MD): NCCOS Biogeography Team in cooperation with the National Marine Sanctuary Program. 145 p.

NCCOS. 2007. A biogeographic assessment off North/Central California: to support the joint management plan review for Cordell Bank, Gulf of the Farallones, and Monterey Bay National Marine Sanctuaries: phase II – environmental setting and update to marine birds and mammals. Silver Spring (MD): NCCOS Biogeography Branch, R.G. Ford Consulting Co. and Oikonos Ecosystem Knowledge, in cooperation with the National Marine Sanctuary Program. NOAA Technical Memorandum NOS NCCOS 40. 240 p.

[NOAA NGDC] National Oceanic and Atmospheric Administration National Geophysical Data Center. 2003a. U.S. Coastal Relief Model Vol. 7 – Central Pacific. NOAA National Centers for Environmental Information. https://doi.org/10.7289/V50Z7152.

NOAA NGDC. 2003b. U.S. Coastal Relief Model Vol. 8 – Northwest Pacific. NOAA National Centers for Environmental Information. https://doi.org/10.7289/V5H12ZXJ.

NOAA NGDC. 2012. U.S. Coastal Relief Model – Southern California Version 2. NOAA National Centers for Environmental Information. https://doi.org/10.7289/V5V985ZM.

Newton KM, Croll DA, Nevins HM, Benson SR, Harvey JT, Tershy BR. 2009. At-sea mortality of seabirds based on beachcast and offshore surveys. Marine Ecology Progress Series. 392:295-305.

Nur N, Jahncke J, Herzog MP, Howar J, Hyrenbach KD, Zamon JE, Ainley DG, Wiens JA, Morgan K, Ballance LT et al. 2011. Where the wild things are: predicting hotspots of seabird aggregations in the California Current System. Ecological Applications. 21(6):2241-2257.

Nychka D, Furrer R, Paige J, Sain S. 2015. fields: tools for spatial data. R package version 8.2-1.

Oedekoven CS, Ainley DG, Spear LB. 2001. Variable responses of seabirds to change in marine climate: California Current, 1985-1994. Marine Ecology Progress Series. 212:265-281.

Pebesma EJ, Bivand RS. 2005. Classes and methods for spatial data in R. R News. 5(2):9-13.

Philbrick VA, Fiedler PC, Ballance LT, Demer DA. 2003. Report of the ecosystem studies conducted during the 2001 Oregon, California, and Washington (ORCAWALE) marine mammal survey on the research vessels *David Starr Jordan* and *McArthur*. US Department of Commerce, National Oceanic and Atmospheric Administration, National Marine Fisheries Service, Southwest Fisheries Science Center. NOAA Technical Memorandum NMFS SWFSC 349.

Phillips EM, Horne JK, Zamon JE. 2017. Predator-prey interactions influenced by a dynamic river plume. Canadian Journal of Fisheries and Aquatic Sciences. 74(9):1375-1390.

Pinheiro J, Bates D, DebRoy S, Sarkar D, R Core Team. 2019. nlme: linear and nonlinear mixed effects models. R package version 3.1-139.

Porter A, Phillips S. 2016. Determining the infrastructure needs to support offshore floating wind and marine hydrokinetic facilities on the Pacific West Coast and Hawaii. Camarillo (CA): US Department of the Interior, Bureau of Ocean Energy Management, Pacific OCS Region. OCS Study BOEM 2016-011. 238 p.

QGIS.org. 2020. QGIS Geographic Information System. Open Source Geospatial Foundation Project.

R Core Team. 2019. R: a language and environment for statistical computing. Vienna (Austria): R Foundation for Statistical Computing.

R Special Interest Group on Databases. 2014. DBI: R database interface. R package version 0.3.1.

Raphael MG, Baldwin J, Falxa GA, Huff MH, Lance M, Miller SL, Pearson SF, Ralph CJ, Strong C, Thompson C. 2007. Regional population monitoring of the marbled murrelet: field and analytical methods. Portland (OR): US Department of Agriculture, Forest Service, Pacific Northwest Research Station. General Technical Report PNW-GTR-716. 70 p.

Raphael MG, Shirk AJ, Falxa GA, Pearson SF. 2015. Habitat associations of marbled murrelets during the nesting season in nearshore waters along the Washington to California coast. Journal of Marine Systems. 146:17-25.

Renner M, Parrish JK, Piatt JF, Kuletz KJ, Edwards AE, Hunt GL Jr. 2013. Modeled distribution and abundance of a pelagic seabird reveal trends in relation to fisheries. Marine Ecology Progress Series. 484:259-277.

Rintoul C, Langabeer-Schlagenhauf B, Hyrenbach KD, Morgan KH, Sydeman WJ. 2006. Atlas of California Current marine bird and mammal distributions: version 1. Petaluma (CA): PRBO Conservation Science. Unpublished report.

Roberts JJ, Best BD, Dunn DC, Treml EA, Halpin PN. 2010. Marine Geospatial Ecology Tools: an integrated framework for ecological geoprocessing with ArcGIS, Python, R, MATLAB, and C++. Environmental Modelling & Software. 25(10):1197-1207.

Robinson Willmott J, Forcey G, Kent A. 2013. The relative vulnerability of migratory bird species to offshore wind energy projects on the Atlantic Outer Continental Shelf: an assessment method and database. Final Report to the U.S. Department of the Interior, Bureau of Ocean Energy Management, Office of Renewable Energy Programs. OCS Study BOEM 2013-207. 275 p.

Robin X, Turck N, Hainard A, Tiberti N, Lisacek F, Sanchez J.-C, Müller M. 2011. pROC: an open-source package for R and S+ to analyze and compare ROC curves. BMC Bioinformatics. 12:77.

Santora JA, Rolston S, Sydeman WJ. 2011. Spatial organization of krill and seabirds in the central California Current. ICES Journal of Marine Science. 68(7):1391-1402.

Sarkar D. 2008. Lattice: multivariate data visualization with R. New York (NY): Springer.

Schmid M, Potapov S, Pfahlberg A, Hothorn T. 2010. Estimation and regularization techniques for regression models with multidimensional prediction functions. Statistics and Computing. 20(2):139-150.

Scott-Hayward LAS, Mackenzie ML, Donovan CR, Walker CG, Ashe E. 2014. Complex Region Spatial Smoother (CReSS). Journal of Computational and Graphical Statistics. 23(2):340-360.

Spear L, Nur N, Ainley DG. 1992. Estimating absolute densities of flying seabirds using analyses of relative movement. The Auk. 109(2):385-389.

Spear LB, Ainley DG, Nur N, Howell SNG. 1995. Population size and factors affecting at-sea distributions of four endangered procellariids in the tropical Pacific. The Condor. 97(3):613-638.

Studwell AJ, Hines E, Elliott ML, Howar J, Holzman B, Nur N, Jahncke J. 2017. Modeling nonresident seabird foraging distributions to inform ocean zoning in Central California. PLoS ONE. 12(1):e0169517.

Suryan RM, Kuletz KJ, Parker-Stetter SL, Ressler PH, Renner M, Horne JK, Farley EV, Labunski EA. 2016. Temporal shifts in seabird populations and spatial coherence with prey in the southeastern Bering Sea. Marine Ecology Progress Series. 549:199-215.

Takekawa JY, Perry WM, Adams J, Felis JJ, Williams LL, Yee JL, Orthmeyer DL, Mason JW, McChesney GJ, McIver WR, et al. 2017. At-sea distribution and abundance of seabirds and marine mammals off southern California GIS resource database: aerial seabird and marine mammal surveys off southern California, 1999-2002. US Geological Survey data release.

Tasker ML, Jones PH, Dixon T, Blake BF. 1984. Counting seabirds at sea from ships: a review of methods employed and a suggestion for a standardized approach. The Auk. 101:567-577.

Veit RR, McGowan JA, Ainley DG, Wahl TR, Pyle P. 1997. Apex marine predator declines ninety percent in association with changing oceanic climate. Global Change Biology. 3:23-28.

Venables WN, Ripley BD. 2002. Modern applied statistics with S. 4th ed. New York (NY): Springer.

Weatherall P, Marks KM, Jakobsson M, Schmitt T, Tani S, Arndt JE, Rovere M, Chayes D, Ferrini V, Wigley R. 2015. A new digital bathymetric model of the world's oceans. Earth and Space Science. 2(8):331-345.

Wessel P, Smith WHF. 1996. A global, self-consistent, hierarchical, high-resolution shoreline database. Journal of Geophysical Research. 101(B4):8741-8743.

Wickham H. 2007. Reshaping data with the reshape package. Journal of Statistical Software. 21(12).

Wickham H, James DA, Falcon S. 2014. RSQLite: SQLite Interface for R. R package version 1.0.0.

Winiarski KJ, Miller DL, Paton PWC, McWilliams SR. 2014. A spatial conservation prioritization approach for protecting marine birds given proposed offshore wind energy development. Biological Conservation. 169:79-88.

Winship AJ, Kinlan BP, Ballance LT, Joyce T, Leirness JB, Costa BM, Poti M, Miller PI. 2016. Seabirds. In: Costa BM and Kendall MS, editors. Marine biogeographic assessment of the Main Hawaiian Islands. Bureau of Ocean Energy Management and National Oceanic and Atmospheric Administration. OCS Study BOEM 2016-035 and NOAA Technical Memorandum NOS NCCOS 214. 359 p.

Winship AJ, Kinlan BP, White TP, Leirness JB, Christensen J. 2018. Modeling at-sea density of marine birds to support Atlantic marine renewable energy planning: final report. Sterling (VA): US Department of the Interior, Bureau of Ocean Energy Management, Office of Renewable Energy Programs. OCS Study BOEM 2018-010. 67 p.

Wood SN. 2011. Fast stable restricted maximum likelihood and marginal likelihood estimation of semiparametric generalized linear models. Journal of the Royal Statistical Society (B). 73(1):3-36.

Wood SN. 2017. Generalized additive models: an introduction with R. 2nd ed. Boca Raton (FL): Chapman and Hall/CRC.

Yee TW. 2015. VGAM: vector generalized linear and additive models. R package version 0.9-8.

Yen PPW, Sydeman WJ, Bograd SJ, Hyrenbach KD. 2006. Spring-time distributions of migratory marine birds in the southern California Current: oceanic eddy associations and coastal habitat hotspots over 17 years. Deep-Sea Research Part II: Topical Studies in Oceanography. 53:399-418.

Zamon JE, Phillips EM, Guy TJ. 2014. Marine bird aggregations associated with the tidally-driven plume and plume fronts of the Columbia River. Deep-Sea Research Part II: Topical Studies in Oceanography. 107:85-95.

Zeileis A, Leisch F, Hornik K, Kleiber C. 2002. strucchange: an R package for testing for structural change in linear regression models. Journal of Statistical Software. 7(2).

Zeileis A. 2004. Econometric computing with HC and HAC covariance matrix estimators. Journal of Statistical Software. 11(10).

Zeileis A, Grothendieck G. 2005. zoo: S3 infrastructure for regular and irregular time series. Journal of Statistical Software. 14(6).

Zeileis A. 2006. Object-oriented computation of sandwich estimators. Journal of Statistical Software. 16(9).

Zeileis A, Kleiber C, Jackman S. 2008. Regression models for count data in R. Journal of Statistical Software. 27(8).

Appendix A: Survey Dataset Information

Table A-1. Survey program information

Survey Name	Institutions	Principal Investigators	Platform Details	Transect Width (m)	References
Applied California Current Ecosystem Studies (ACCESS)	Point Blue Conservation Science, Cordell Bank NMS, Greater Farallones NMS	Jaime Jahncke, Danielle Lipski, Jan Roletto	Moss Landing Marine Laboratories R/V *John H. Martin* and NOAA R/V *Fulmar*	200	McGowan et al. 2013; Manugian et al. 2015; Studwell et al. 2017
California Cooperative Oceanic Fisheries Investigations (CalCOFI)[a]	Farallon Institute, SIO	Richard Veit, David Hyrenbach, William Sydeman	NOAA Ships *Bell M. Shimada*, *David Starr Jordan*, *Reuben Lasker* and SIO R/Vs *New Horizon*, *Robert Gordon Sproul*, *Roger Revelle*, *Sally Ride*	300	Veit et al. 1997; Hyrenbach and Veit 2003; Yen et al. 2006
California Current Cetacean and Ecosystem Assessment Survey (CalCurCEAS)	NOAA Southwest Fisheries Science Center	Lisa T. Ballance	R/V *Ocean Starr*	200-300[d]	
California Seabird Ecology Study (CDAS dataset code: SBECOL)[a]	UCSC, MMS	Kenneth Briggs	Partenavia P-68/P-68-Observer fixed-wing aircraft	50	Briggs et al. 1987a; Briggs et al. 1987b; CDAS 2009
Collaborative Survey of Cetacean Abundance and the Pelagic Ecosystem (CSCAPE)	NOAA Southwest Fisheries Science Center	Lisa T. Ballance	NOAA Ships *David Starr Jordan* and *McArthur II*	300	Forney 2007
Equatorial Pacific Ocean Climate Studies (EPOCS)[a]	H. T. Harvey & Associates, NOAA Environmental Research Laboratories	David Ainley, Larry Spear	NOAA Ships *Discoverer* and *Researcher*	250-600[e]	Spear et al. 1995
Juvenile Salmon Ocean Ecosystem Survey (JSOES)	NOAA Northwest Fisheries Science Center	Jeannette E. Zamon	F/Vs *Chellissa*, *Frosti*, *Miss Sue*, *Pacifc Fury*, *Piky*	300	Zamon et al. 2014; Phillips et al. 2017
Marine Mammal and Seabird Surveys of Central and Northern California (CDAS dataset codes: CLALL1 and CLALL2)[a]	UCSC, MMS	Thomas Dohl, Kenneth Briggs	Partenavia P-68/P-68-Observer fixed-wing aircraft	50	Briggs et al. 1983; CDAS 2009
Northwest Forest Plan Marbled Murrelet Monitoring Program Zone 2	USFS Pacific Northwest Research Station, WDFW	Scott Pearson, William McIver	R/V *Almar*	300	Raphael et al. 2007; Falxa and Raphael 2016; McIver et al. 2019

Survey Name	Institutions	Principal Investigators	Platform Details	Transect Width (m)	References
Northwest Forest Plan Marbled Murrelet Monitoring Program Zones 3-5[a,b]	USFS Pacific Northwest Research Station, CDFW	Craig Strong, William McIver		110	Raphael et al. 2007; Falxa and Raphael 2016; McIver et al. 2019
Olympic Coast NMS Seabird and Marine Mammal Surveys[c]	Olympic Coast NMS	C. Edward Bowlby, Liam Antrim	NOAA Ship *McArthur II*	300	Calambokidis et al. 2004; Lopez et al. 2011
Olympic Coast NMS Pelagic Seabird Surveys[c]	Olympic Coast NMS	Liam Antrim	NOAA Ship *McArthur II* and NOAA R/V *Tatoosh*	300	
Oregon and Washington Marine Mammal and Seabird Surveys (CDAS dataset code: OWPELB)[a]	Ebasco Environmental, Ecological Consulting, Inc., MMS	G. A. Green, Michael L. Bonnell, Kenneth Briggs	Partenavia P-68/P-68-Observer fixed-wing aircraft	50	Briggs et al. 1991; CDAS 2009
Oregon, California, and Washington Line-transect Expedition (ORCAWALE)	NOAA Southwest Fisheries Science Center	Lisa T. Ballance	NOAA Ships *David Starr Jordan* and *McArthur*	200-300[d]	Philbrick et al. 2003; Appler et al. 2004
Pacific Coast Winter Sea Duck Survey	WDFW, Sea Duck Joint Venture	Joseph Evenson	Partenavia P-68 fixed-wing aircraft	200	Evenson et al. 2011
Pacific Continental Shelf Environmental Assessment (PaCSEA)	USGS Western Ecological Research Center	Josh Adams	Partenavia P-68/P-68-Observer and Commander AC-500 fixed-wing aircraft	75-150[e]	Adams et al. 2014, 2016
Pacific Orca Distribution Survey (PODS)	NOAA Northwest Fisheries Science Center	Bradley Hanson, Dawn Noren, Jeannette E. Zamon	NOAA Ships *Bell M. Shimada* and *McArthur II*	300	Hanson et al. 2010
Pelagic Juvenile Rockfish Recruitment and Ecosystem Assessment Survey[a]	Farallon Institute, NOAA Southwest Fisheries Science Center	David Ainley, William Sydeman	NOAA Ships *David Starr Jordan* and *McArthur II*	300	Ainley and Hyrenbach 2010; Santora et al. 2011
Santa Barbara Channel Surveys (CDAS dataset code: MMSSBC)[a]	UCSC, CDFW Office of Spill Prevention and Response, MMS	Michael L. Bonnell	Partenavia P-68/P-68-Observer fixed-wing aircraft	50	CDAS 2009
Southern California Bight Surveys	USGS Western Ecological Research Center, MMS	Josh Adams, John Takekawa	Partenavia P-68/P-68-Observer fixed-wing aircraft	50-100[e]	Mason et al. 2007; Takekawa et al. 2017
Wind to Whales	UCSC, Moss Landing Marine Laboratories	Donald Croll, James Harvey	Moss Landing Marine Laboratories R/V *John H. Martin* and NOAA R/V *Fulmar*	100-300[e]	Newton et al. 2009

[a] contained pre-segmented data

[b] only used in Marbled Murrelet models

[c] current point of contact: Jeannette E. Waddell (Olympic Coast NMS)

[d] varied by species

[e] varied by observation conditions and number of observers

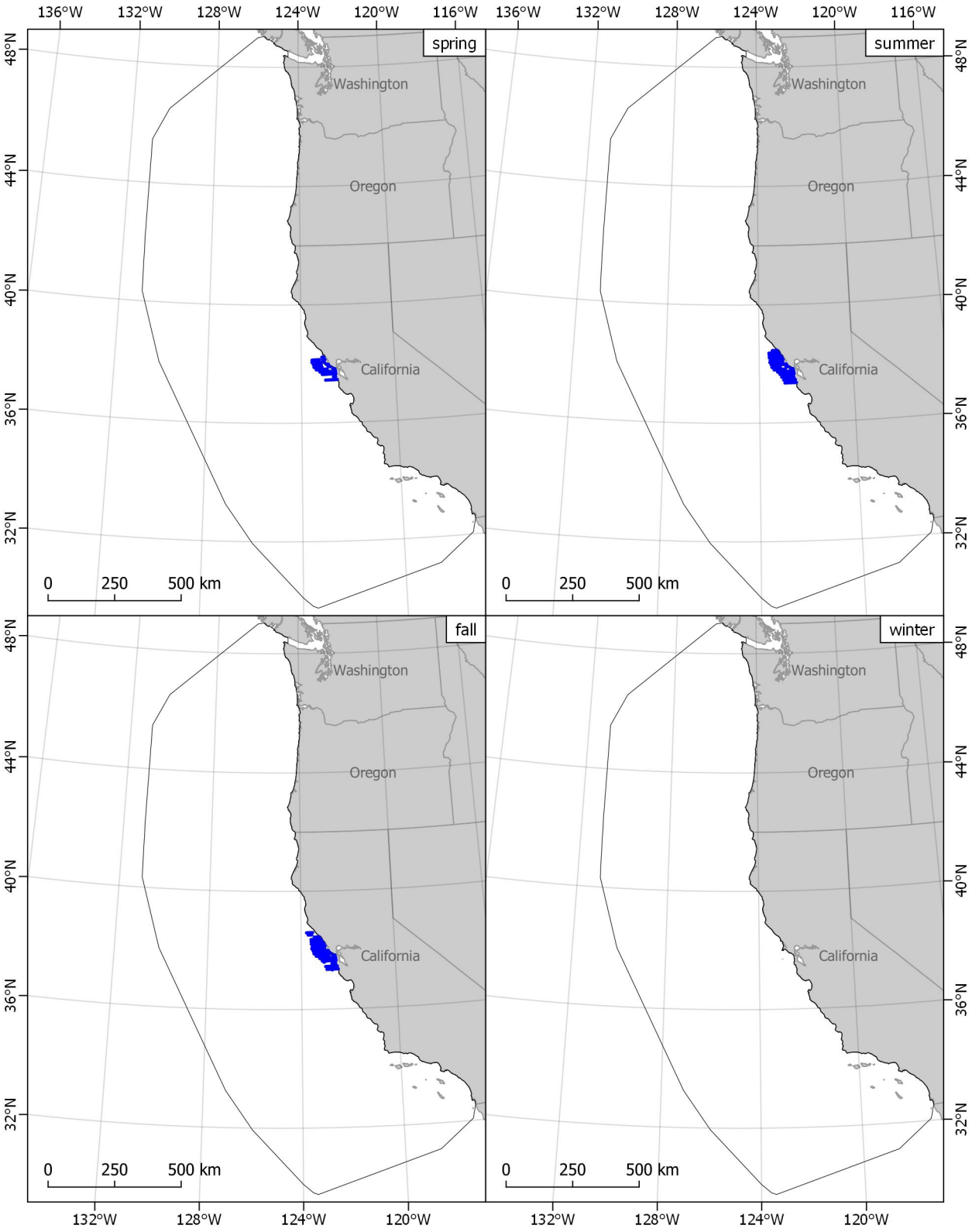

Figure A-1. Applied California Current Ecosystem Studies (ACCESS)

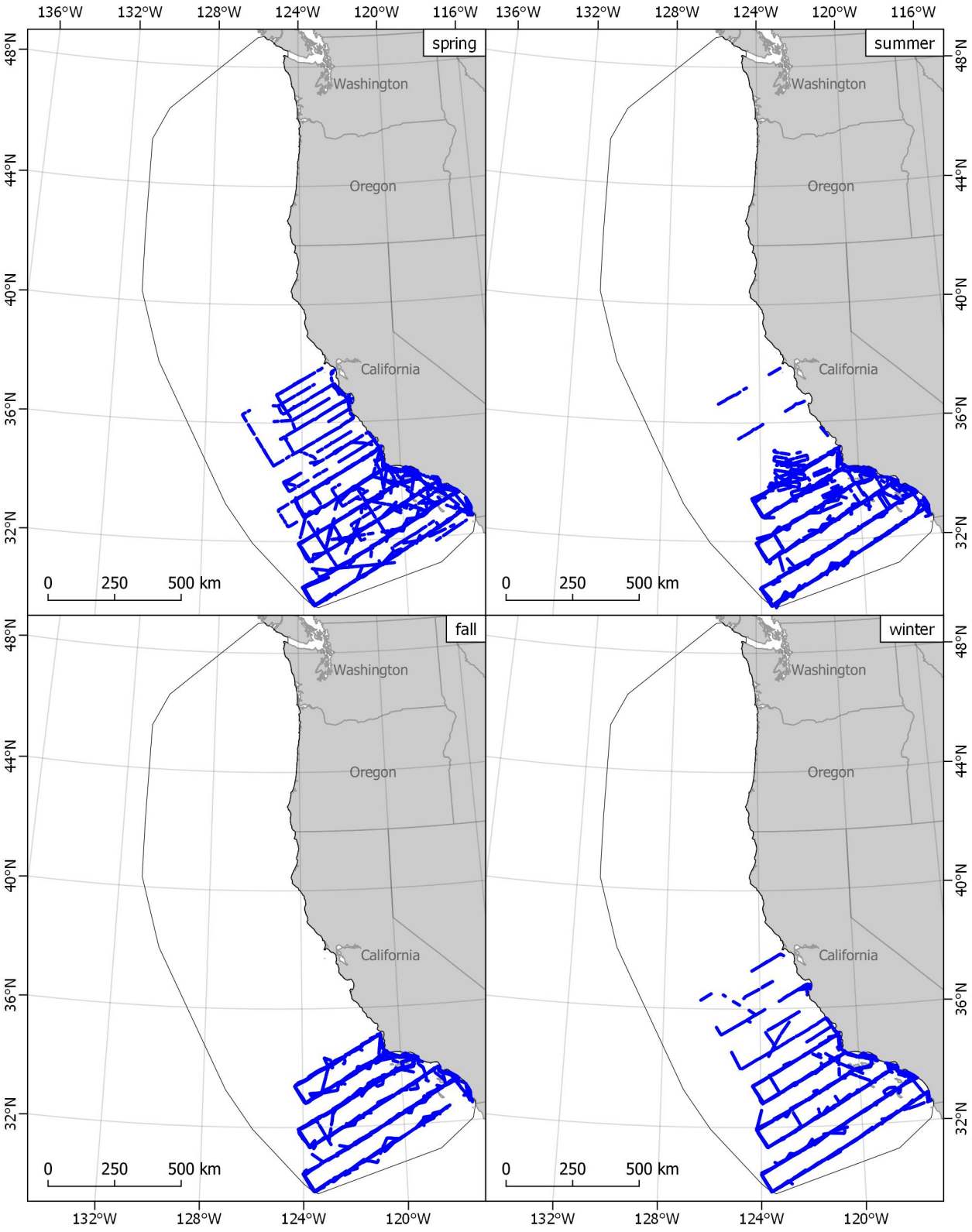

Figure A-2. California Cooperative Oceanic Fisheries Investigations (CalCOFI)

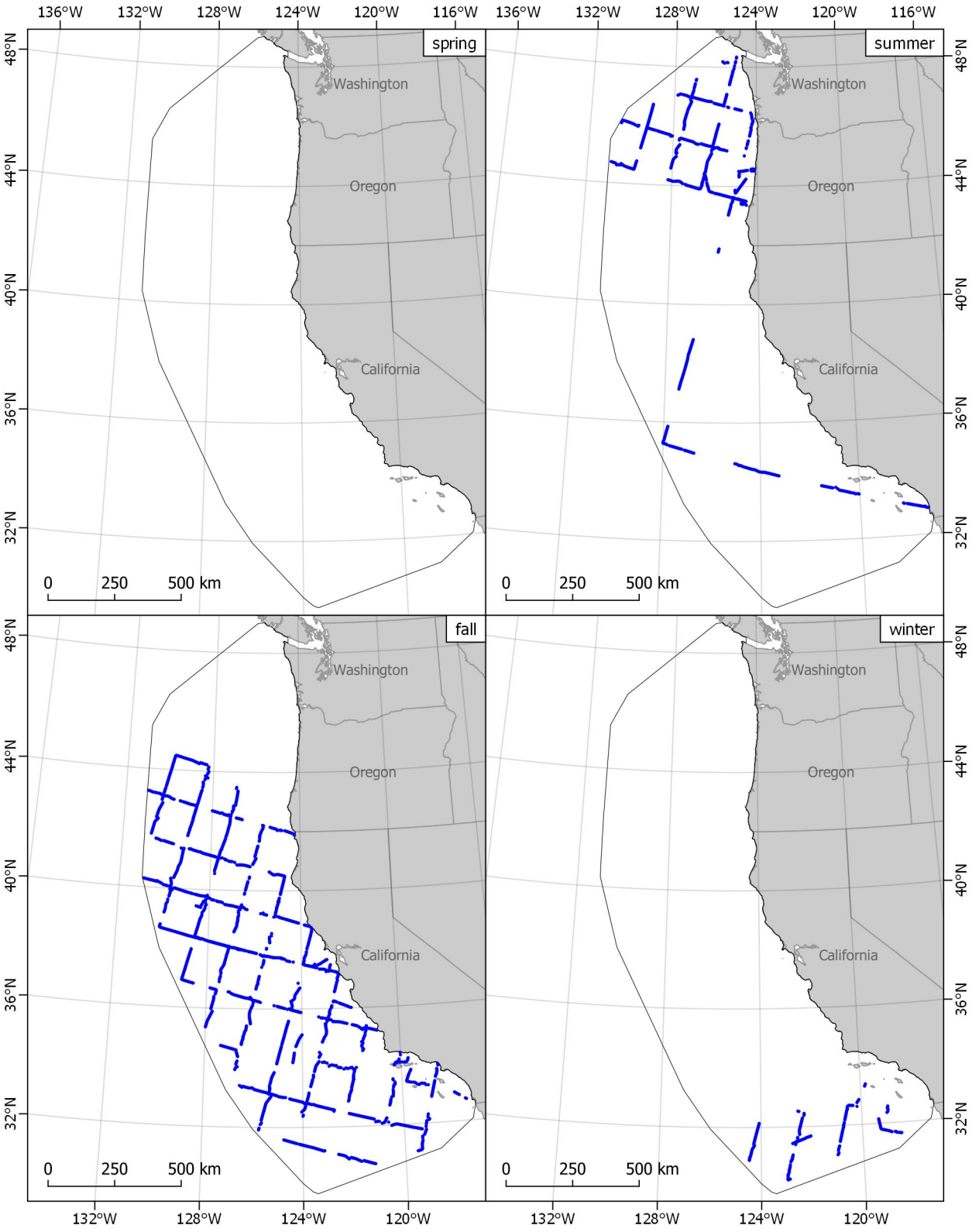

Figure A-3. California Current Cetacean and Ecosystem Assessment Survey (CalCurCEAS)

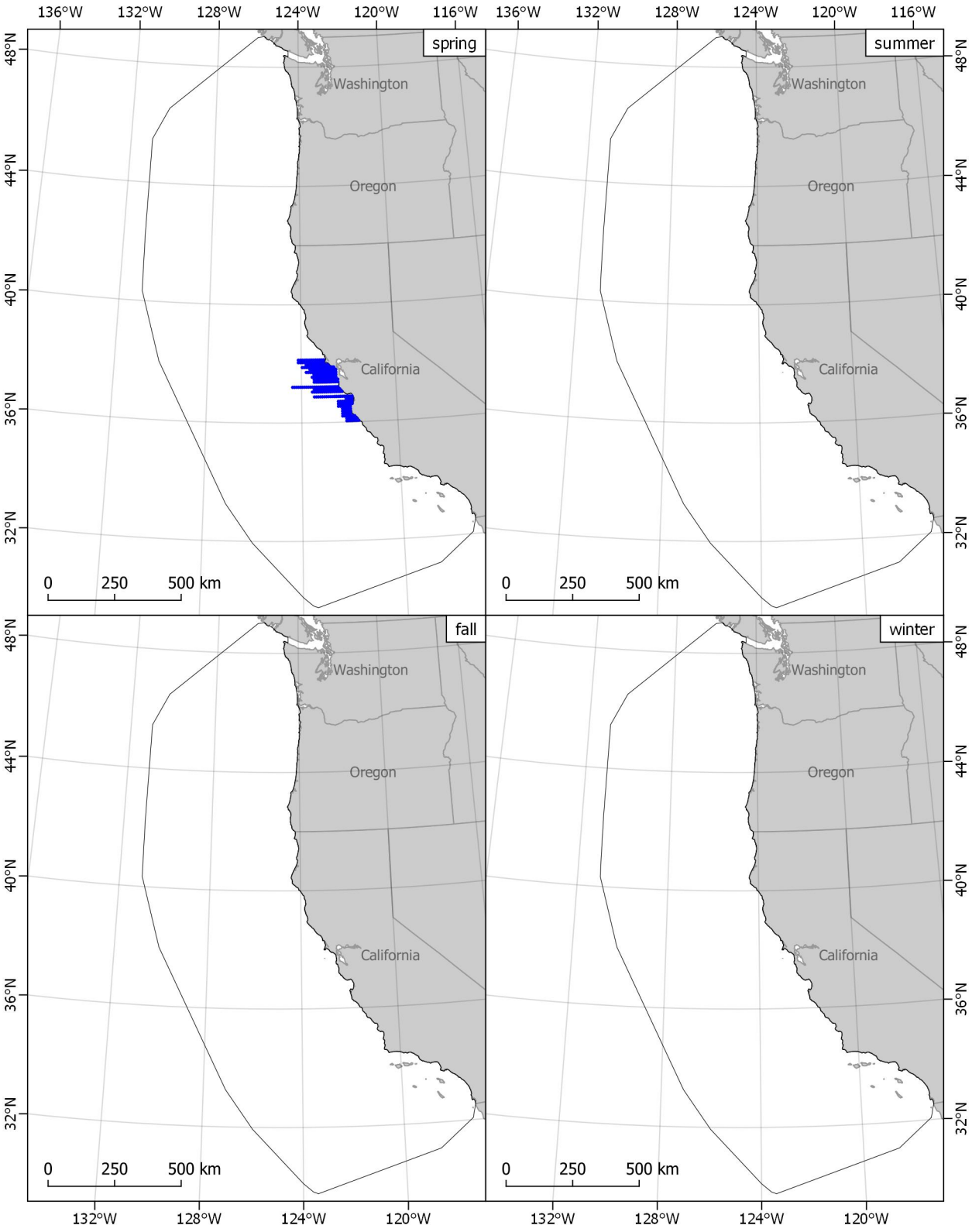

Figure A-4. California Seabird Ecology Study

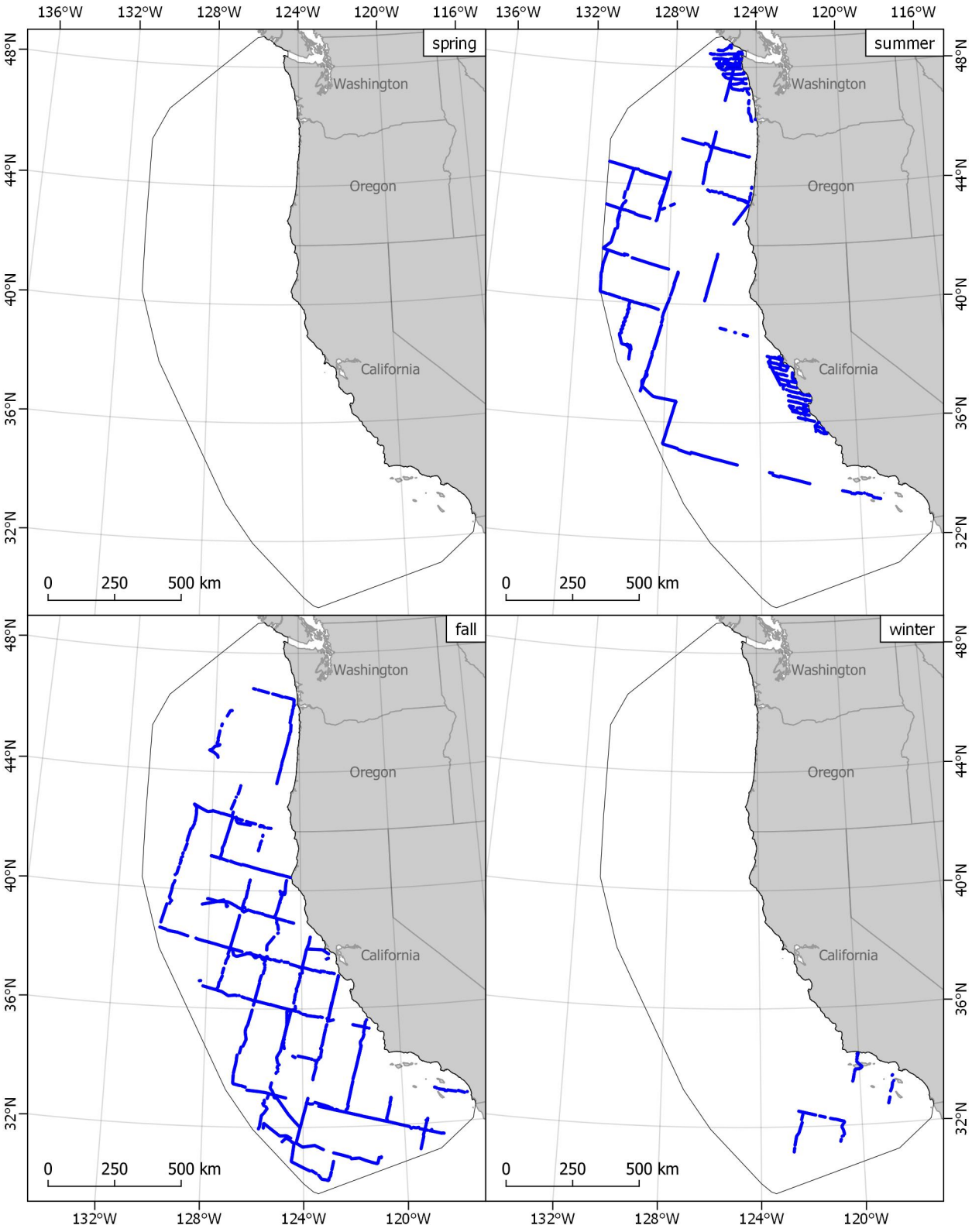

Figure A-5. Collaborative Survey of Cetacean Abundance and the Pelagic Ecosystem (CSCAPE)

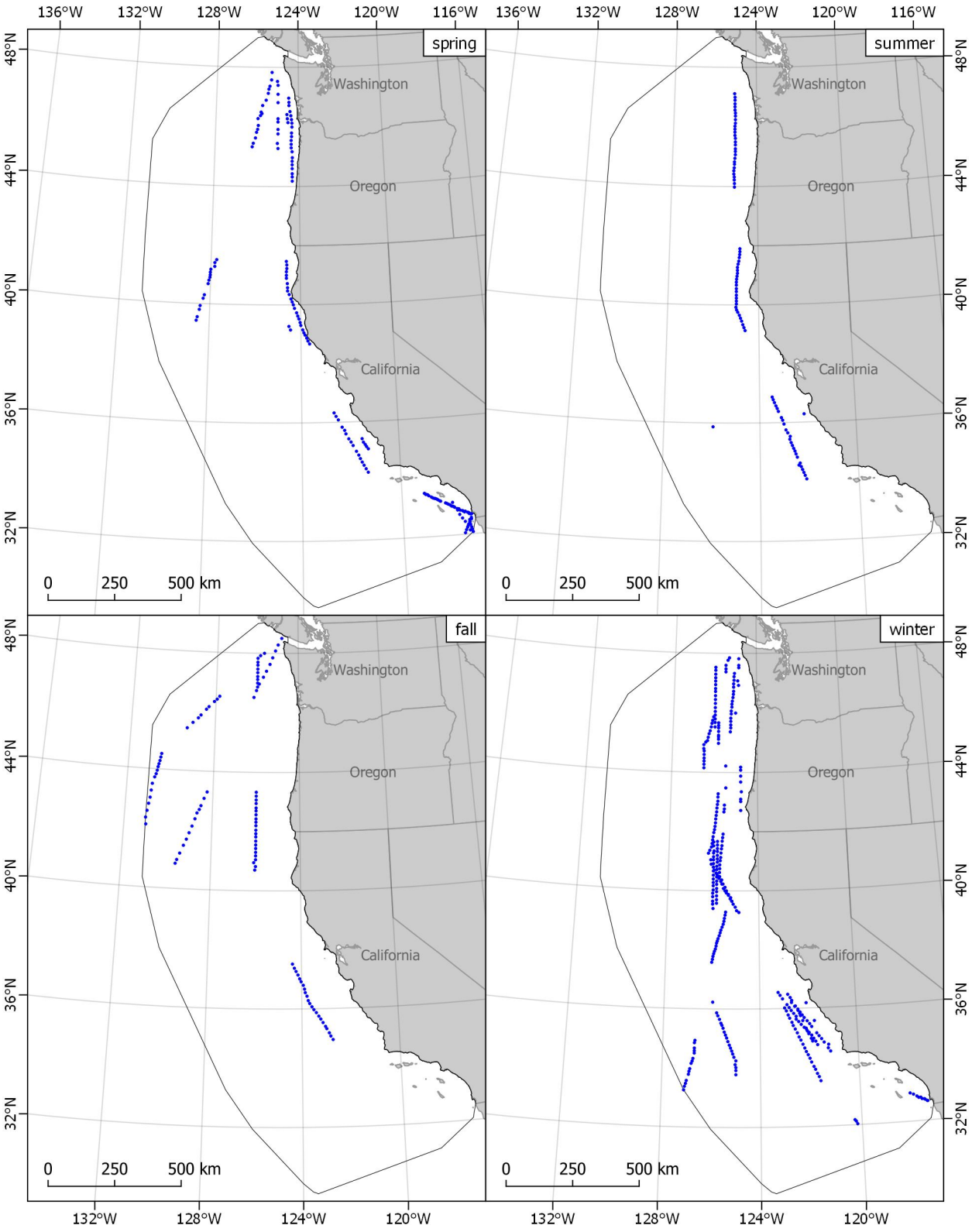

Figure A-6. Equatorial Pacific Ocean Climate Studies (EPOCS)

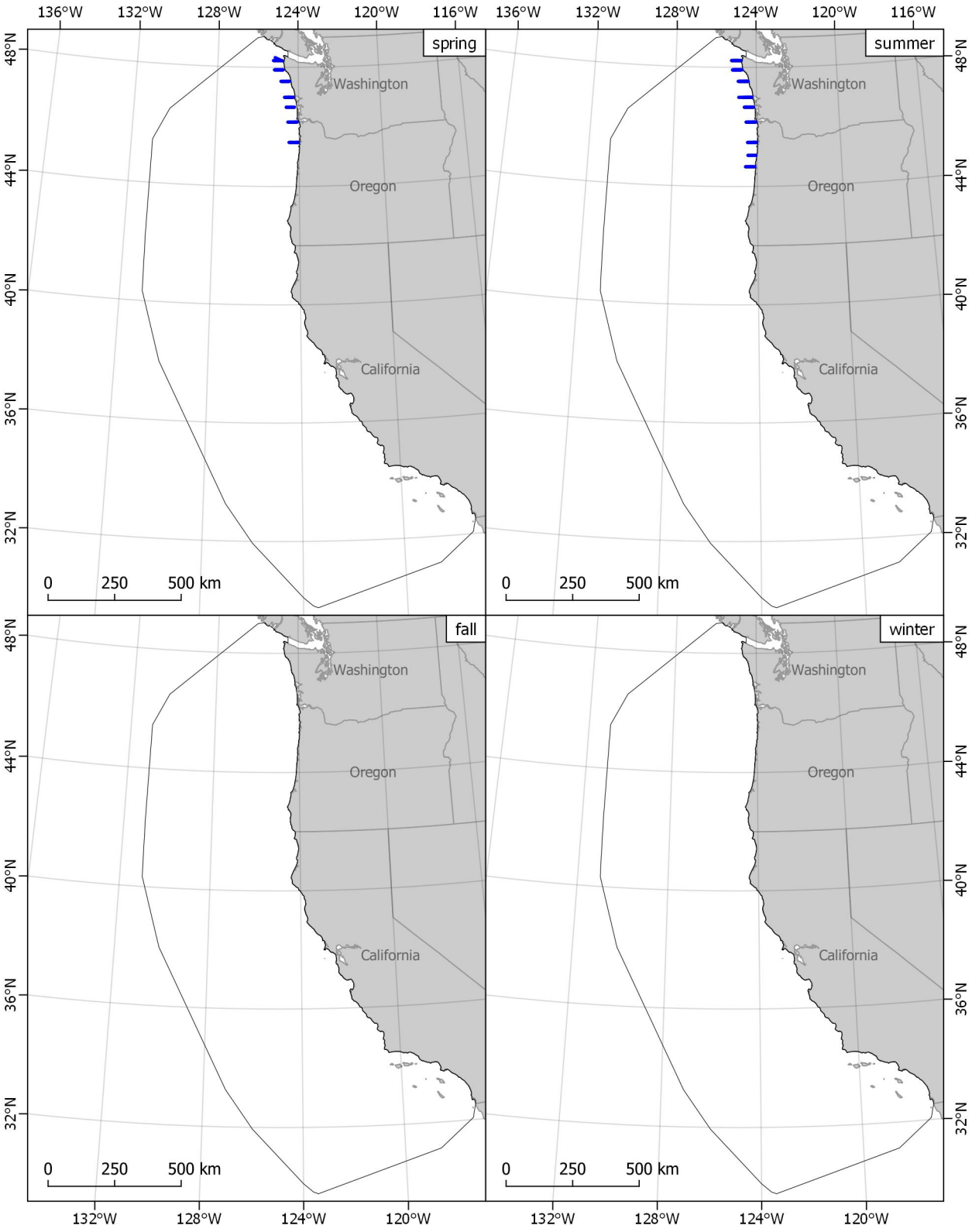

Figure A-7. Juvenile Salmon Ocean Ecosystem Survey (JSOES)

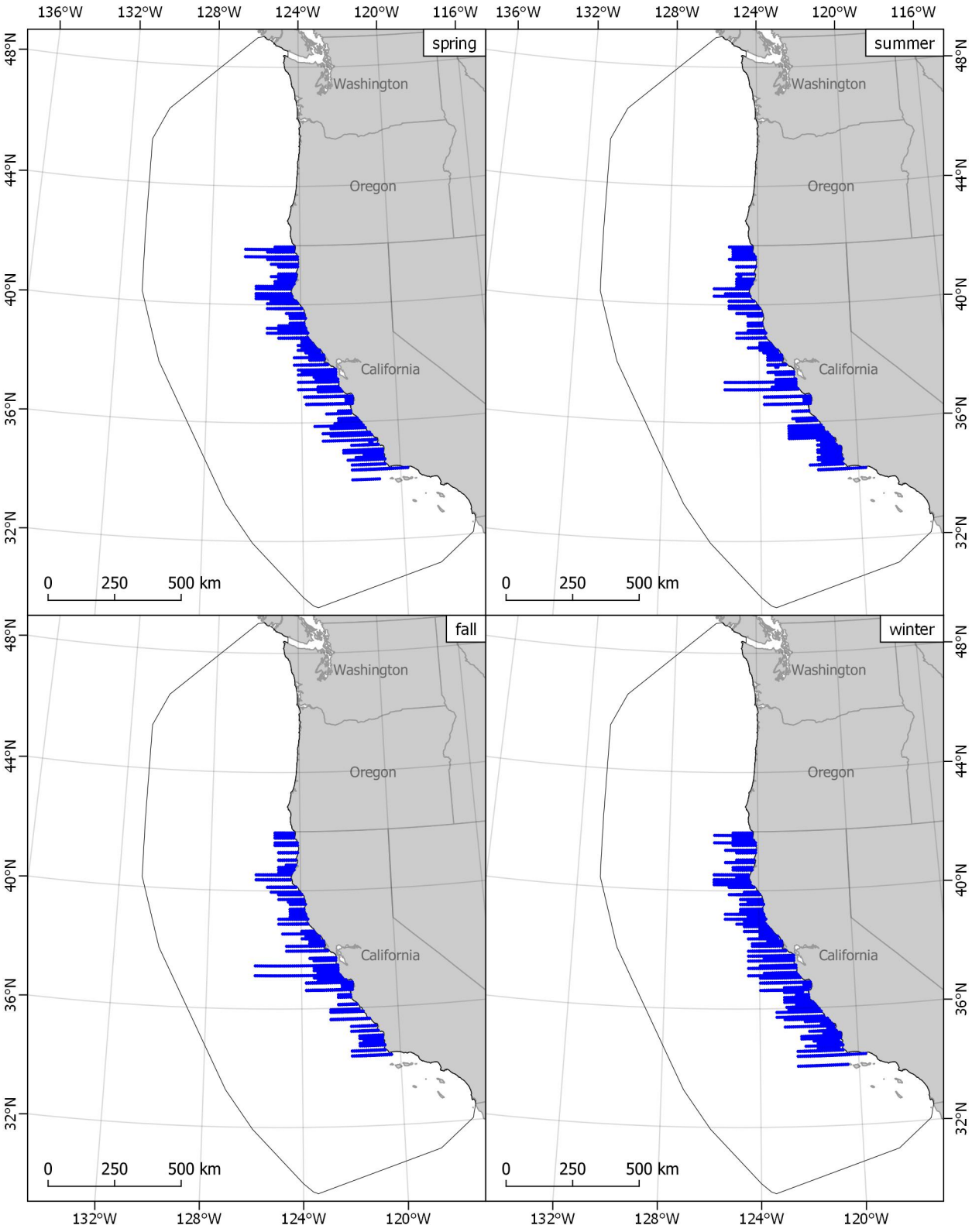

Figure A-8. Marine Mammal and Seabird Surveys of Central and Northern California

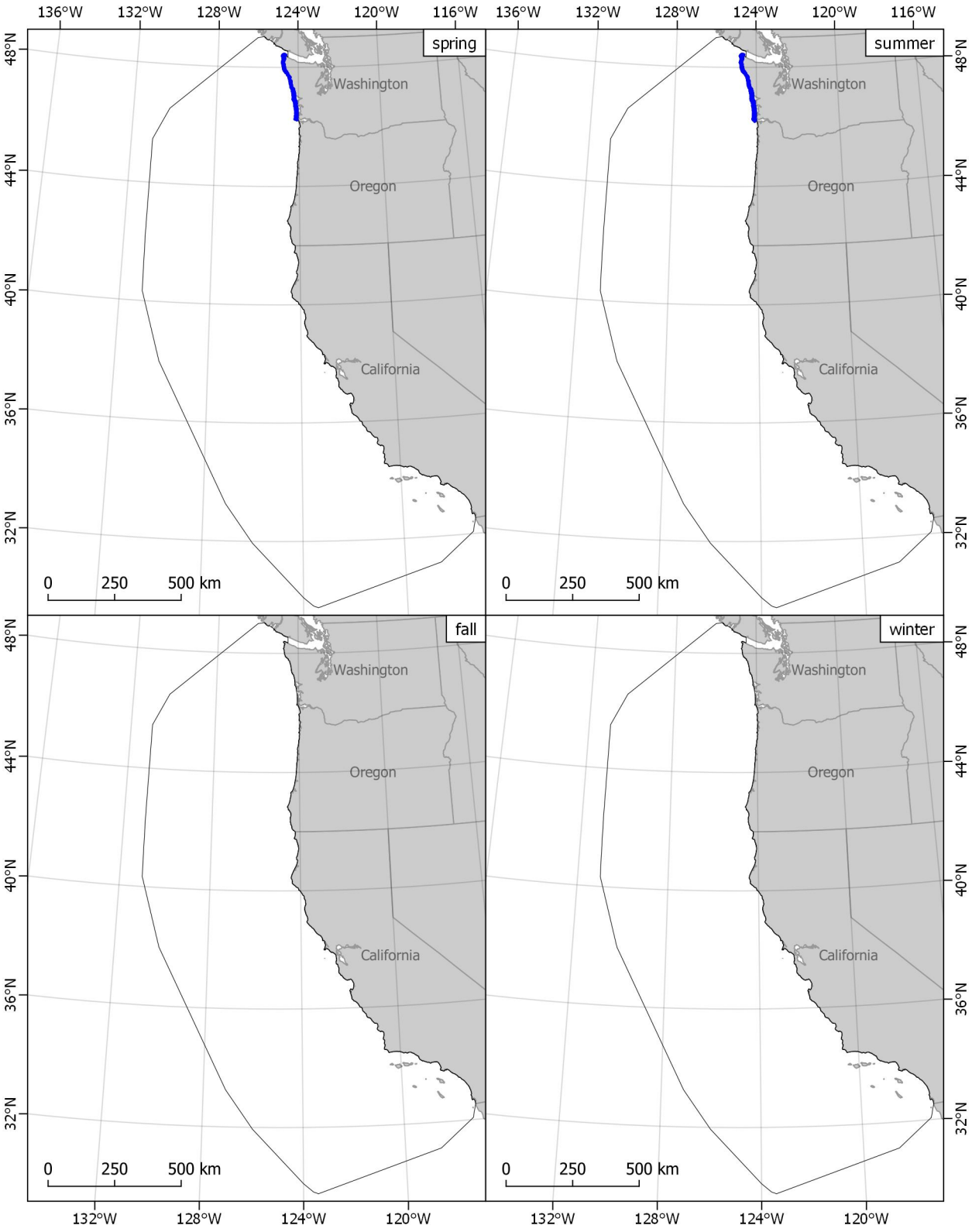

Figure A-9. Northwest Forest Plan Marbled Murrelet Monitoring Program Zone 2

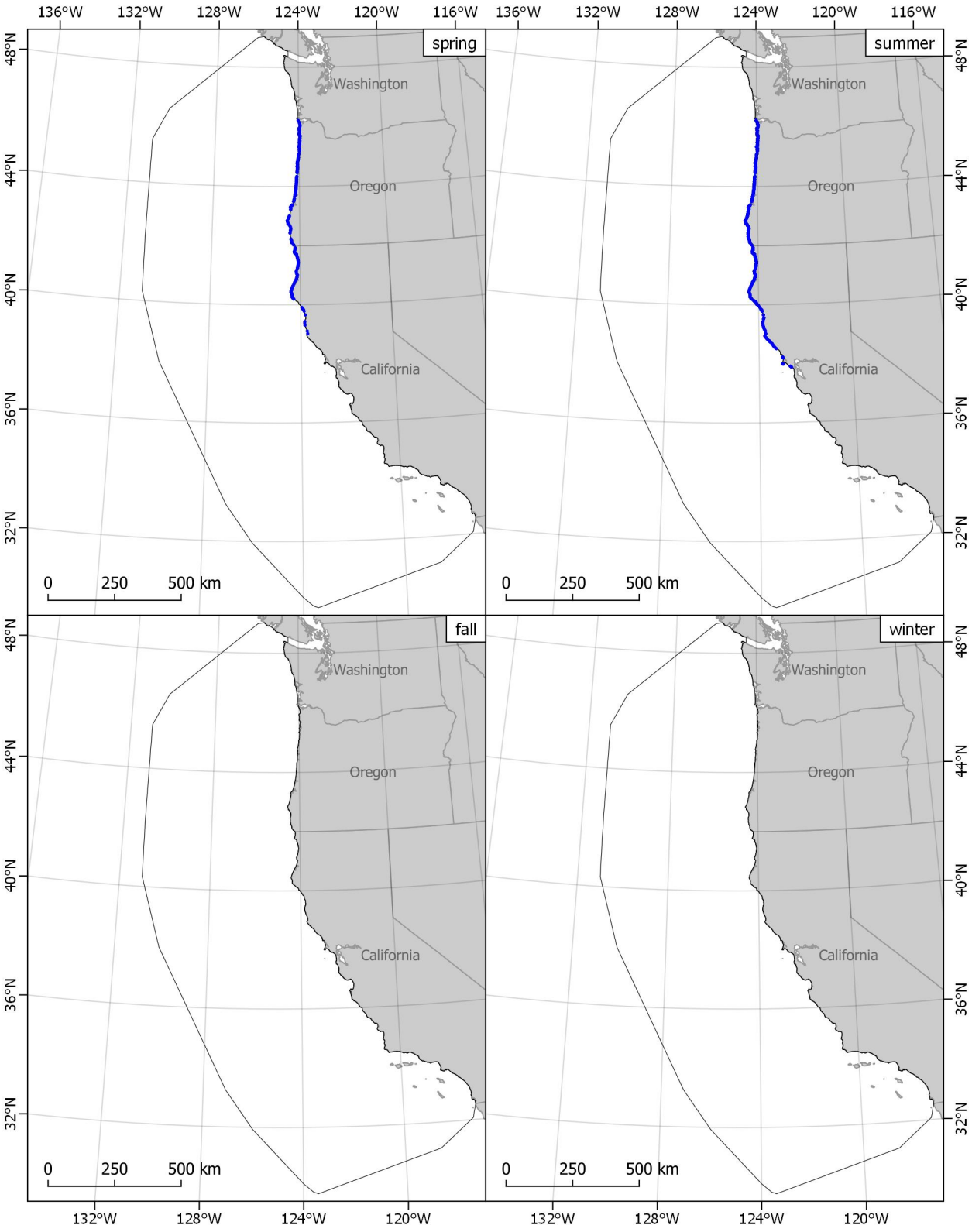

Figure A-10. Northwest Forest Plan Marbled Murrelet Monitoring Program Zones 3-5

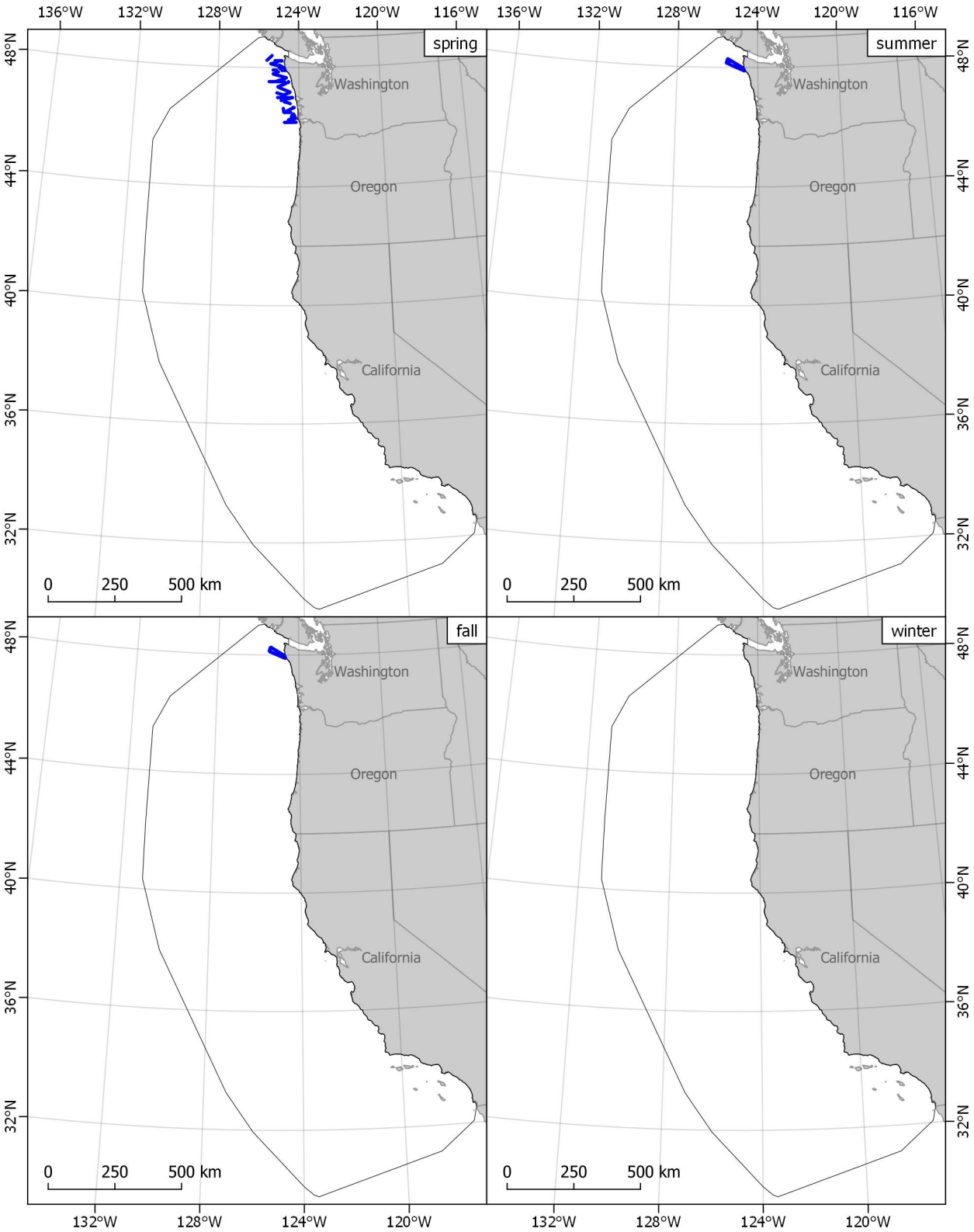

Figure A-11. Olympic Coast NMS Pelagic Seabird Surveys

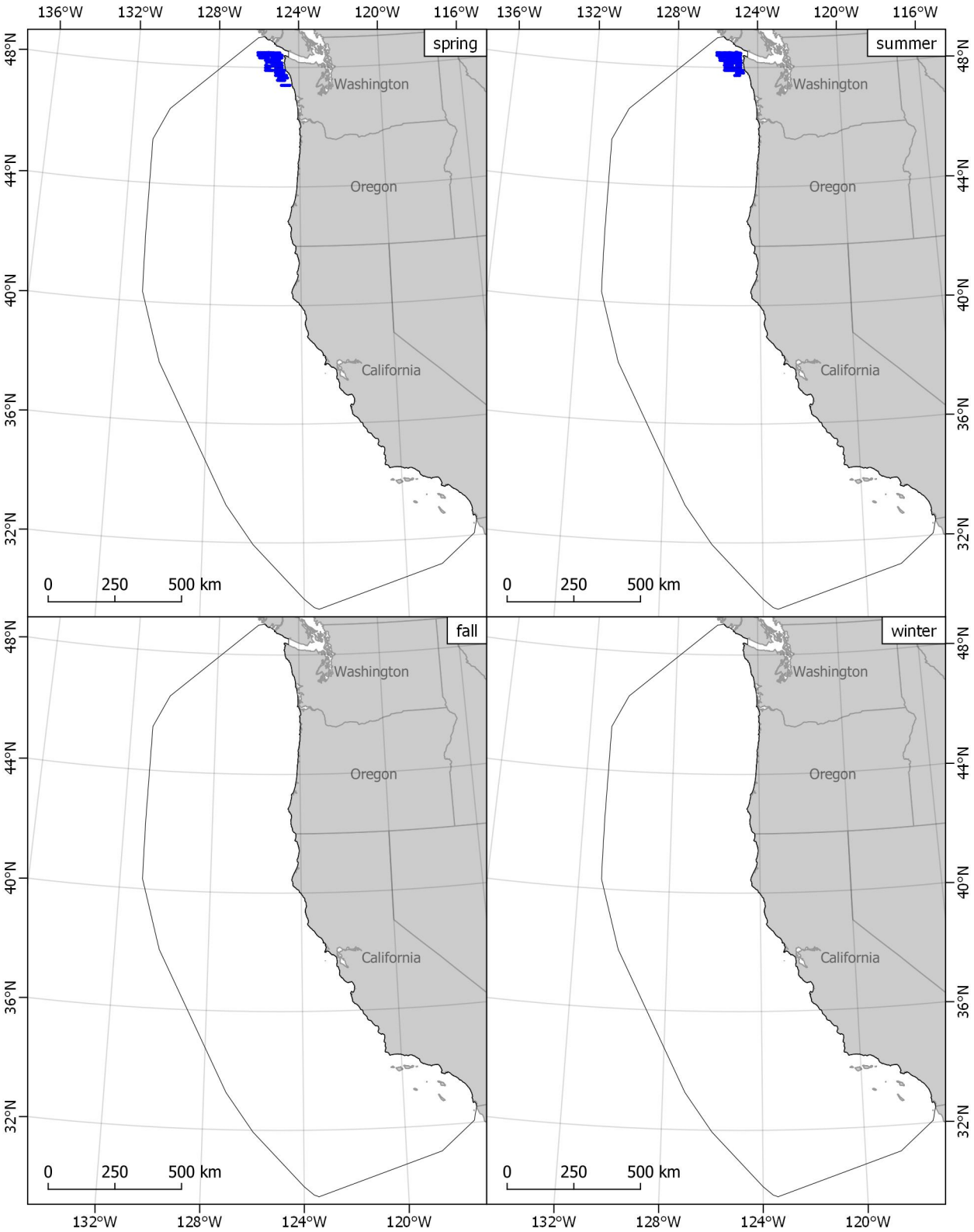

Figure A-12. Olympic Coast NMS Seabird and Marine Mammal Surveys

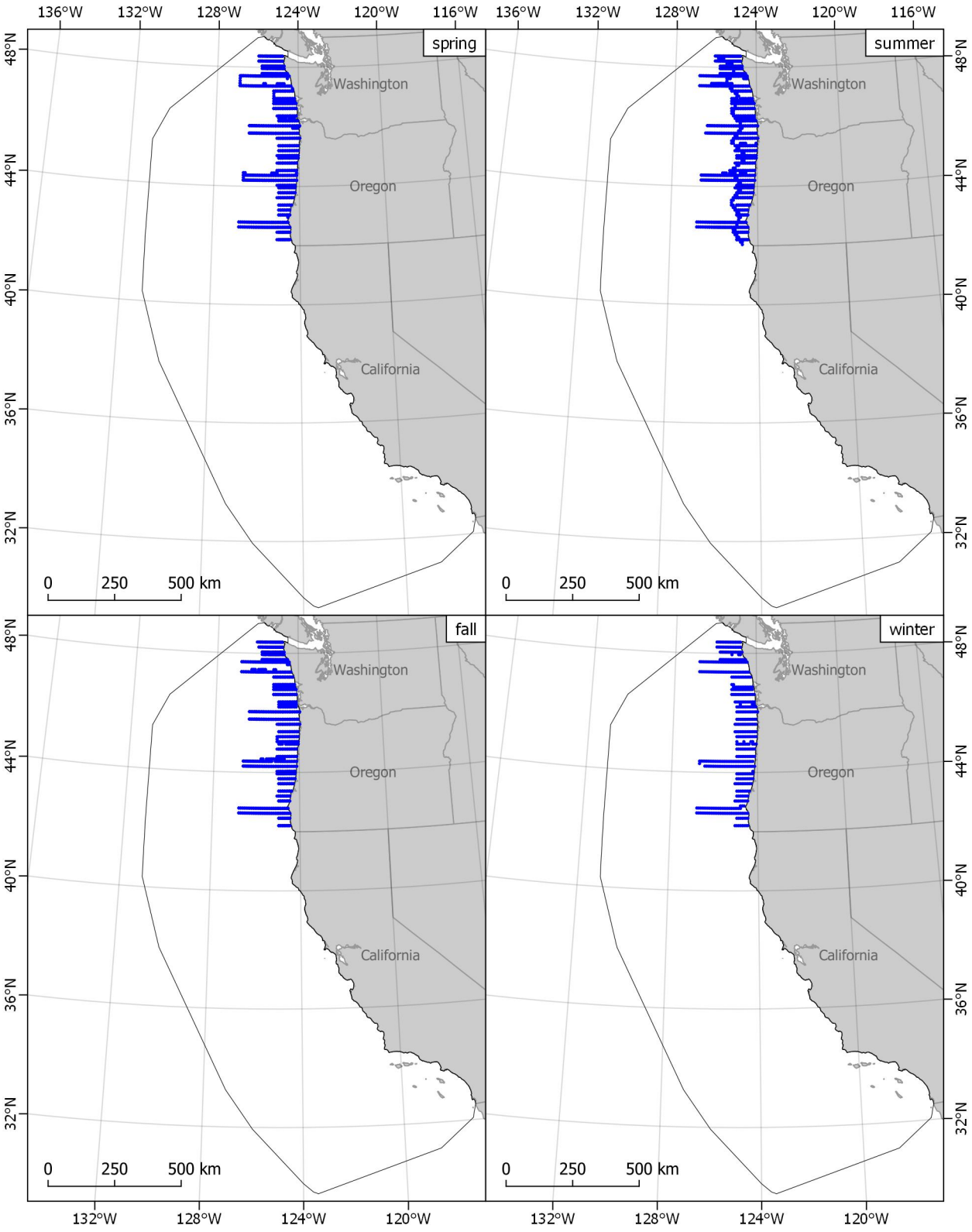

Figure A-13. Oregon and Washington Marine Mammal and Seabird Surveys

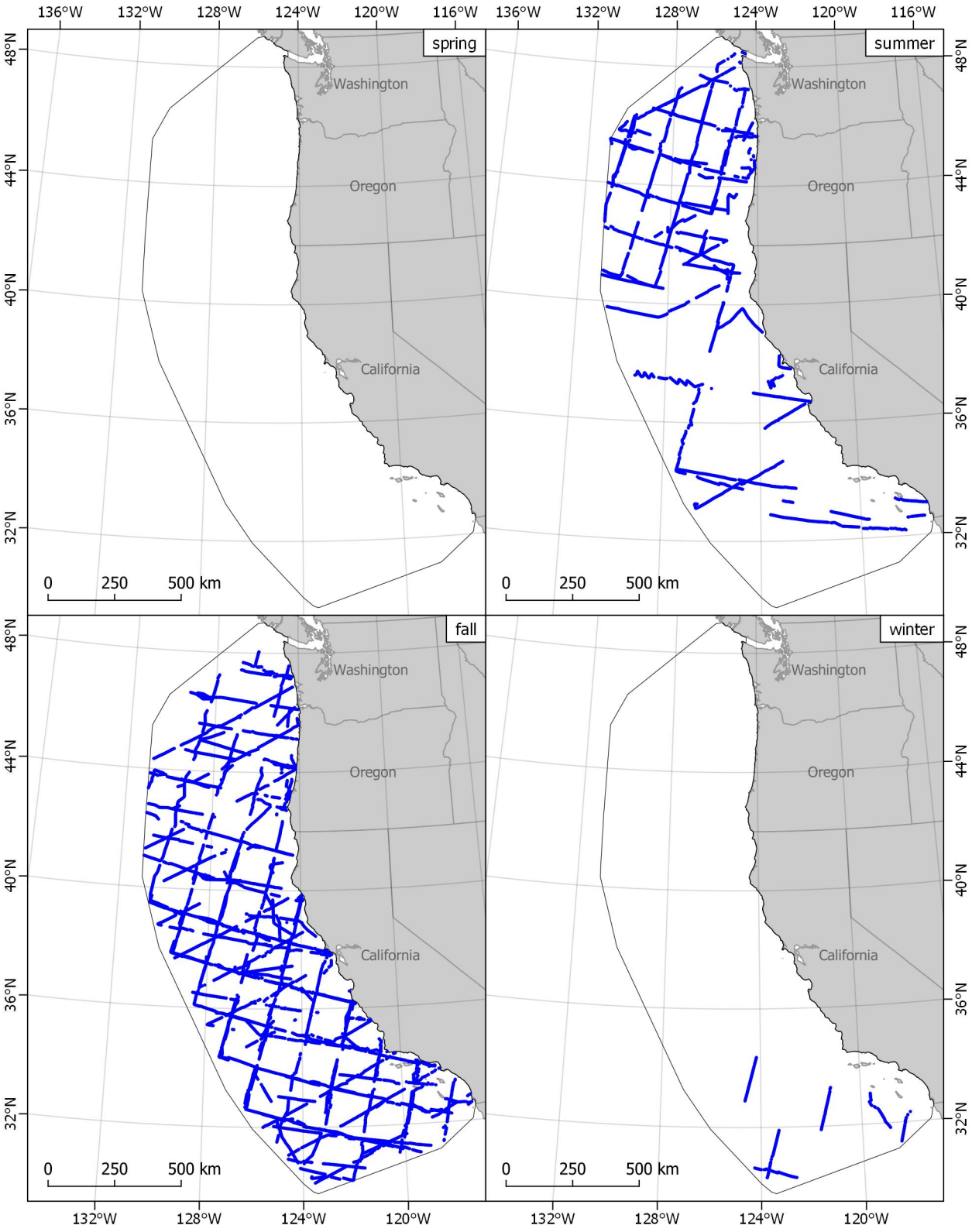

Figure A-14. Oregon, California, and Washington Line-transect Expedition (ORCAWALE)

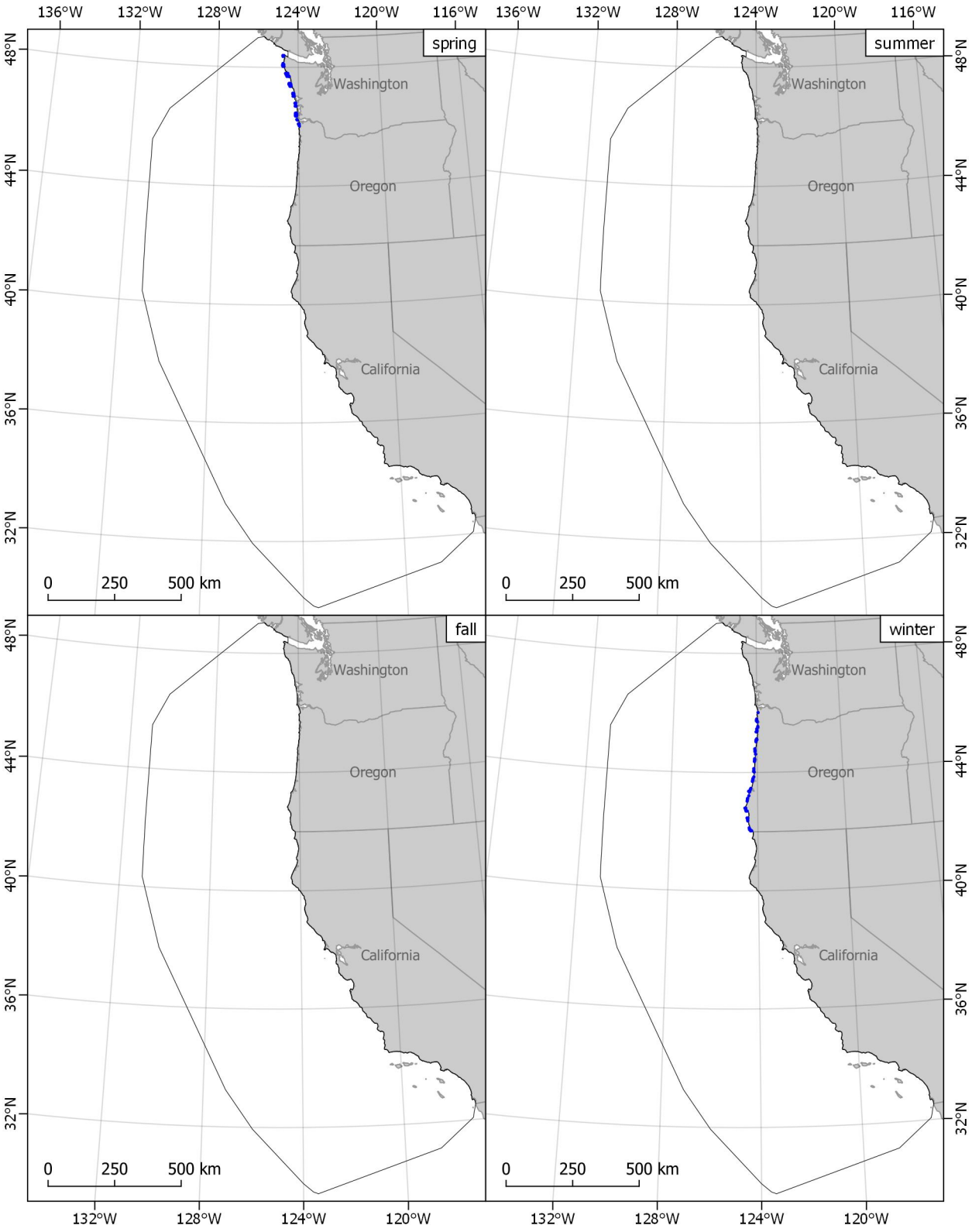

Figure A-15. Pacific Coast Winter Sea Duck Survey

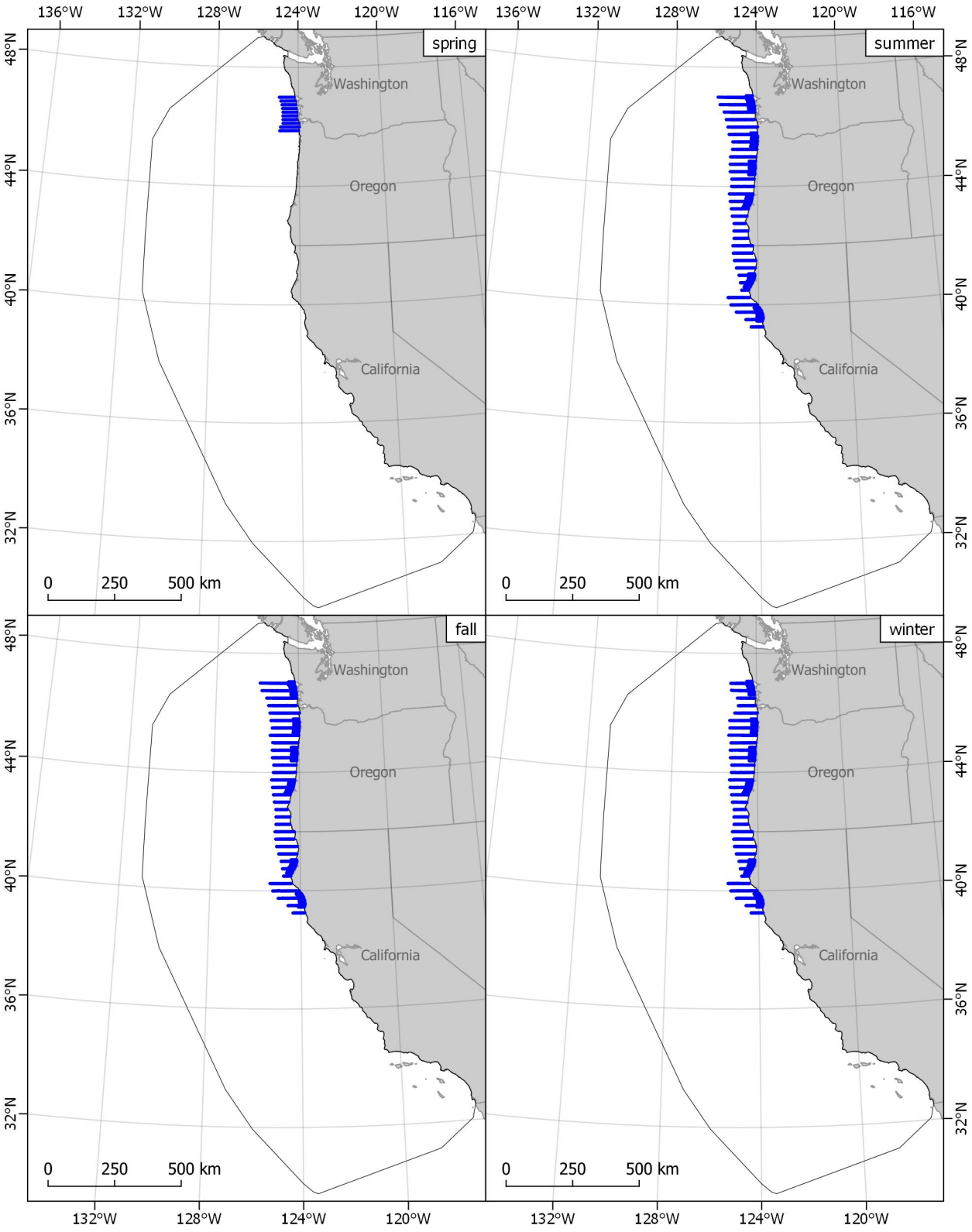

Figure A-16. Pacific Continental Shelf Environmental Assessment (PaCSEA)

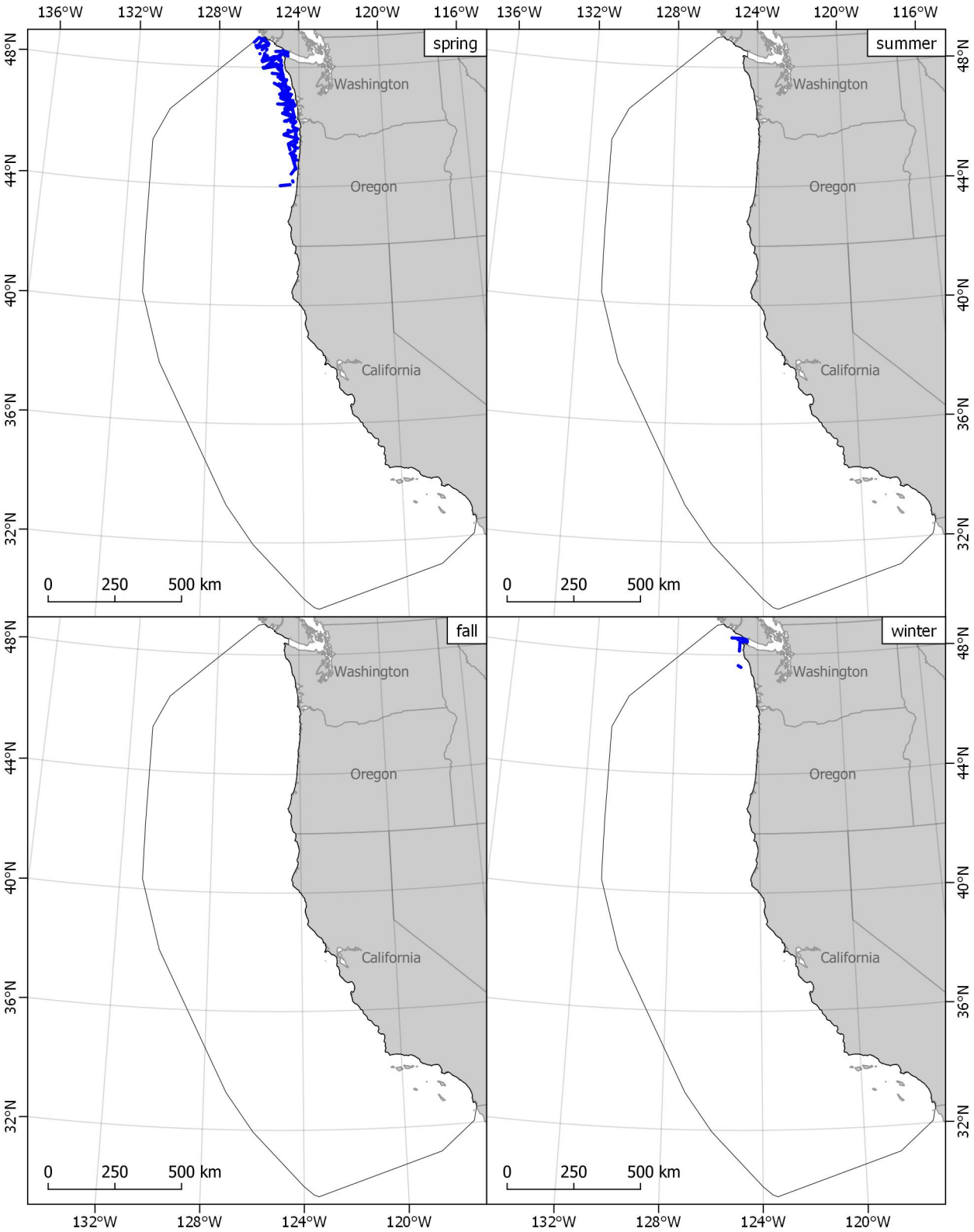

Figure A-17. Pacific Orca Distribution Survey (PODS)

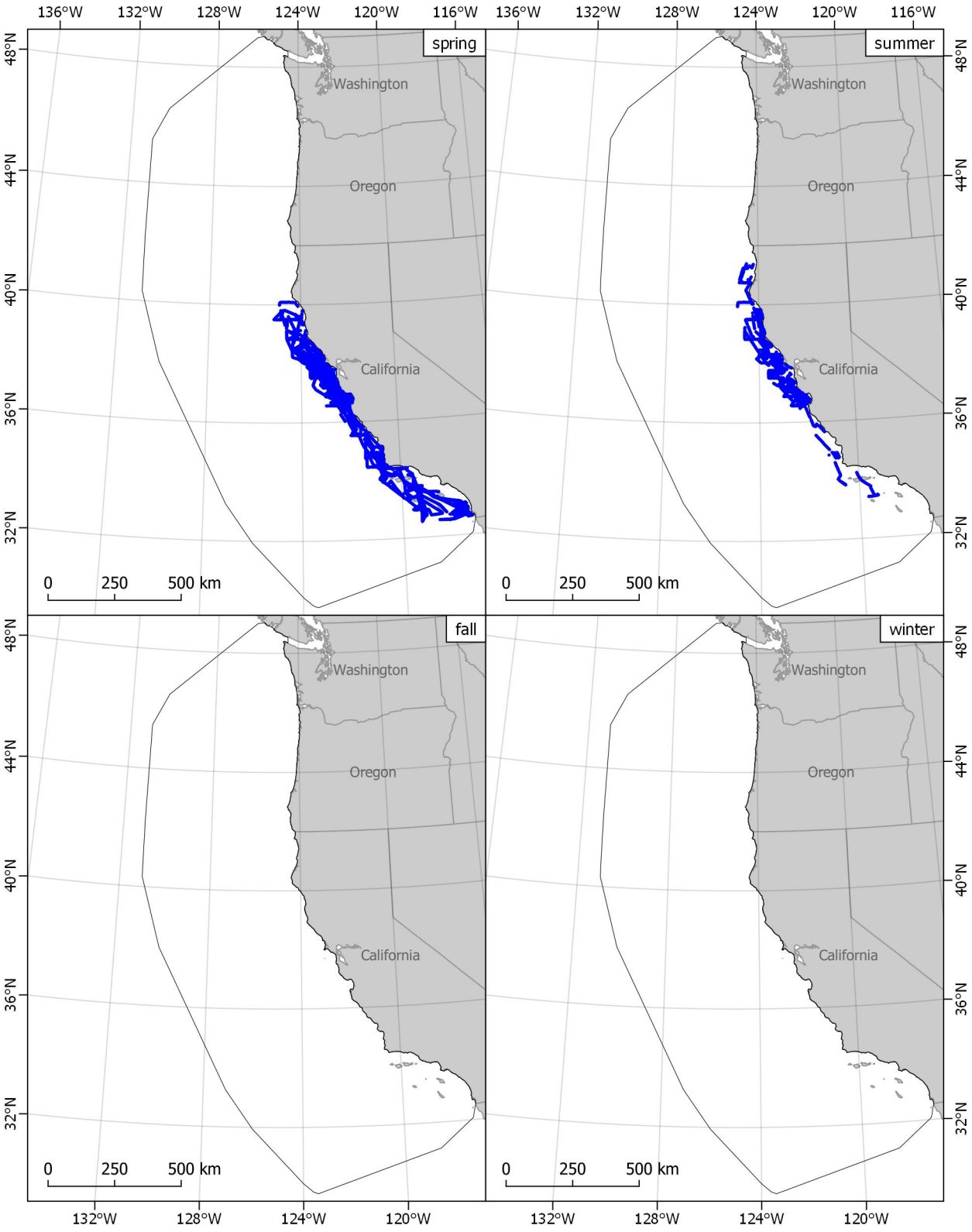

Figure A-18. Pelagic Juvenile Rockfish Recruitment and Ecosystem Assessment Survey

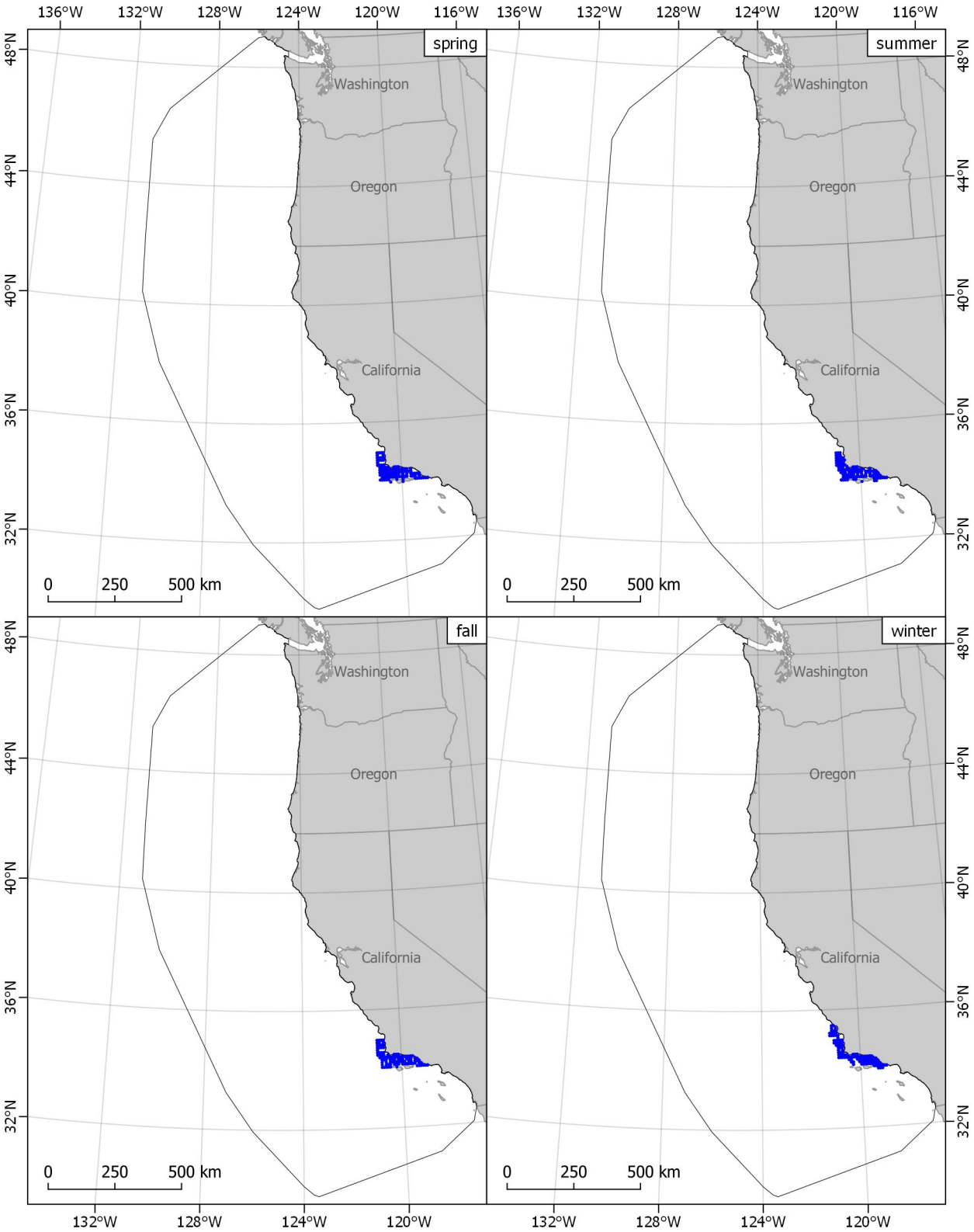

Figure A-19. Santa Barbara Channel Surveys

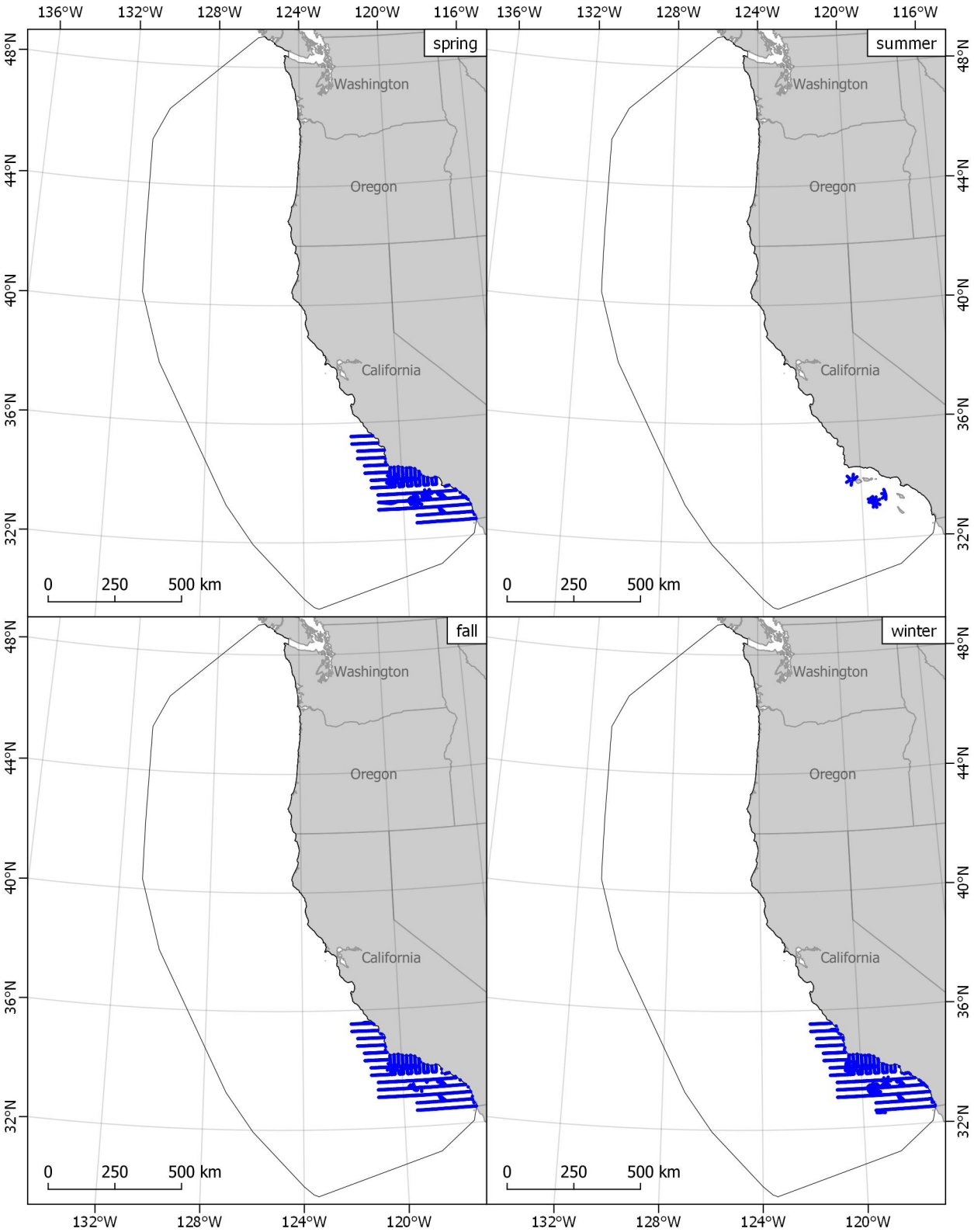

Figure A-20. Southern California Bight Surveys

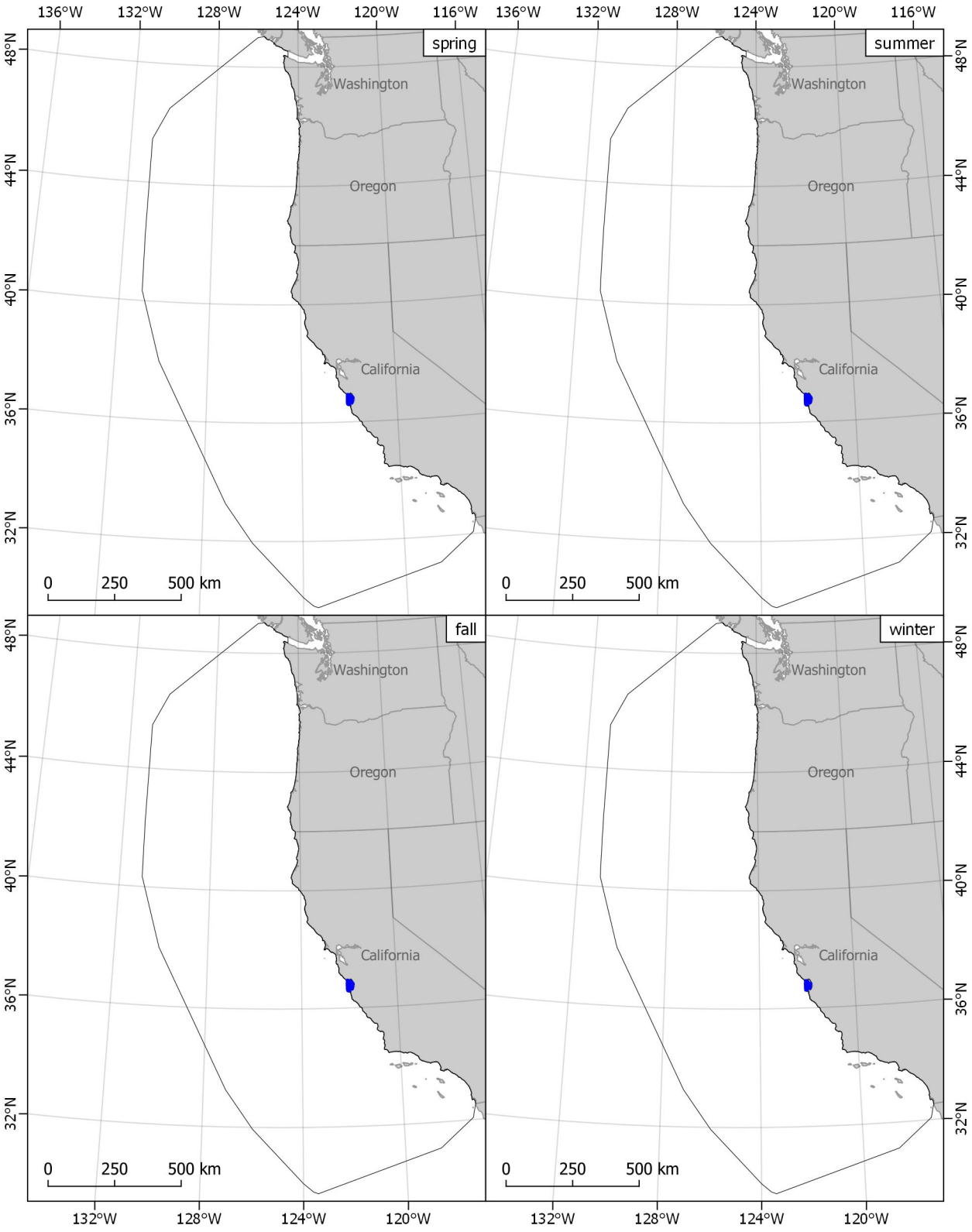

Figure A-21. Wind to Whales

Appendix B: Predictor Variable Figures

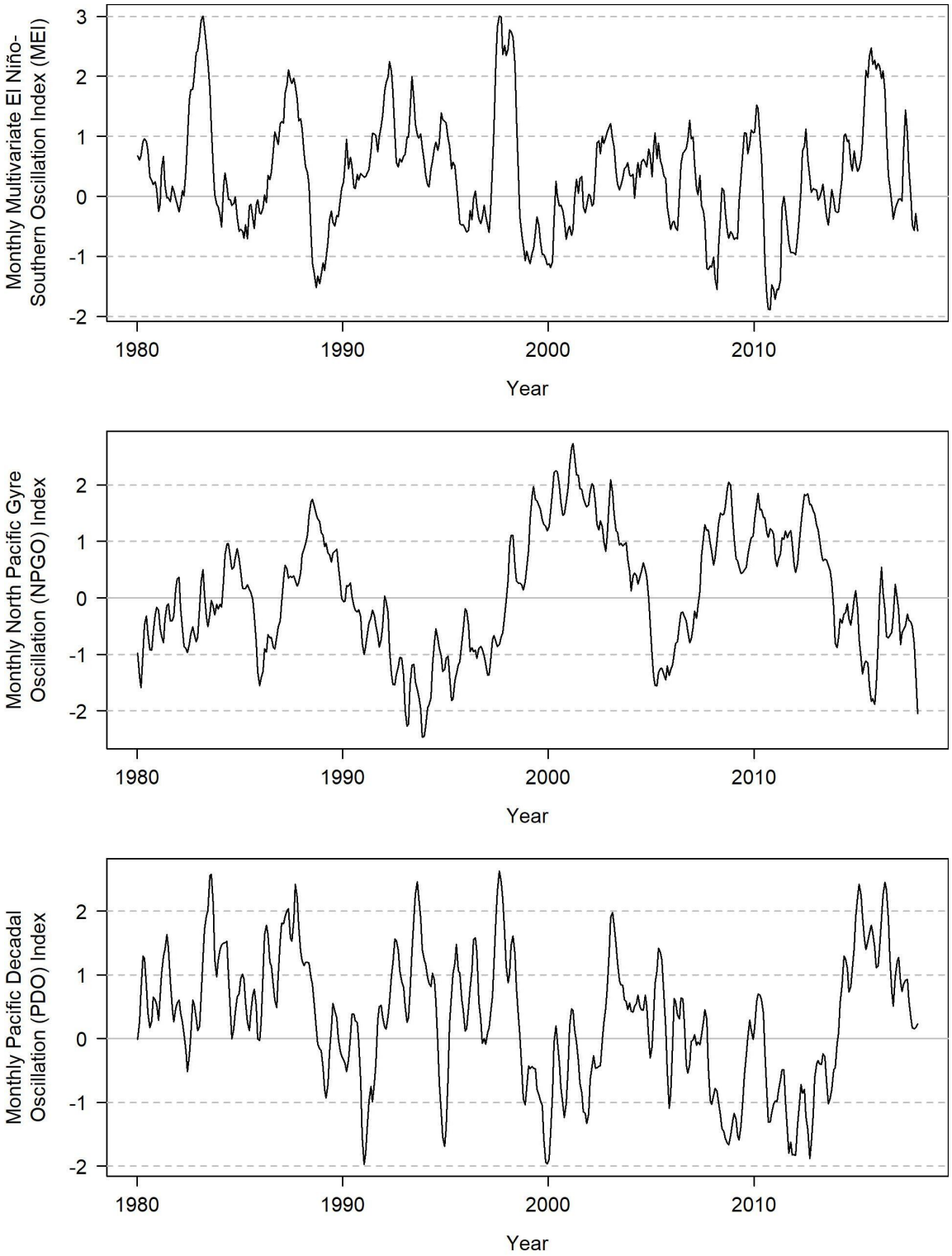

Figure B-1. Temporal climate index predictors

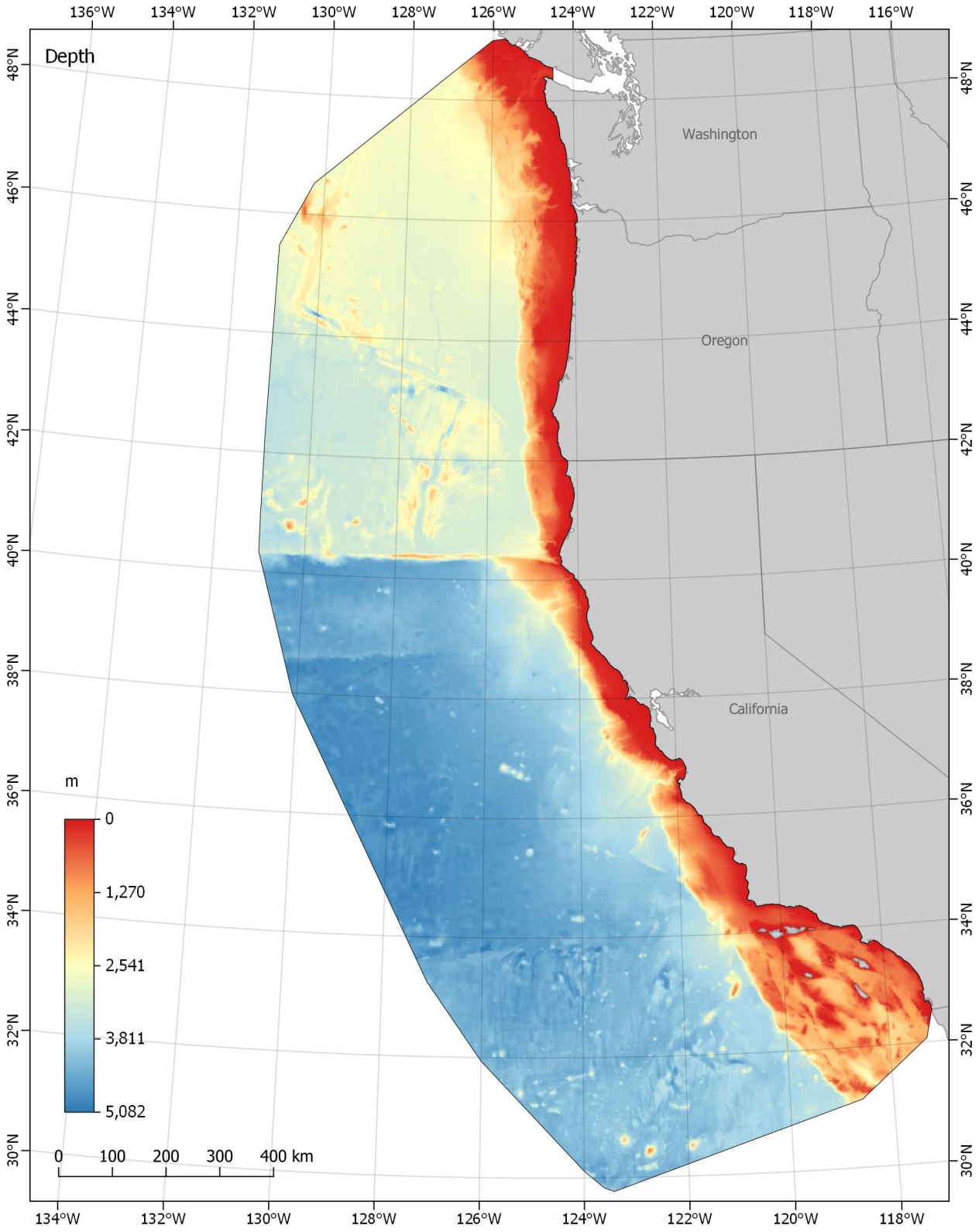

Figure B-2. Seafloor depth

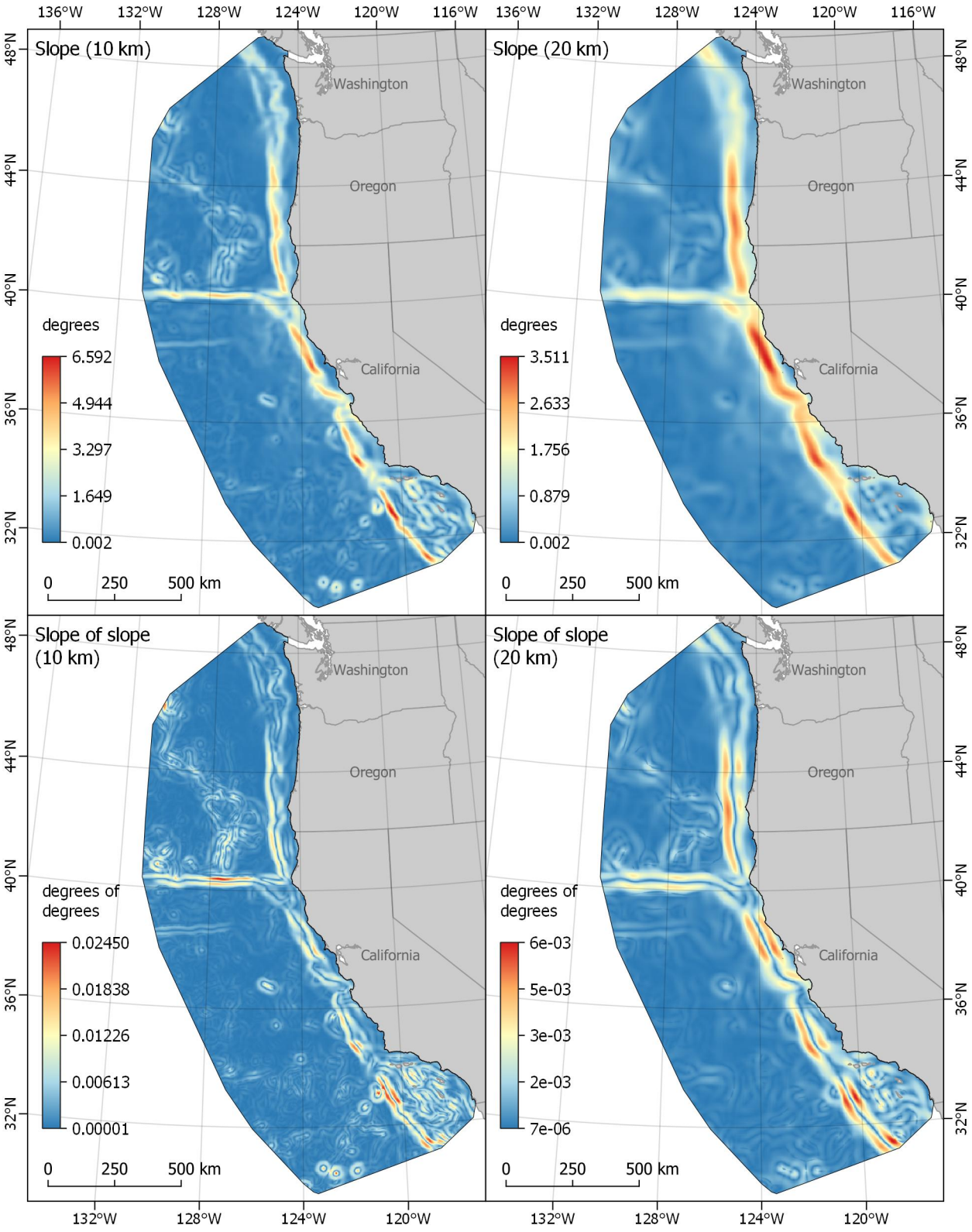

Figure B-3. Seafloor slope (top panel) and slope of slope (bottom panel)

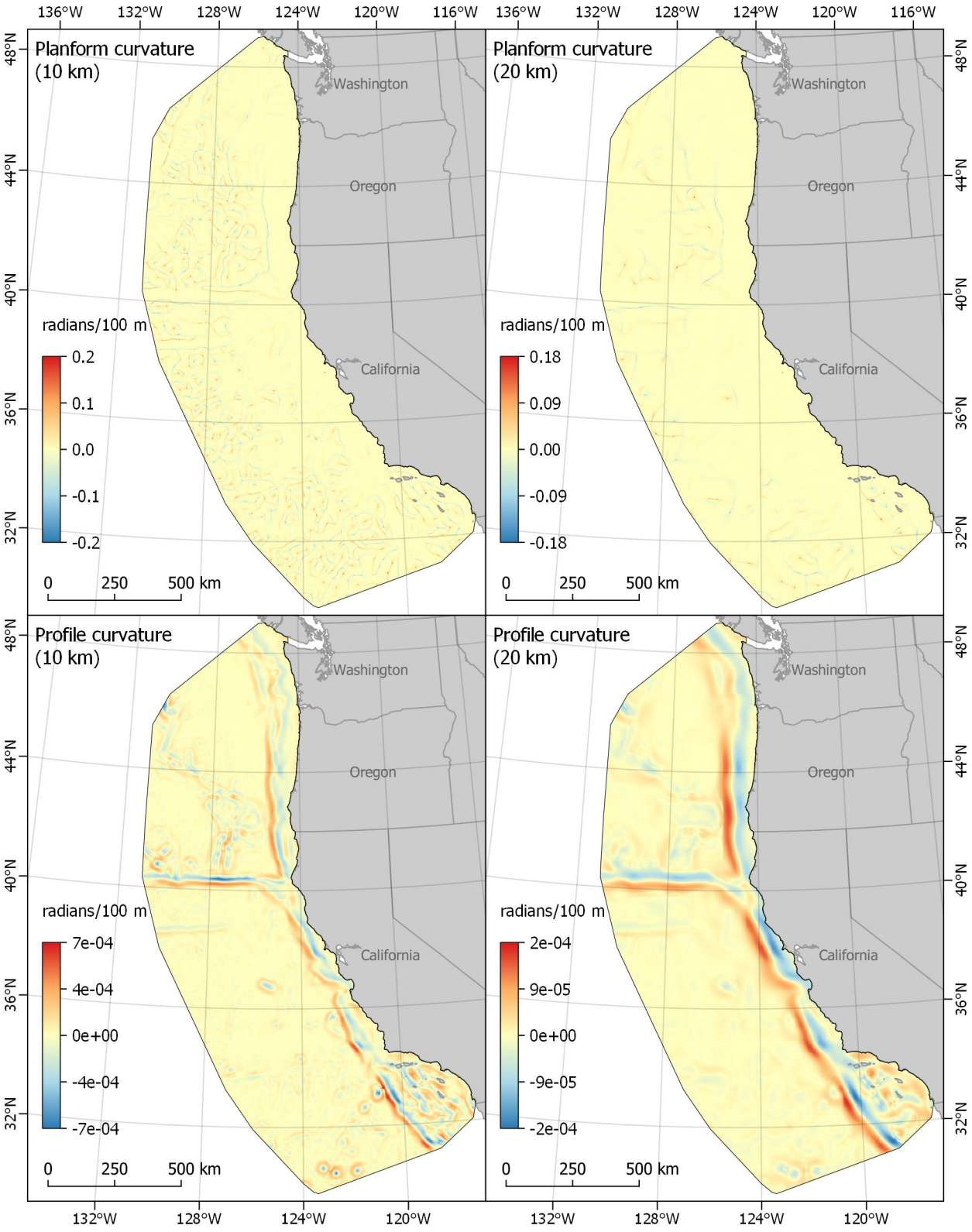

Figure B-4. Seafloor planform curvature (top panel) and profile curvature (bottom panel)

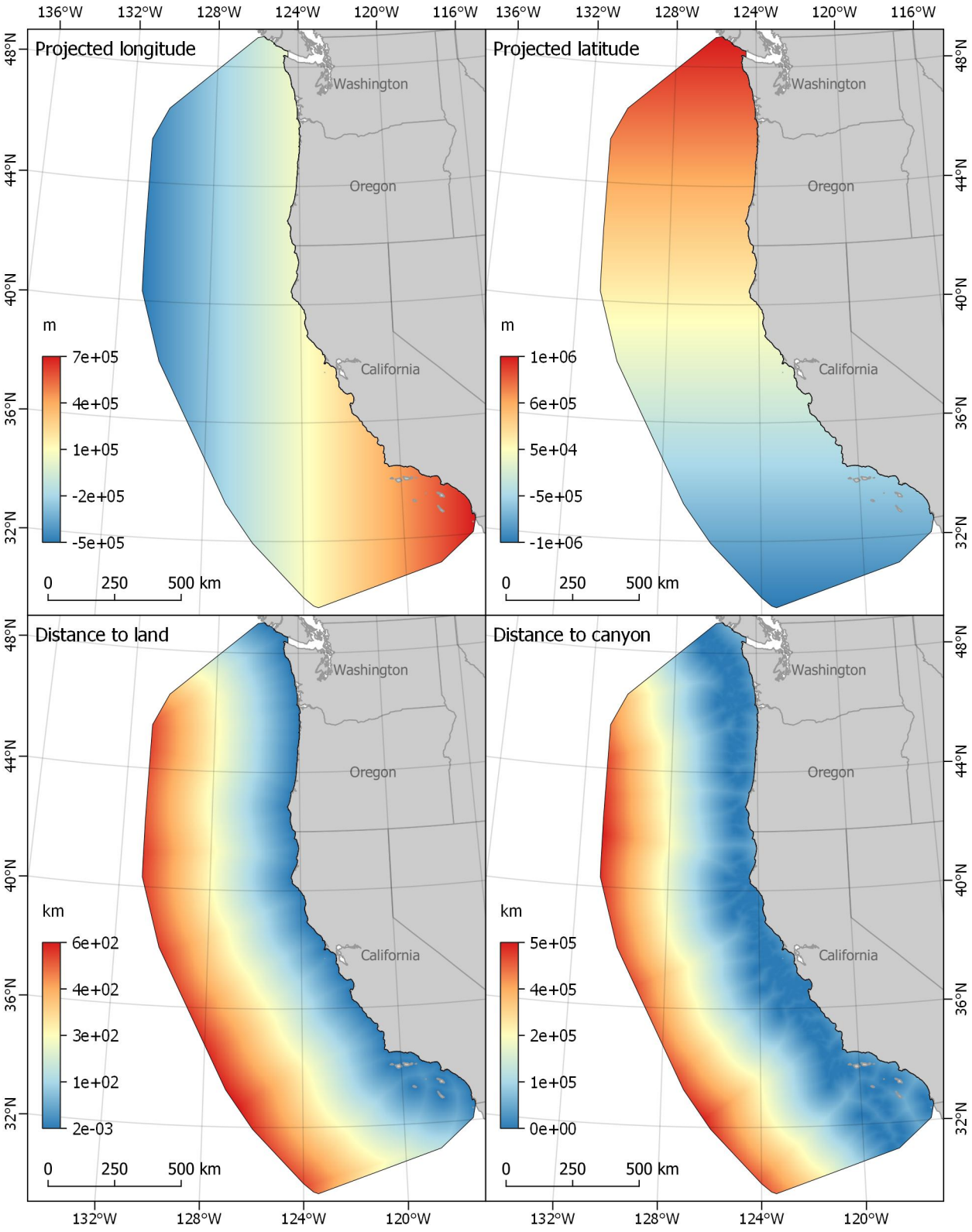

Figure B-5. Projected geographic coordinates (top panel) and distance to nearest land and nearest canyon (bottom panel)

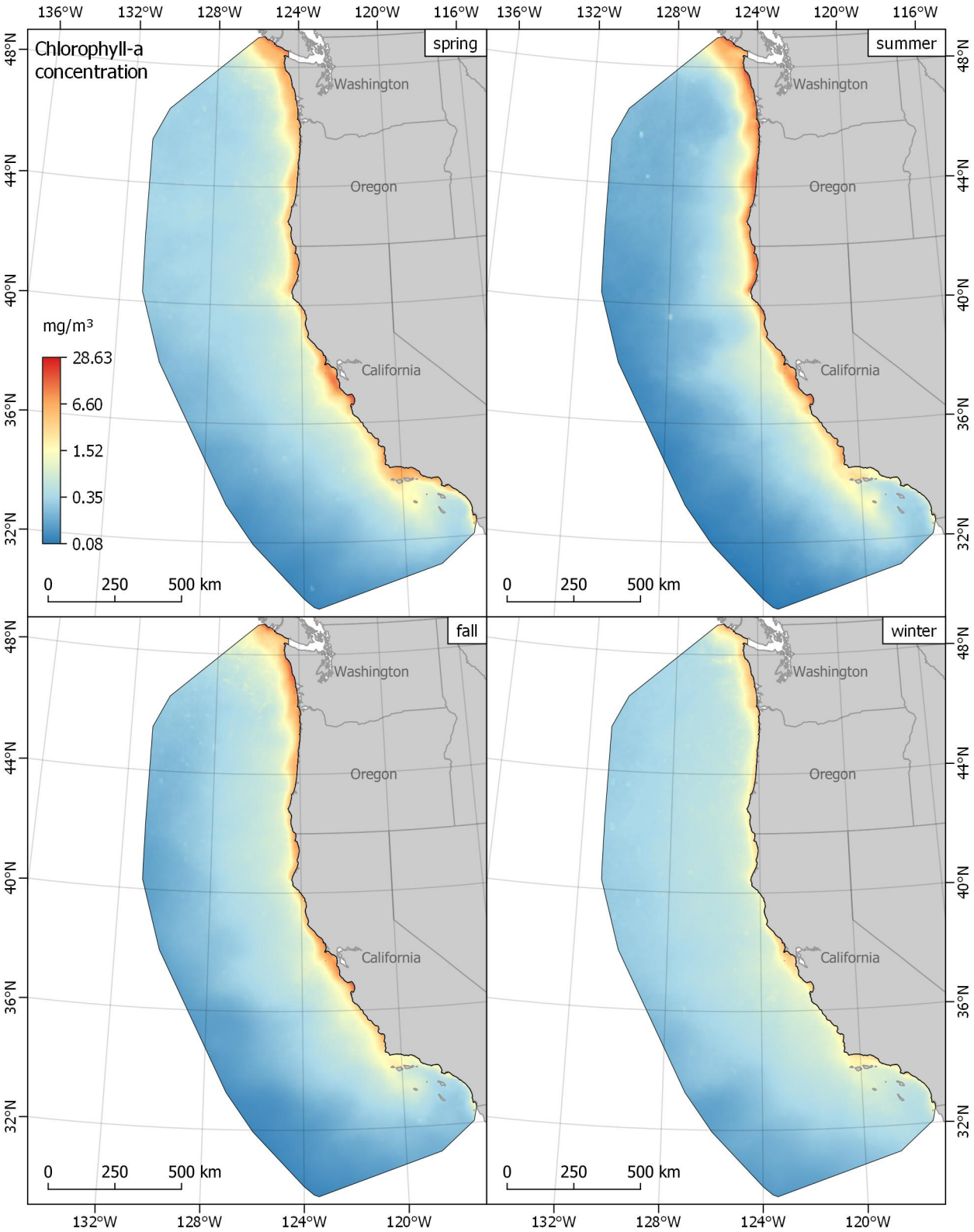

Figure B-6. Seasonal chlorophyll-a concentration
Color gradient is linear on the natural logarithmic scale

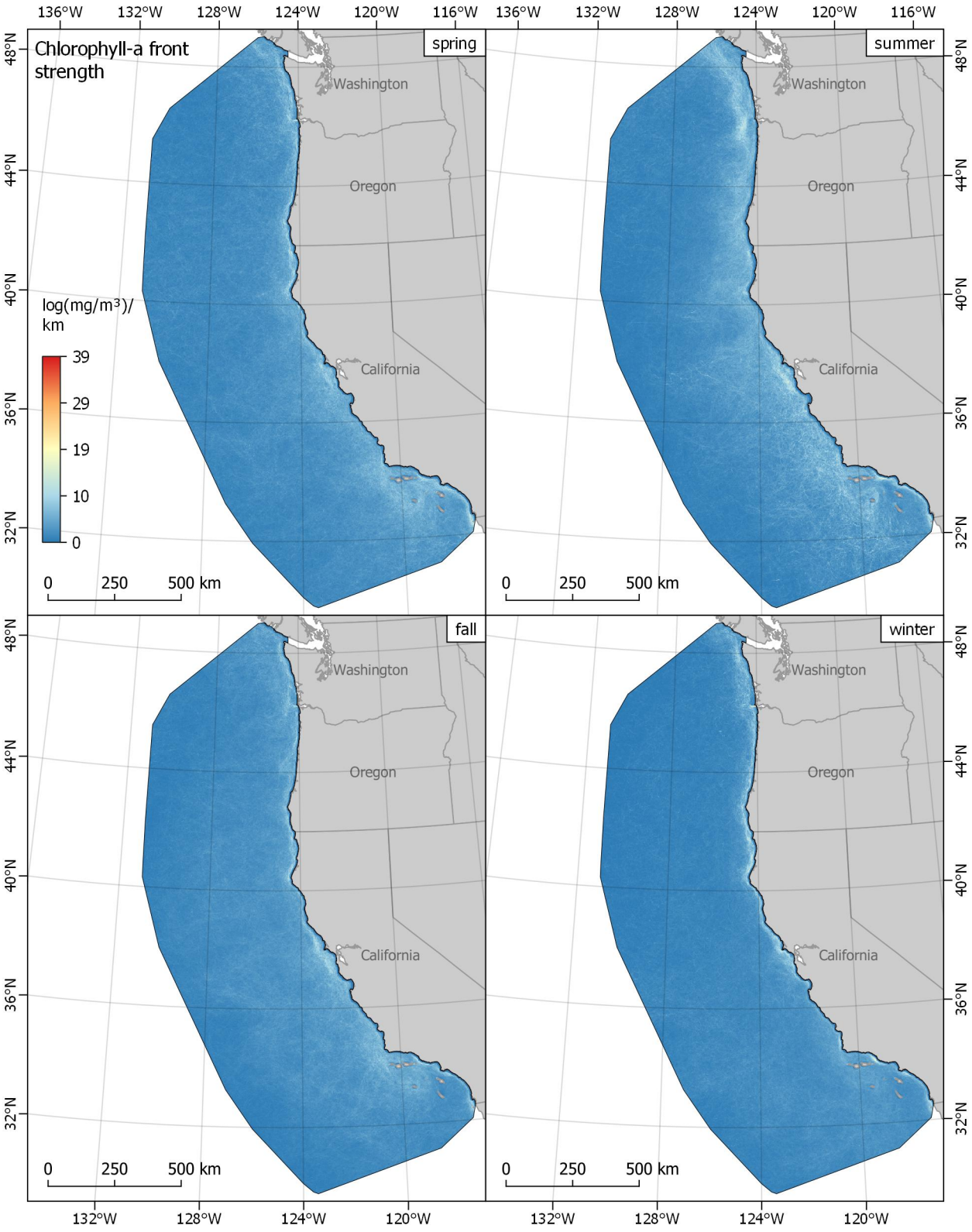

Figure B-7. Seasonal chlorophyll-a front strength

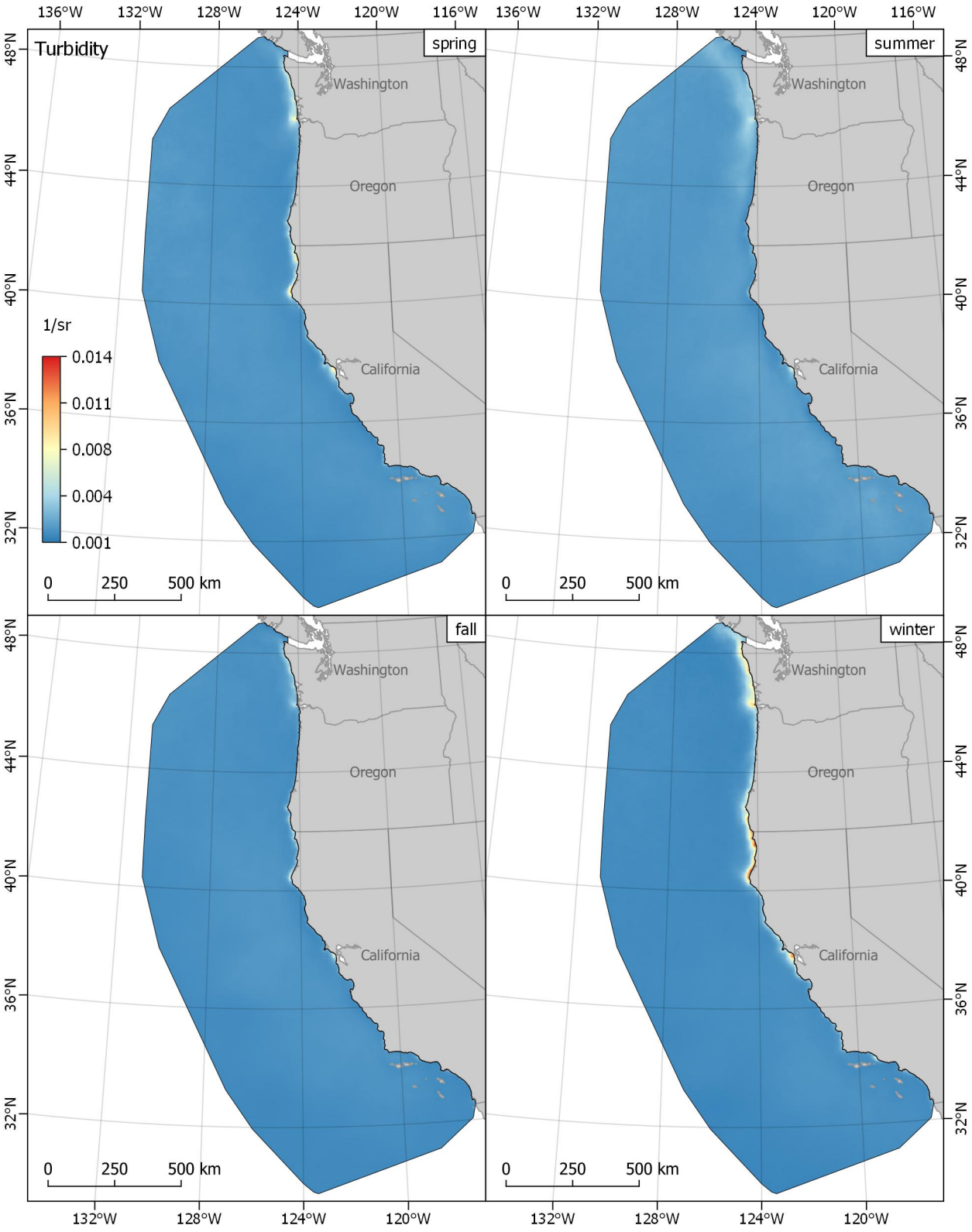

Figure B-8. Seasonal turbidity

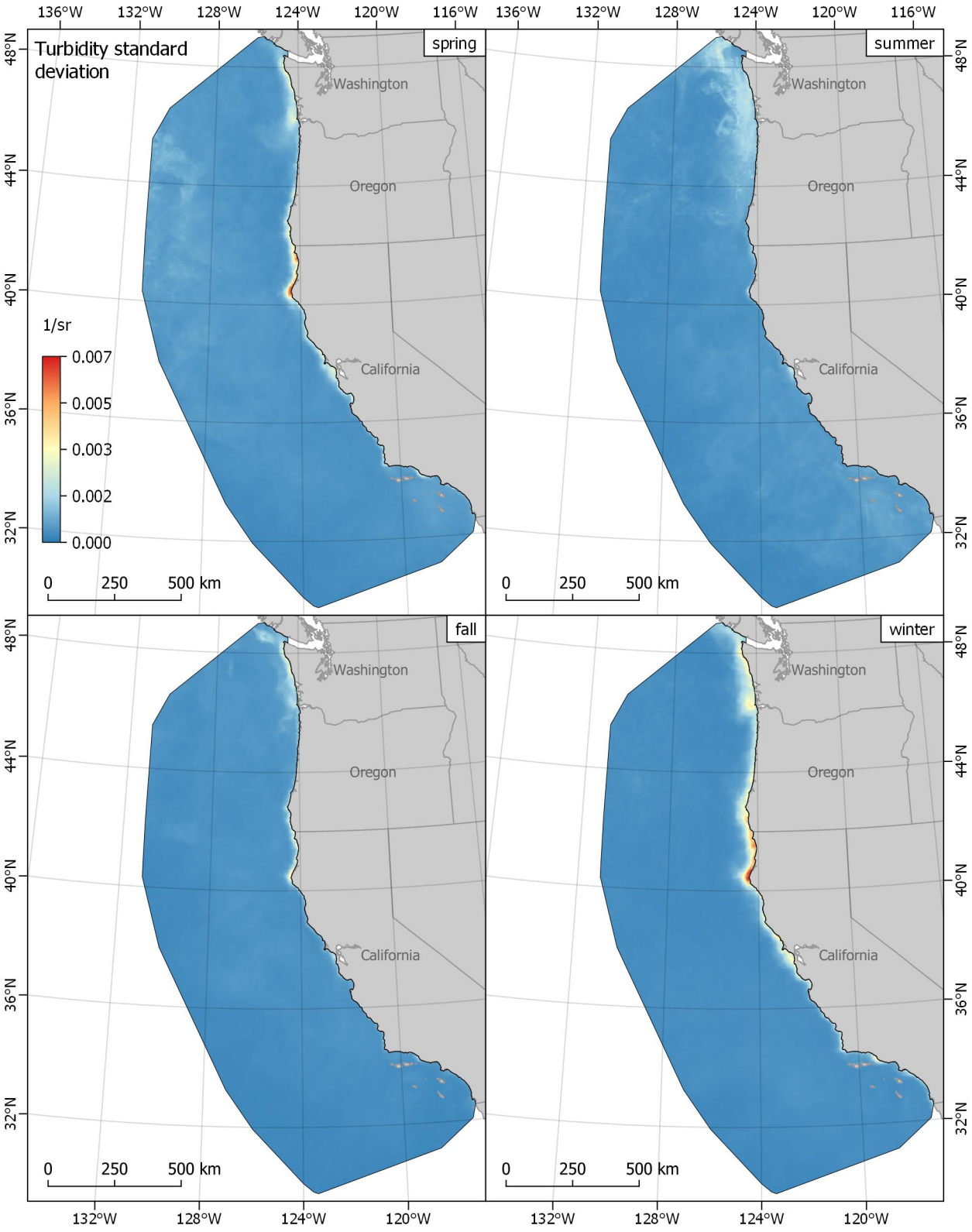

Figure B-9. Seasonal turbidity standard deviation

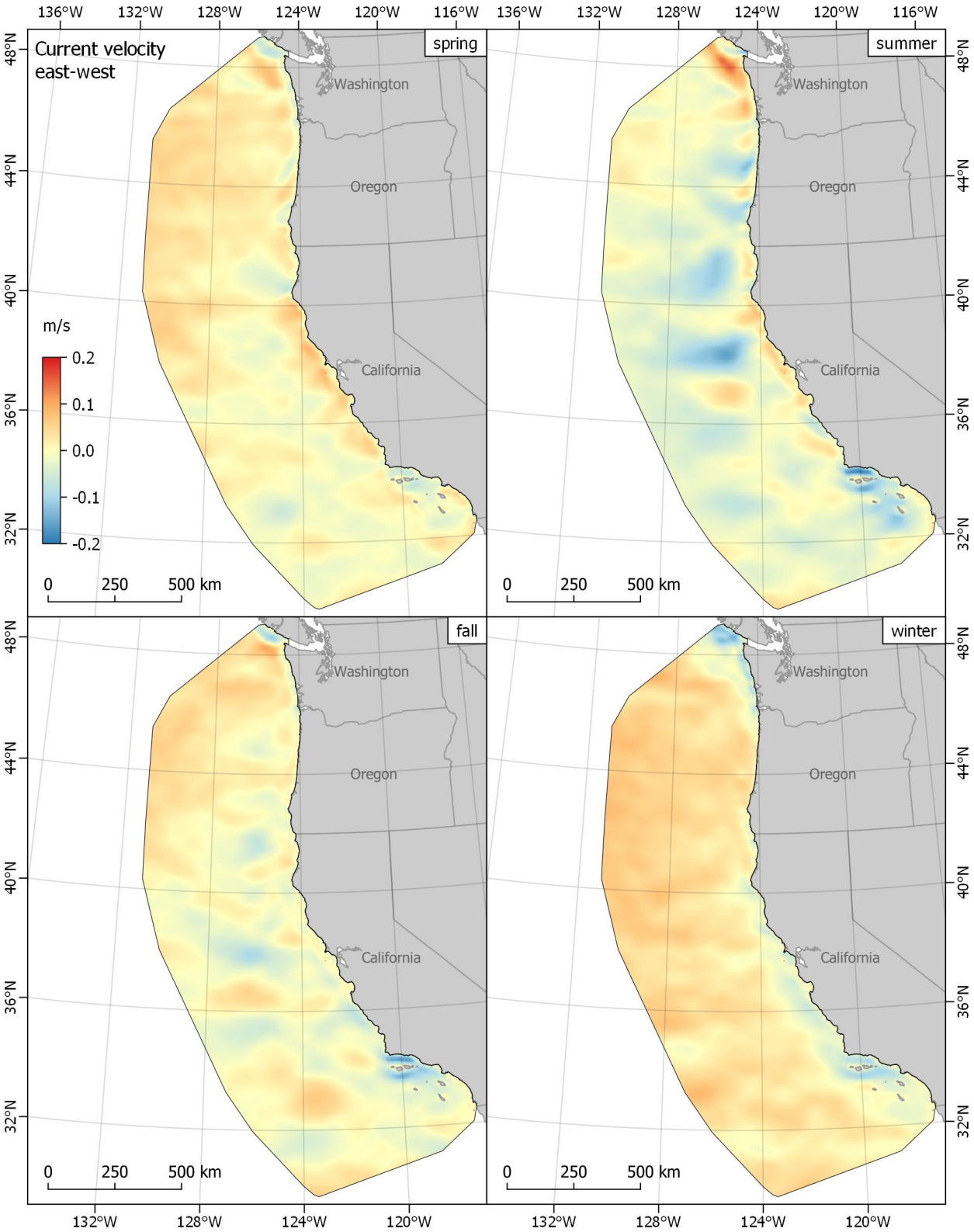

Figure B-10. Seasonal surface current velocity east-west

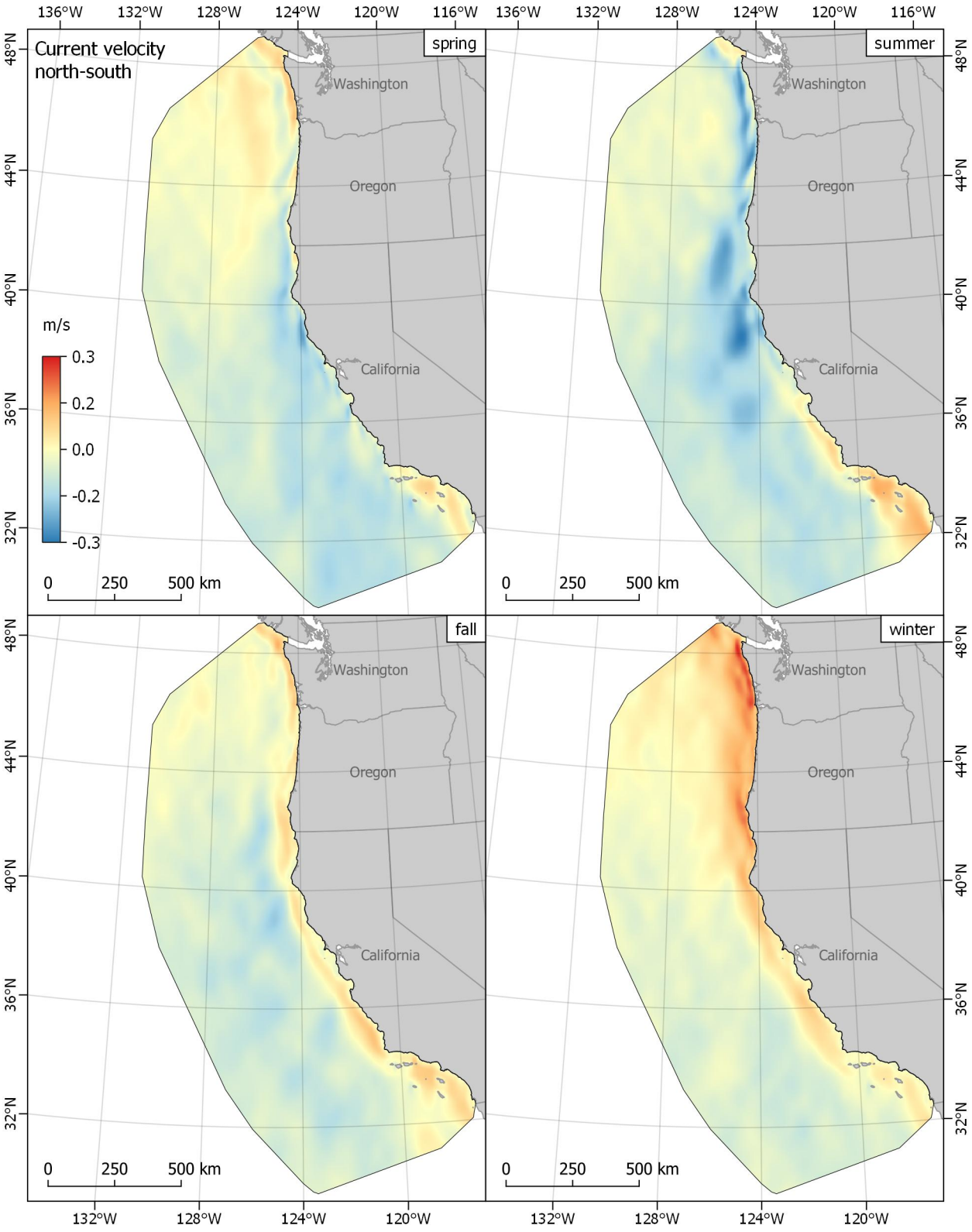

Figure B-11. Seasonal surface current velocity north-south

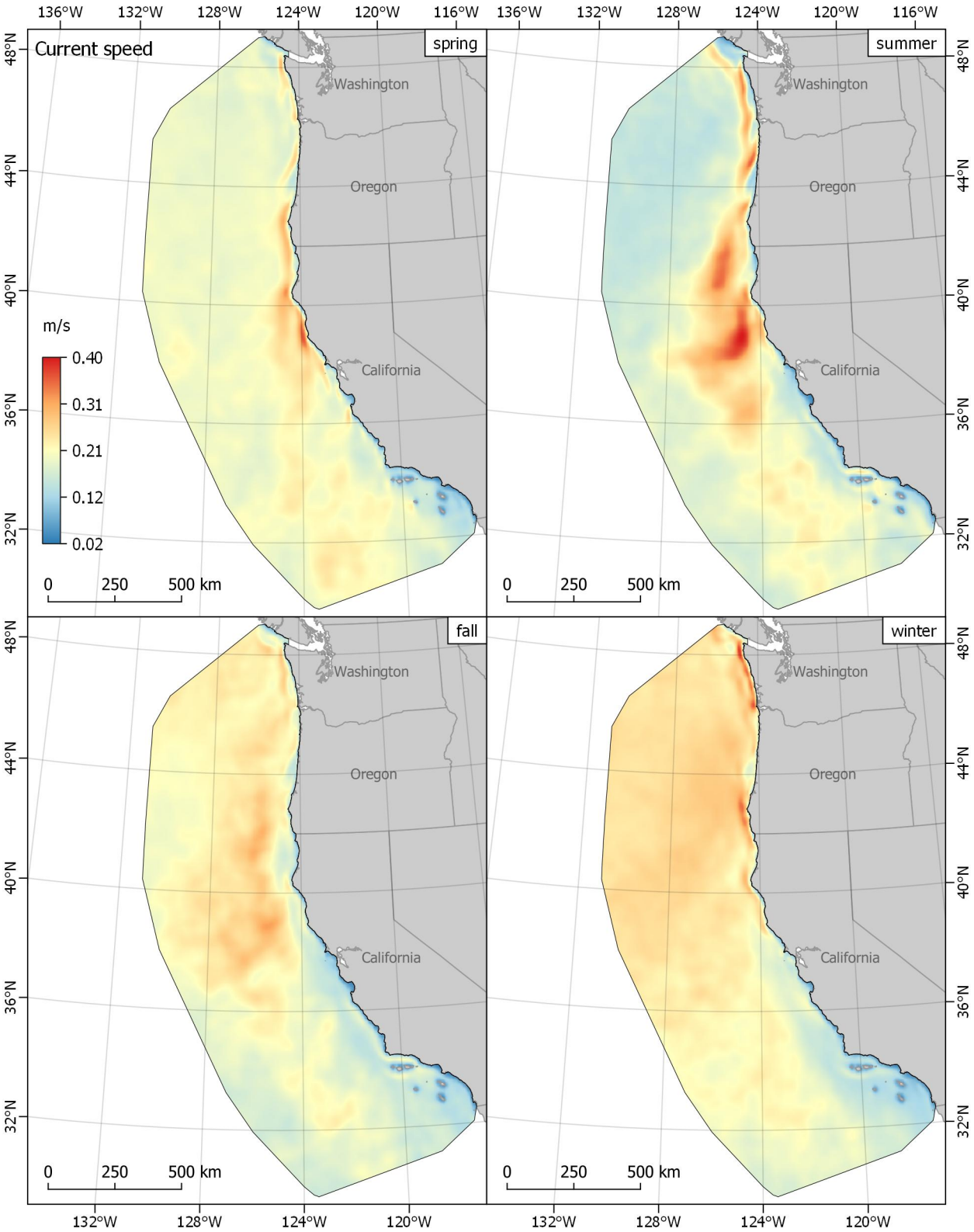

Figure B-12. Seasonal surface current speed

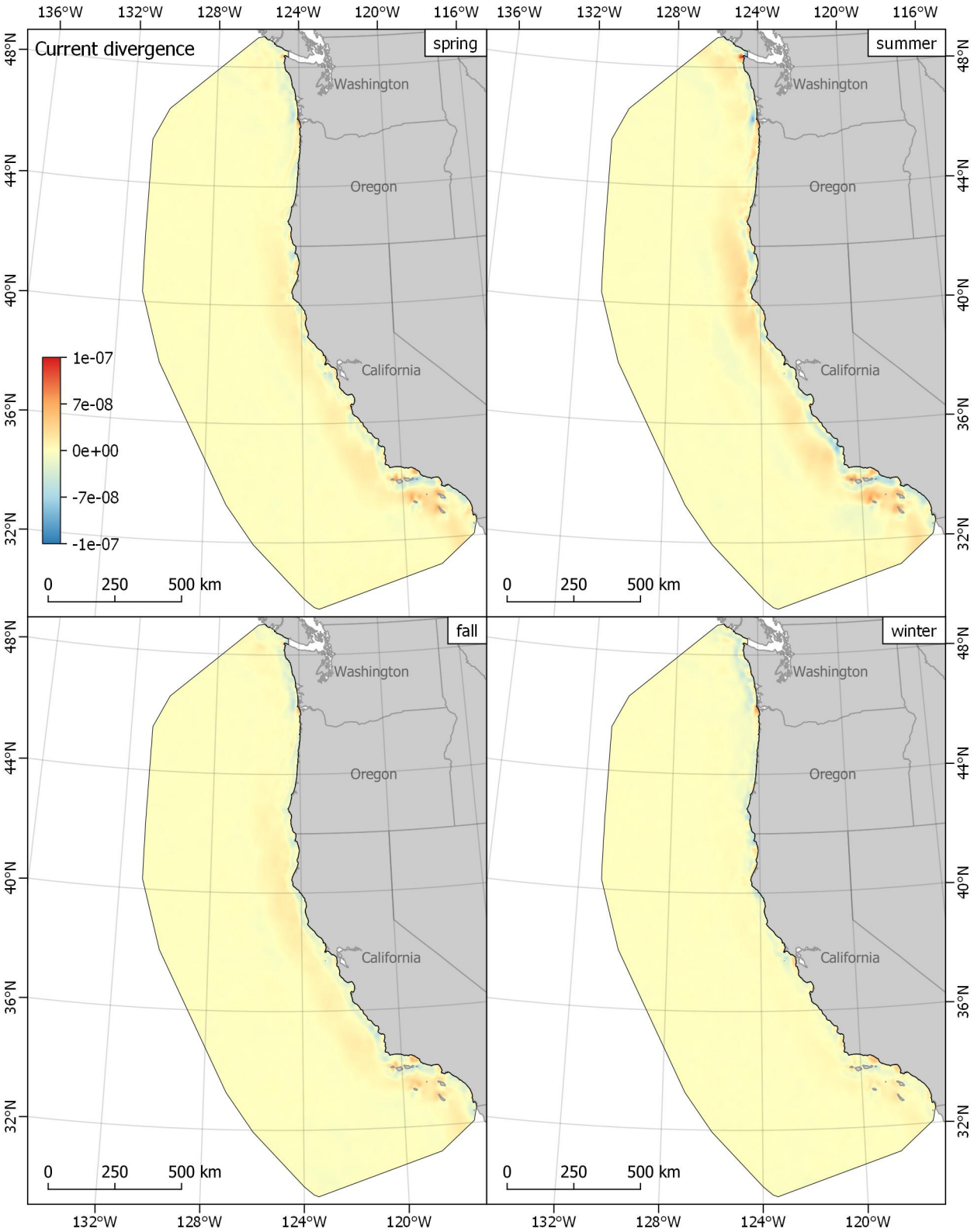

Figure B-13. Seasonal surface current divergence
Positive values = divergence, negative values = convergence

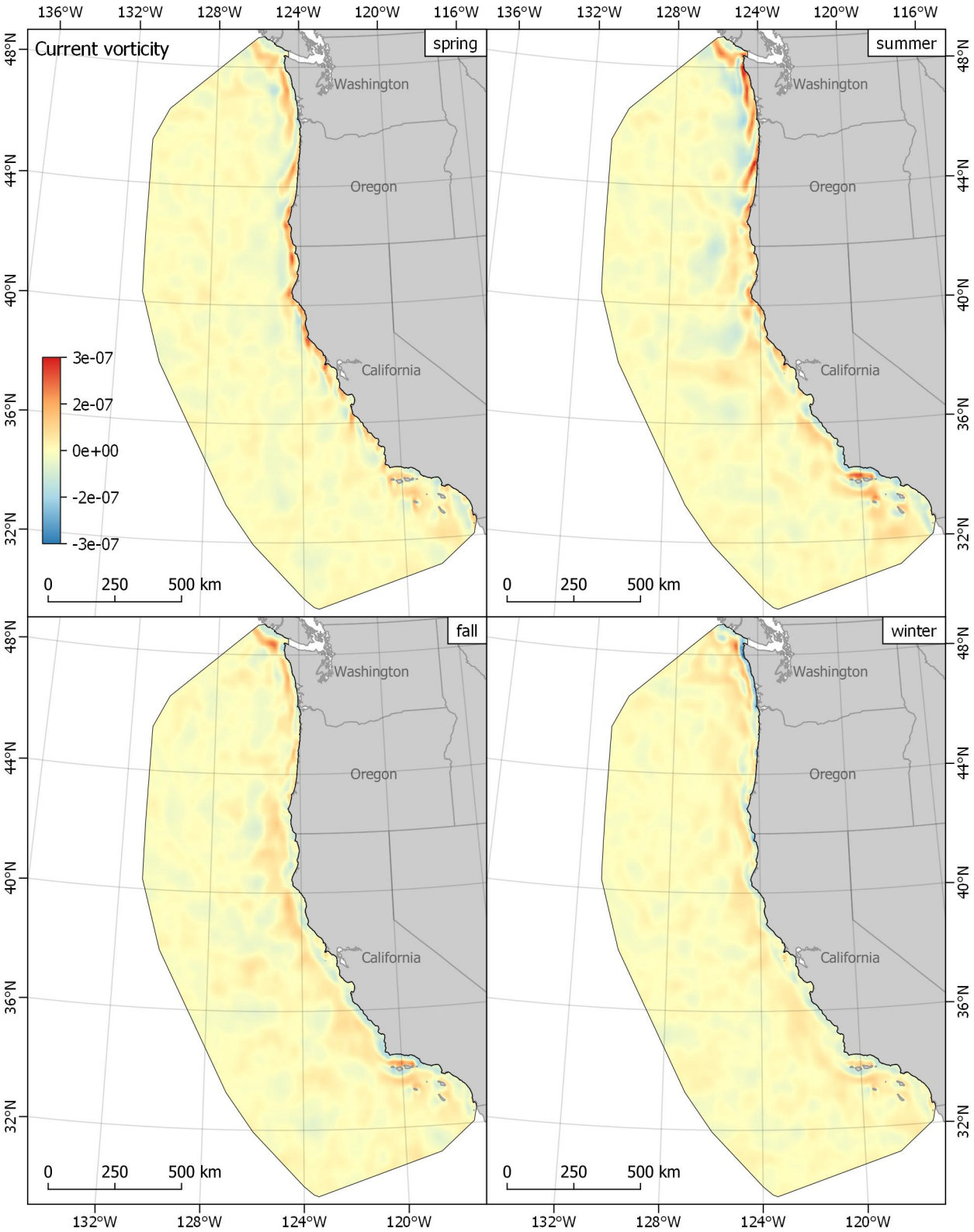

Figure B-14. Seasonal surface current vorticity
Positive values = counterclockwise, negative values = clockwise

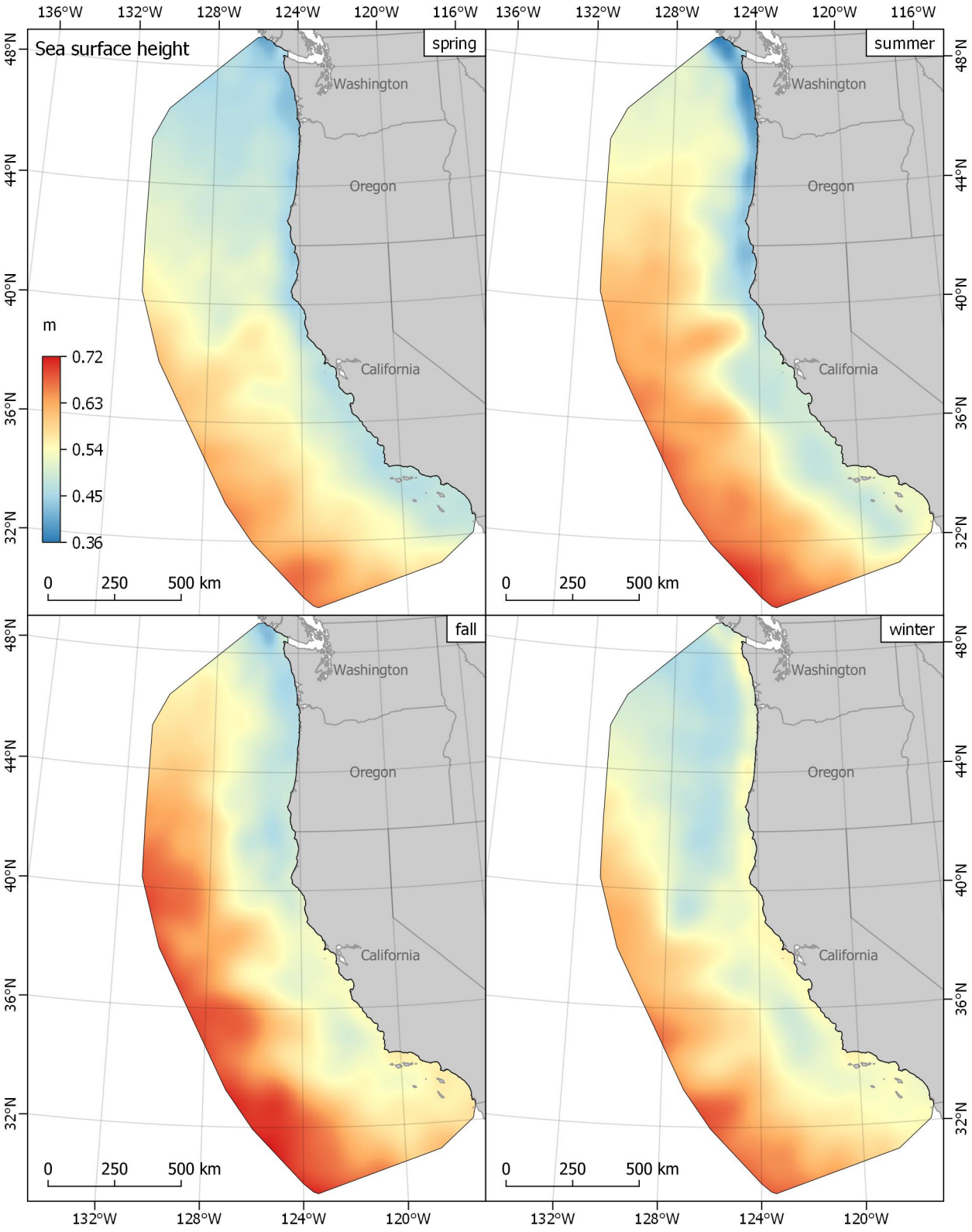

Figure B-15. Seasonal surface height

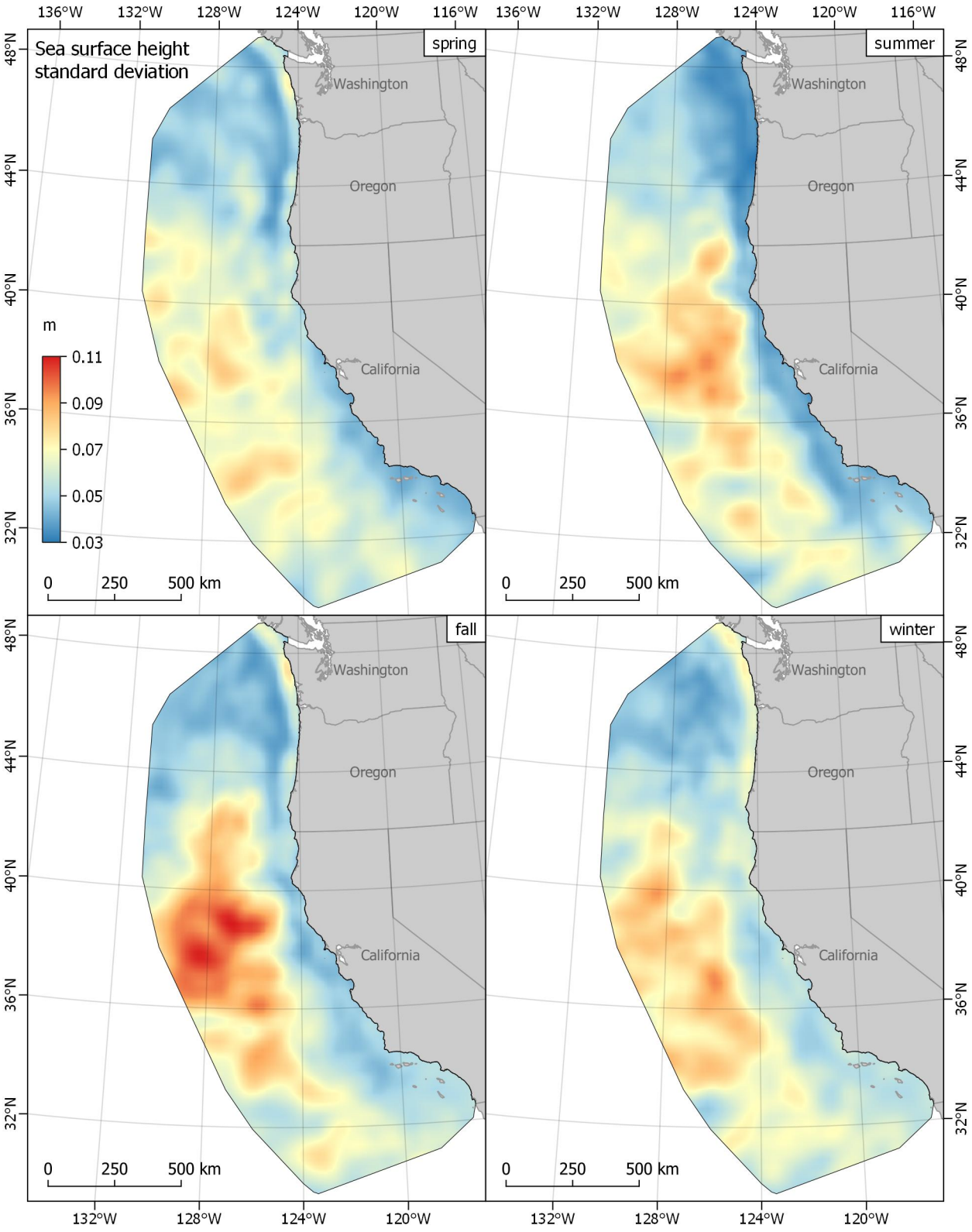

Figure B-16. Seasonal surface height standard deviation

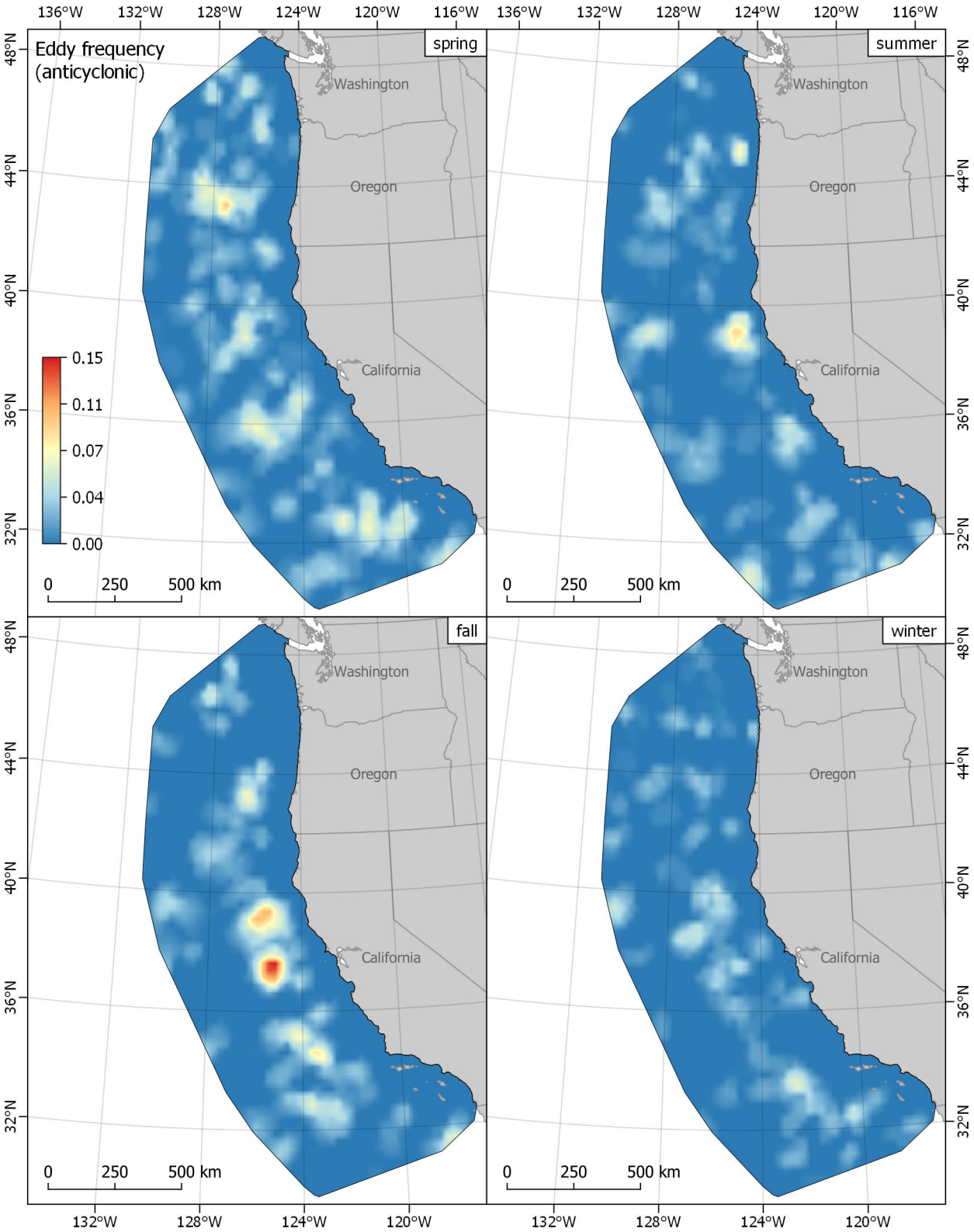

Figure B-17. Seasonal anticyclonic eddy frequency

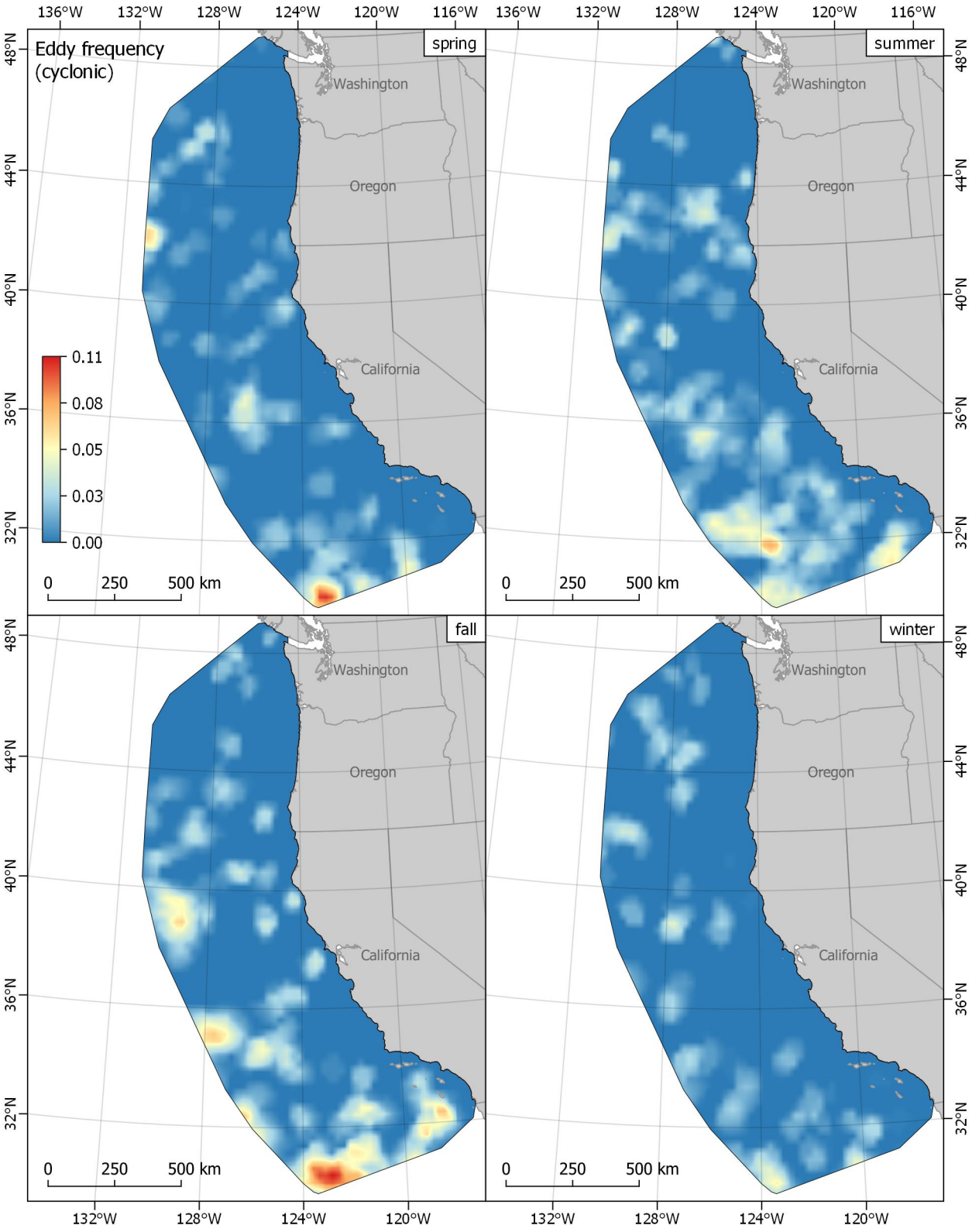

Figure B-18. Seasonal cyclonic eddy frequency

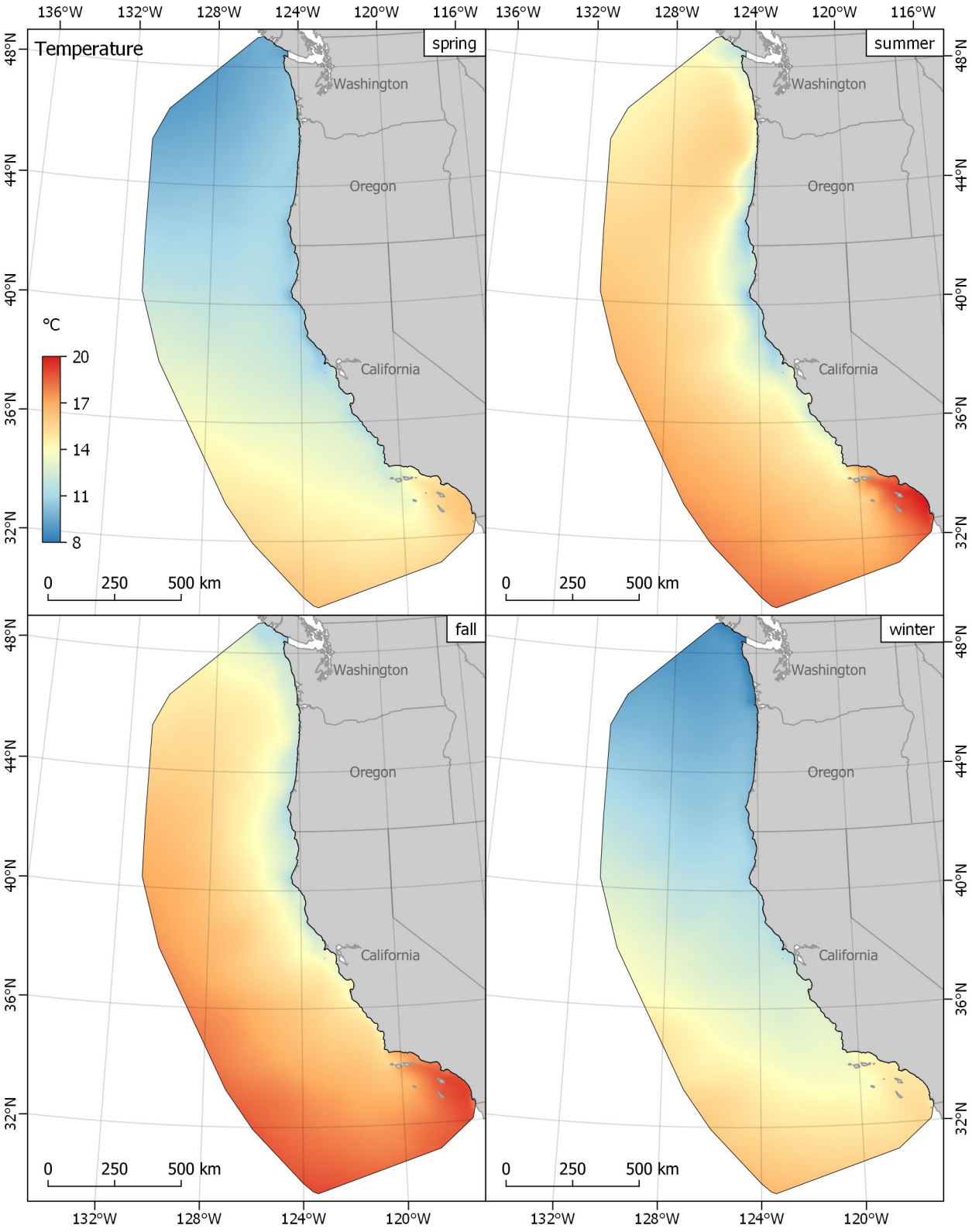

Figure B-19. Seasonal surface temperature

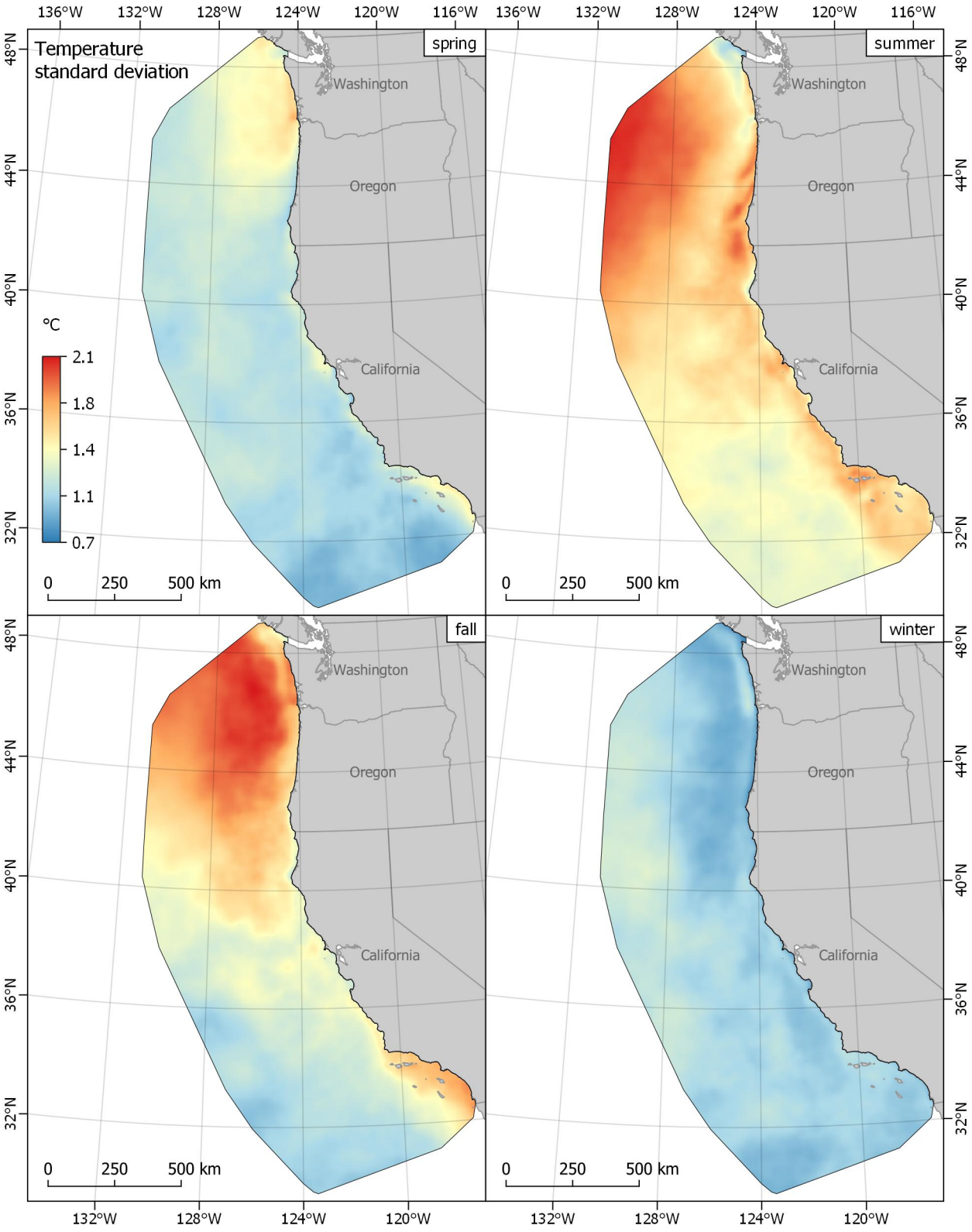

Figure B-20. Seasonal surface temperature standard deviation

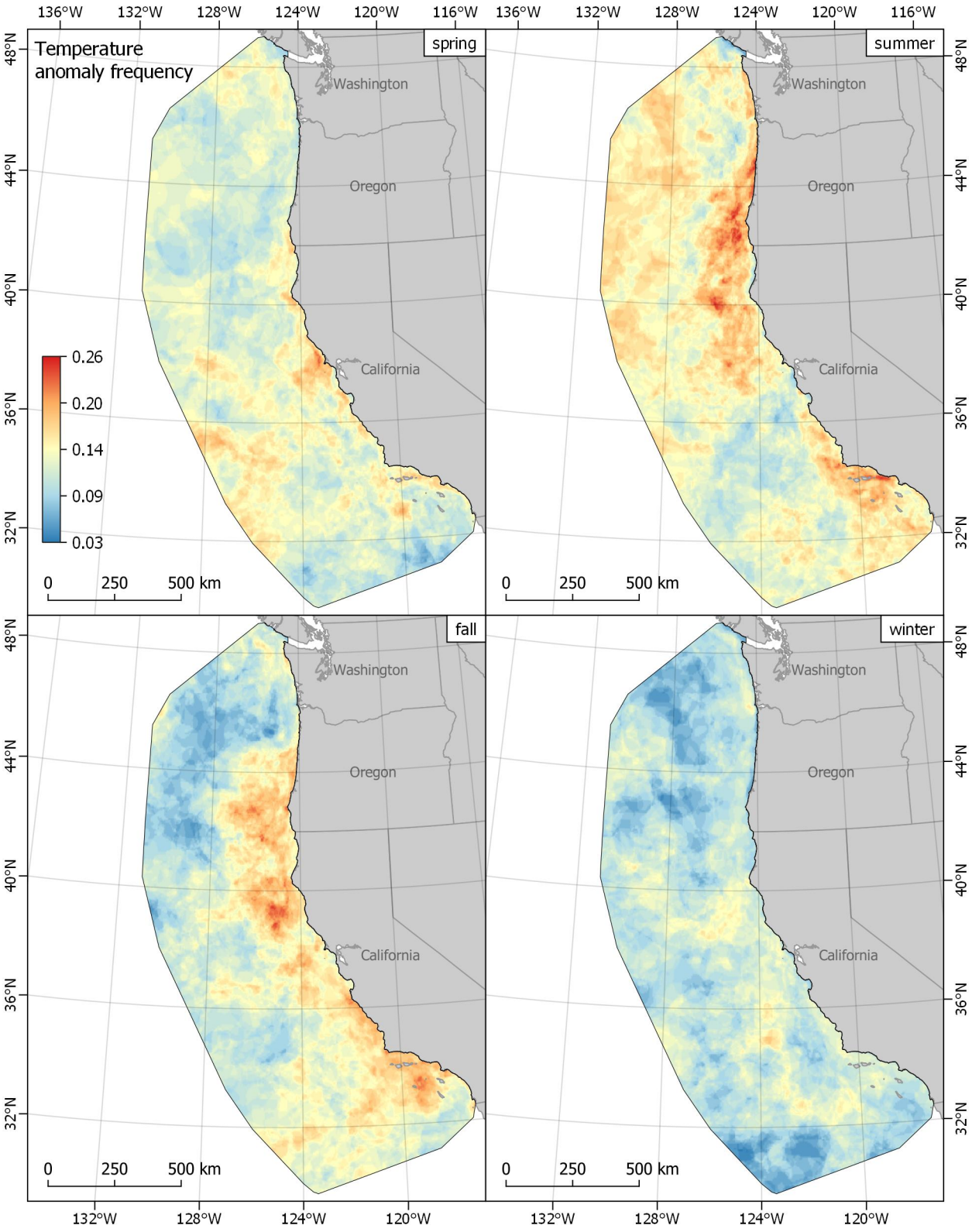

Figure B-21. Seasonal surface temperature anomaly frequency

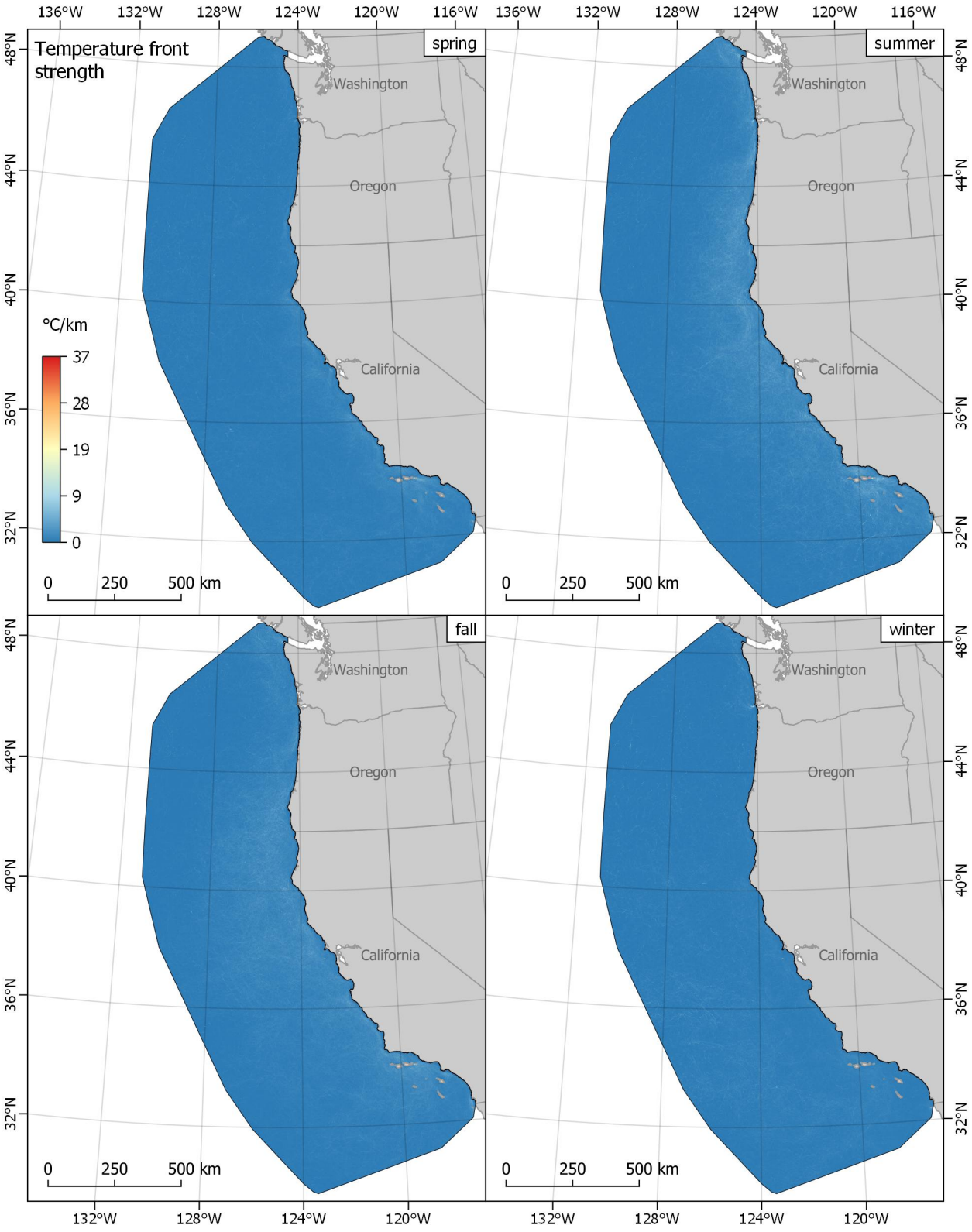

Figure B-22. Seasonal surface temperature front strength

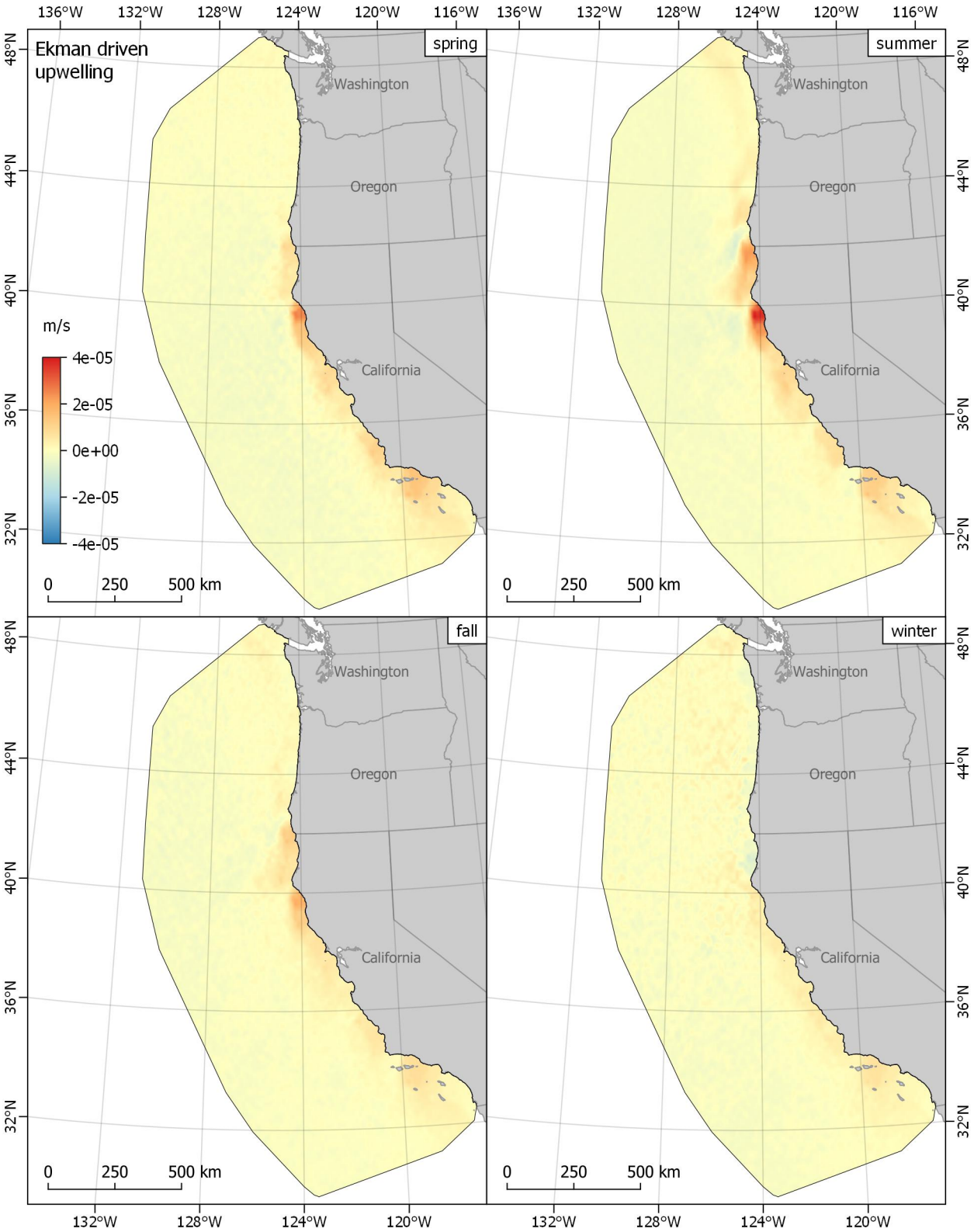

Figure B-23. Seasonal Ekman driven upwelling
Positive values = upwelling, negative values = downwelling

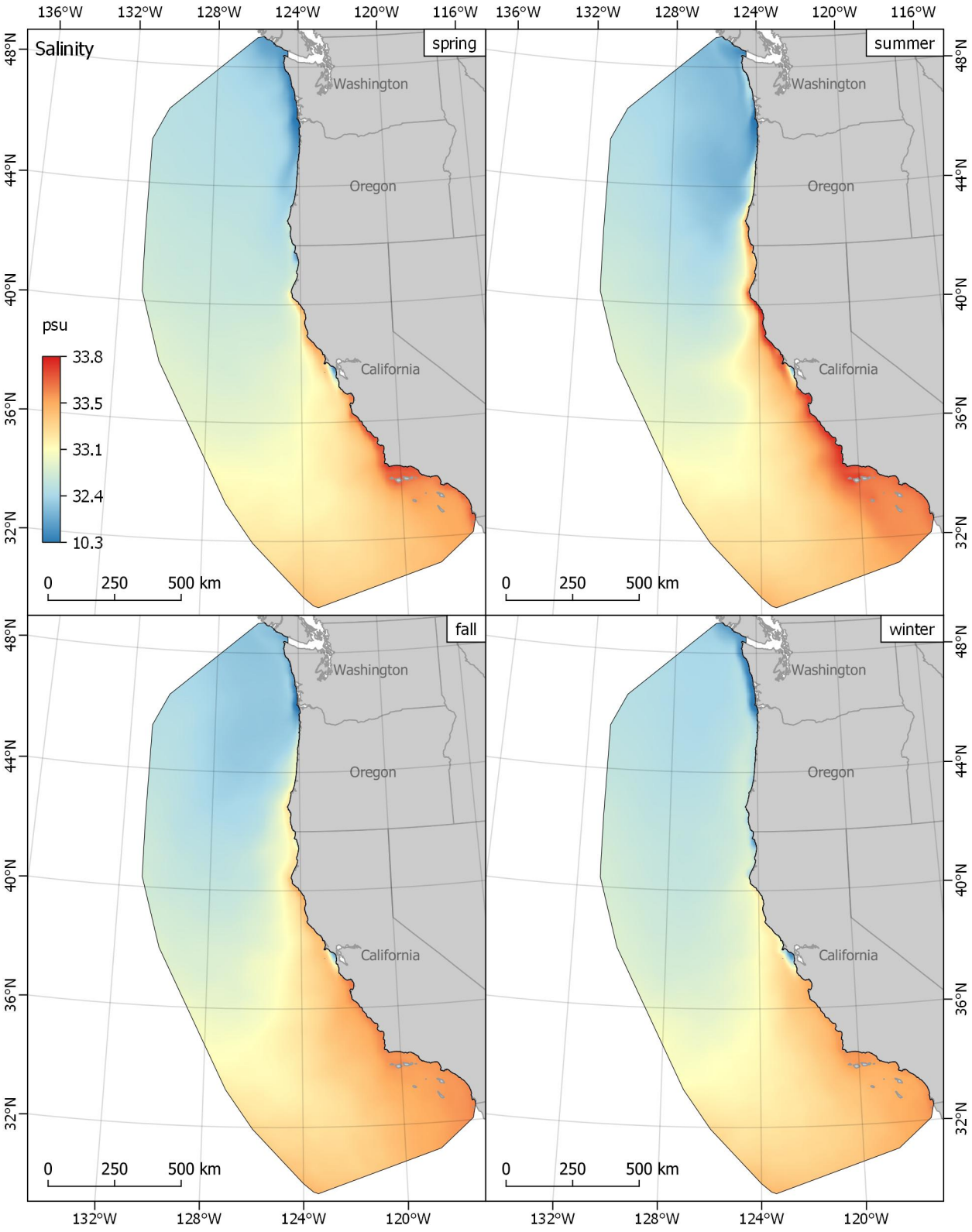

Figure B-24. Seasonal salinity
Color gradient is linear on the exponential scale

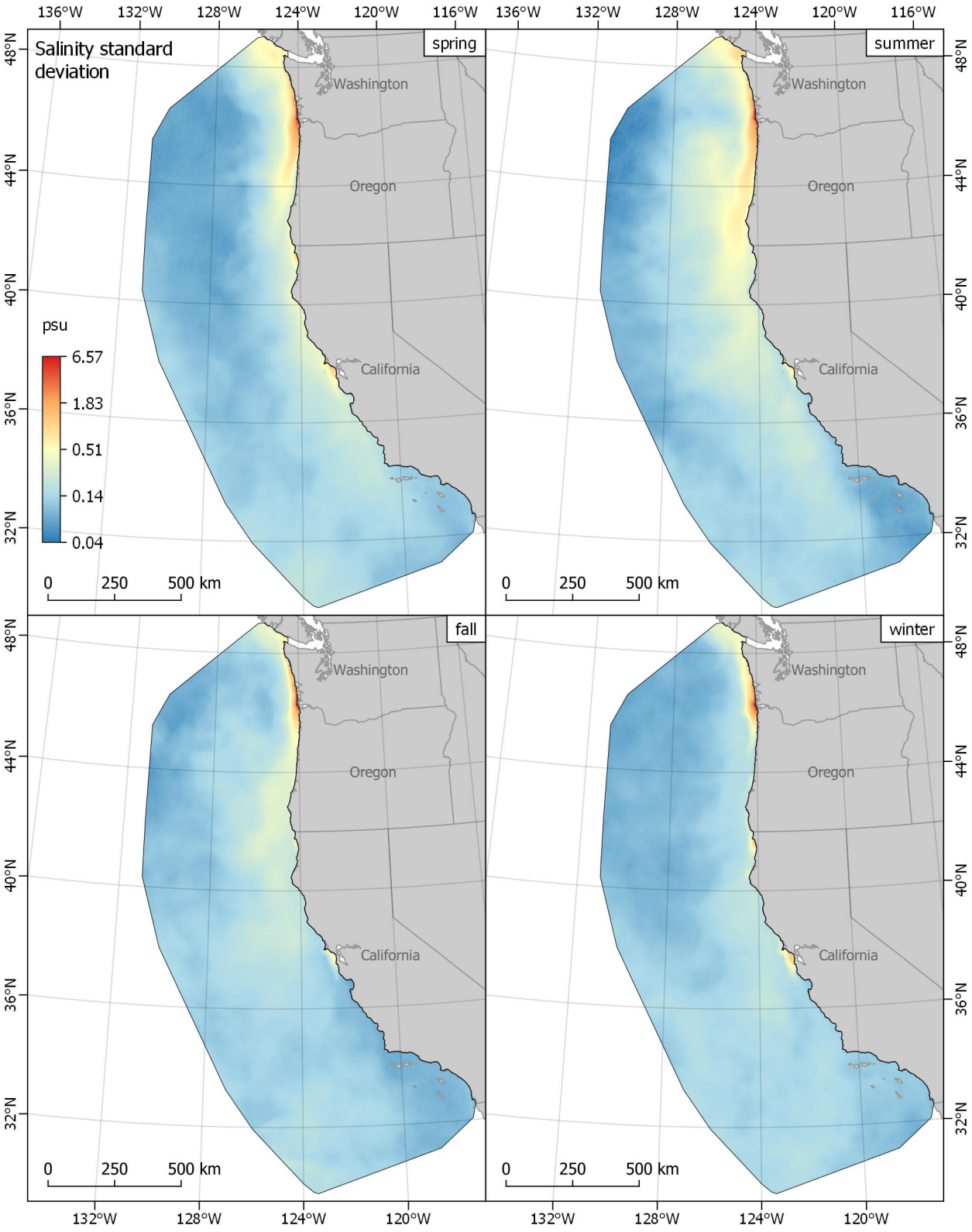

Figure B-25. Seasonal salinity standard deviation
Color gradient is linear on the natural logarithmic scale

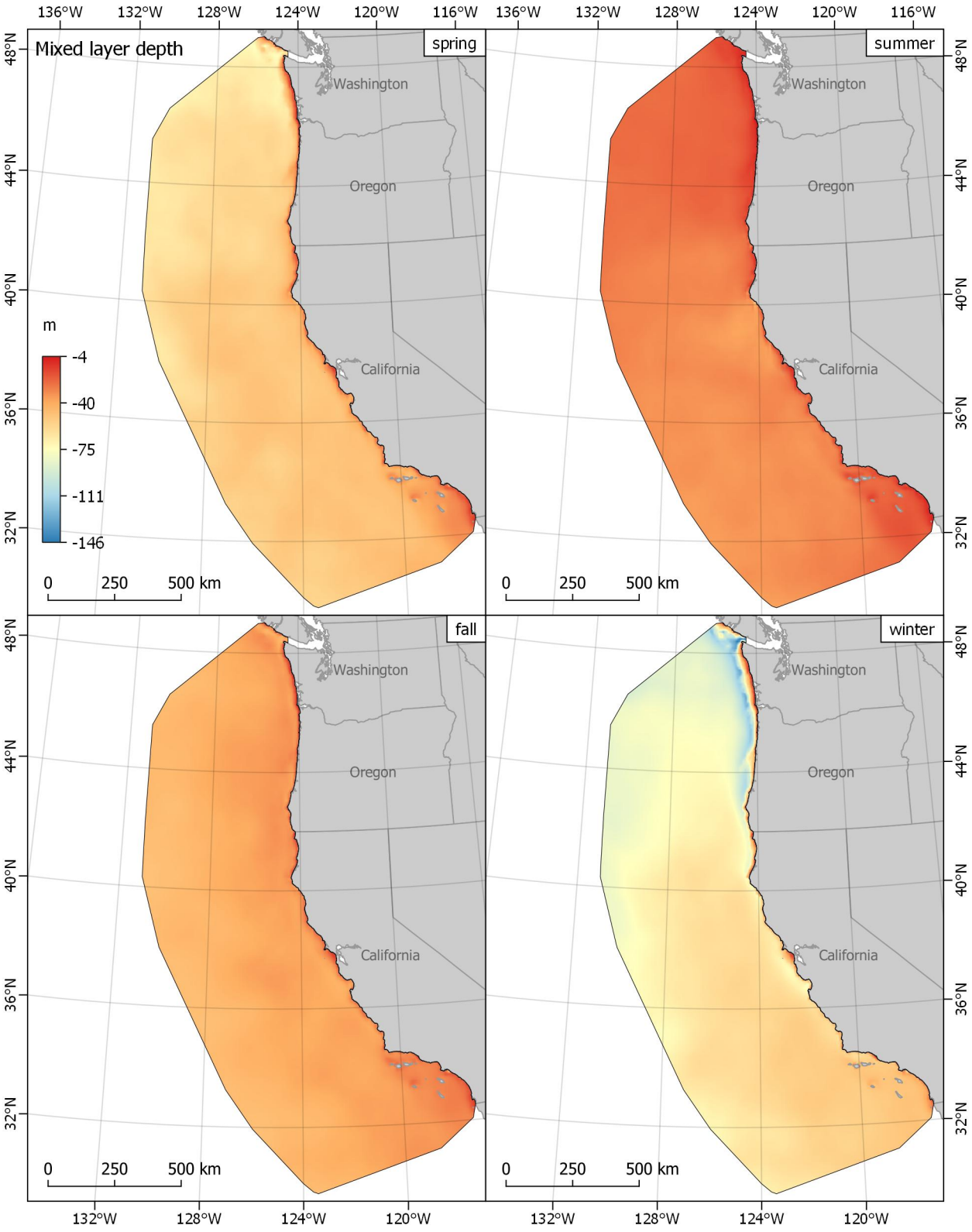

Figure B-26. Seasonal mixed layer depth

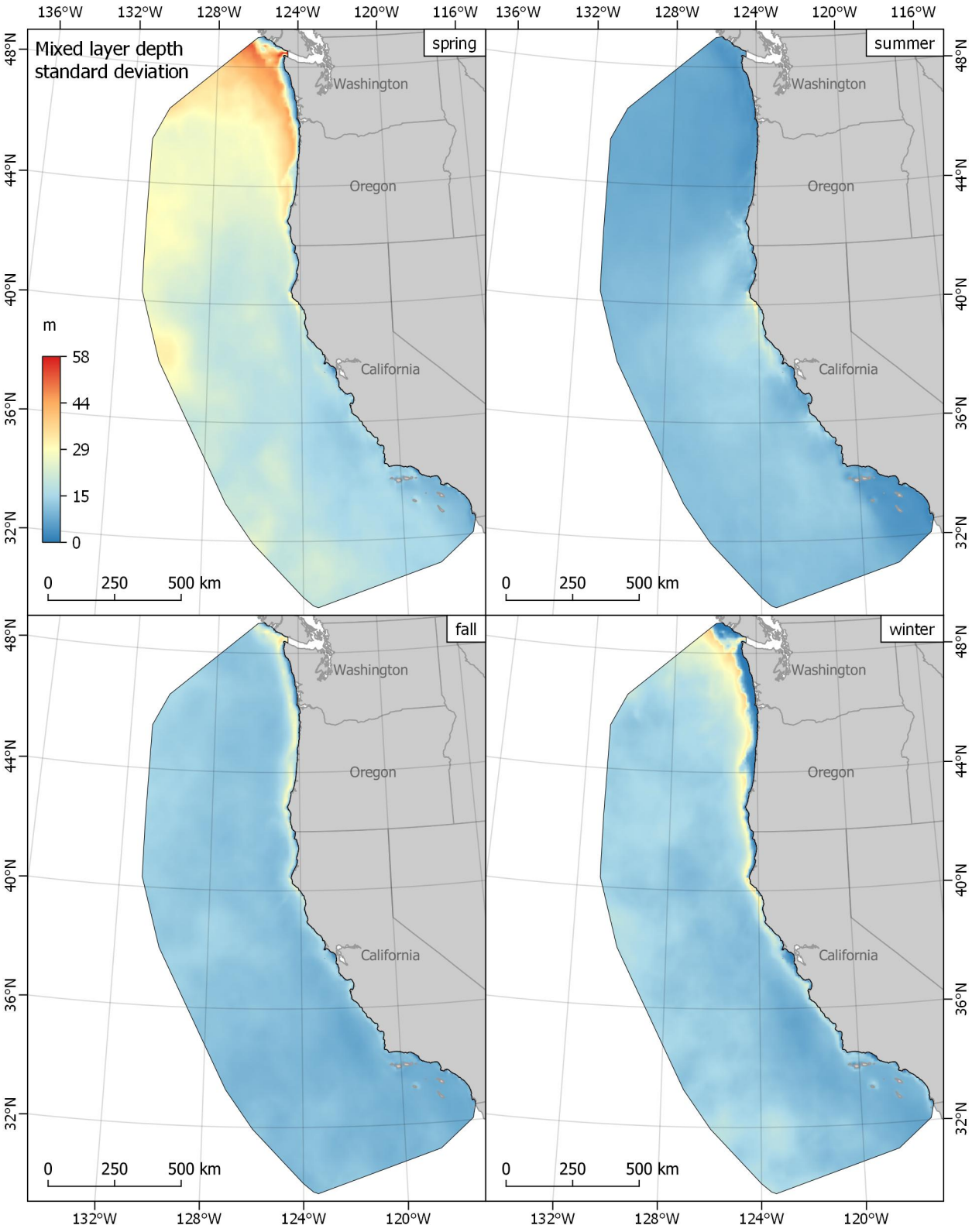

Figure B-27. Seasonal mixed layer depth standard deviation

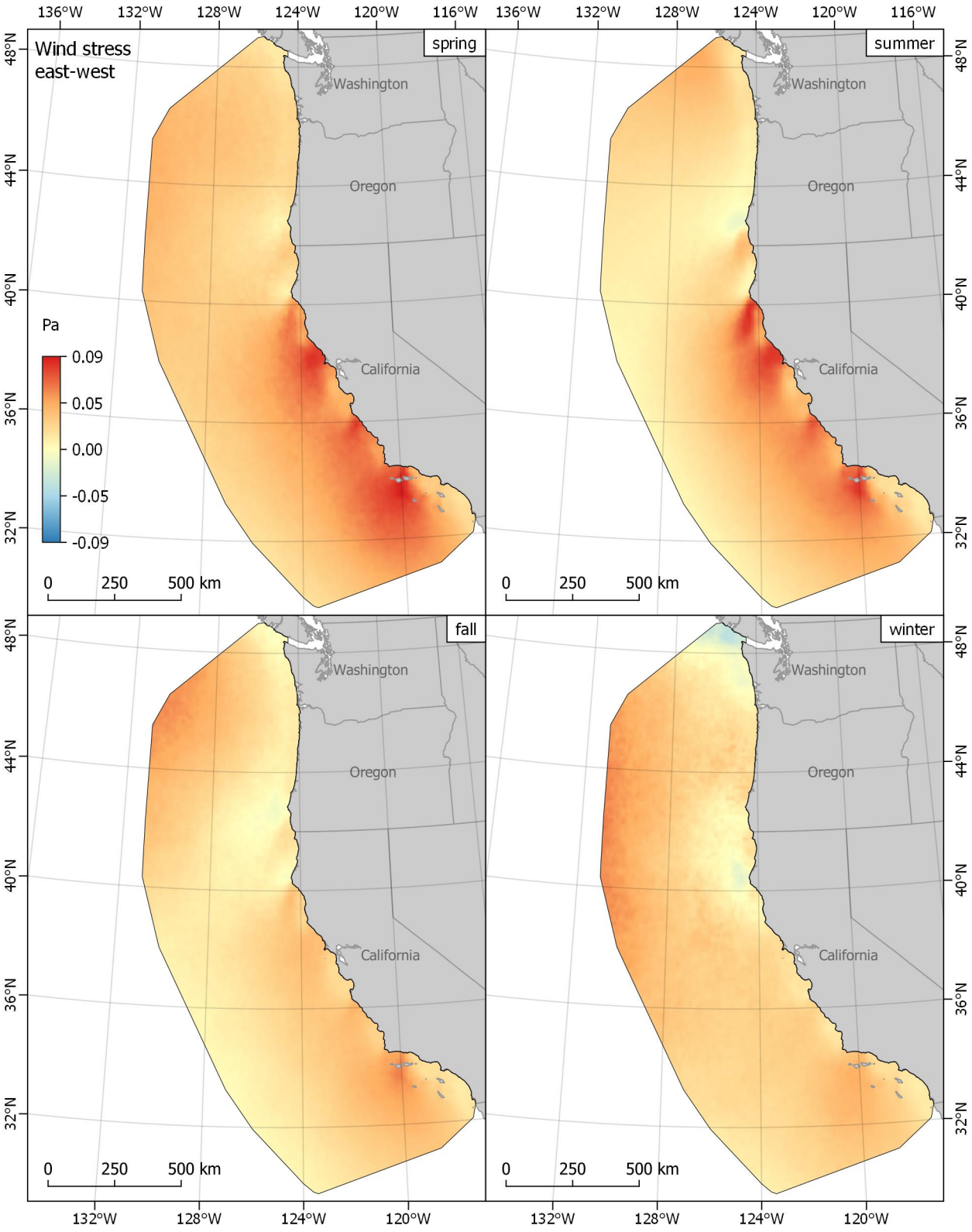

Figure B-28. Seasonal wind stress east-west

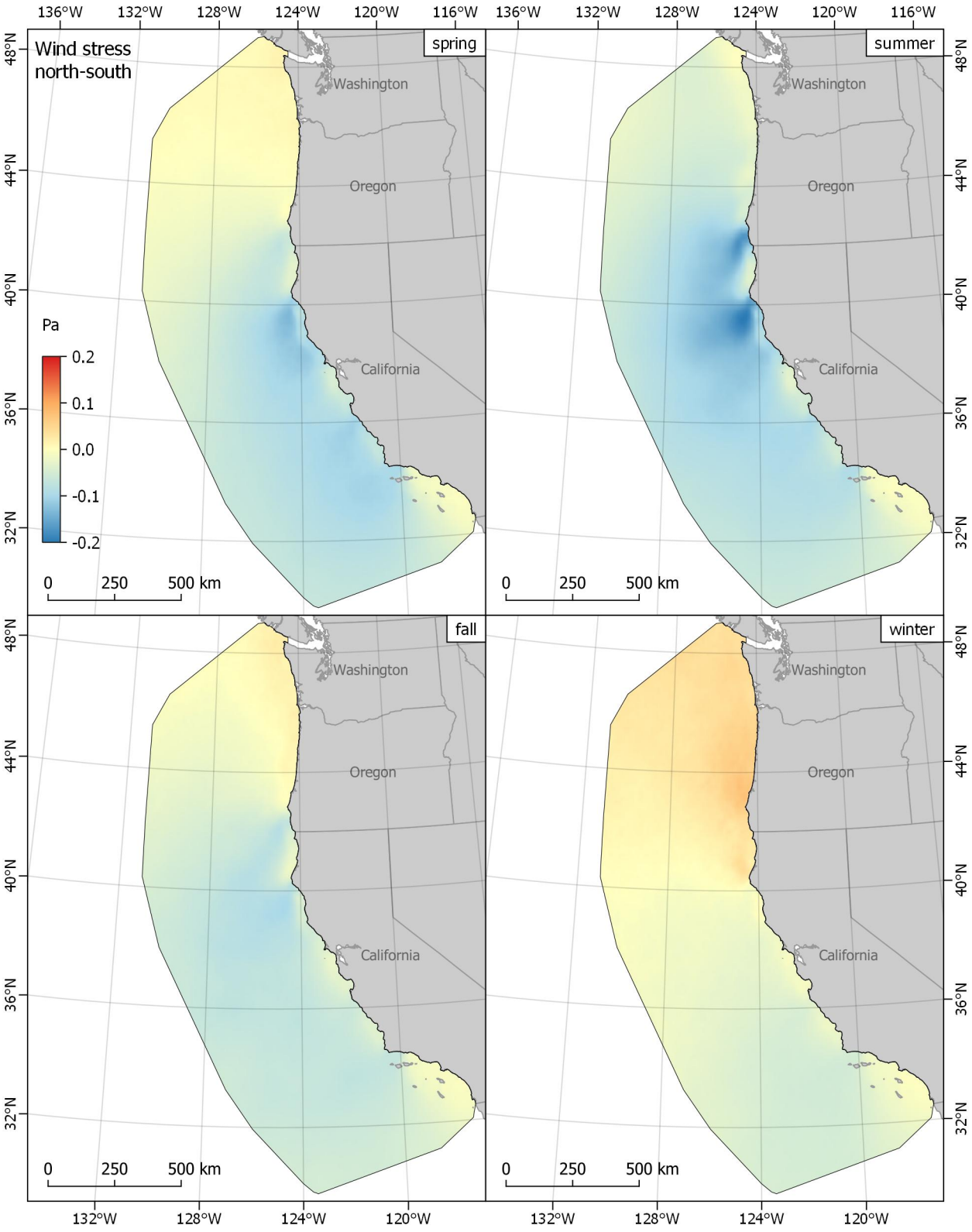

Figure B-29. Seasonal wind stress north-south

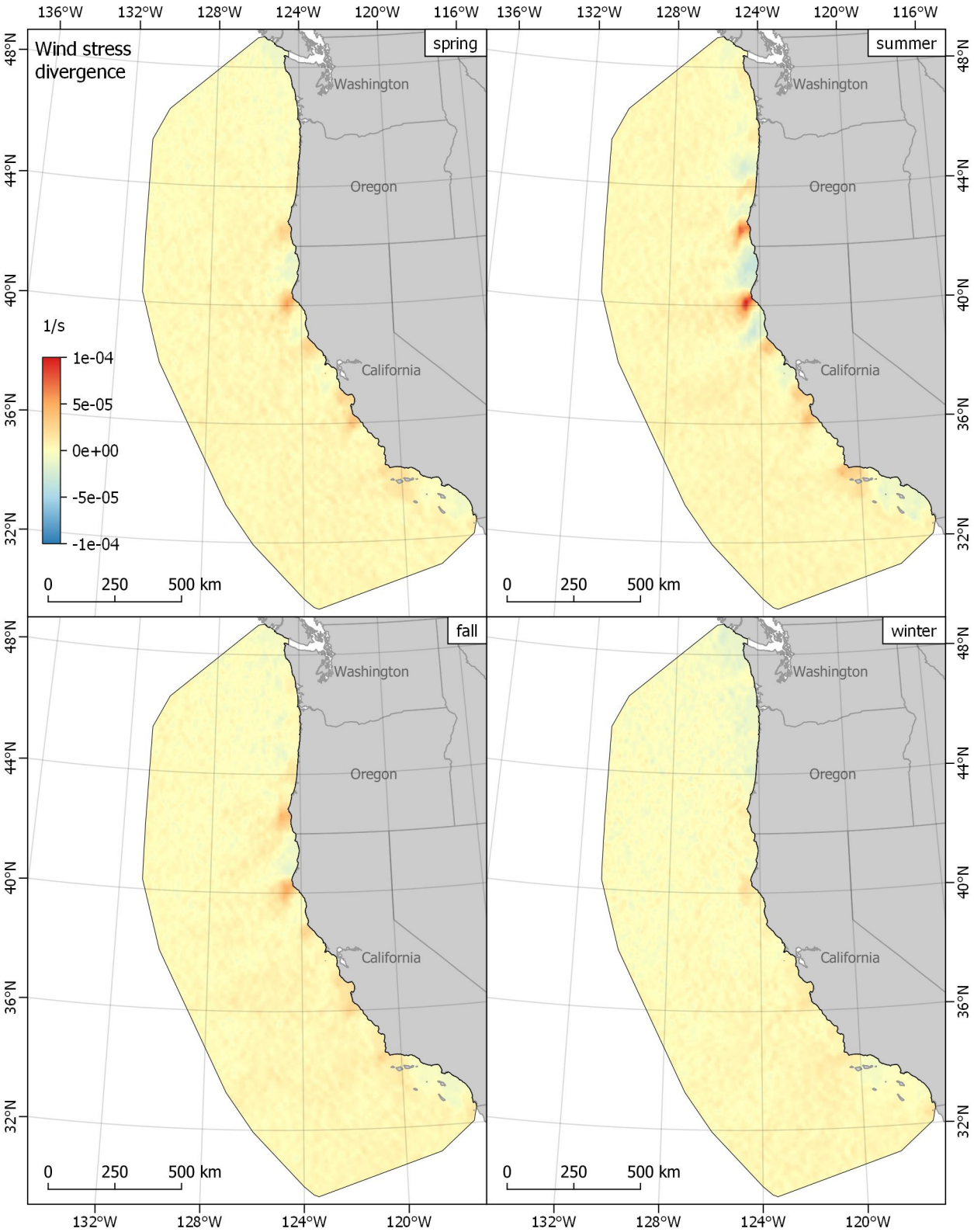

Figure B-30. Seasonal wind stress divergence
Positive values = divergence, negative values = convergence

Appendix C: Multibeam Bathymetry Dataset Information

Table C-1. Multibeam bathymetry datasets included in bathymetry synthesis

Dataset	Data Source	Grid Resolution	Coordinate System
MBARI_Axial_Volcano_40m	Monterey Bay Aquarium Research Institute	40 x 40 m	WGS84
MBARI_Central_Gorda_Ridge_40m	Monterey Bay Aquarium Research Institute	40 x 40 m	WGS84
MBARI_Cleft_Segment_A_30m	Monterey Bay Aquarium Research Institute	30 x 30 m	WGS84
MBARI_Eel_River_Basin_10m	Monterey Bay Aquarium Research Institute	10 x 10 m	WGS84
MBARI_Escanaba_Trough_40m	Monterey Bay Aquarium Research Institute	40 x 40 m	WGS84
MBARI_Guide_to_Gumdrop_Seamounts_30m	Monterey Bay Aquarium Research Institute	30 x 30 m	WGS84
MBARI_Mendocino_Fracture_Zone_20m	Monterey Bay Aquarium Research Institute	20 x 20 m	WGS84
MBARI_Monterey_Bay_40m	Monterey Bay Aquarium Research Institute	40 x 40 m	WGS84
MBARI_North_Gorda_Ridge_40m	Monterey Bay Aquarium Research Institute	40 x 40 m	WGS84
MBARI_Northern_California_Transit_1A_40m	Monterey Bay Aquarium Research Institute	40 x 40 m	WGS84
MBARI_Northern_California_Transit_1B_40m	Monterey Bay Aquarium Research Institute	40 x 40 m	WGS84
MBARI_Northern_California_Transit_1C_40m	Monterey Bay Aquarium Research Institute	40 x 40 m	WGS84
MBARI_Northern_California_Transit_1D_40m	Monterey Bay Aquarium Research Institute	40 x 40 m	WGS84
MBARI_Northern_California_Transit_1E_10m	Monterey Bay Aquarium Research Institute	10 x 10 m	WGS84
MBARI_Northern_California_Transit_1F_20m	Monterey Bay Aquarium Research Institute	20 x 20 m	WGS84
MBARI_Northern_California_Transit_1G_10m	Monterey Bay Aquarium Research Institute	10 x 10 m	WGS84
MBARI_Northern_California_Transit_1H_10m	Monterey Bay Aquarium Research Institute	10 x 10 m	WGS84
MBARI_Oregon_Margin_40m	Monterey Bay Aquarium Research Institute	40 x 40 m	WGS84
MBARI_President_Jackson_Seamounts_30m	Monterey Bay Aquarium Research Institute	30 x 30 m	WGS84
MBARI_Santa_Barbara_Basin_40m	Monterey Bay Aquarium Research Institute	40 x 40 m	WGS84
MBARI_Santa_Barbara_Basin_Rodriguez_Seamount_40m	Monterey Bay Aquarium Research Institute	40 x 40 m	WGS84
MBARI_Taney_Seamounts_40m	Monterey Bay Aquarium Research Institute	40 x 40 m	WGS84
MBARI_Transit_2A_40m	Monterey Bay Aquarium Research Institute	40 x 40 m	WGS84
MBARI_Transit_2B_40m	Monterey Bay Aquarium Research Institute	40 x 40 m	WGS84
MBARI_Transit_3A_40m	Monterey Bay Aquarium Research Institute	40 x 40 m	WGS84
MBARI_Transit_3B_40m	Monterey Bay Aquarium Research Institute	40 x 40 m	WGS84

Dataset	Data Source	Grid Resolution	Coordinate System
MBARI_Transit_3C_40m	Monterey Bay Aquarium Research Institute	40 x 40 m	WGS84
MBARI_Vance_Seamounts_40m	Monterey Bay Aquarium Research Institute	40 x 40 m	WGS84
EX0801_MB_10m_UTM_Zone10N	NOAA Office of Exploration and Research	10 x 10 m	WGS84, UTM Zone 10N
EX0903_Mendocino_Central_bathy	NOAA Office of Exploration and Research	50 x 50 m	WGS84
EX0903_Mendocino_East_bathy	NOAA Office of Exploration and Research	50 x 50 m	WGS84
EX0903_Mendocino_West_bathy	NOAA Office of Exploration and Research	50 x 50 m	WGS84
EX0904_Geog_LatLong_50m_All	NOAA Office of Exploration and Research	50 x 50 m	WGS84
EX0905_Geog_LatLong_100m_All	NOAA Office of Exploration and Research	100 x 100 m	WGS84
EX0907_Geog_LatLong_100m_Transit	NOAA Office of Exploration and Research	100 x 100 m	WGS84
EX0907_Geog_LatLong_50m_Sanctuary	NOAA Office of Exploration and Research	50 x 50 m	WGS84
EX1101_MB_FNL_CINMS_30m_WGS84	NOAA Office of Exploration and Research	30 x 30 m	WGS84
EX1101_MB_FNL_Hancock_109_Seamnts_25m_WGS84	NOAA Office of Exploration and Research	25 x 25 m	WGS84
EX1101_MB_FNL_PatchTest_50m_WGS84	NOAA Office of Exploration and Research	50 x 50 m	WGS84
EX1101_MB_FNL_SanJuanSeamnt_75m_WGS84	NOAA Office of Exploration and Research	75 x 75 m	WGS84
EX1101_MB_FNL_SouthMBNMS_25m_WGS84	NOAA Office of Exploration and Research	25 x 25 m	WGS84
EX1101_MB_FNL_SurRidge_30m_WGS84	NOAA Office of Exploration and Research	30 x 30 m	WGS84
EX1101_MB_FNL_Transit_North_50m_WGS84	NOAA Office of Exploration and Research	50 x 50 m	WGS84
EX1101_MB_FNL_Transit_South_50m_WGS84	NOAA Office of Exploration and Research	50 x 50 m	WGS84
EX1102_MB_FNL_50m_WGS84	NOAA Office of Exploration and Research	50 x 50 m	WGS84
ocnms_multibeam_2011	Olympic Coast NMS	8 x 8 m	NAD83, UTM Zone 10N
wa_offshr_25m	OSU Active Tectonics and Seafloor Mapping Lab	25 x 25 m	WGS84, UTM Zone 10N
tn174_50m	University of Washington	50 x 50 m	WGS84, UTM Zone 10N
tn177_35m	University of Washington	35 x 35 m	WGS84, UTM Zone 10N
tn207_35m	University of Washington	35 x 35 m	WGS84, UTM Zone 10N
tn252_n_50m	University of Washington	50 x 50 m	WGS84, UTM Zone 10N
Farallon_Escarpment_10m	USGS	10 x 10 m	NAD83, UTM Zone 10N
s_ca_merged_intercontinental_25mbathy	USGS	25 x 25 m	NAD83, UTM Zone 11N

Appendix D: Model Performance Metrics

Table D-1. Model performance metrics of the final selected model for each species/group-season combination
Model performance metrics were calculated using the full (i.e., non-bootstrapped) dataset.

Species	Season	Distribution	*M*	PDE	AUC	r_G	Median AE	Mean AE	RMSE
Scoter spp.	spring	ZINB	18,063	66.6%	0.98	0.30	0.00	1.25	11.89
Scoter spp.	summer	ZINB	17,724	77.0%	0.99	0.37	0.00	1.18	14.79
Scoter spp.	fall	ZINB	20,000	41.1%	0.95	0.14	0.83	1.95	5.68
Scoter spp.	winter	ZINB	14,207	68.7%	0.99	0.29	0.02	1.11	6.46
Western/Clark's Grebe	spring	ZINB	20,000	61.2%	0.98	0.16	0.10	1.78	1.58
Western/Clark's Grebe	fall	ZINB	19,181	69.6%	0.99	0.17	0.23	1.70	1.47
Western/Clark's Grebe	winter	ZINB	19,667	69.2%	0.99	0.26	0.01	1.17	9.00
Phalarope spp.	spring	ZIP	6,463	53.8%	0.79	0.32	0.20	1.44	95.77
Phalarope spp.	summer	ZINB	19,999	38.0%	0.87	0.31	0.11	1.46	16.02
Phalarope spp.	fall	ZINB	19,999	30.1%	0.78	0.25	0.27	1.58	24.98
Phalarope spp.	winter	ZIP	11,607	37.2%	0.85	0.29	0.38	1.58	2.88
South Polar Skua	fall	ZINB	19,220	36.0%	0.88	0.10	0.43	1.85	0.07
Pomarine Jaeger	spring	ZIP	19,997	28.7%	0.87	0.17	0.37	1.71	0.18
Pomarine Jaeger	summer	ZIP	16,063	18.4%	0.86	0.09	0.55	1.98	0.08
Pomarine Jaeger	fall	ZIP	19,007	18.8%	0.82	0.19	0.54	1.82	0.24
Pomarine Jaeger	winter	ZIP	19,986	30.0%	0.87	0.18	0.34	1.74	0.18
Parasitic/Long-tailed Jaeger	spring	ZIP	18,158	19.9%	0.87	0.09	0.60	1.92	0.07
Parasitic/Long-tailed Jaeger	summer	ZIP	19,989	31.5%	0.91	0.16	0.26	1.77	0.17
Parasitic/Long-tailed Jaeger	fall	ZINB	19,237	32.0%	0.84	0.19	0.34	1.64	0.38
Jaeger spp.	spring	ZIP	19,997	25.6%	0.86	0.19	0.47	1.73	0.20
Jaeger spp.	summer	ZINB	19,634	30.1%	0.84	0.15	0.40	1.80	0.20
Jaeger spp.	fall	ZIP	19,979	21.8%	0.79	0.23	0.56	1.69	0.45
Jaeger spp.	winter	ZIP	19,971	27.5%	0.86	0.19	0.41	1.74	0.19
Common Murre	spring	ZINB	19,983	66.9%	0.96	0.57	0.00	1.07	26.31
Common Murre	summer	ZINB	18,732	74.8%	0.98	0.68	0.00	0.81	47.57

Species	Season	Distribution	*M*	PDE	AUC	r_G	Median AE	Mean AE	RMSE
Common Murre	fall	ZINB	17,356	72.1%	0.98	0.50	0.00	1.05	9.76
Common Murre	winter	ZINB	18,013	58.3%	0.96	0.48	0.01	1.11	12.41
Pigeon Guillemot	spring	ZINB	18,130	65.6%	0.98	0.25	0.04	1.16	0.69
Pigeon Guillemot	summer	ZINB	19,156	74.2%	0.99	0.37	0.01	0.93	1.16
Marbled Murrelet	spring	ZINB	15,046	75.5%	1.00	0.27	0.02	0.90	0.72
Marbled Murrelet	summer	ZINB	18,518	70.7%	0.99	0.47	0.01	0.92	2.45
Scripps's/Guadalupe/Craveri's Murrelet	spring	ZINB	20,000	45.7%	0.95	0.12	0.32	1.85	0.21
Ancient Murrelet	spring	ZINB	18,573	65.4%	0.98	0.17	0.04	1.70	0.91
Cassin's Auklet	spring	ZIP	17,444	40.8%	0.88	0.36	0.26	1.43	5.15
Cassin's Auklet	summer	ZIP	18,256	47.5%	0.91	0.37	0.10	1.29	5.02
Cassin's Auklet	fall	ZINB	19,997	49.8%	0.91	0.35	0.05	1.49	5.41
Cassin's Auklet	winter	ZINB	19,988	37.5%	0.85	0.41	0.23	1.31	5.10
Rhinoceros Auklet	spring	ZINB	19,988	55.7%	0.92	0.41	0.08	1.19	4.68
Rhinoceros Auklet	summer	ZINB	19,953	70.7%	0.97	0.50	0.00	1.05	20.96
Rhinoceros Auklet	fall	ZINB	19,998	57.7%	0.93	0.31	0.05	1.43	1.08
Rhinoceros Auklet	winter	ZINB	19,966	44.2%	0.85	0.33	0.18	1.35	10.84
Tufted Puffin	spring	ZINB	19,978	65.1%	0.98	0.20	0.03	1.25	0.86
Tufted Puffin	summer	ZINB	19,789	75.2%	0.99	0.36	0.01	1.03	2.68
Black-legged Kittiwake	spring	ZINB	19,632	58.8%	0.96	0.32	0.03	1.27	2.32
Black-legged Kittiwake	fall	ZIP	19,650	41.2%	0.94	0.15	0.31	1.95	0.23
Black-legged Kittiwake	winter	ZINB	19,954	42.5%	0.88	0.37	0.23	1.41	1.78
Sabine's Gull	spring	ZINB	18,330	38.5%	0.86	0.17	0.22	1.65	1.31
Sabine's Gull	summer	ZINB	19,090	41.0%	0.90	0.11	0.25	1.61	0.28
Sabine's Gull	fall	ZIP	12,204	53.3%	0.94	0.18	0.20	1.54	1.27
Bonaparte's Gull	spring	ZINB	19,678	45.0%	0.91	0.19	0.10	1.49	2.47
Bonaparte's Gull	fall	ZINB	18,125	45.4%	0.94	0.19	0.11	1.49	3.79
Bonaparte's Gull	winter	ZINB	19,996	57.7%	0.92	0.17	0.03	1.10	5.89
Heermann's Gull	summer	ZINB	19,999	52.8%	0.95	0.24	0.08	1.56	0.52
Heermann's Gull	fall	ZINB	19,997	61.0%	0.97	0.27	0.03	1.38	1.30

Species	Season	Distribution	*M*	PDE	AUC	r_G	Median AE	Mean AE	RMSE
Heermann's Gull	winter	ZINB	19,973	71.9%	0.97	0.26	0.04	1.29	1.27
California Gull	spring	ZINB	20,000	42.6%	0.89	0.33	0.18	1.45	3.70
California Gull	summer	ZINB	19,998	55.8%	0.93	0.26	0.09	1.26	0.71
California Gull	fall	ZINB	19,832	63.8%	0.93	0.44	0.03	1.03	5.80
California Gull	winter	ZIP	9,449	57.1%	0.91	0.44	0.10	1.20	10.84
Herring/Iceland Gull	spring	ZINB	19,945	46.0%	0.92	0.21	0.16	1.67	0.45
Herring/Iceland Gull	summer	ZINB	19,560	55.3%	0.94	0.14	0.18	1.64	0.23
Herring/Iceland Gull	fall	ZINB	18,162	54.4%	0.91	0.27	0.07	1.39	1.95
Herring/Iceland Gull	winter	ZINB	19,064	42.1%	0.87	0.32	0.13	1.43	3.34
Western/Glaucous-winged Gull	spring	ZINB	19,991	47.1%	0.89	0.56	0.29	1.07	6.36
Western/Glaucous-winged Gull	summer	ZINB	19,990	59.0%	0.94	0.55	0.07	1.04	4.74
Western/Glaucous-winged Gull	fall	ZINB	16,533	58.1%	0.91	0.53	0.05	1.08	9.08
Western/Glaucous-winged Gull	winter	ZINB	19,998	57.2%	0.88	0.49	0.11	1.25	20.04
Caspian Tern	spring	ZINB	19,996	66.1%	0.97	0.13	0.10	1.15	0.46
Caspian Tern	summer	ZINB	17,692	68.1%	0.98	0.29	0.01	0.90	1.56
Common/Arctic Tern	spring	ZINB	20,000	22.4%	0.83	0.06	0.64	1.95	0.19
Common/Arctic Tern	summer	ZINB	16,672	48.4%	0.94	0.18	0.12	1.45	0.78
Common/Arctic Tern	fall	ZINB	17,147	49.6%	0.92	0.20	0.10	1.38	1.15
Royal/Elegant Tern	spring	ZINB	18,620	75.2%	0.98	0.15	0.10	1.49	0.86
Royal/Elegant Tern	summer	ZINB	19,186	59.4%	0.97	0.19	0.05	1.58	0.58
Royal/Elegant Tern	fall	ZINB	18,490	65.5%	0.95	0.12	0.14	1.74	0.54
Red-throated Loon	spring	ZINB	19,996	62.7%	0.96	0.15	0.08	1.65	0.29
Red-throated Loon	summer	ZIP	19,961	60.2%	0.99	0.17	0.04	1.44	0.25
Common Loon	spring	ZIP	17,686	47.1%	0.94	0.20	0.11	1.47	0.42
Common Loon	summer	ZIP	19,081	55.9%	0.98	0.19	0.03	1.47	0.19
Loon spp.	spring	ZINB	19,995	55.6%	0.93	0.37	0.05	1.26	3.23
Loon spp.	summer	ZIP	17,590	65.2%	0.98	0.36	0.01	0.94	0.91
Loon spp.	fall	ZIP	12,525	63.1%	0.97	0.25	0.04	1.26	2.15
Loon spp.	winter	ZINB	18,609	58.1%	0.94	0.29	0.05	1.45	1.79

Species	Season	Distribution	*M*	PDE	AUC	r_G	Median AE	Mean AE	RMSE
Laysan Albatross	spring	ZINB	19,874	21.9%	0.86	0.09	0.57	1.97	0.07
Laysan Albatross	winter	ZIP	19,994	46.9%	0.95	0.20	0.21	1.45	0.12
Black-footed Albatross	spring	ZINB	19,998	45.1%	0.89	0.41	0.24	1.28	0.88
Black-footed Albatross	summer	ZINB	19,992	44.8%	0.89	0.35	0.23	1.36	0.75
Black-footed Albatross	fall	ZINB	19,985	38.2%	0.86	0.25	0.33	1.46	0.40
Black-footed Albatross	winter	ZIP	19,999	35.7%	0.92	0.21	0.21	1.70	0.17
Fork-tailed Storm-Petrel	spring	ZIP	17,213	39.4%	0.96	0.23	0.17	1.59	0.53
Fork-tailed Storm-Petrel	summer	ZINB	18,581	71.9%	0.96	0.28	0.01	1.20	3.68
Fork-tailed Storm-Petrel	fall	ZINB	14,405	49.7%	0.95	0.19	0.07	1.56	3.39
Fork-tailed Storm-Petrel	winter	ZIP	19,334	48.6%	0.97	0.18	0.22	1.49	0.17
Leach's Storm-Petrel	spring	ZINB	19,998	50.0%	0.92	0.32	0.08	1.37	0.78
Leach's Storm-Petrel	summer	ZINB	19,995	52.3%	0.92	0.50	0.17	1.07	1.13
Leach's Storm-Petrel	fall	ZIP	19,538	39.6%	0.89	0.41	0.15	1.32	1.41
Leach's Storm-Petrel	winter	ZIP	19,989	44.5%	0.93	0.36	0.09	1.35	0.55
Ashy Storm-Petrel	spring	ZINB	18,534	33.0%	0.86	0.10	0.36	1.67	1.06
Ashy Storm-Petrel	summer	ZIP	1,326	2.5%	0.94	0.12	0.85	2.07	5.50
Ashy Storm-Petrel	fall	ZINB	18,835	61.6%	0.90	0.14	0.08	1.27	3.22
Black Storm-Petrel	spring	ZINB	17,472	59.3%	0.96	0.16	0.14	1.37	0.43
Black Storm-Petrel	summer	ZINB	18,770	60.4%	0.95	0.21	0.06	1.45	1.48
Black Storm-Petrel	fall	ZINB	18,155	46.4%	0.90	0.10	0.25	1.61	0.36
Northern Fulmar	spring	ZIP	19,968	40.6%	0.89	0.32	0.27	1.46	0.97
Northern Fulmar	summer	ZINB	19,994	59.1%	0.95	0.31	0.04	1.17	5.79
Northern Fulmar	fall	ZIP	19,530	60.6%	0.91	0.38	0.12	1.04	1.73
Northern Fulmar	winter	ZINB	19,997	44.4%	0.85	0.36	0.28	1.36	1.45
Murphy's Petrel	spring	ZINB	18,700	40.0%	0.93	0.12	0.34	1.73	0.09
Cook's Petrel	spring	ZINB	17,258	50.1%	0.95	0.21	0.10	1.59	0.59
Cook's Petrel	summer	ZINB	19,999	52.4%	0.95	0.24	0.05	1.52	0.57
Cook's Petrel	fall	ZIP	19,718	26.7%	0.90	0.11	0.30	1.85	0.12
Buller's Shearwater	summer	ZINB	19,994	54.7%	0.96	0.21	0.05	1.43	0.86

Species	Season	Distribution	*M*	PDE	AUC	r_G	Median AE	Mean AE	RMSE
Buller's Shearwater	fall	ZINB	17,447	37.5%	0.86	0.17	0.22	1.71	0.79
Pink-footed Shearwater	spring	ZINB	19,999	44.4%	0.89	0.35	0.16	1.37	1.85
Pink-footed Shearwater	summer	ZINB	16,899	50.1%	0.91	0.37	0.09	1.30	10.21
Pink-footed Shearwater	fall	ZINB	19,526	51.9%	0.90	0.32	0.07	1.34	4.40
Short-tailed/Sooty/Flesh-footed Shearwater	spring	ZINB	19,997	47.3%	0.87	0.52	0.11	1.29	67.56
Short-tailed/Sooty/Flesh-footed Shearwater	summer	ZINB	16,790	51.5%	0.90	0.50	0.07	1.42	169.38
Short-tailed/Sooty/Flesh-footed Shearwater	fall	ZIP	8,431	49.0%	0.84	0.36	0.11	1.41	24.20
Short-tailed/Sooty/Flesh-footed Shearwater	winter	ZIP	19,964	29.5%	0.87	0.18	0.32	1.62	0.23
Black-vented Shearwater	spring	ZINB	19,408	64.6%	0.98	0.15	0.05	1.27	2.04
Black-vented Shearwater	fall	ZINB	17,418	67.0%	0.98	0.26	0.01	1.41	7.36
Black-vented Shearwater	winter	ZINB	16,040	71.7%	0.97	0.23	0.02	1.14	6.40
Brandt's Cormorant	spring	ZINB	17,753	62.7%	0.95	0.30	0.03	1.19	2.43
Brandt's Cormorant	summer	ZINB	17,266	61.0%	0.96	0.30	0.02	1.25	5.99
Pelagic Cormorant	spring	ZINB	12,857	73.2%	0.99	0.29	0.02	0.77	2.01
Pelagic Cormorant	summer	ZINB	13,039	76.6%	0.99	0.43	0.00	0.71	2.67
Double-crested Cormorant	spring	ZINB	19,994	60.5%	0.96	0.18	0.06	1.34	1.05
Double-crested Cormorant	summer	ZINB	16,098	71.2%	0.98	0.29	0.00	1.30	13.12
Cormorant spp.	fall	ZINB	19,530	67.6%	0.96	0.31	0.02	1.31	2.57
Cormorant spp.	winter	ZINB	16,545	67.0%	0.96	0.35	0.02	1.23	2.86
Brown Pelican	spring	ZINB	18,787	63.2%	0.95	0.26	0.02	1.39	1.12
Brown Pelican	summer	ZINB	19,749	59.0%	0.95	0.33	0.01	1.34	4.36
Brown Pelican	fall	ZINB	18,706	56.8%	0.94	0.30	0.02	1.42	4.32
Brown Pelican	winter	ZINB	19,983	57.3%	0.96	0.29	0.04	1.40	0.79

Appendix E: Maps of Predicted Density and Coefficient of Variation

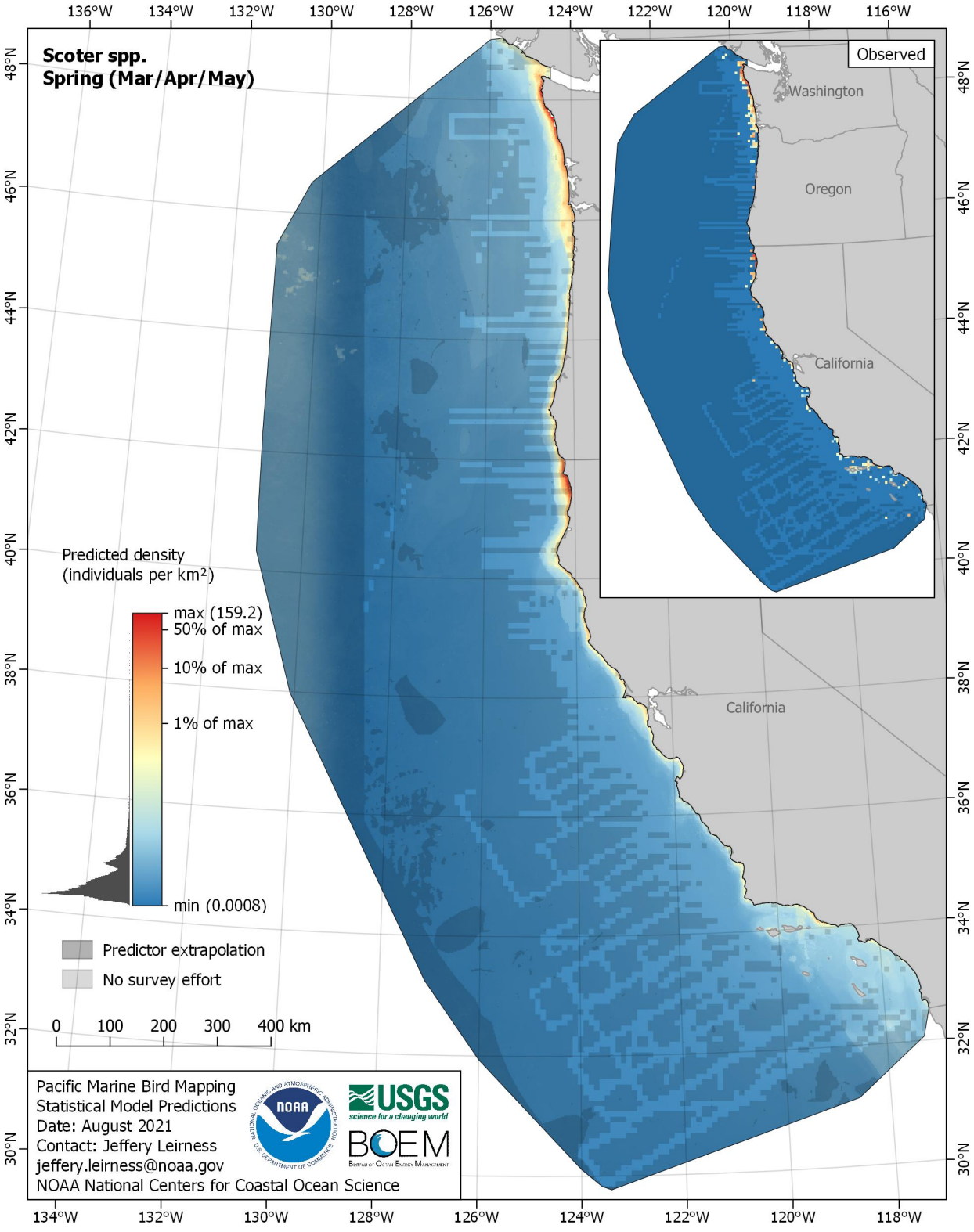

Figure E-1. Predicted density for Scoter spp. (*Melanitta spp.*) in the spring season

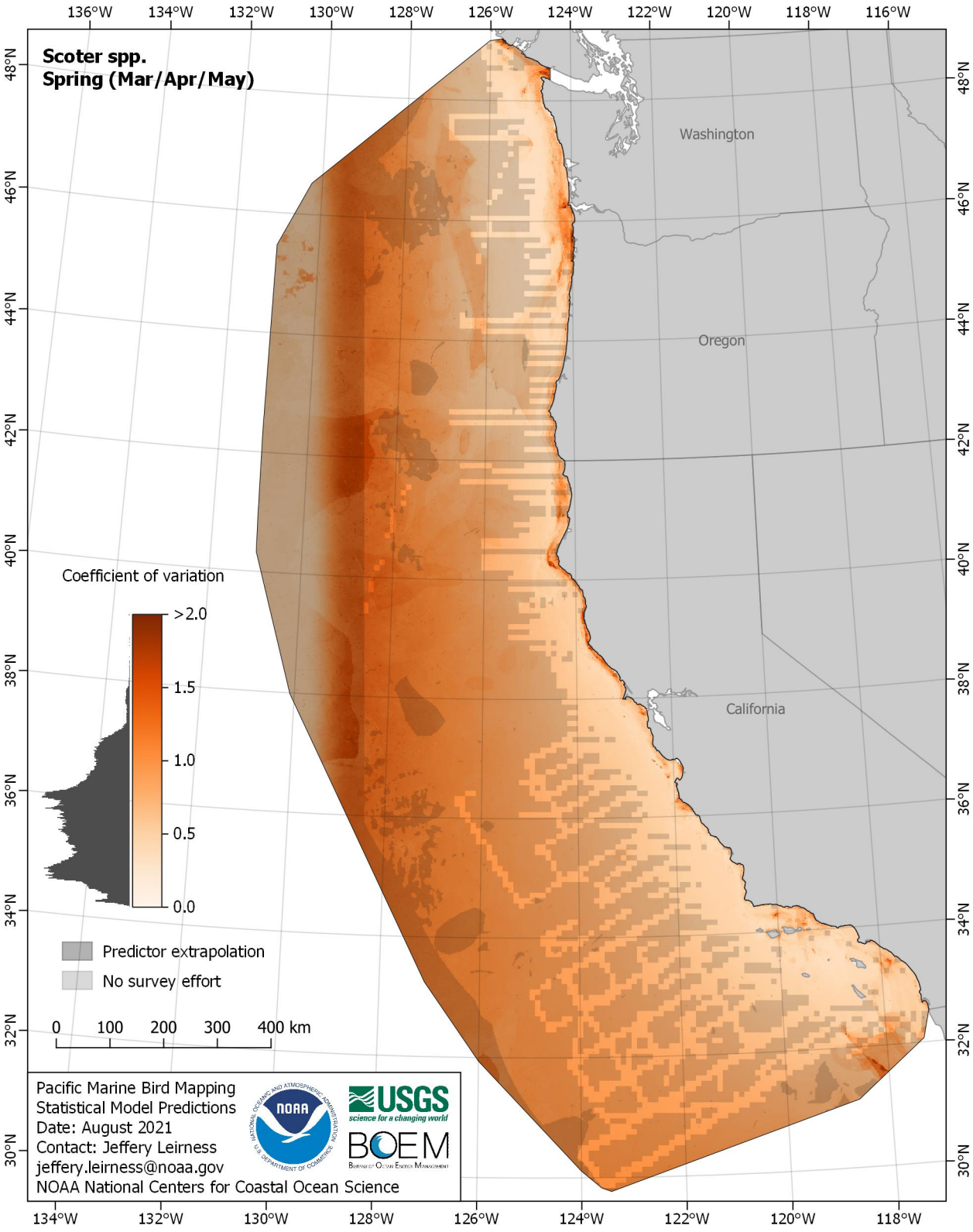

Figure E-2. Coefficient of variation for Scoter spp. (*Melanitta spp.*) in the spring season

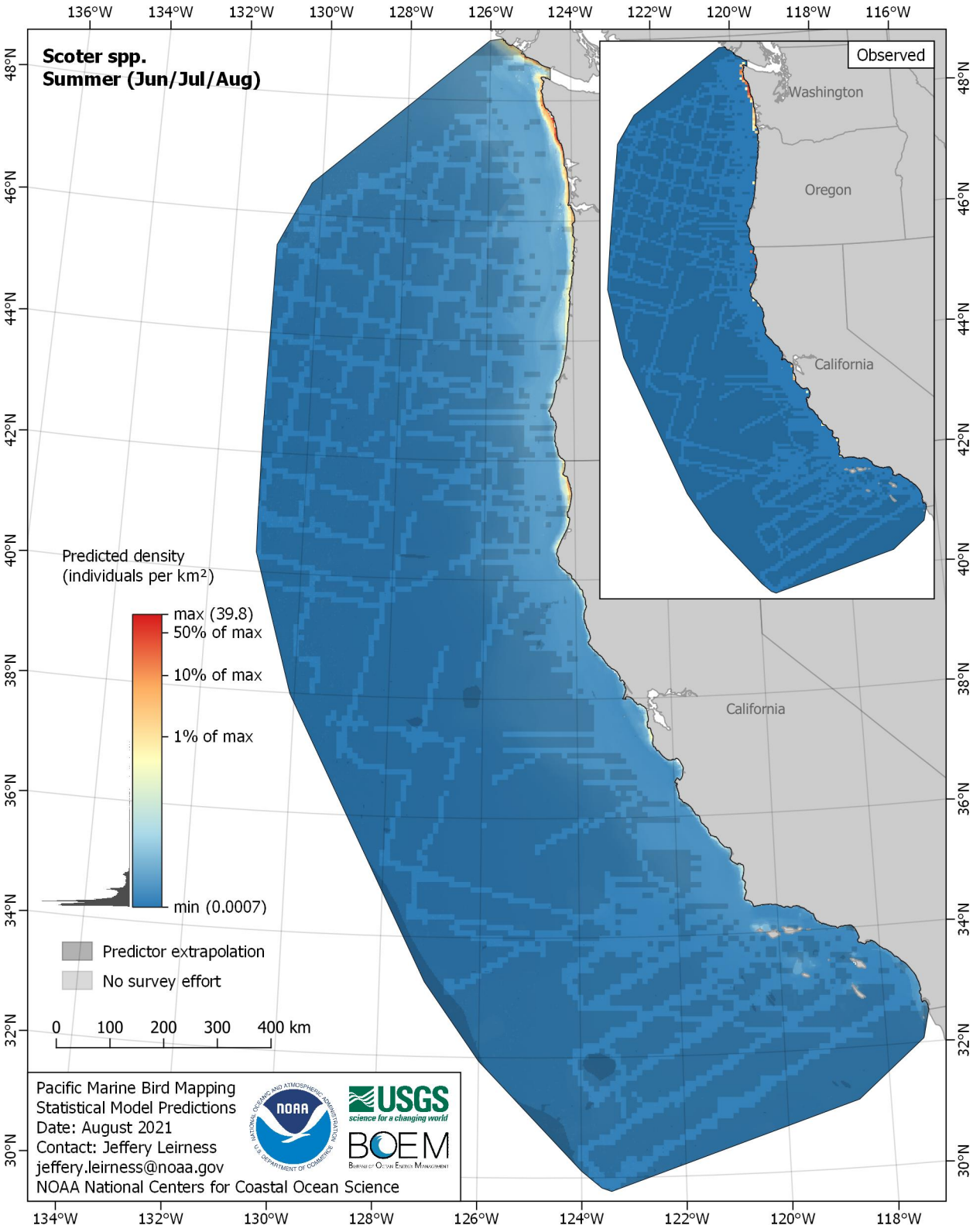

Figure E-3. Predicted density for Scoter spp. (*Melanitta spp.*) in the summer season

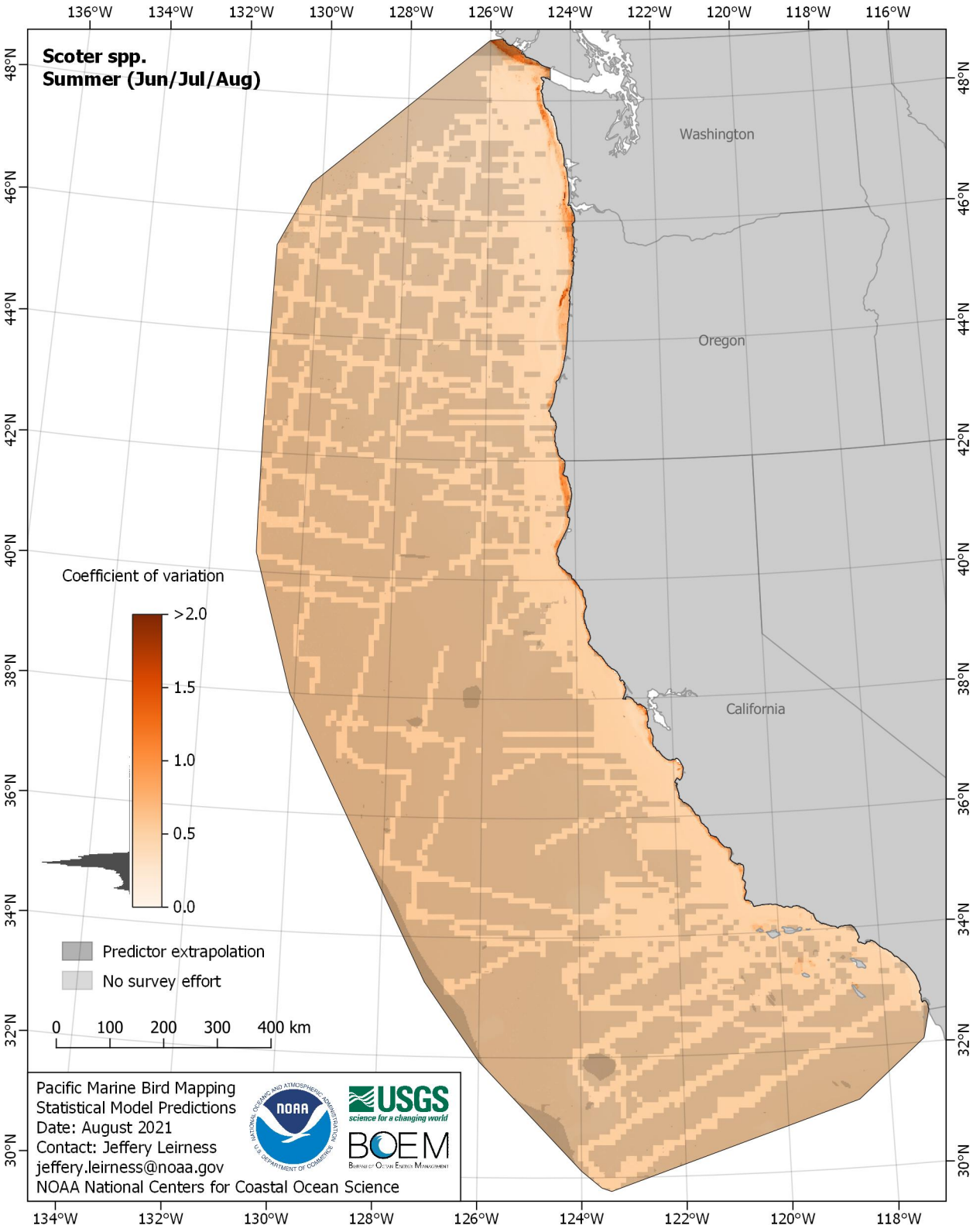

Figure E-4. Coefficient of variation for Scoter spp. (*Melanitta spp.*) in the summer season

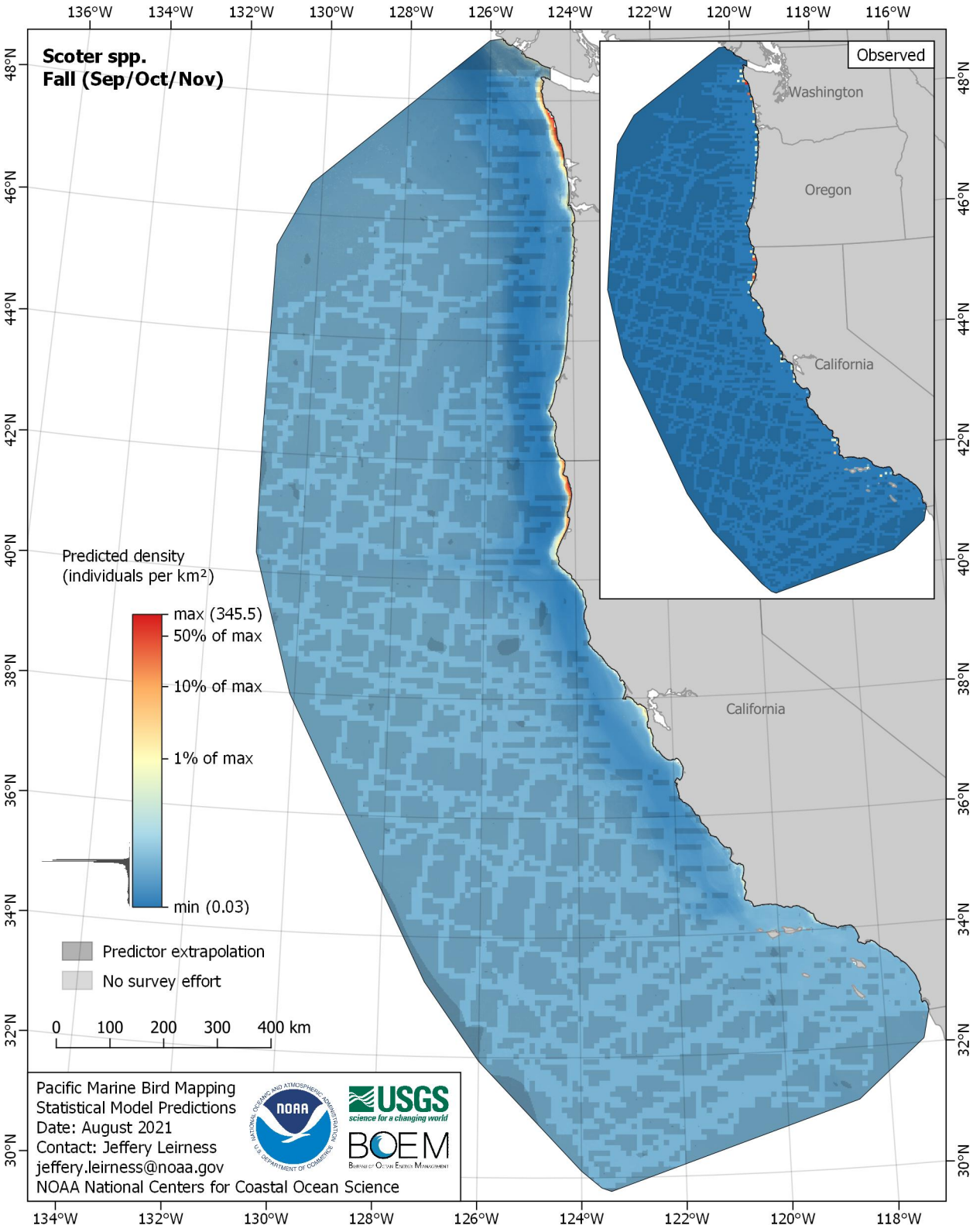

Figure E-5. Predicted density for Scoter spp. (*Melanitta spp.*) in the fall season

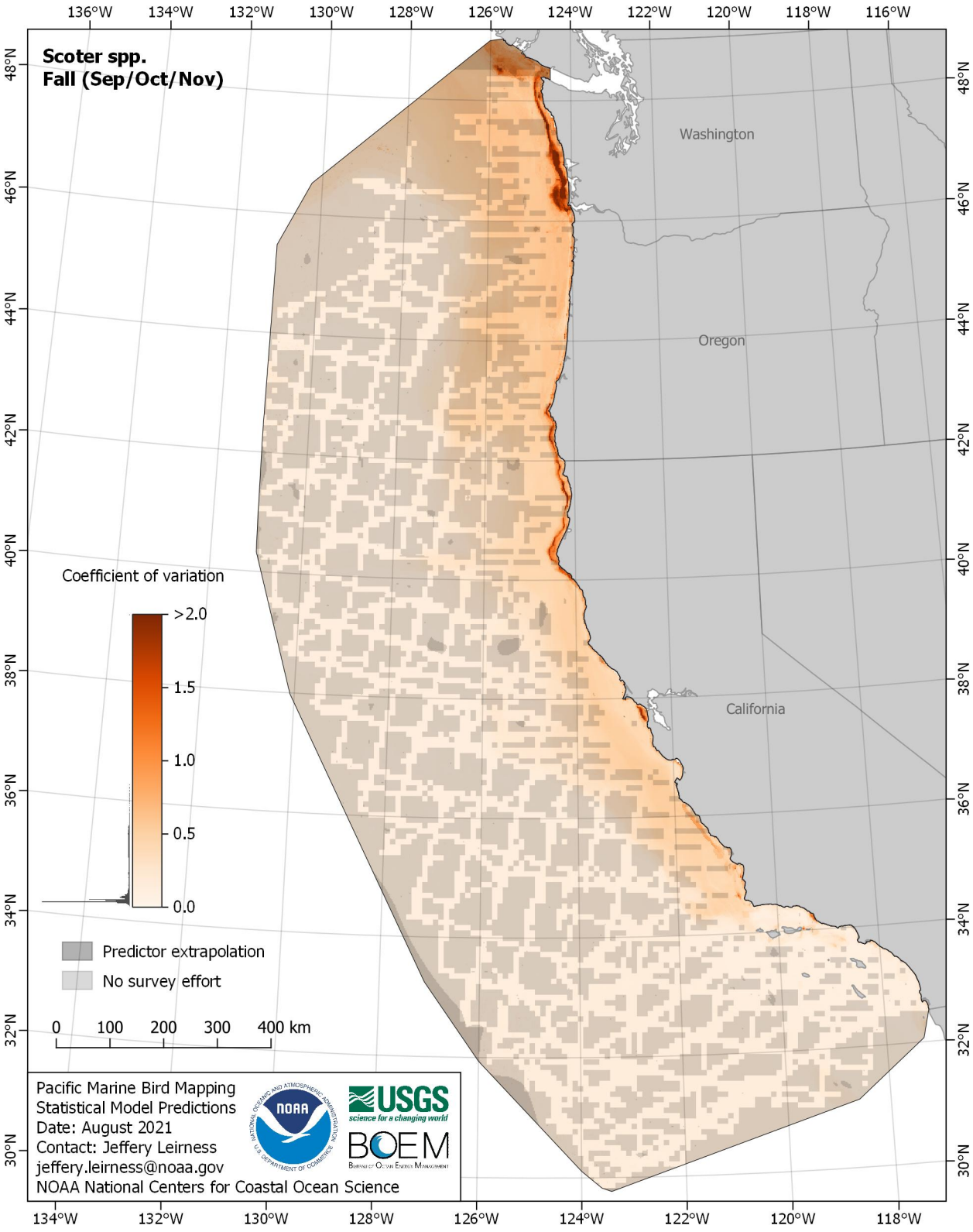

Figure E-6. Coefficient of variation for Scoter spp. (*Melanitta spp.*) in the fall season

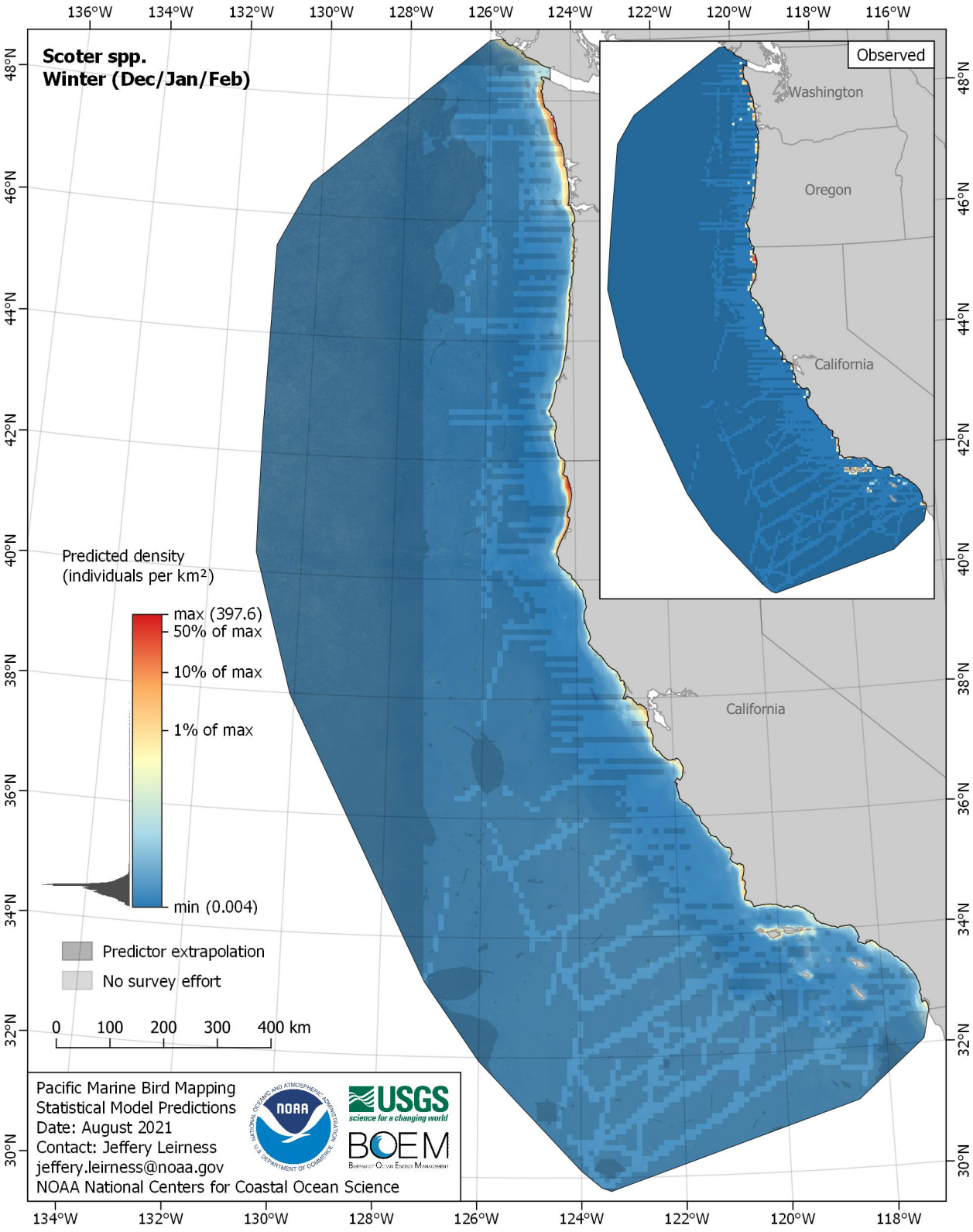

Figure E-7. Predicted density for Scoter spp. (*Melanitta spp.*) in the winter season

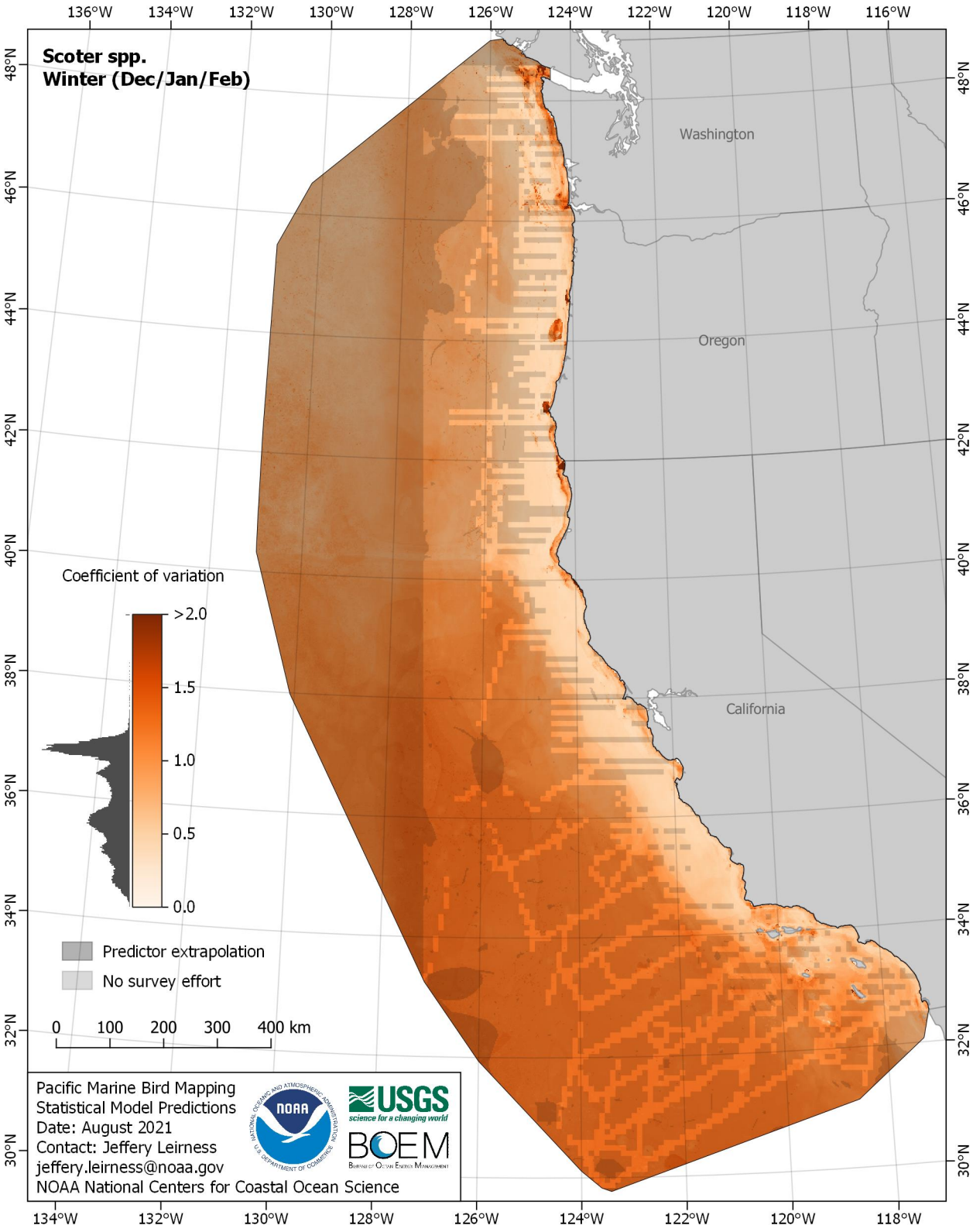

Figure E-8. Coefficient of variation for Scoter spp. (*Melanitta spp.*) in the winter season

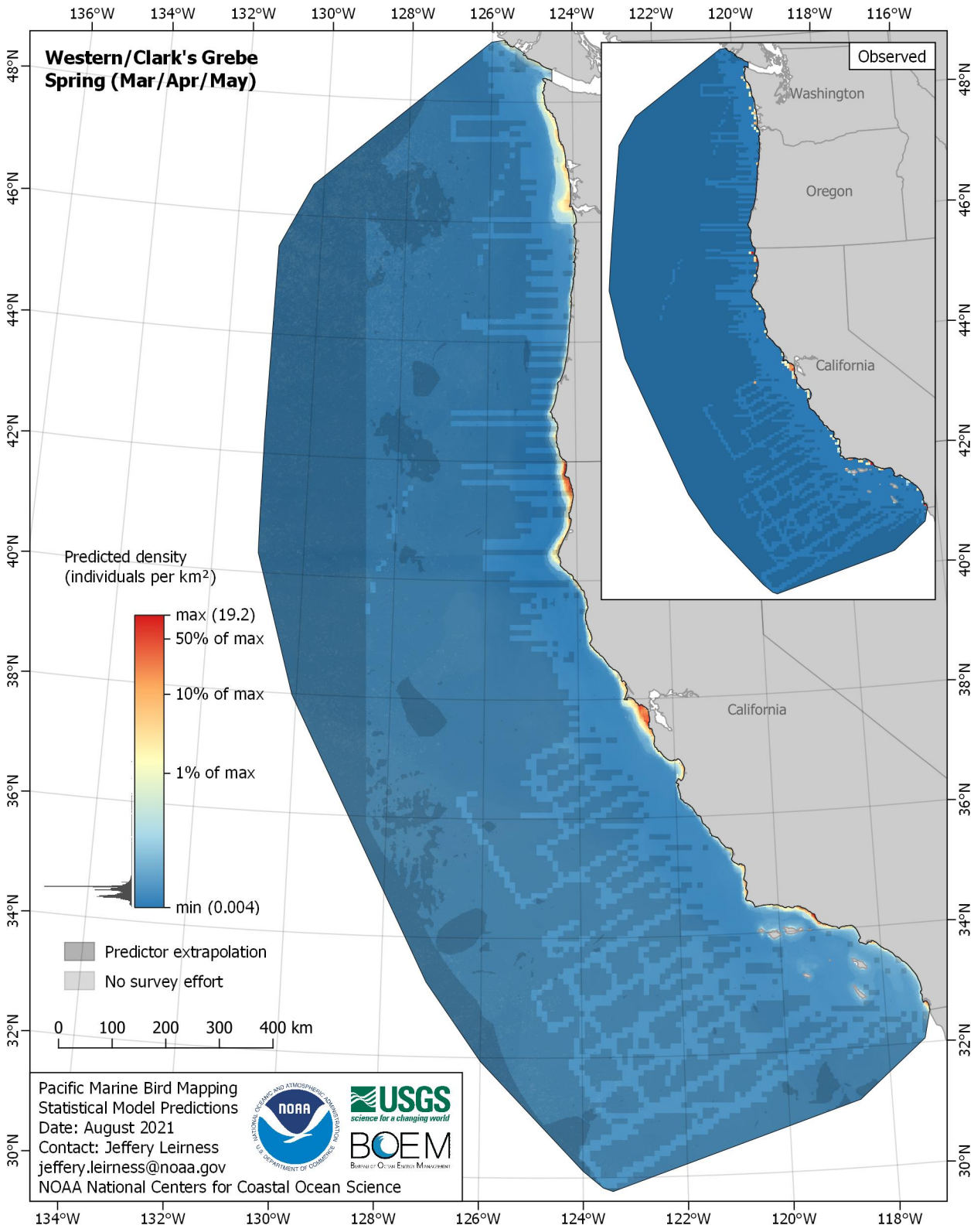

Figure E-9. Predicted density for Western/Clark's Grebe (*Aechmophorus occidentalis/clarkii*) in the spring season

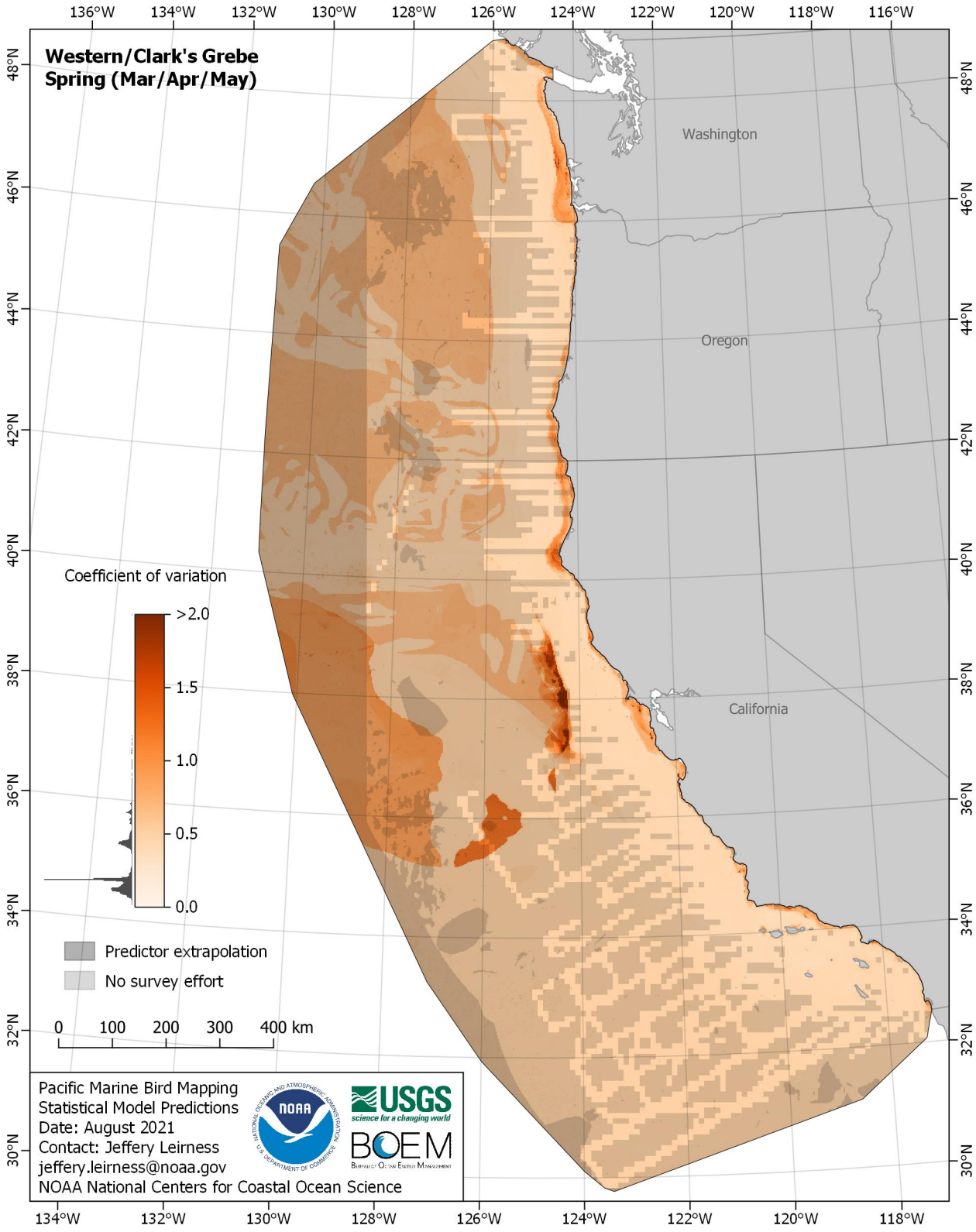

Figure E-10. Coefficient of variation for Western/Clark's Grebe (*Aechmophorus occidentalis/clarkii*) in the spring season

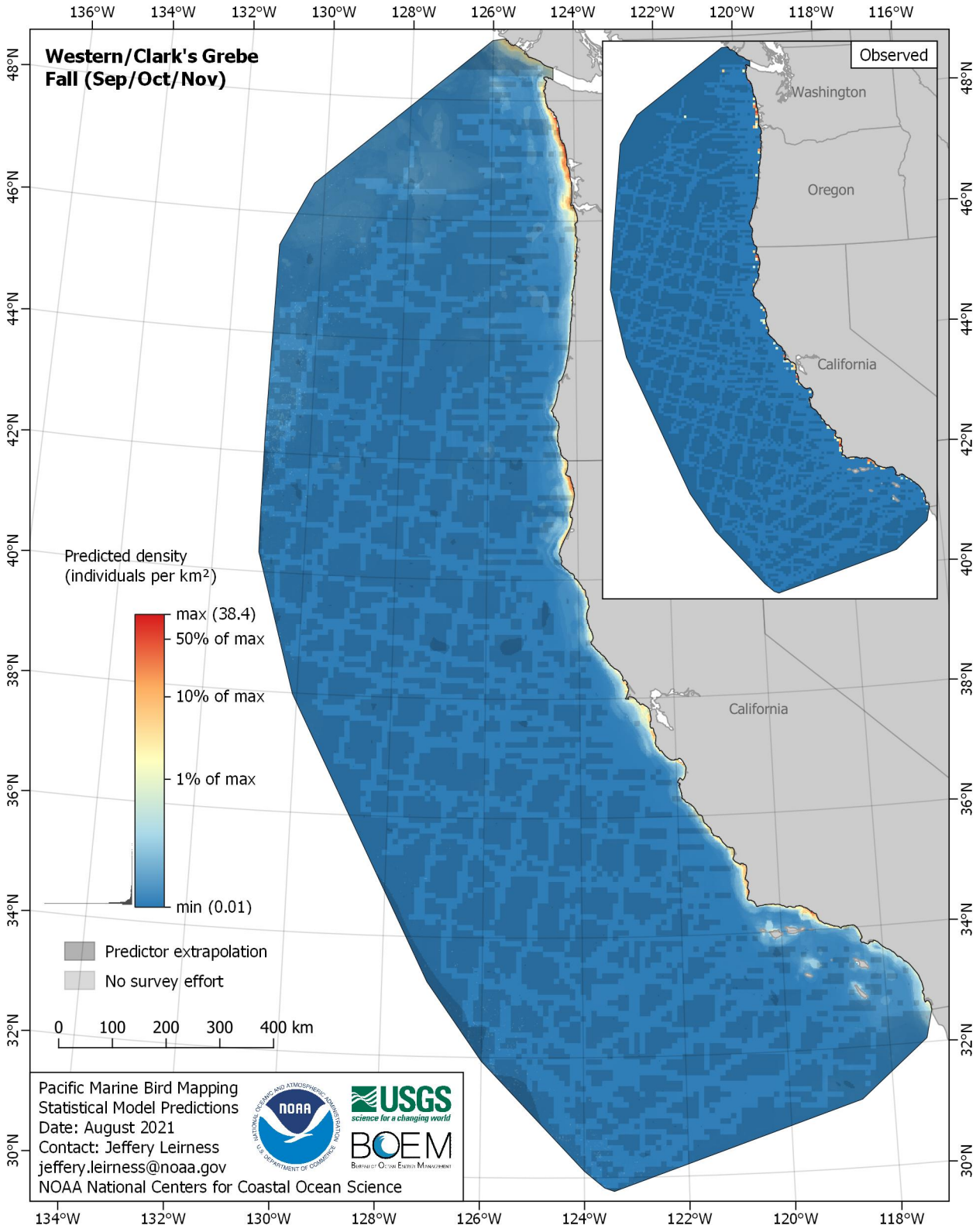

Figure E-11. Predicted density for Western/Clark's Grebe (*Aechmophorus occidentalis/clarkii*) in the fall season

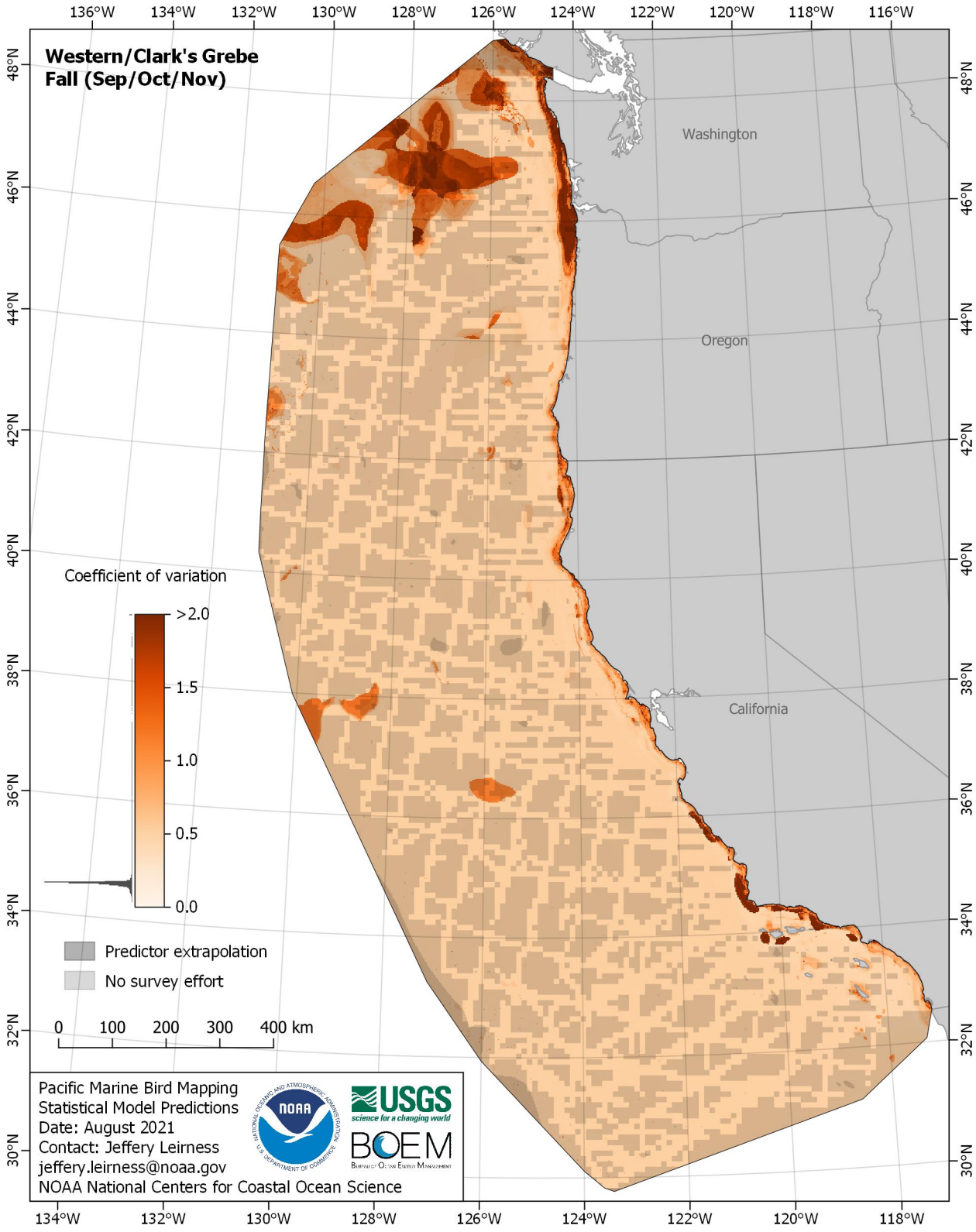

Figure E-12. Coefficient of variation for Western/Clark's Grebe (*Aechmophorus occidentalis/clarkii*) in the fall season

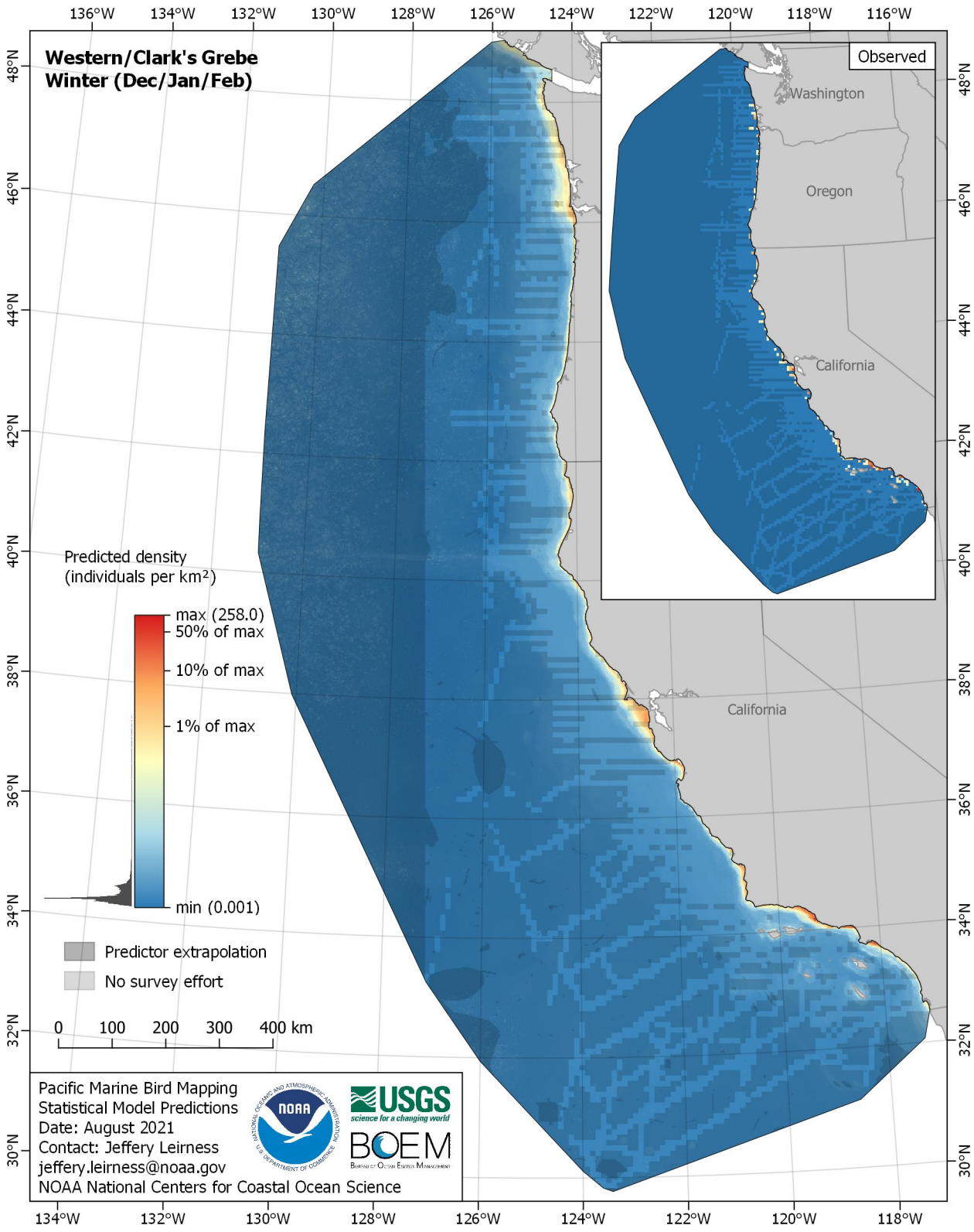

Figure E-13. Predicted density for Western/Clark's Grebe (*Aechmophorus occidentalis/clarkii*) in the winter season

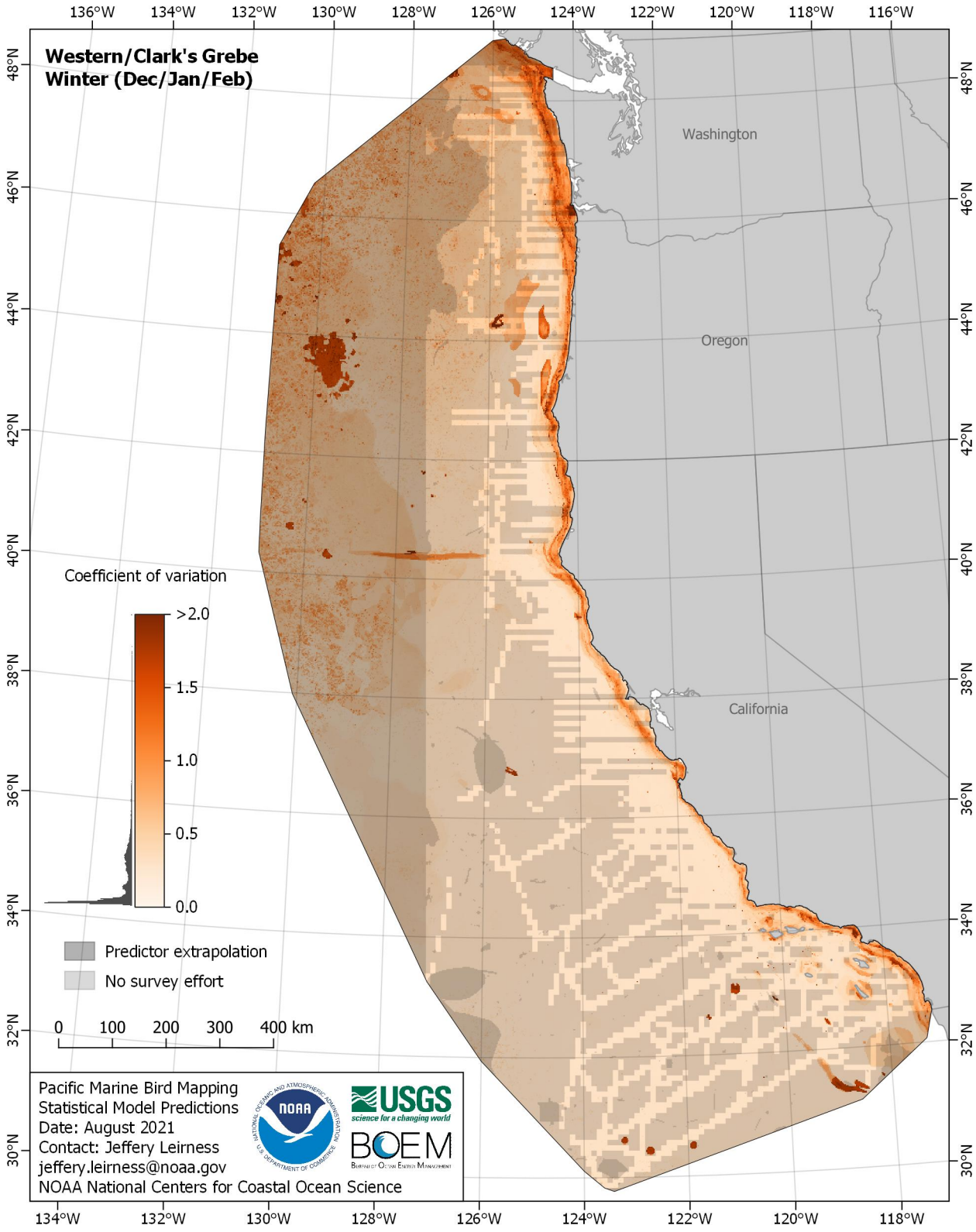

Figure E-14. Coefficient of variation for Western/Clark's Grebe (*Aechmophorus occidentalis/clarkii*) in the winter season

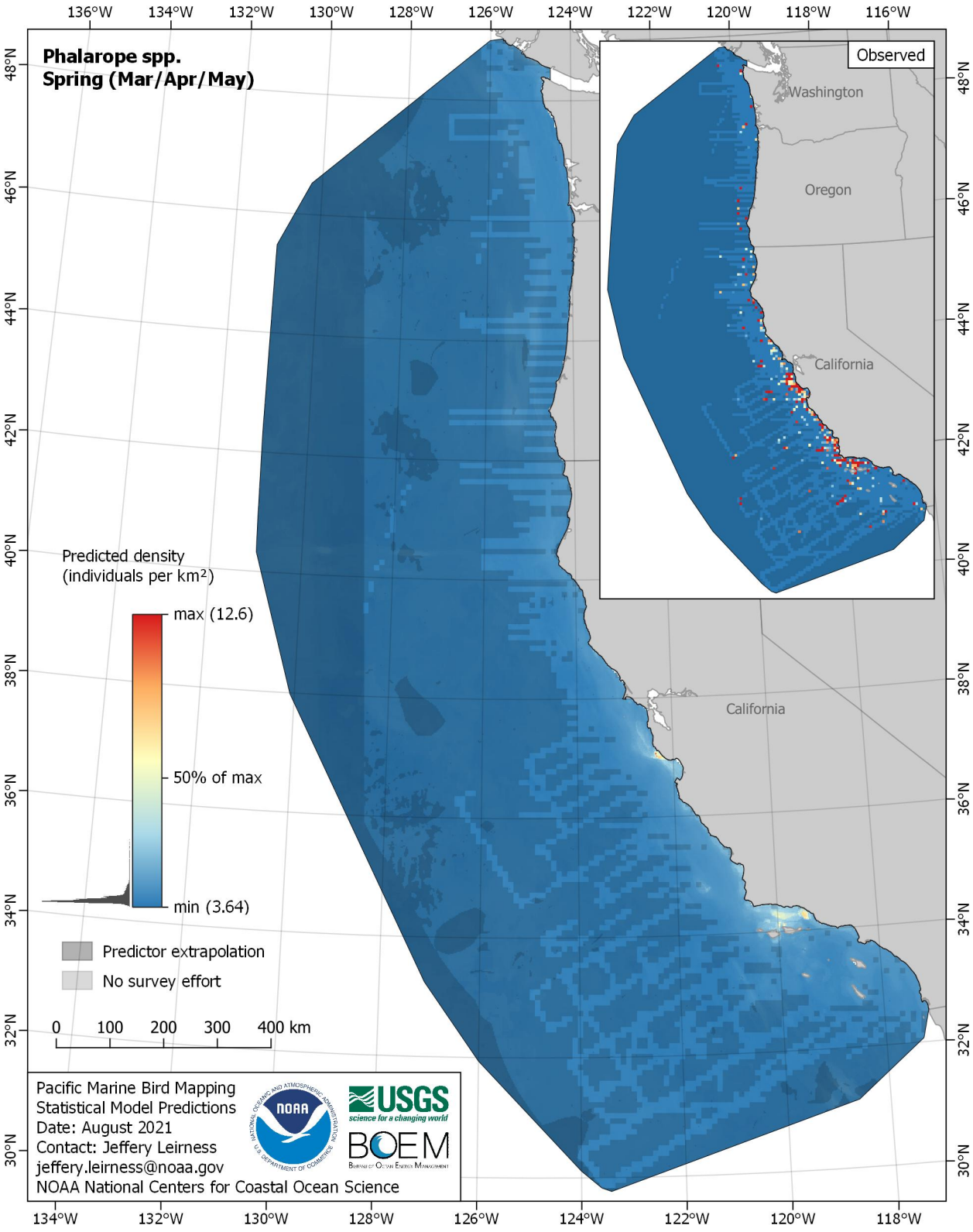

Figure E-15. Predicted density for Phalarope spp. (*Phalaropus spp.*) in the spring season

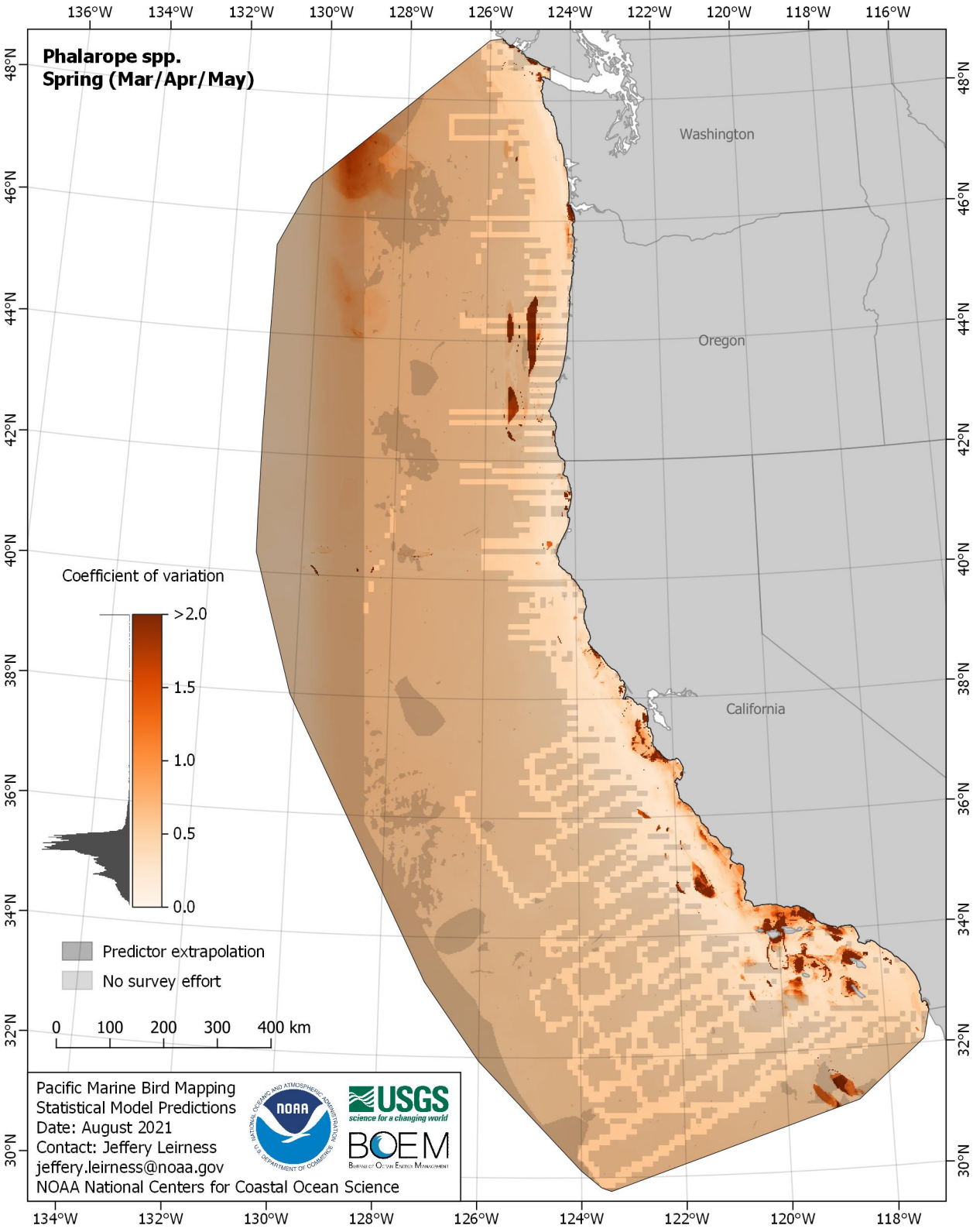

Figure E-16. Coefficient of variation for Phalarope spp. (*Phalaropus spp.*) in the spring season

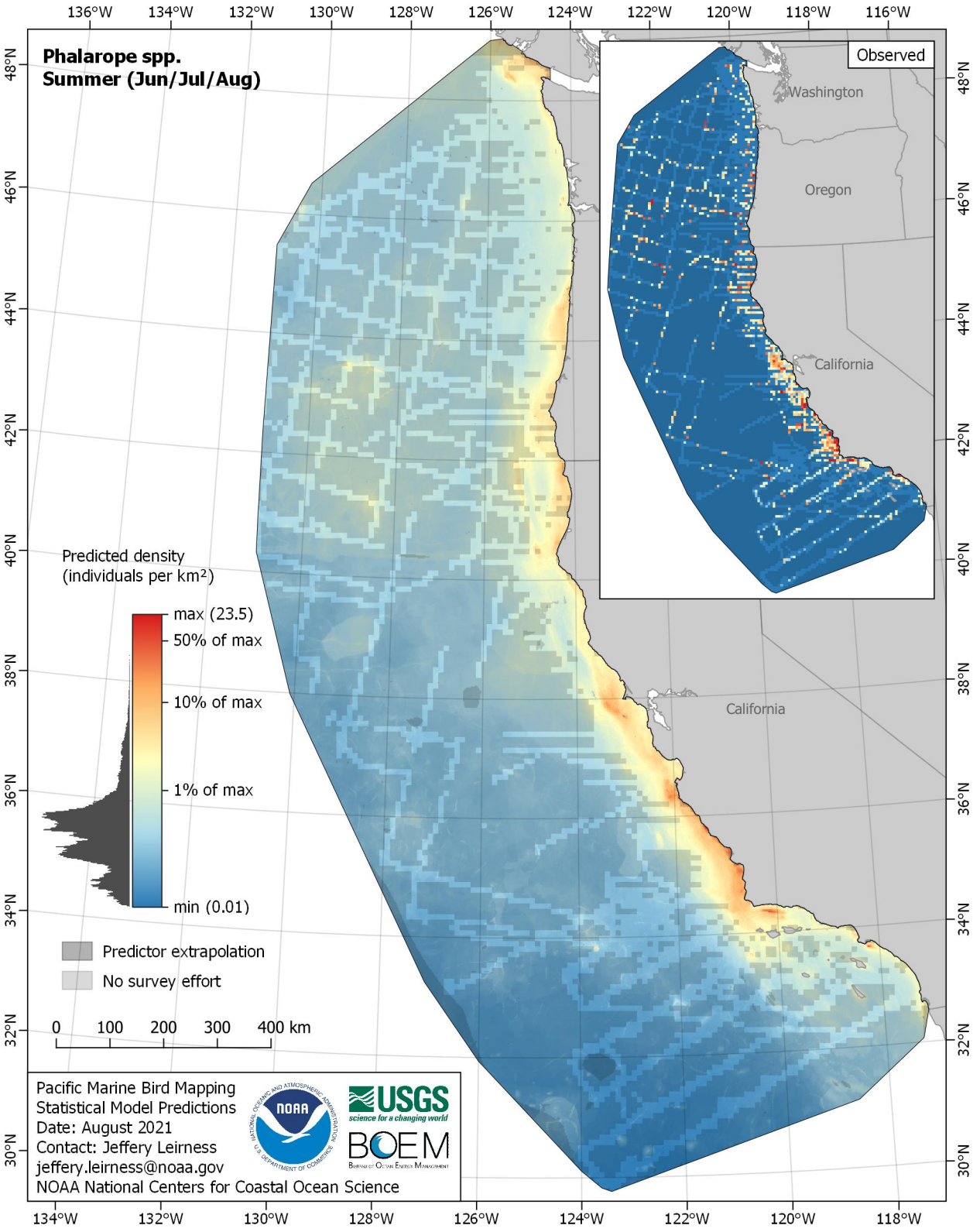

Figure E-17. Predicted density for Phalarope spp. (*Phalaropus spp.*) in the summer season

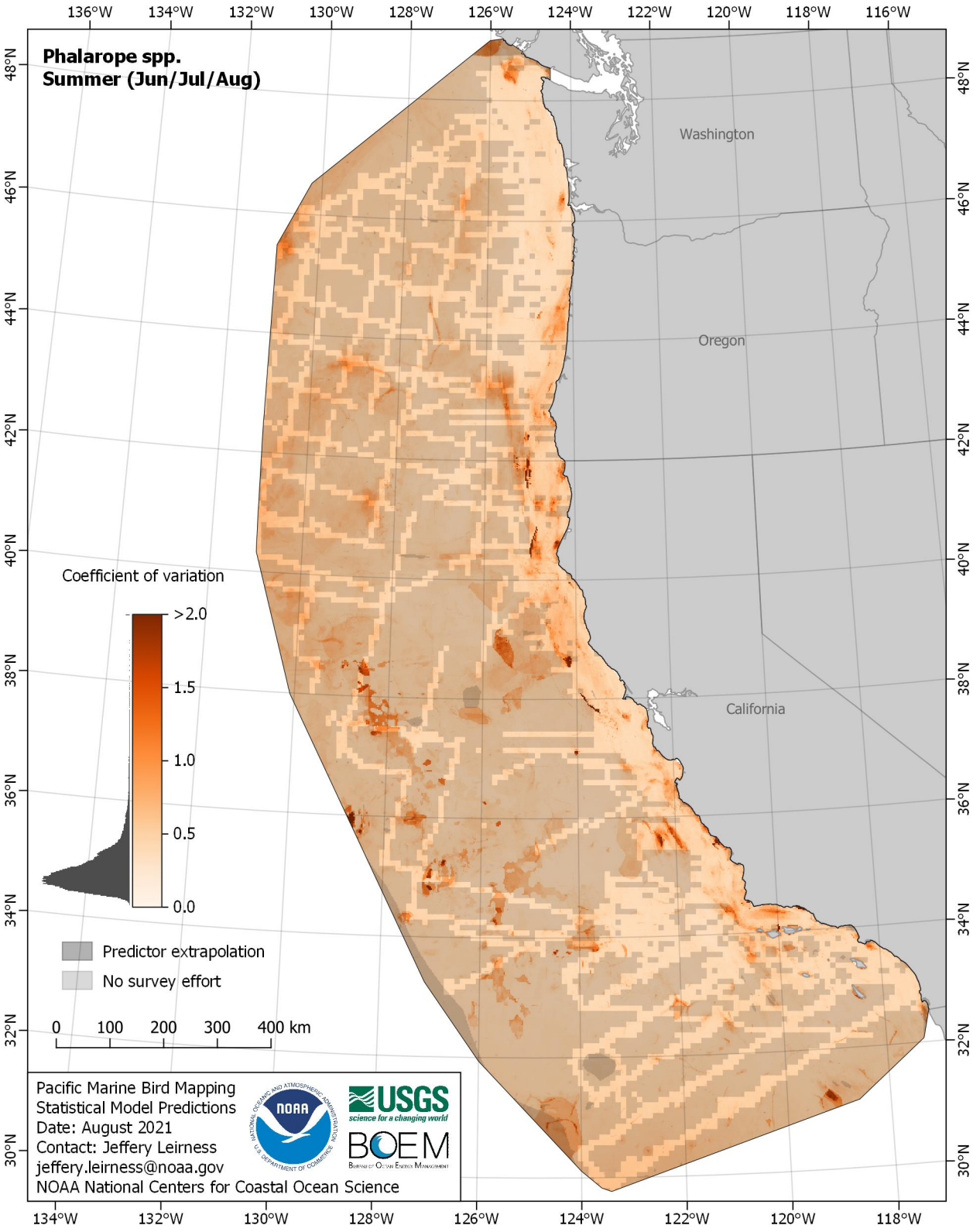

Figure E-18. Coefficient of variation for Phalarope spp. (*Phalaropus spp.*) in the summer season

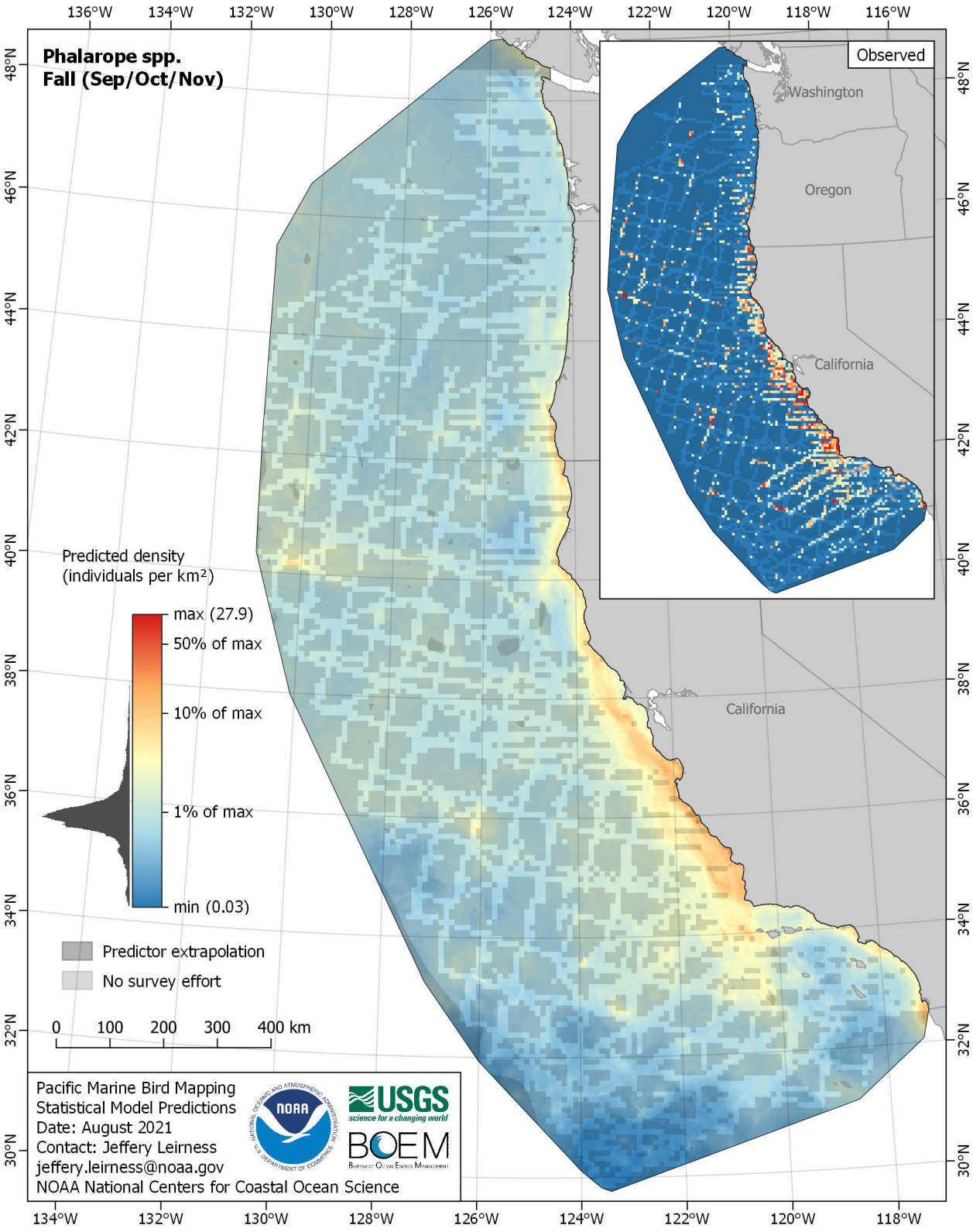

Figure E-19. Predicted density for Phalarope spp. (*Phalaropus spp.*) in the fall season

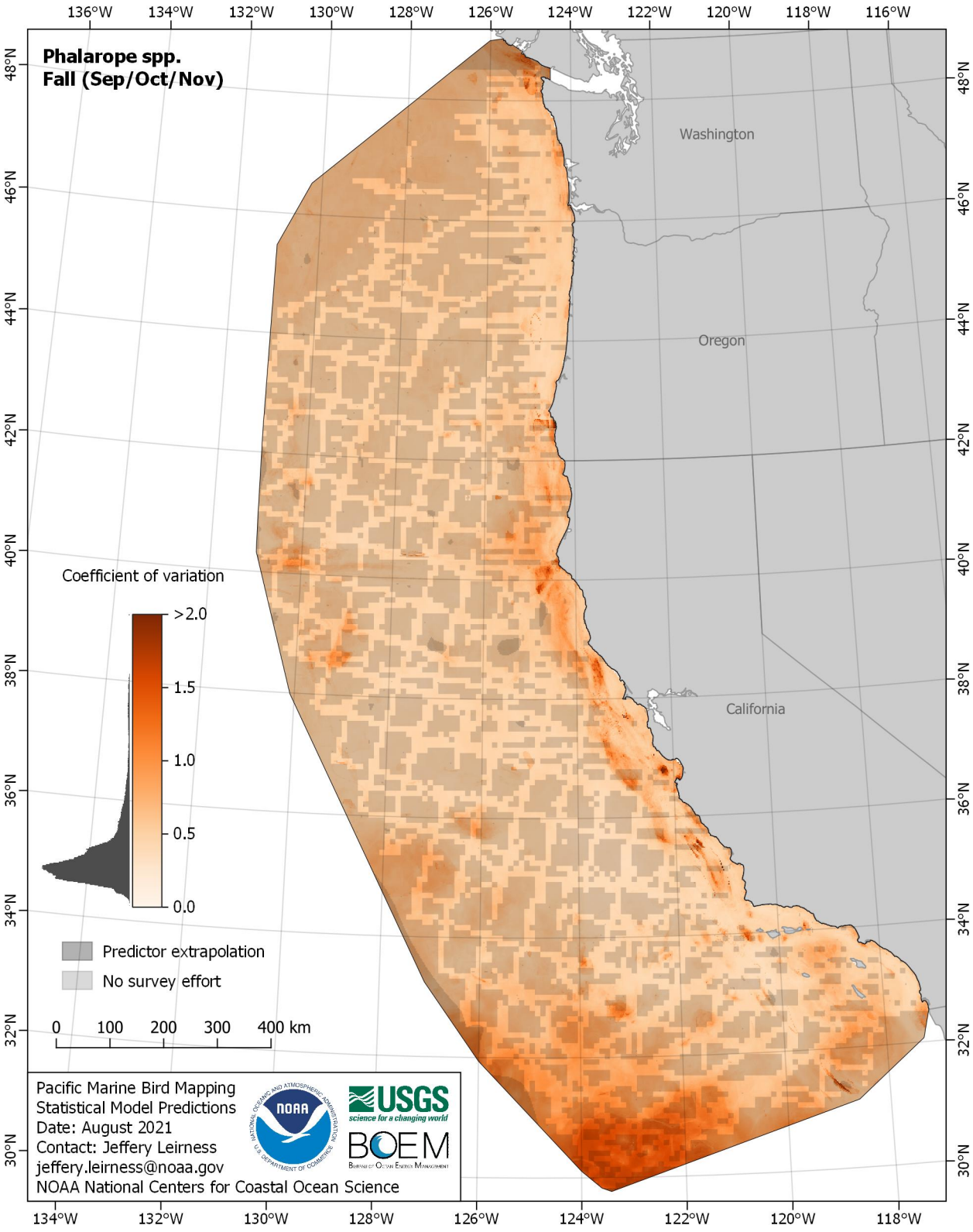

Figure E-20. Coefficient of variation for Phalarope spp. (*Phalaropus spp.*) in the fall season

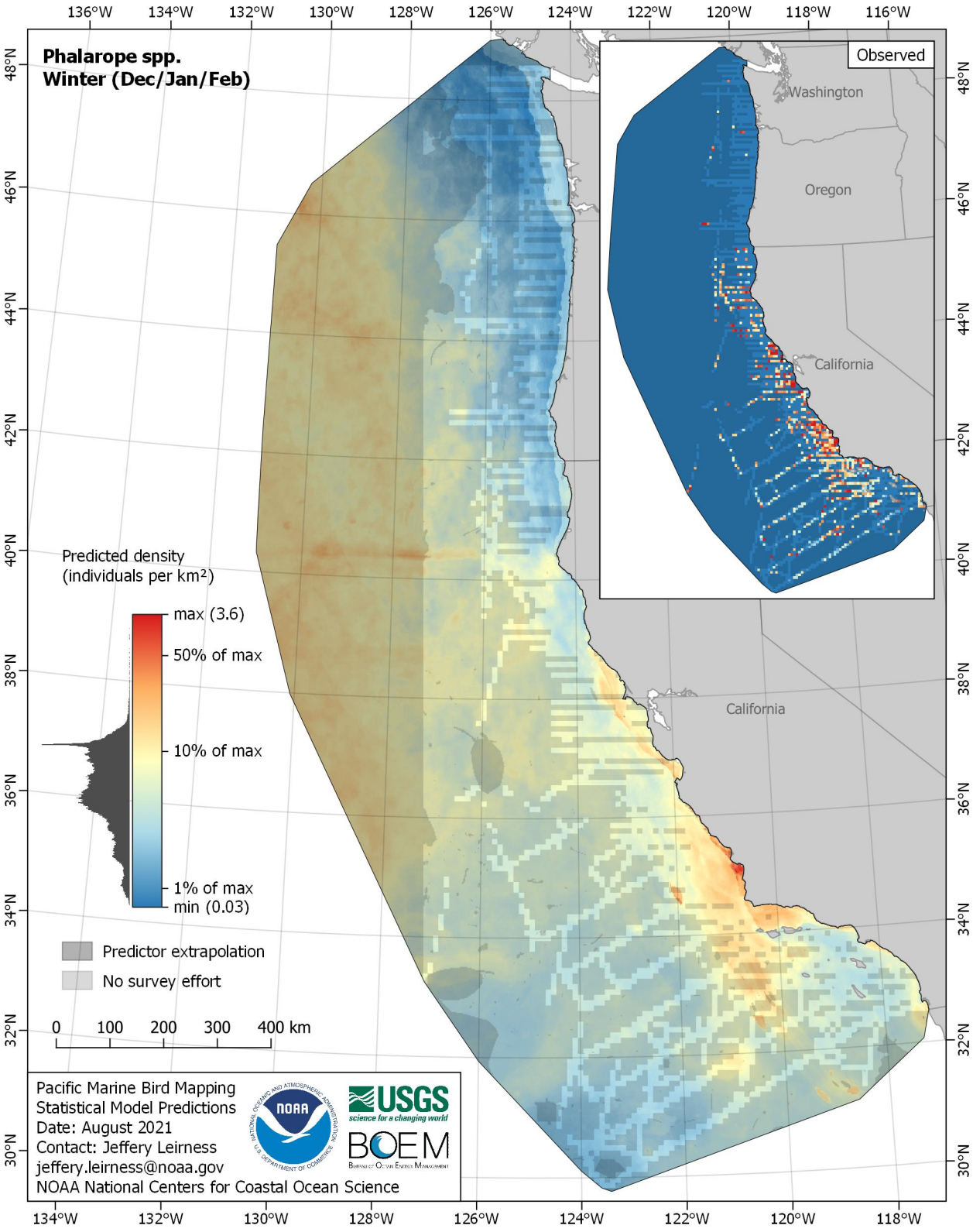

Figure E-21. Predicted density for Phalarope spp. (*Phalaropus spp.*) in the winter season

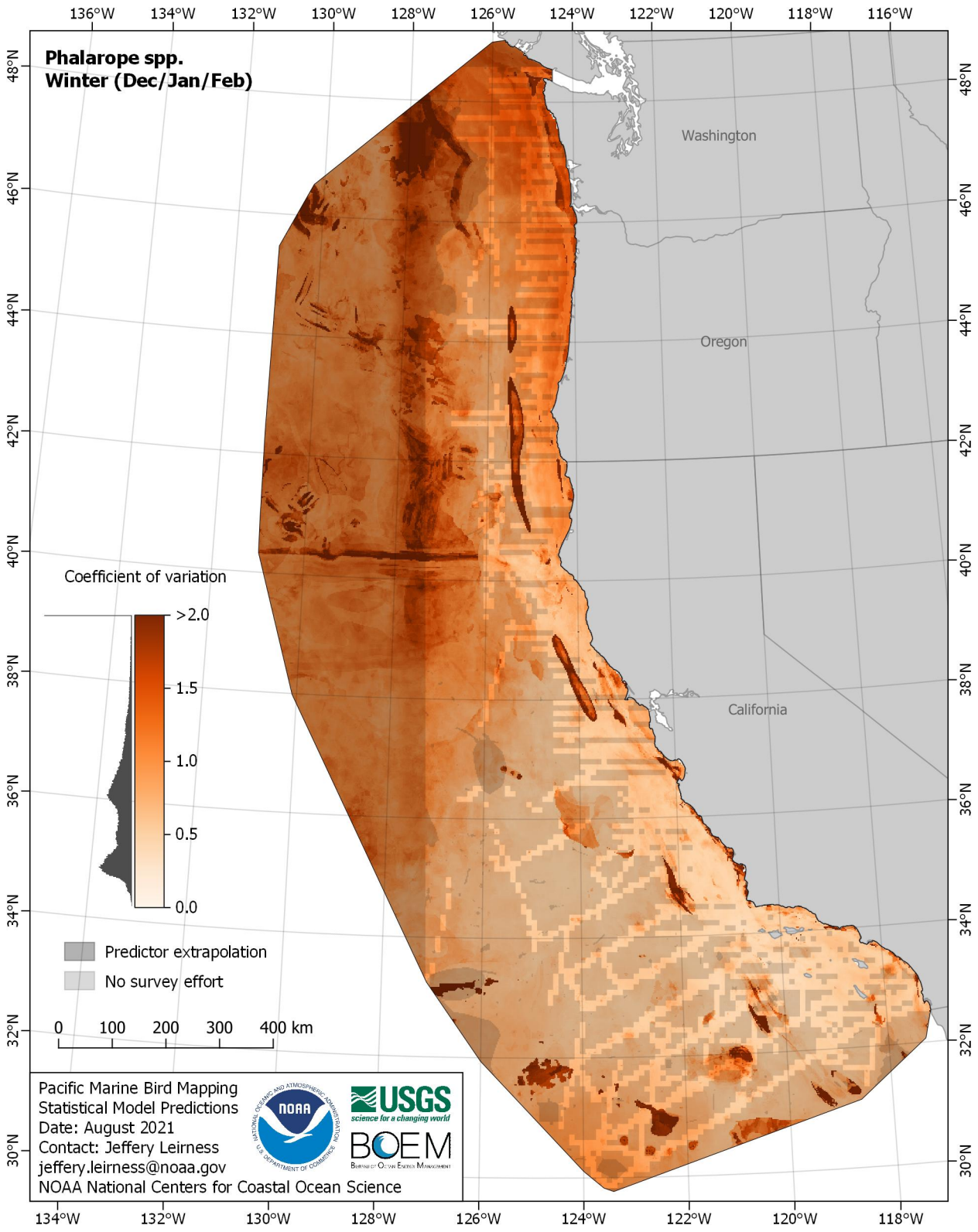

Figure E-22. Coefficient of variation for Phalarope spp. (*Phalaropus spp.*) in the winter season

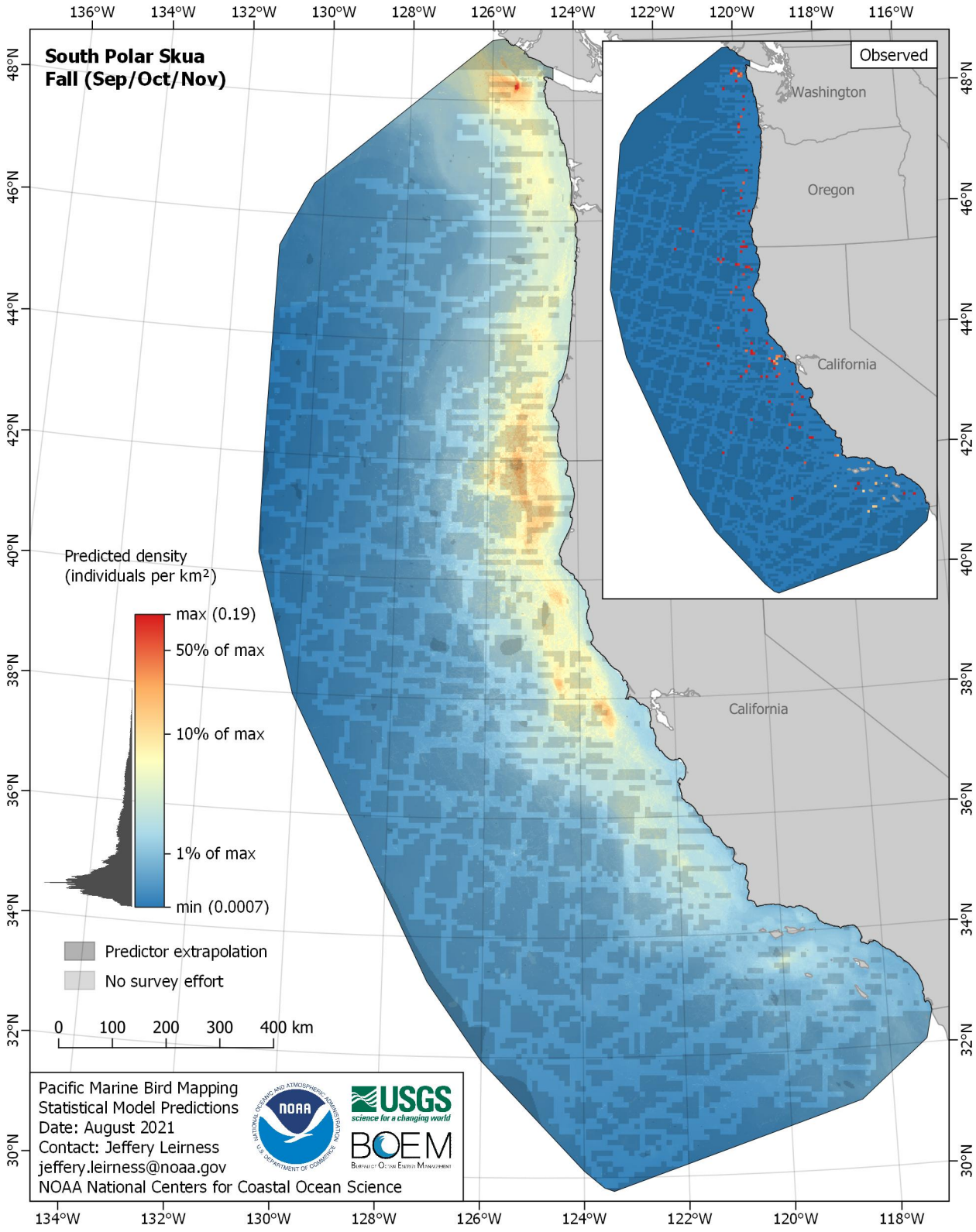

Figure E-23. Predicted density for South Polar Skua (*Stercorarius maccormicki*) in the fall season

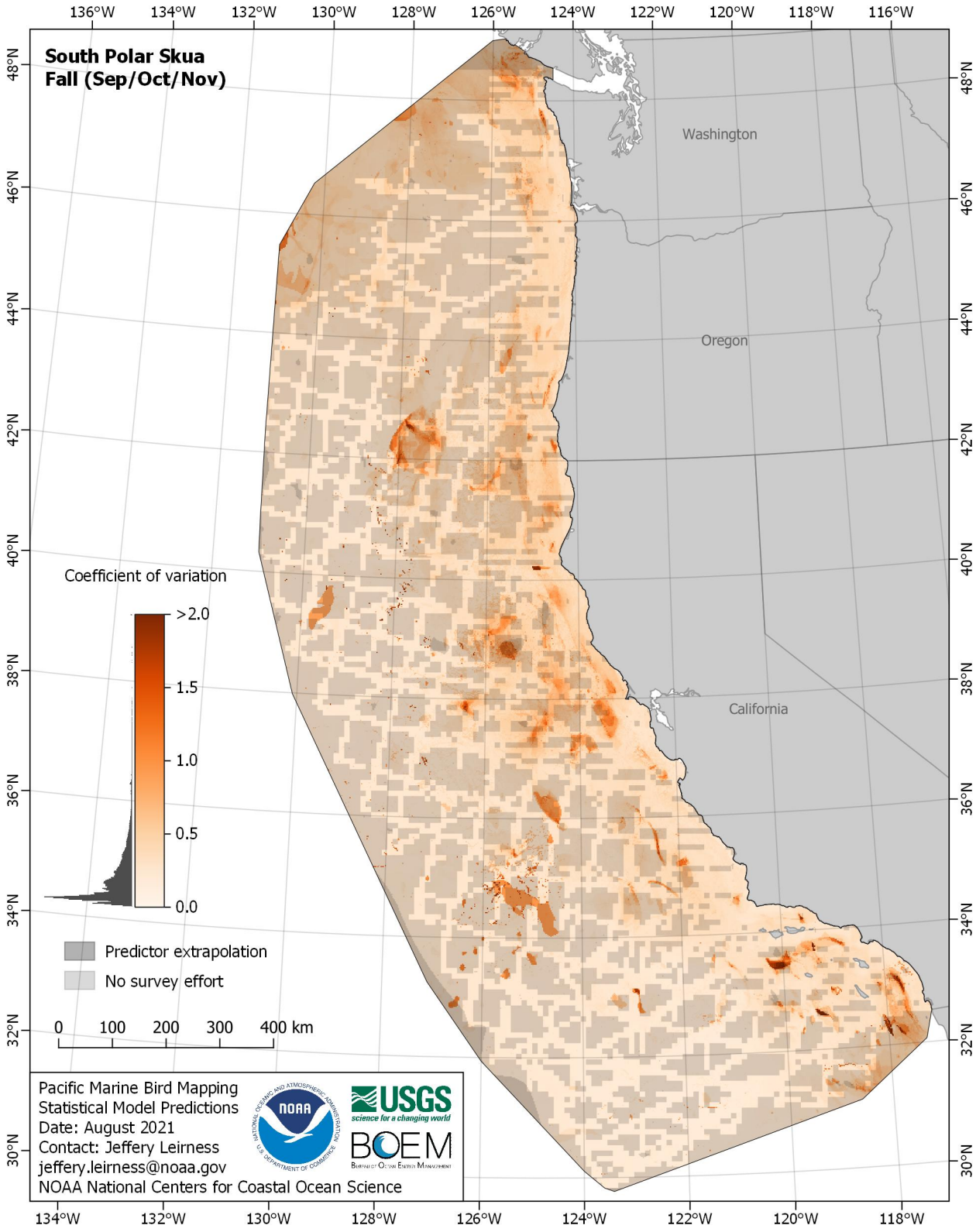

Figure E-24. Coefficient of variation for South Polar Skua (*Stercorarius maccormicki*) in the fall season

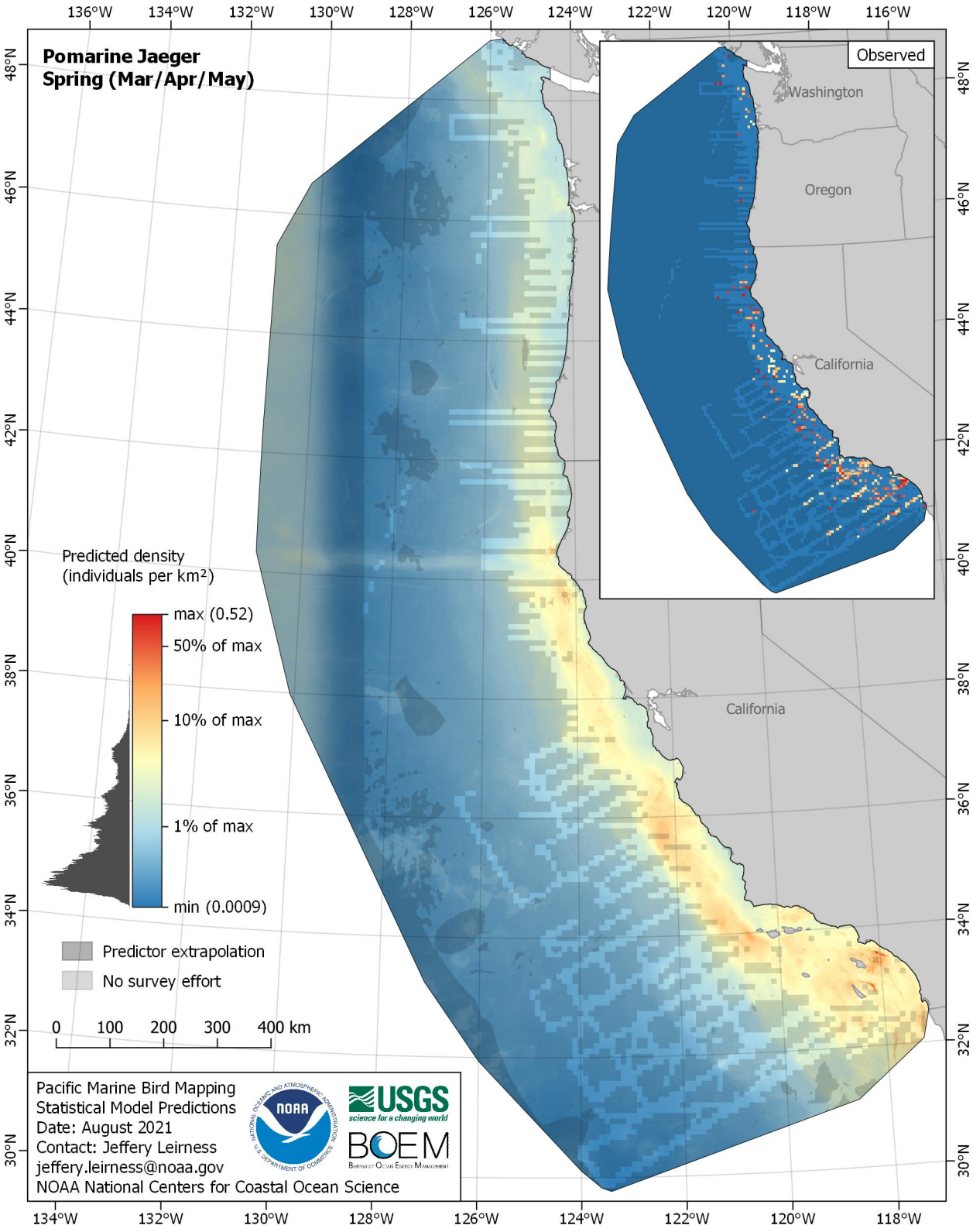

Figure E-25. Predicted density for Pomarine Jaeger (*Stercorarius pomarinus*) in the spring season

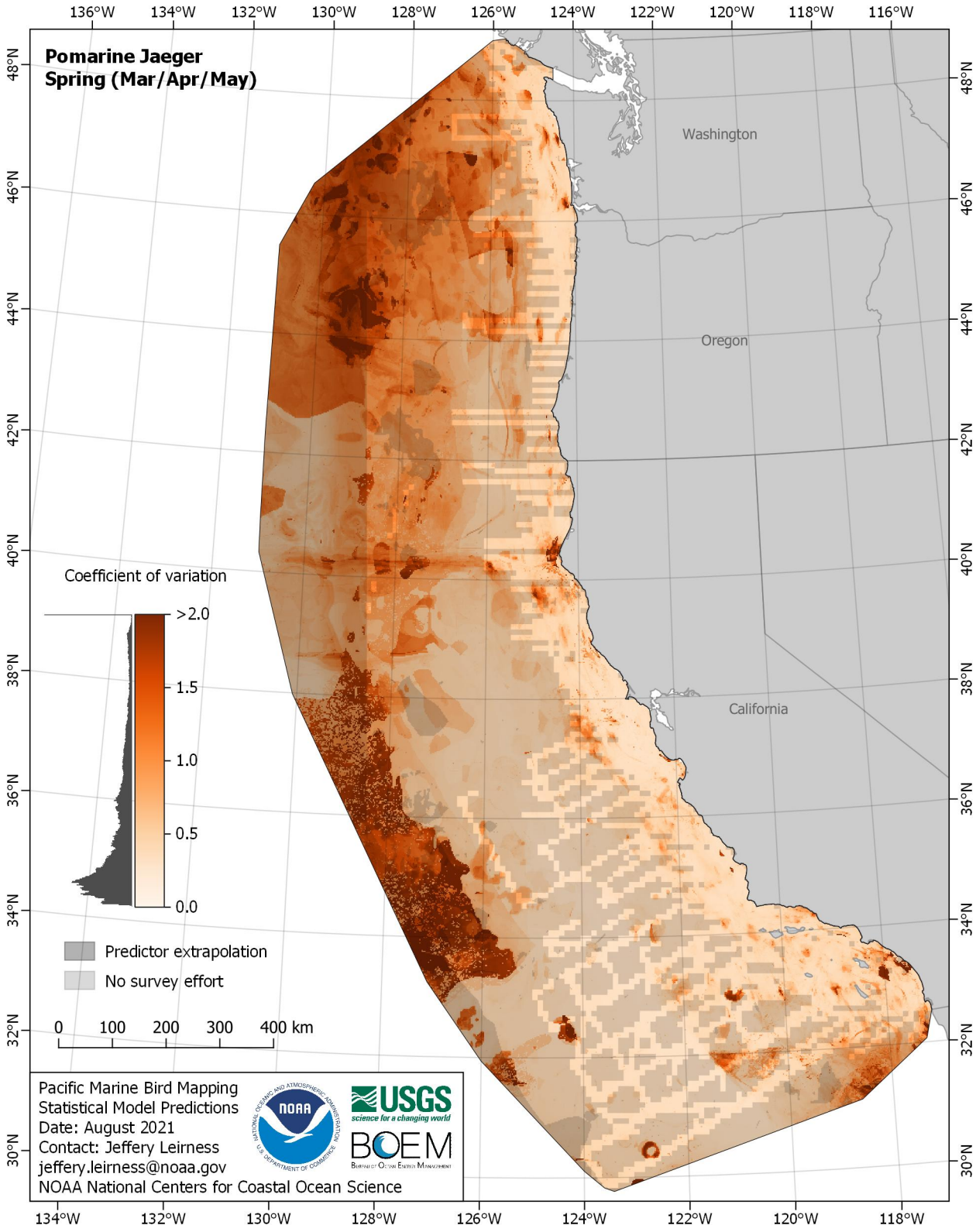

Figure E-26. Coefficient of variation for Pomarine Jaeger (*Stercorarius pomarinus*) in the spring season

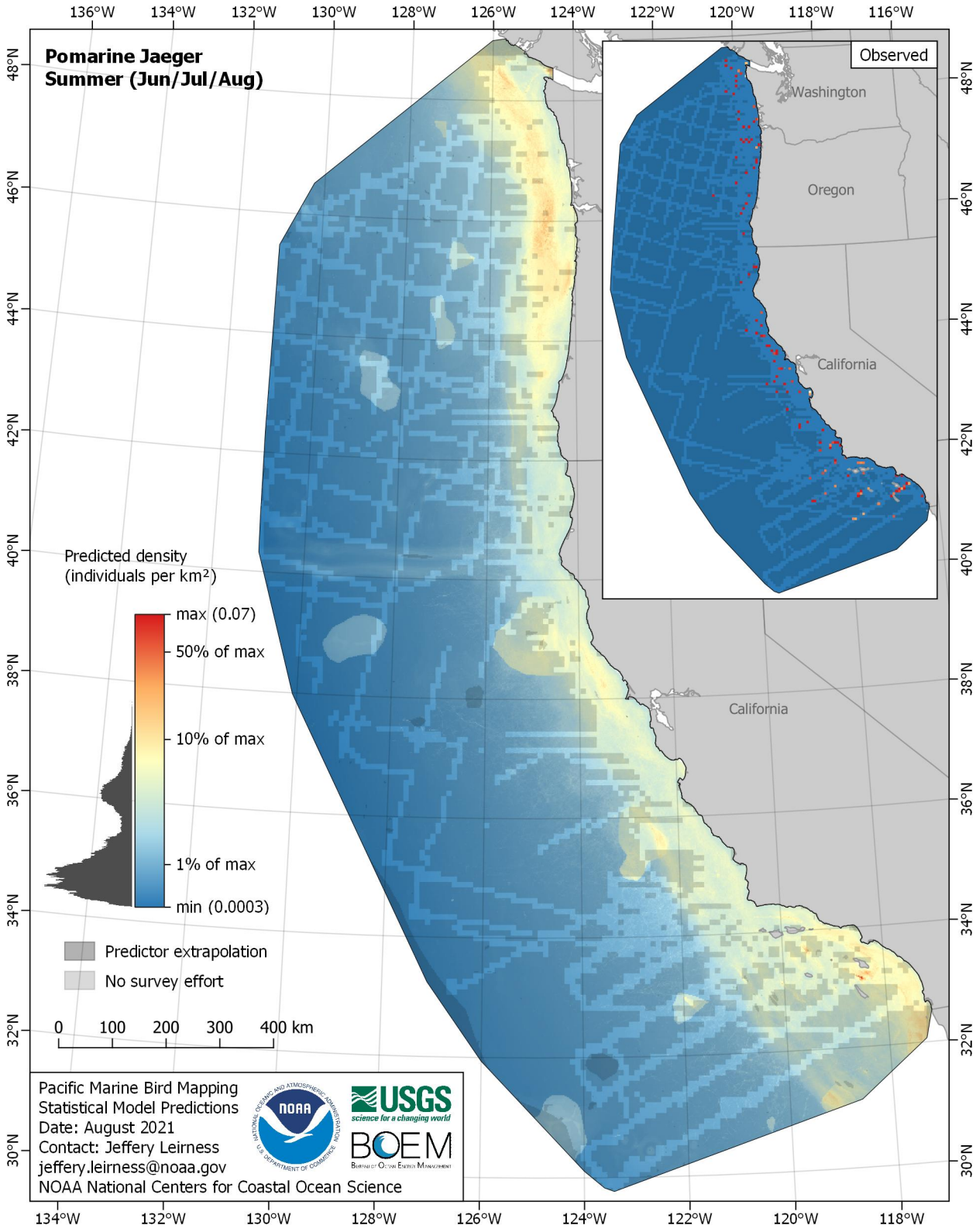

Figure E-27. Predicted density for Pomarine Jaeger (*Stercorarius pomarinus*) in the summer season

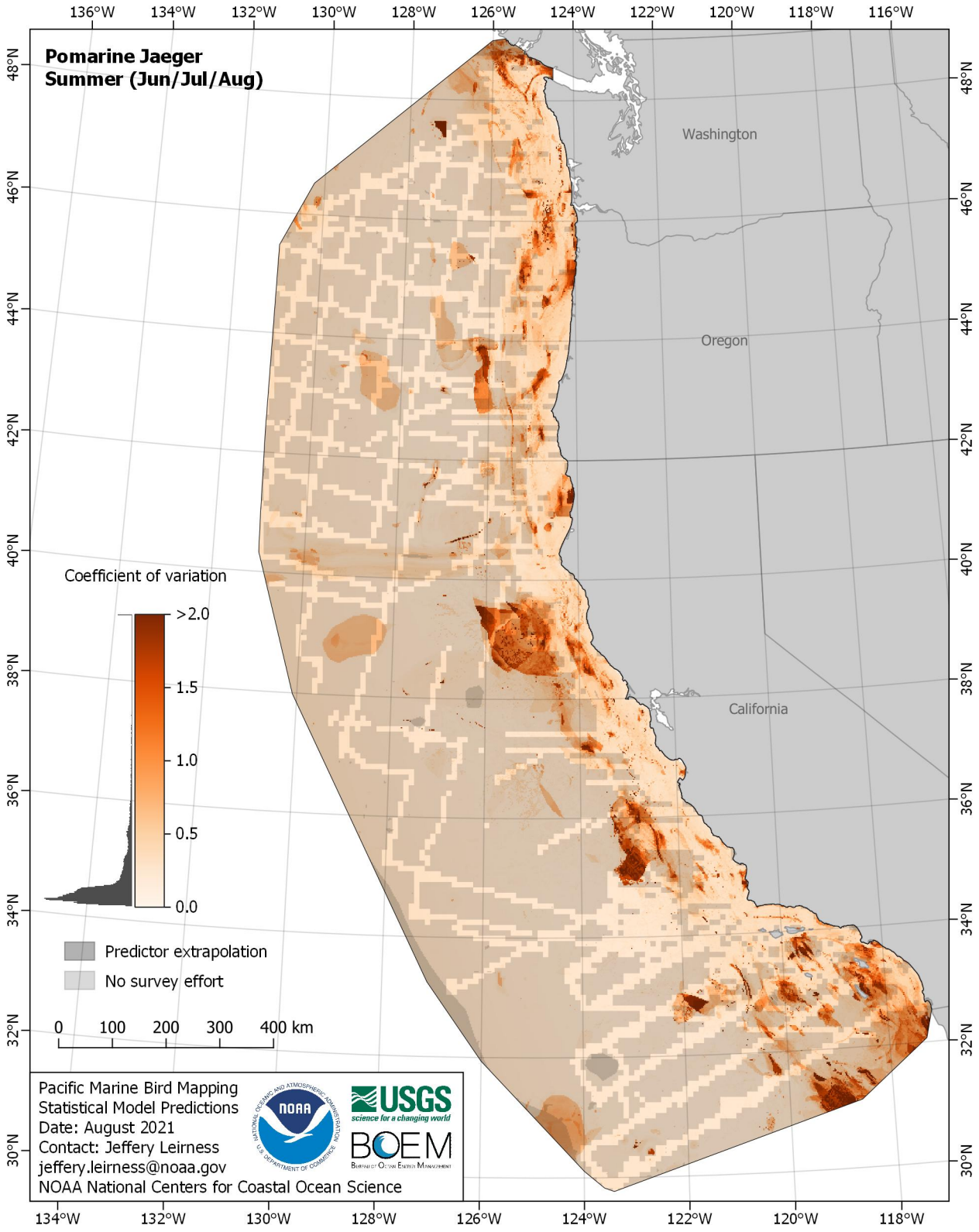

Figure E-28. Coefficient of variation for Pomarine Jaeger (*Stercorarius pomarinus*) in the summer season

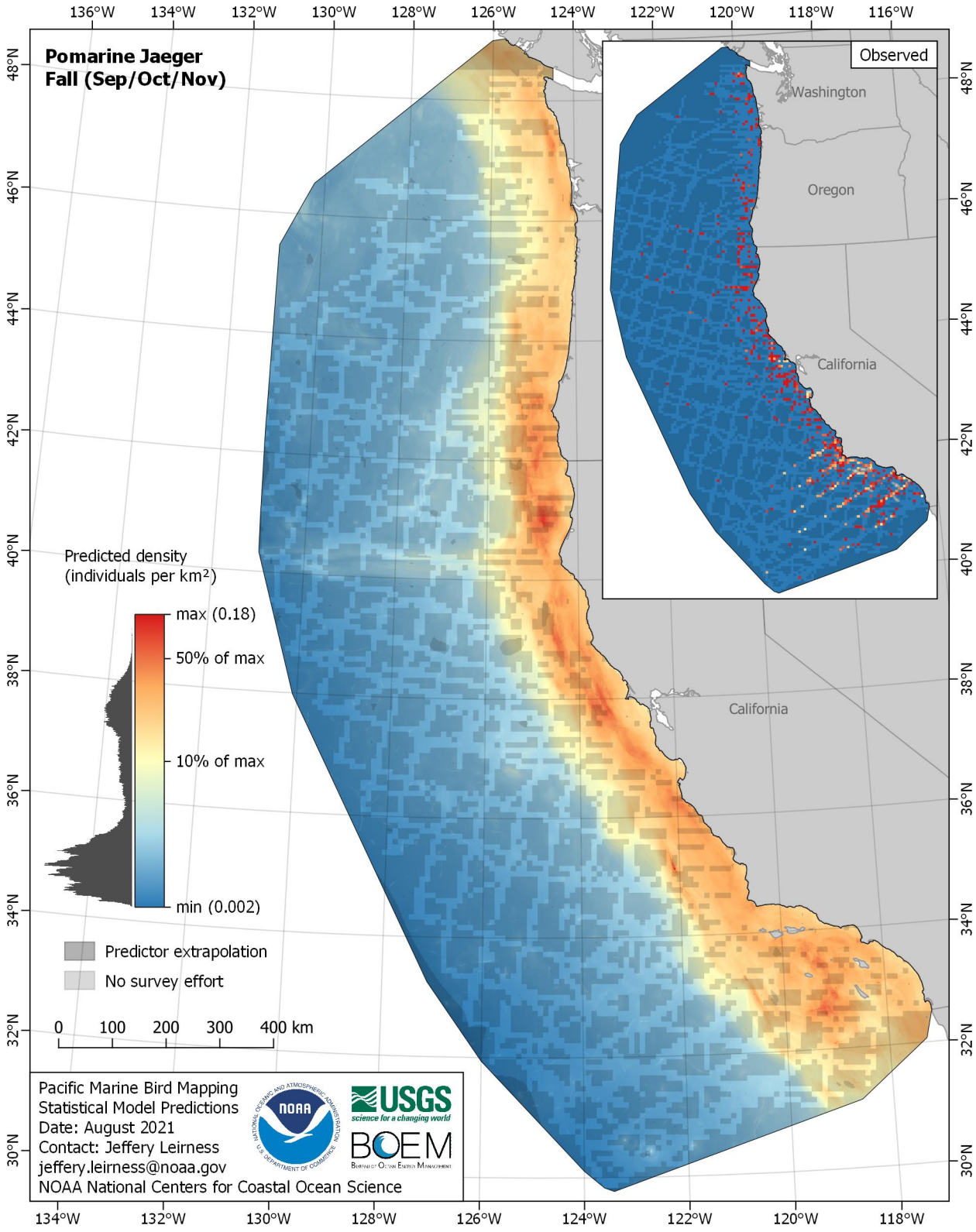

Figure E-29. Predicted density for Pomarine Jaeger (*Stercorarius pomarinus*) in the fall season

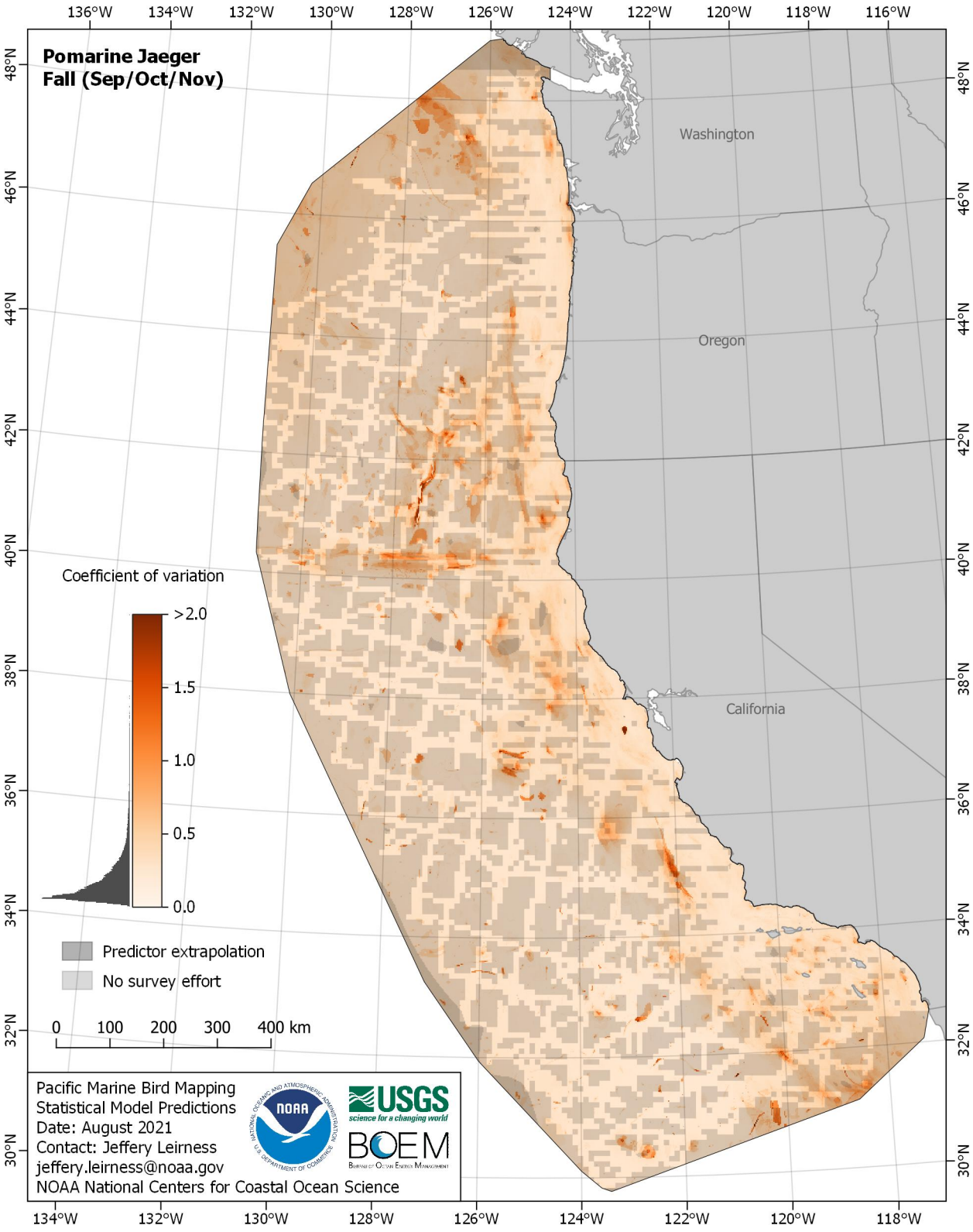

Figure E-30. Coefficient of variation for Pomarine Jaeger (*Stercorarius pomarinus*) in the fall season

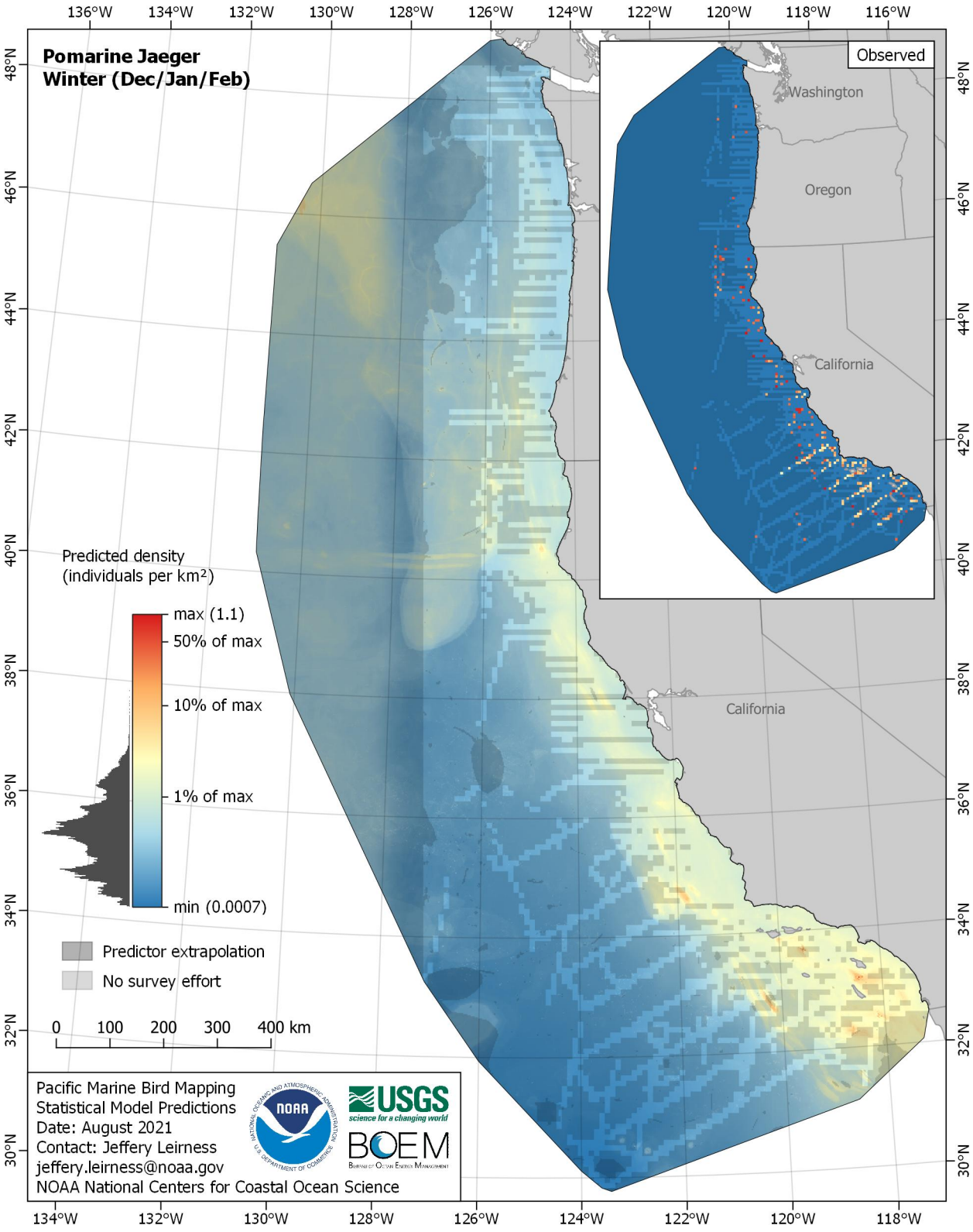

Figure E-31. Predicted density for Pomarine Jaeger (*Stercorarius pomarinus*) in the winter season

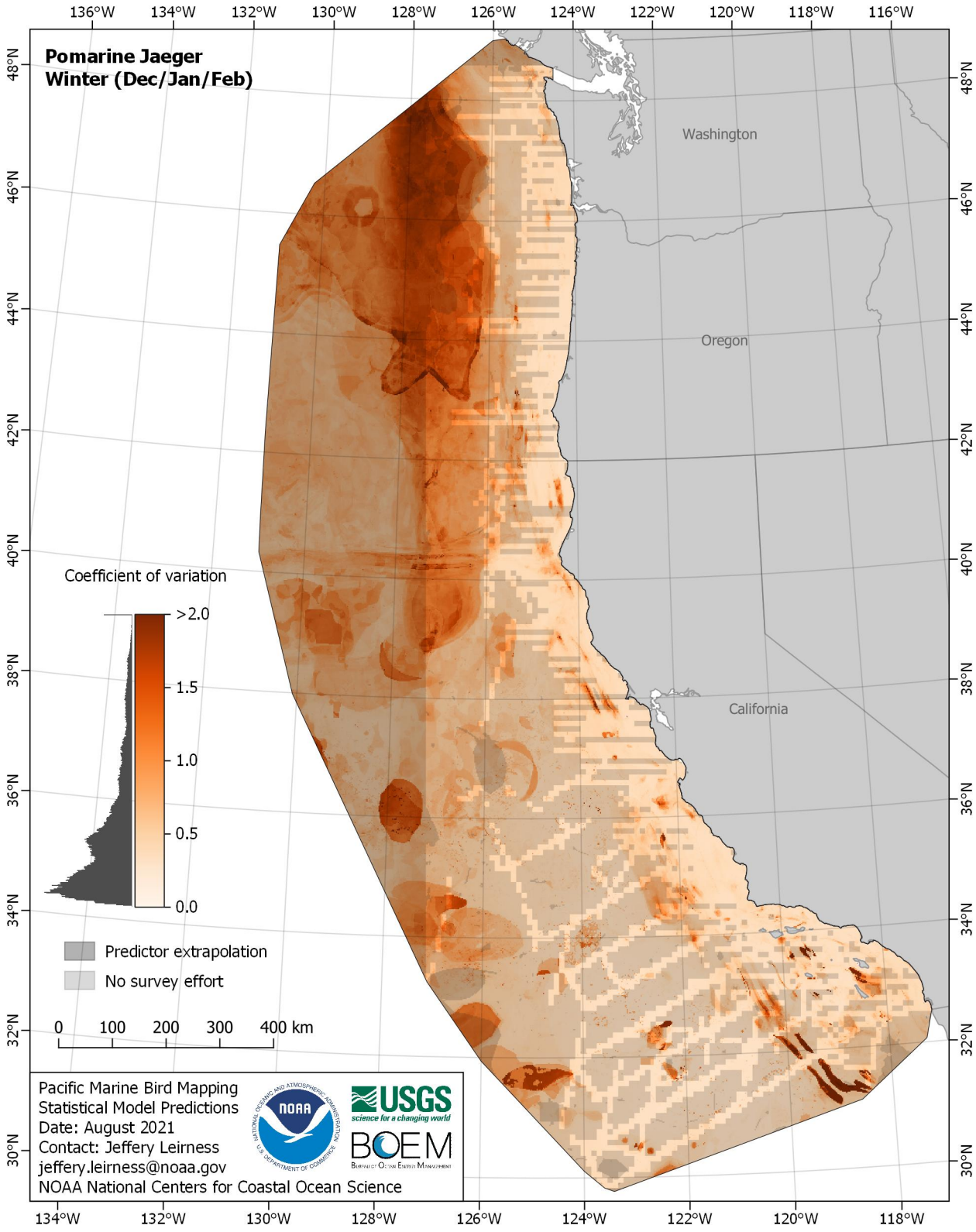

Figure E-32. Coefficient of variation for Pomarine Jaeger (*Stercorarius pomarinus*) in the winter season

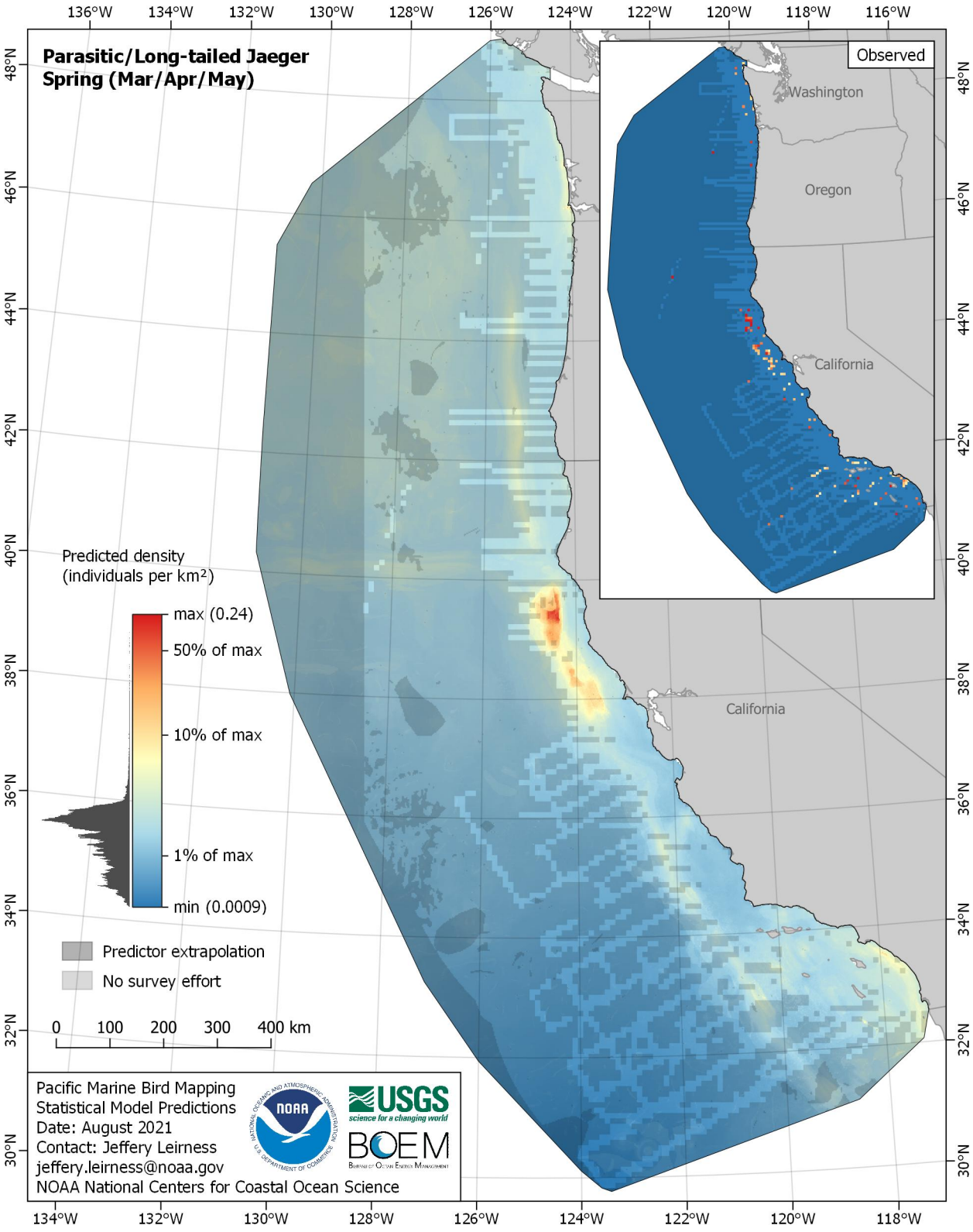

Figure E-33. Predicted density for Parasitic/Long-tailed Jaeger (*Stercorarius parasiticus/longicaudus*) in the spring season

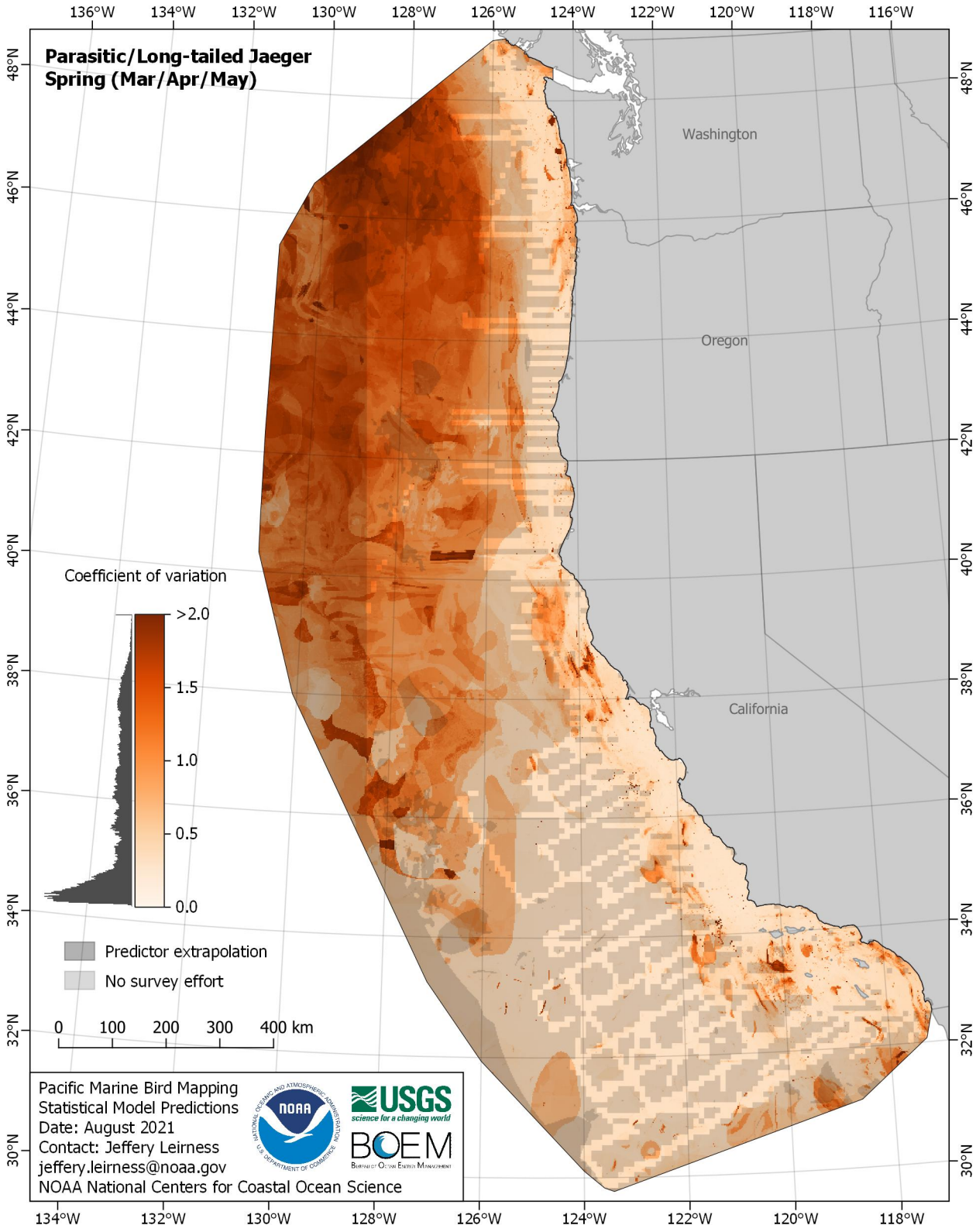

Figure E-34. Coefficient of variation for Parasitic/Long-tailed Jaeger (*Stercorarius parasiticus/longicaudus*) in the spring season

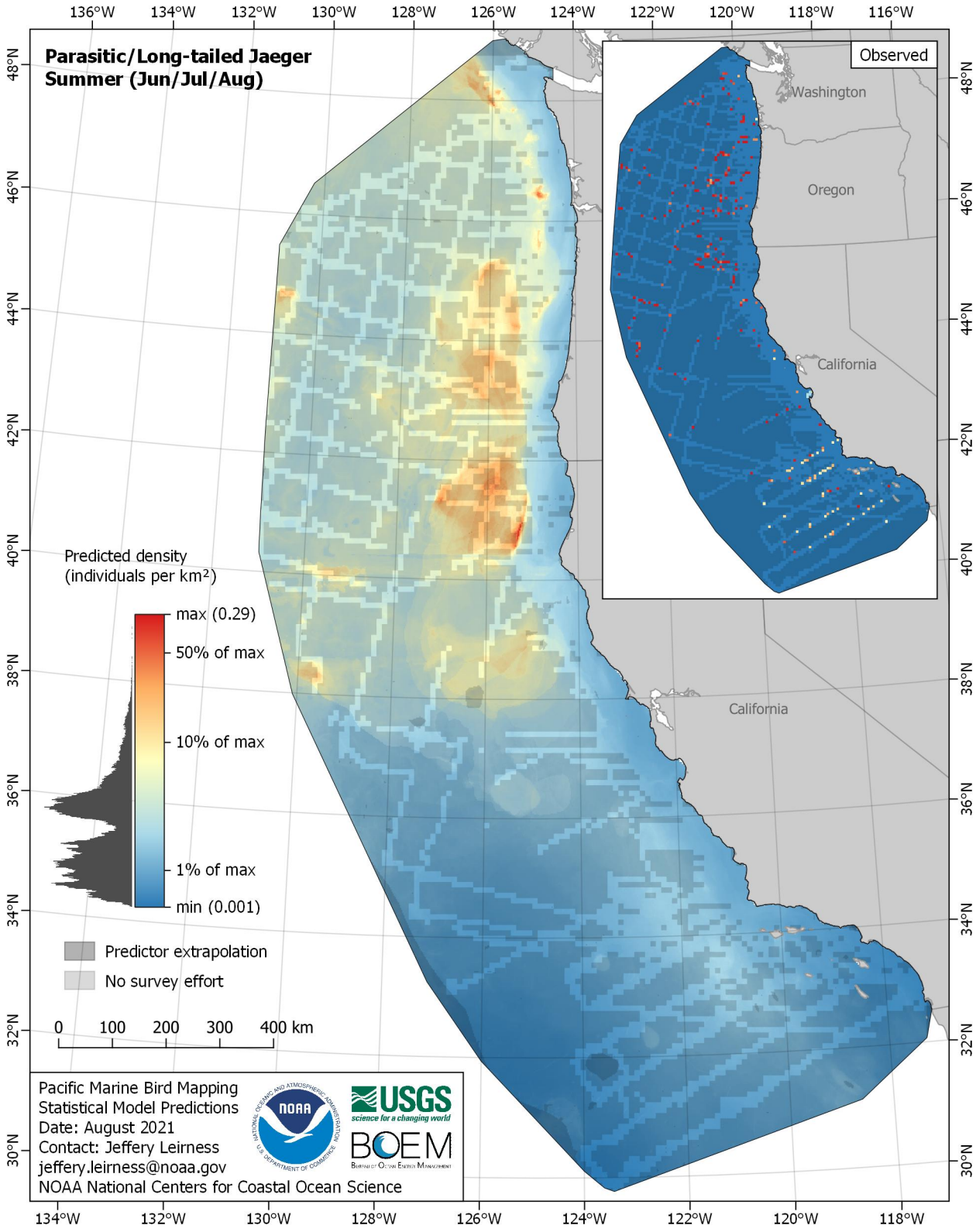

Figure E-35. Predicted density for Parasitic/Long-tailed Jaeger (Stercorarius parasiticus/longicaudus) in the summer season

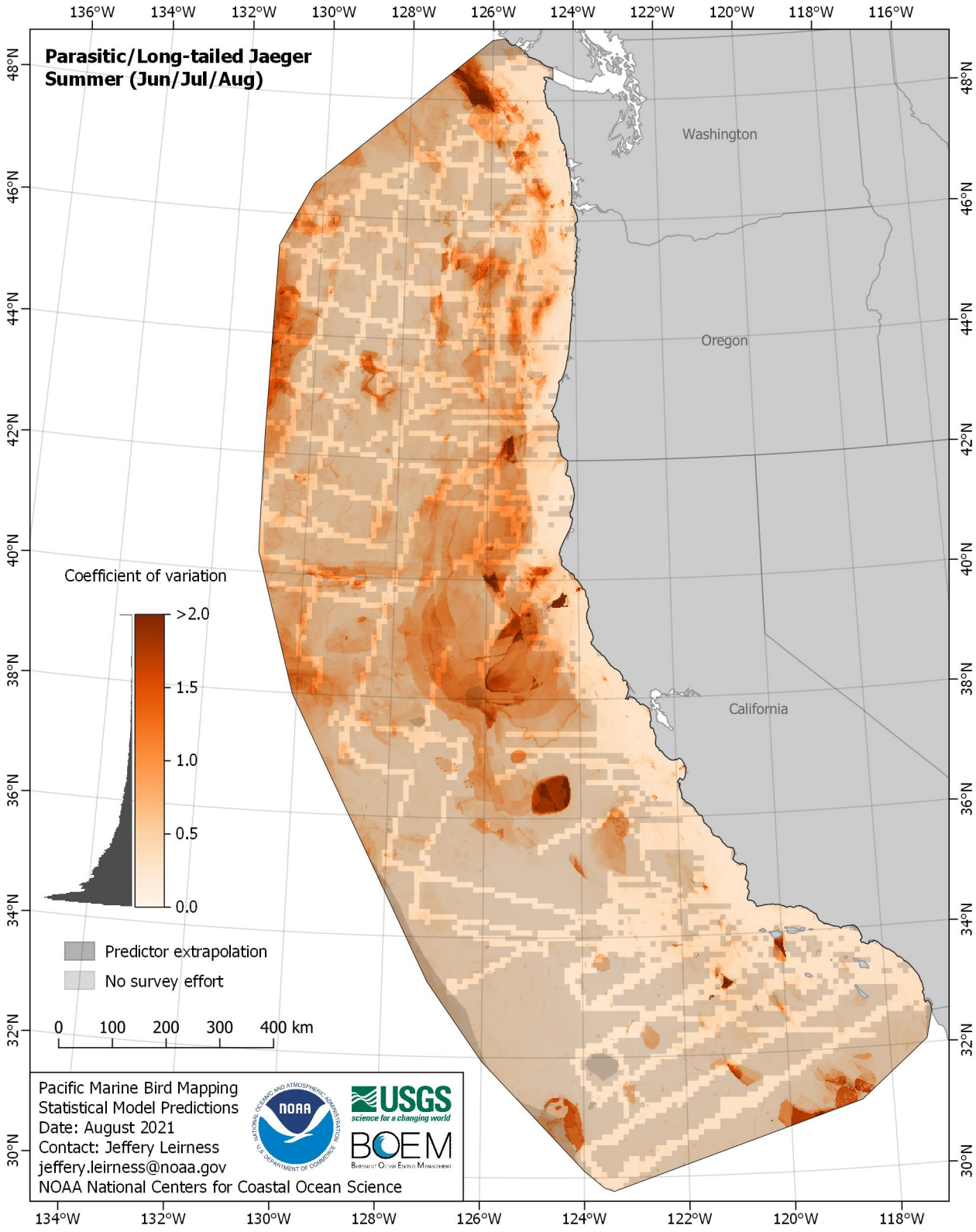

Figure E-36. Coefficient of variation for Parasitic/Long-tailed Jaeger (*Stercorarius parasiticus/longicaudus*) in the summer season

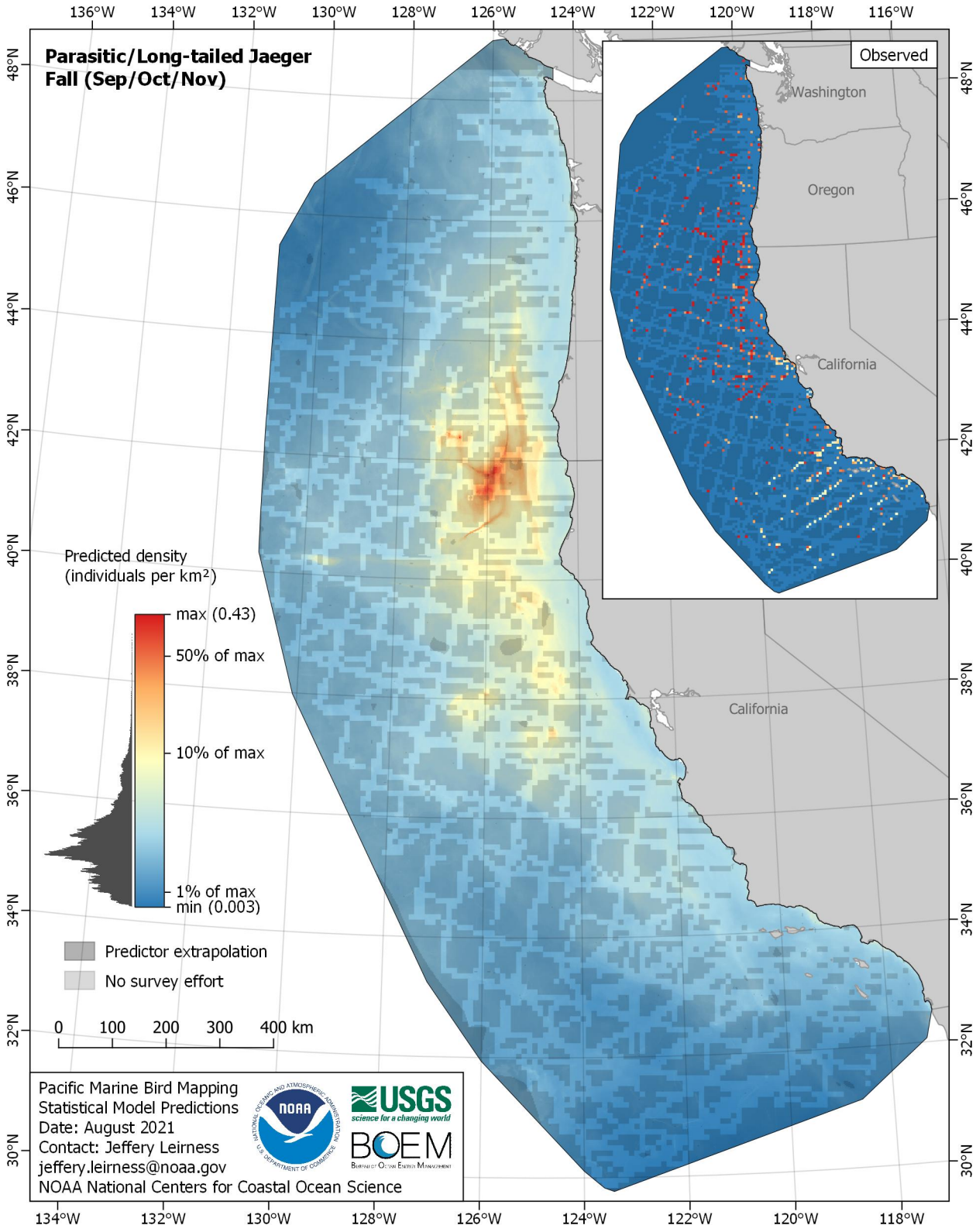

Figure E-37. Predicted density for Parasitic/Long-tailed Jaeger (*Stercorarius parasiticus/longicaudus*) in the fall season

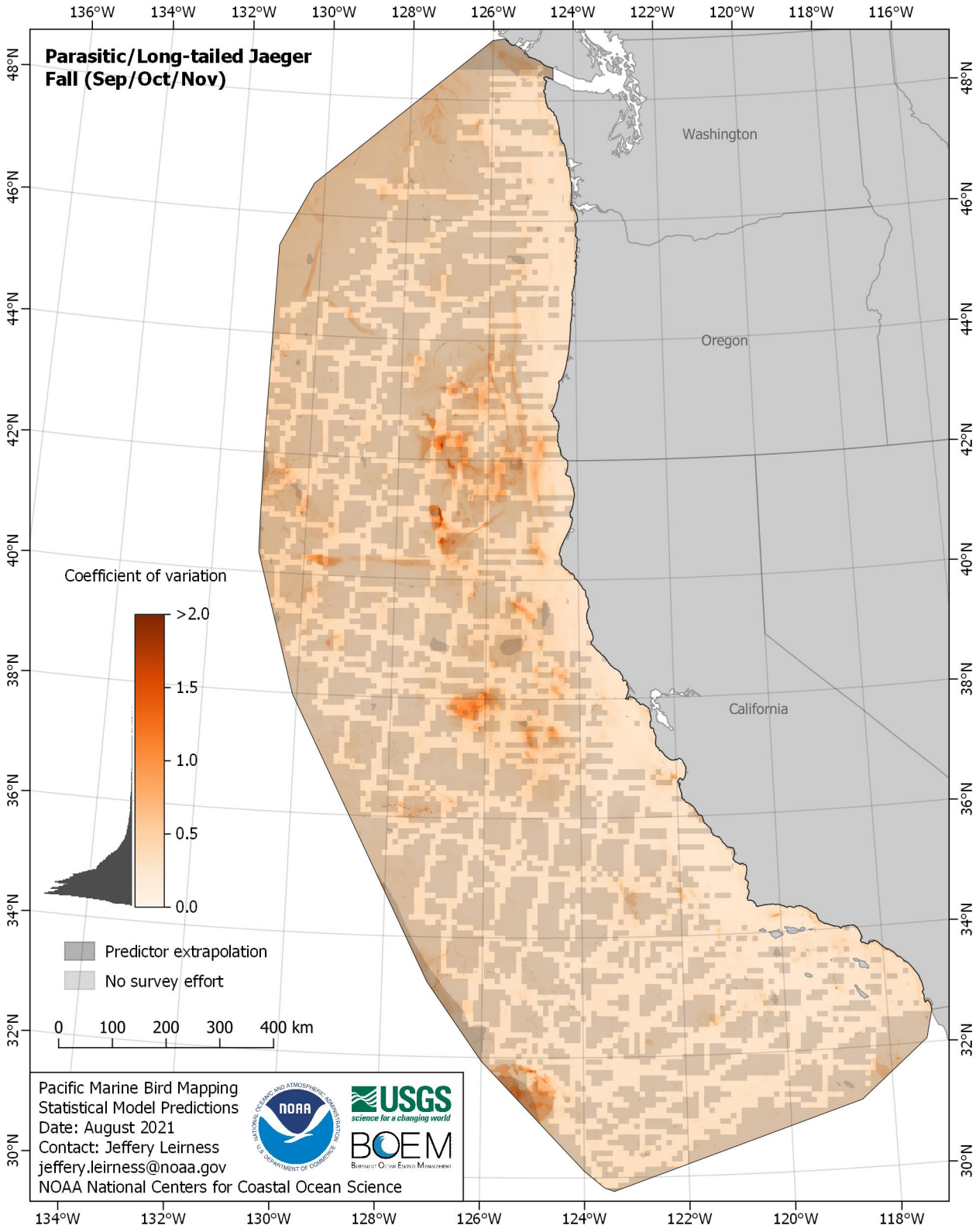

Figure E-38. Coefficient of variation for Parasitic/Long-tailed Jaeger (*Stercorarius parasiticus/longicaudus*) in the fall season

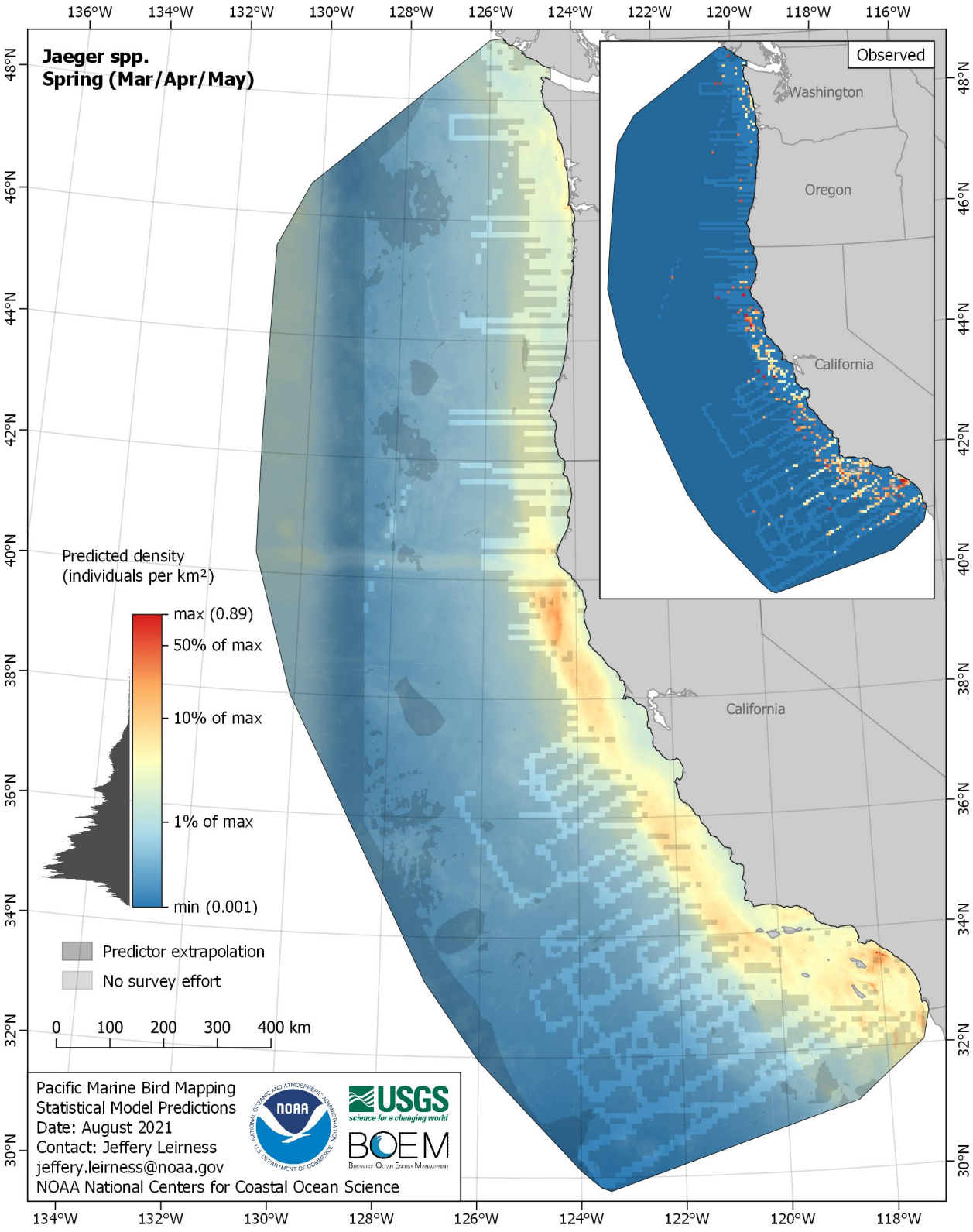

Figure E-39. Predicted density for Jaeger spp. (*Stercorarius pomarinus/parasiticus/longicaudus*) in the spring season

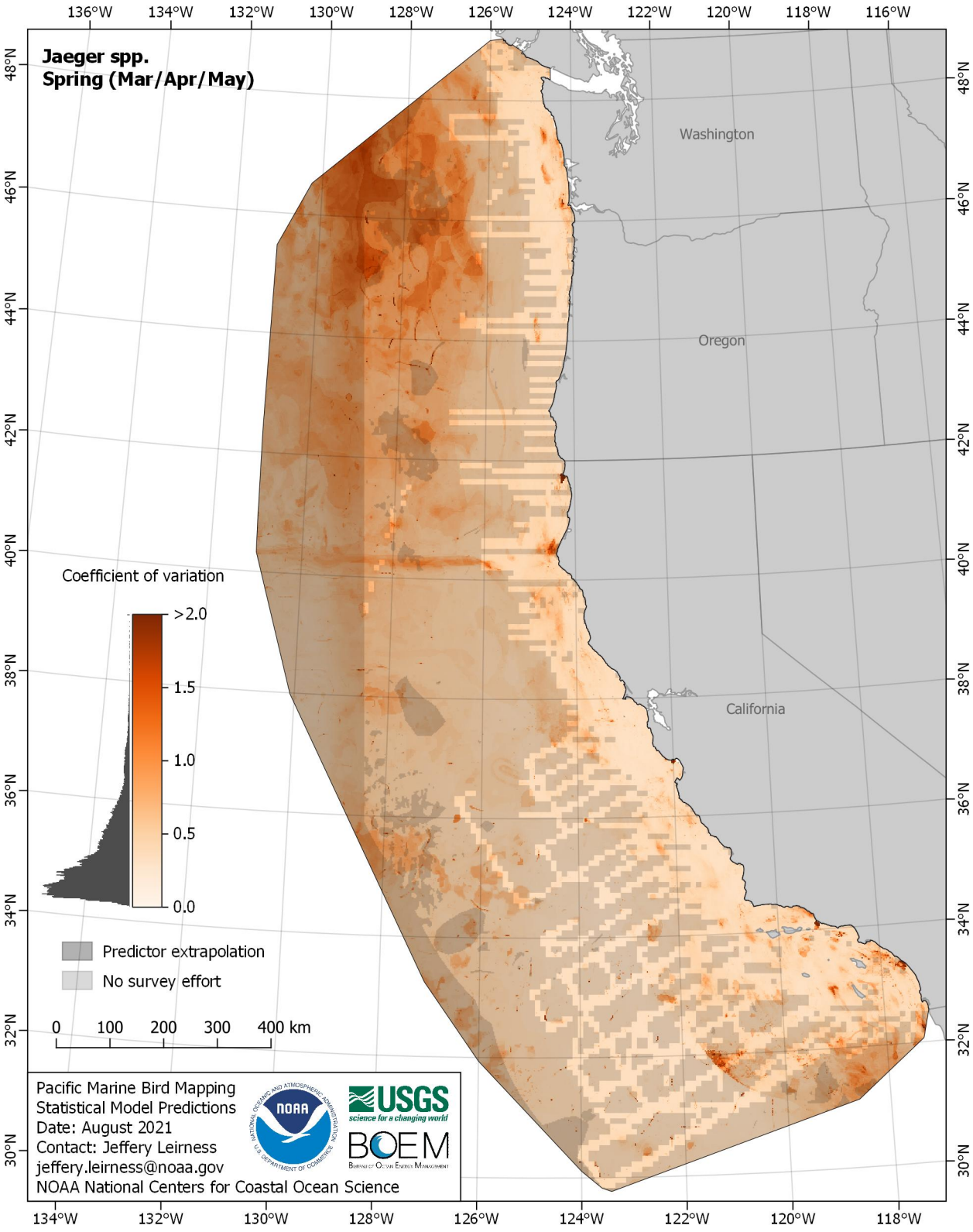

Figure E-40. Coefficient of variation for Jaeger spp. (*Stercorarius pomarinus/parasiticus/longicaudus*) in the spring season

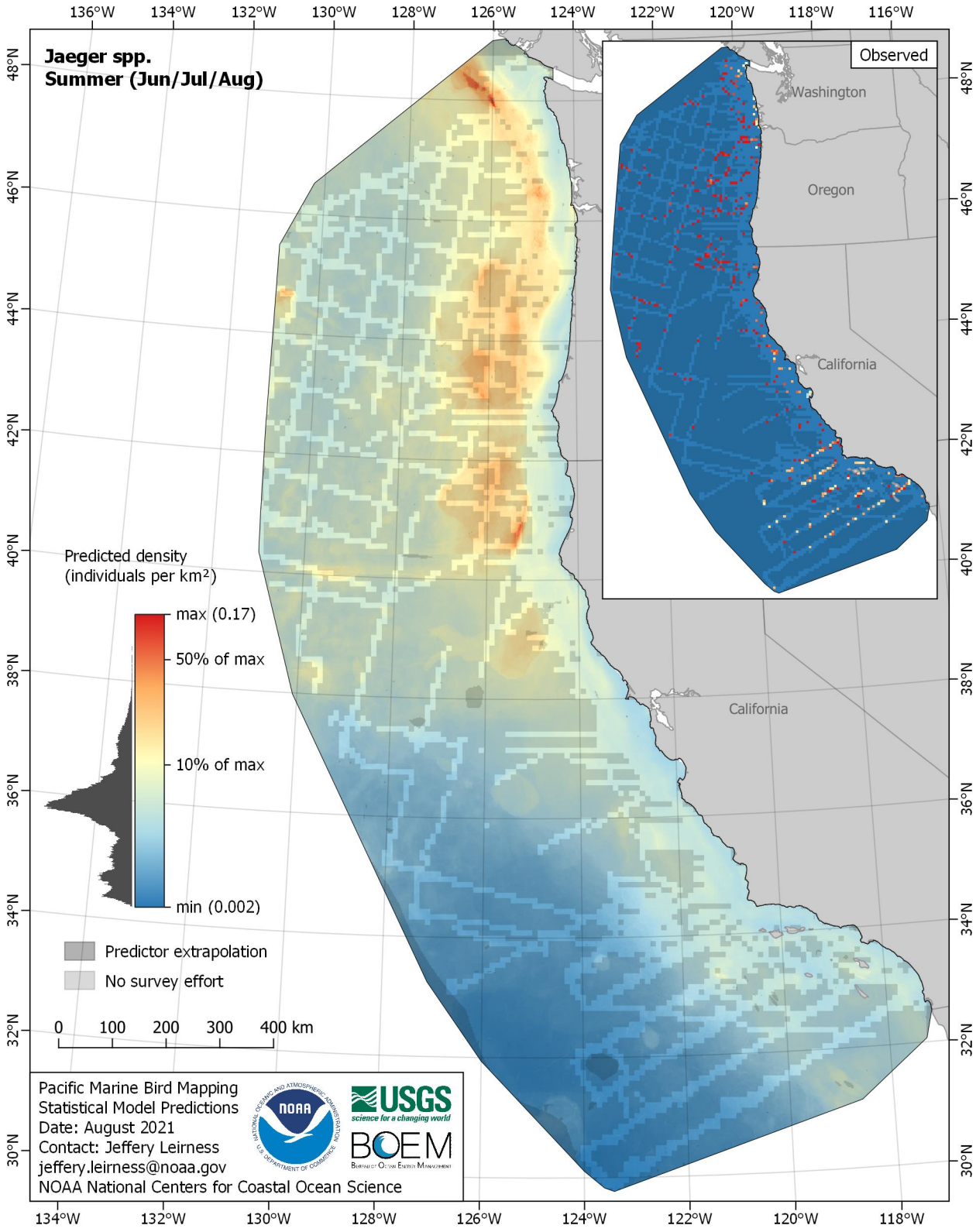

Figure E-41. Predicted density for Jaeger spp. (*Stercorarius pomarinus/parasiticus/longicaudus*) in the summer season

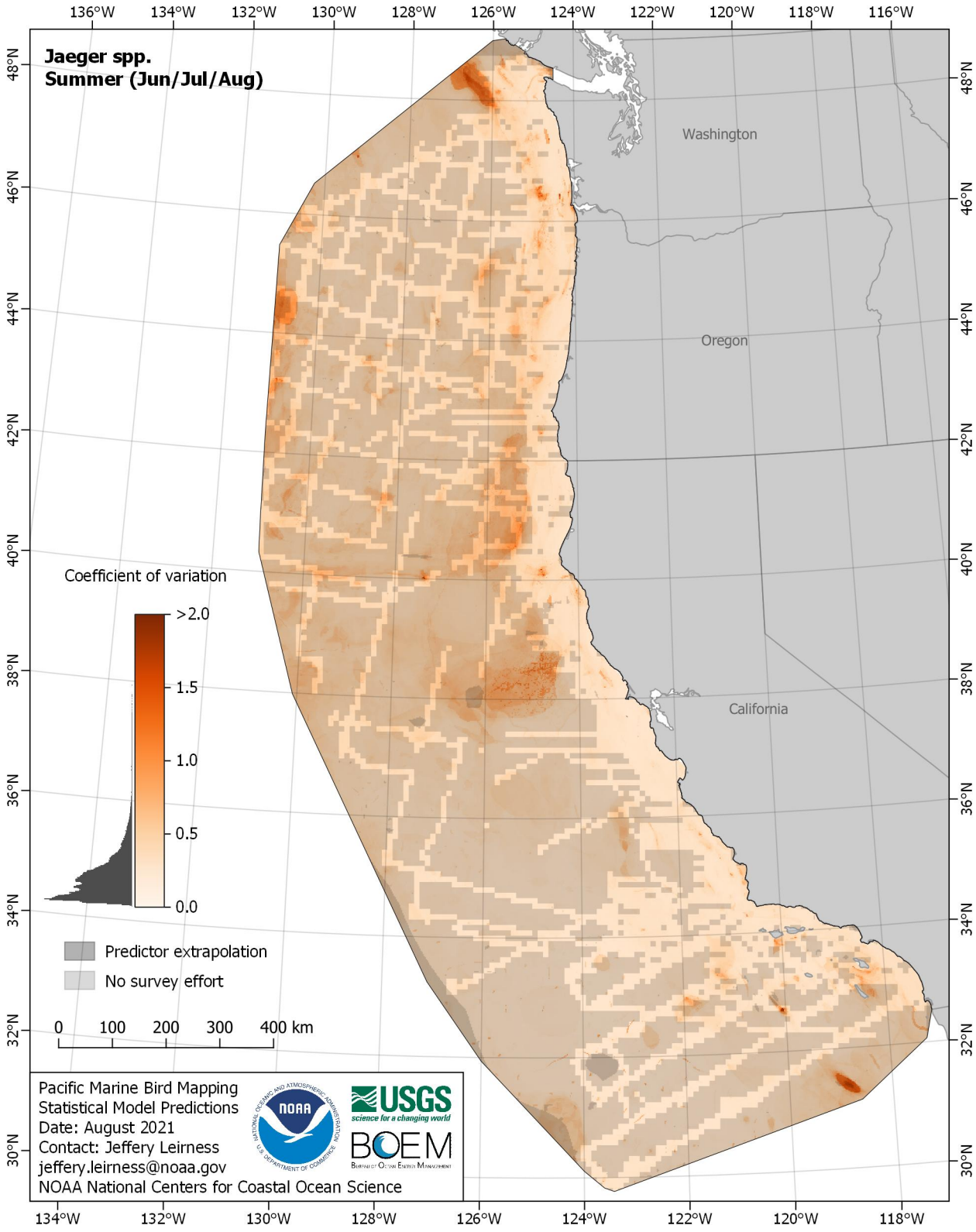

Figure E-42. Coefficient of variation for Jaeger spp. (*Stercorarius pomarinus/parasiticus/longicaudus*) in the summer season

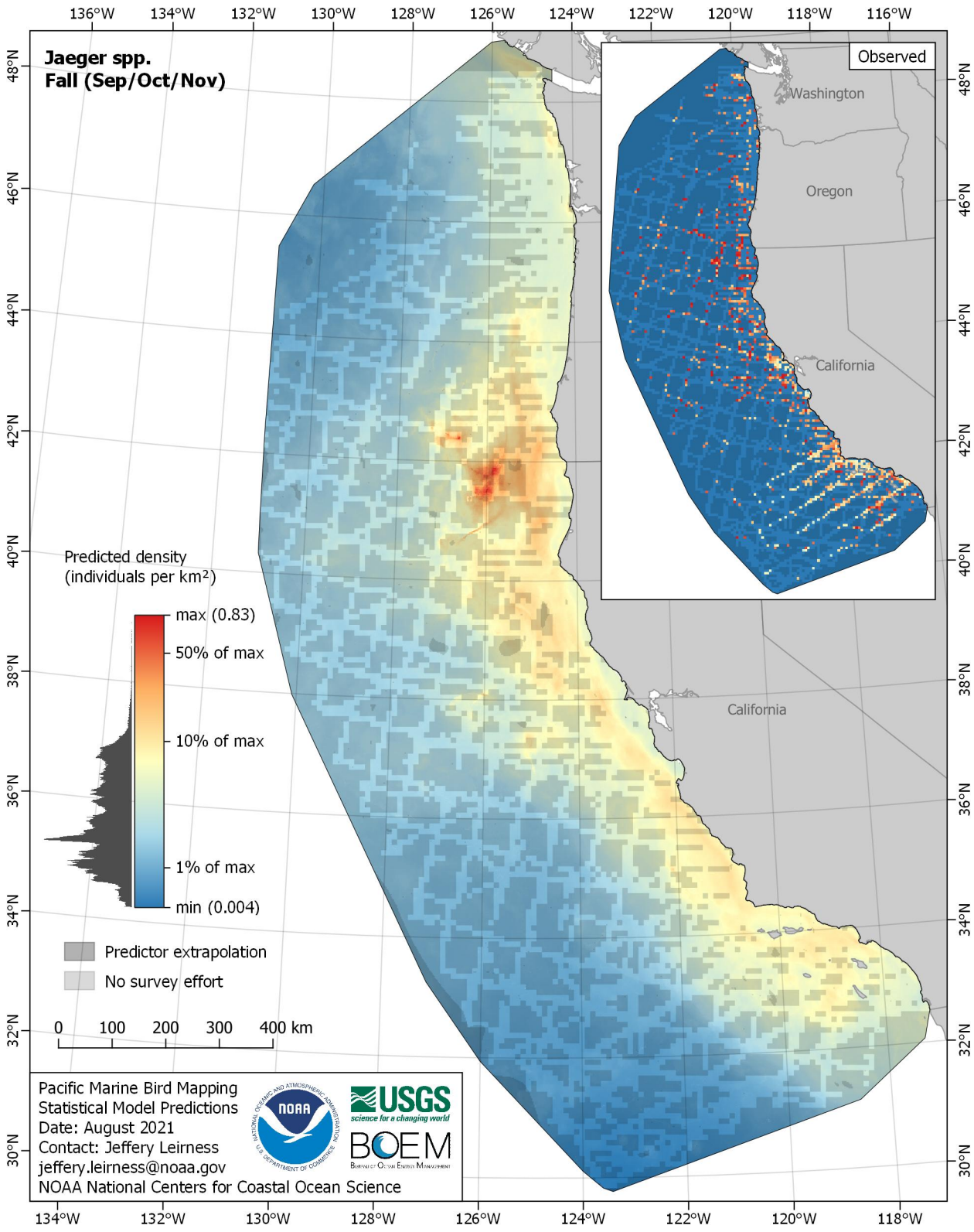

Figure E-43. Predicted density for Jaeger spp. (*Stercorarius pomarinus/parasiticus/longicaudus*) in the fall season

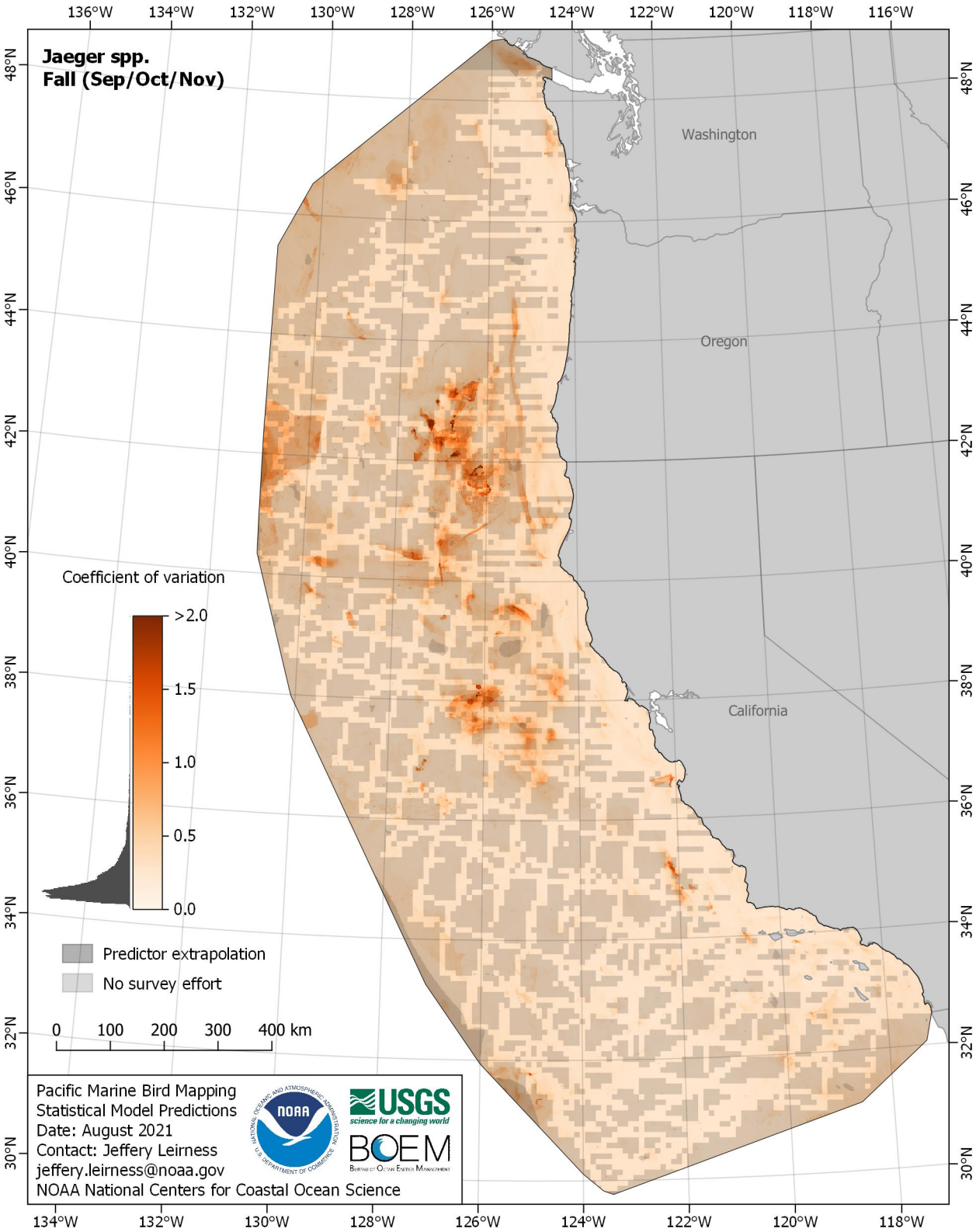

Figure E-44. Coefficient of variation for Jaeger spp. (*Stercorarius pomarinus/parasiticus/longicaudus*) in the fall season

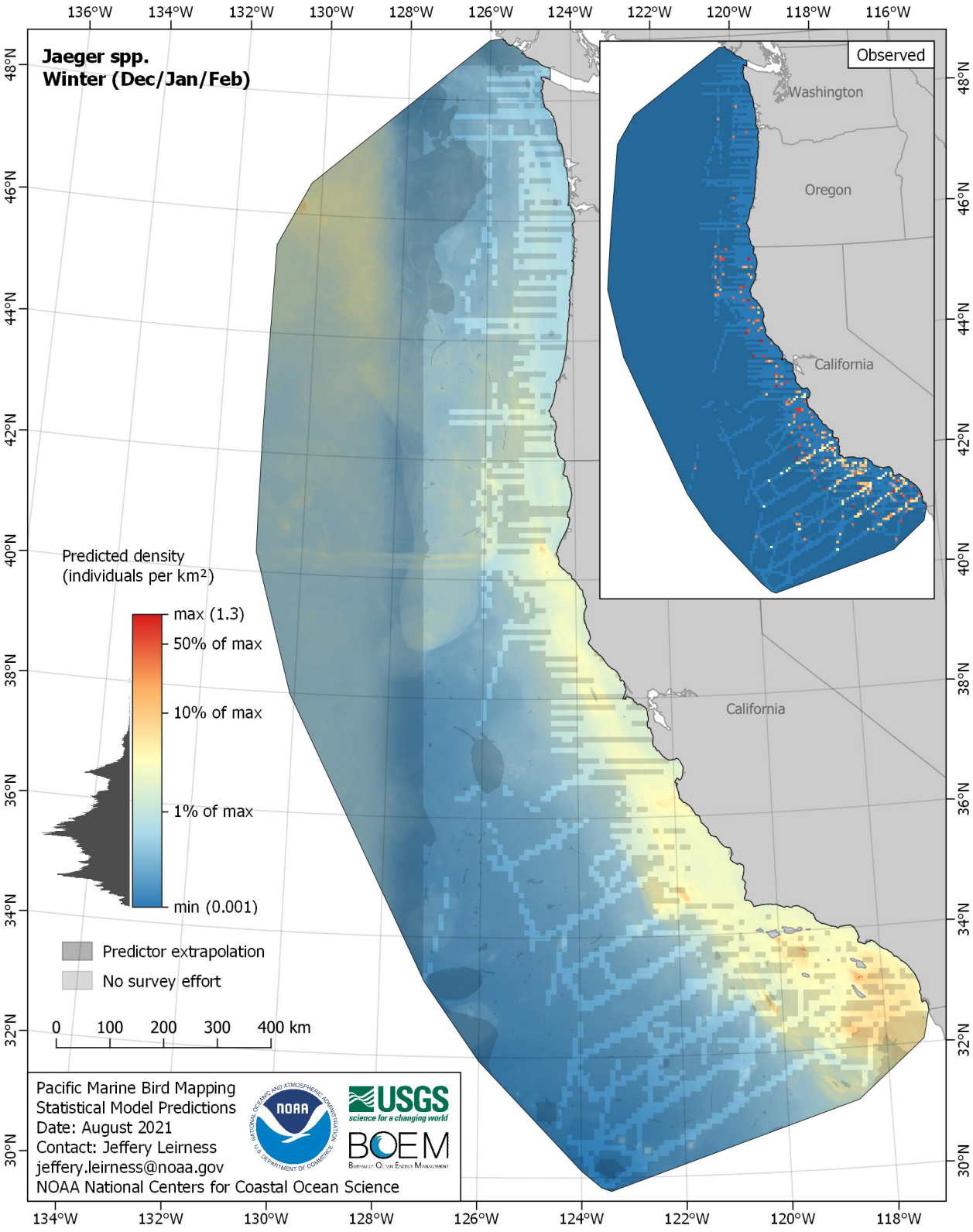

Figure E-45. Predicted density for Jaeger spp. (*Stercorarius pomarinus/parasiticus/longicaudus*) in the winter season

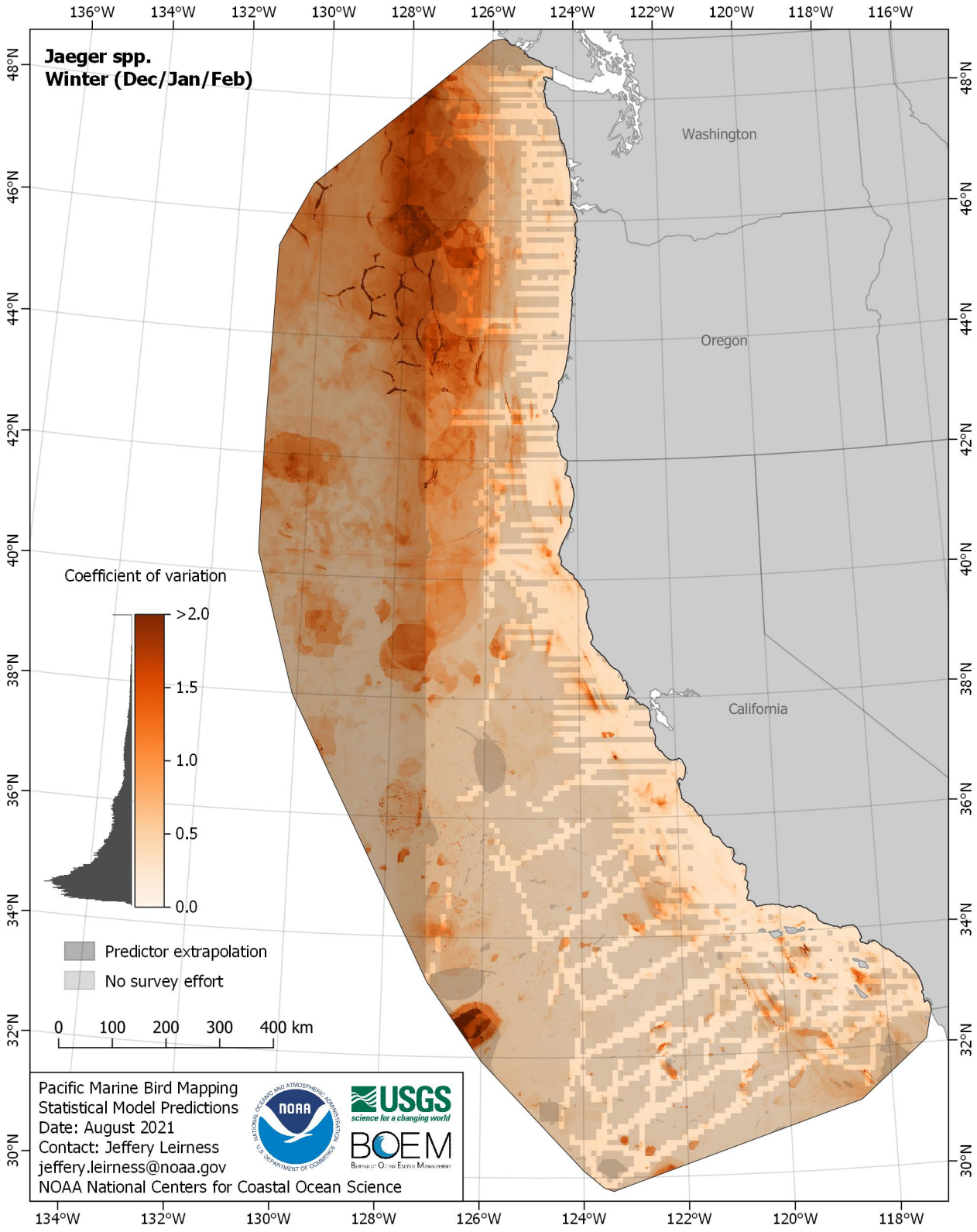

Figure E-46. Coefficient of variation for Jaeger spp. (*Stercorarius pomarinus/parasiticus/longicaudus*) in the winter season

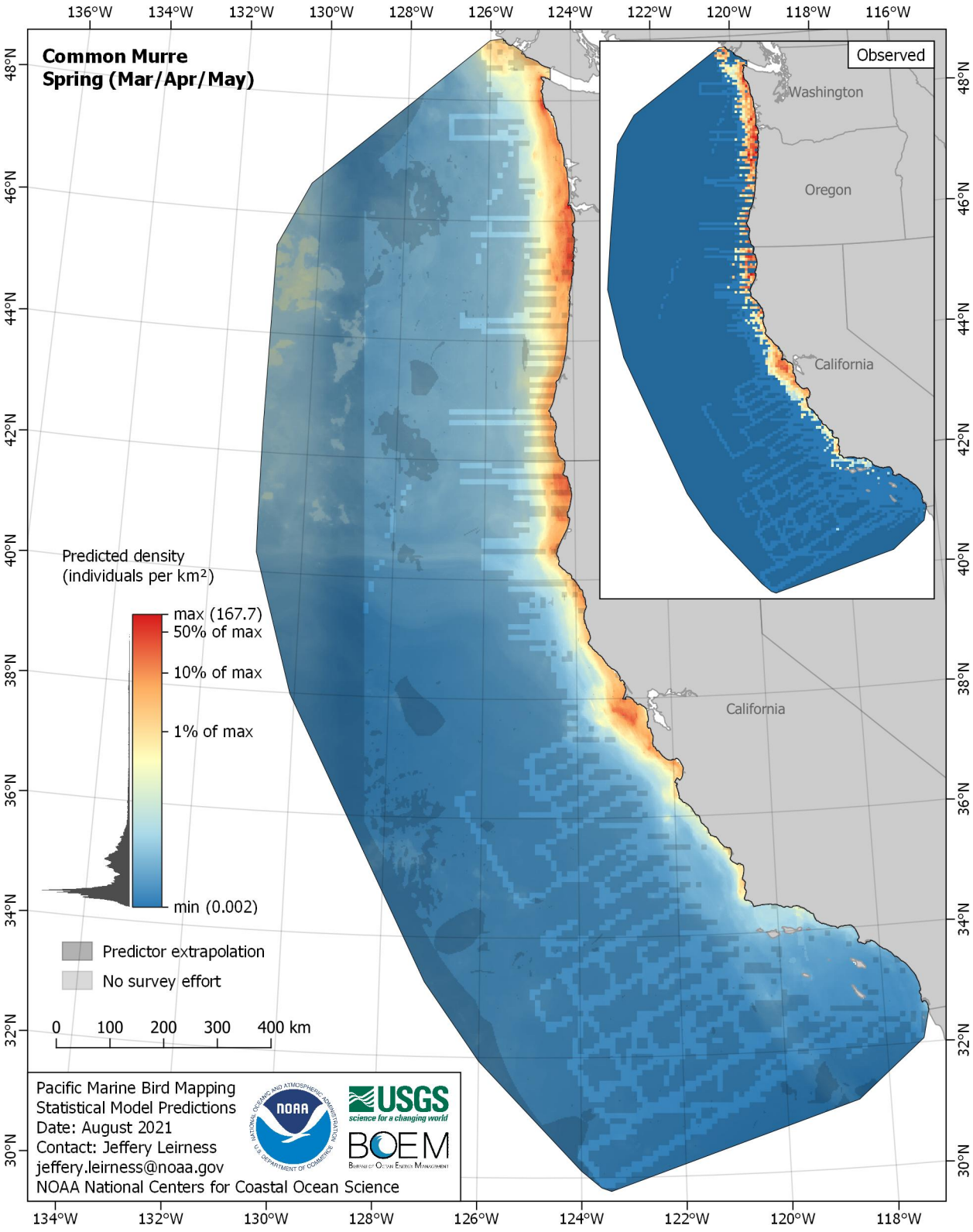

Figure E-47. Predicted density for Common Murre (*Uria aalge*) in the spring season

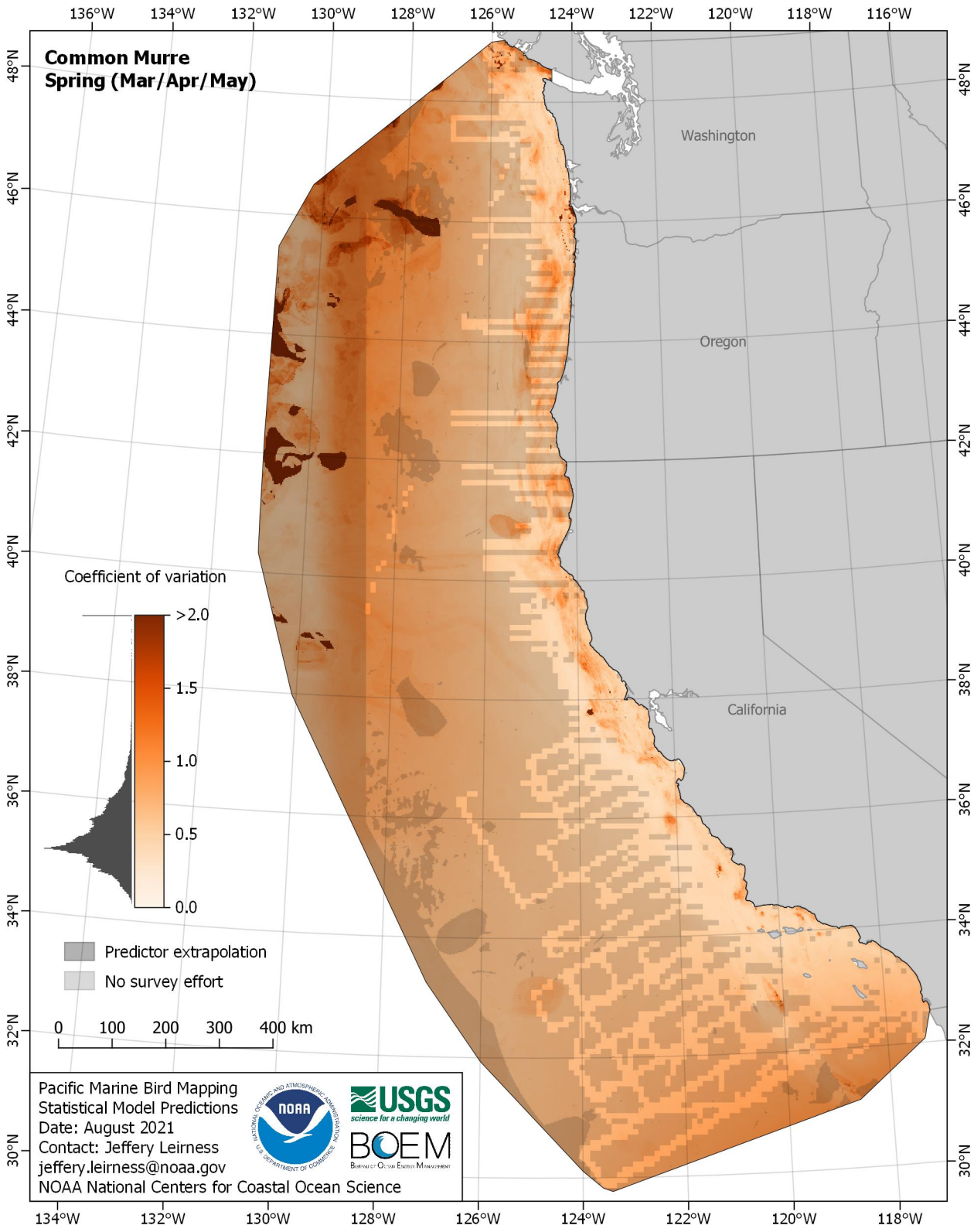

Figure E-48. Coefficient of variation for Common Murre (*Uria aalge*) in the spring season

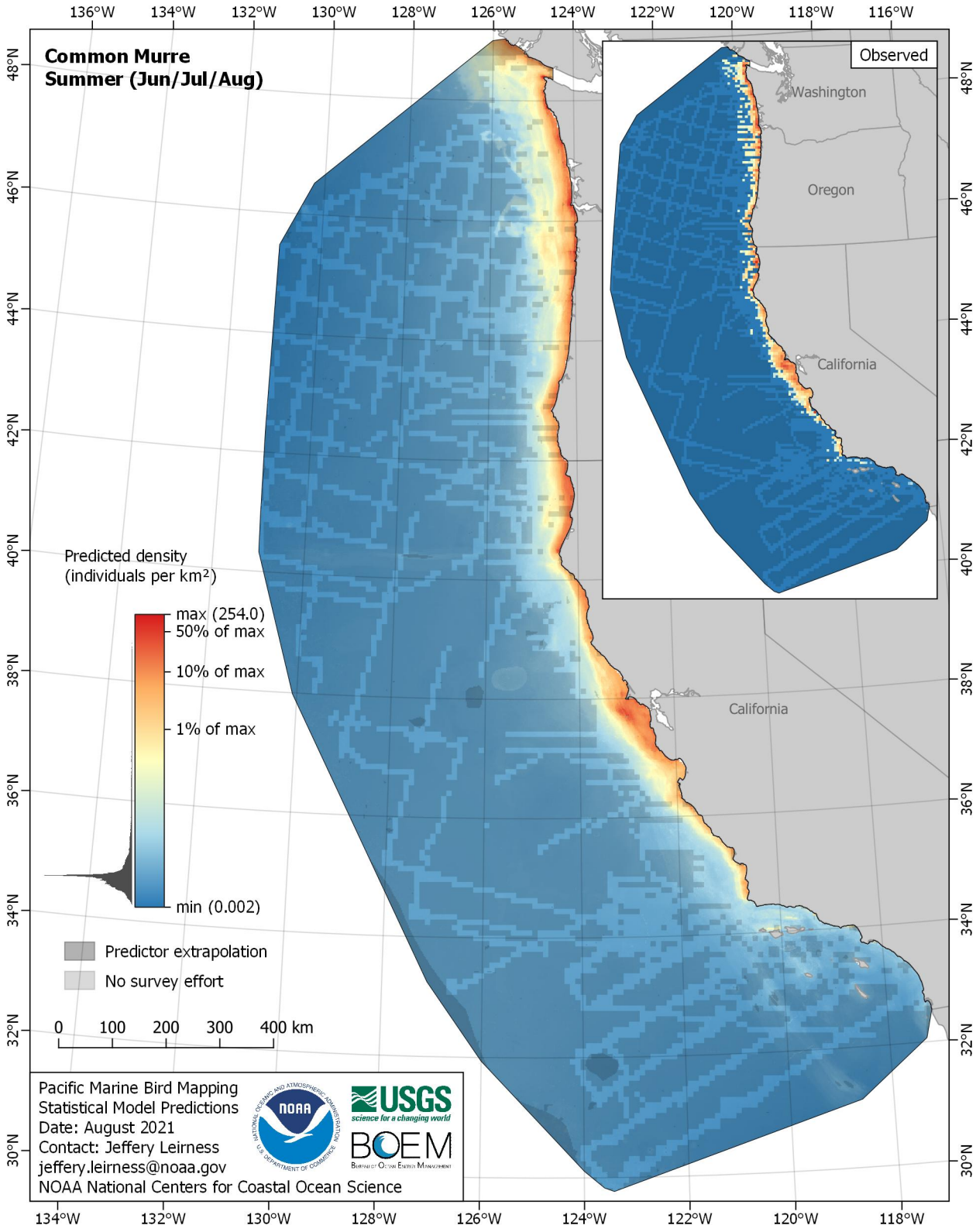

Figure E-49. Predicted density for Common Murre (*Uria aalge*) in the summer season

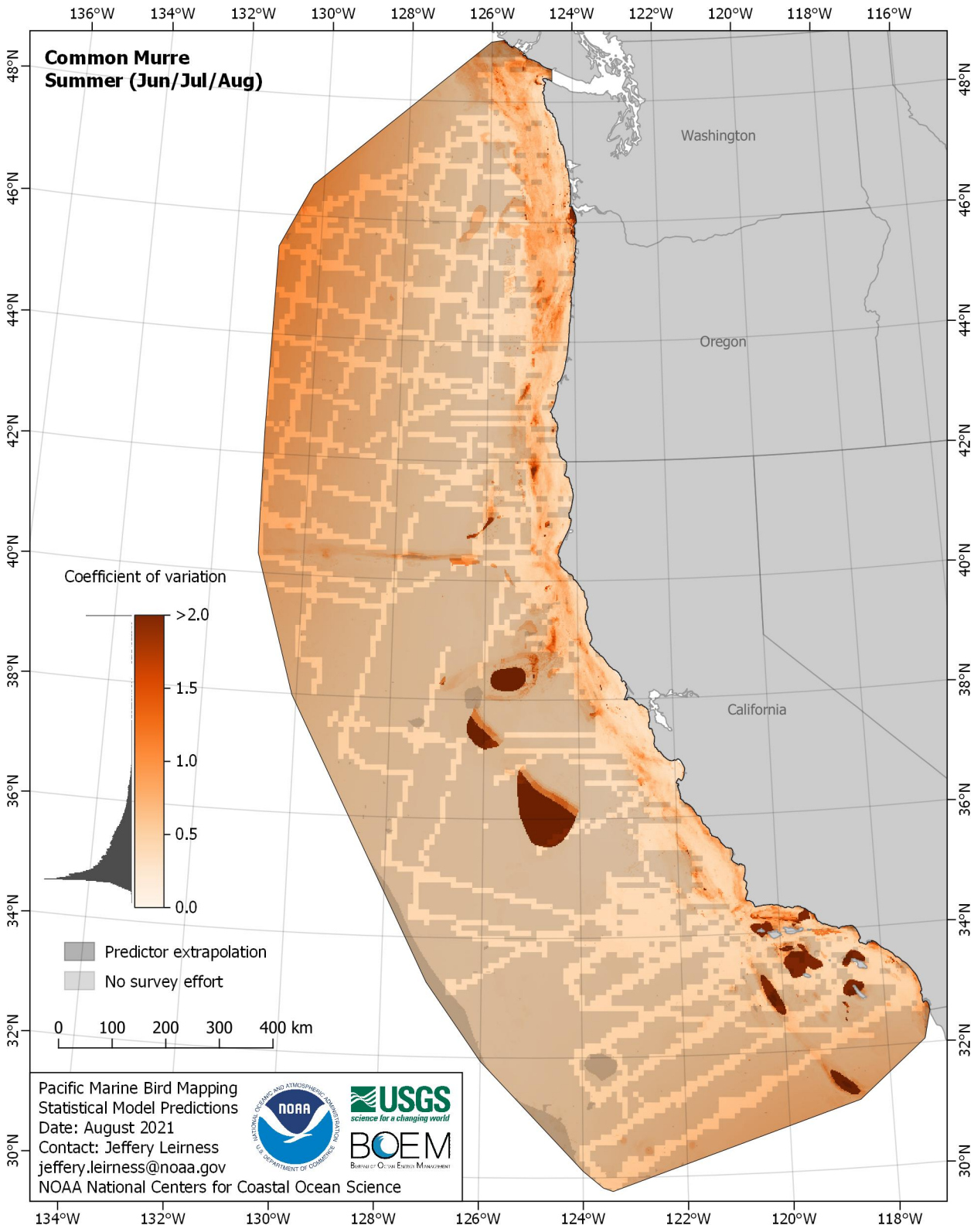

Figure E-50. Coefficient of variation for Common Murre (*Uria aalge*) in the summer season

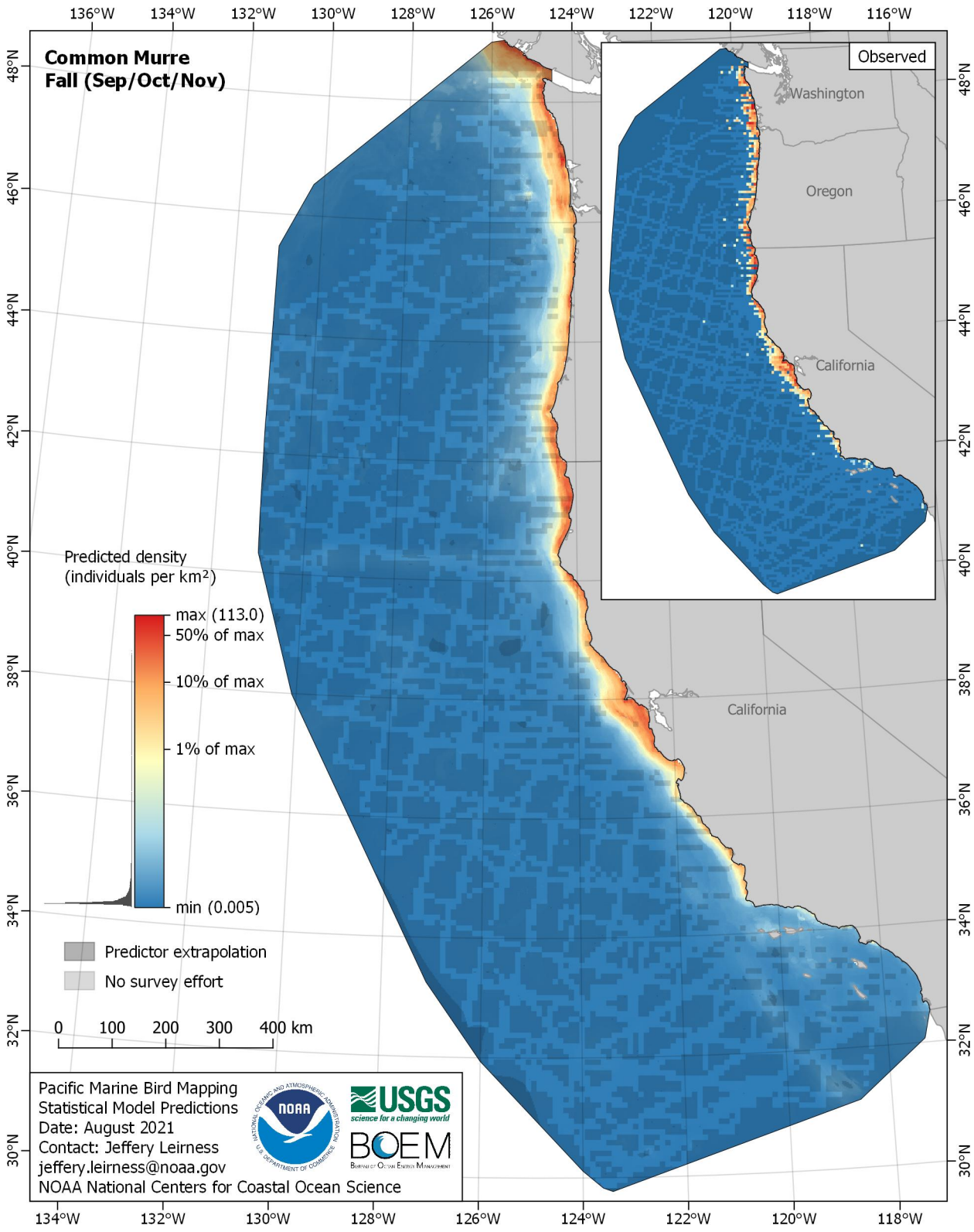

Figure E-51. Predicted density for Common Murre (*Uria aalge*) in the fall season

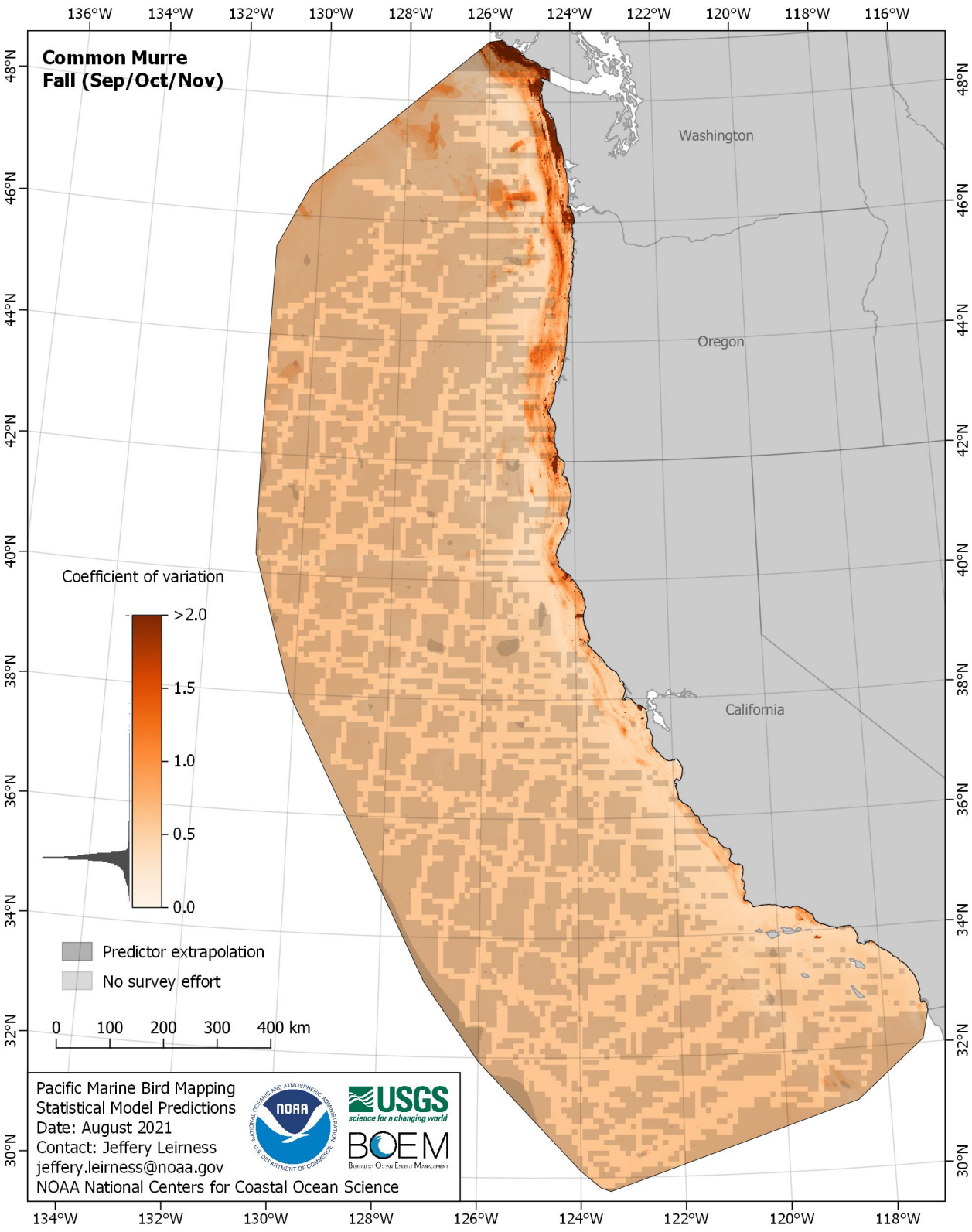

Figure E-52. Coefficient of variation for Common Murre (*Uria aalge*) in the fall season

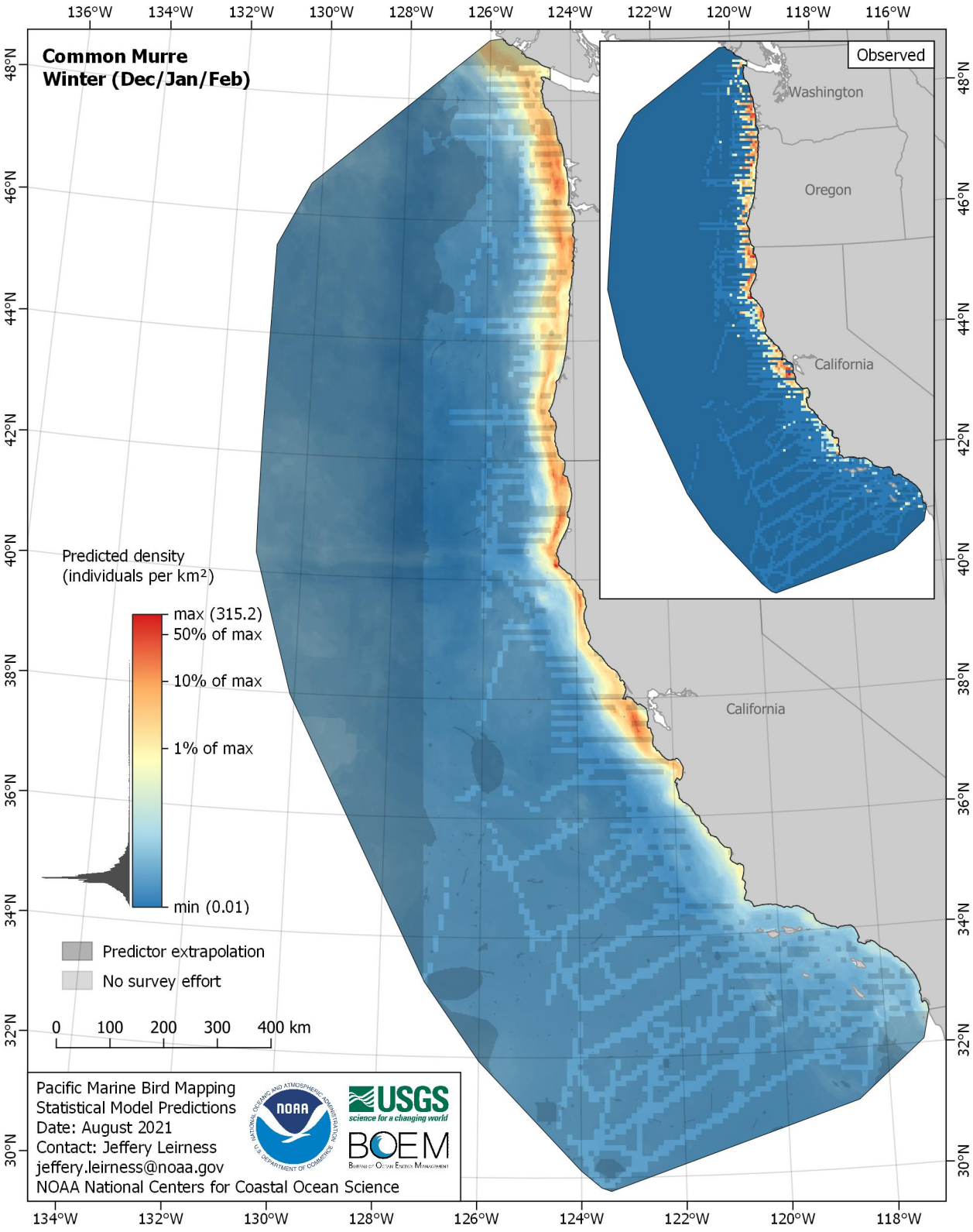

Figure E-53. Predicted density for Common Murre (*Uria aalge*) in the winter season

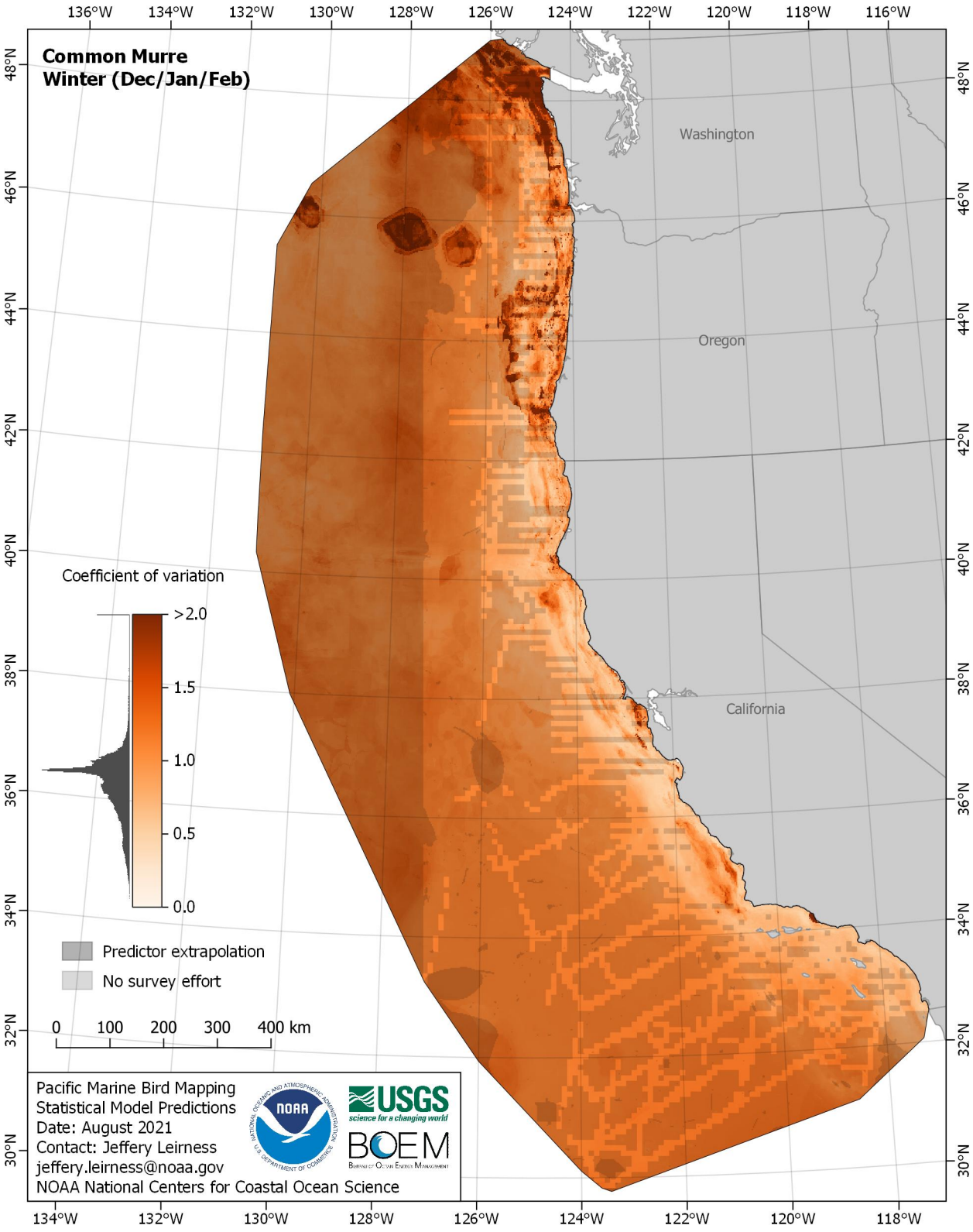

Figure E-54. Coefficient of variation for Common Murre (*Uria aalge*) in the winter season

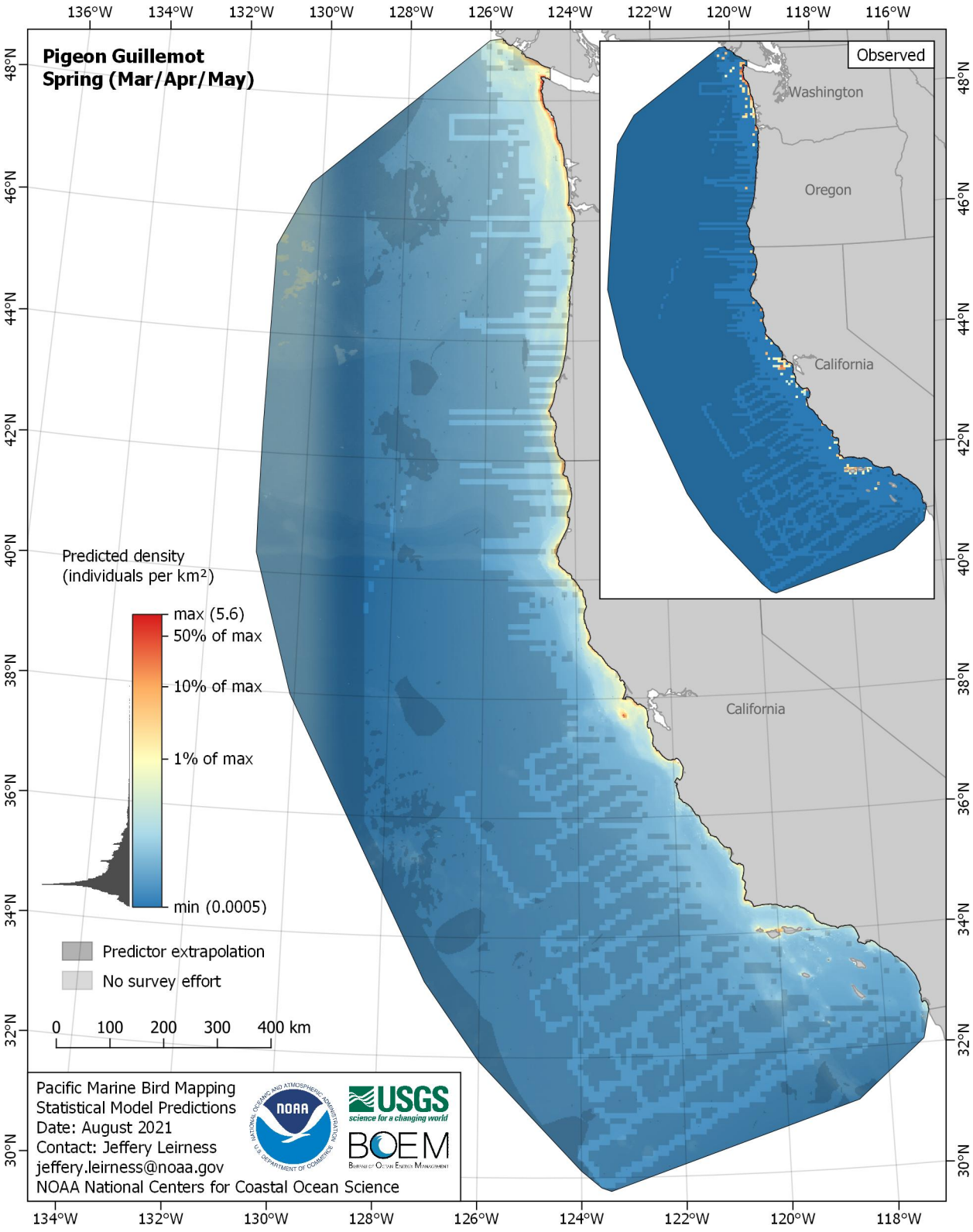

Figure E-55. Predicted density for Pigeon Guillemot (*Cepphus columba*) in the spring season

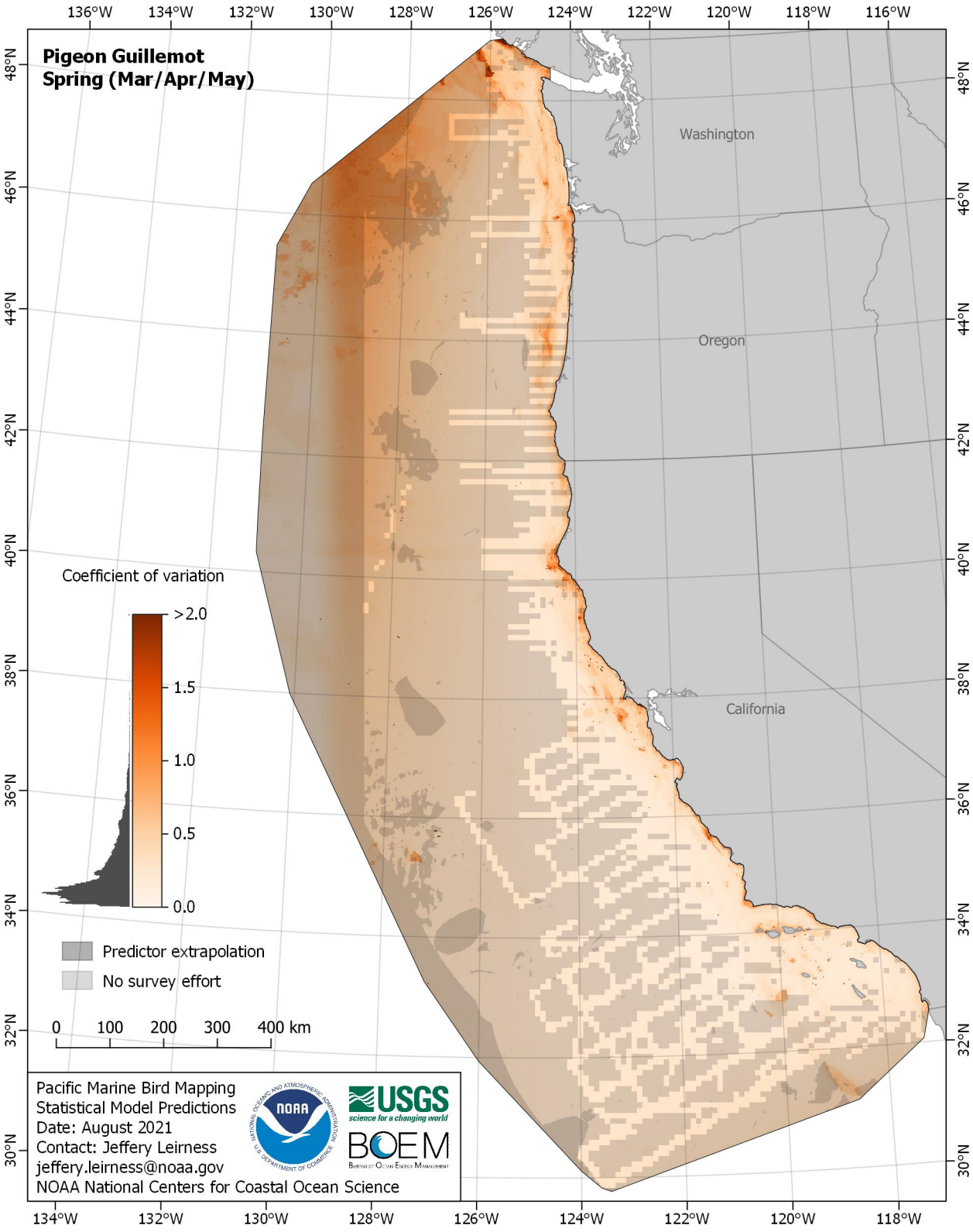

Figure E-56. Coefficient of variation for Pigeon Guillemot (*Cepphus columba*) in the spring season

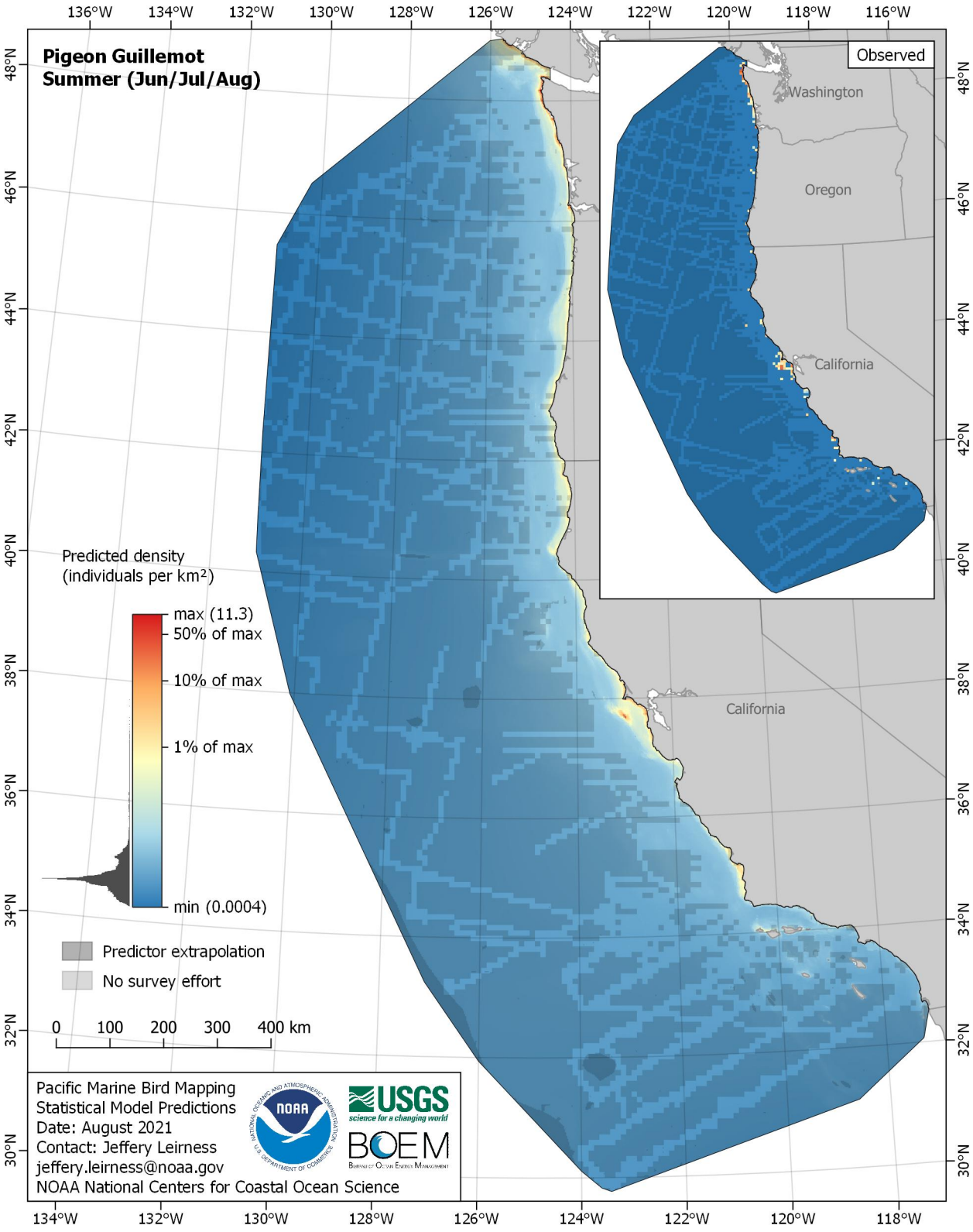

Figure E-57. Predicted density for Pigeon Guillemot (*Cepphus columba*) in the summer season

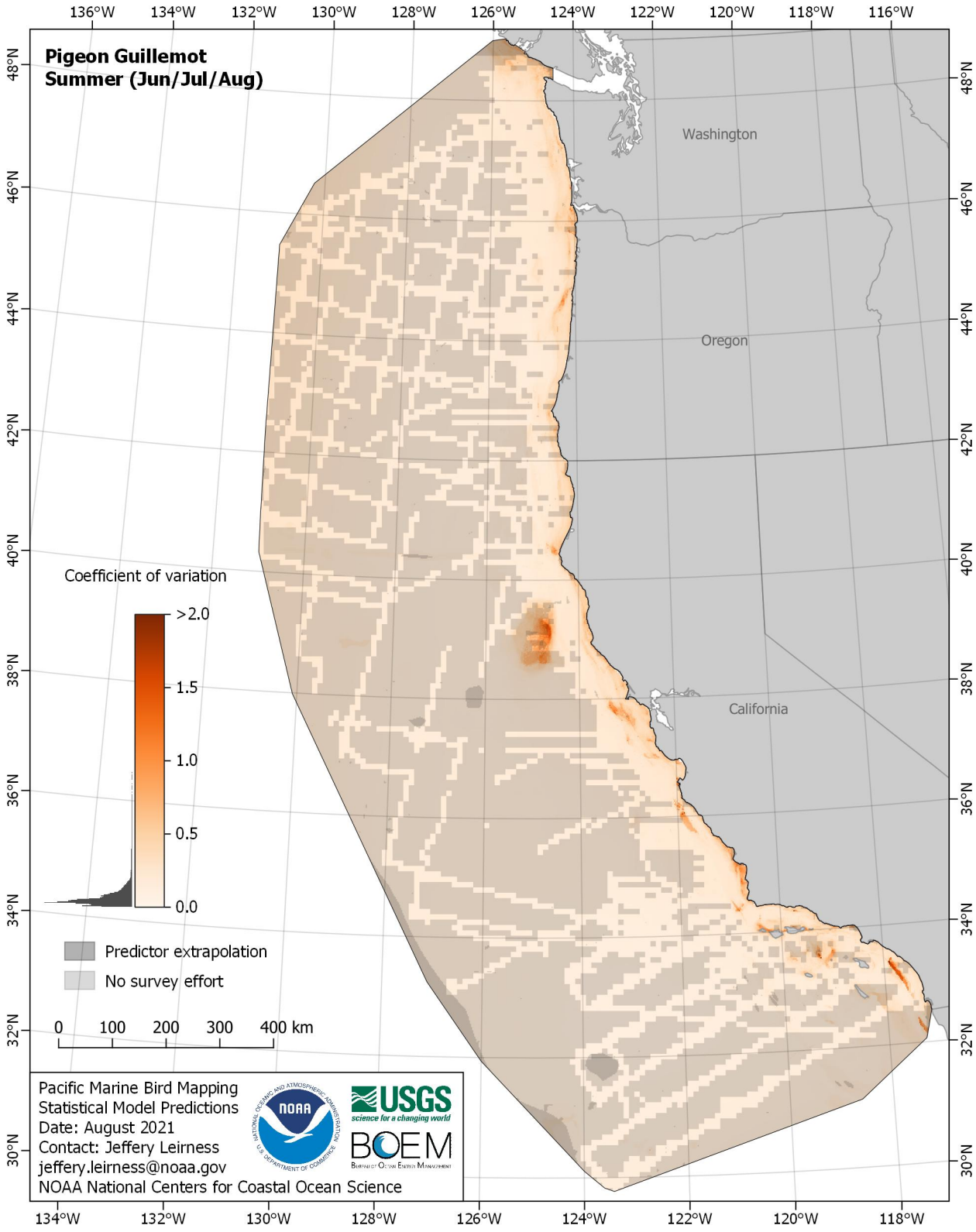

Figure E-58. Coefficient of variation for Pigeon Guillemot (*Cepphus columba*) in the summer season

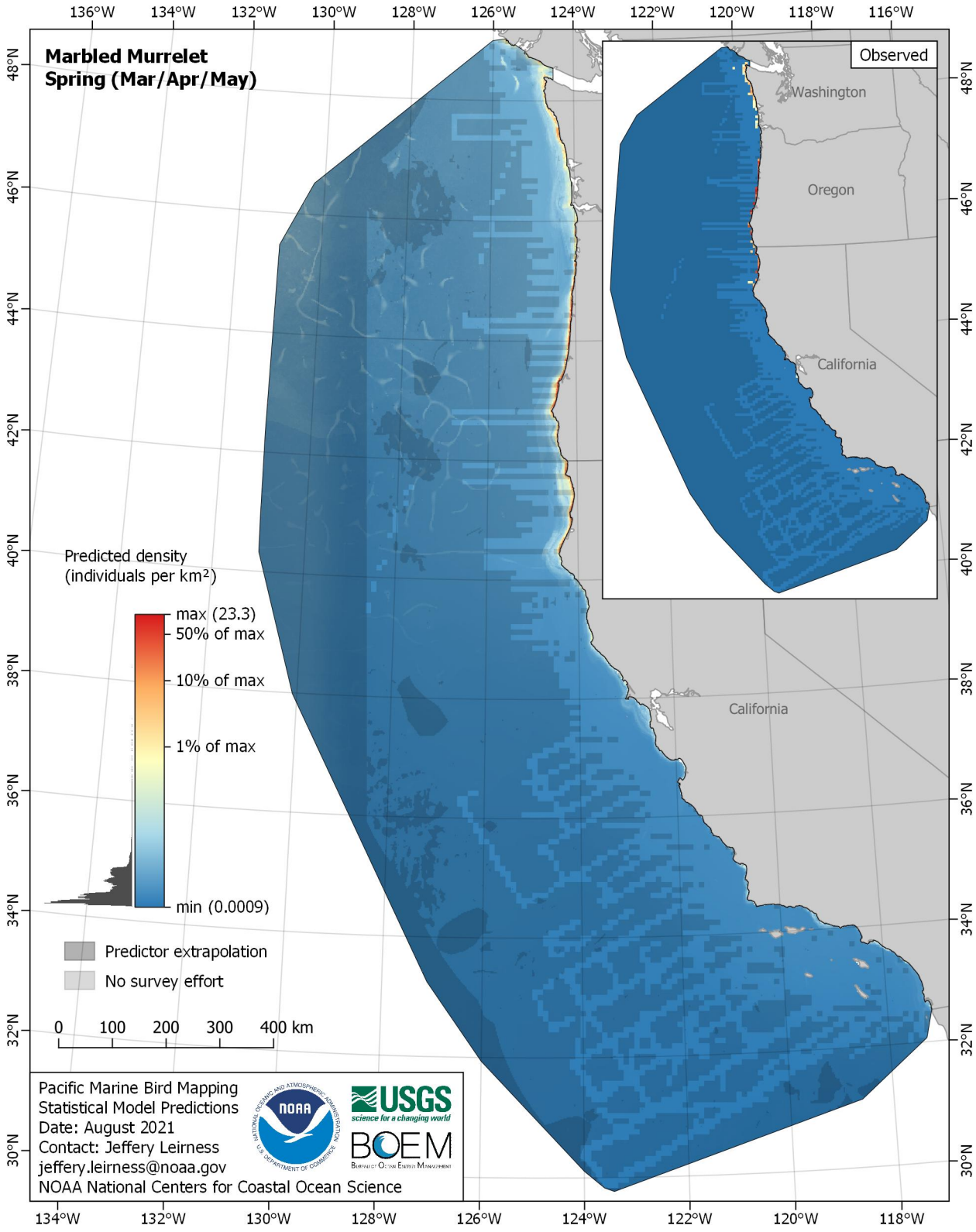

Figure E-59. Predicted density for Marbled Murrelet (*Brachyramphus marmoratus*) in the spring season

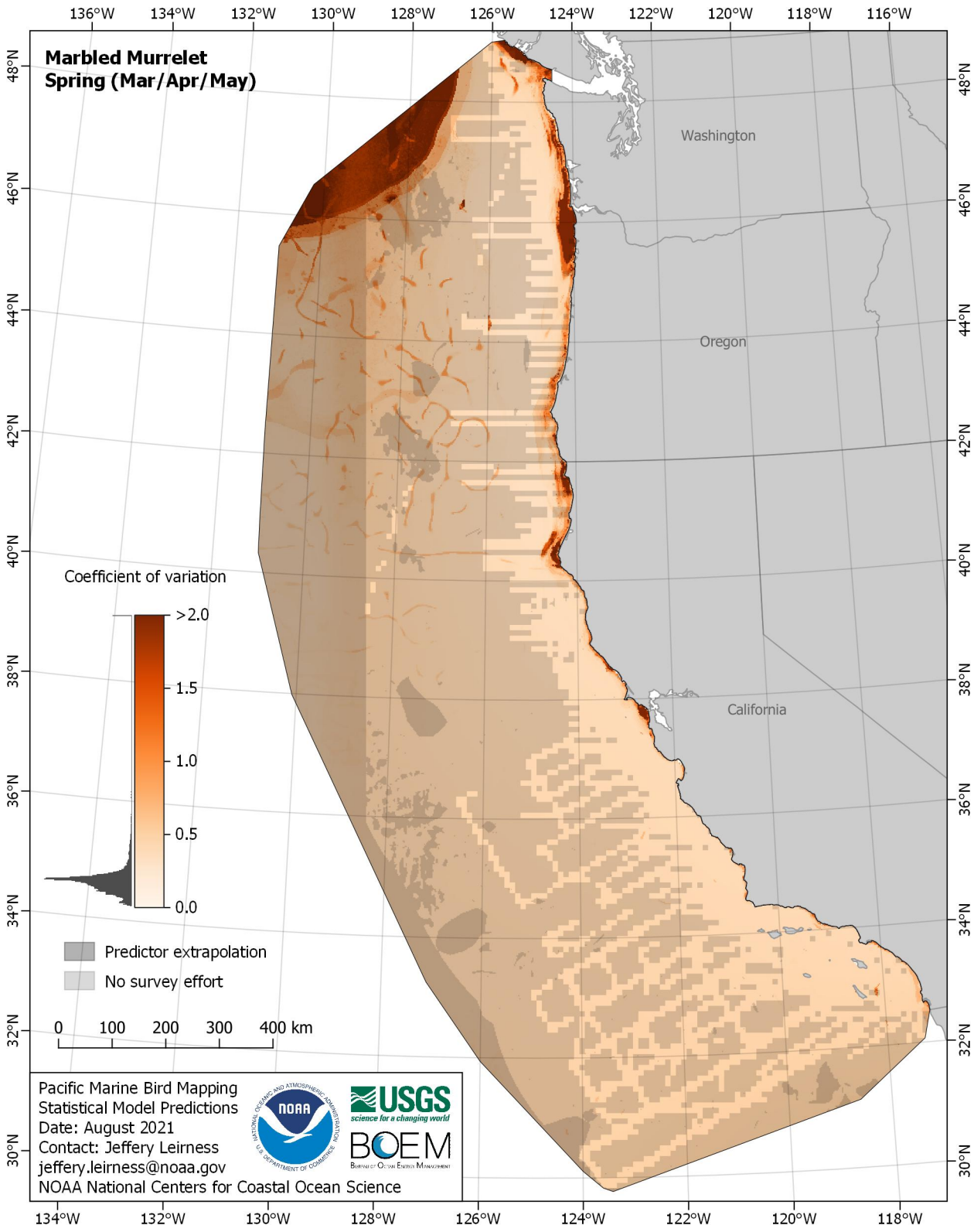

Figure E-60. Coefficient of variation for Marbled Murrelet (*Brachyramphus marmoratus*) in the spring season

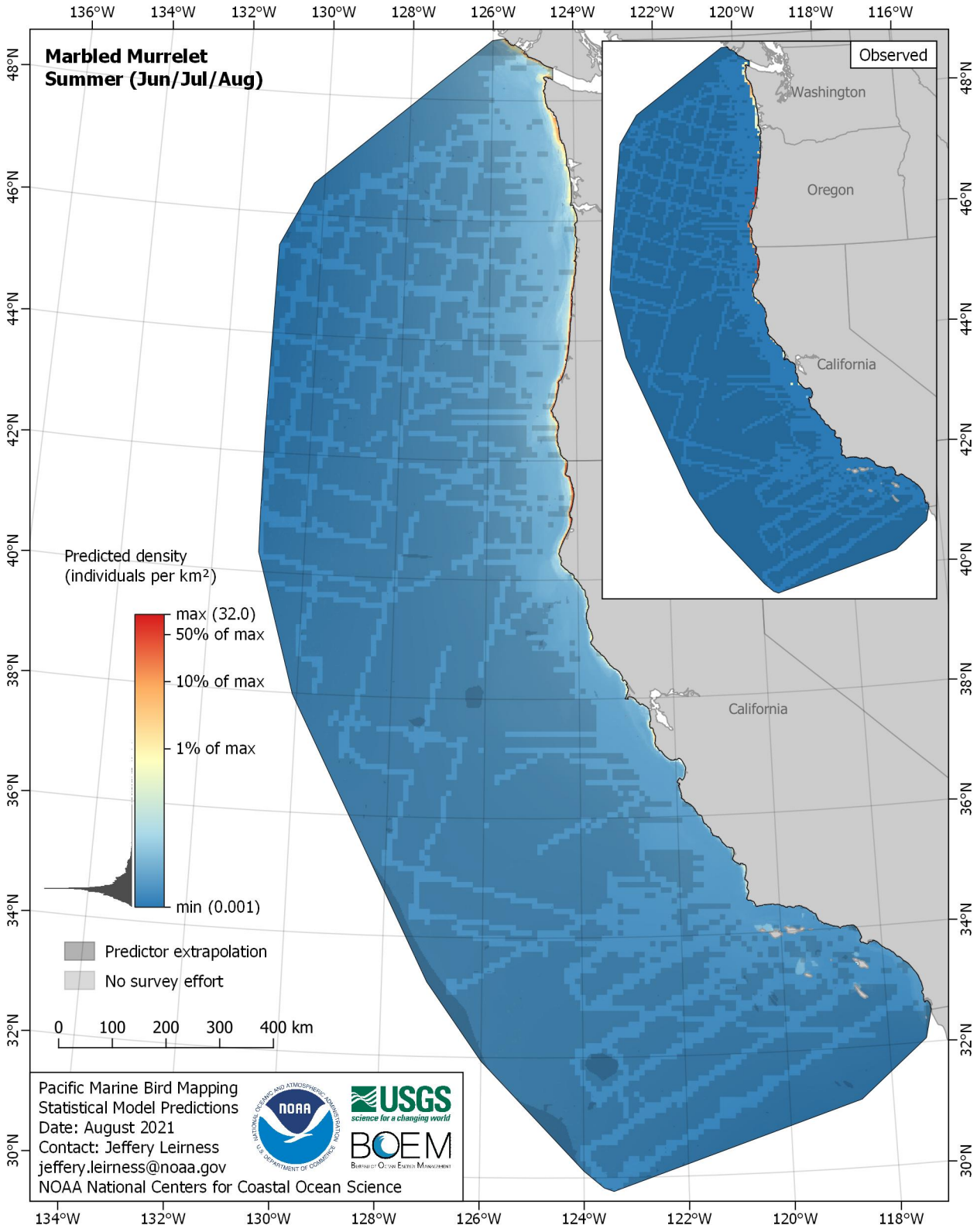

Figure E-61. Predicted density for Marbled Murrelet (*Brachyramphus marmoratus*) in the summer season

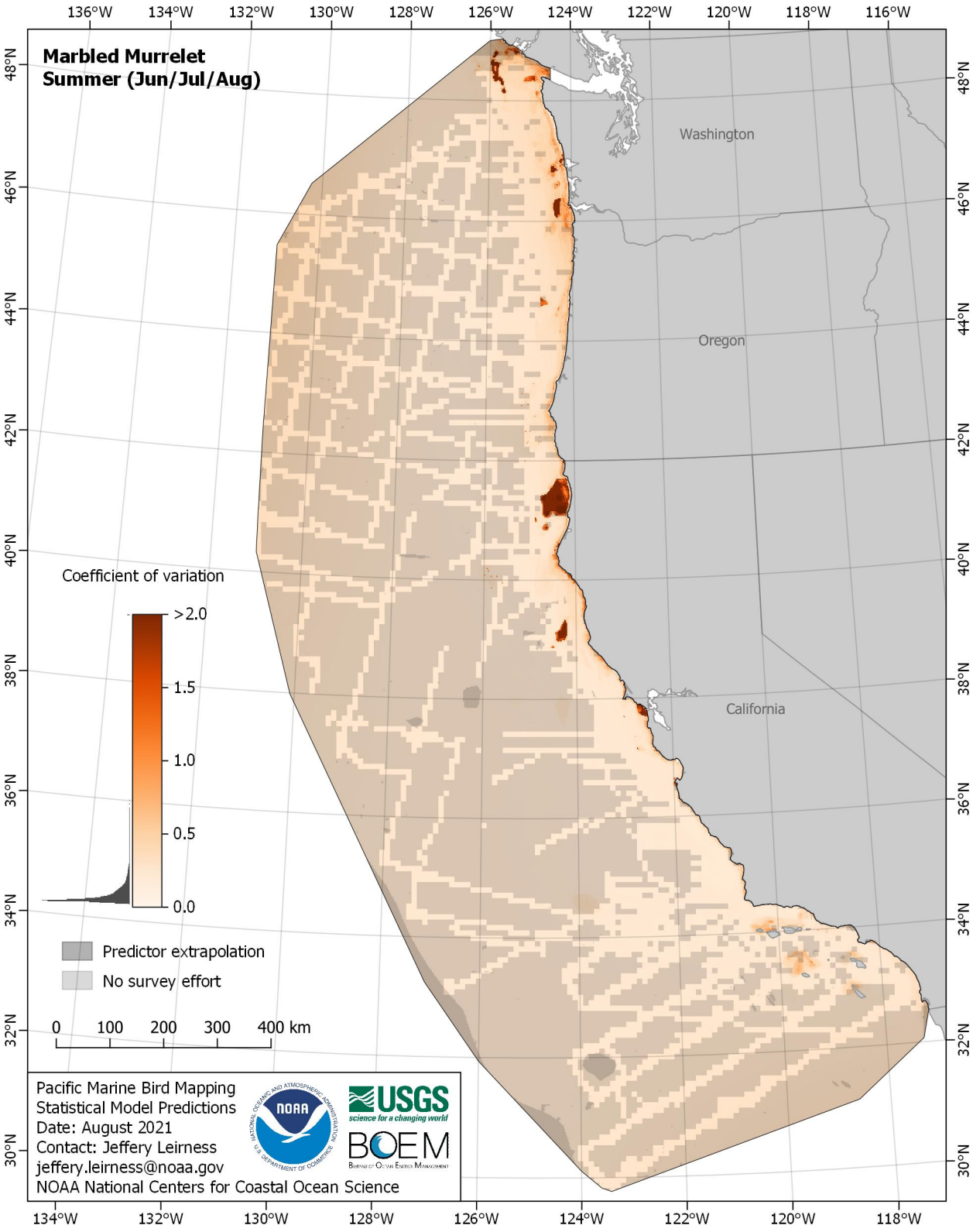

Figure E-62. Coefficient of variation for Marbled Murrelet (*Brachyramphus marmoratus*) in the summer season

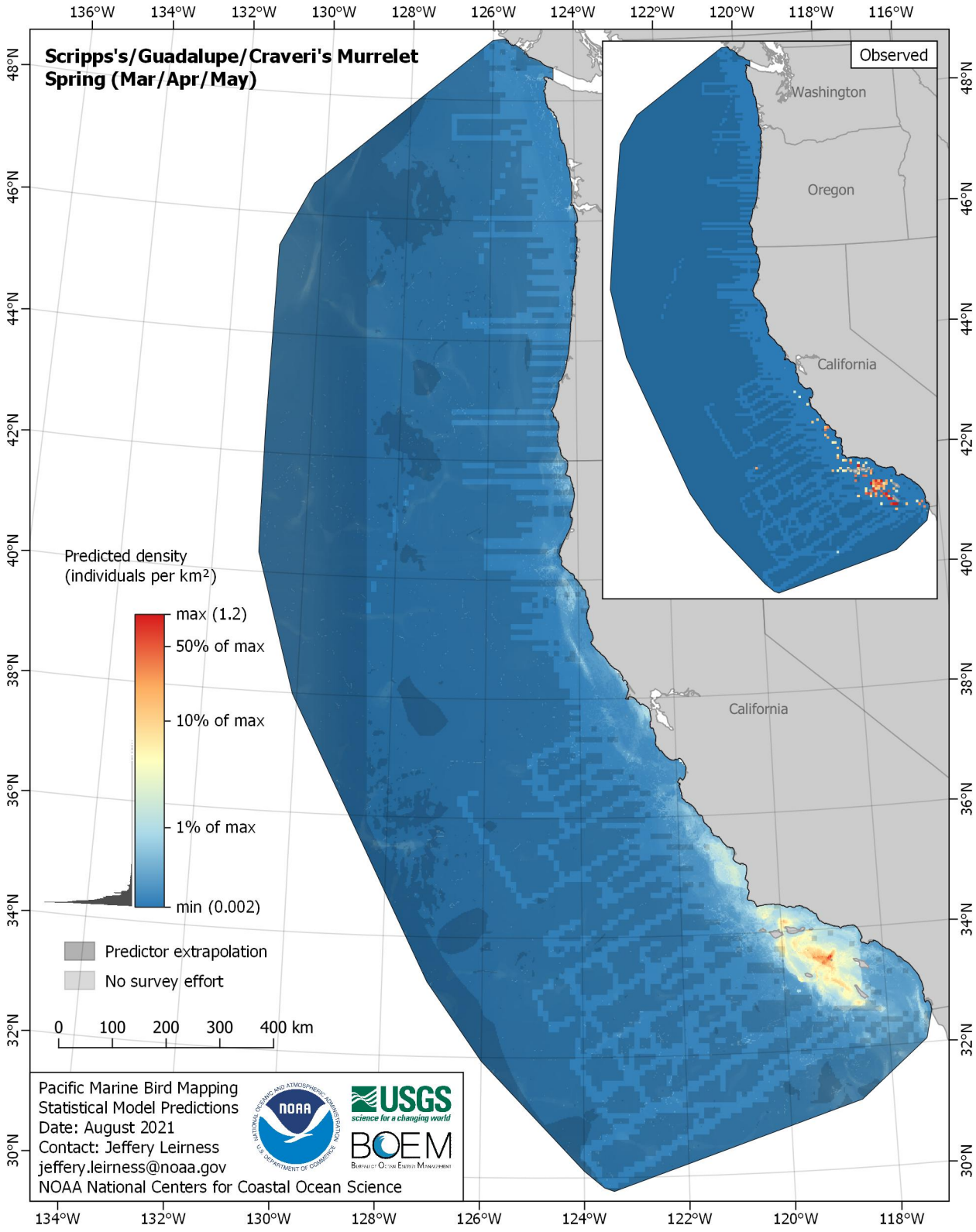

Figure E-63. Predicted density for Scripps's/Guadalupe/Craveri's Murrelet (*Synthliboramphus scrippsi/hypoleucus/craveri*) in the spring season

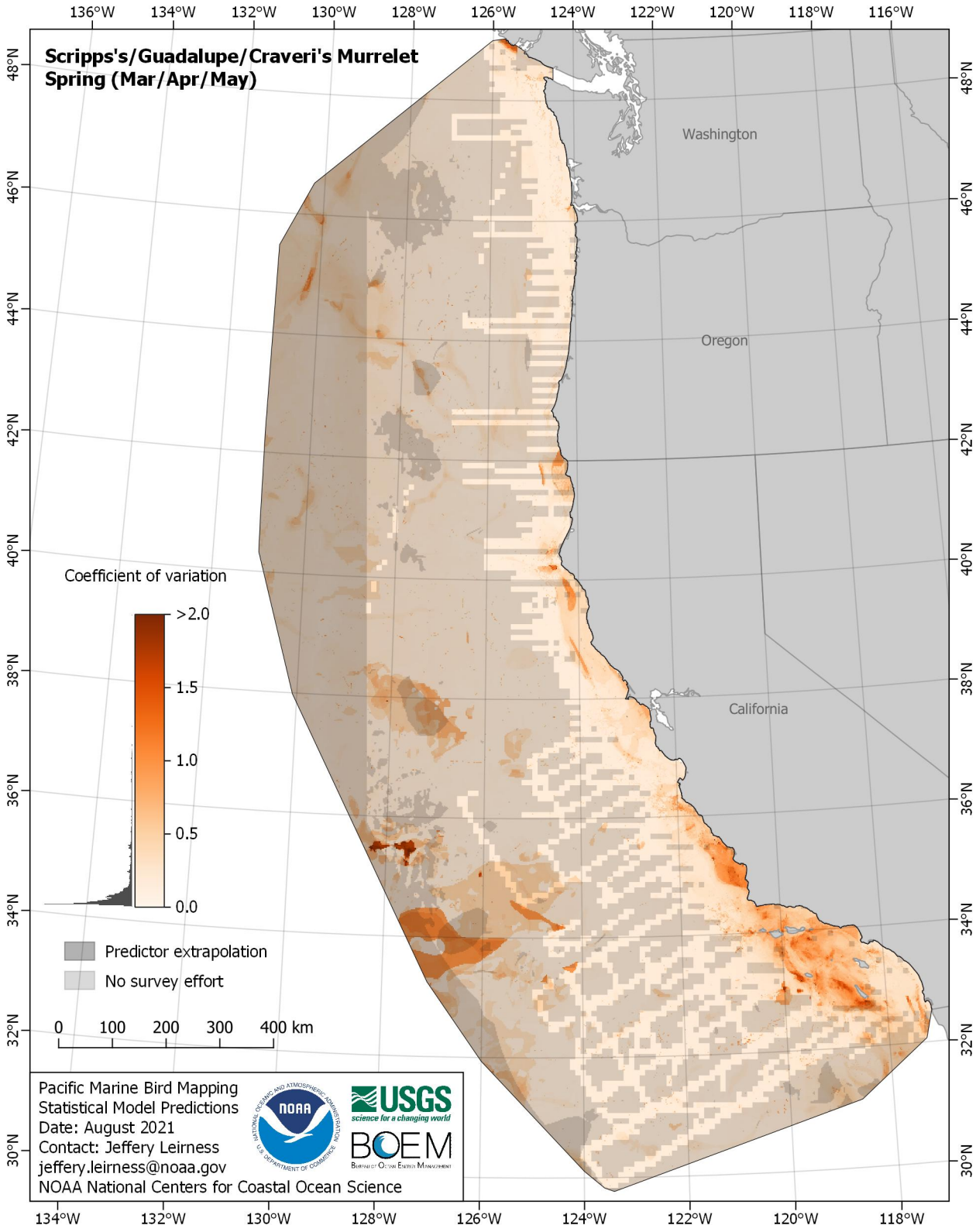

Figure E-64. Coefficient of variation for Scripps's/Guadalupe/Craveri's Murrelet (*Synthliboramphus scrippsi/hypoleucus/craveri*) in the spring season

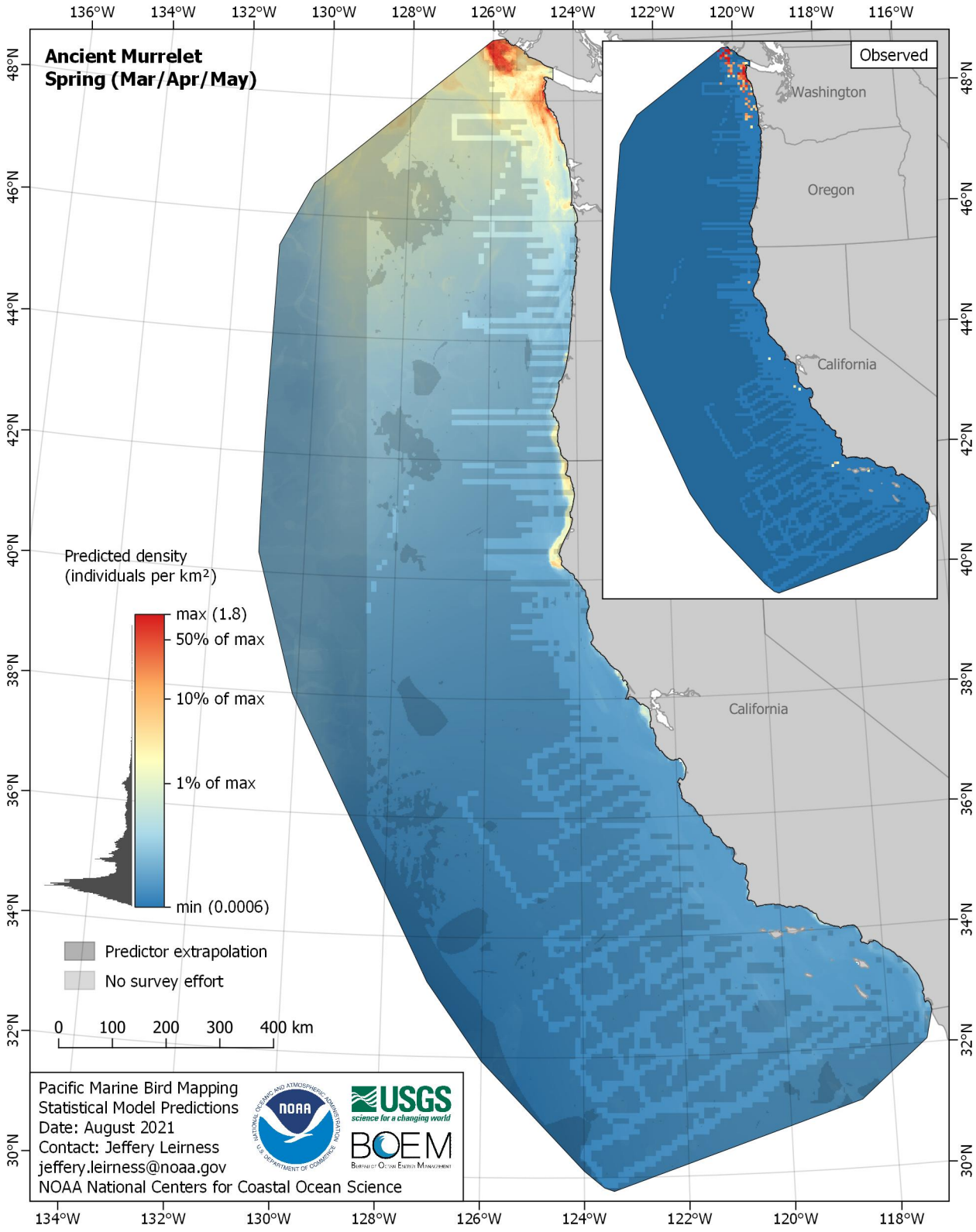

Figure E-65. Predicted density for Ancient Murrelet (*Synthliboramphus antiquus*) in the spring season

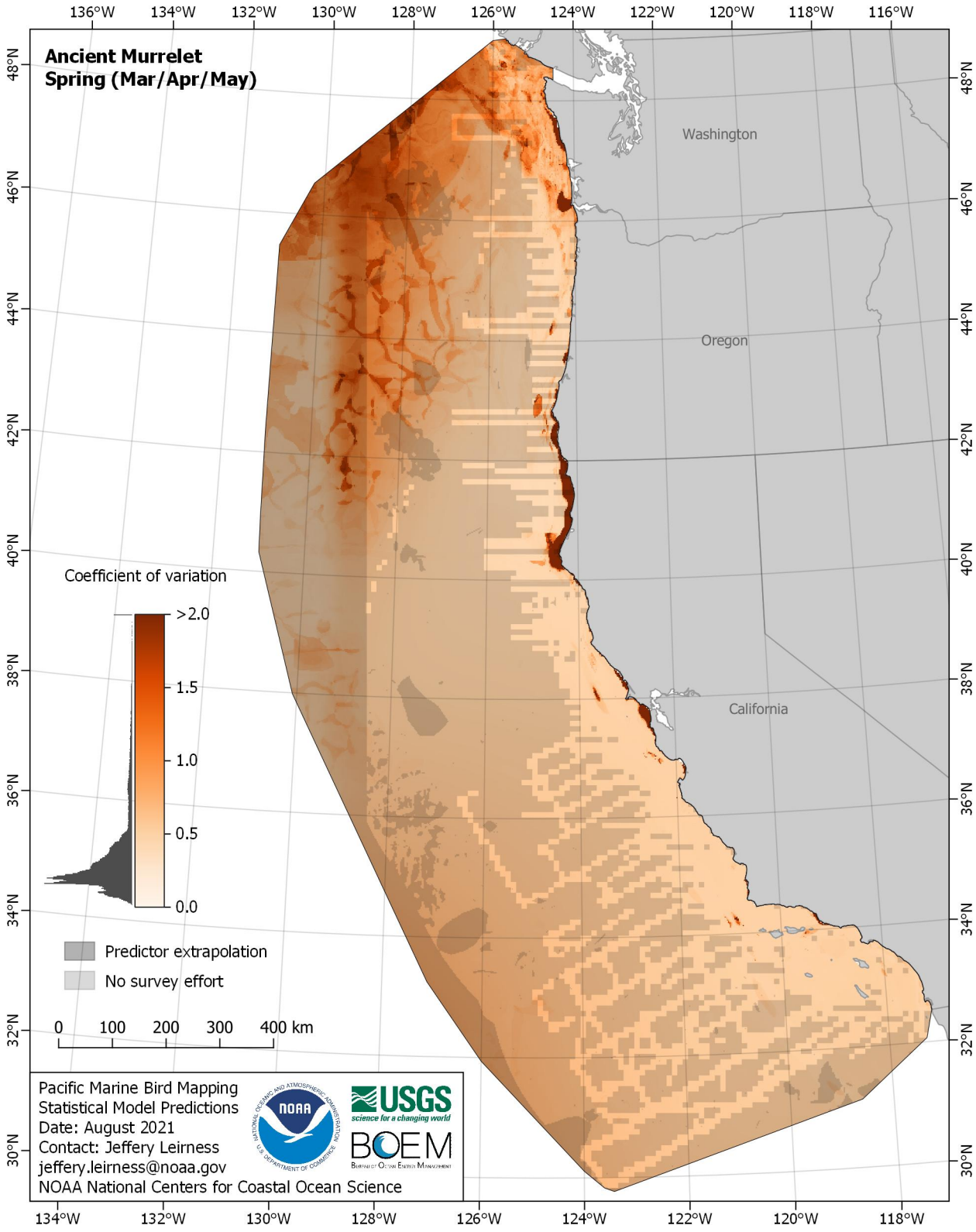

Figure E-66. Coefficient of variation for Ancient Murrelet (*Synthliboramphus antiquus*) in the spring season

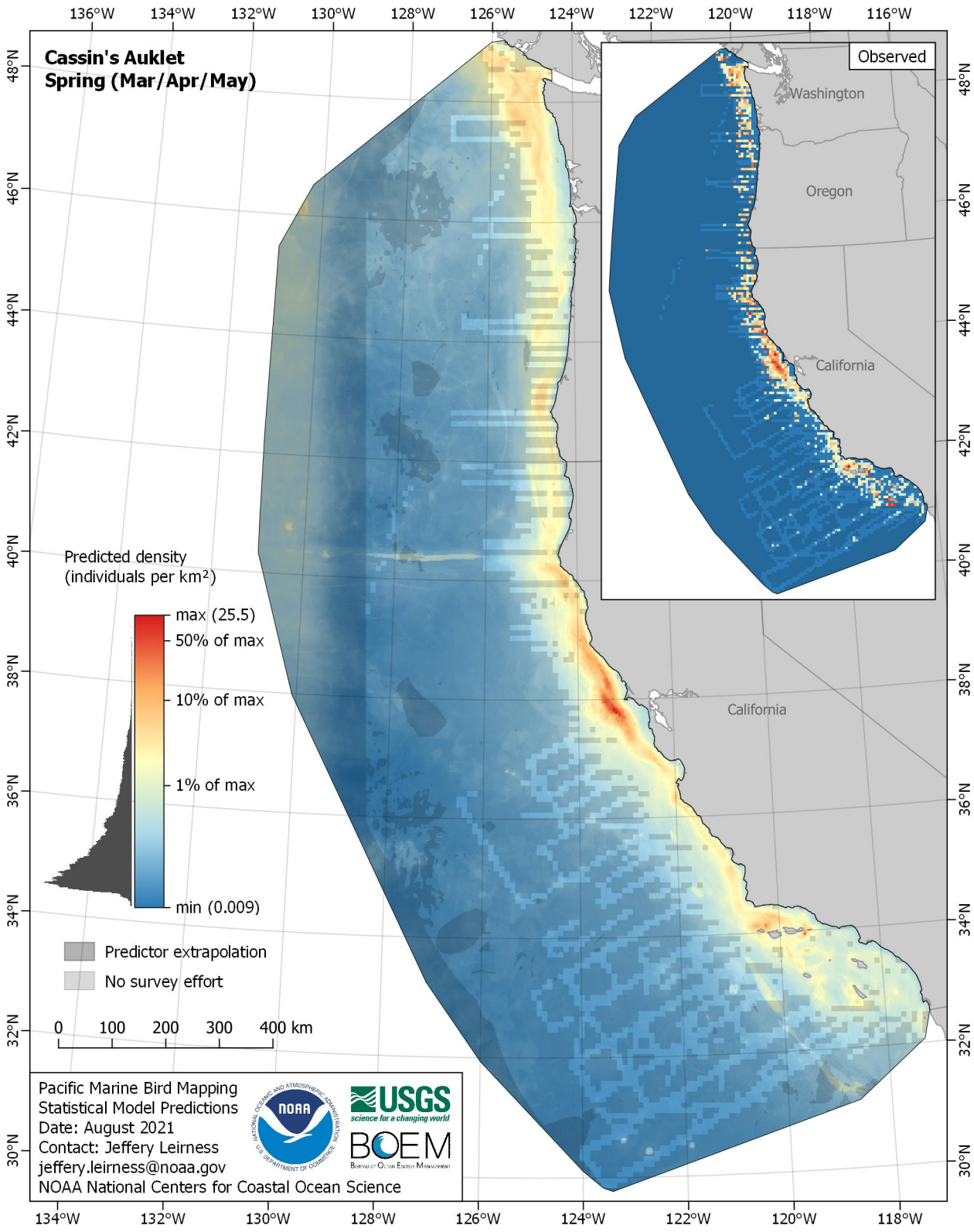

Figure E-67. Predicted density for Cassin's Auklet (*Ptychoramphus aleuticus*) in the spring season

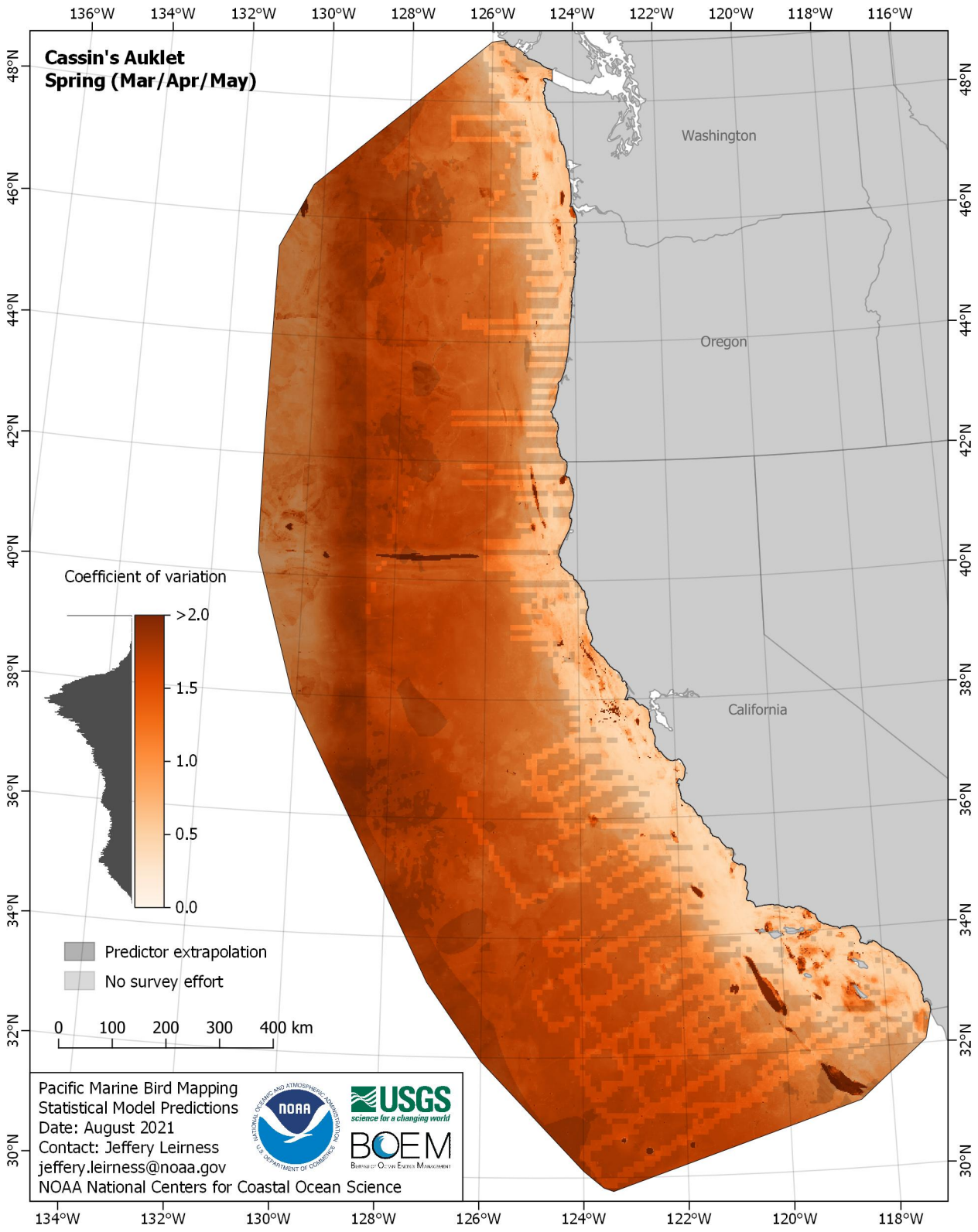

Figure E-68. Coefficient of variation for Cassin's Auklet (*Ptychoramphus aleuticus*) in the spring season

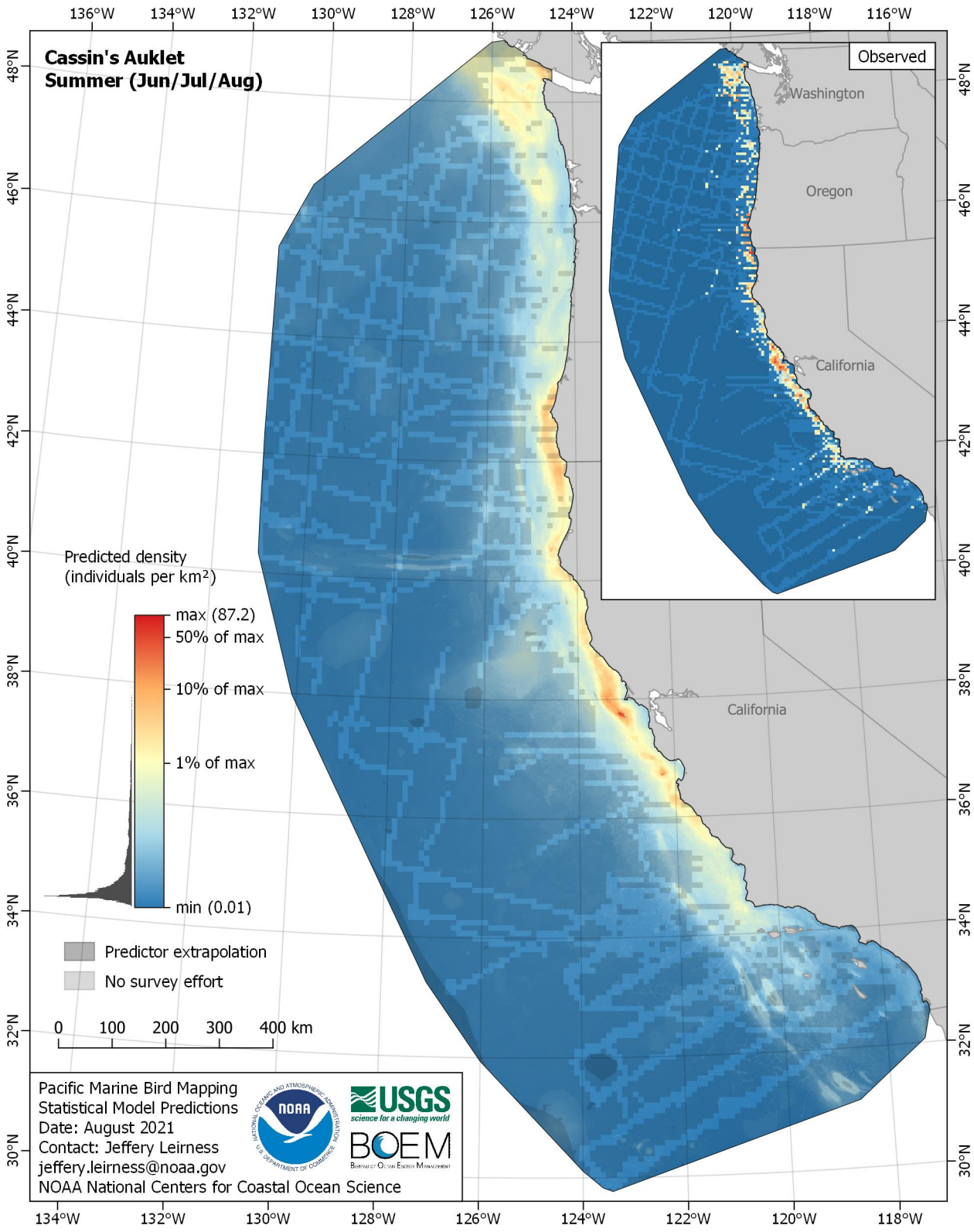

Figure E-69. Predicted density for Cassin's Auklet (*Ptychoramphus aleuticus*) in the summer season

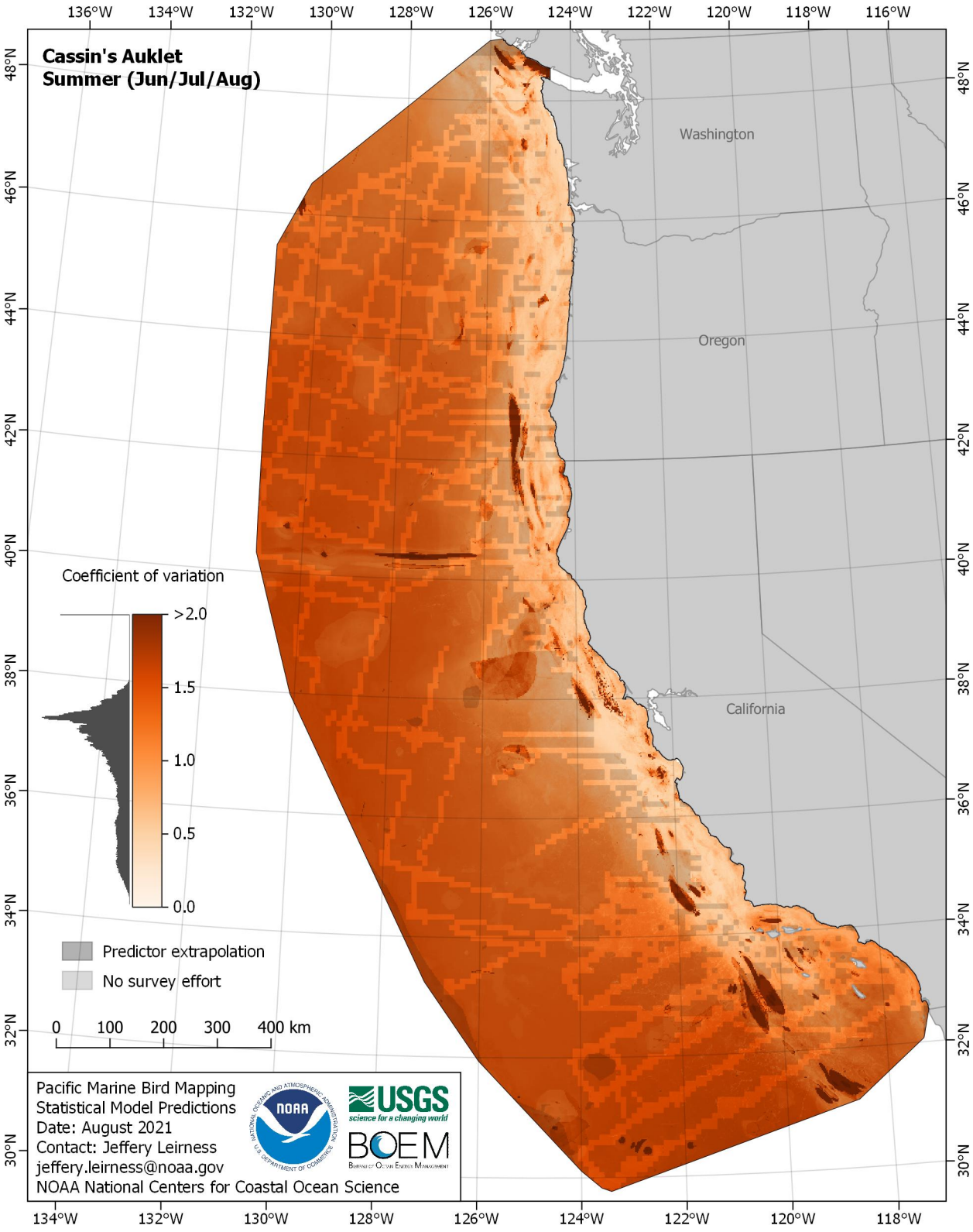

Figure E-70. Coefficient of variation for Cassin's Auklet (*Ptychoramphus aleuticus*) in the summer season

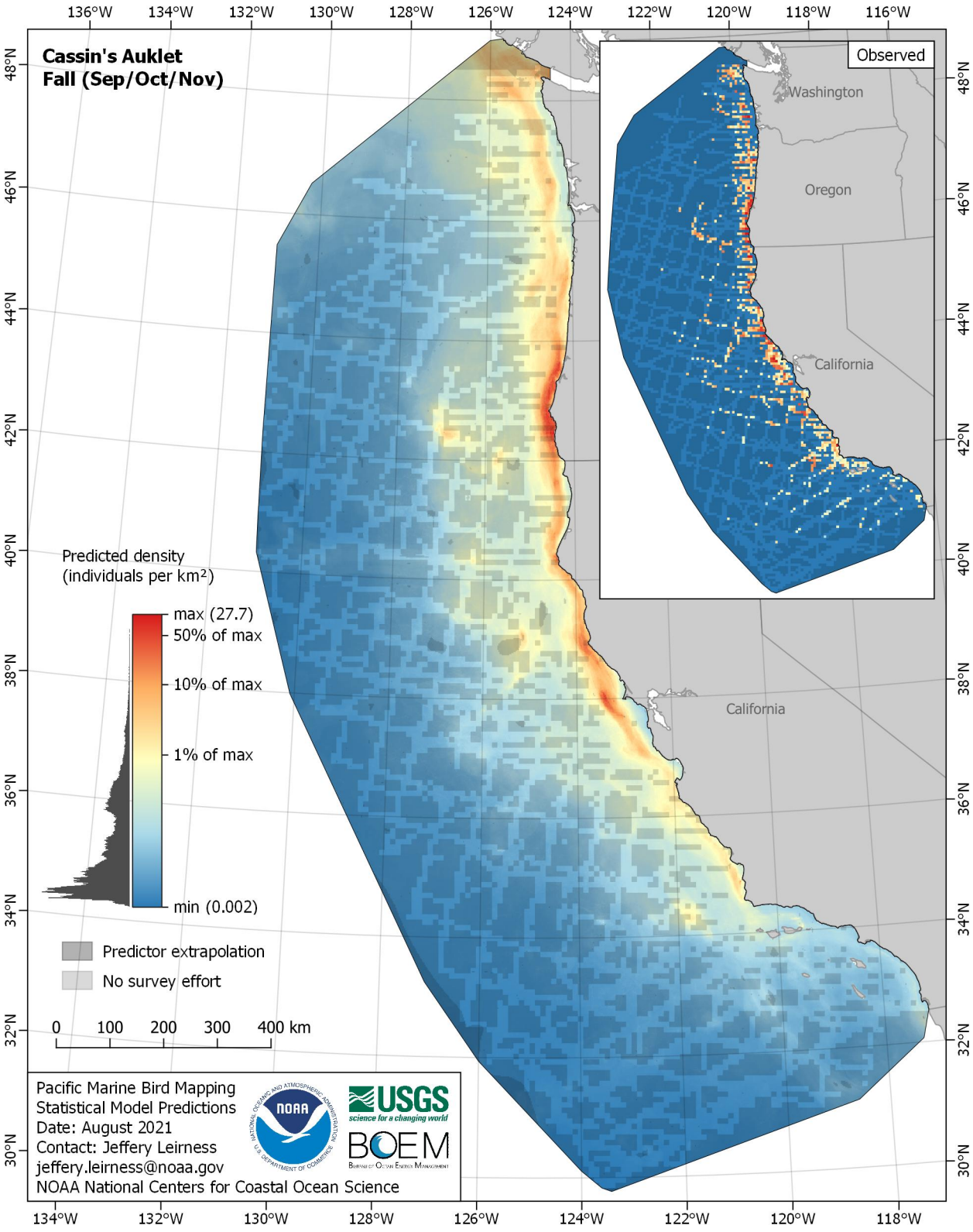

Figure E-71. Predicted density for Cassin's Auklet (*Ptychoramphus aleuticus*) in the fall season

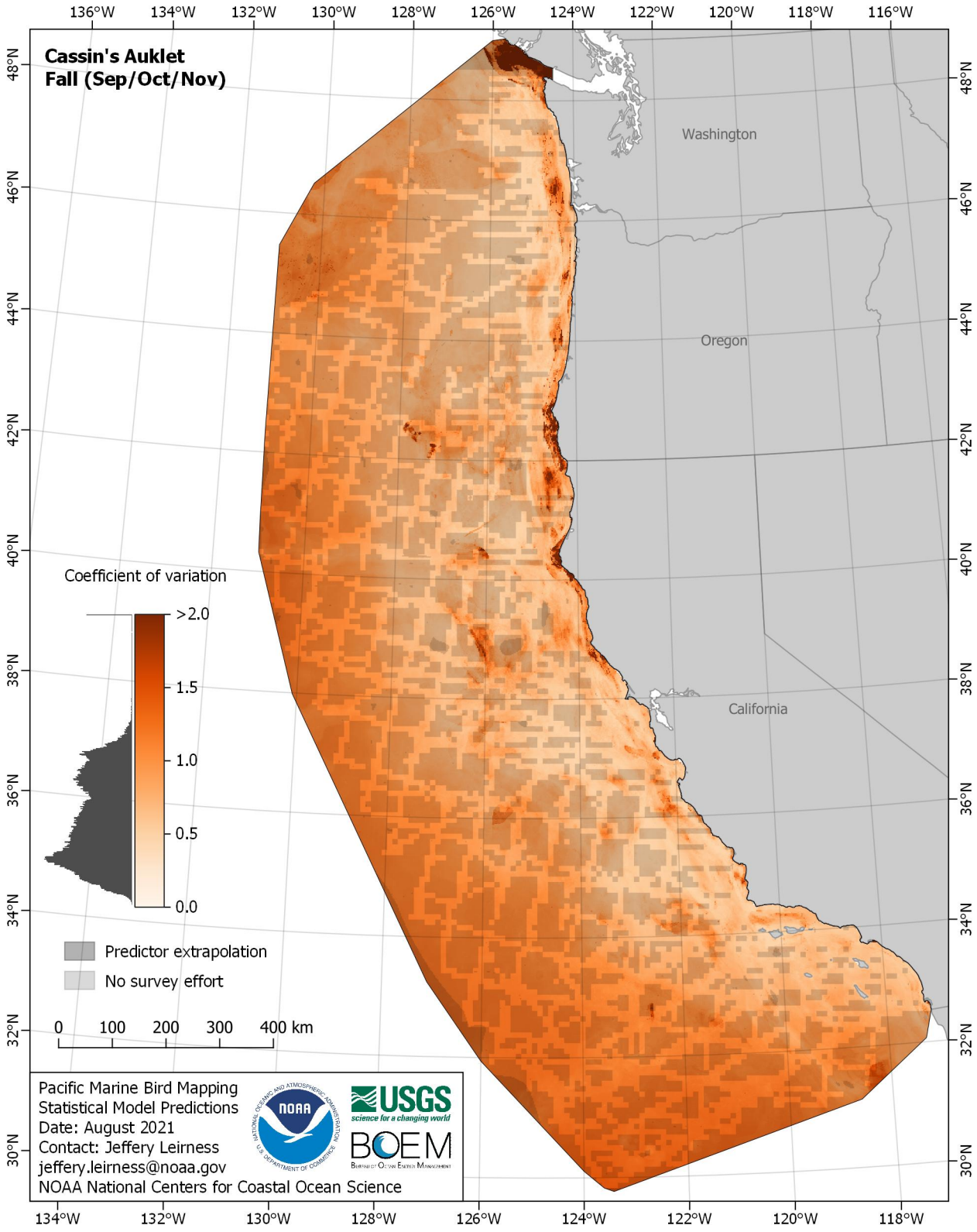

Figure E-72. Coefficient of variation for Cassin's Auklet (*Ptychoramphus aleuticus*) in the fall season

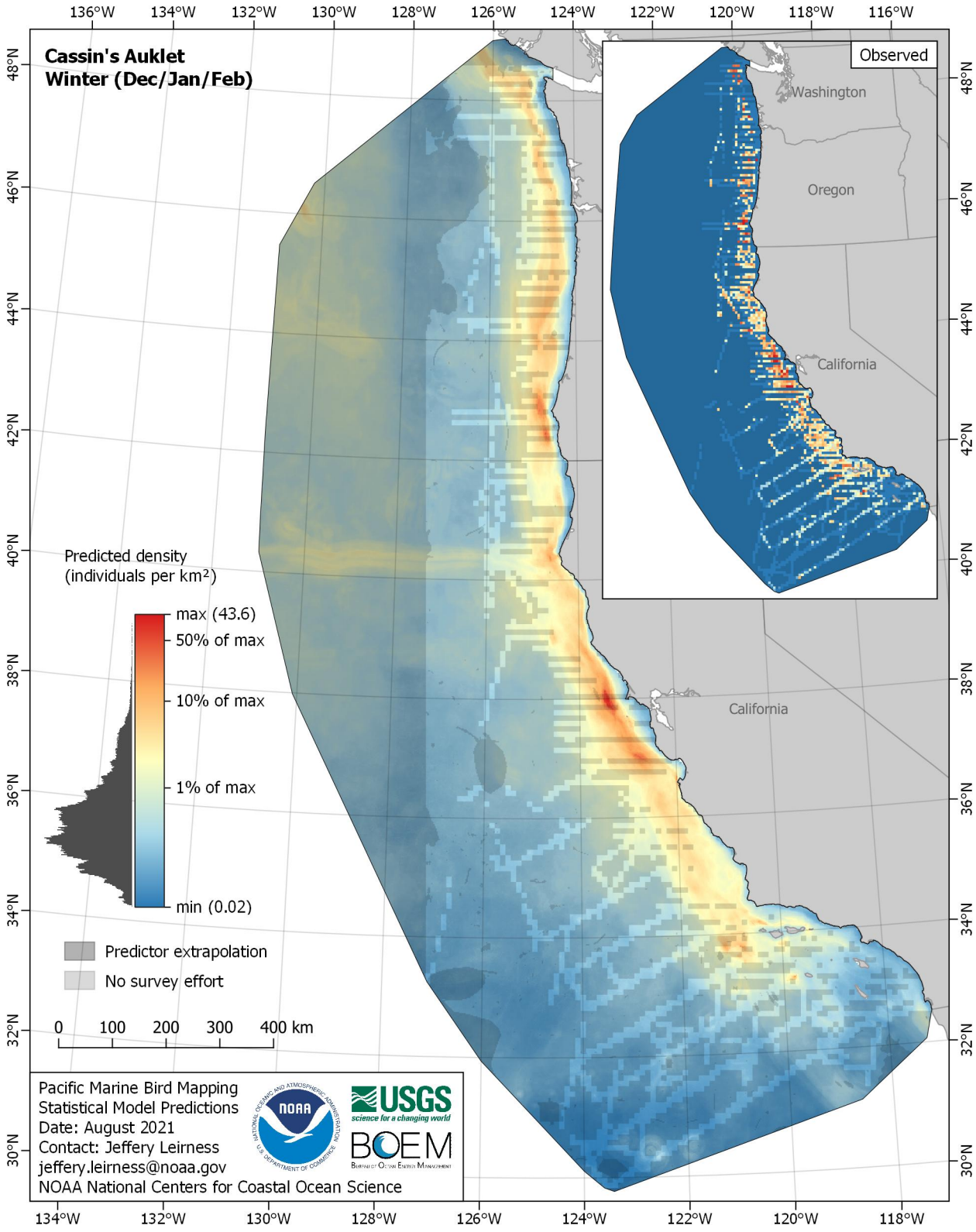

Figure E-73. Predicted density for Cassin's Auklet (*Ptychoramphus aleuticus*) in the winter season

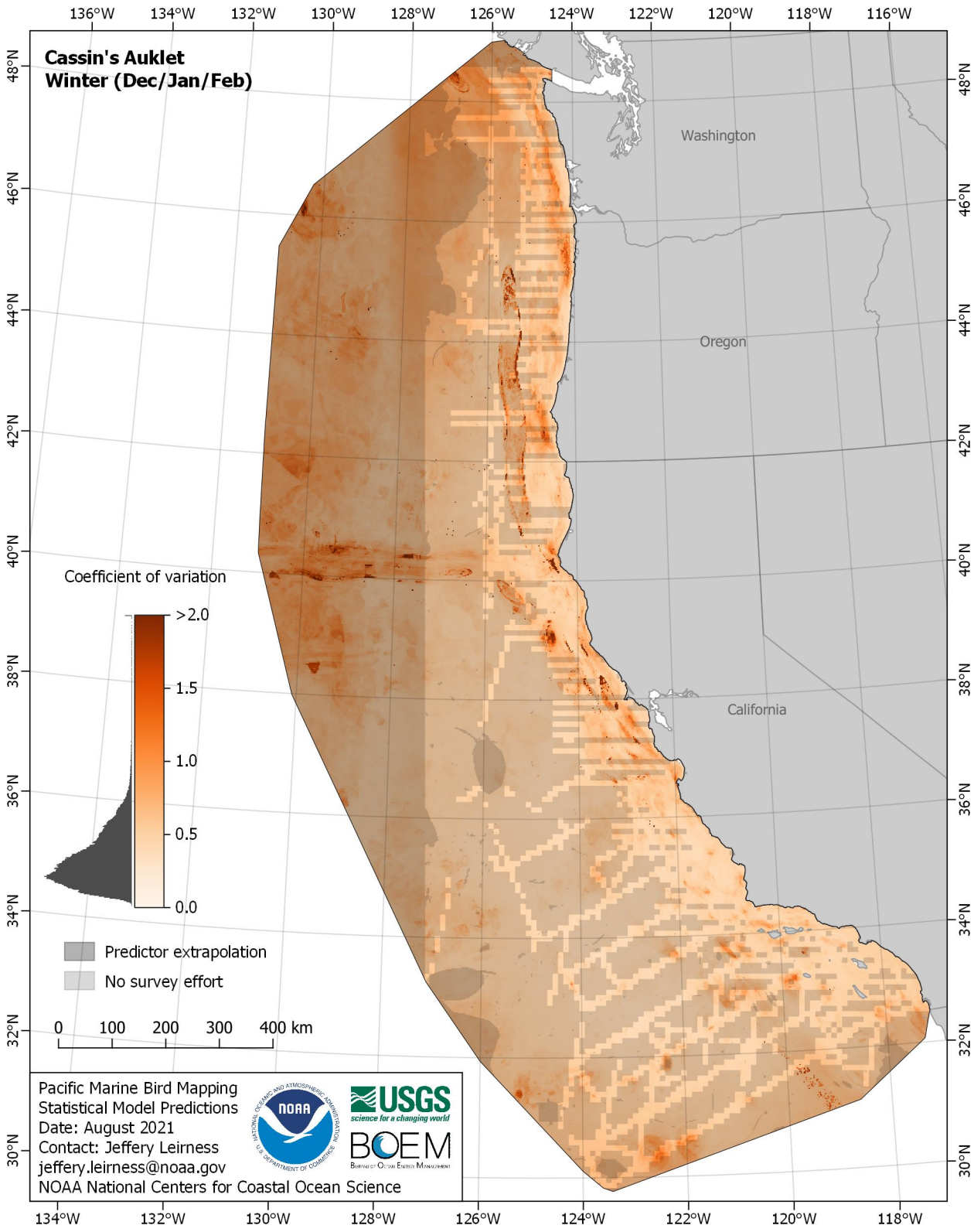

Figure E-74. Coefficient of variation for Cassin's Auklet (*Ptychoramphus aleuticus*) in the winter season

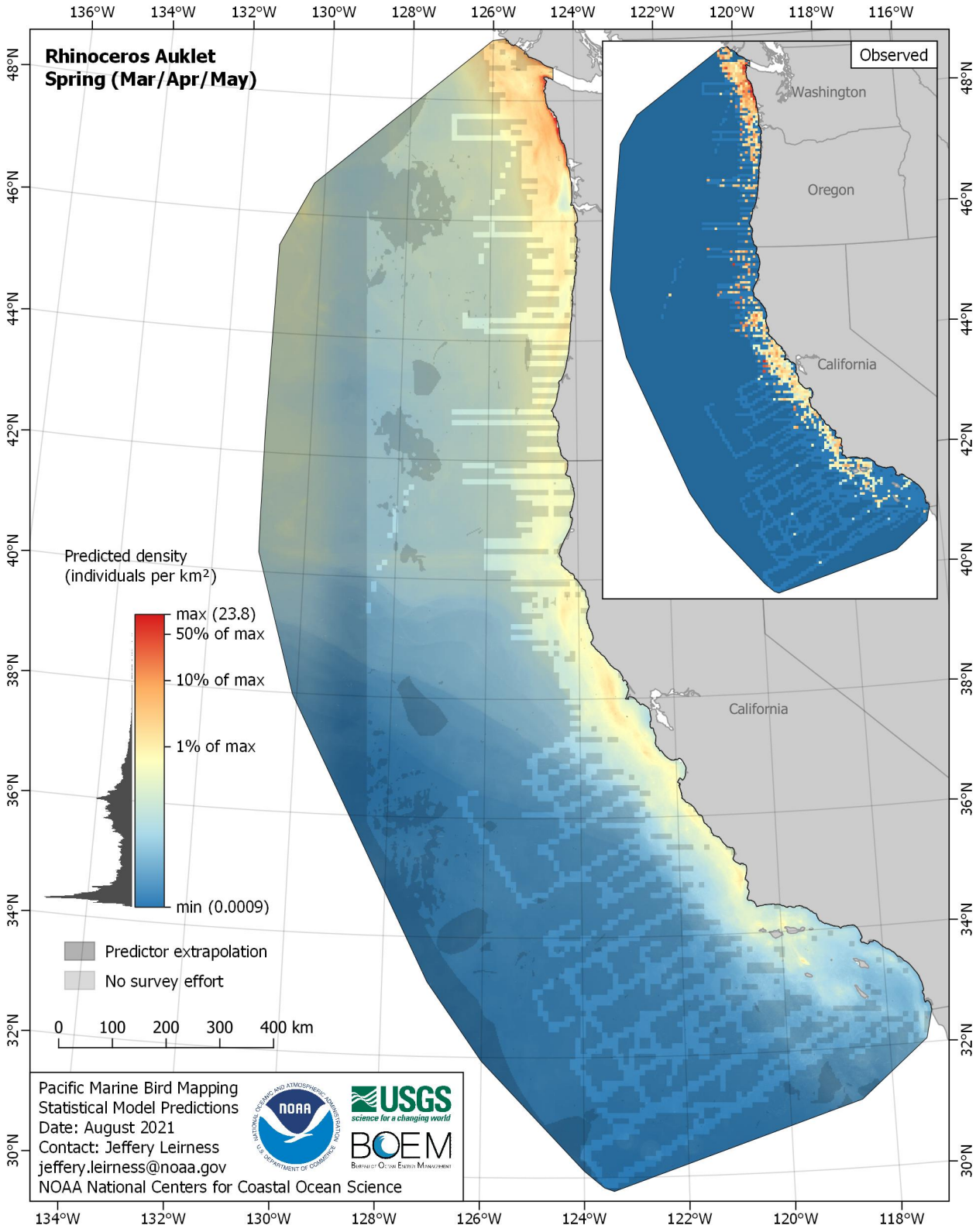

Figure E-75. Predicted density for Rhinoceros Auklet (*Cerorhinca monocerata*) in the spring season

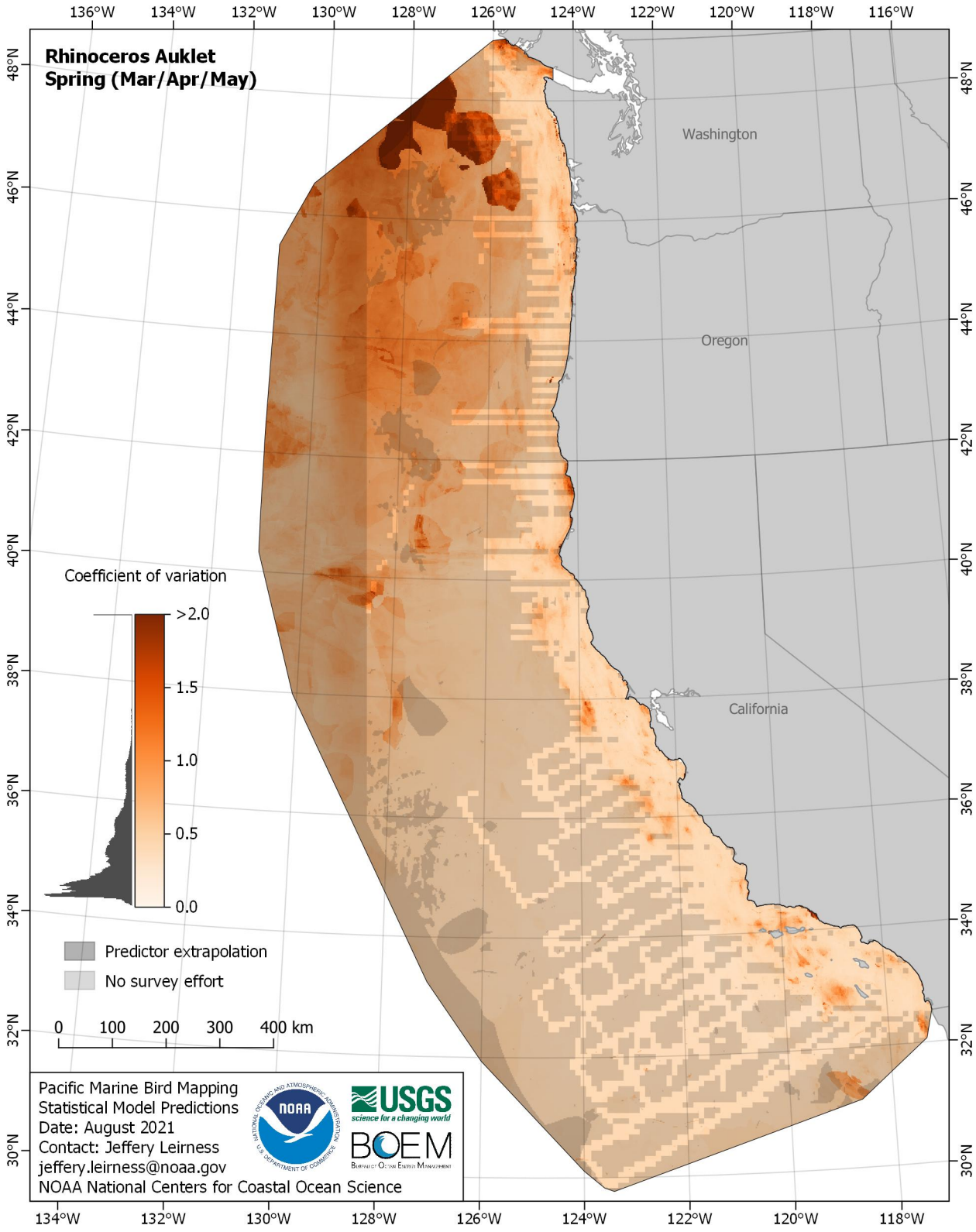

Figure E-76. Coefficient of variation for Rhinoceros Auklet (*Cerorhinca monocerata*) in the spring season

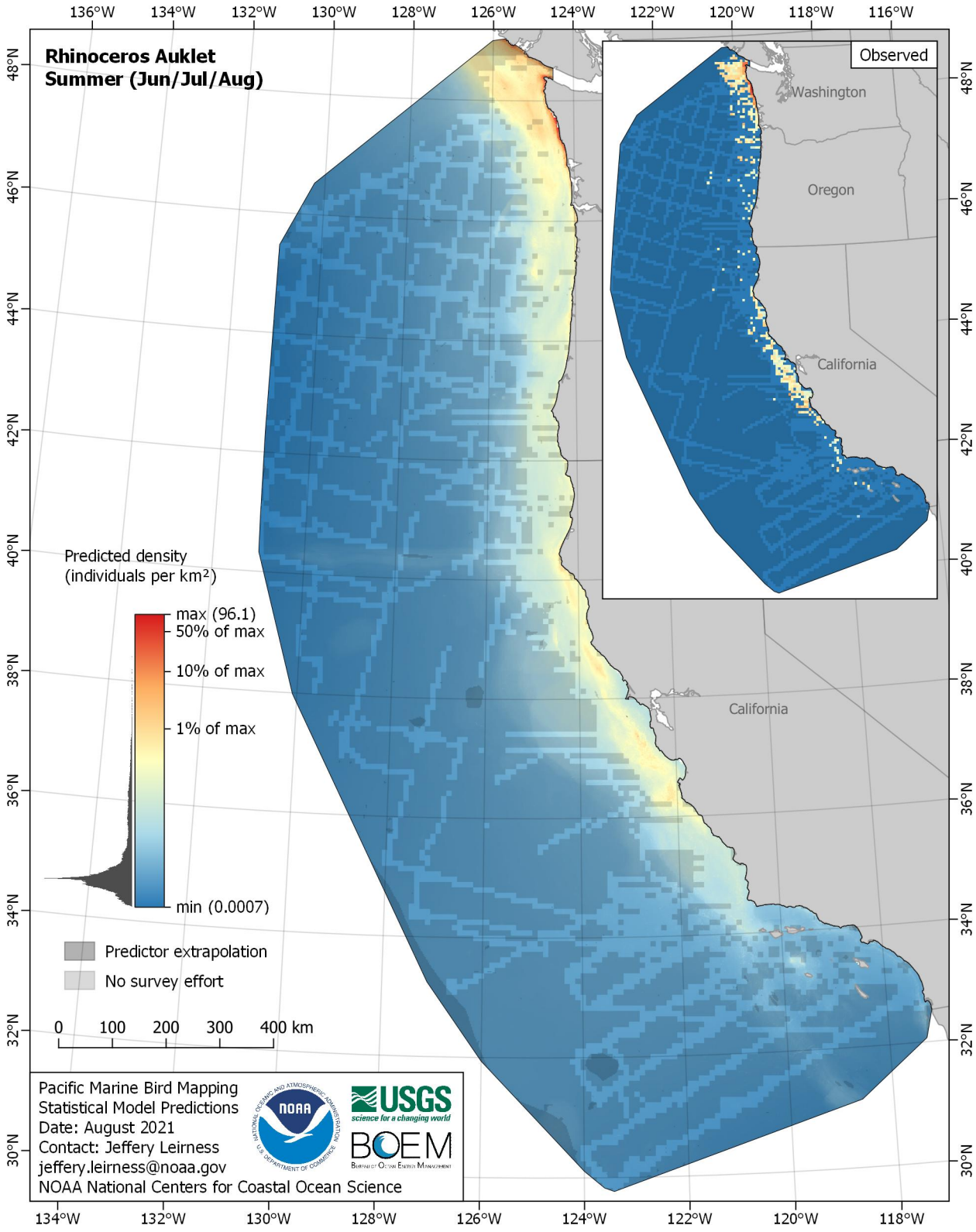

Figure E-77. Predicted density for Rhinoceros Auklet (*Cerorhinca monocerata*) in the summer season

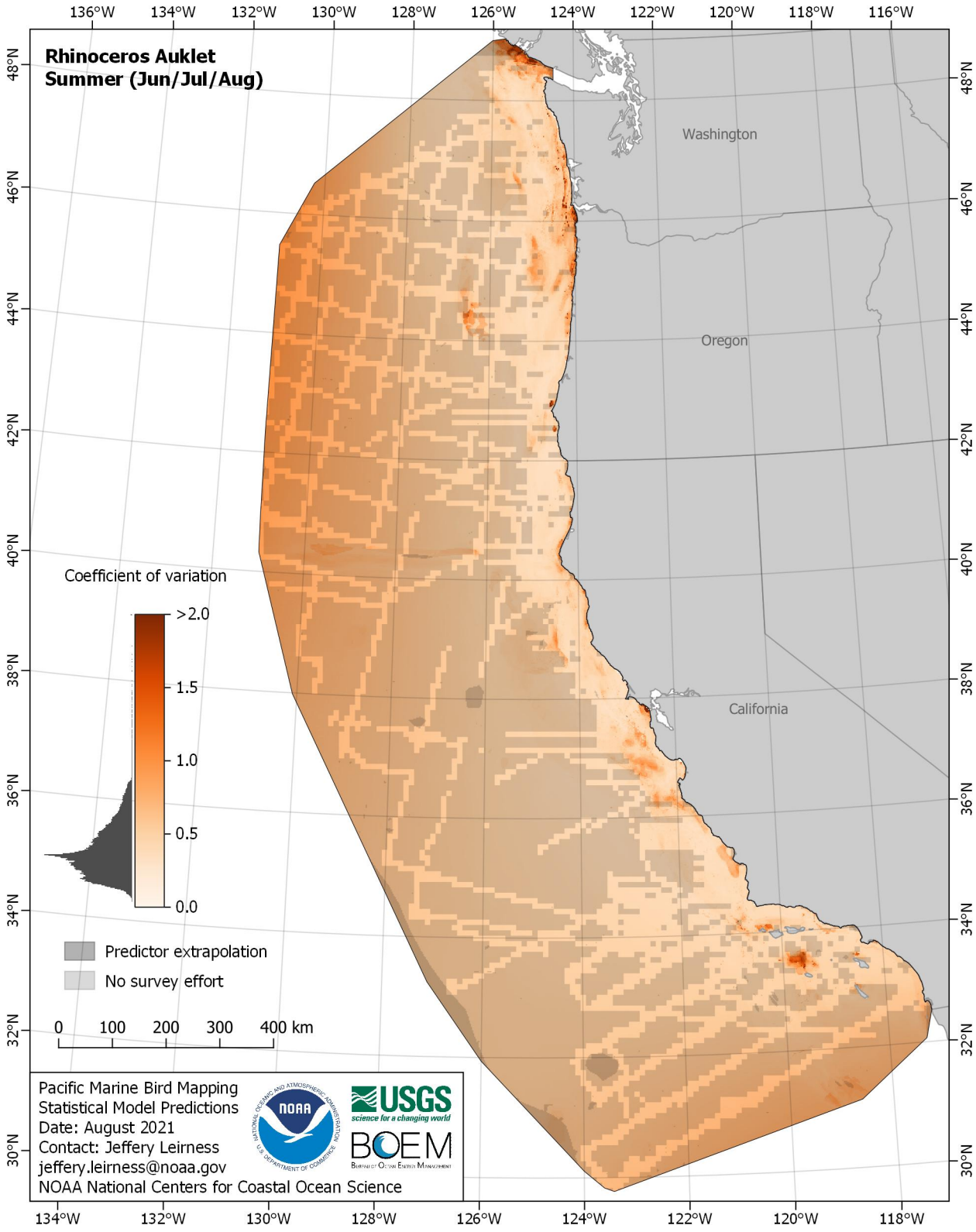

Figure E-78. Coefficient of variation for Rhinoceros Auklet (*Cerorhinca monocerata*) in the summer season

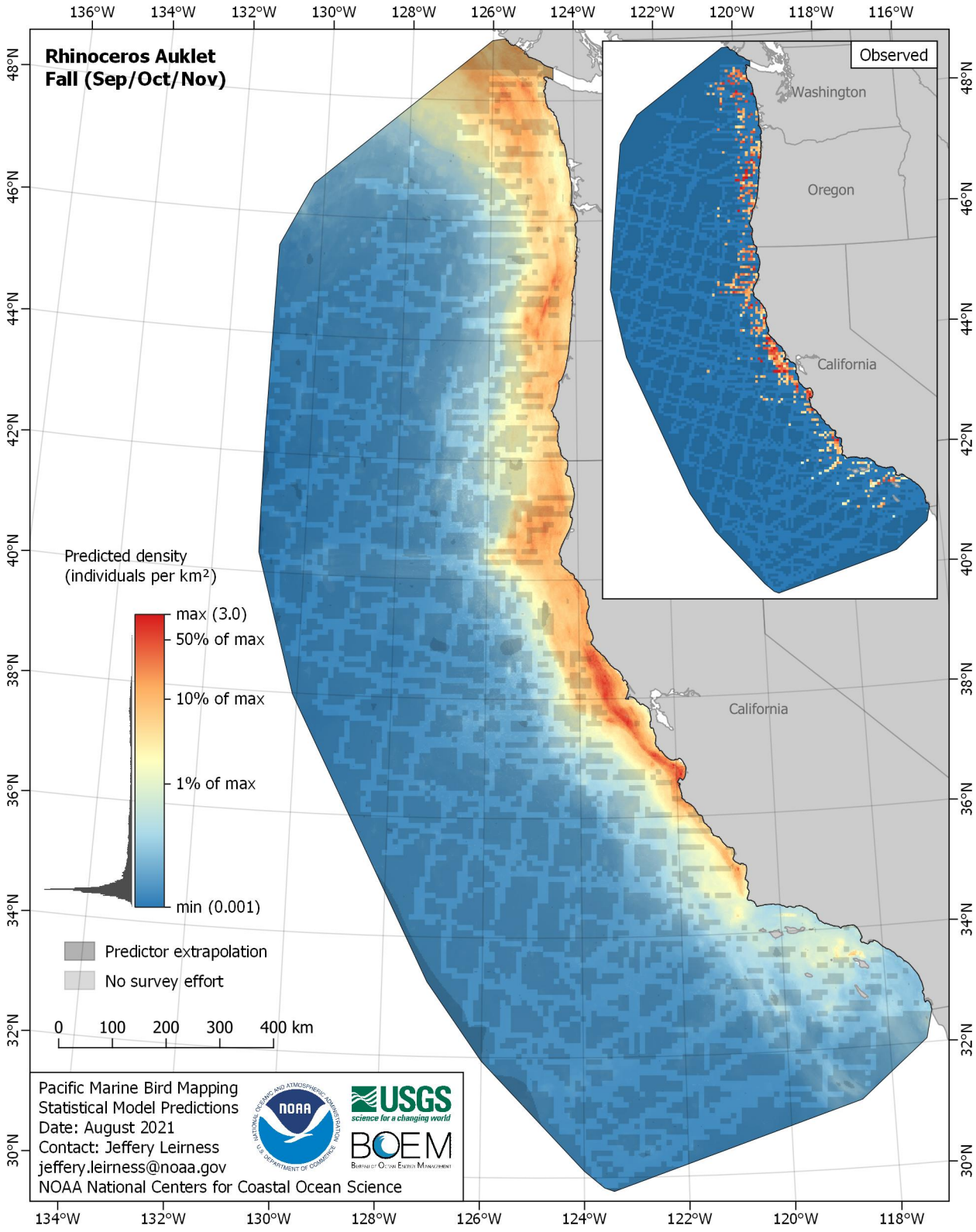

Figure E-79. Predicted density for Rhinoceros Auklet (*Cerorhinca monocerata*) in the fall season

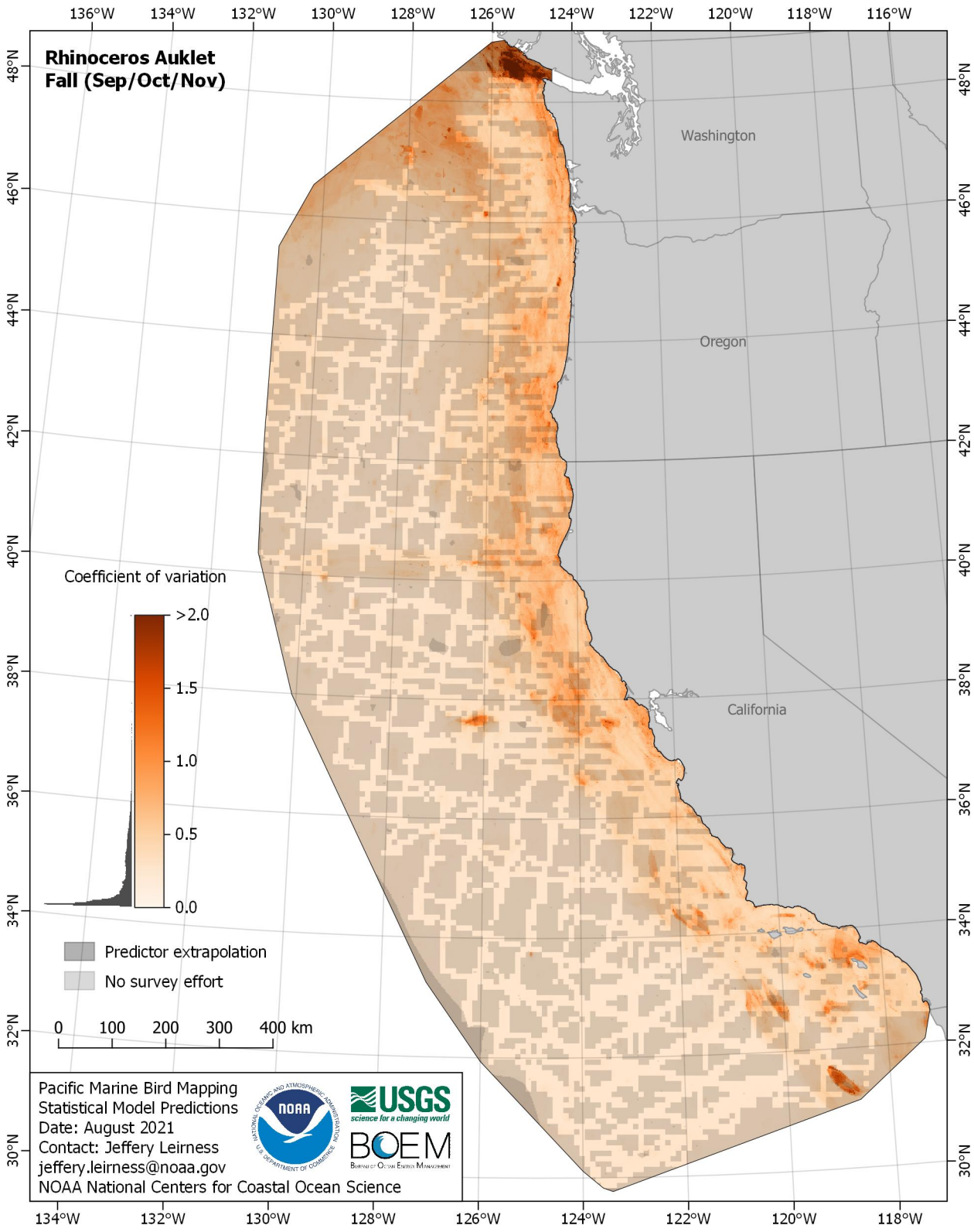

Figure E-80. Coefficient of variation for Rhinoceros Auklet (*Cerorhinca monocerata*) in the fall season

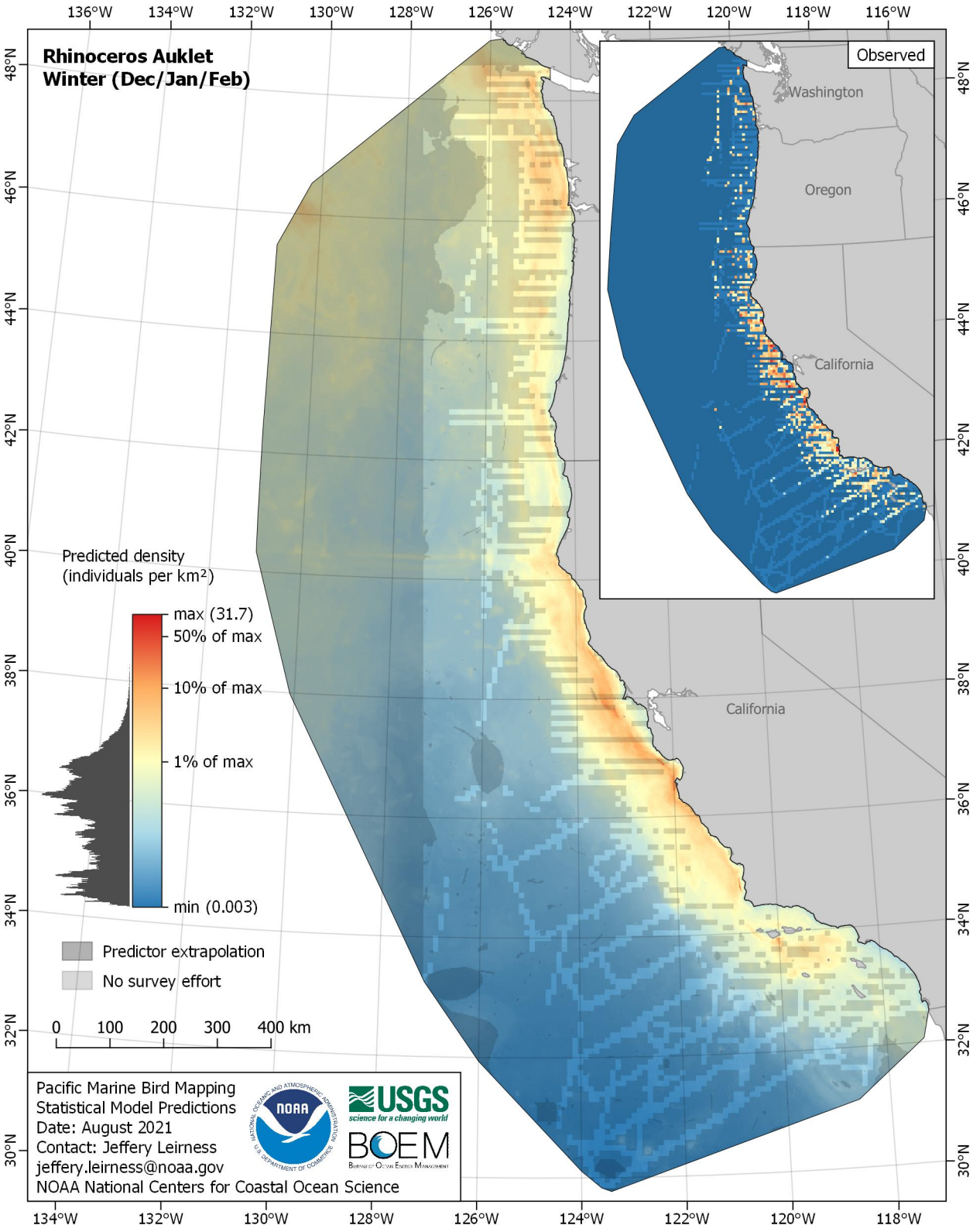

Figure E-81. Predicted density for Rhinoceros Auklet (*Cerorhinca monocerata*) in the winter season

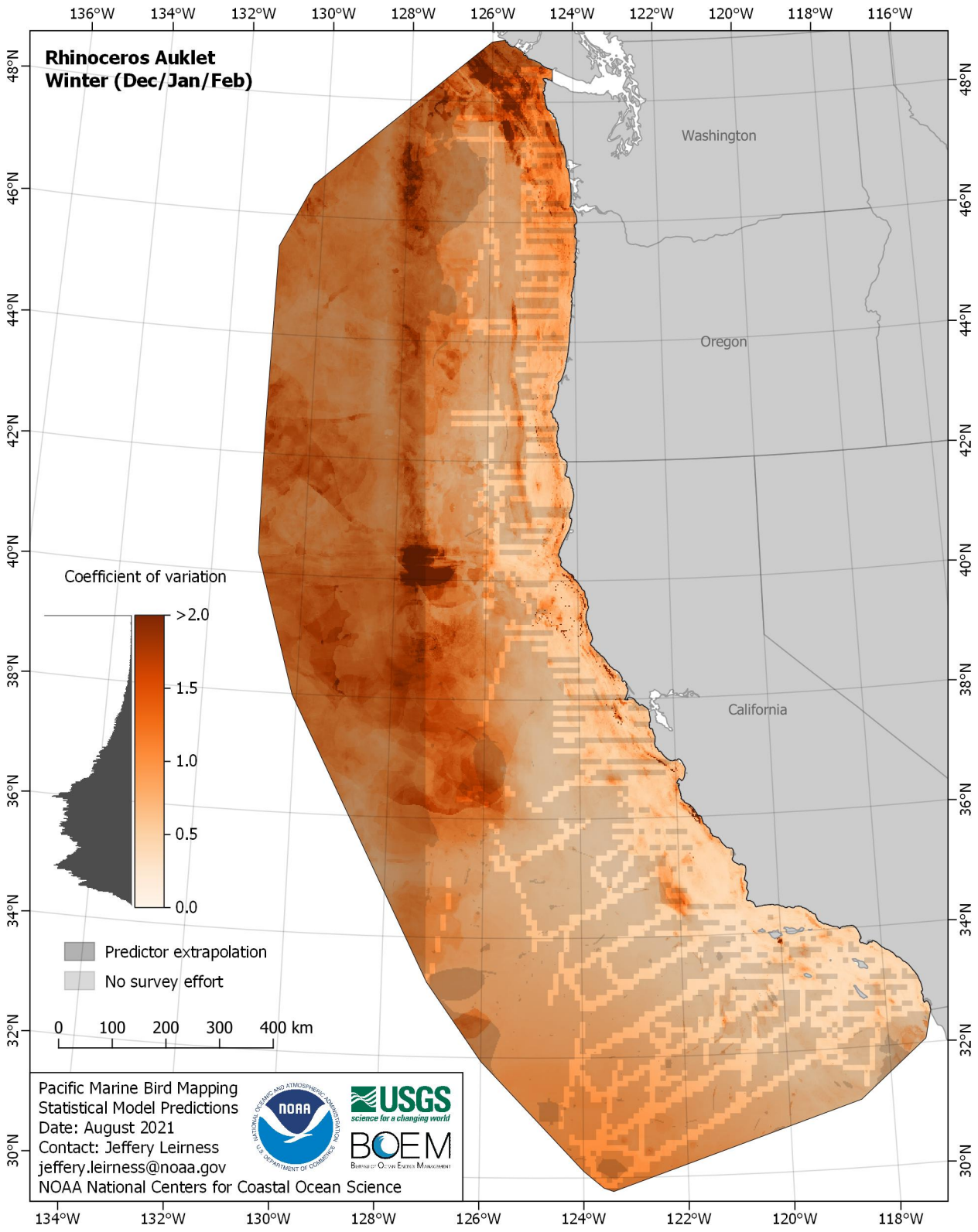

Figure E-82. Coefficient of variation for Rhinoceros Auklet (*Cerorhinca monocerata*) in the winter season

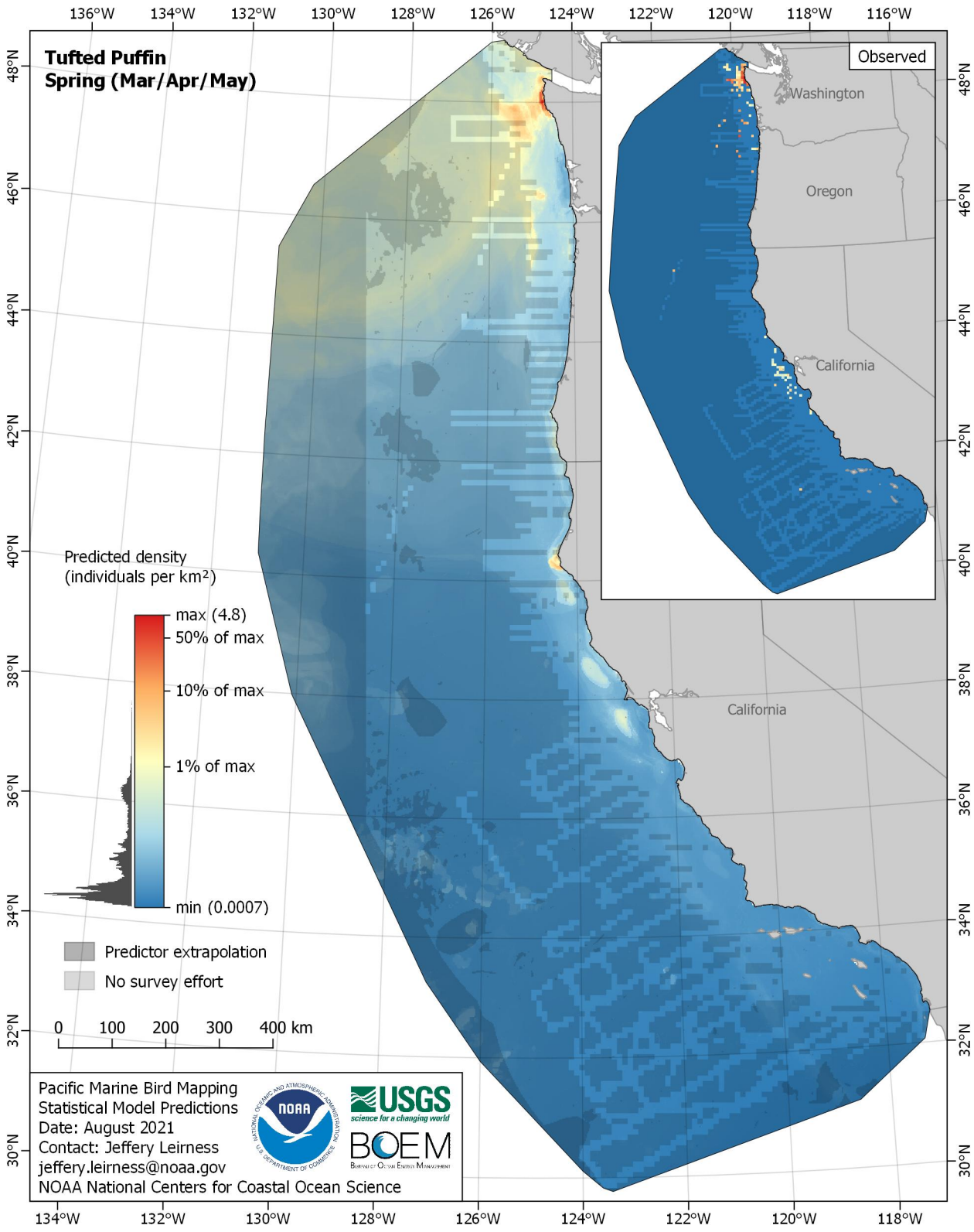

Figure E-83. Predicted density for Tufted Puffin (*Fratercula cirrhata*) in the spring season

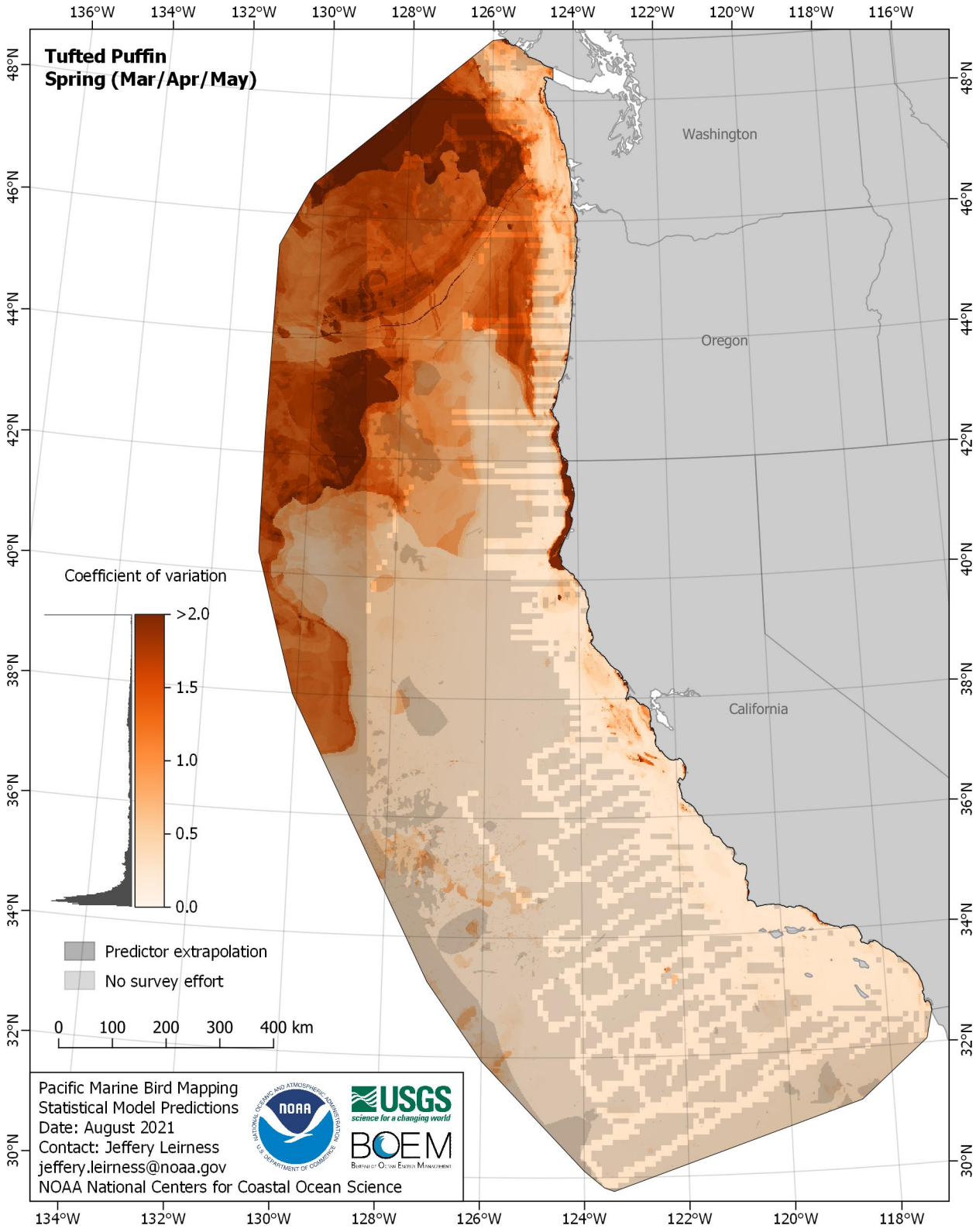

Figure E-84. Coefficient of variation for Tufted Puffin (*Fratercula cirrhata*) in the spring season

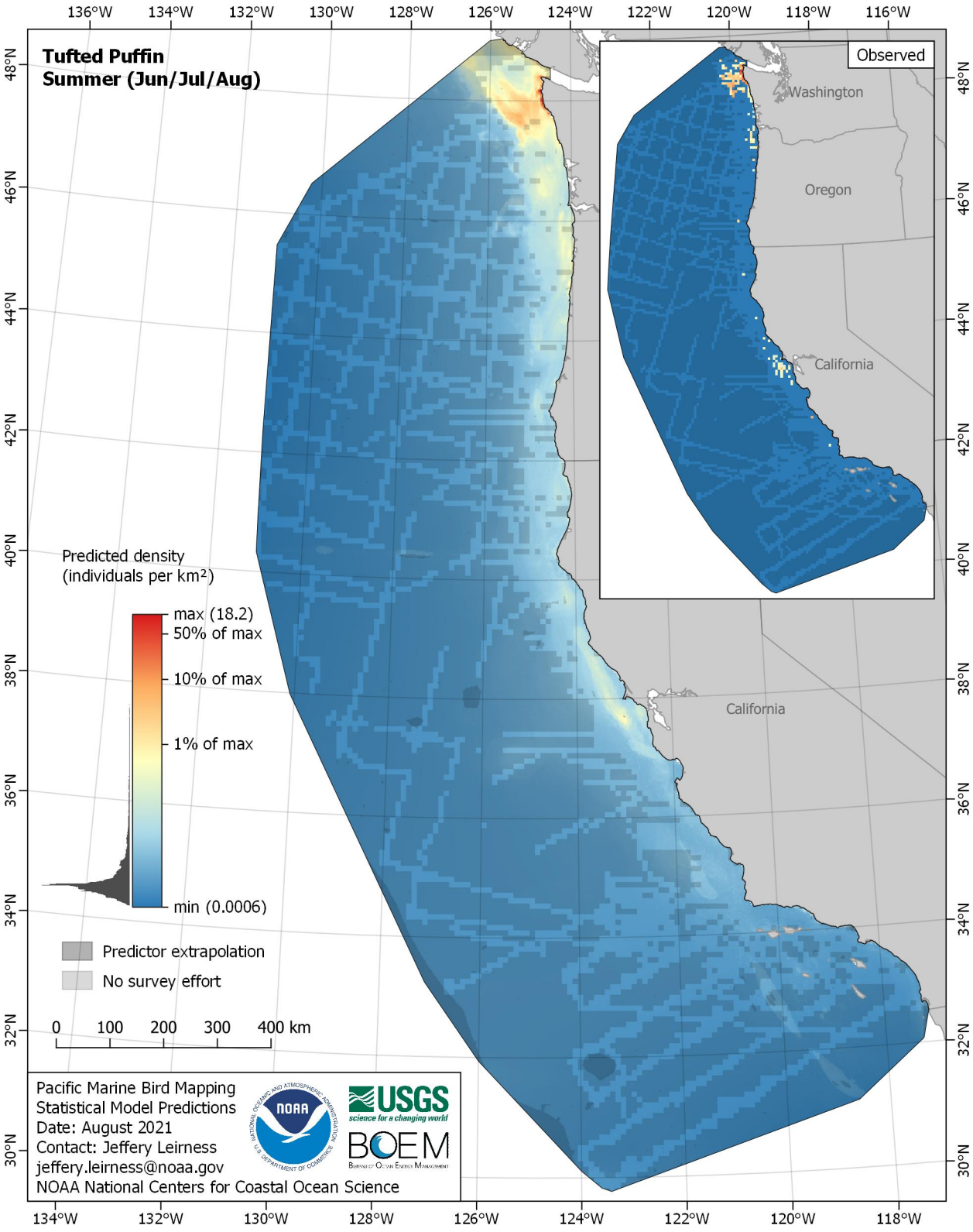

Figure E-85. Predicted density for Tufted Puffin (*Fratercula cirrhata*) in the summer season

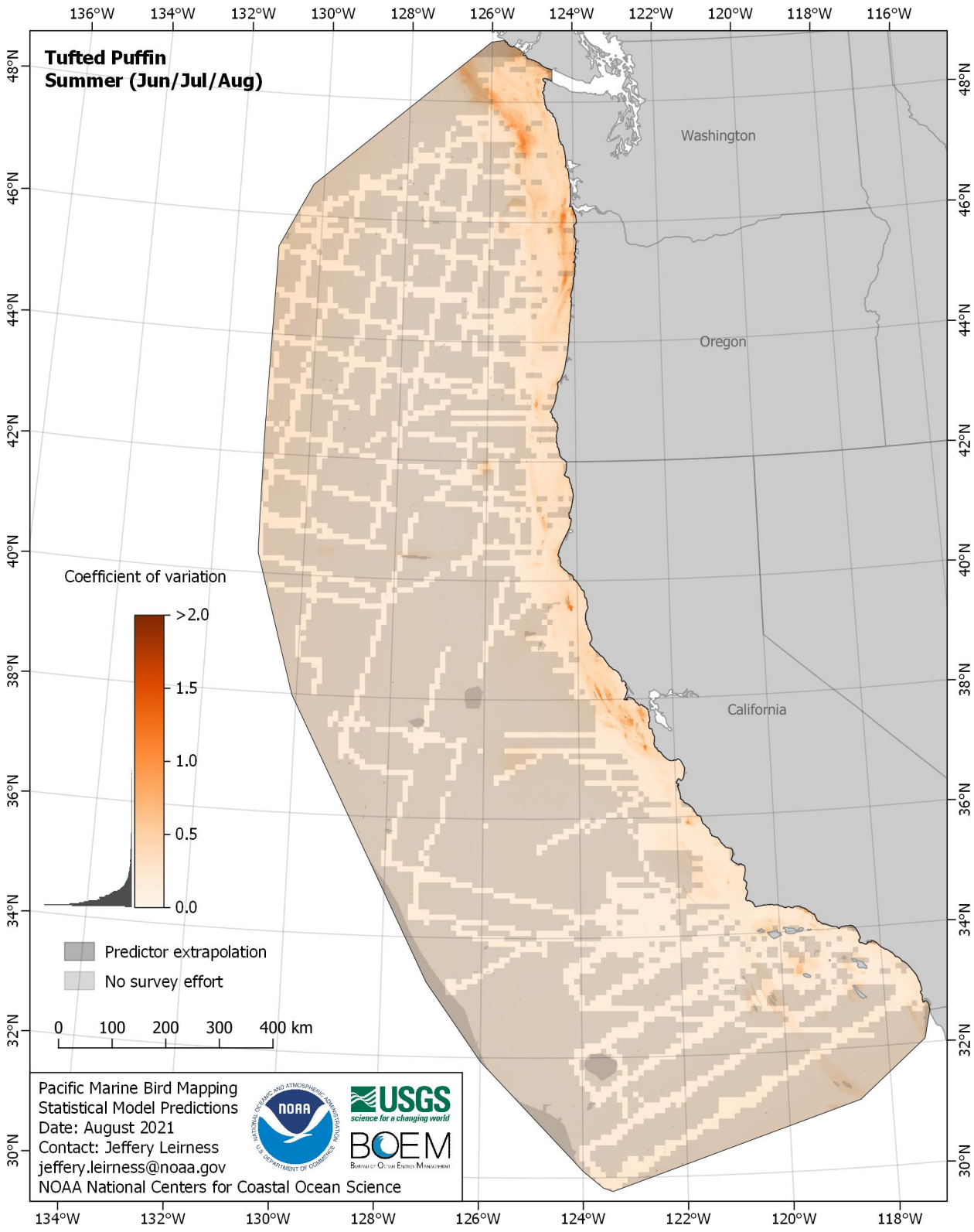

Figure E-86. Coefficient of variation for Tufted Puffin (*Fratercula cirrhata*) in the summer season

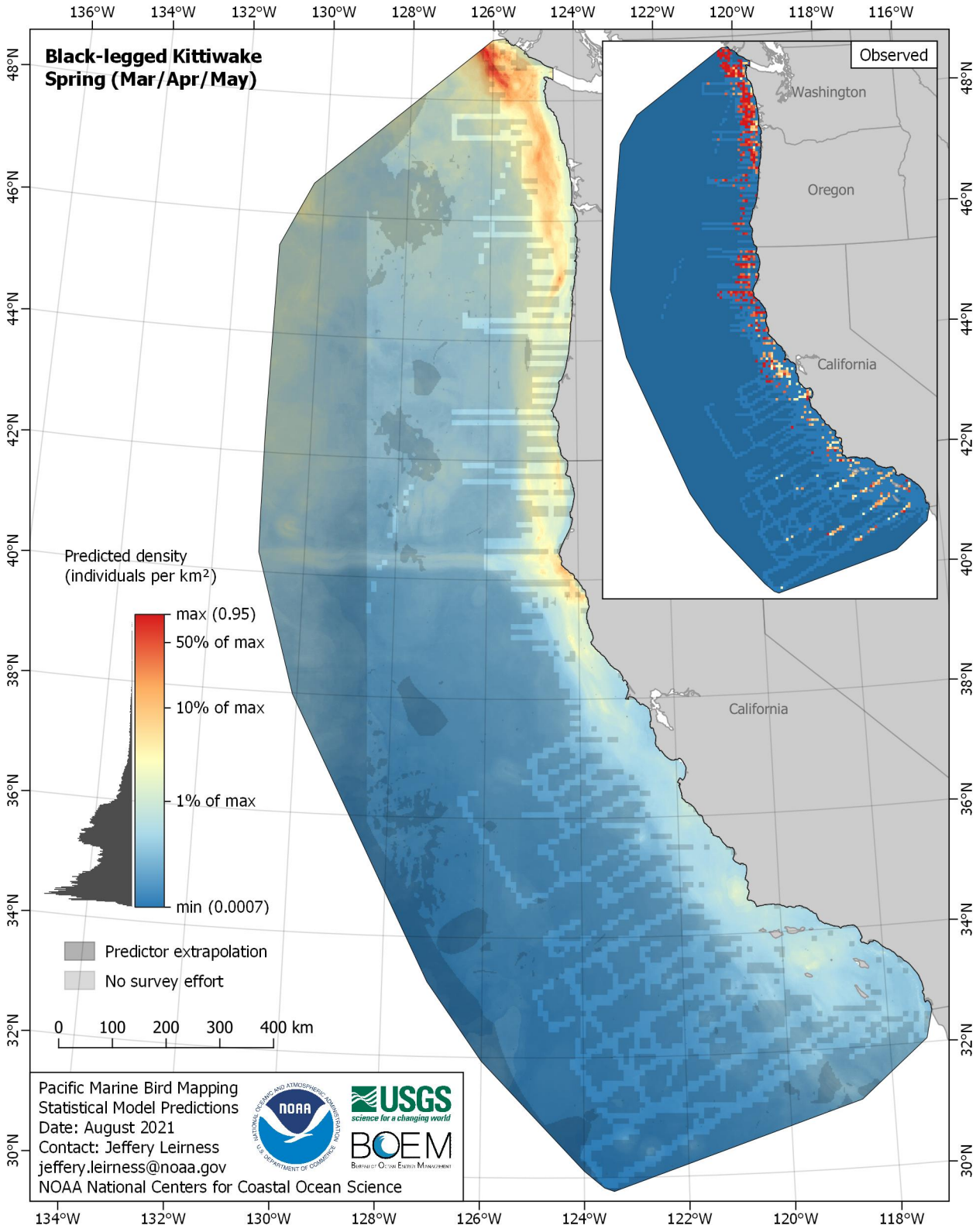

Figure E-87. Predicted density for Black-legged Kittiwake (*Rissa tridactyla*) in the spring season

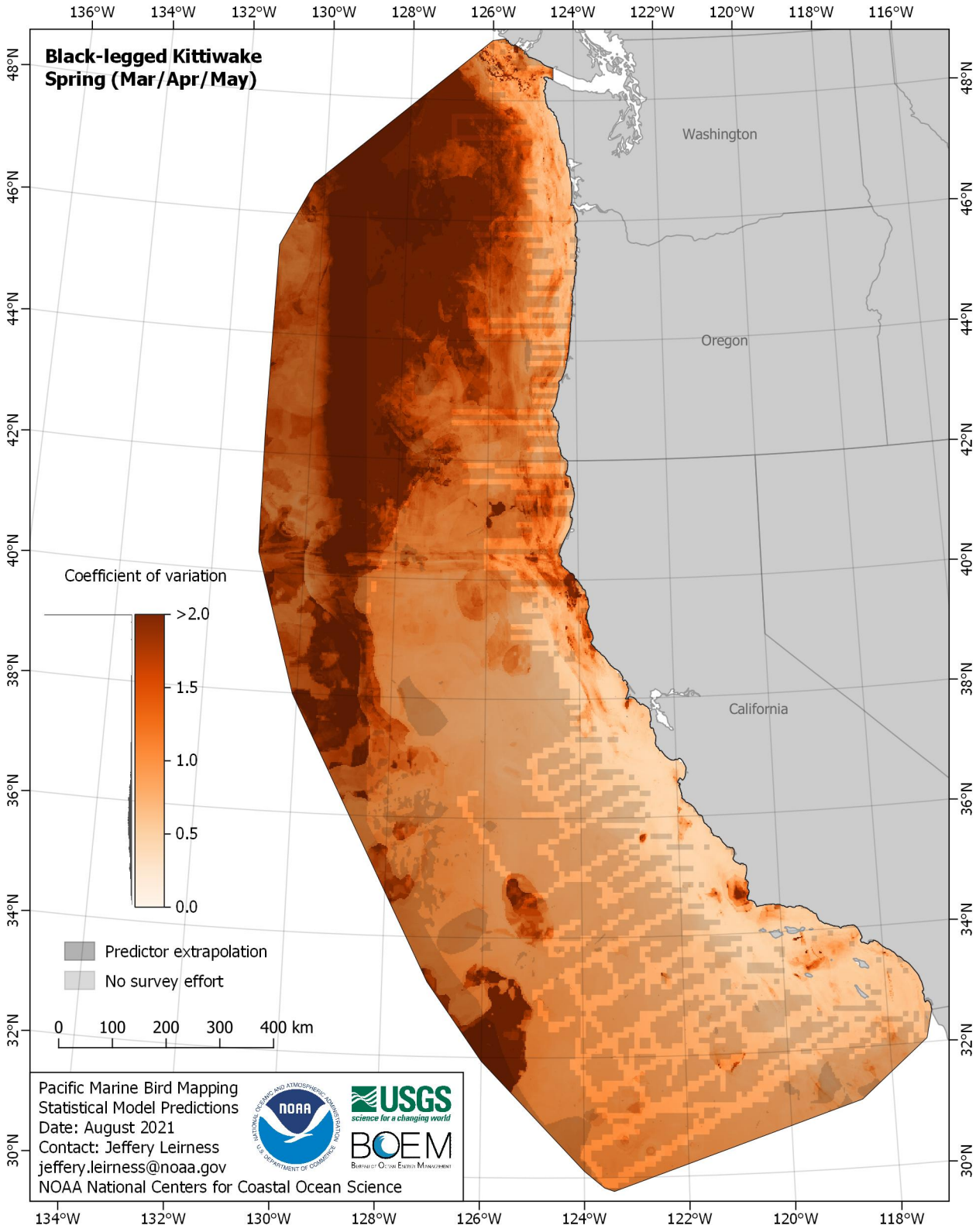

Figure E-88. Coefficient of variation for Black-legged Kittiwake (*Rissa tridactyla*) in the spring season

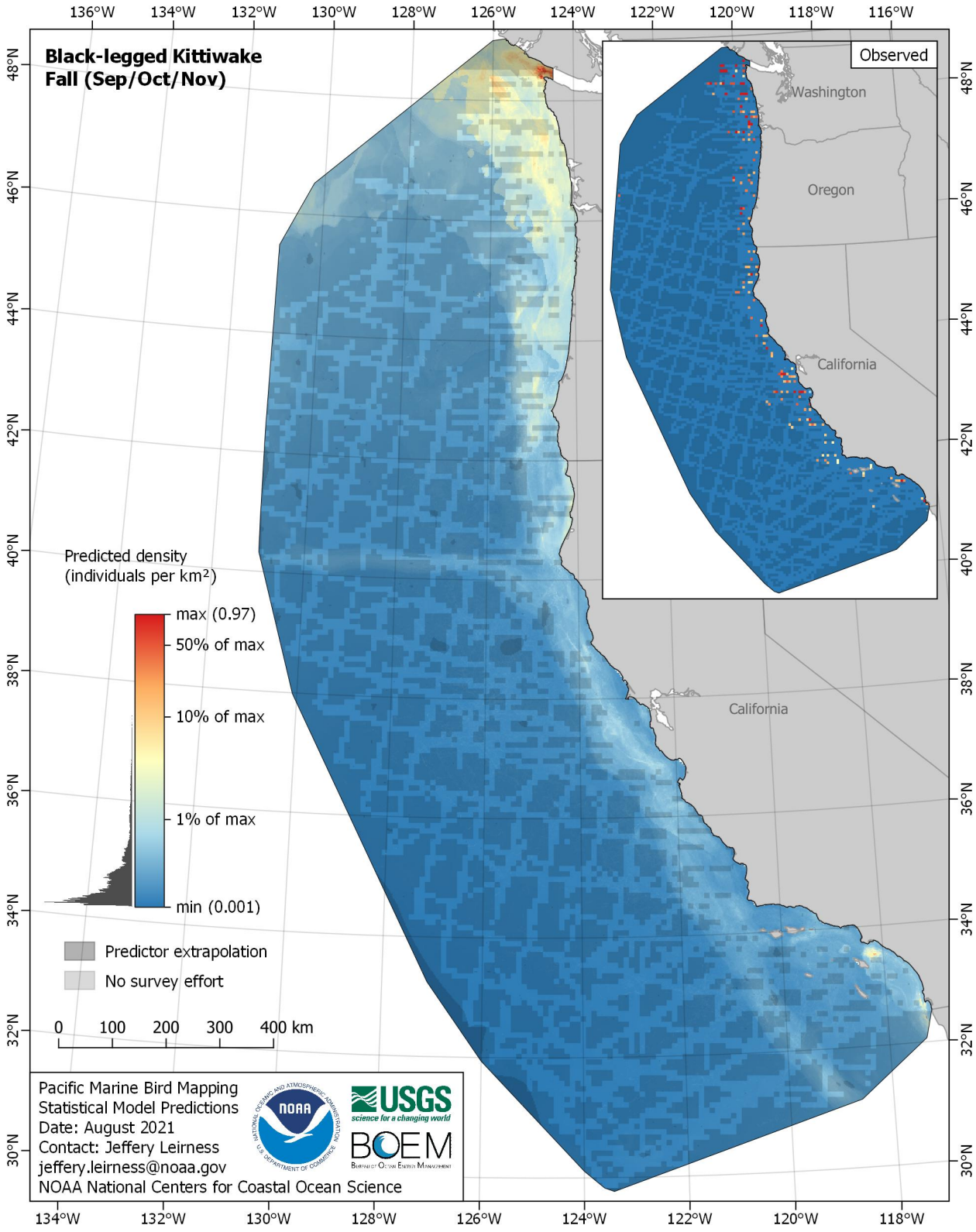

Figure E-89. Predicted density for Black-legged Kittiwake (*Rissa tridactyla*) in the fall season

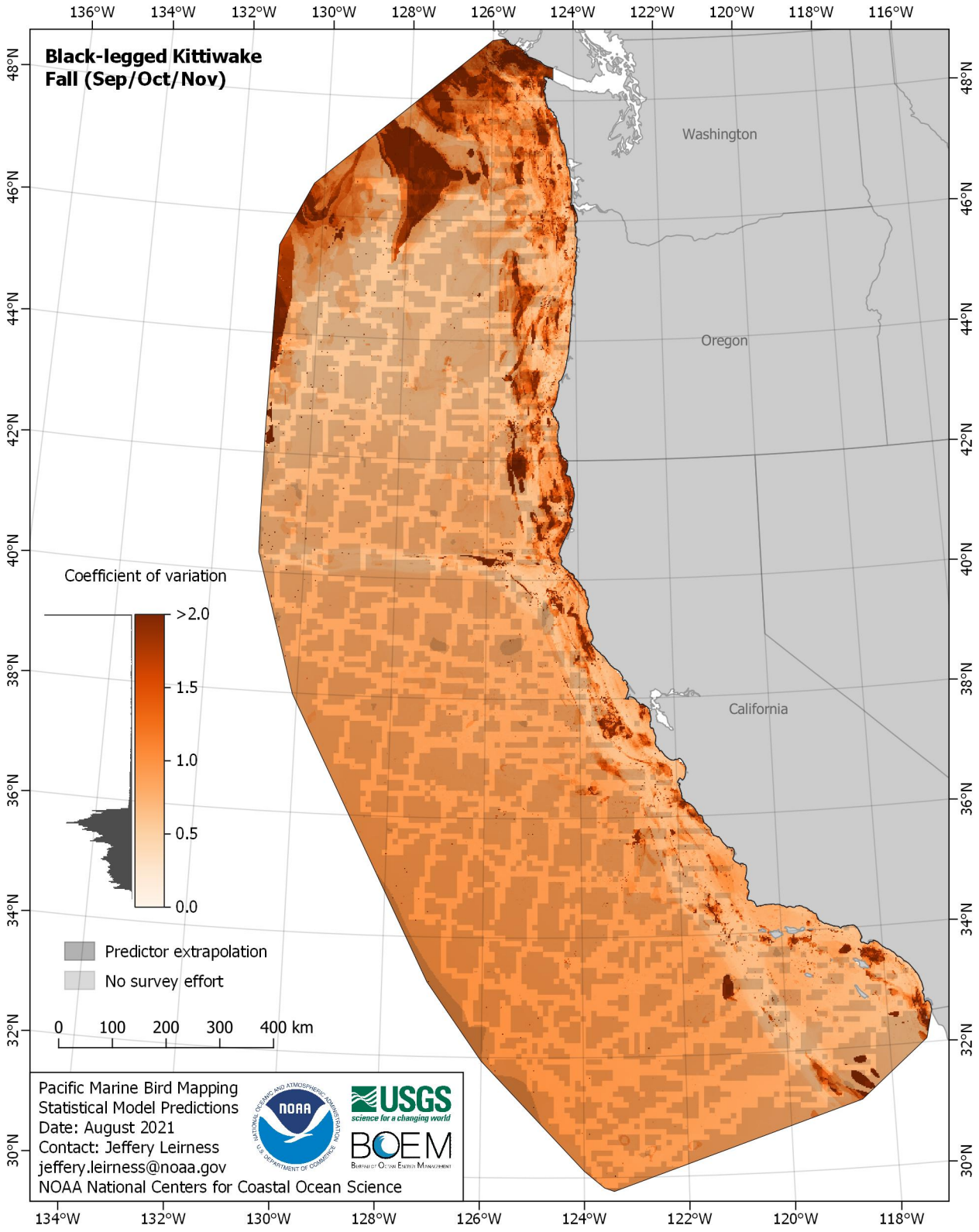

Figure E-90. Coefficient of variation for Black-legged Kittiwake (*Rissa tridactyla*) in the fall season

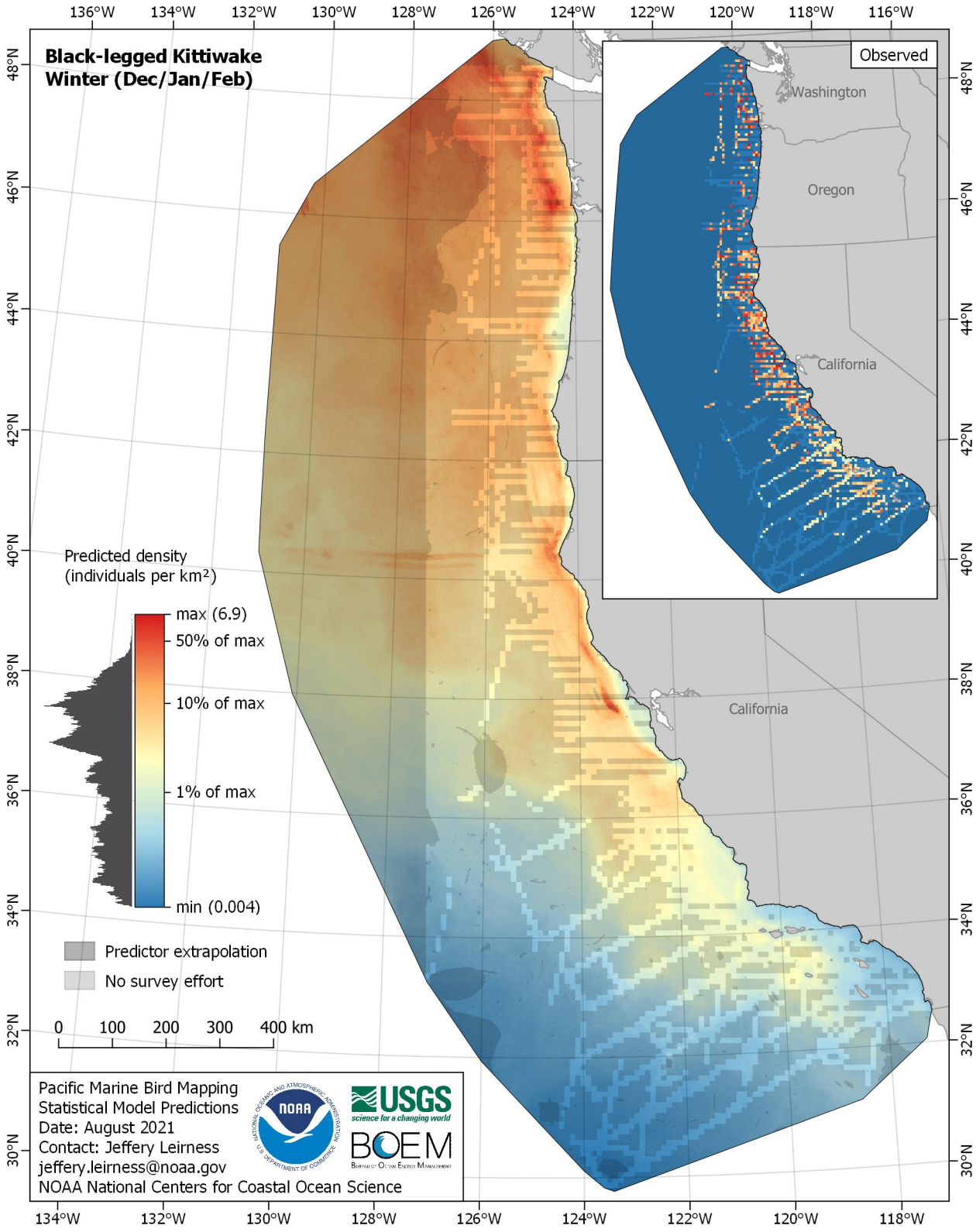

Figure E-91. Predicted density for Black-legged Kittiwake (*Rissa tridactyla*) in the winter season

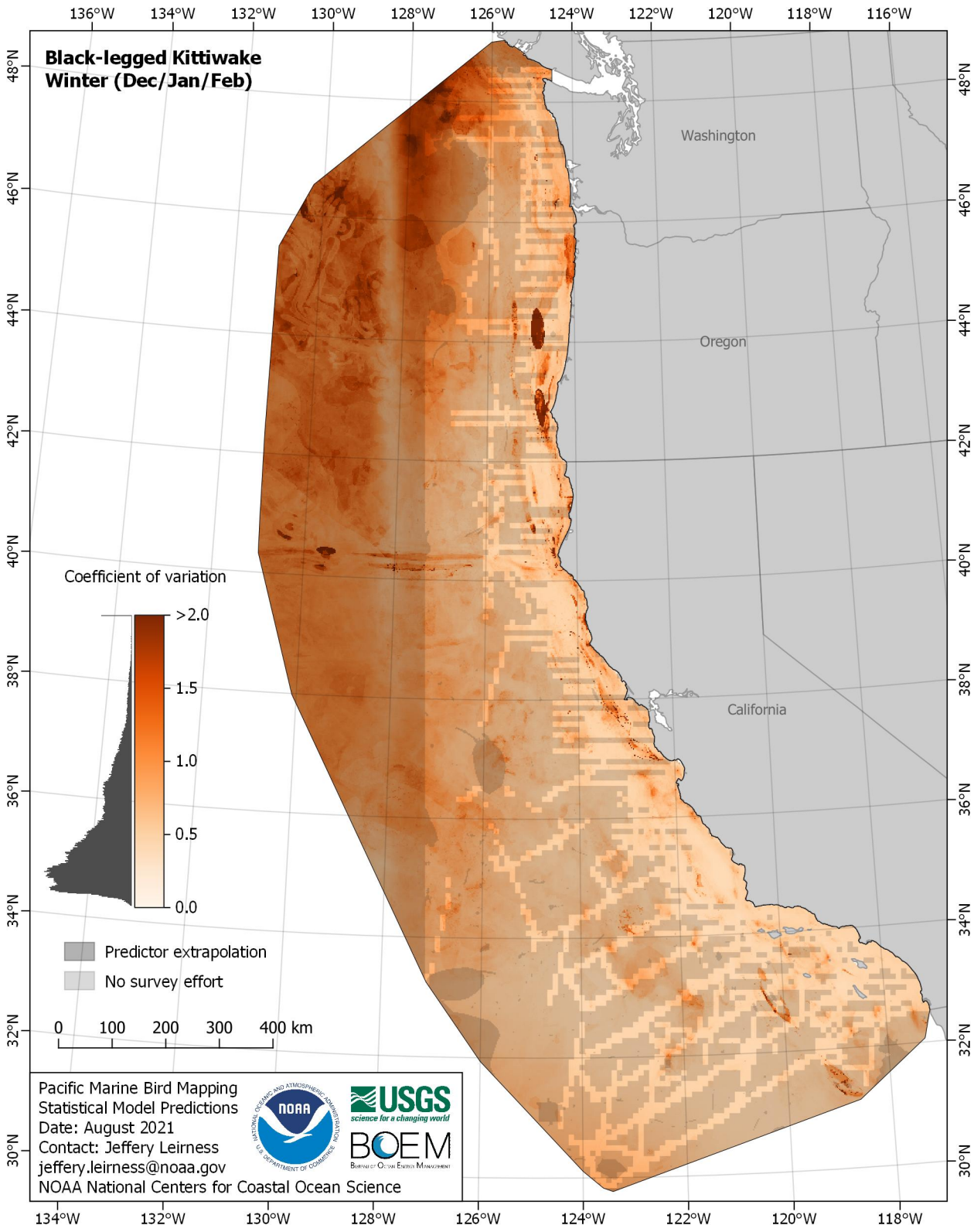

Figure E-92. Coefficient of variation for Black-legged Kittiwake (*Rissa tridactyla*) in the winter season

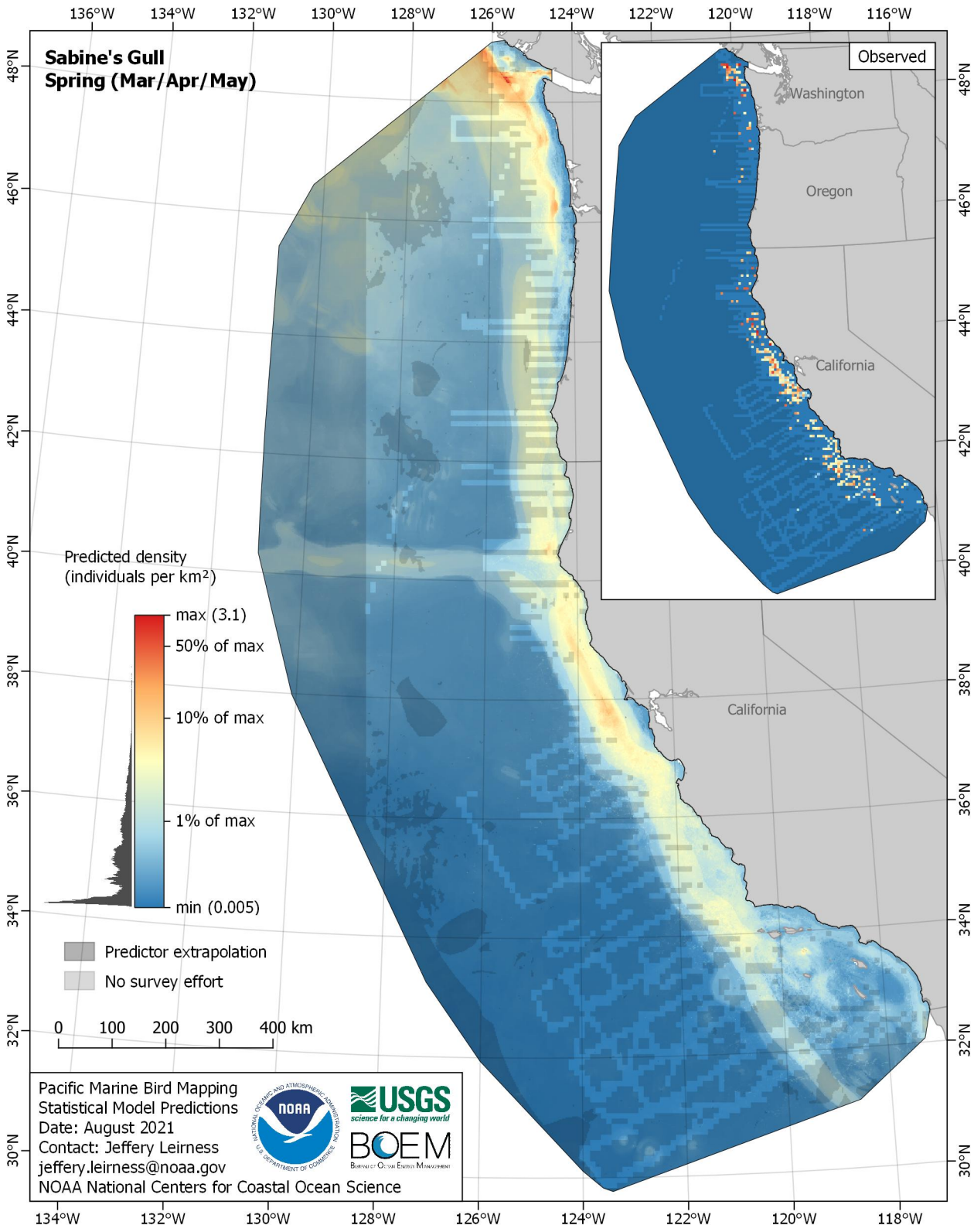

Figure E-93. Predicted density for Sabine's Gull (*Xema sabini*) in the spring season

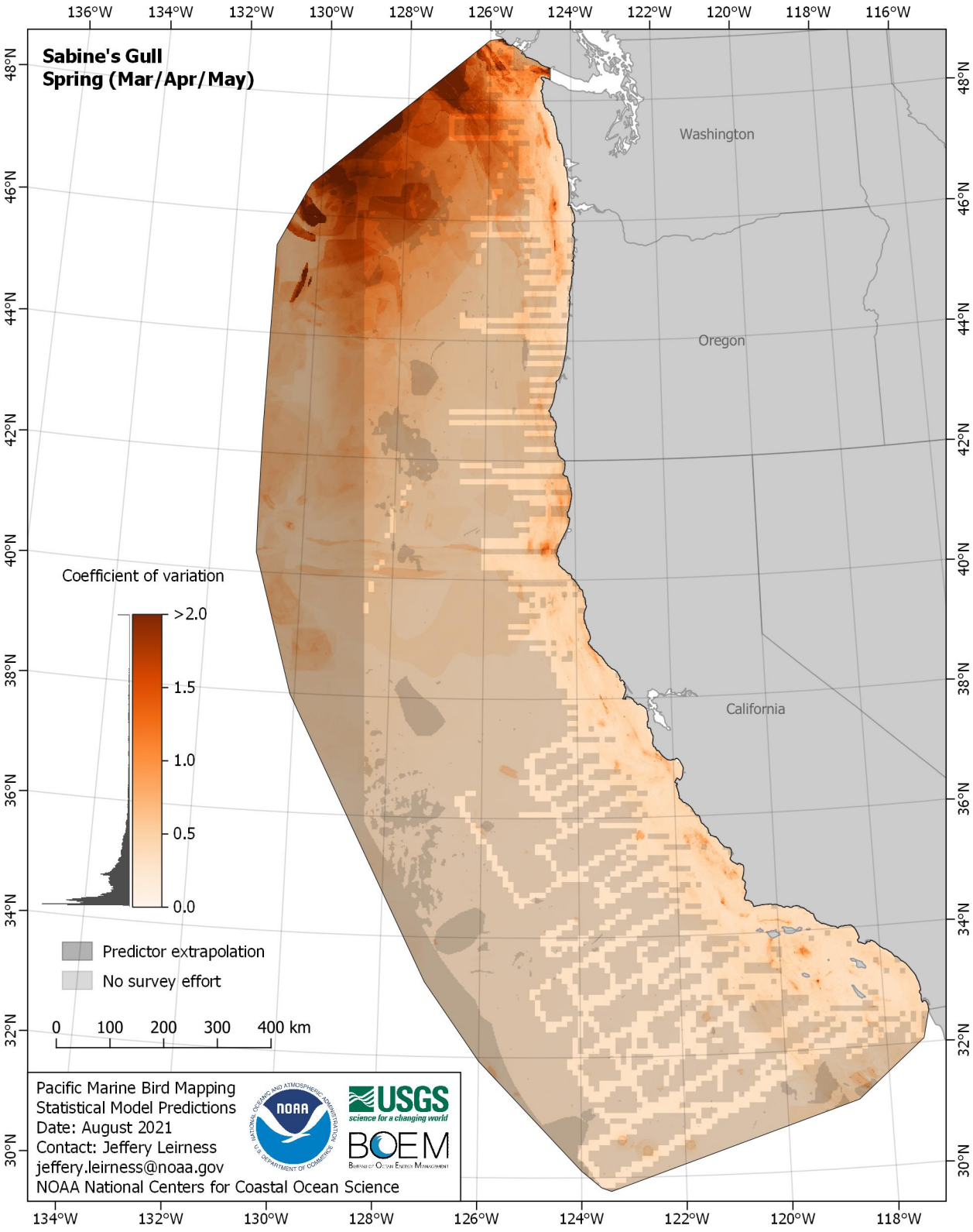

Figure E-94. Coefficient of variation for Sabine's Gull (*Xema sabini*) in the spring season

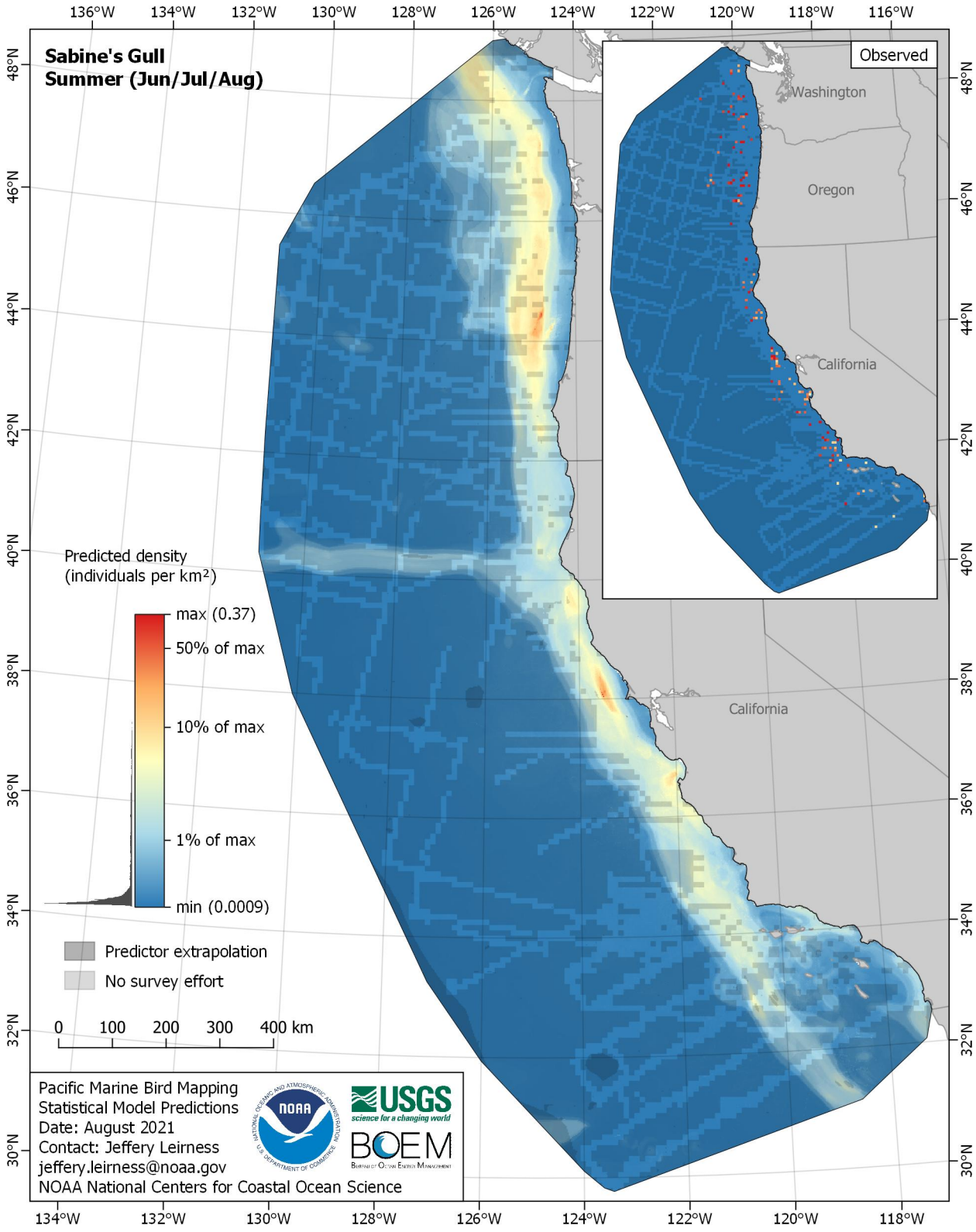

Figure E-95. Predicted density for Sabine's Gull (*Xema sabini*) in the summer season

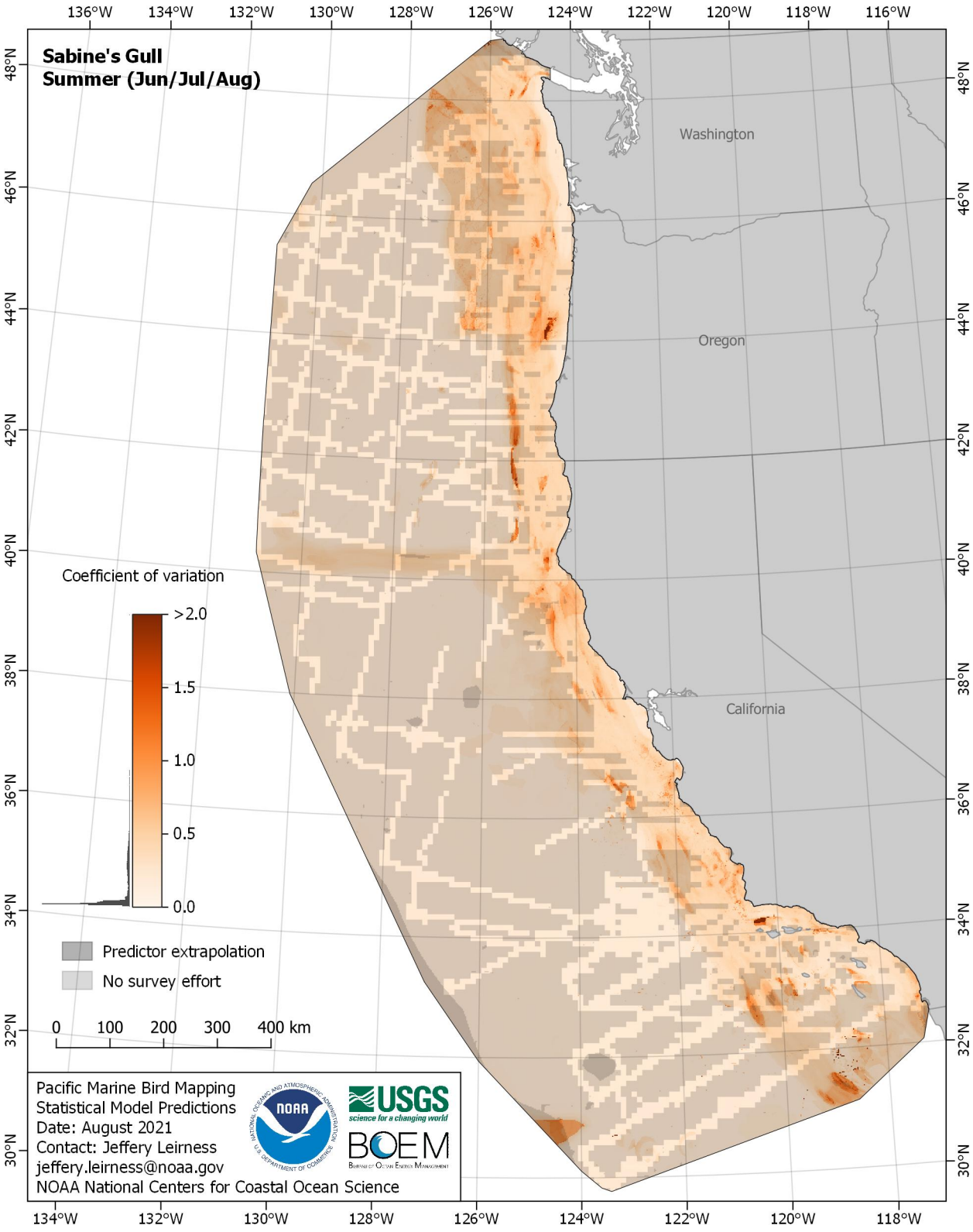

Figure E-96. Coefficient of variation for Sabine's Gull (*Xema sabini*) in the summer season

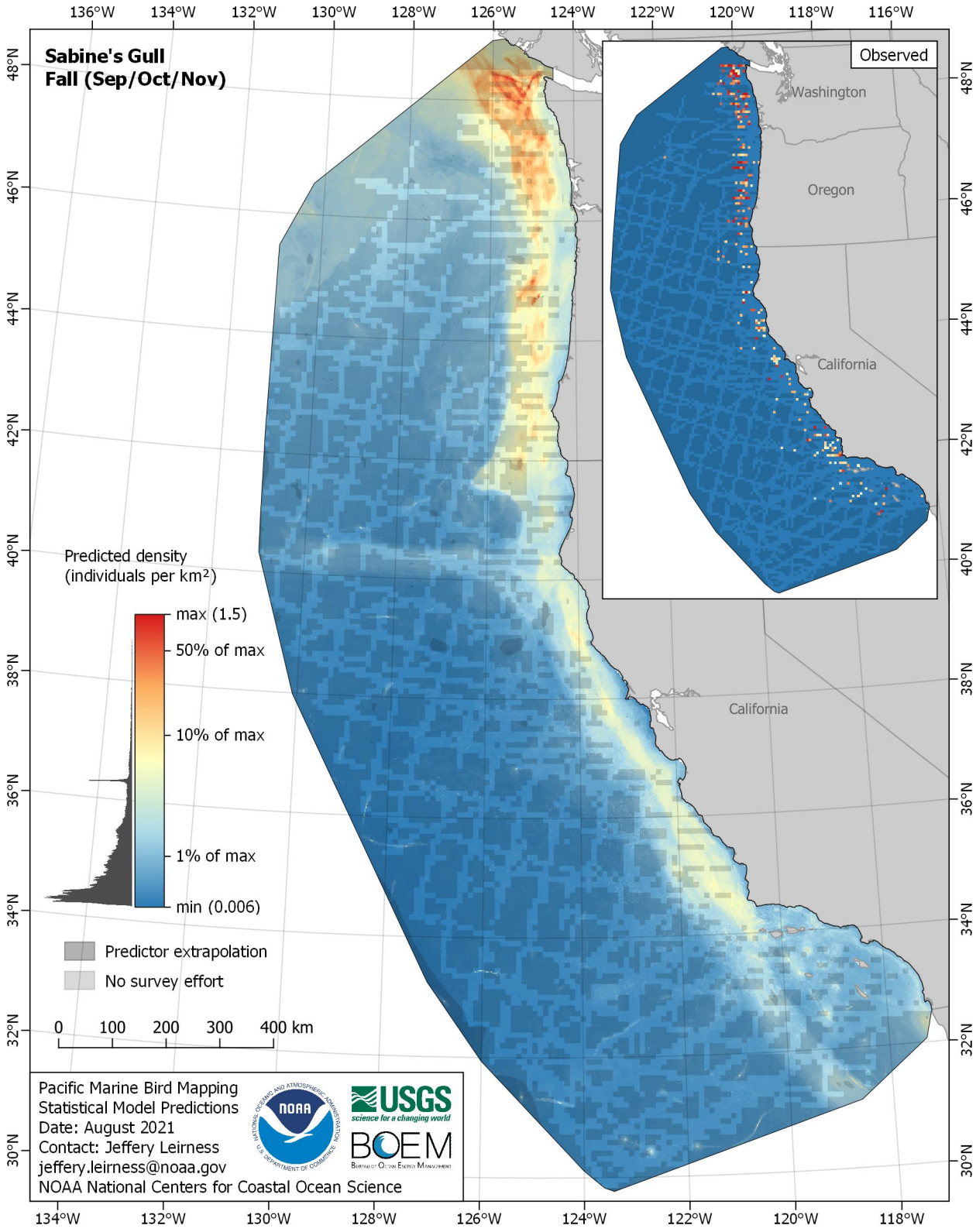

Figure E-97. Predicted density for Sabine's Gull (*Xema sabini*) in the fall season

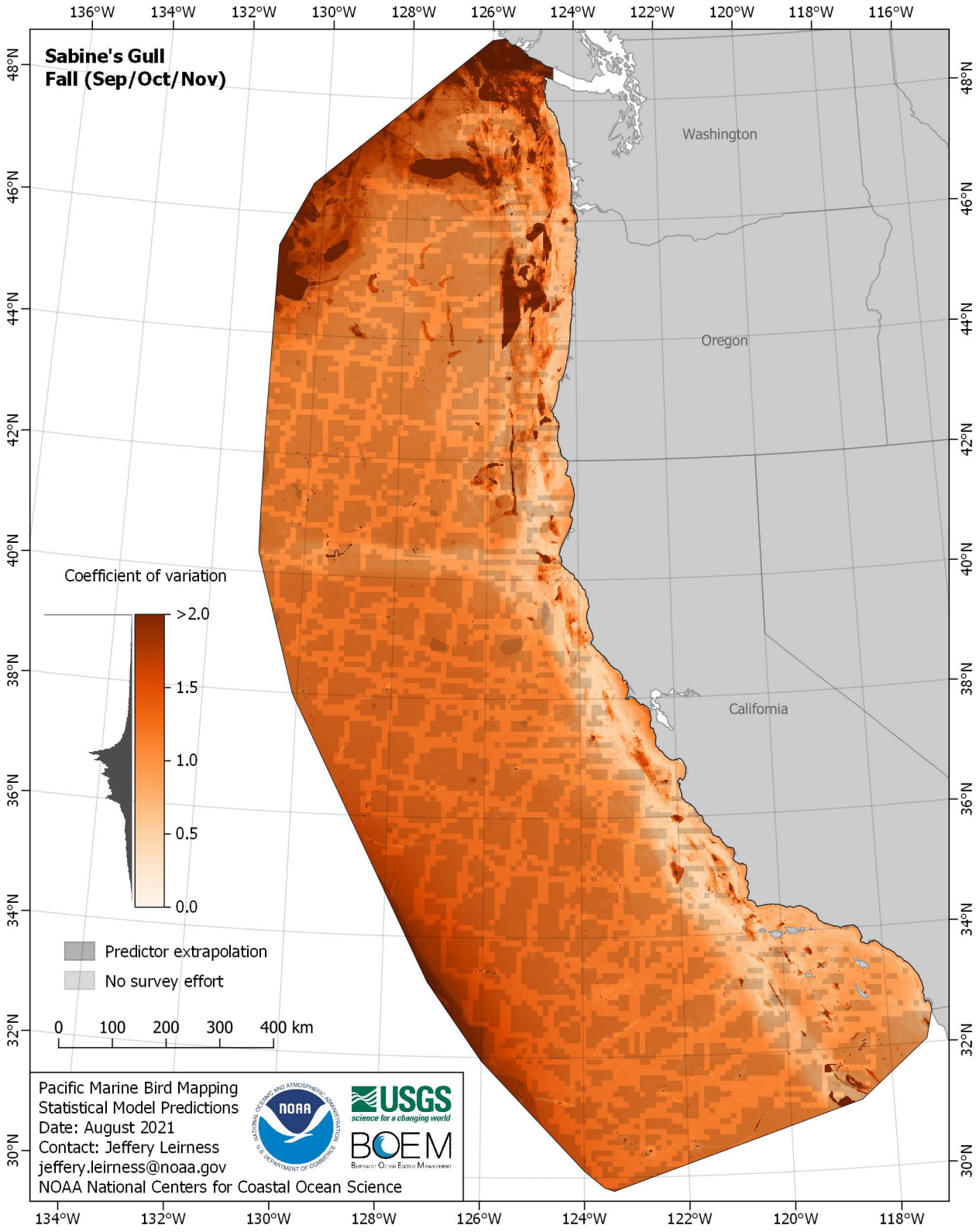

Figure E-98. Coefficient of variation for Sabine's Gull (*Xema sabini*) in the fall season

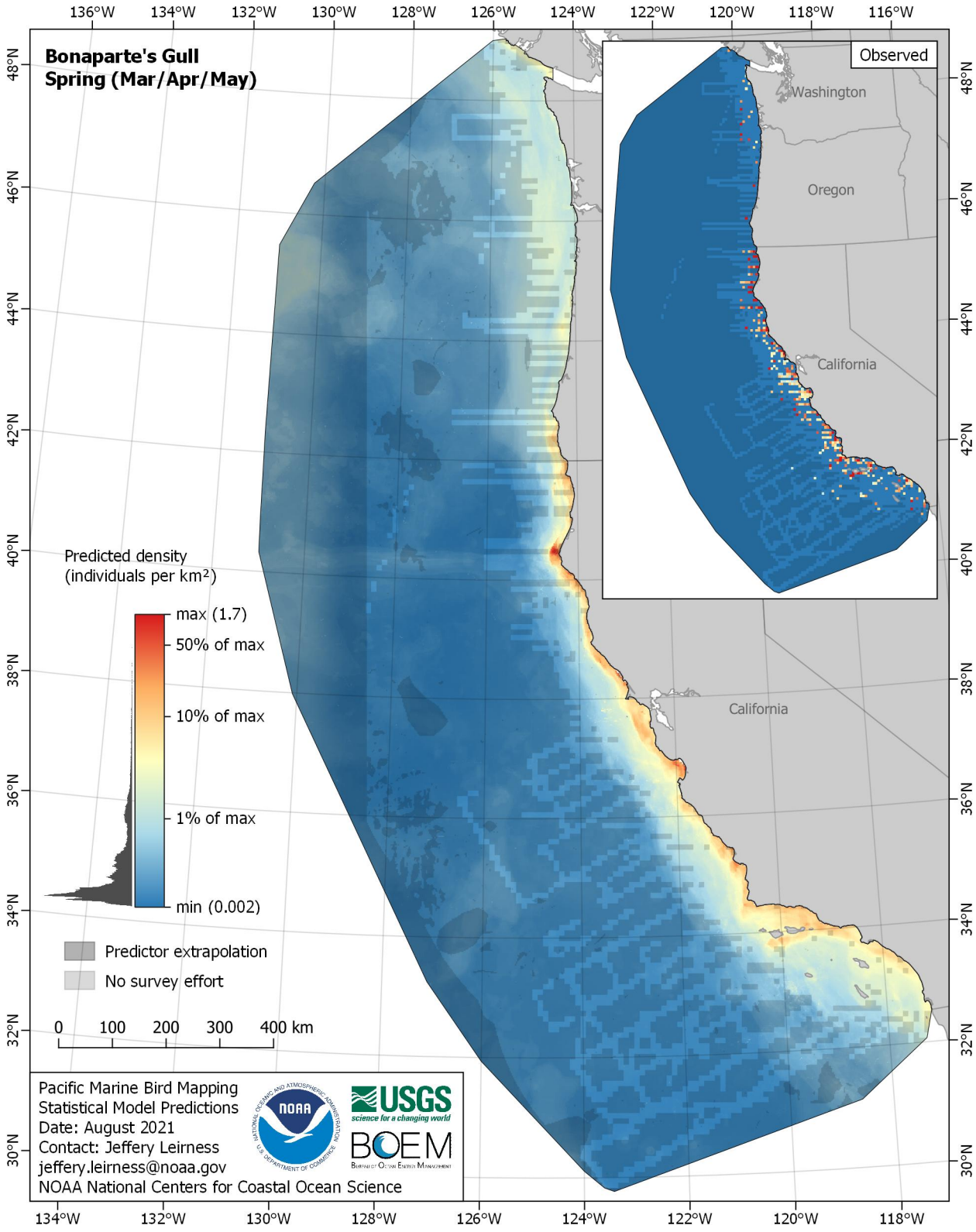

Figure E-99. Predicted density for Bonaparte's Gull (*Chroicocephalus philadelphia*) in the spring season

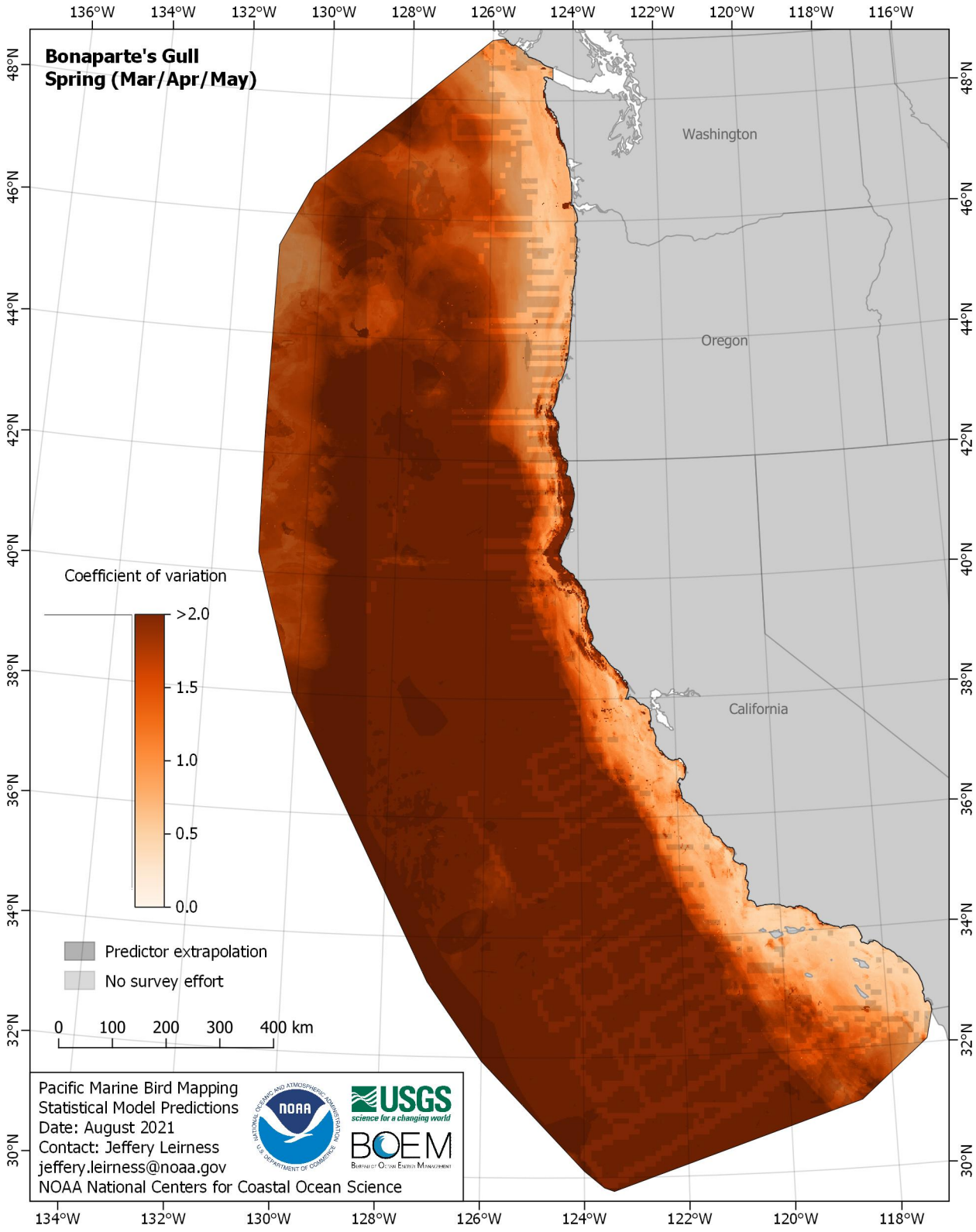

Figure E-100. Coefficient of variation for Bonaparte's Gull (*Chroicocephalus philadelphia*) in the spring season

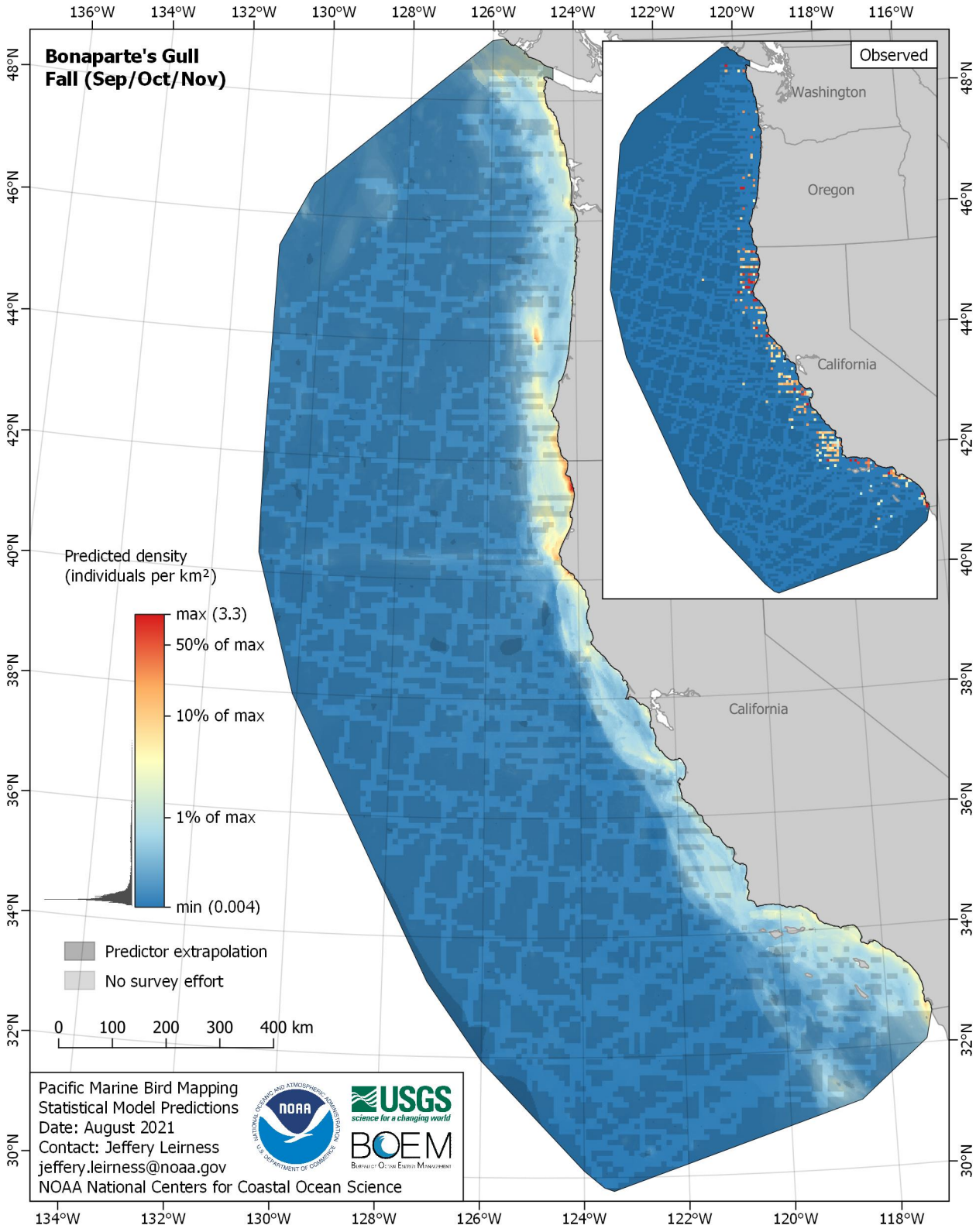

Figure E-101. Predicted density for Bonaparte's Gull (*Chroicocephalus philadelphia*) in the fall season

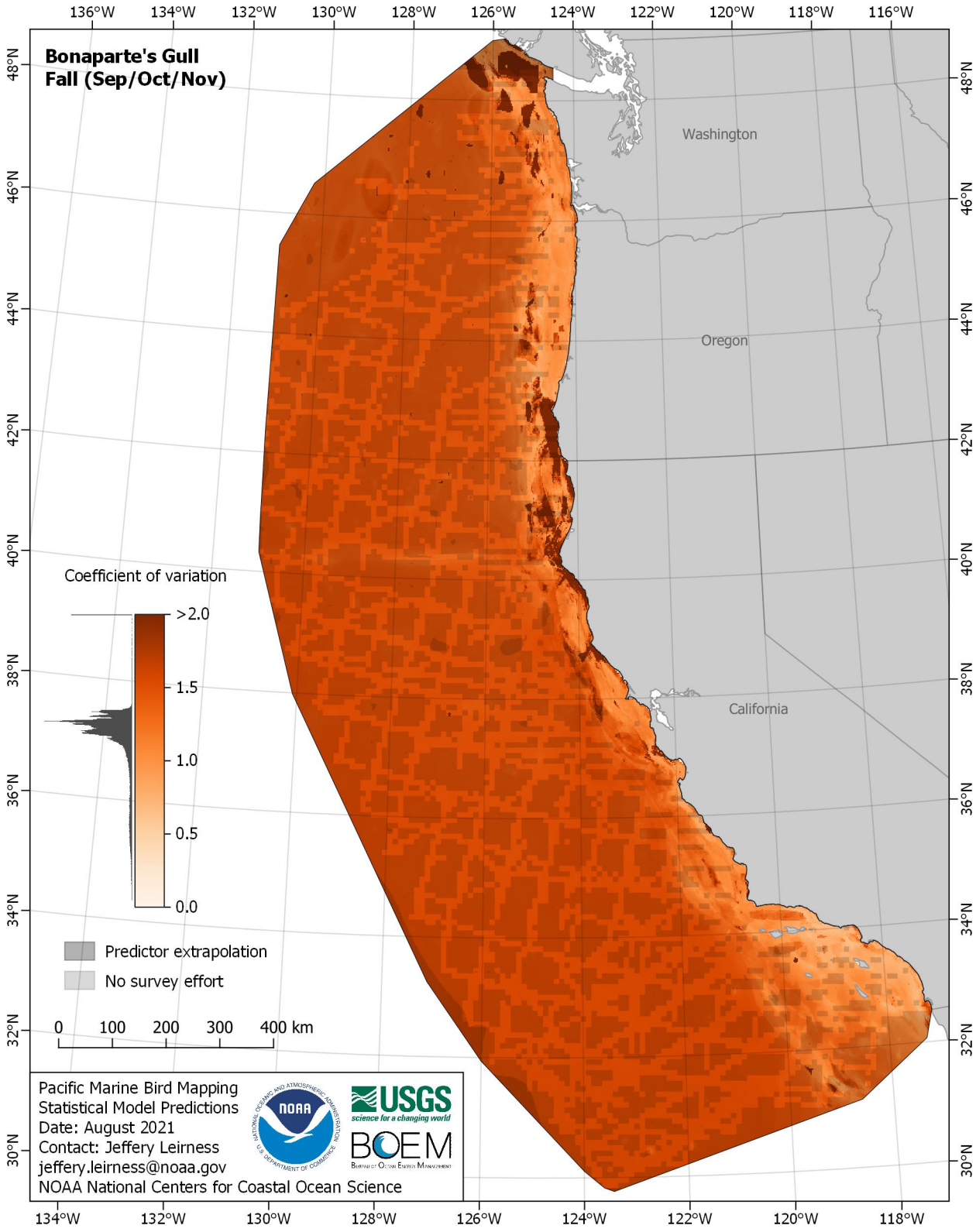

Figure E-102. Coefficient of variation for Bonaparte's Gull (*Chroicocephalus philadelphia*) in the fall season

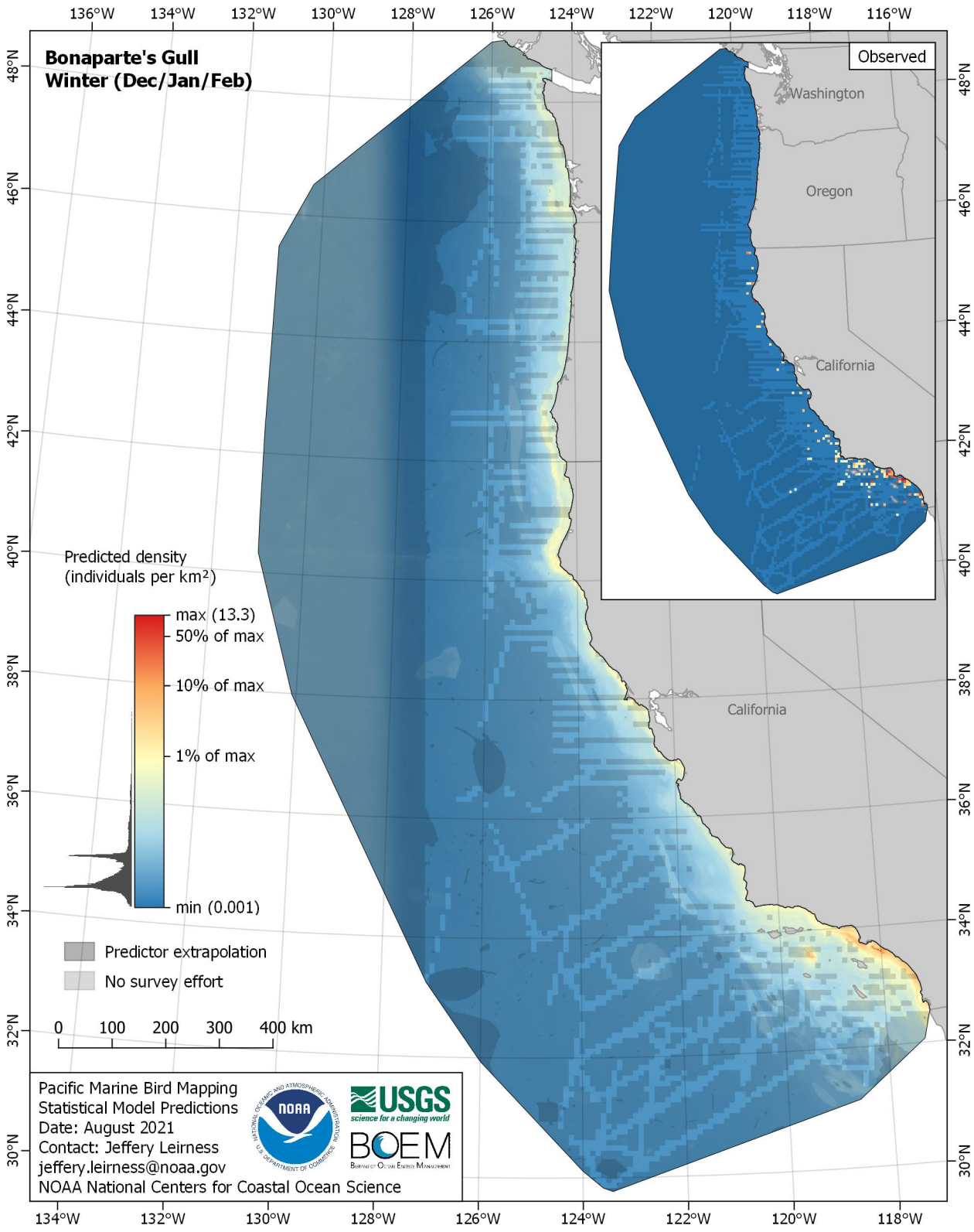

Figure E-103. Predicted density for Bonaparte's Gull (*Chroicocephalus philadelphia*) in the winter season

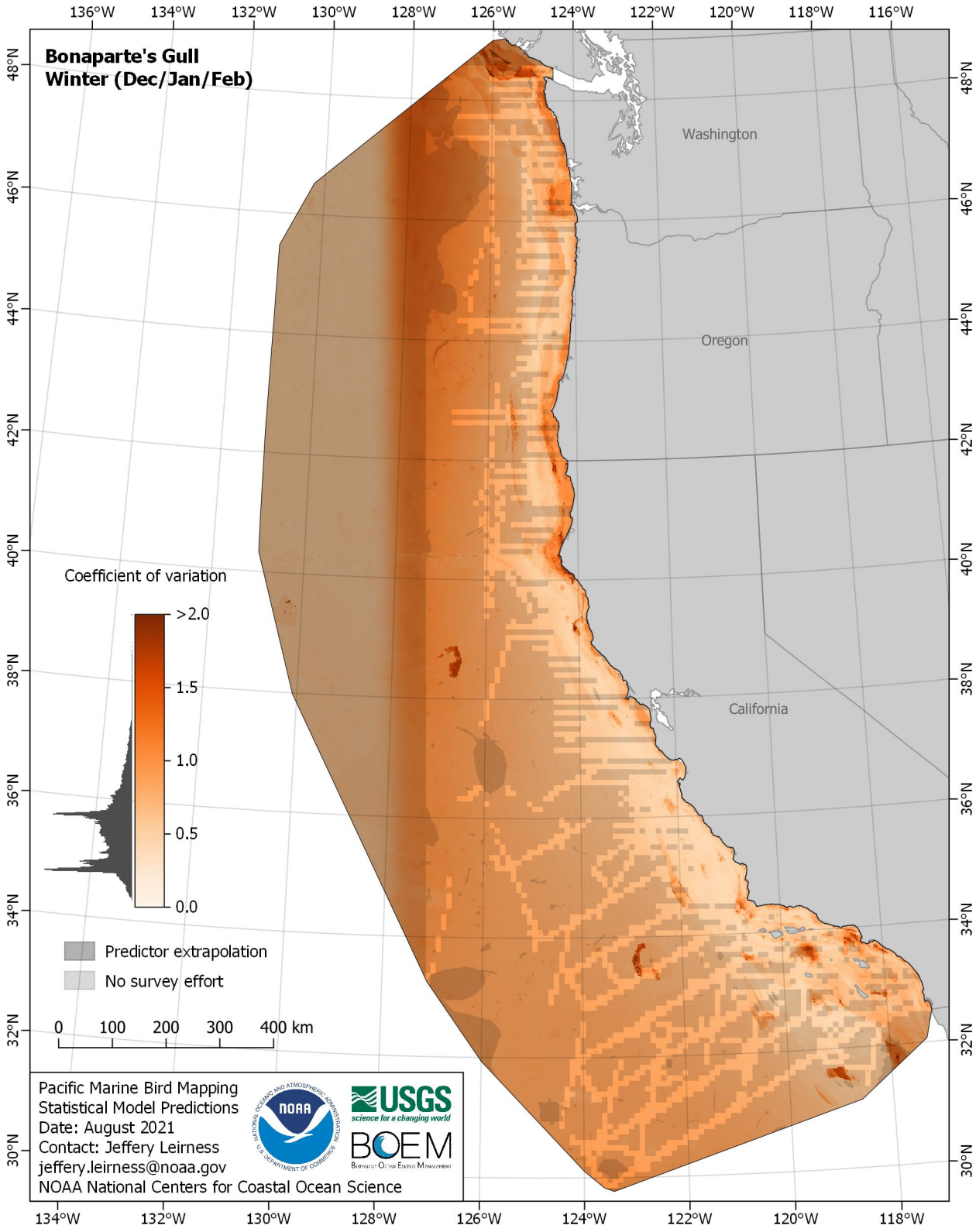

Figure E-104. Coefficient of variation for Bonaparte's Gull (*Chroicocephalus philadelphia*) in the winter season

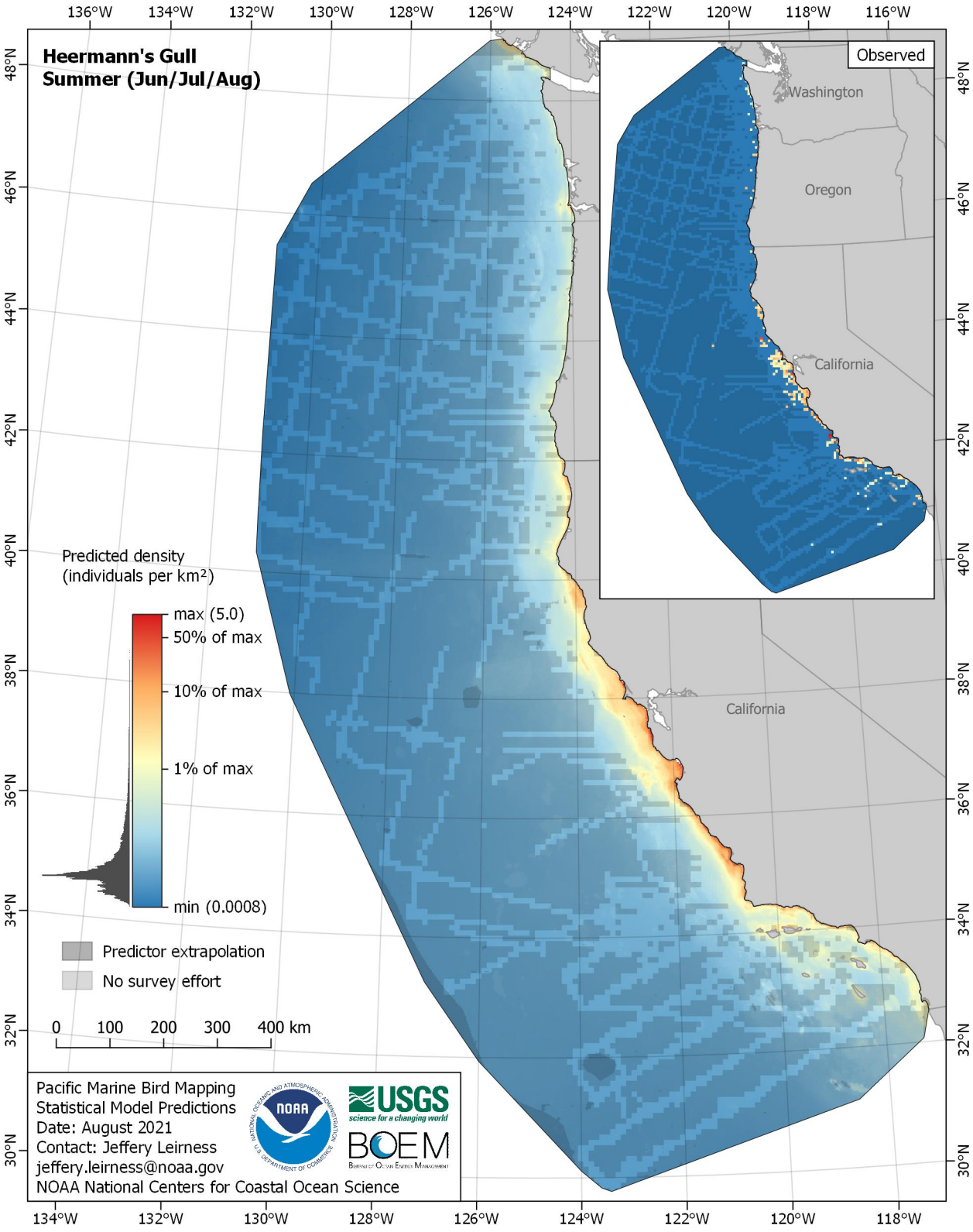

Figure E-105. Predicted density for Heermann's Gull (*Larus heermanni*) in the summer season

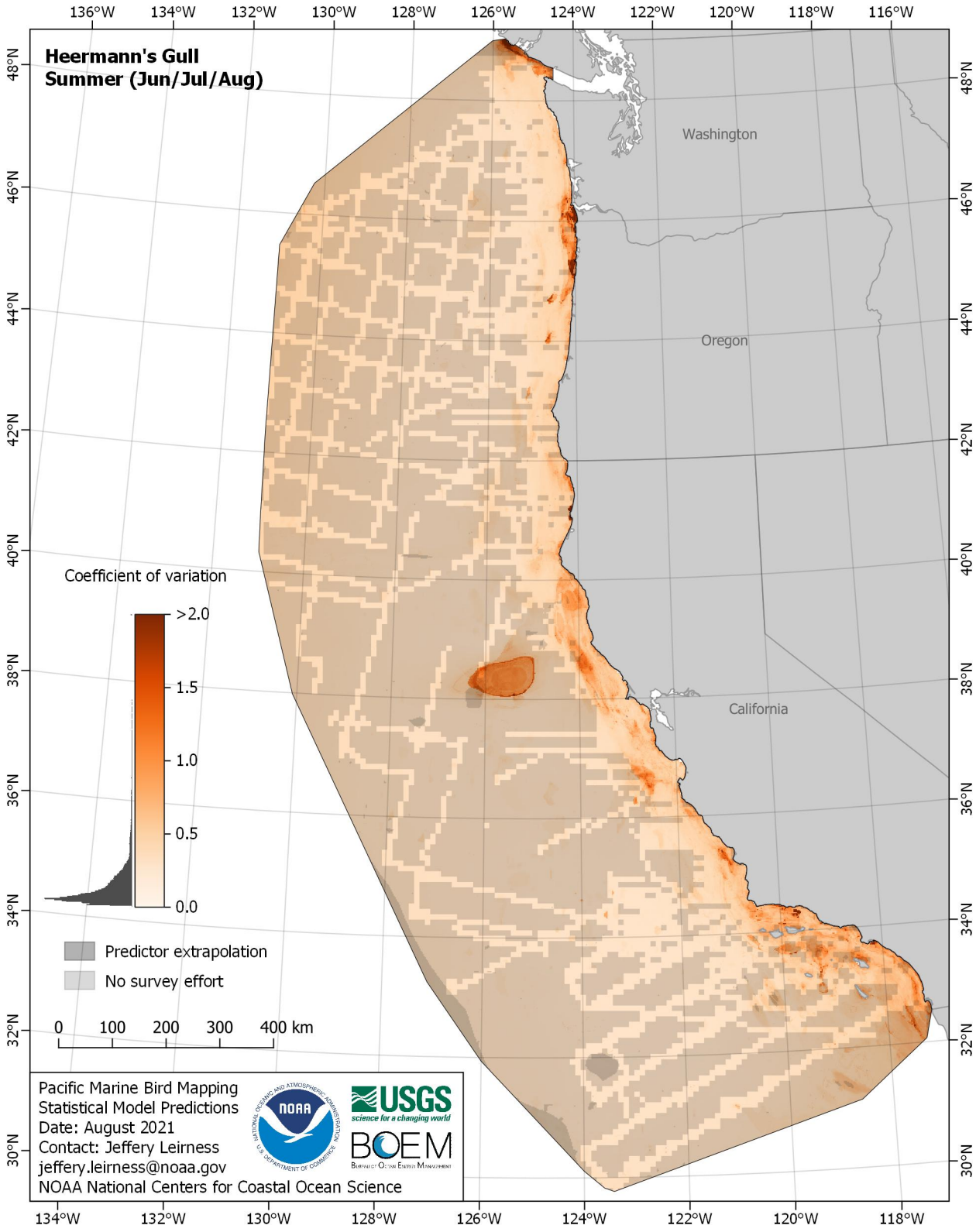

Figure E-106. Coefficient of variation for Heermann's Gull (*Larus heermanni*) in the summer season

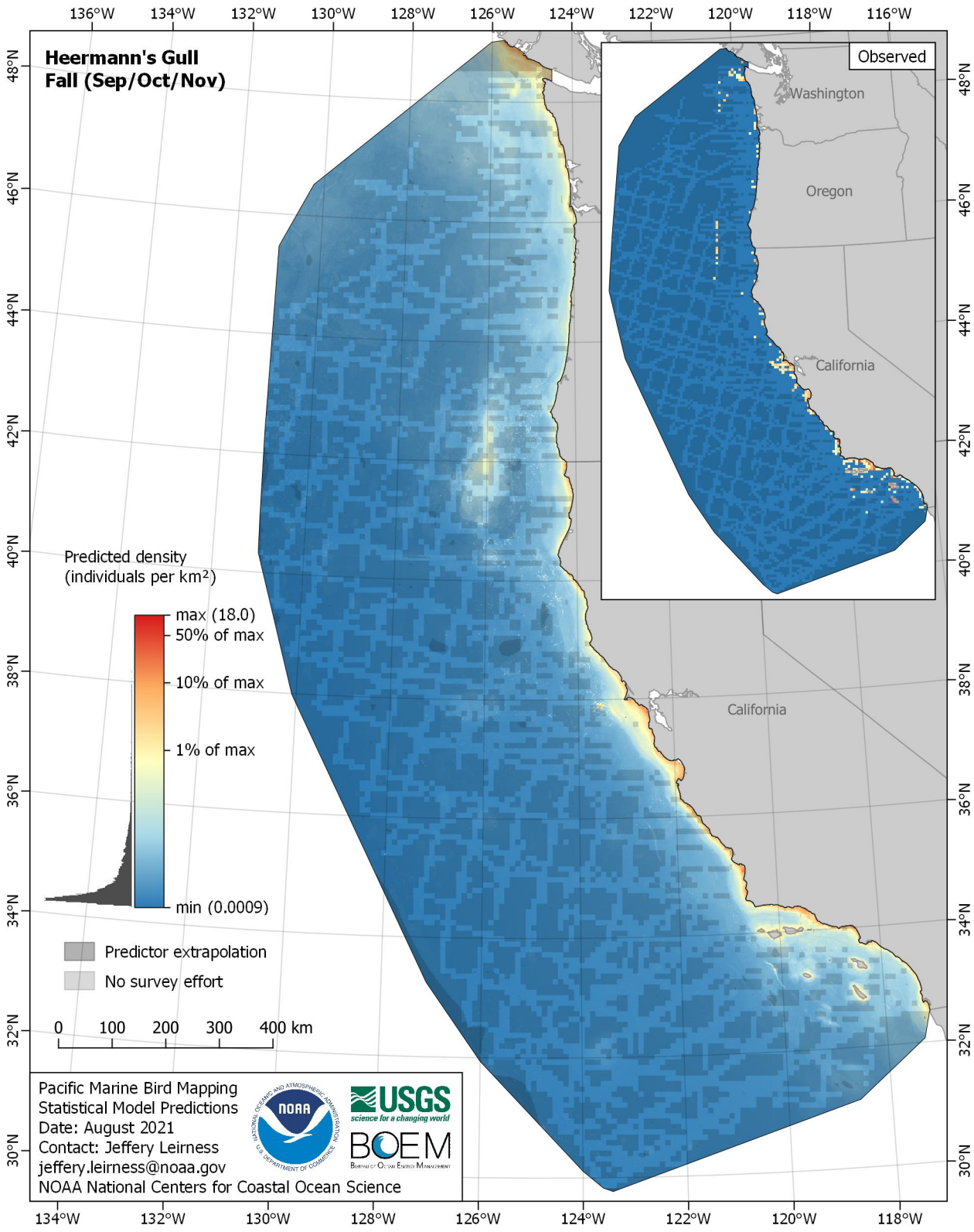

Figure E-107. Predicted density for Heermann's Gull (*Larus heermanni*) in the fall season

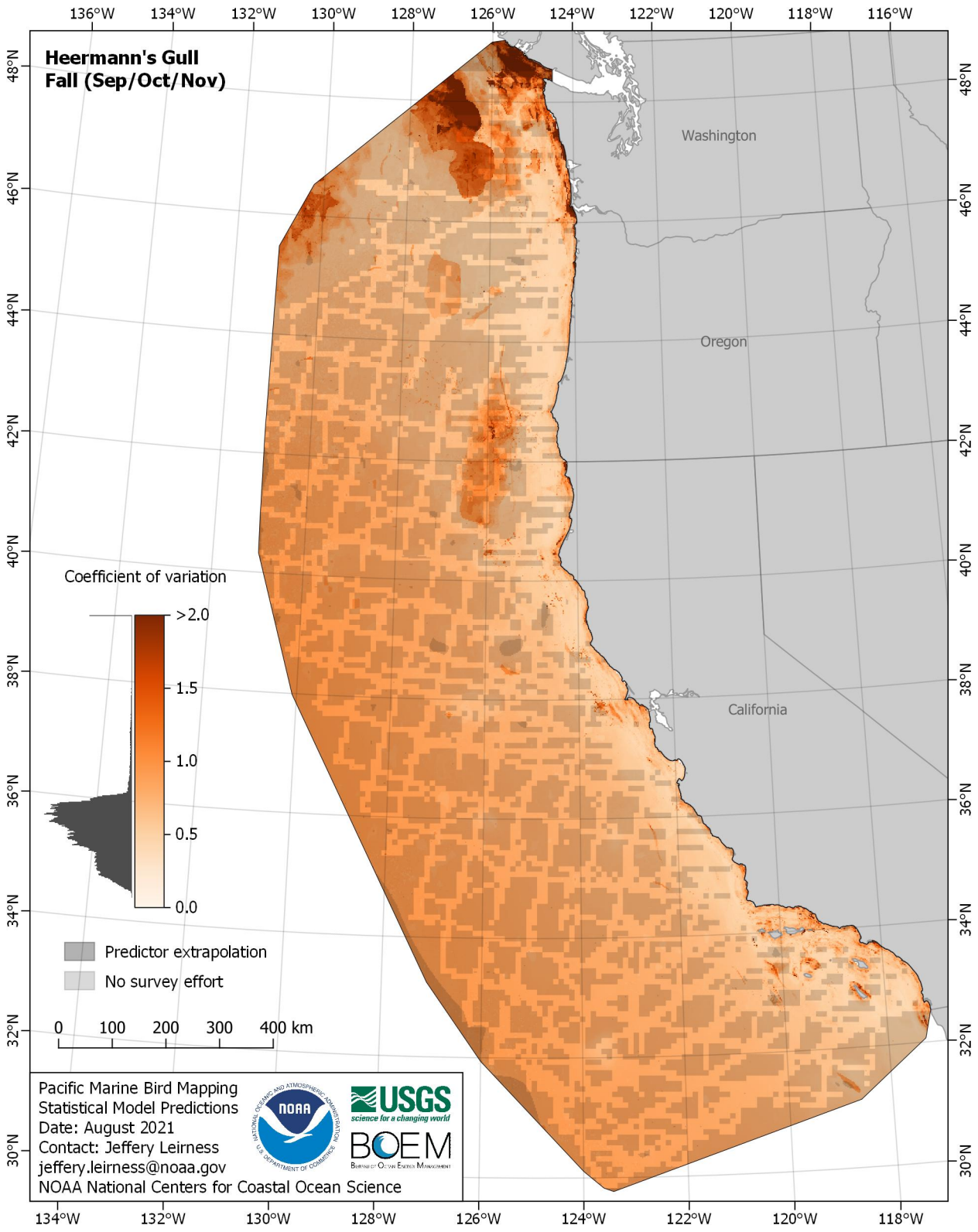

Figure E-108. Coefficient of variation for Heermann's Gull (*Larus heermanni*) in the fall season

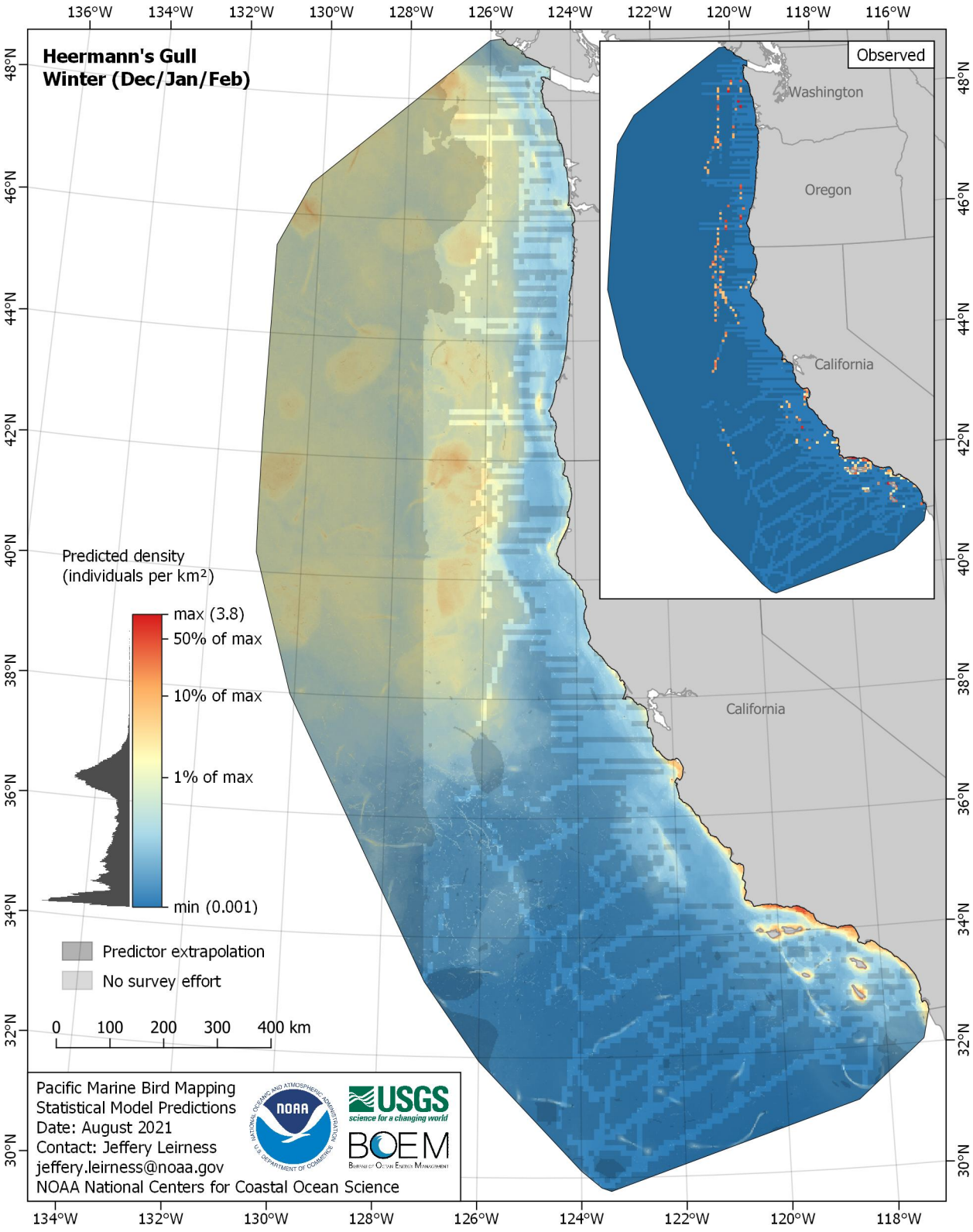

Figure E-109. Predicted density for Heermann's Gull (*Larus heermanni*) in the winter season

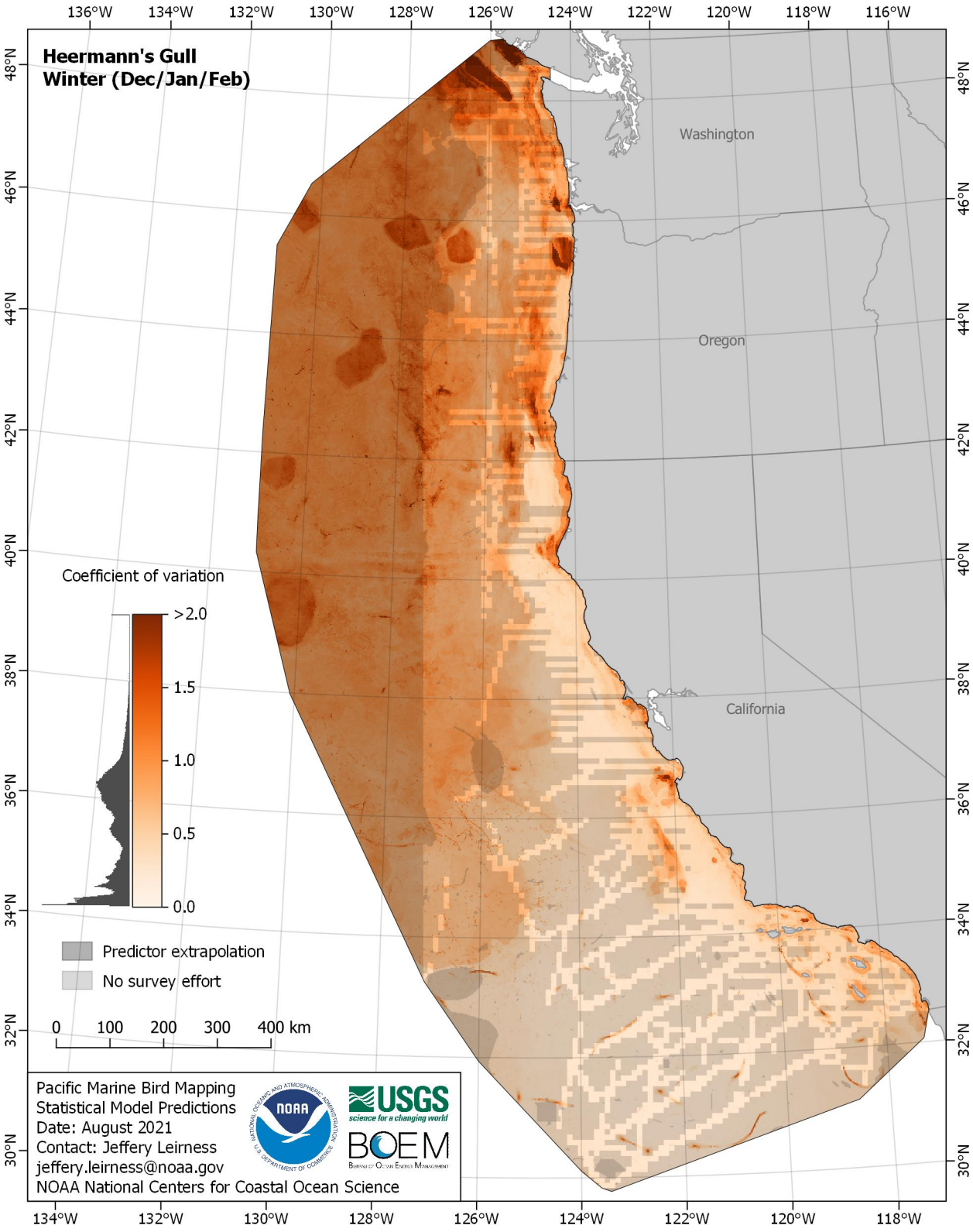

Figure E-110. Coefficient of variation for Heermann's Gull (*Larus heermanni*) in the winter season

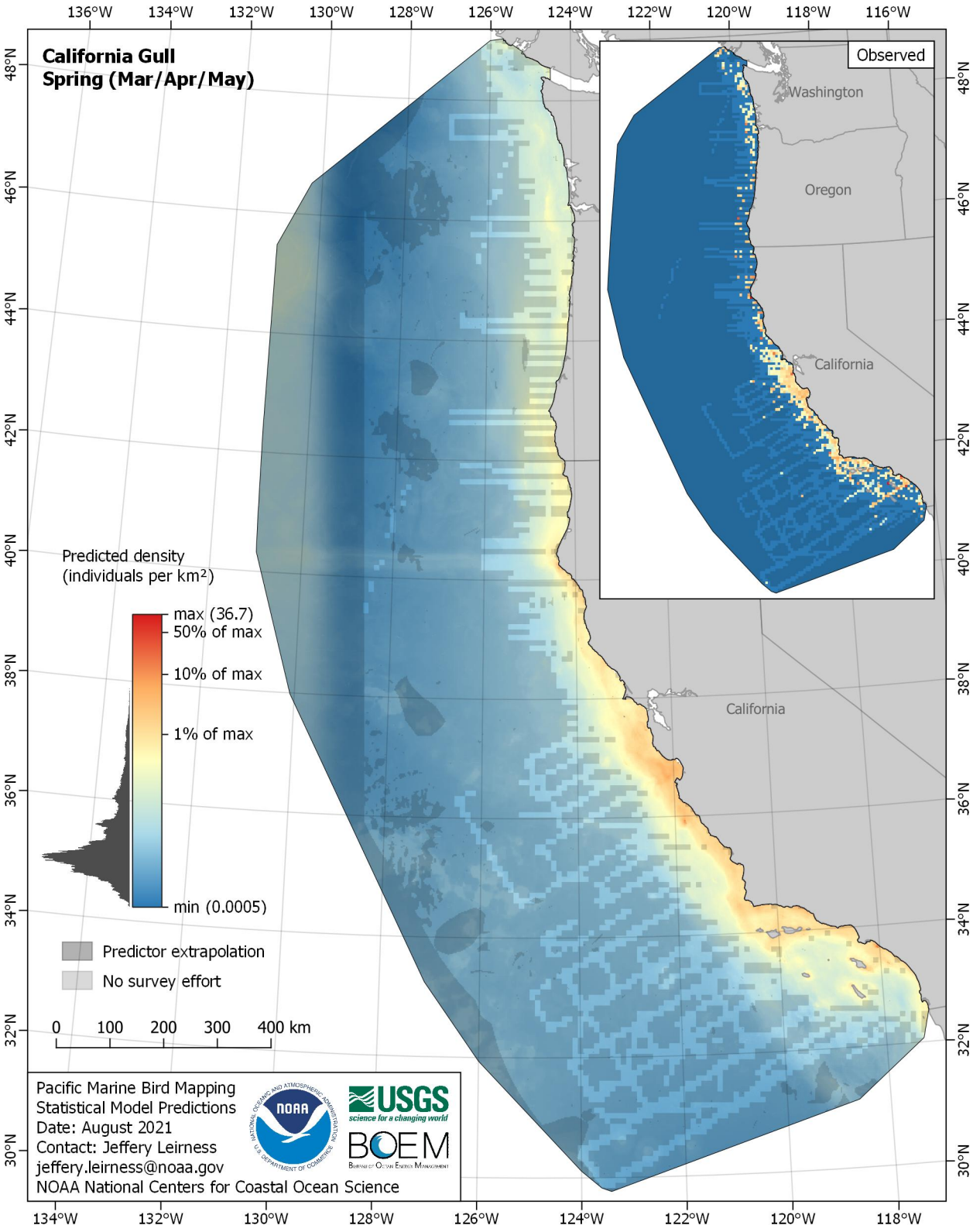

Figure E-111. Predicted density for California Gull (*Larus californicus*) in the spring season

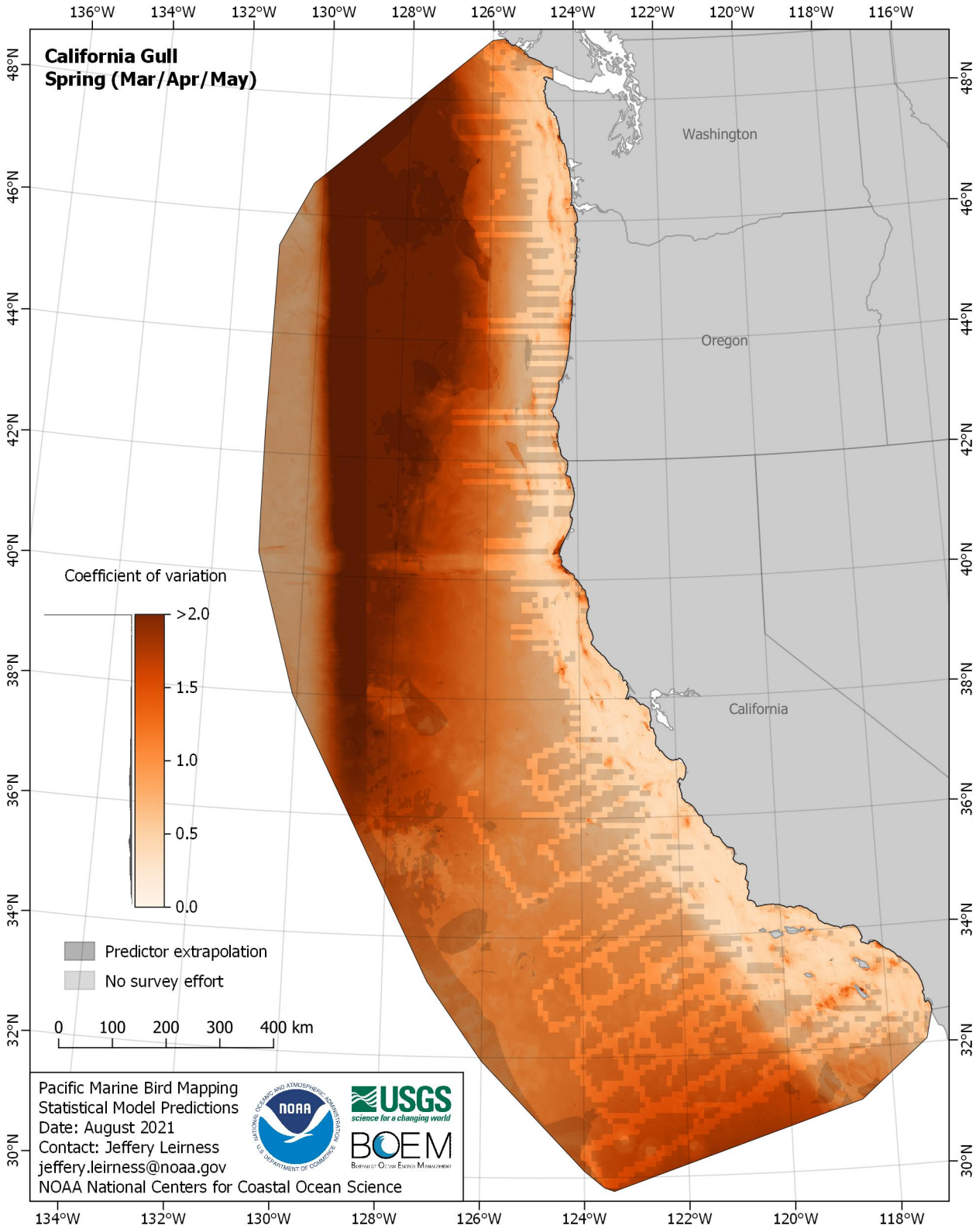

Figure E-112. Coefficient of variation for California Gull (*Larus californicus*) in the spring season

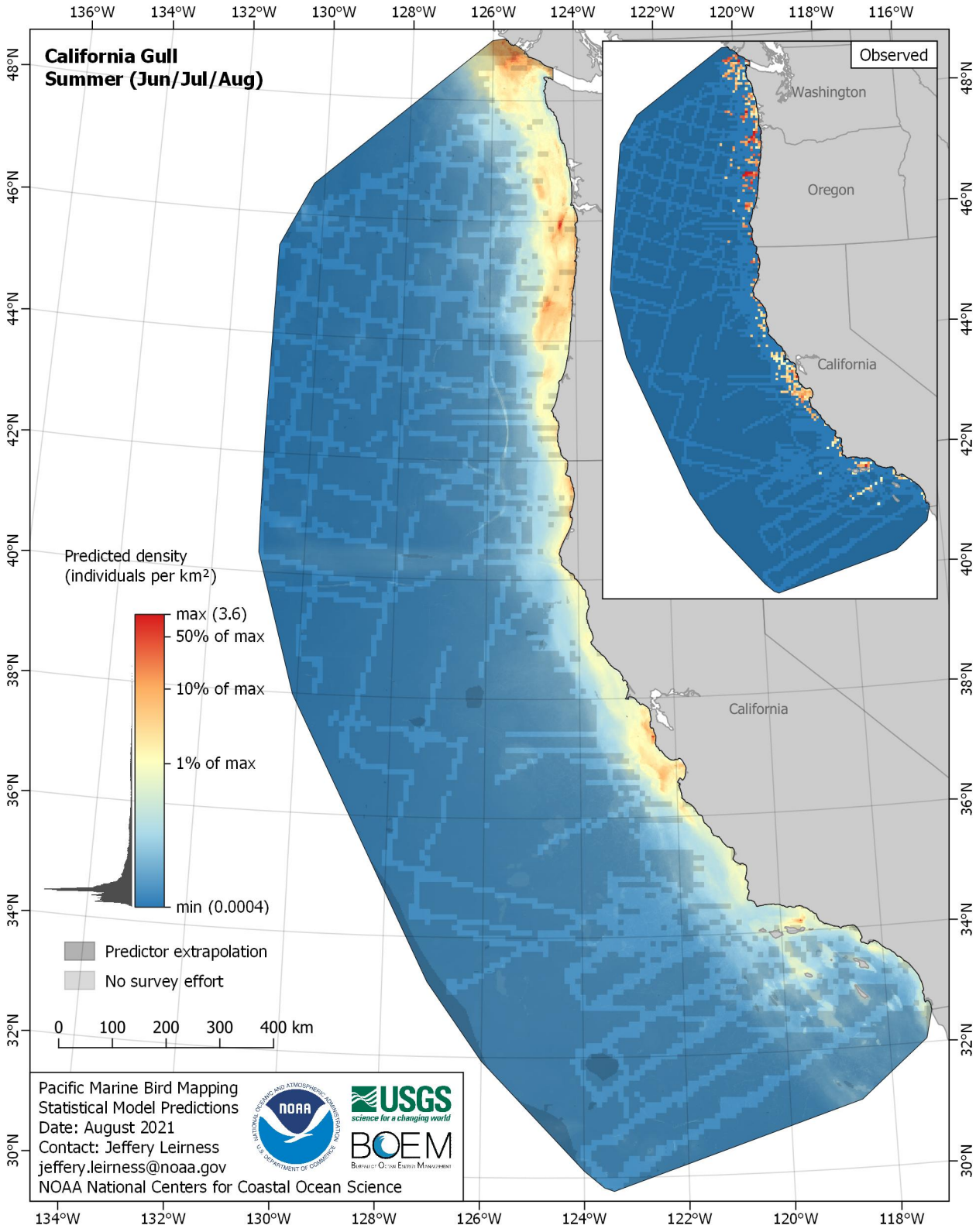

Figure E-113. Predicted density for California Gull (*Larus californicus*) in the summer season

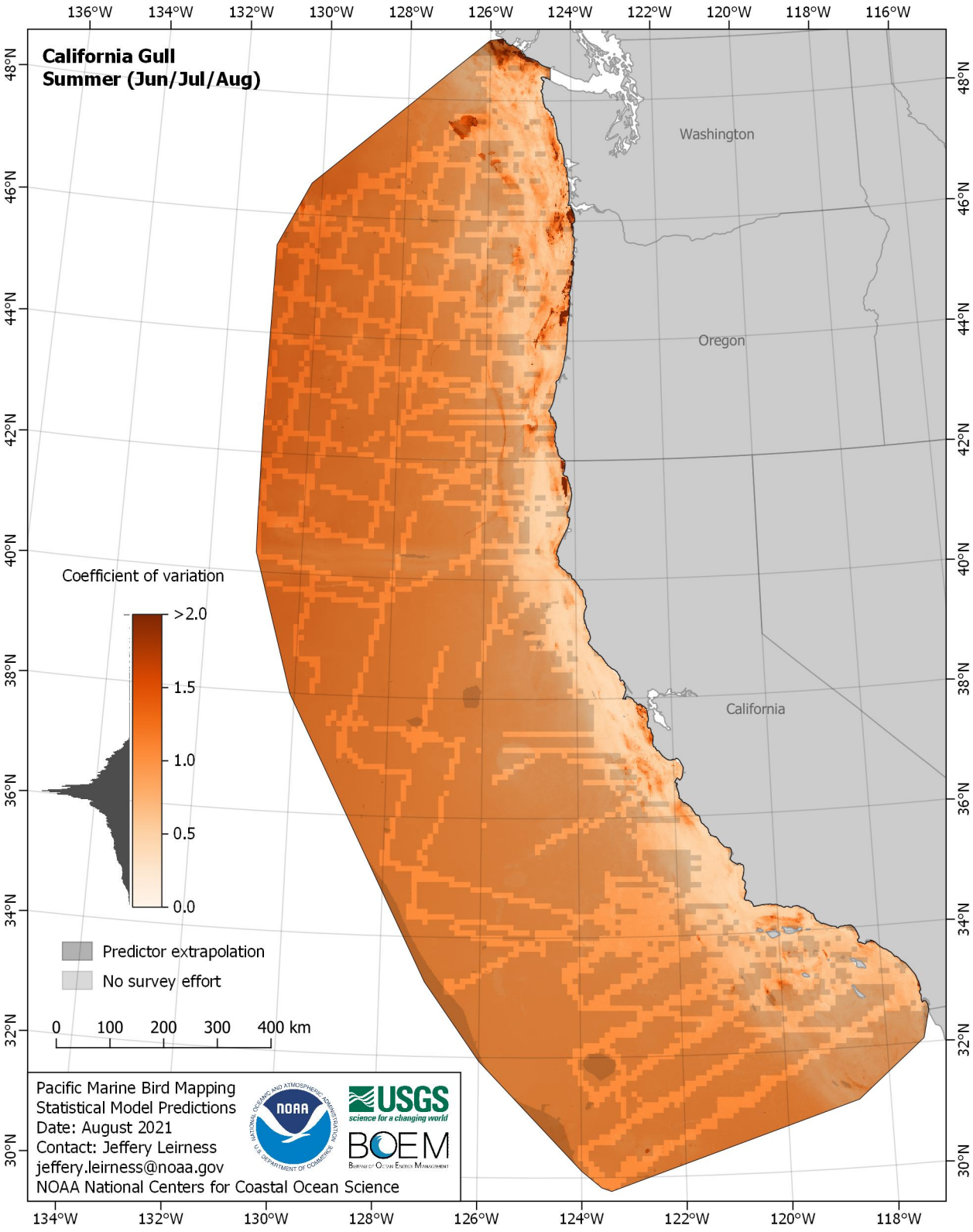

Figure E-114. Coefficient of variation for California Gull (*Larus californicus*) in the summer season

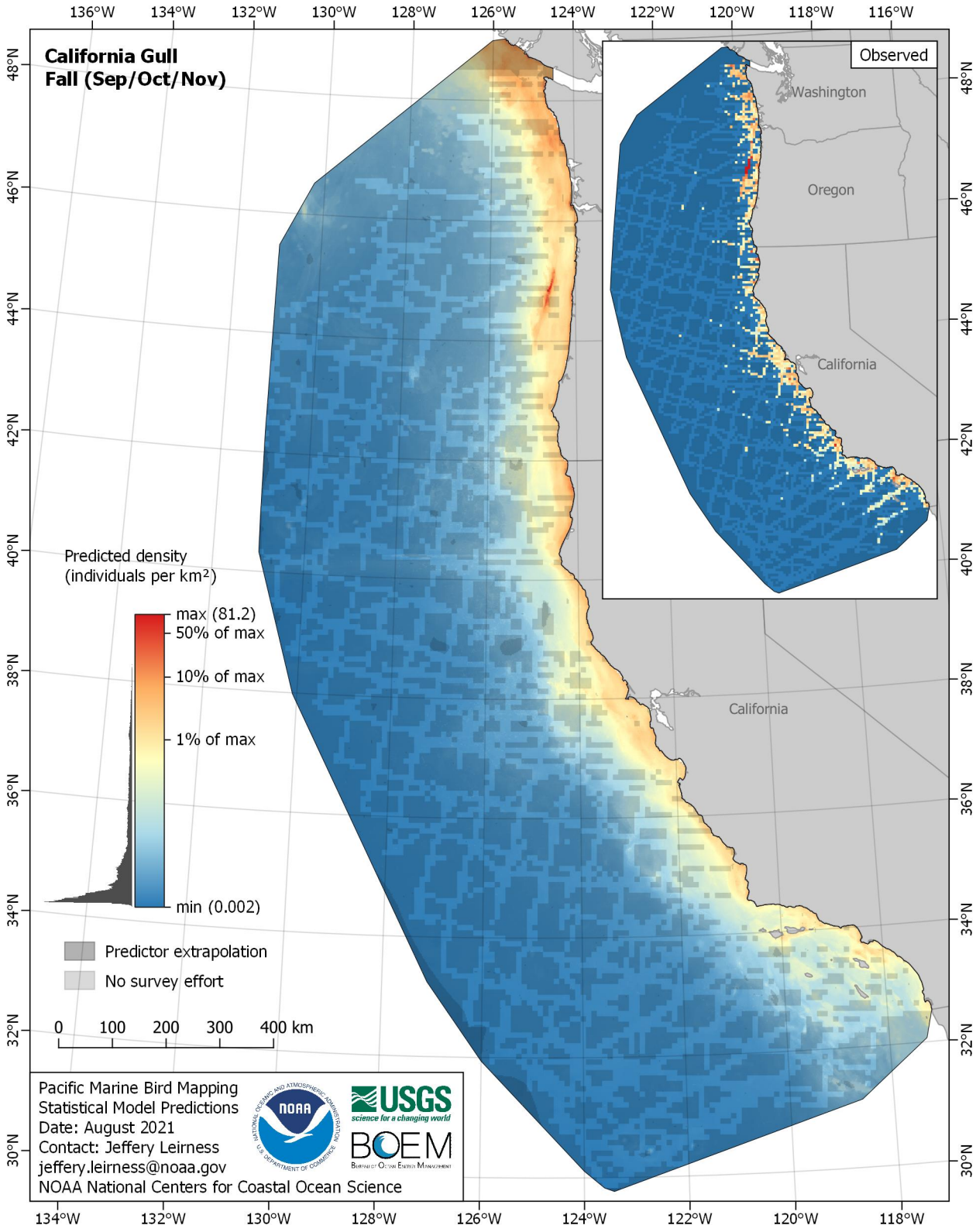

Figure E-115. Predicted density for California Gull (*Larus californicus*) in the fall season

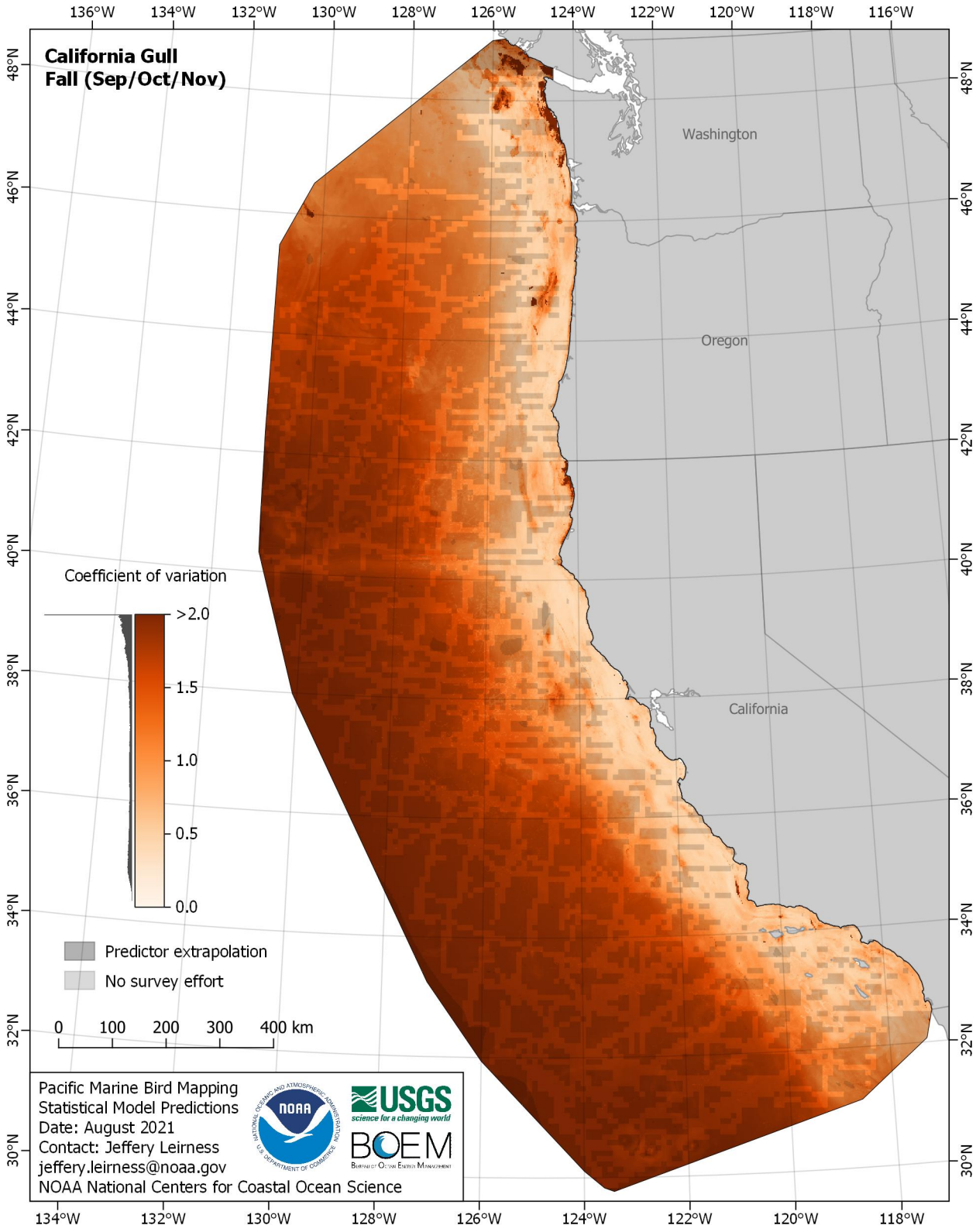

Figure E-116. Coefficient of variation for California Gull (*Larus californicus*) in the fall season

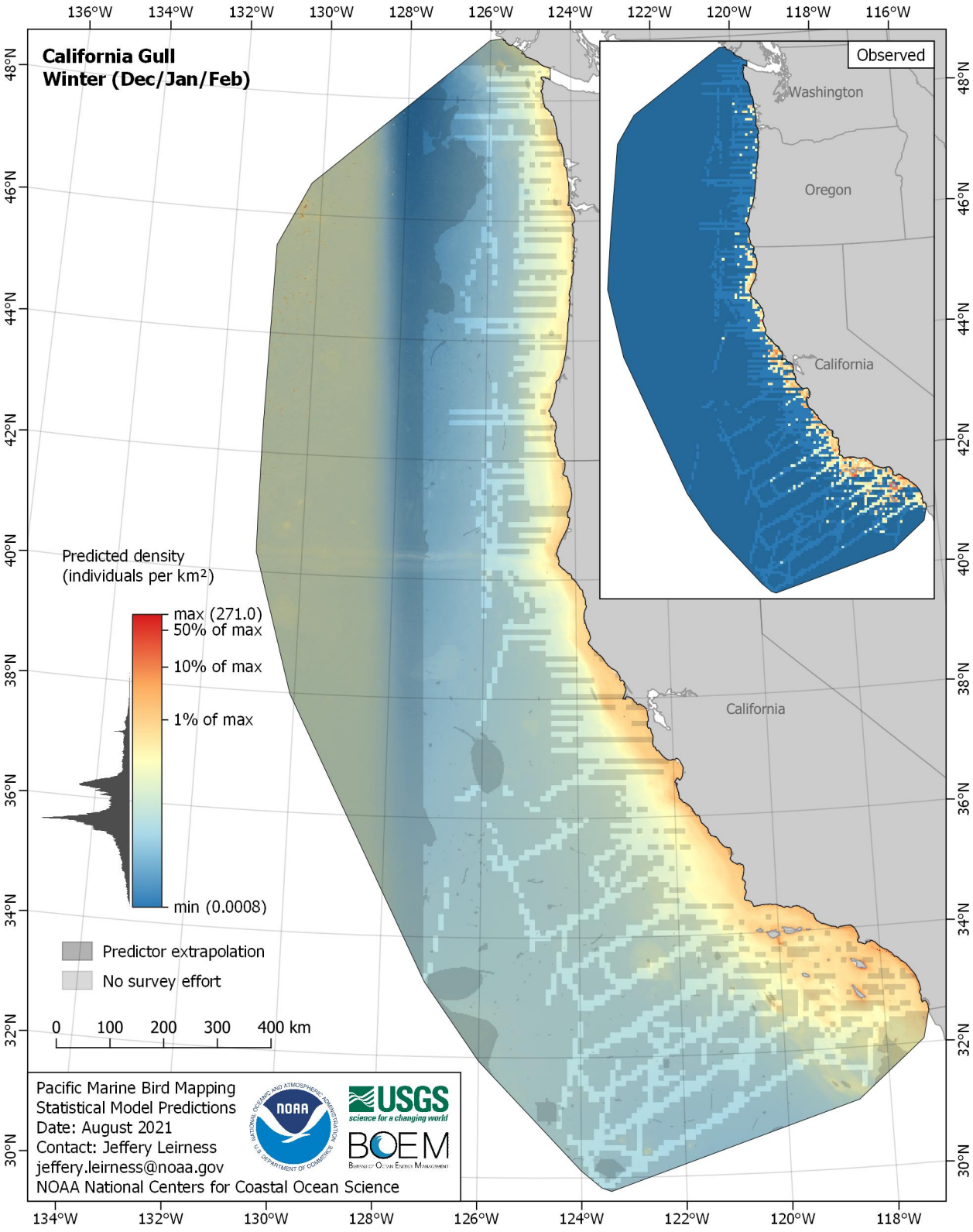

Figure E-117. Predicted density for California Gull (*Larus californicus*) in the winter season

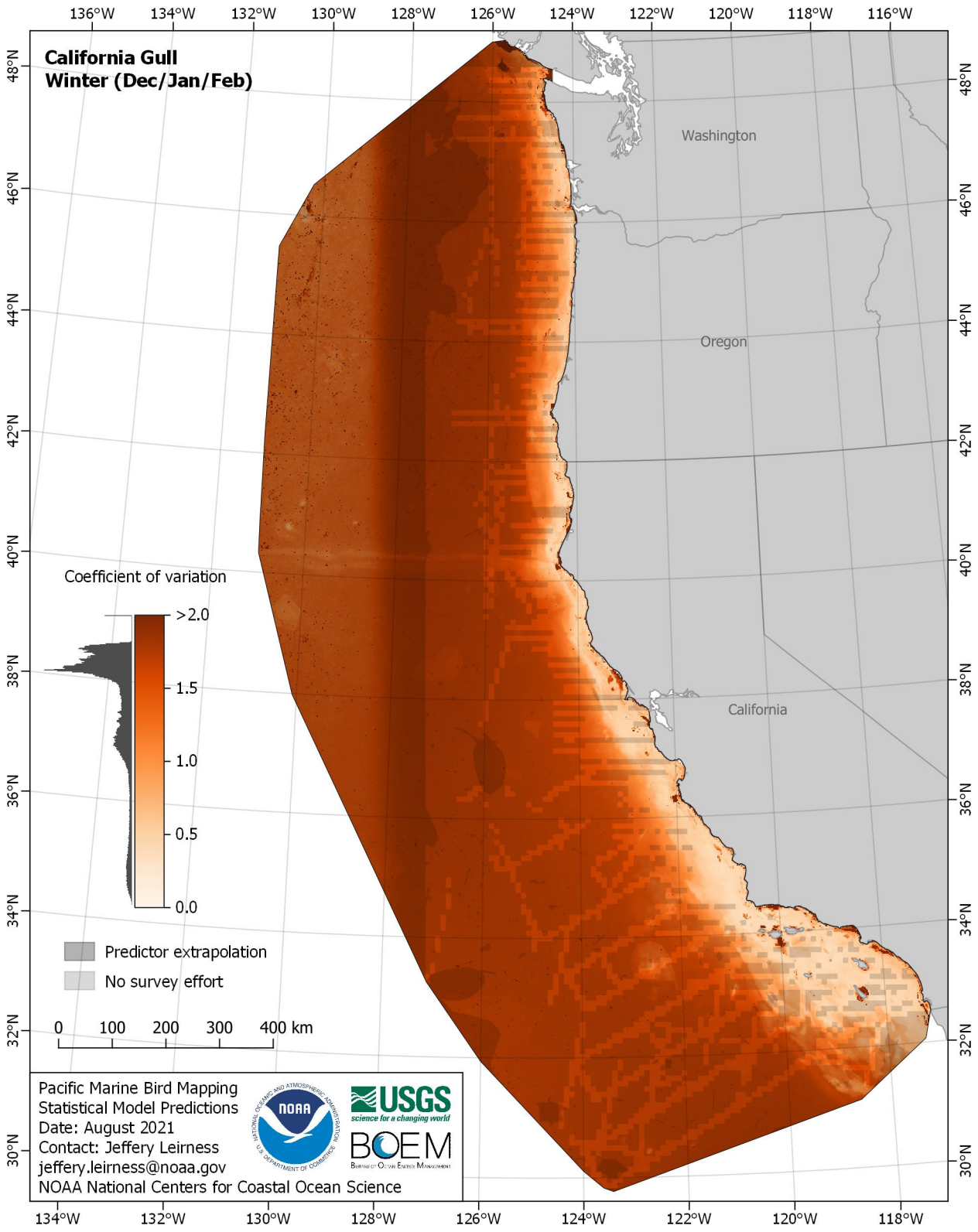

Figure E-118. Coefficient of variation for California Gull (*Larus californicus*) in the winter season

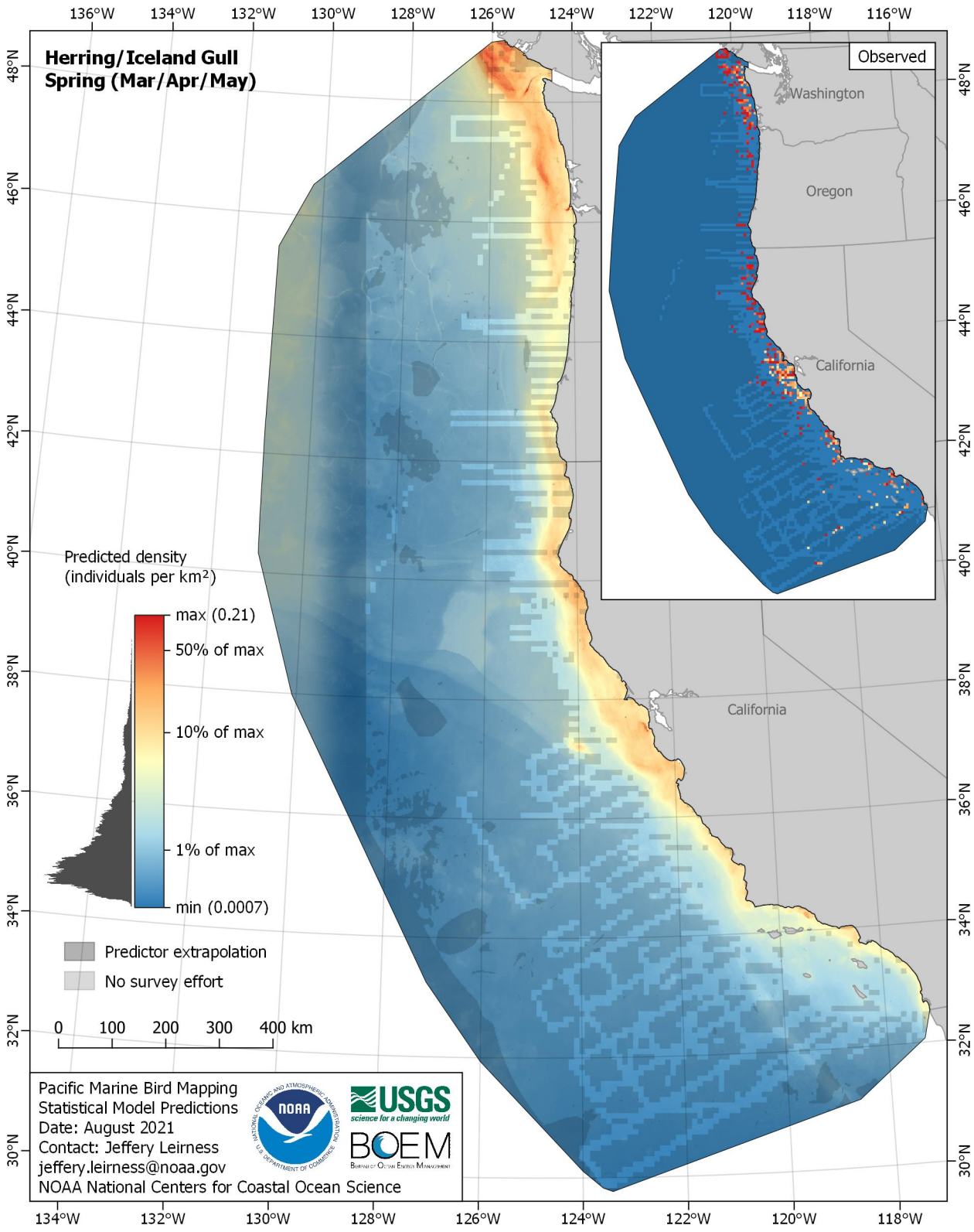

Figure E-119. Predicted density for Herring/Iceland Gull (*Larus argentatus/glaucoides*) in the spring season

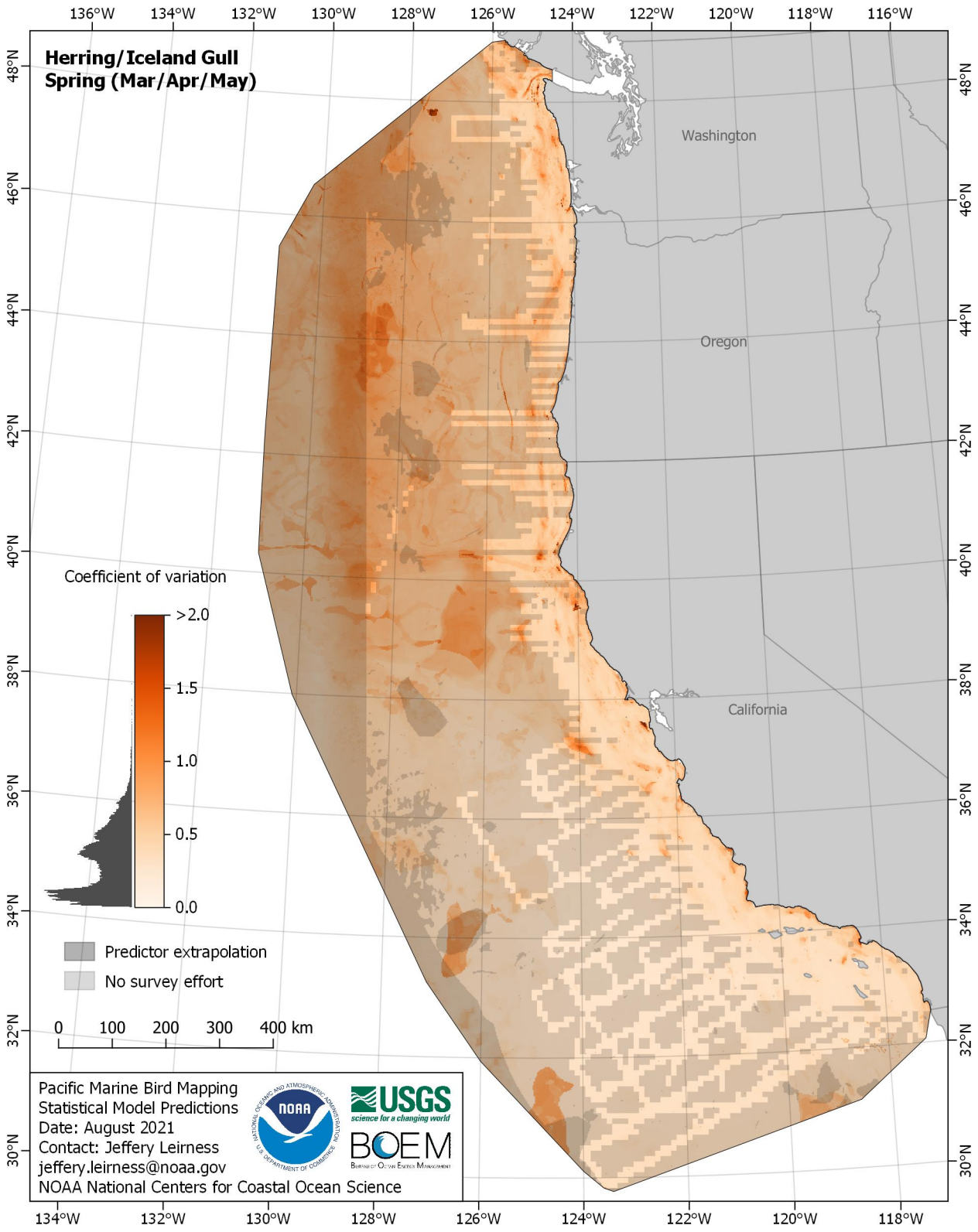

Figure E-120. Coefficient of variation for Herring/Iceland Gull (*Larus argentatus/glaucoides*) in the spring season

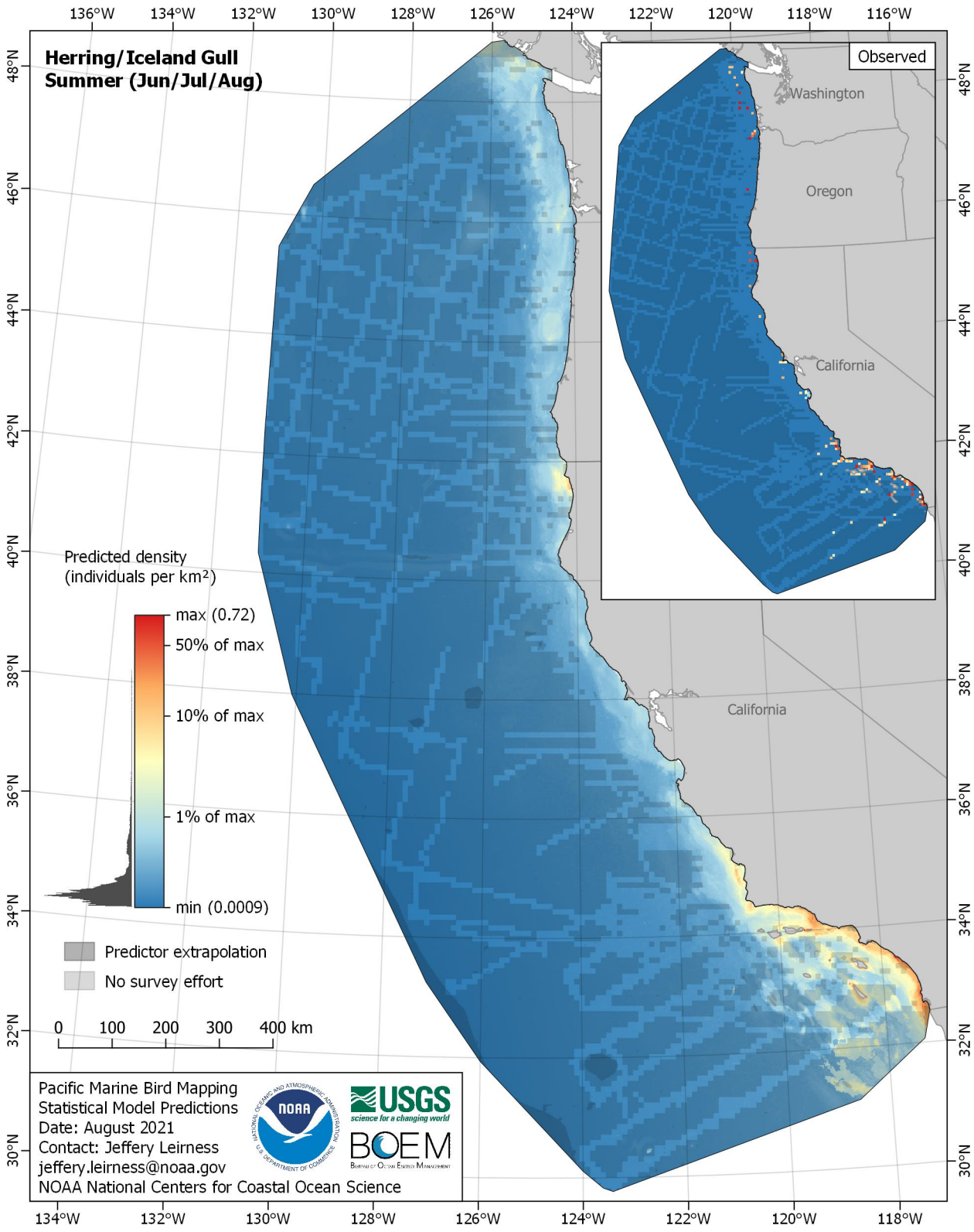

Figure E-121. Predicted density for Herring/Iceland Gull (*Larus argentatus/glaucoides*) in the summer season

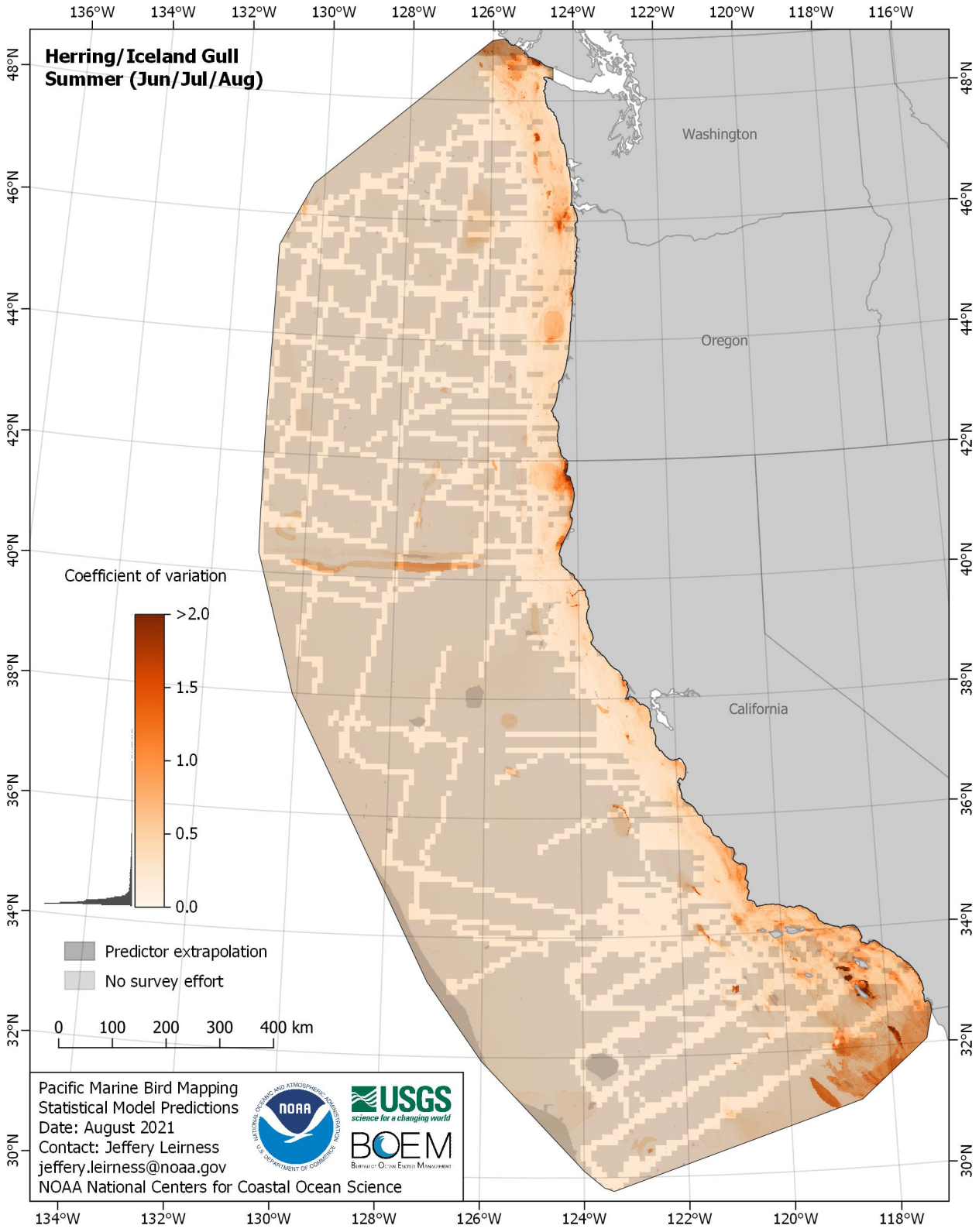

Figure E-122. Coefficient of variation for Herring/Iceland Gull (*Larus argentatus/glaucoides*) in the summer season

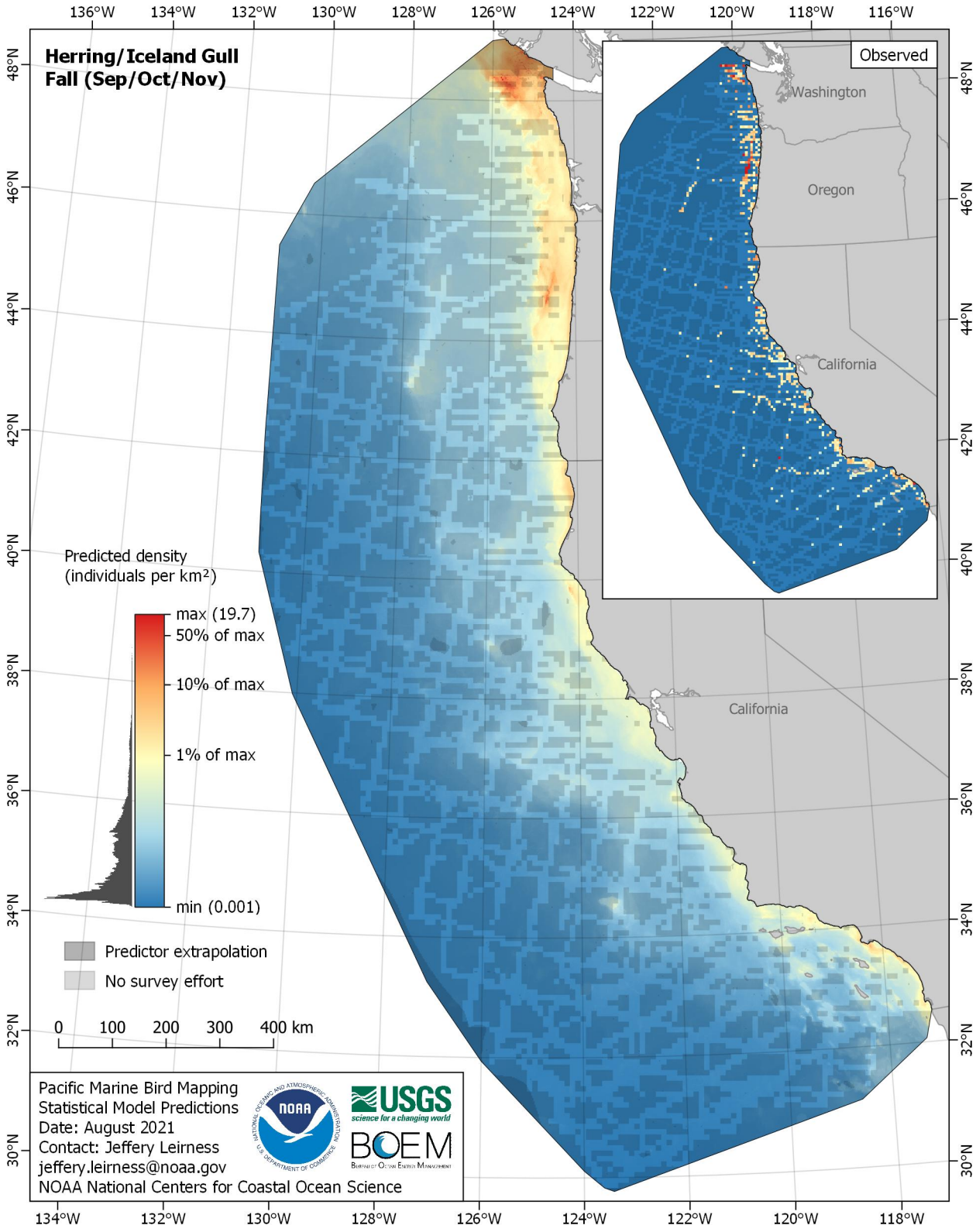

Figure E-123. Predicted density for Herring/Iceland Gull (*Larus argentatus/glaucoides*) in the fall season

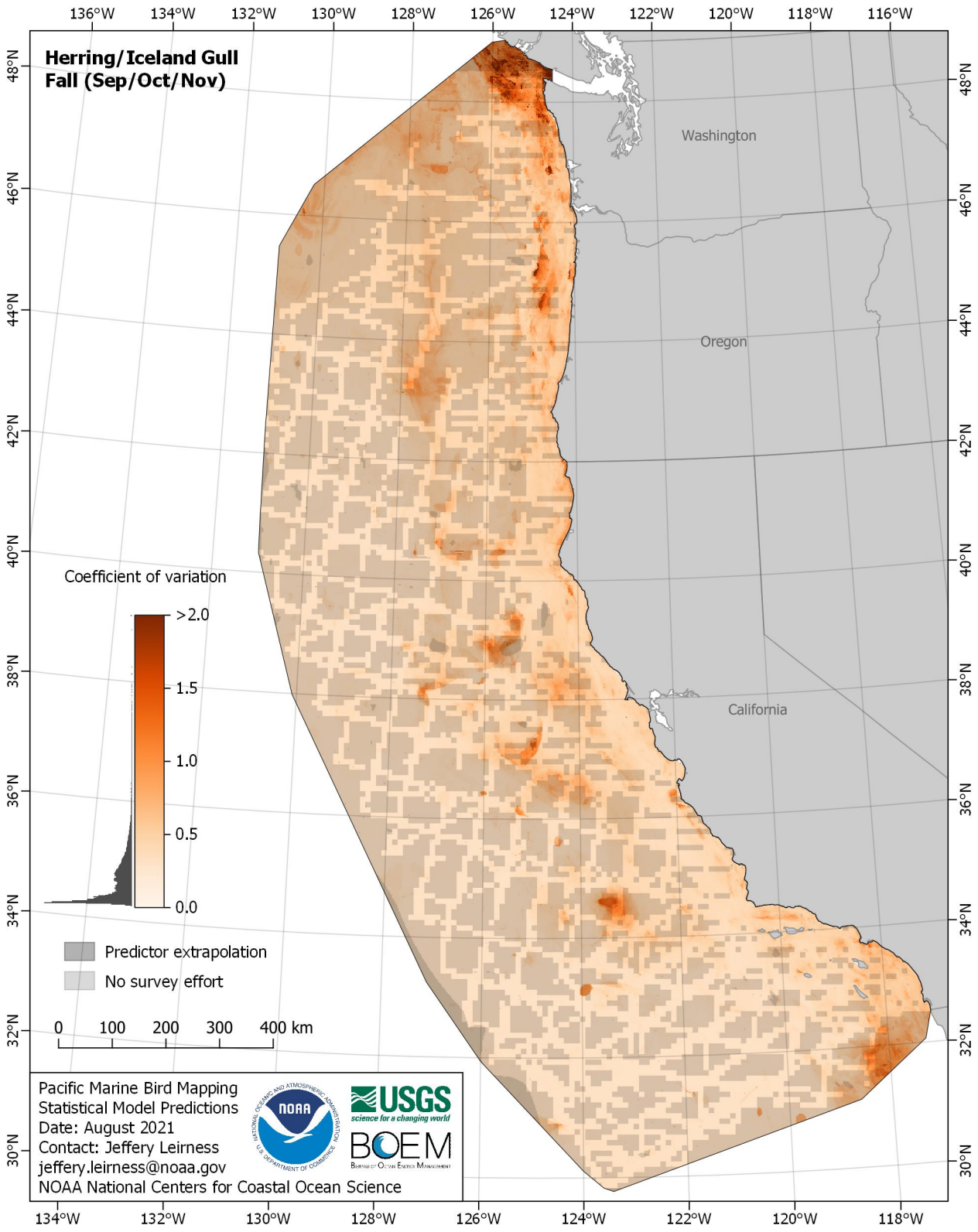

Figure E-124. Coefficient of variation for Herring/Iceland Gull (*Larus argentatus/glaucoides*) in the fall season

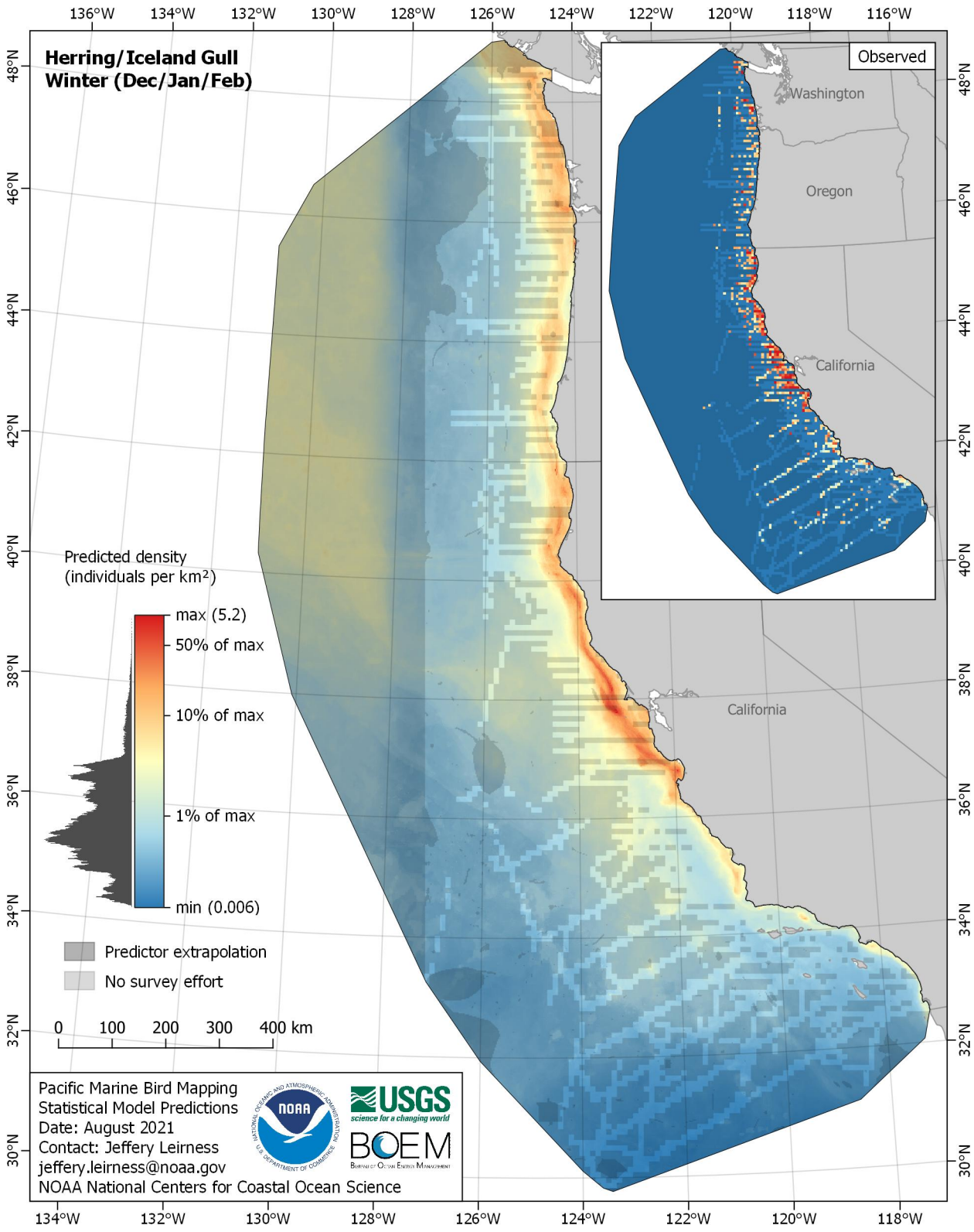

Figure E-125. Predicted density for Herring/Iceland Gull (*Larus argentatus/glaucoides*) in the winter season

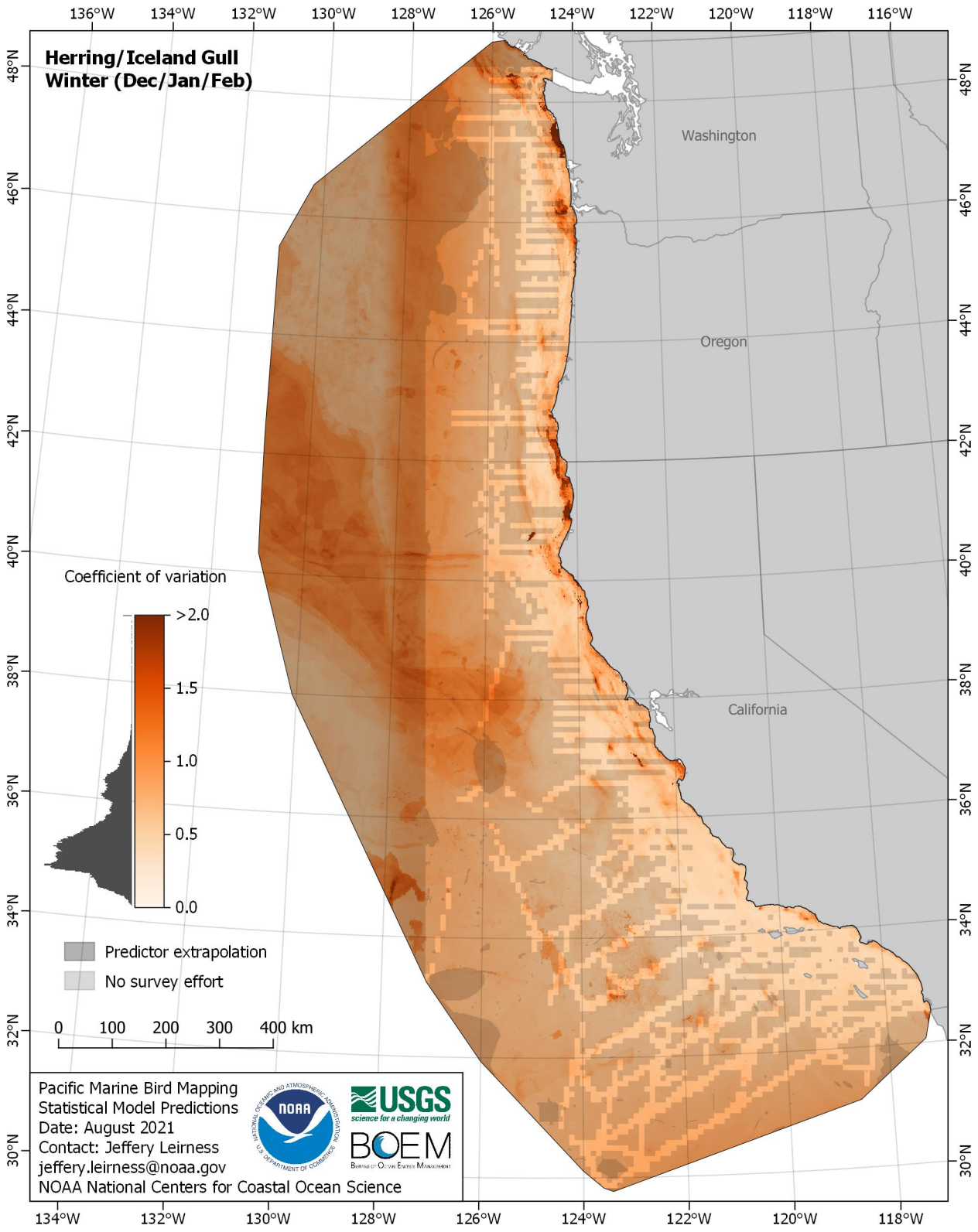

Figure E-126. Coefficient of variation for Herring/Iceland Gull (*Larus argentatus/glaucoides*) in the winter season

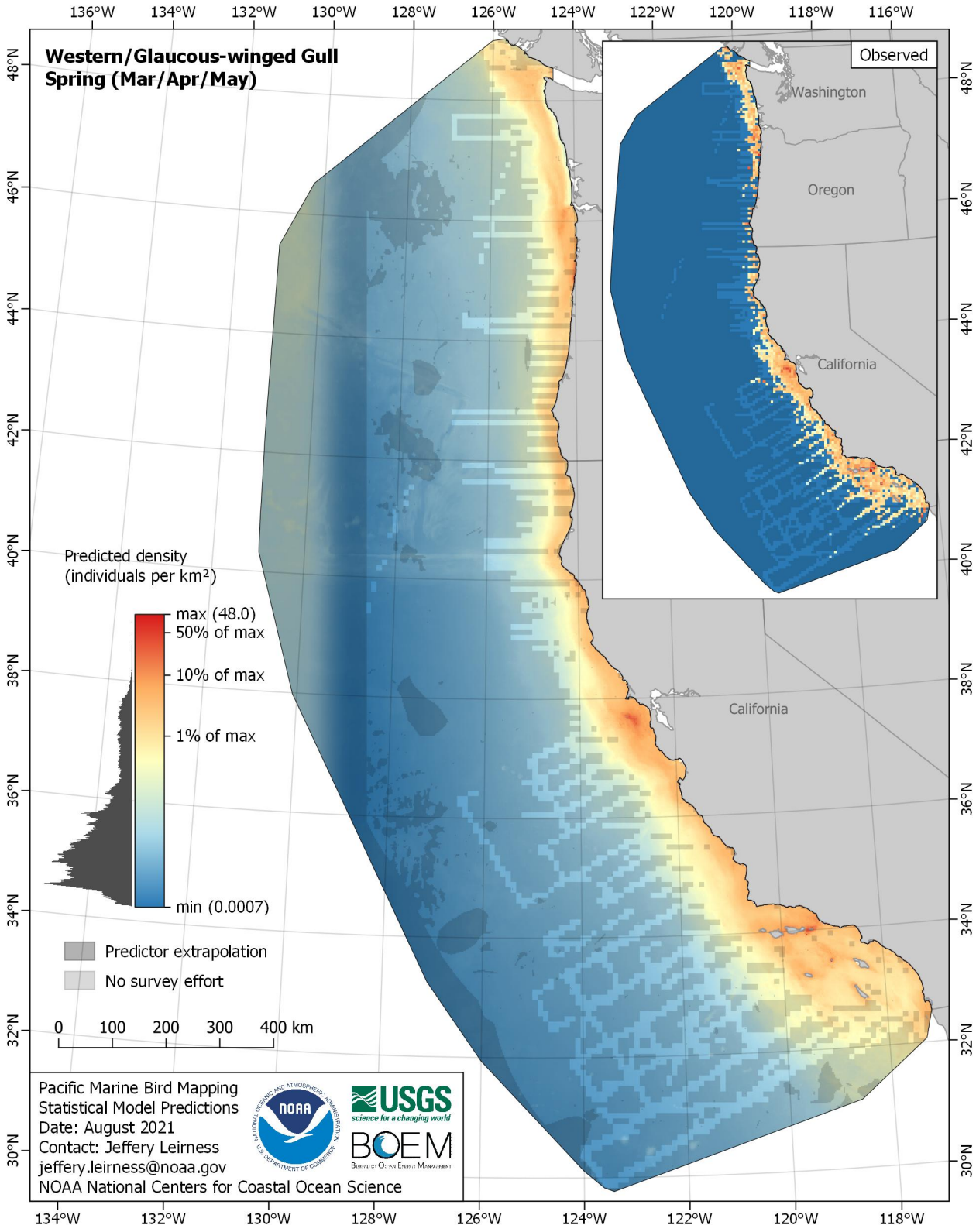

Figure E-127. Predicted density for Western/Glaucous-winged Gull (*Larus occidentalis/glaucescens*) in the spring season

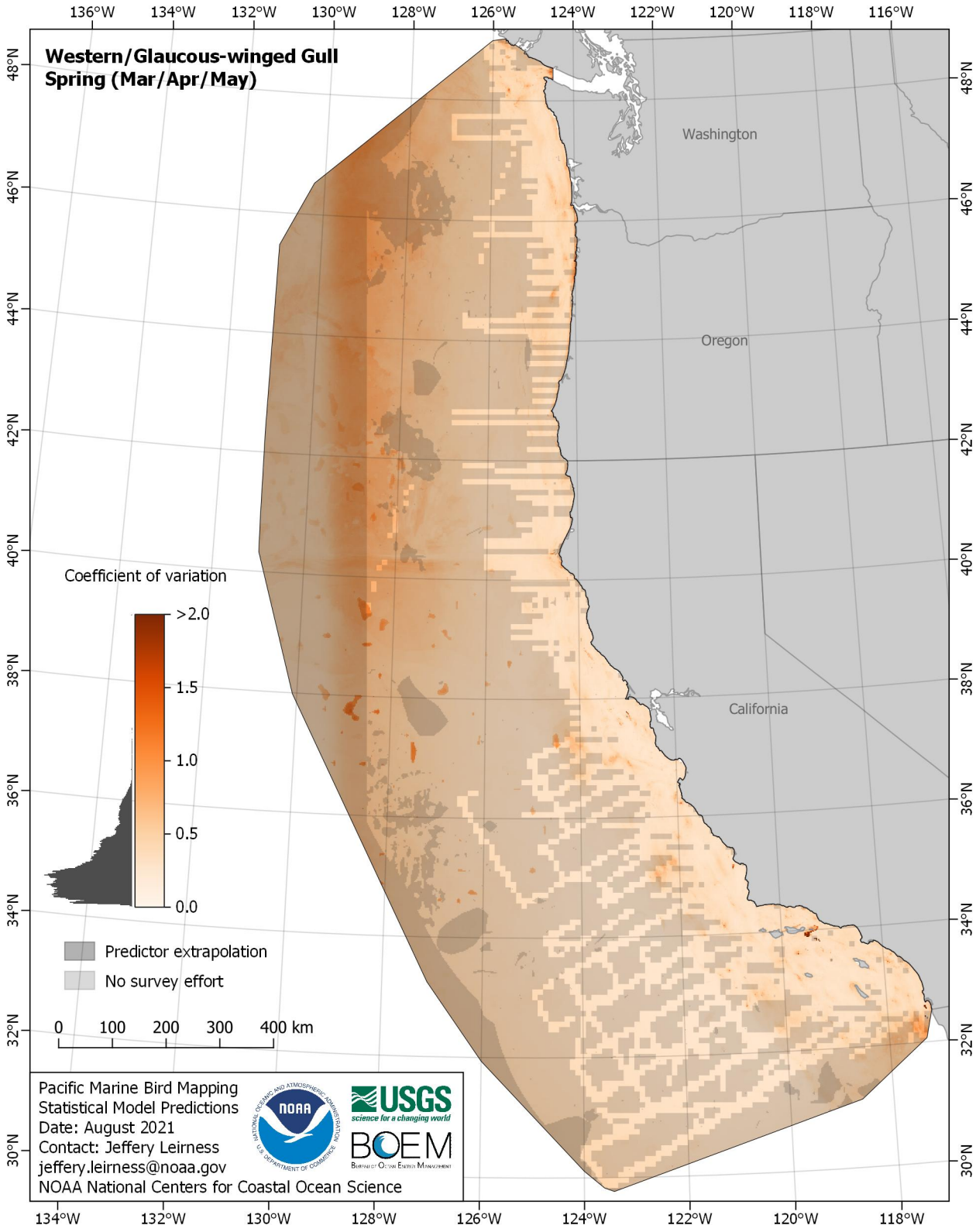

Figure E-128. Coefficient of variation for Western/Glaucous-winged Gull (*Larus occidentalis/glaucescens*) in the spring season

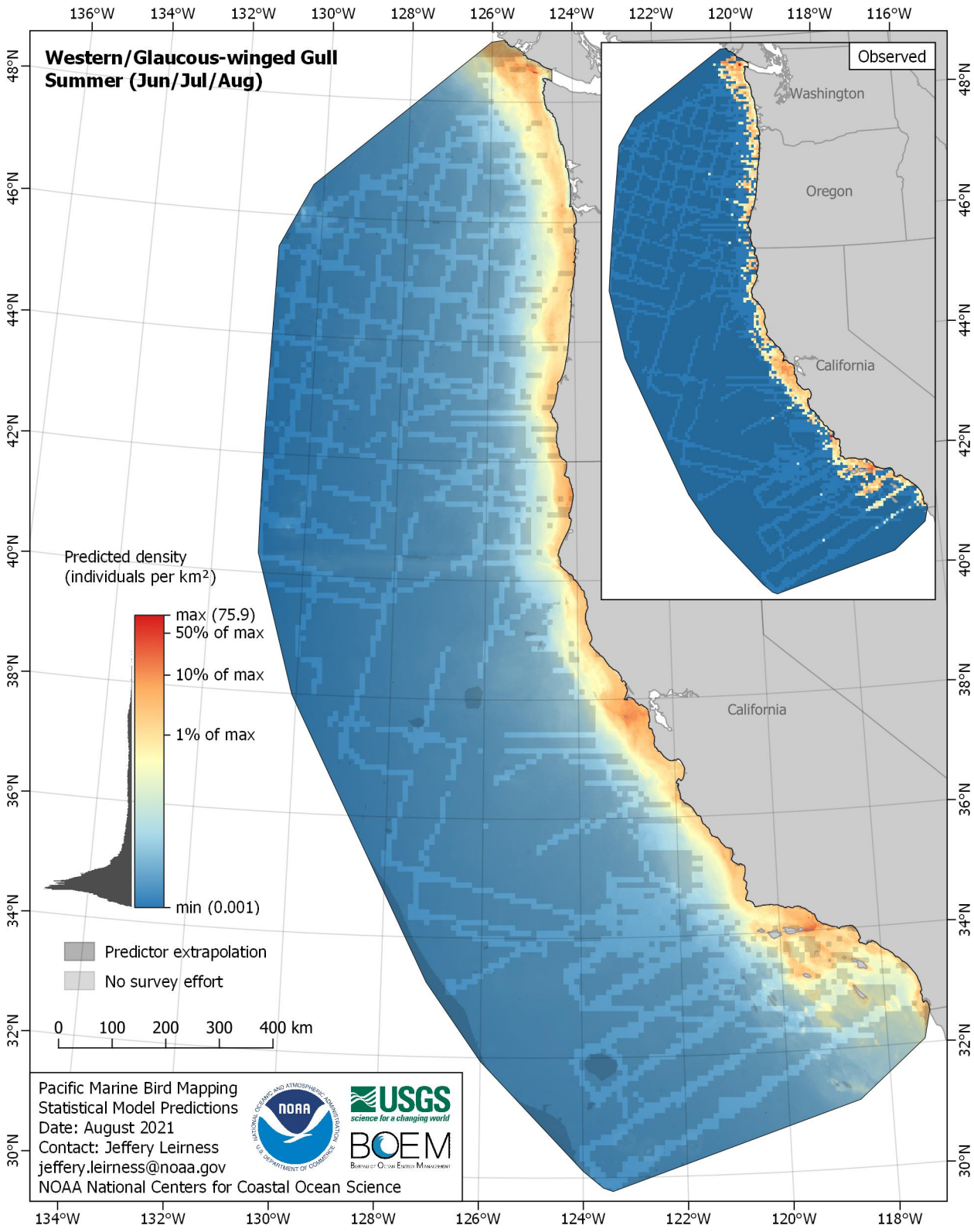

Figure E-129. Predicted density for Western/Glaucous-winged Gull (*Larus occidentalis/glaucescens*) in the summer season

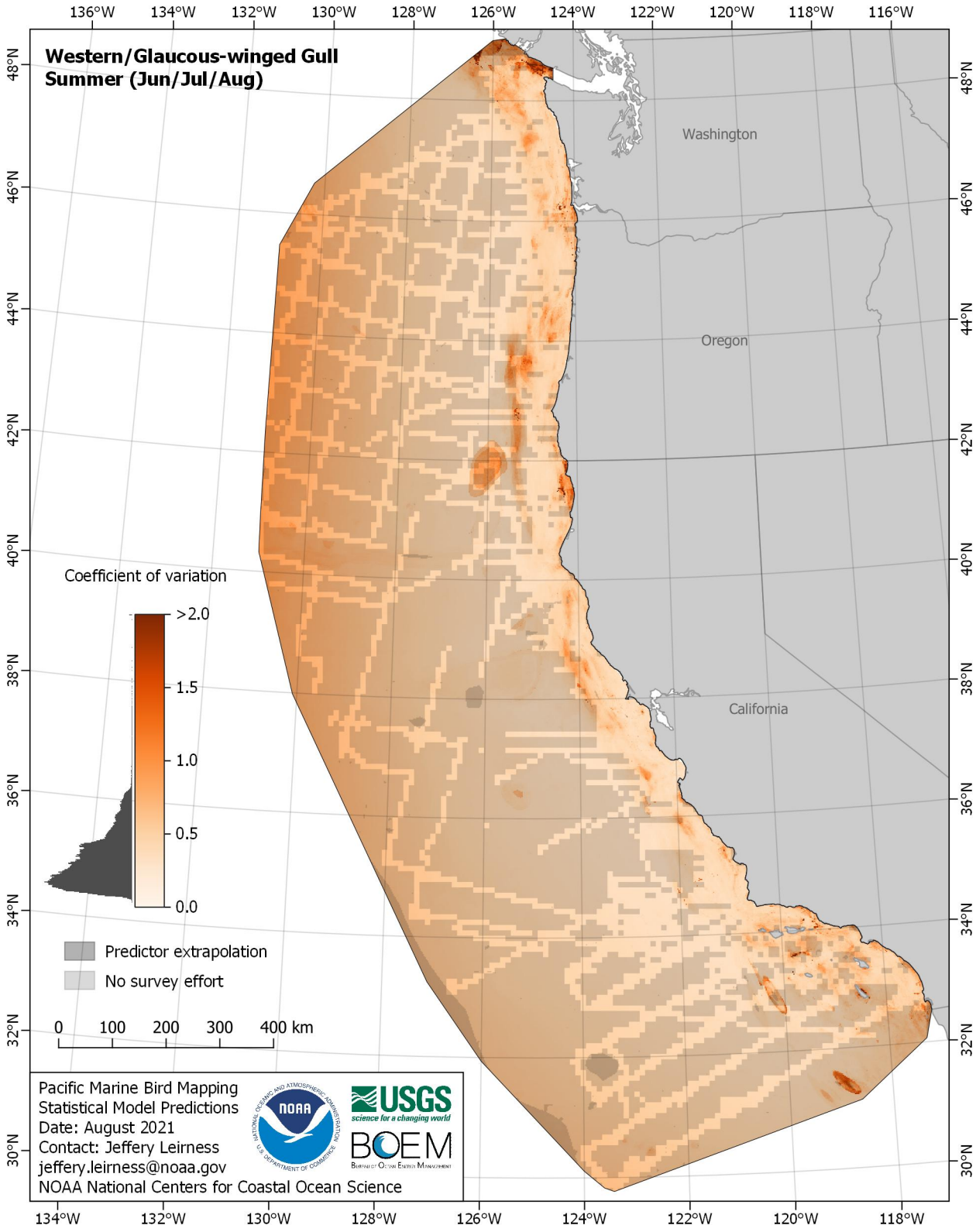

Figure E-130. Coefficient of variation for Western/Glaucous-winged Gull (*Larus occidentalis/glaucescens*) in the summer season

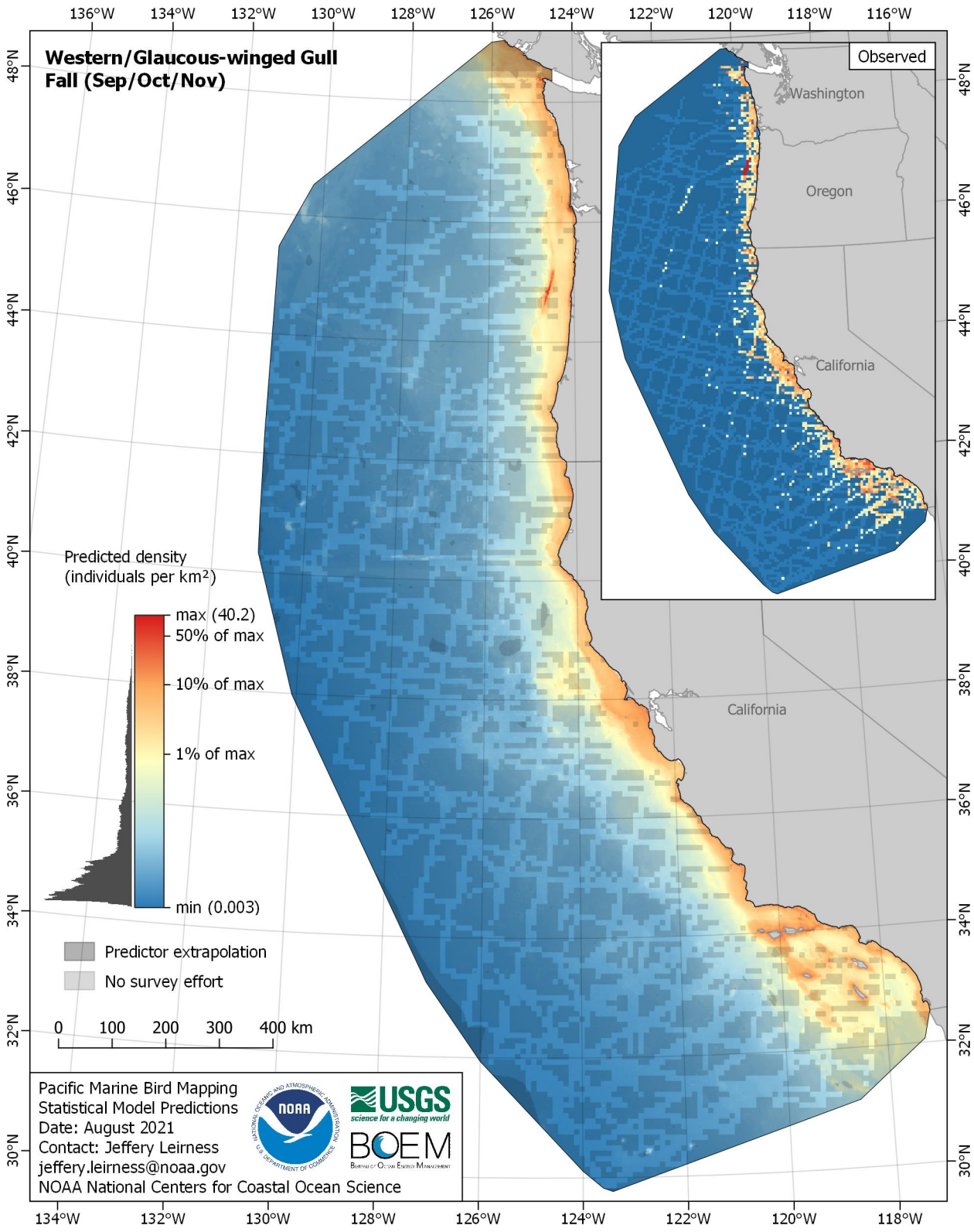

Figure E-131. Predicted density for Western/Glaucous-winged Gull (*Larus occidentalis/glaucescens*) in the fall season

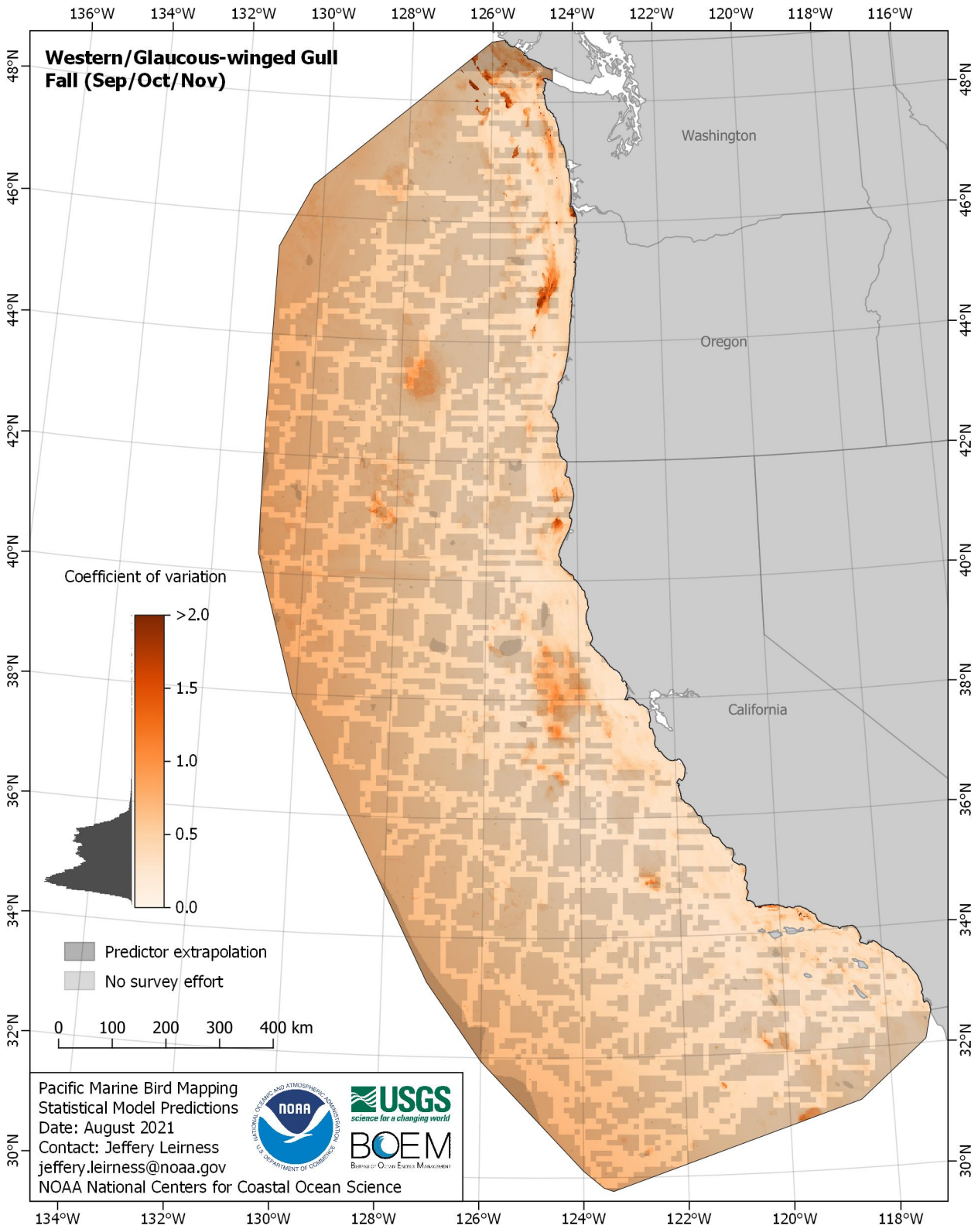

Figure E-132. Coefficient of variation for Western/Glaucous-winged Gull (*Larus occidentalis/glaucescens*) in the fall season

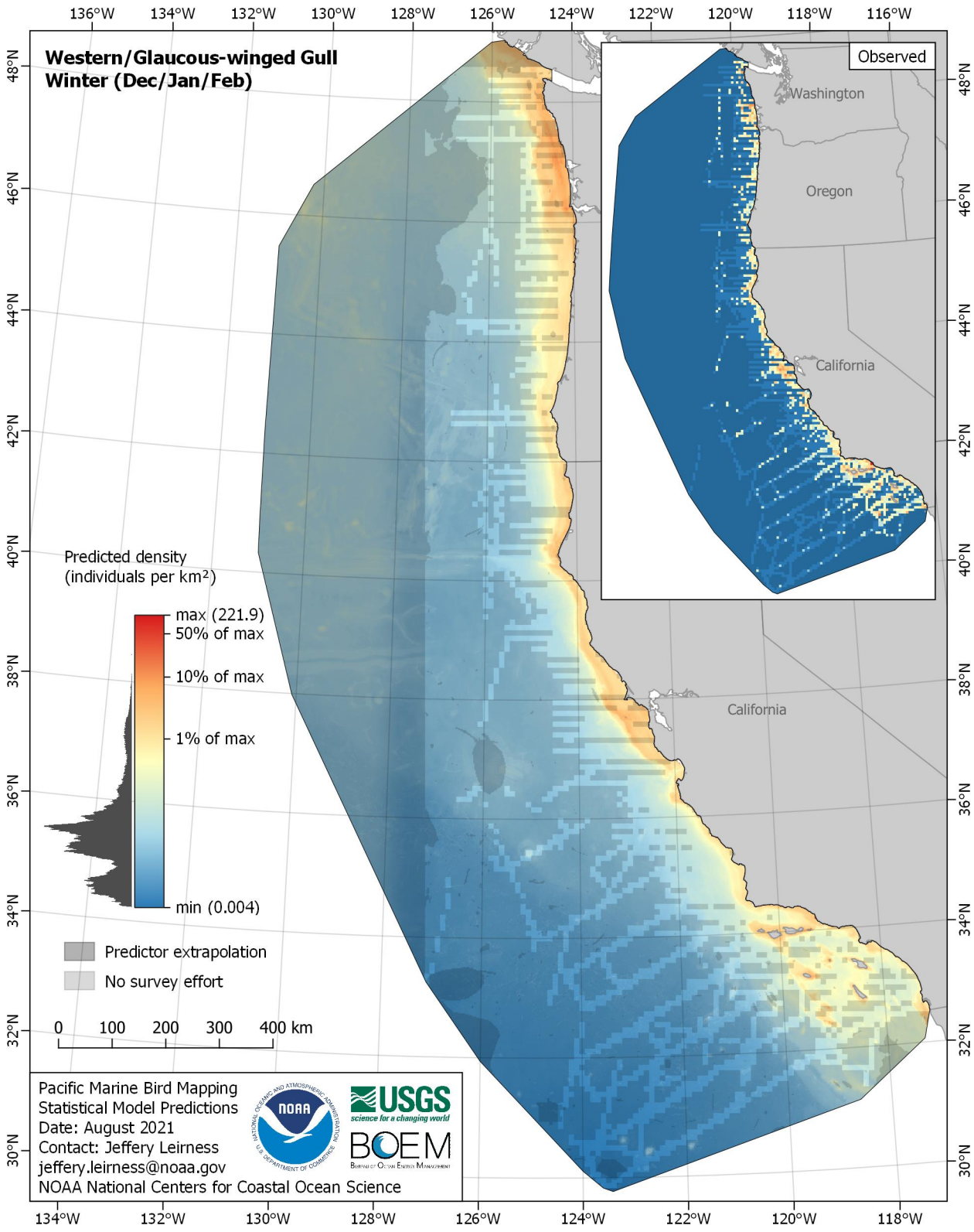

Figure E-133. Predicted density for Western/Glaucous-winged Gull (*Larus occidentalis/glaucescens*) in the winter season

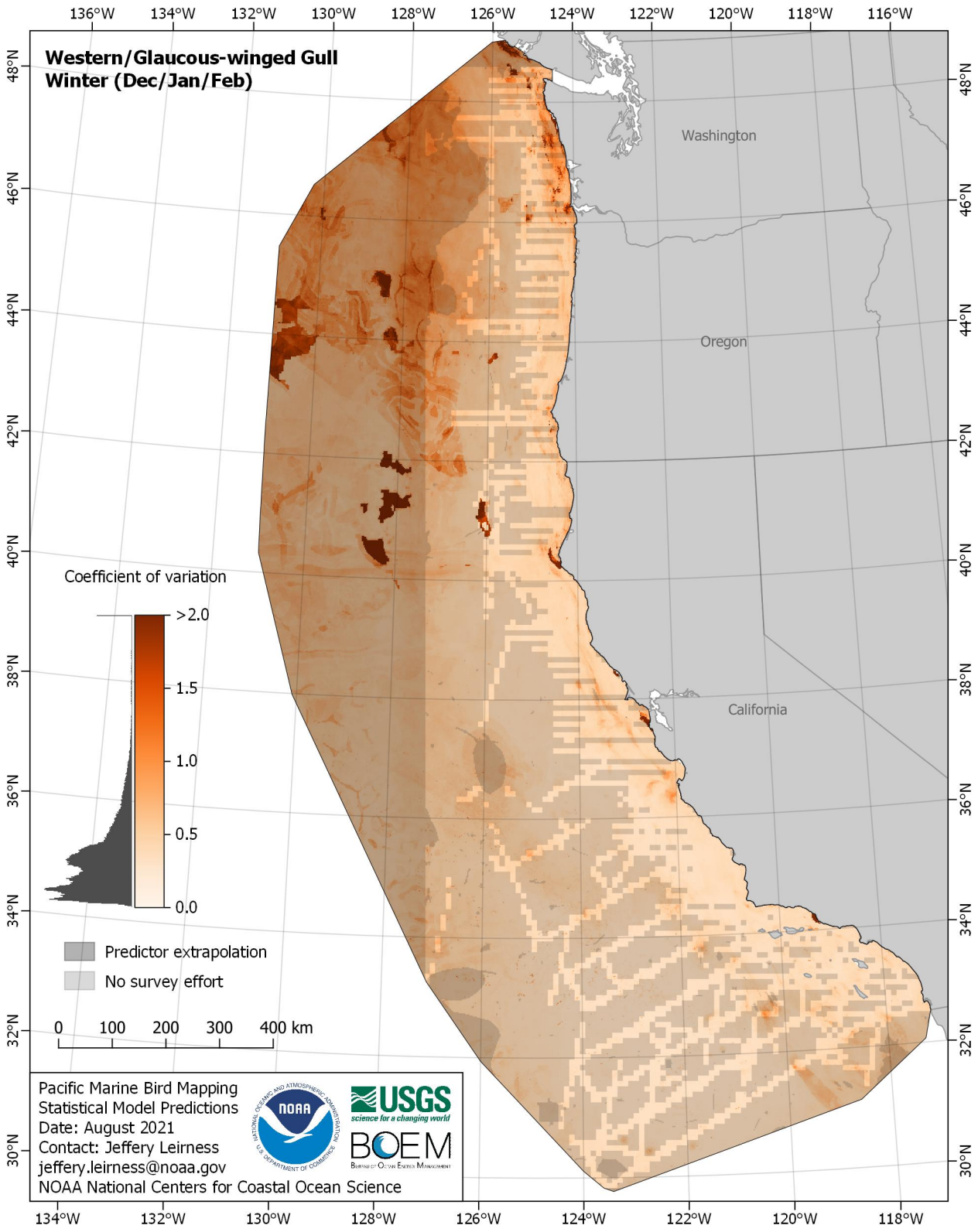

Figure E-134. Coefficient of variation for Western/Glaucous-winged Gull (*Larus occidentalis/glaucescens*) in the winter season

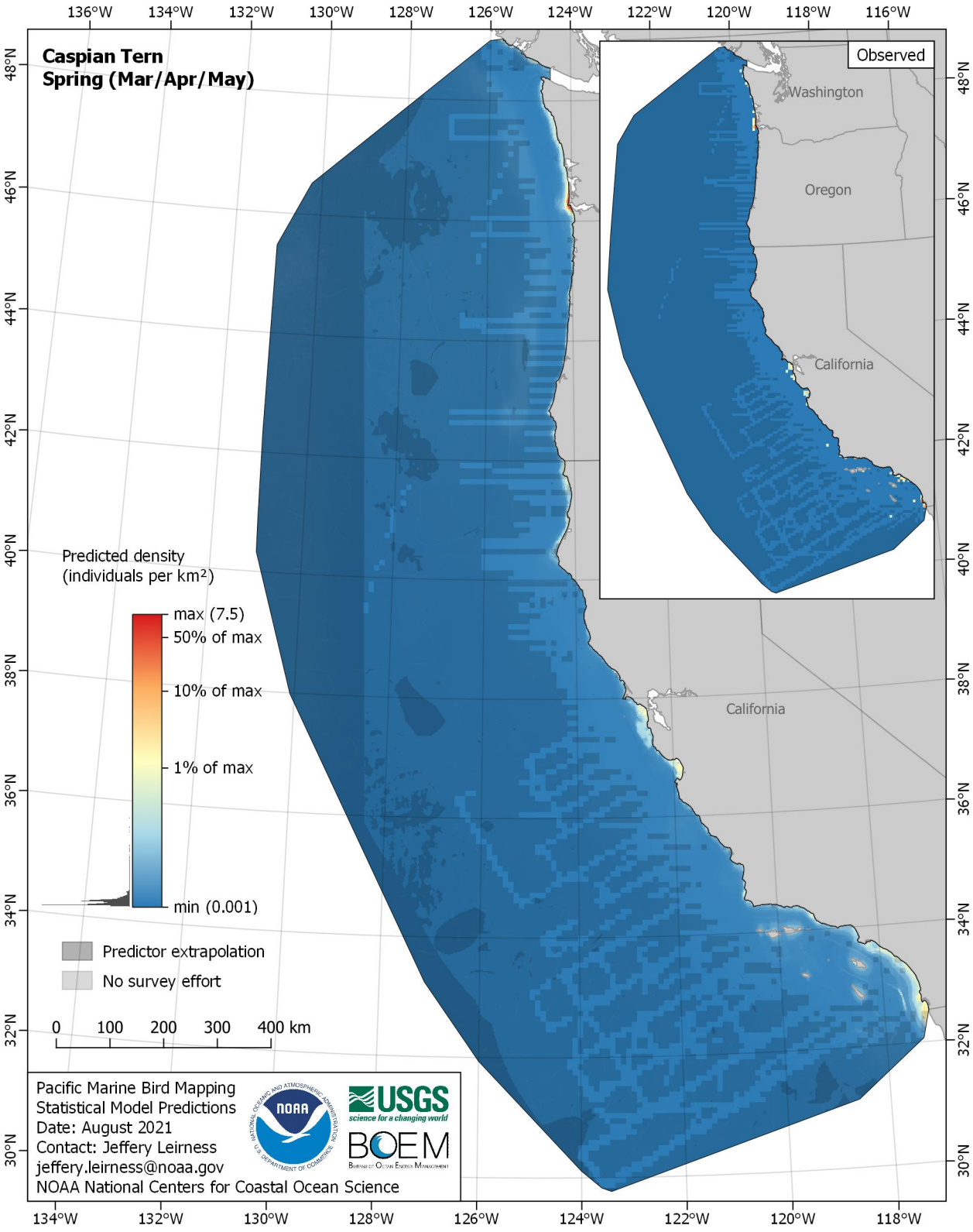

Figure E-135. Predicted density for Caspian Tern (*Hydroprogne caspia*) in the spring season

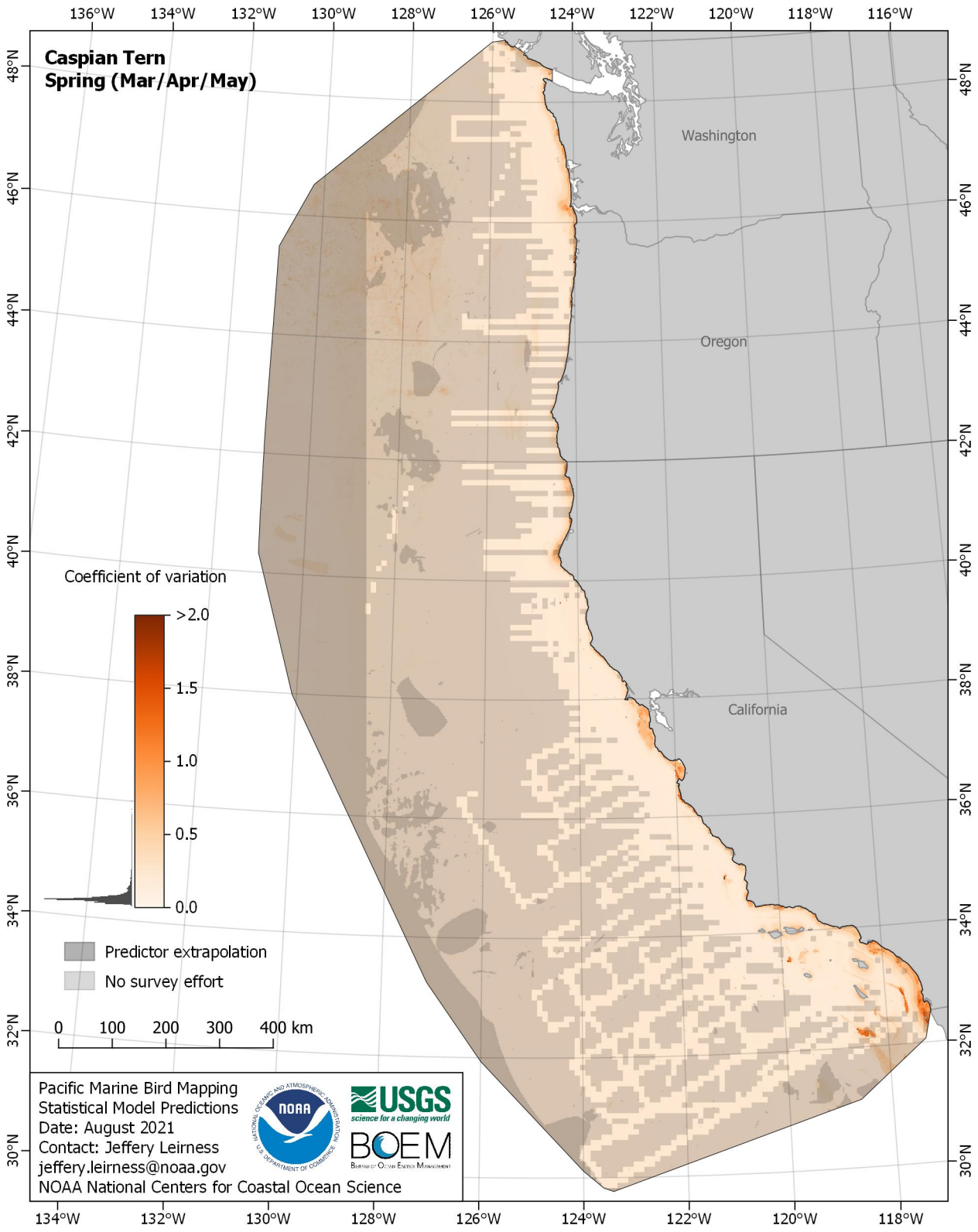

Figure E-136. Coefficient of variation for Caspian Tern (*Hydroprogne caspia*) in the spring season

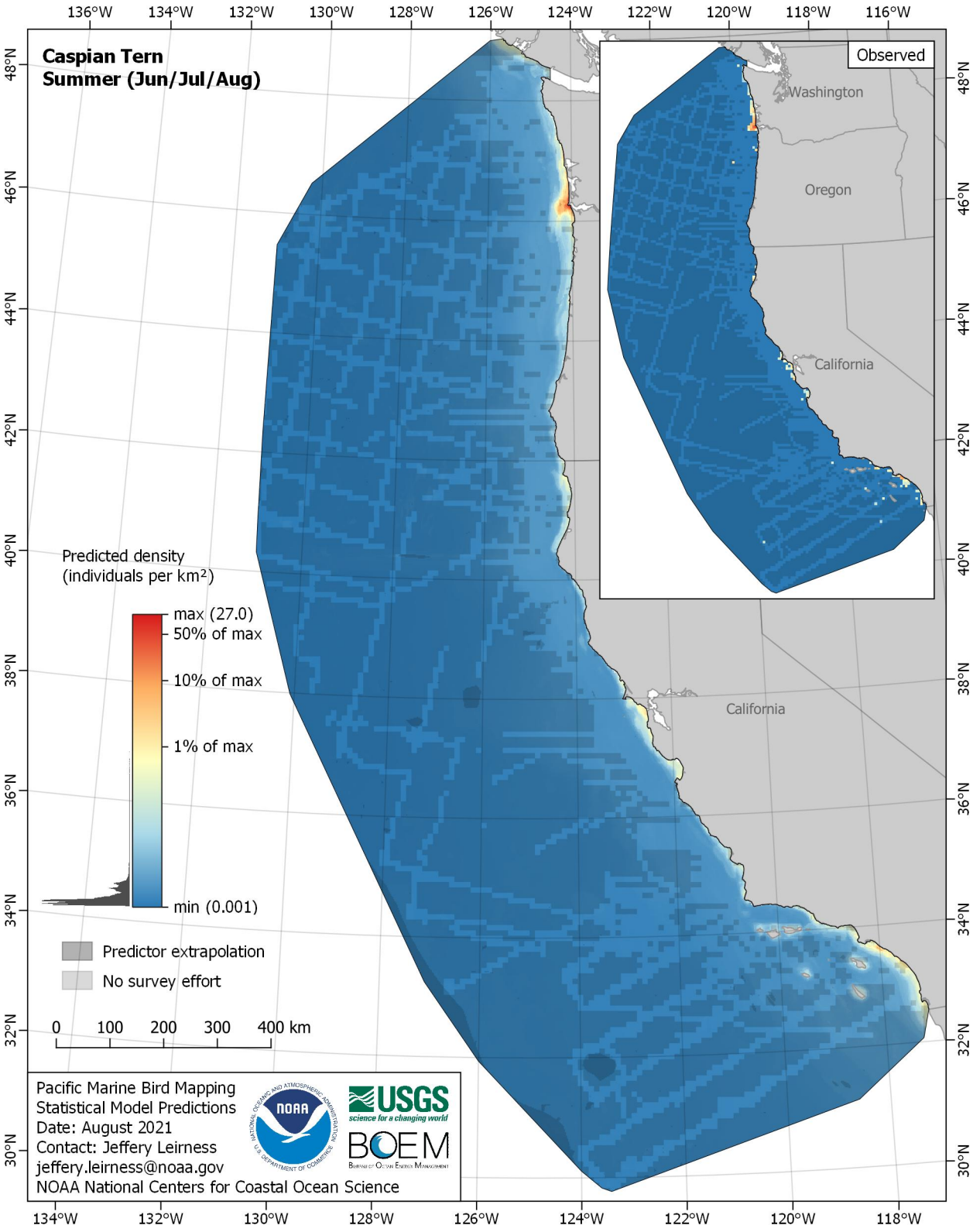

Figure E-137. Predicted density for Caspian Tern (*Hydroprogne caspia*) in the summer season

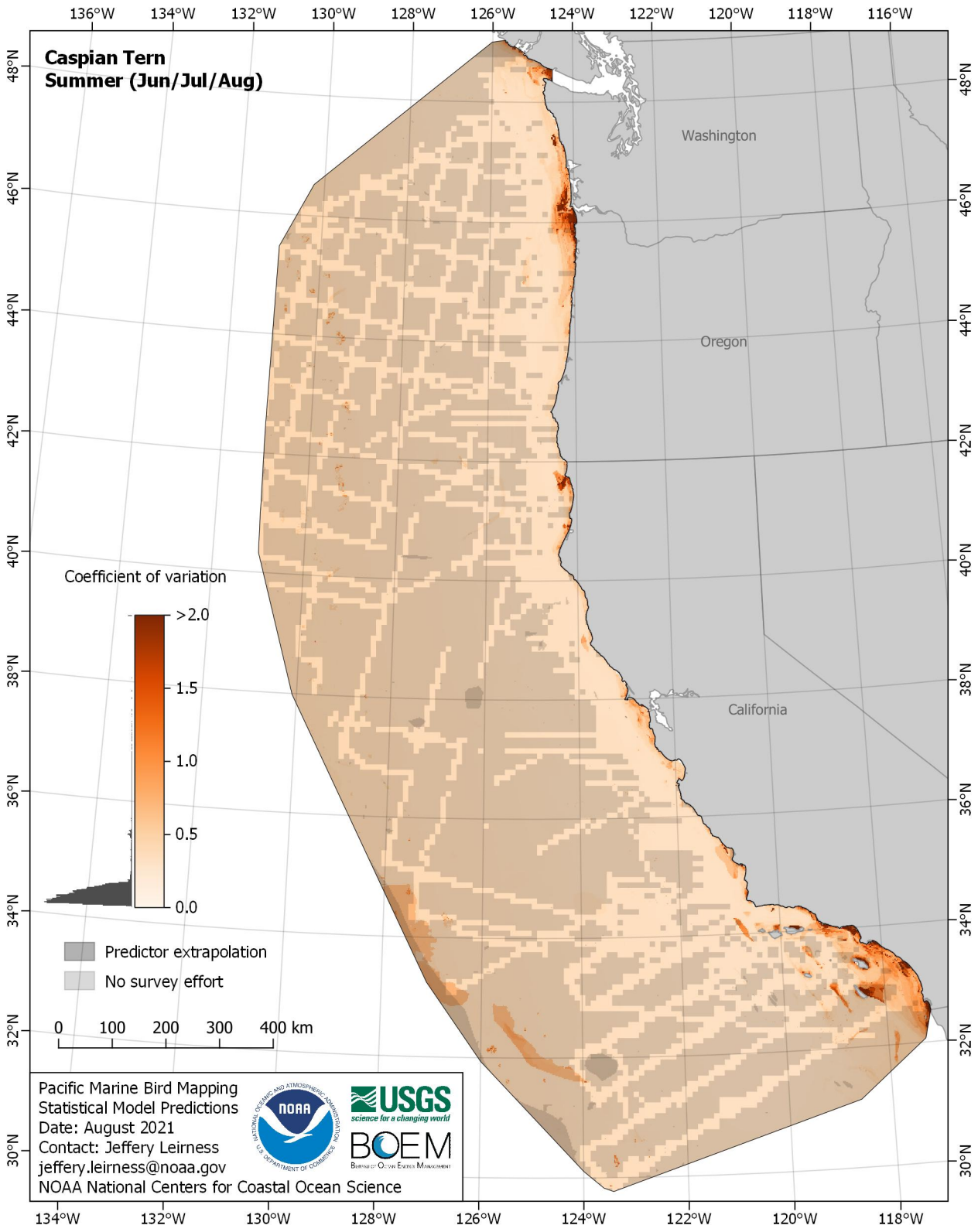

Figure E-138. Coefficient of variation for Caspian Tern (*Hydroprogne caspia*) in the summer season

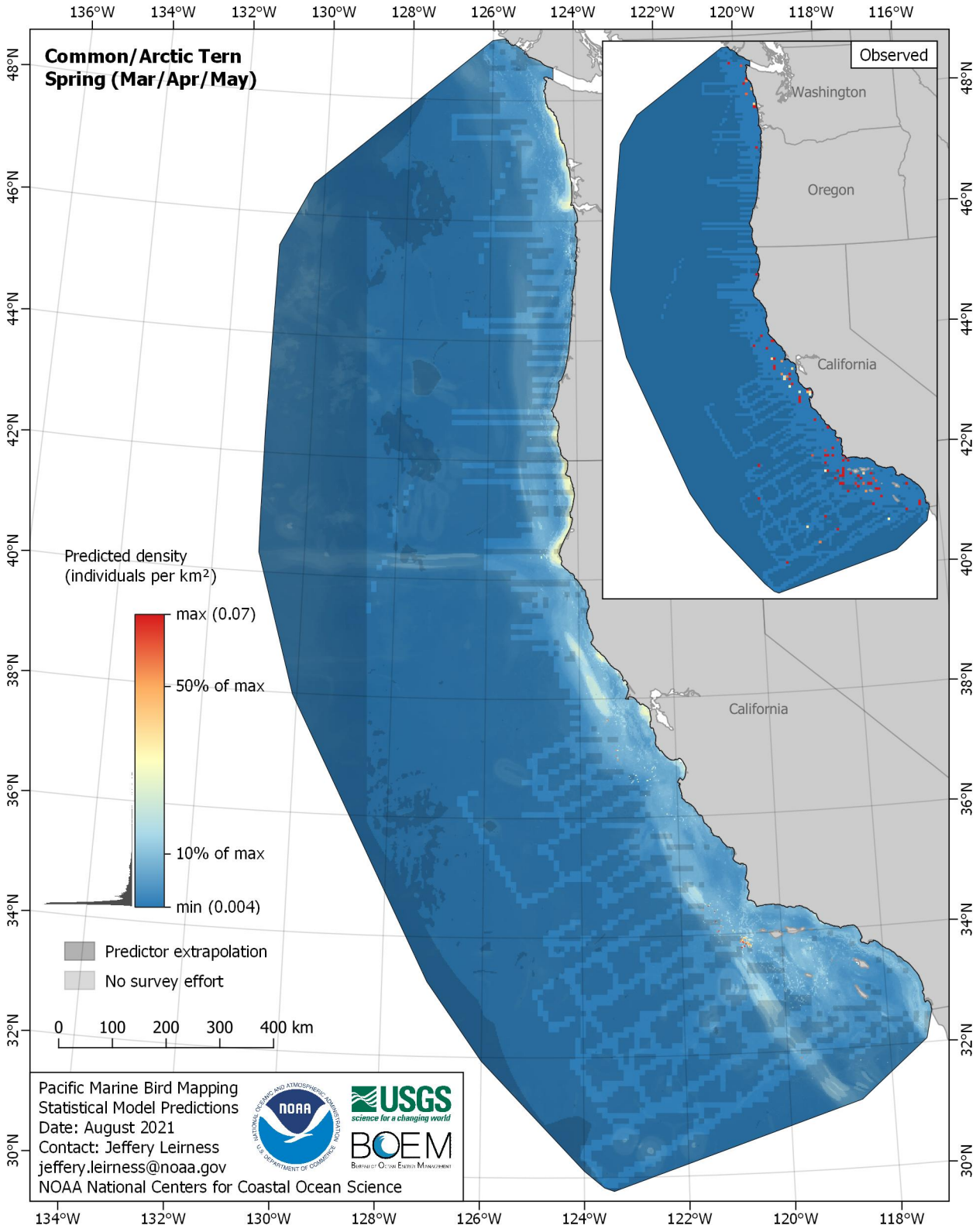

Figure E-139. Predicted density for Common/Arctic Tern (*Sterna hirundo/paradisaea*) in the spring season

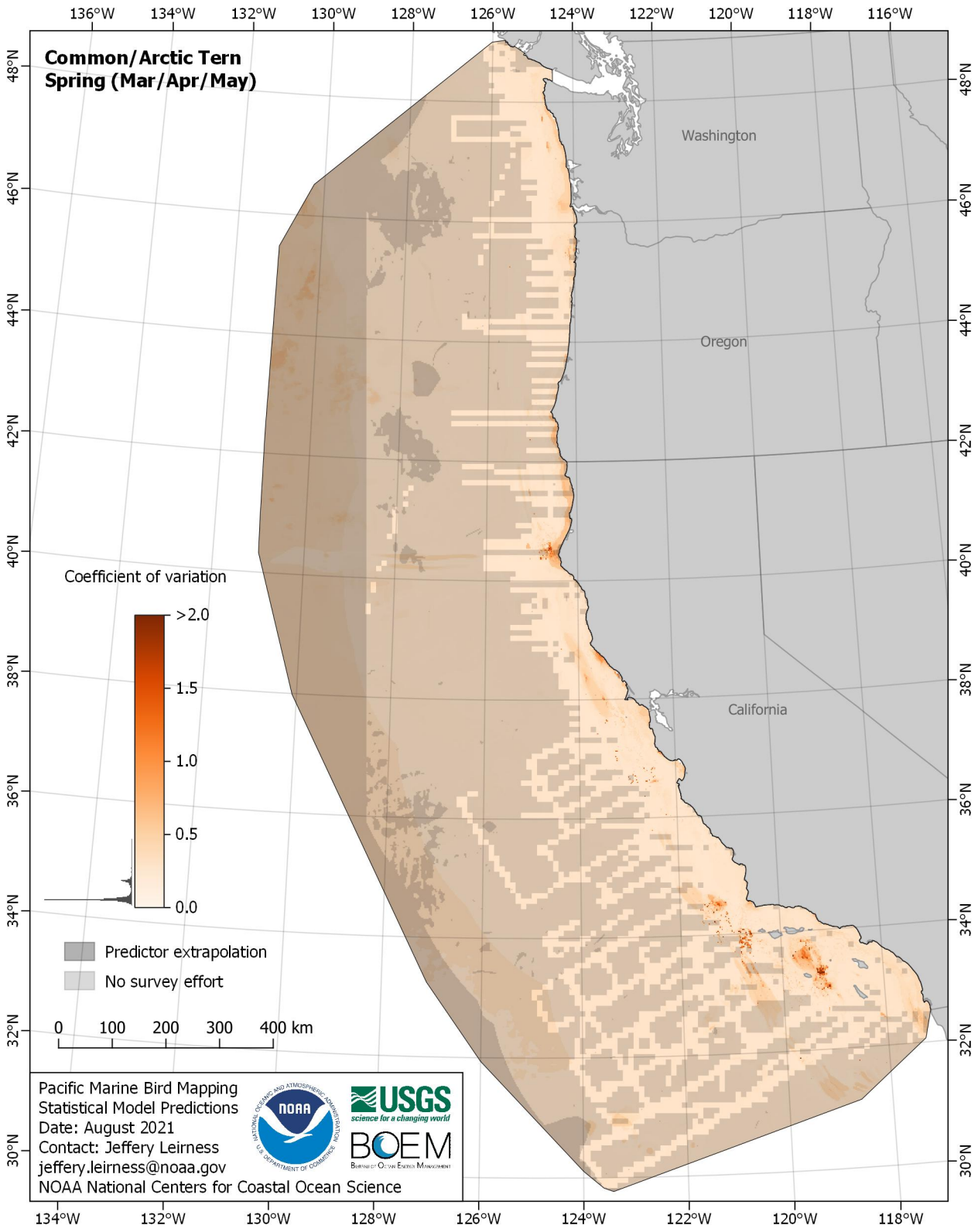

Figure E-140. Coefficient of variation for Common/Arctic Tern (*Sterna hirundo/paradisaea*) in the spring season

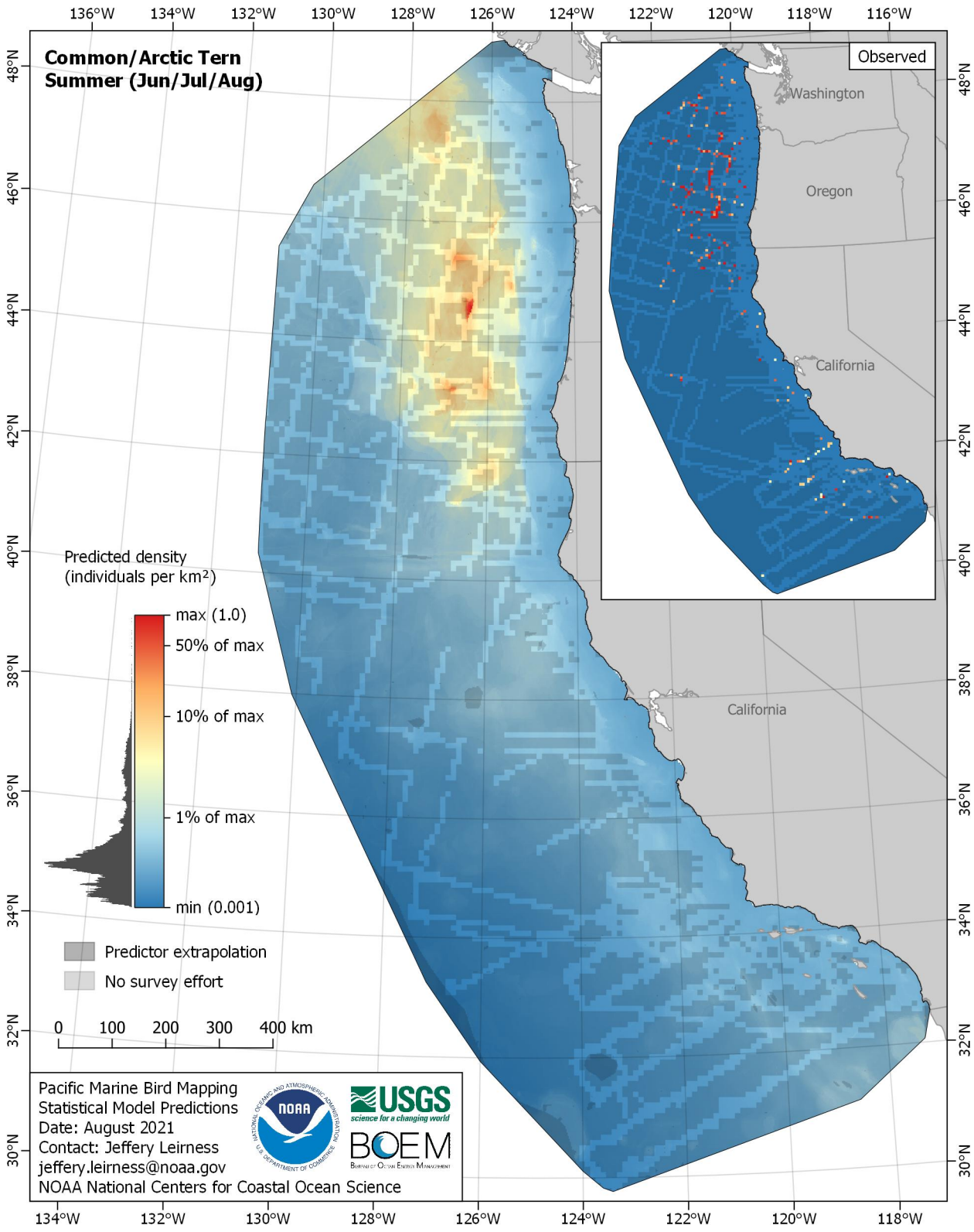

Figure E-141. Predicted density for Common/Arctic Tern (*Sterna hirundo/paradisaea*) in the summer season

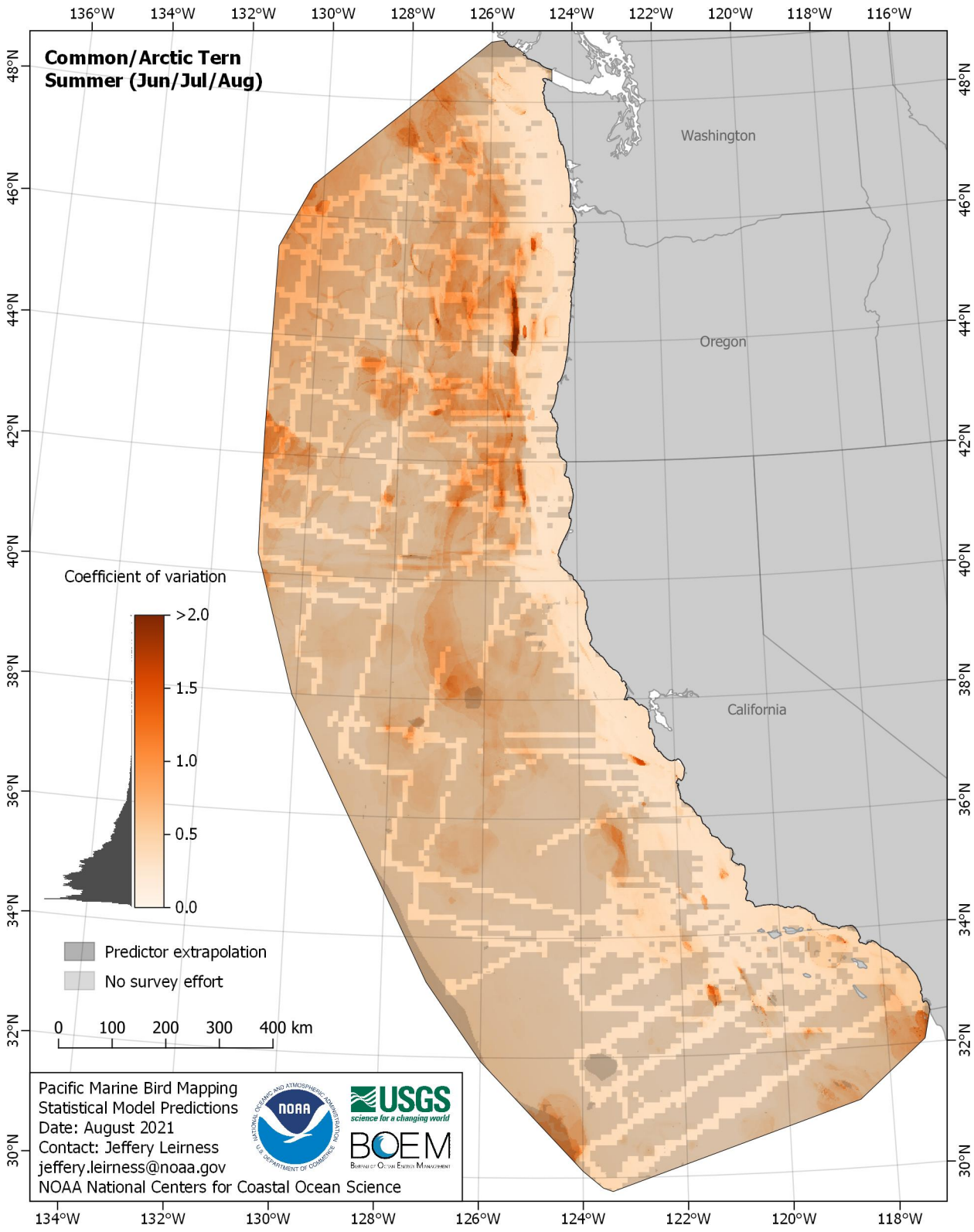

Figure E-142. Coefficient of variation for Common/Arctic Tern (*Sterna hirundo/paradisaea*) in the summer season

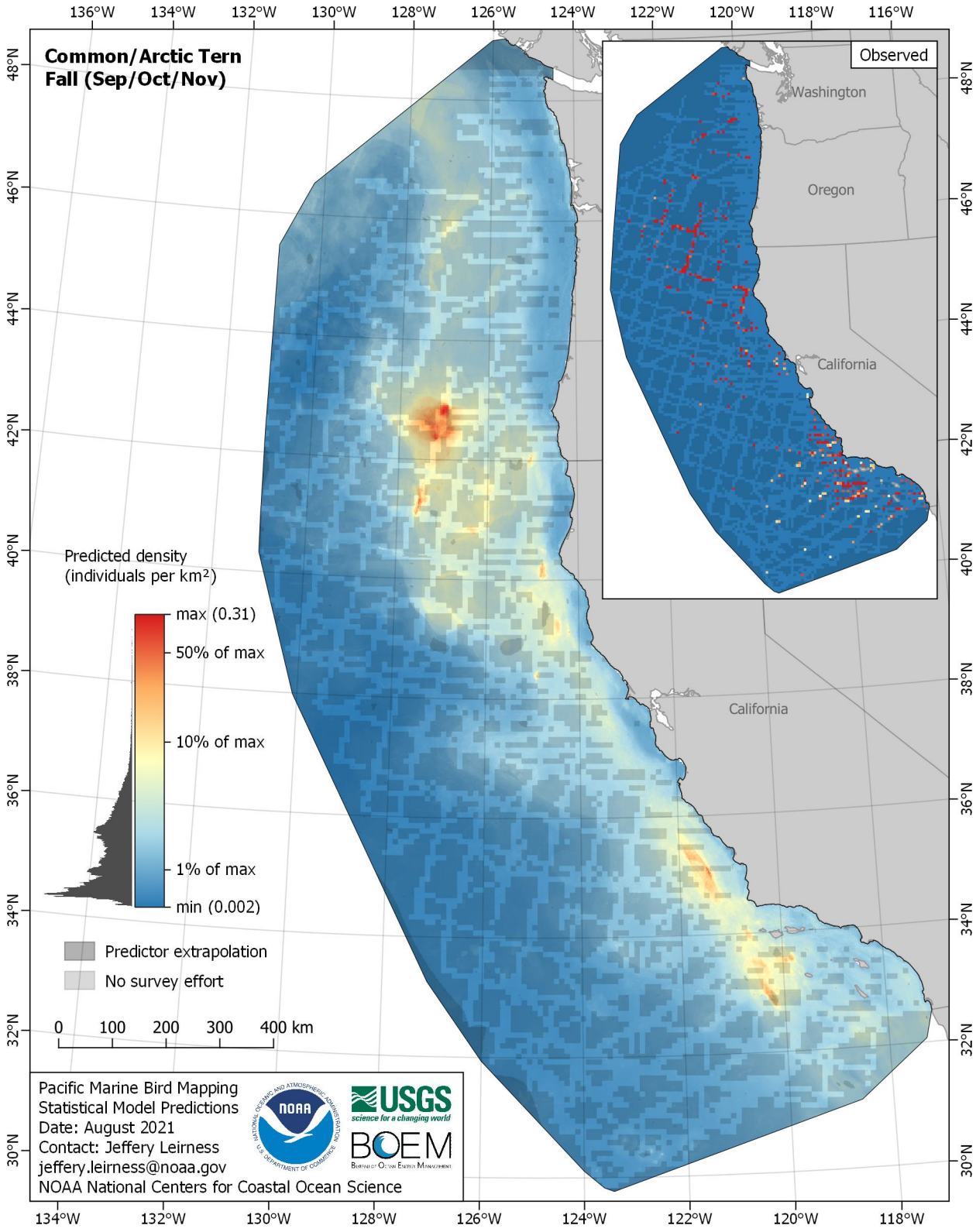

Figure E-143. Predicted density for Common/Arctic Tern (*Sterna hirundo/paradisaea*) in the fall season

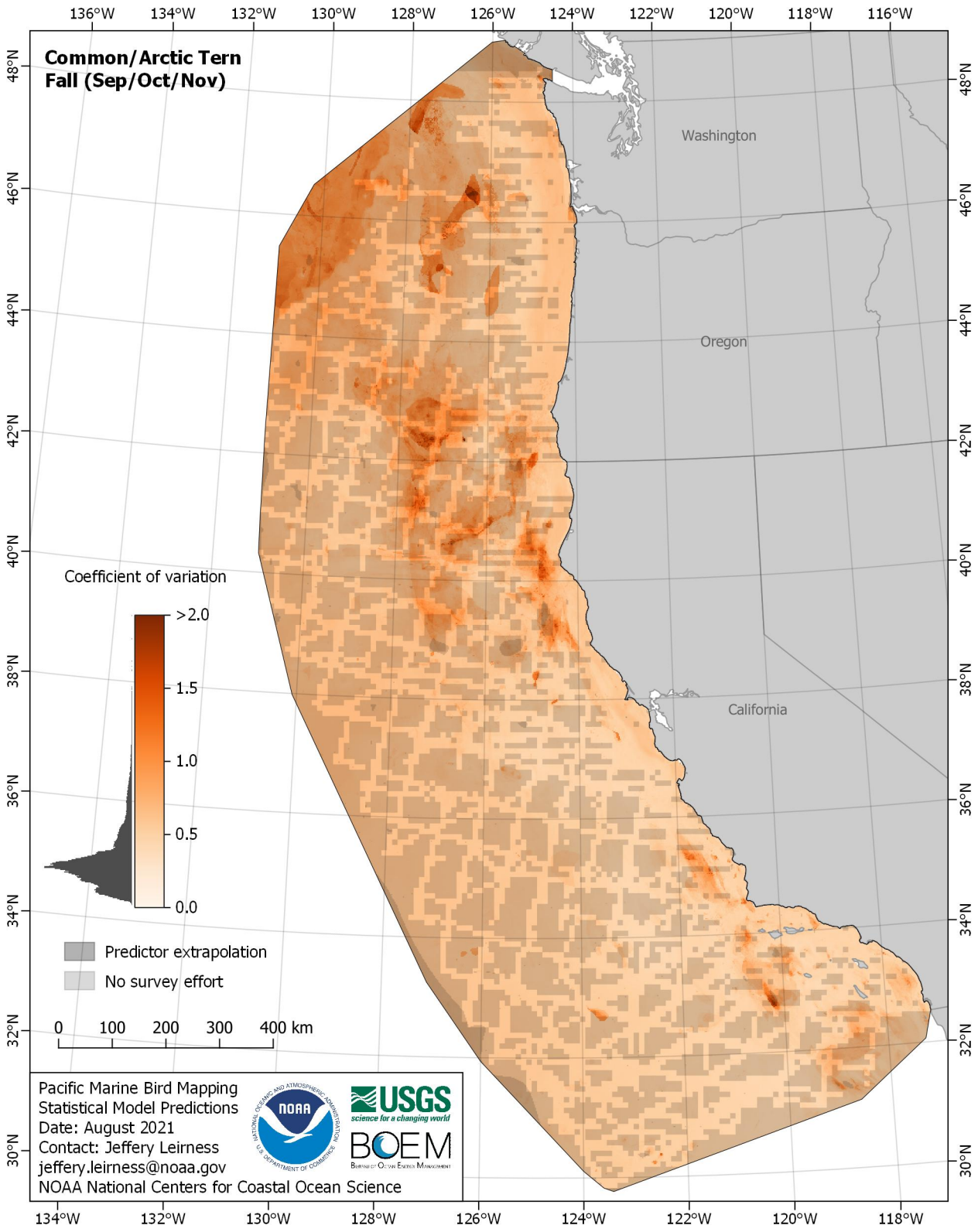

Figure E-144. Coefficient of variation for Common/Arctic Tern (*Sterna hirundo/paradisaea*) in the fall season

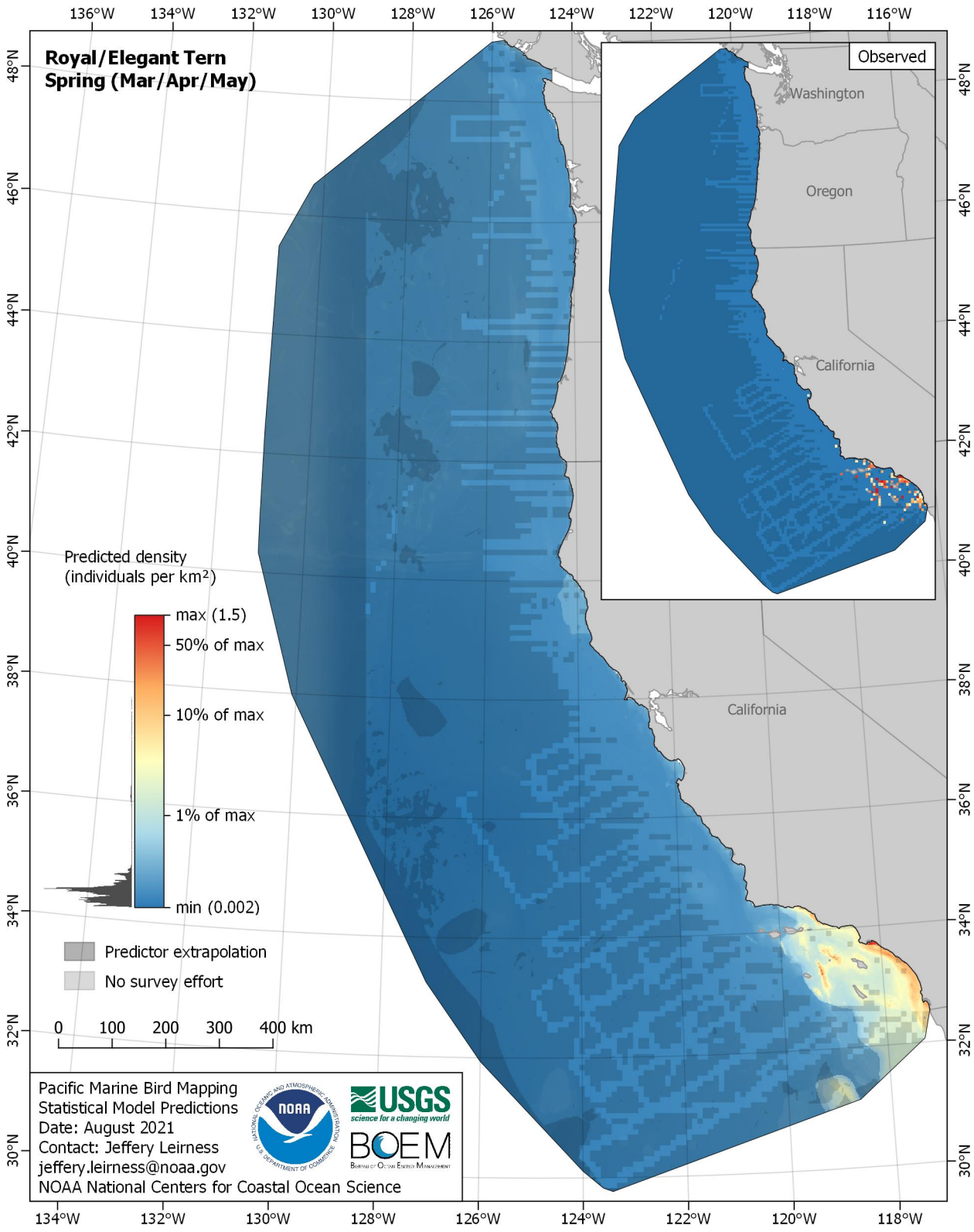

Figure E-145. Predicted density for Royal/Elegant Tern (*Thalasseus maximus/elegans*) in the spring season

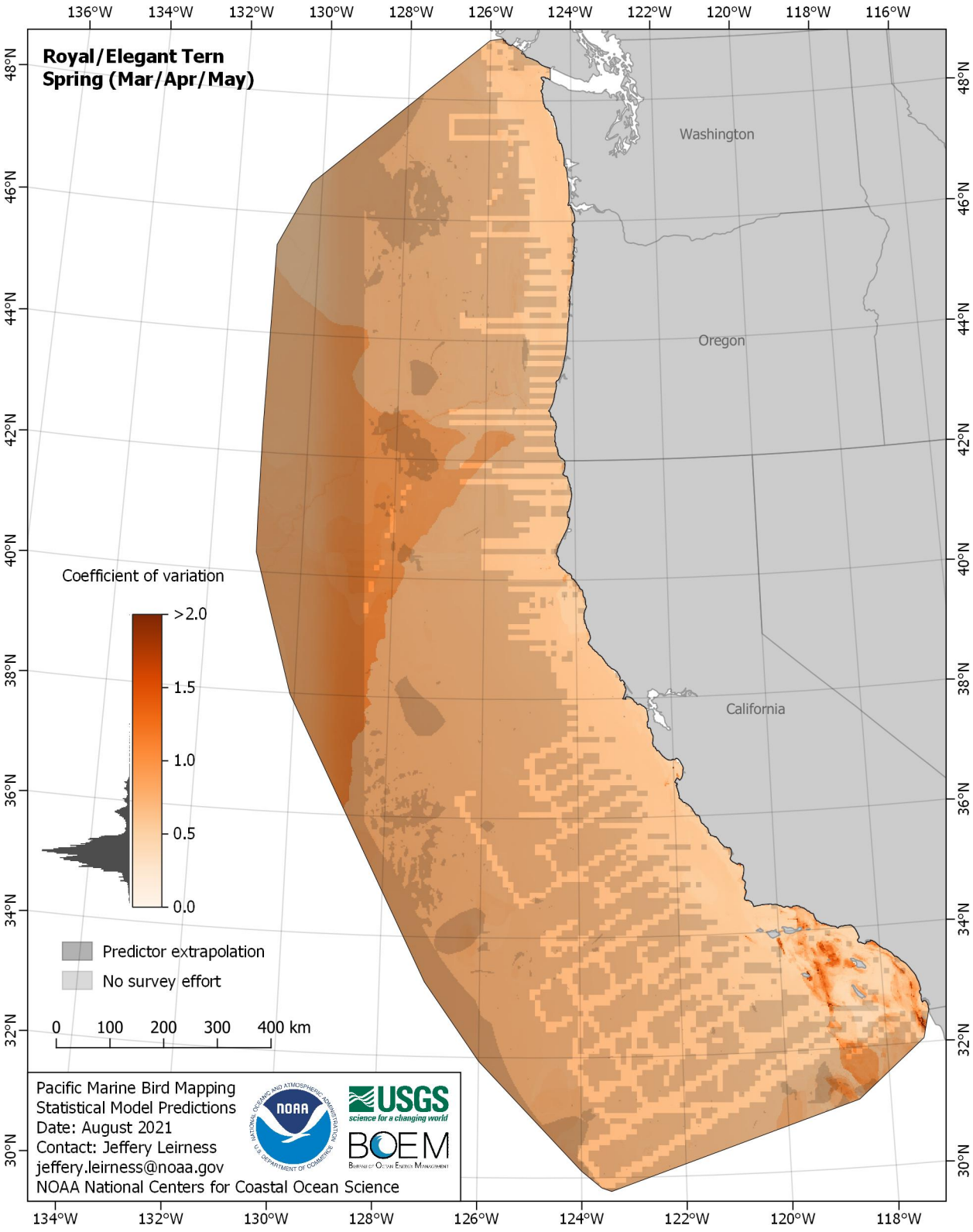

Figure E-146. Coefficient of variation for Royal/Elegant Tern (*Thalasseus maximus/elegans*) in the spring season

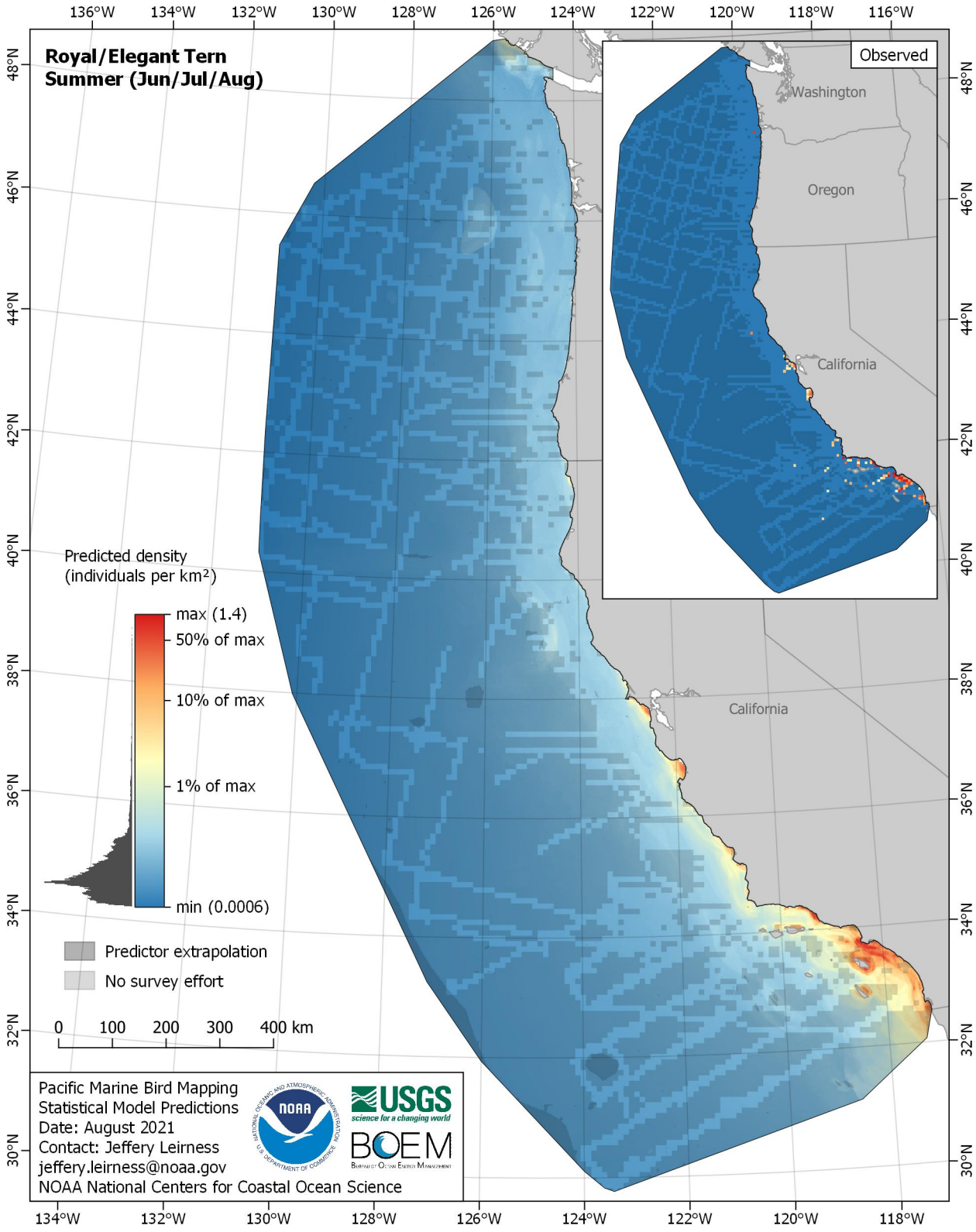

Figure E-147. Predicted density for Royal/Elegant Tern (*Thalasseus maximus/elegans*) in the summer season

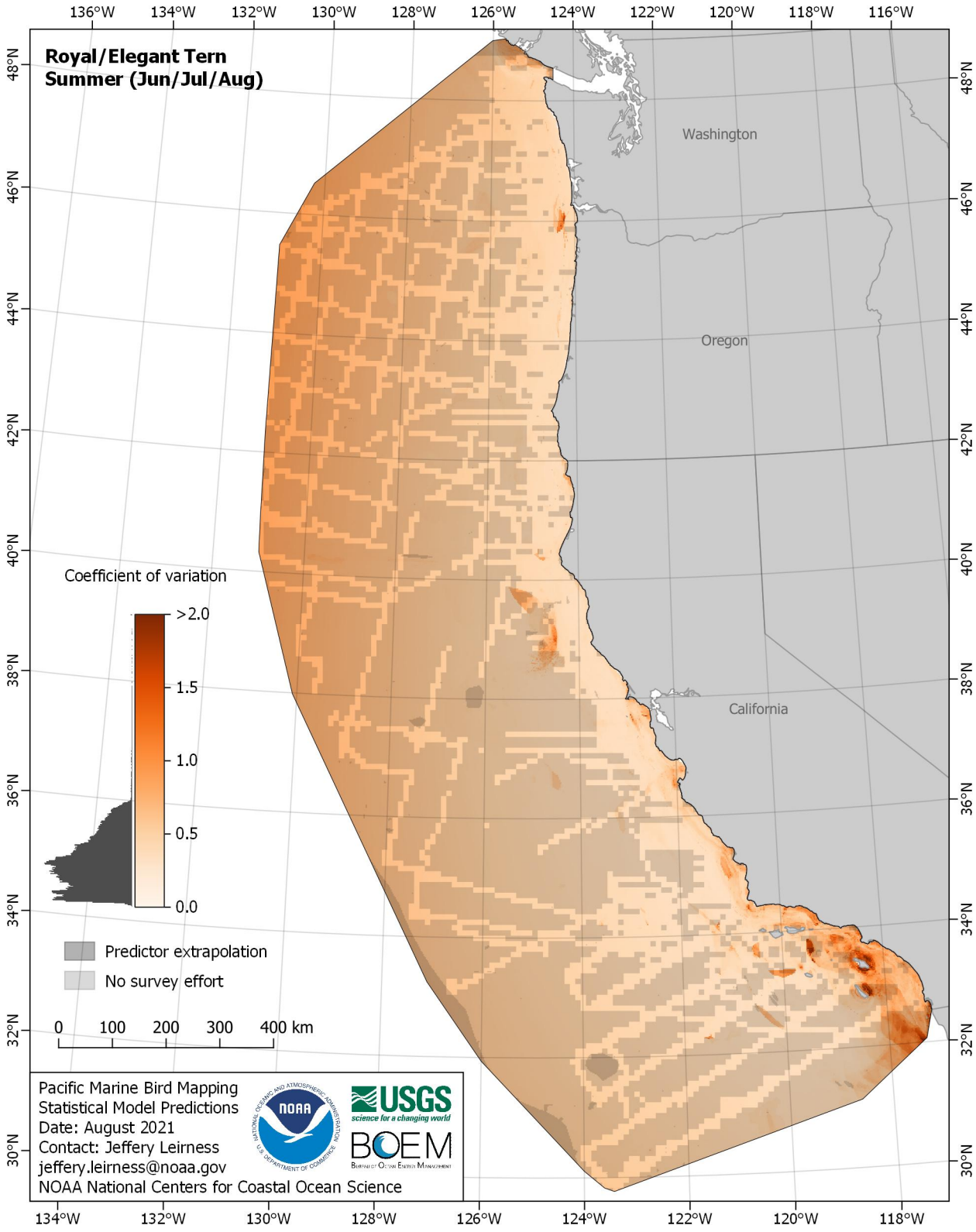

Figure E-148. Coefficient of variation for Royal/Elegant Tern (*Thalasseus maximus/elegans*) in the summer season

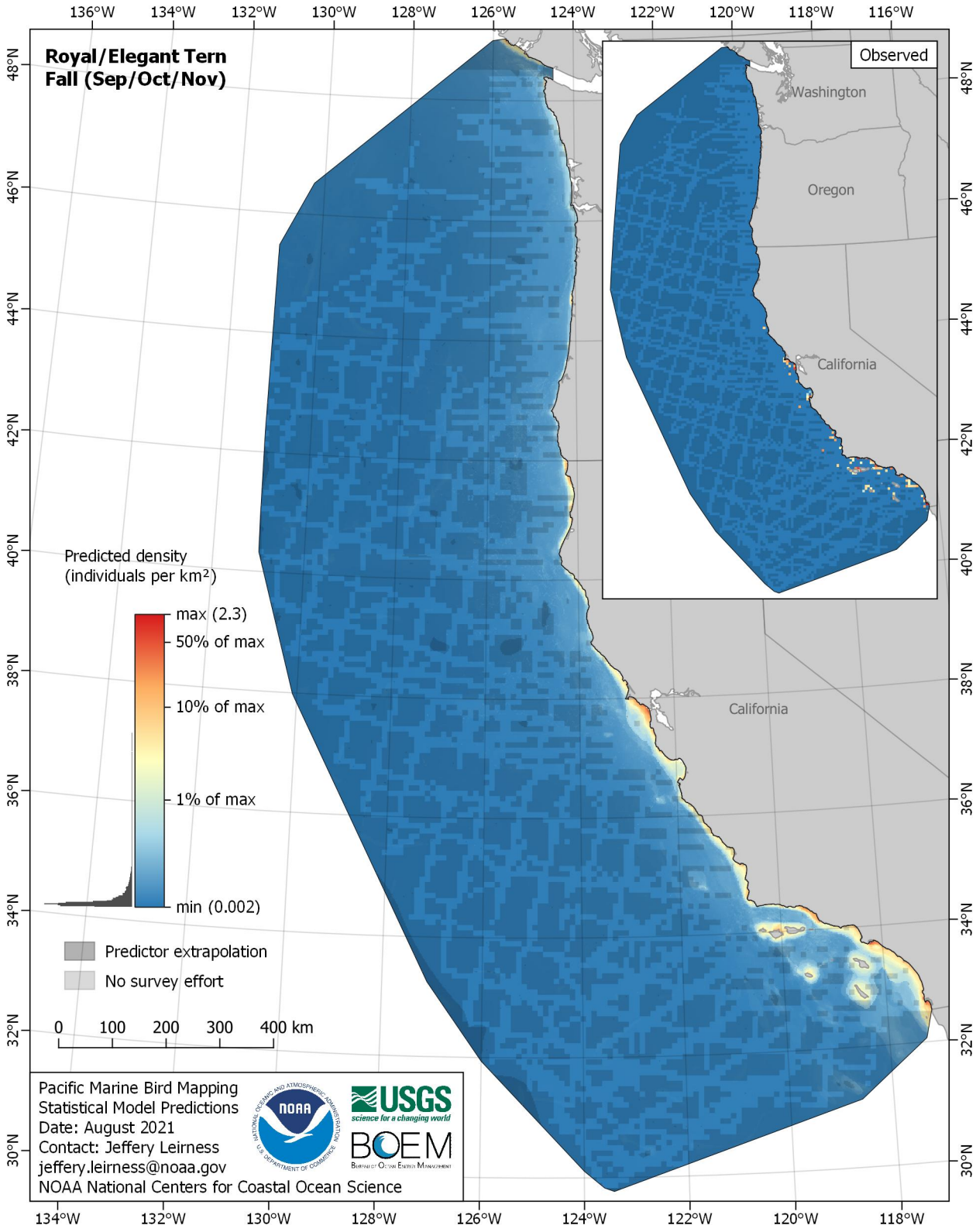

Figure E-149. Predicted density for Royal/Elegant Tern (*Thalasseus maximus/elegans*) in the fall season

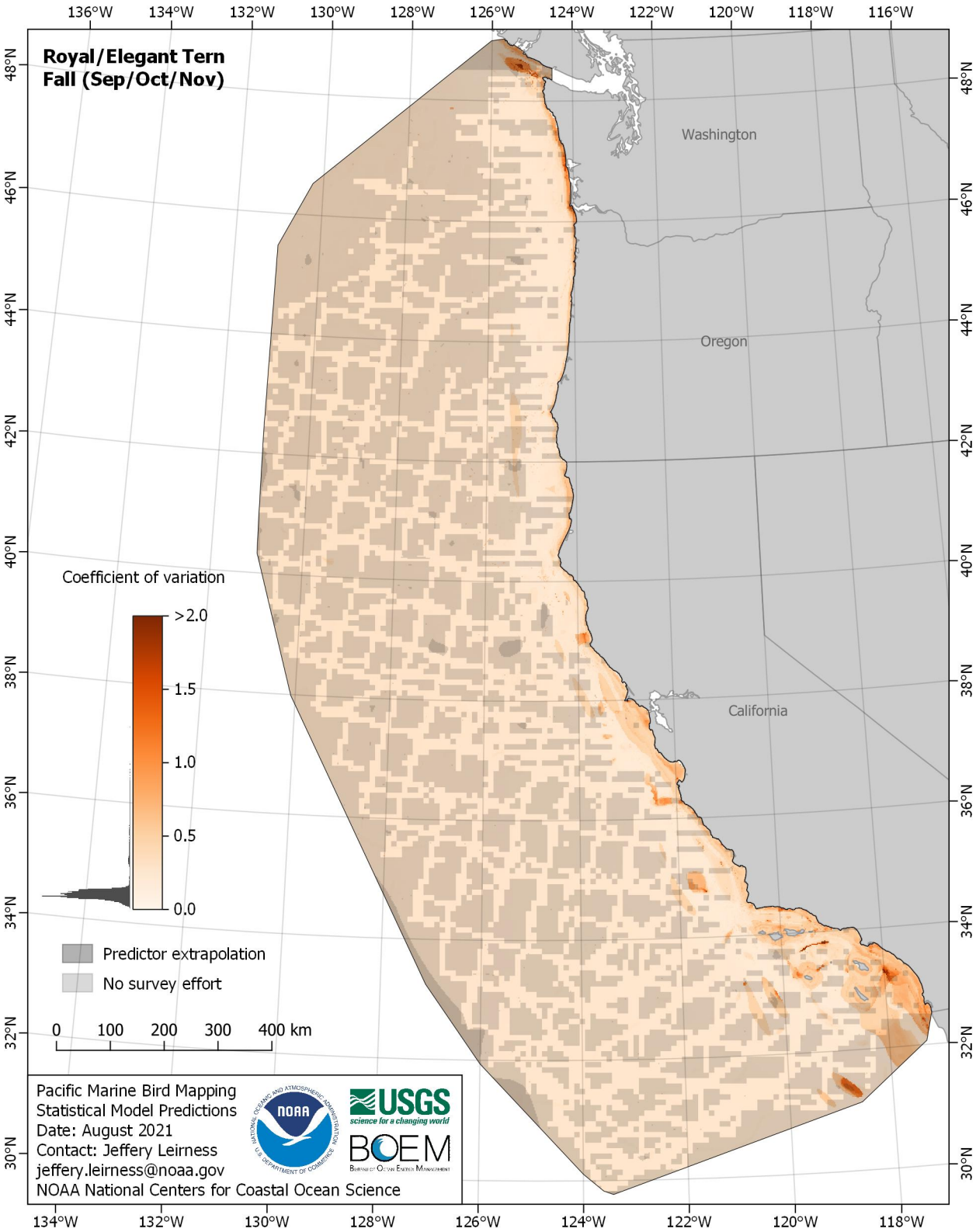

Figure E-150. Coefficient of variation for Royal/Elegant Tern (*Thalasseus maximus/elegans*) in the fall season

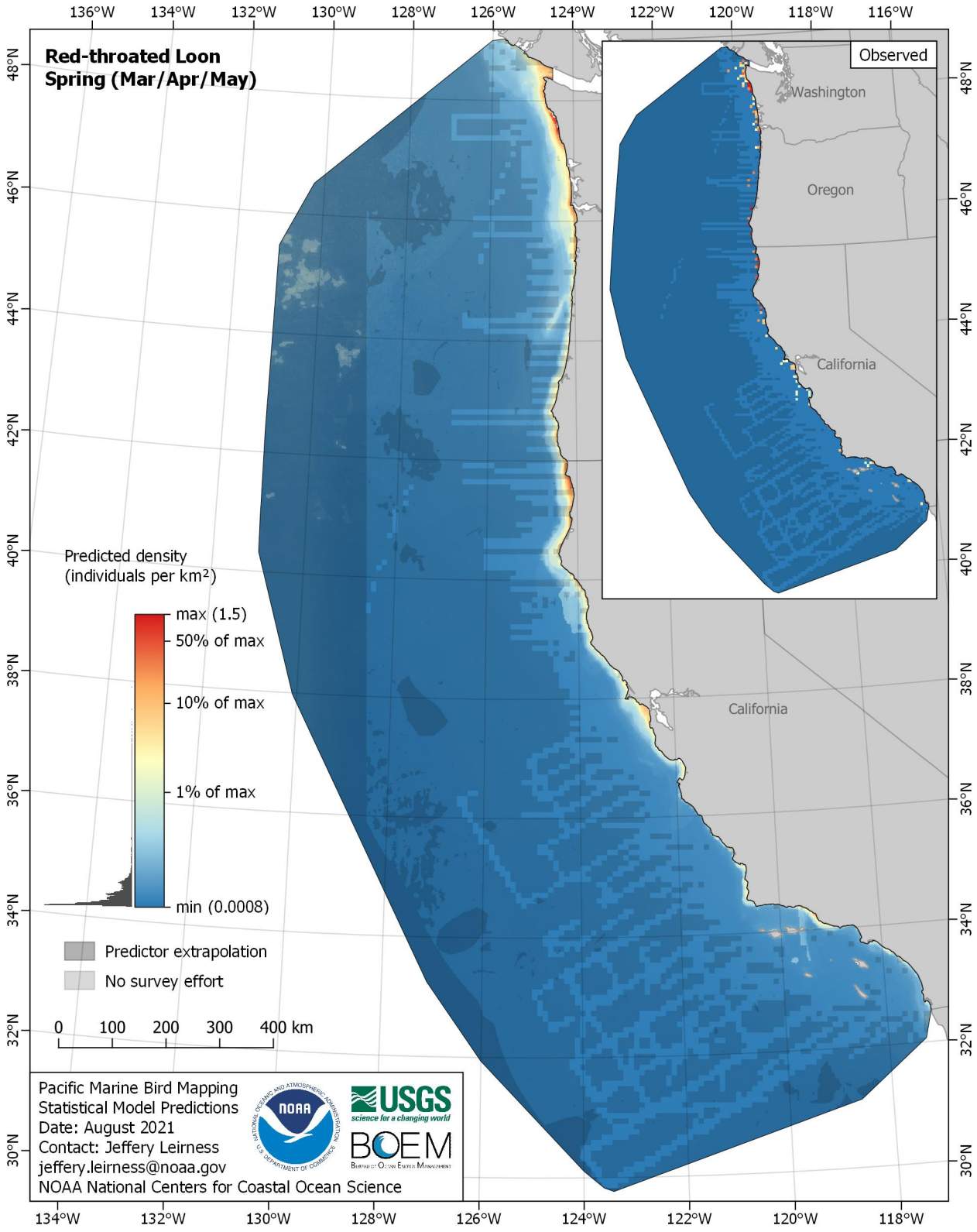

Figure E-151. Predicted density for Red-throated Loon (*Gavia stellata*) in the spring season

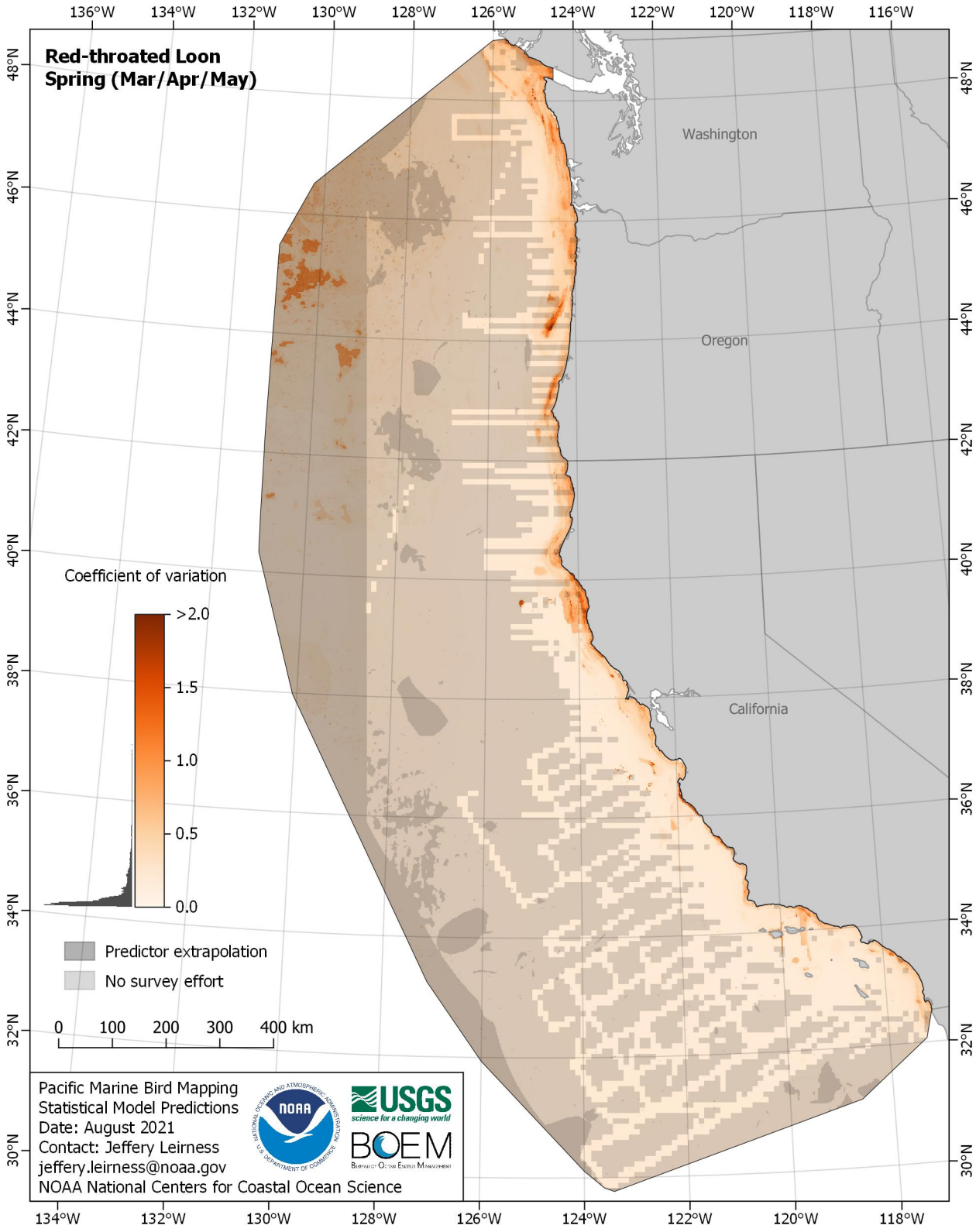

Figure E-152. Coefficient of variation for Red-throated Loon (*Gavia stellata*) in the spring season

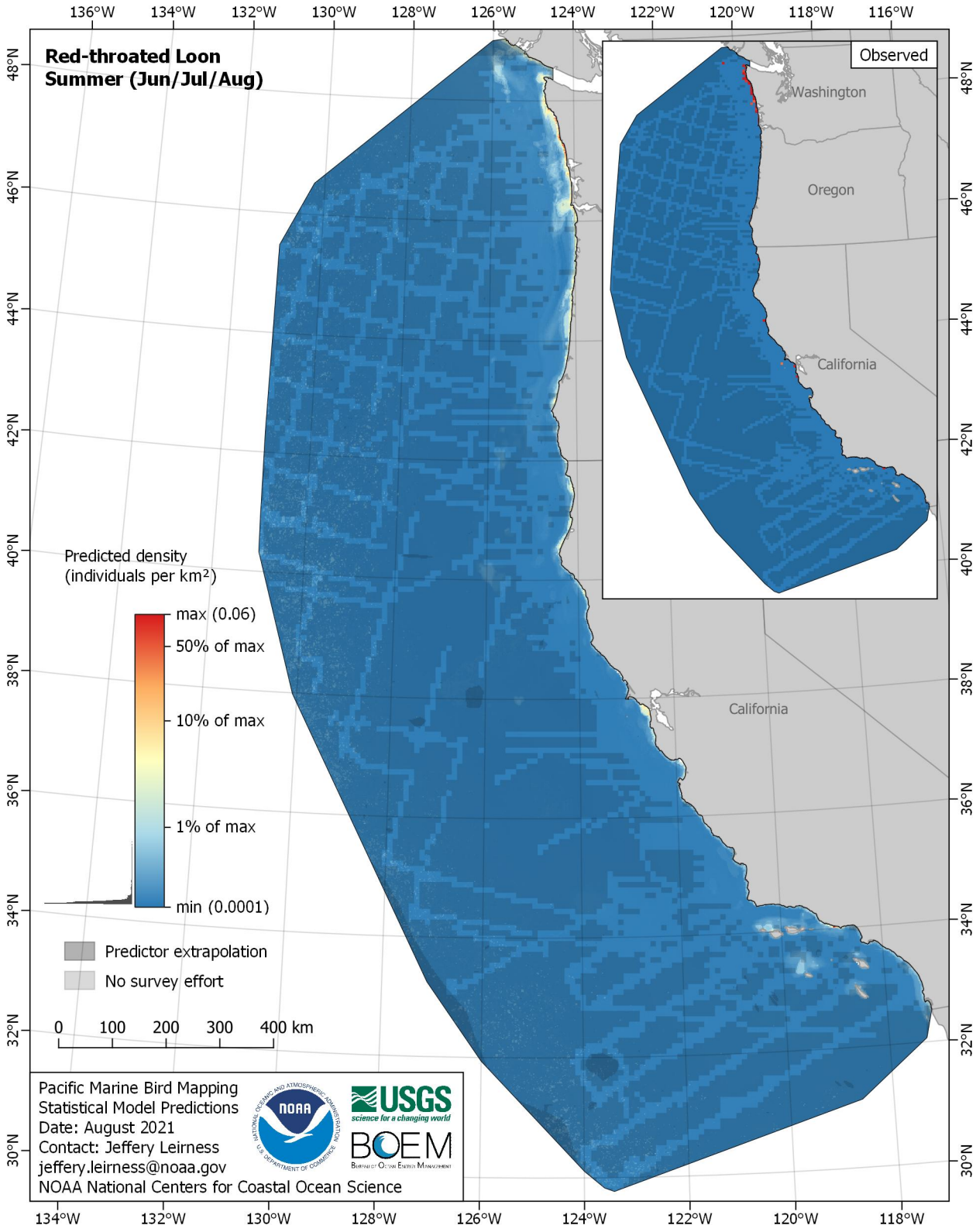

Figure E-153. Predicted density for Red-throated Loon (*Gavia stellata*) in the summer season

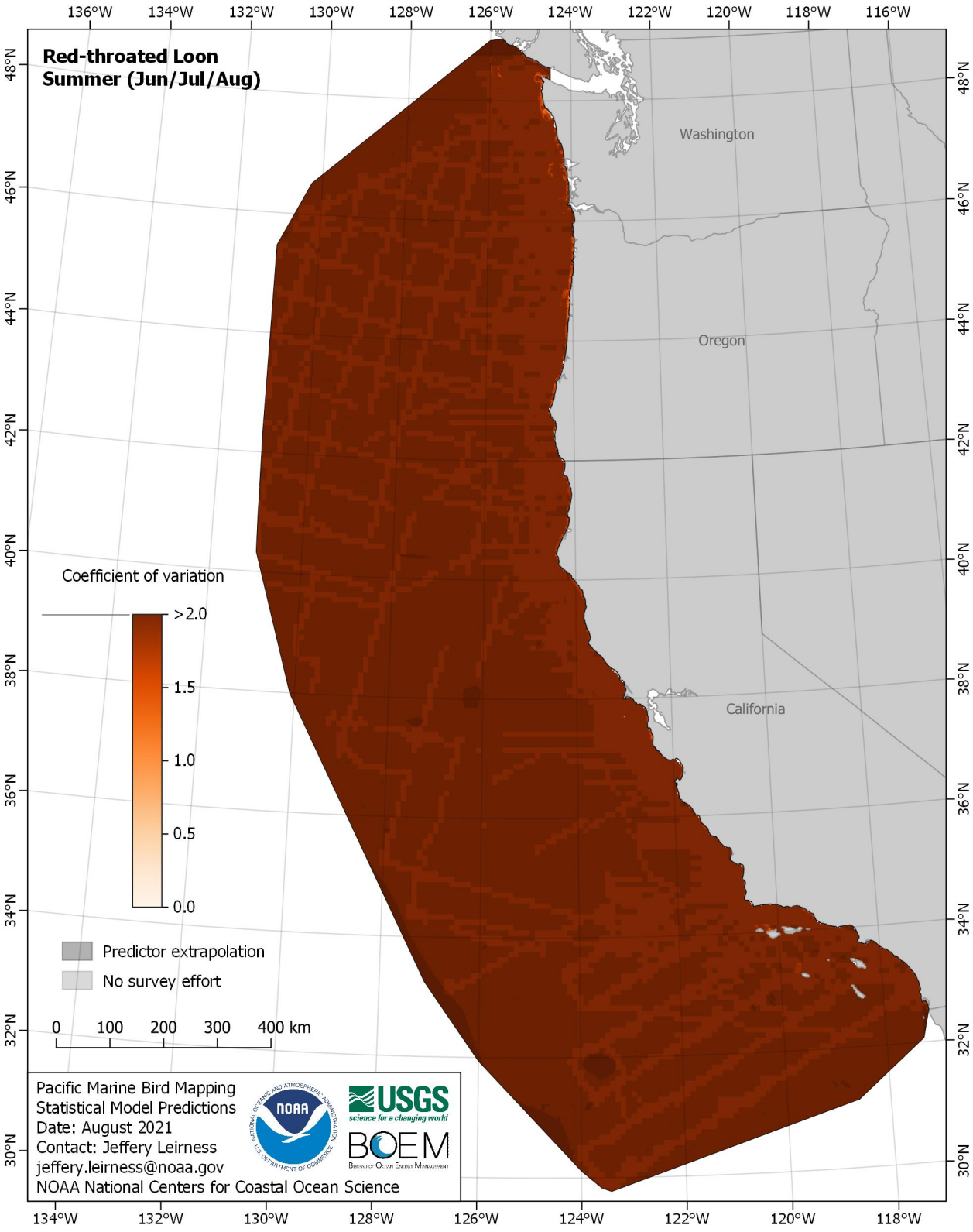

Figure E-154. Coefficient of variation for Red-throated Loon (*Gavia stellata*) in the summer season

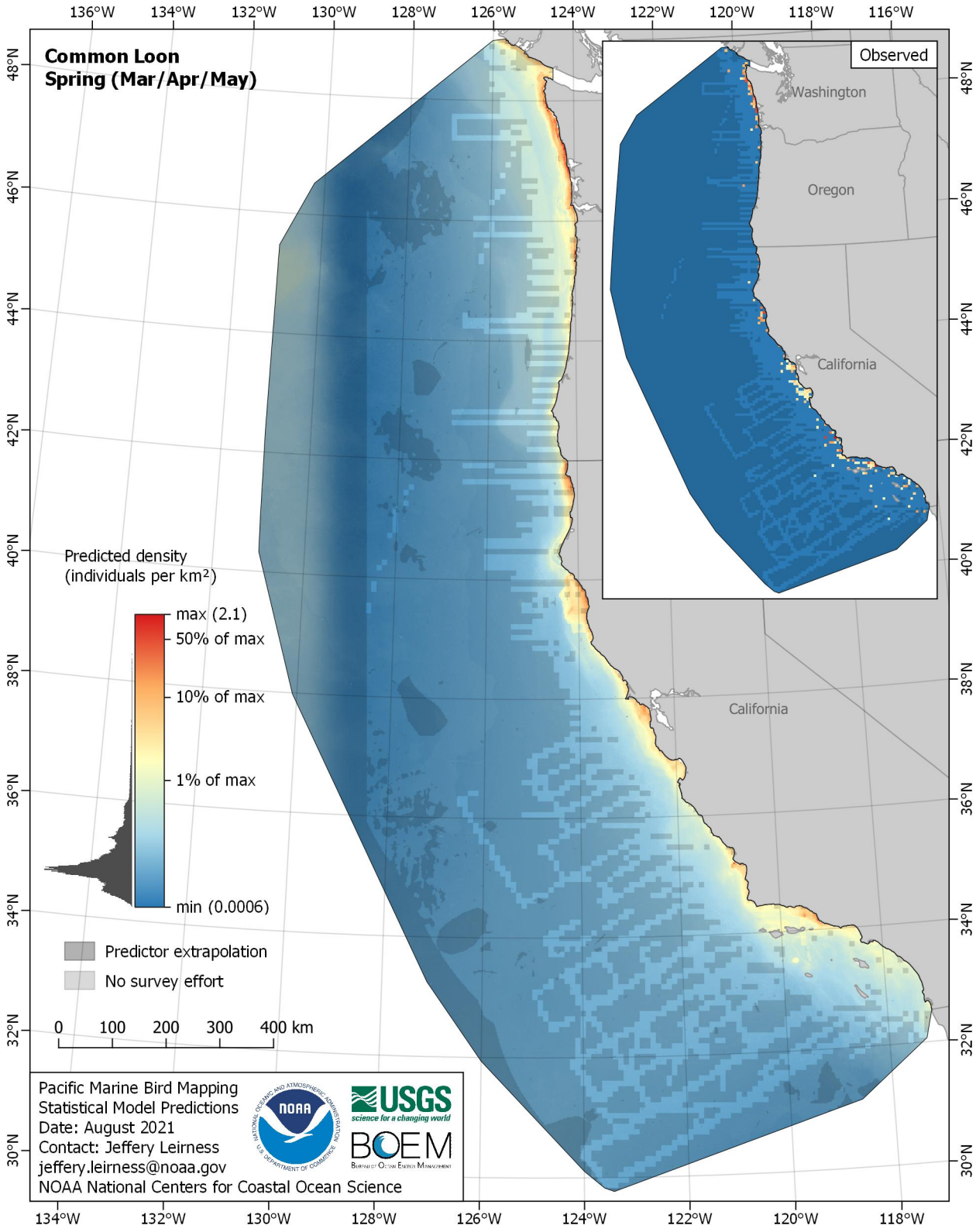

Figure E-155. Predicted density for Common Loon (*Gavia immer*) in the spring season

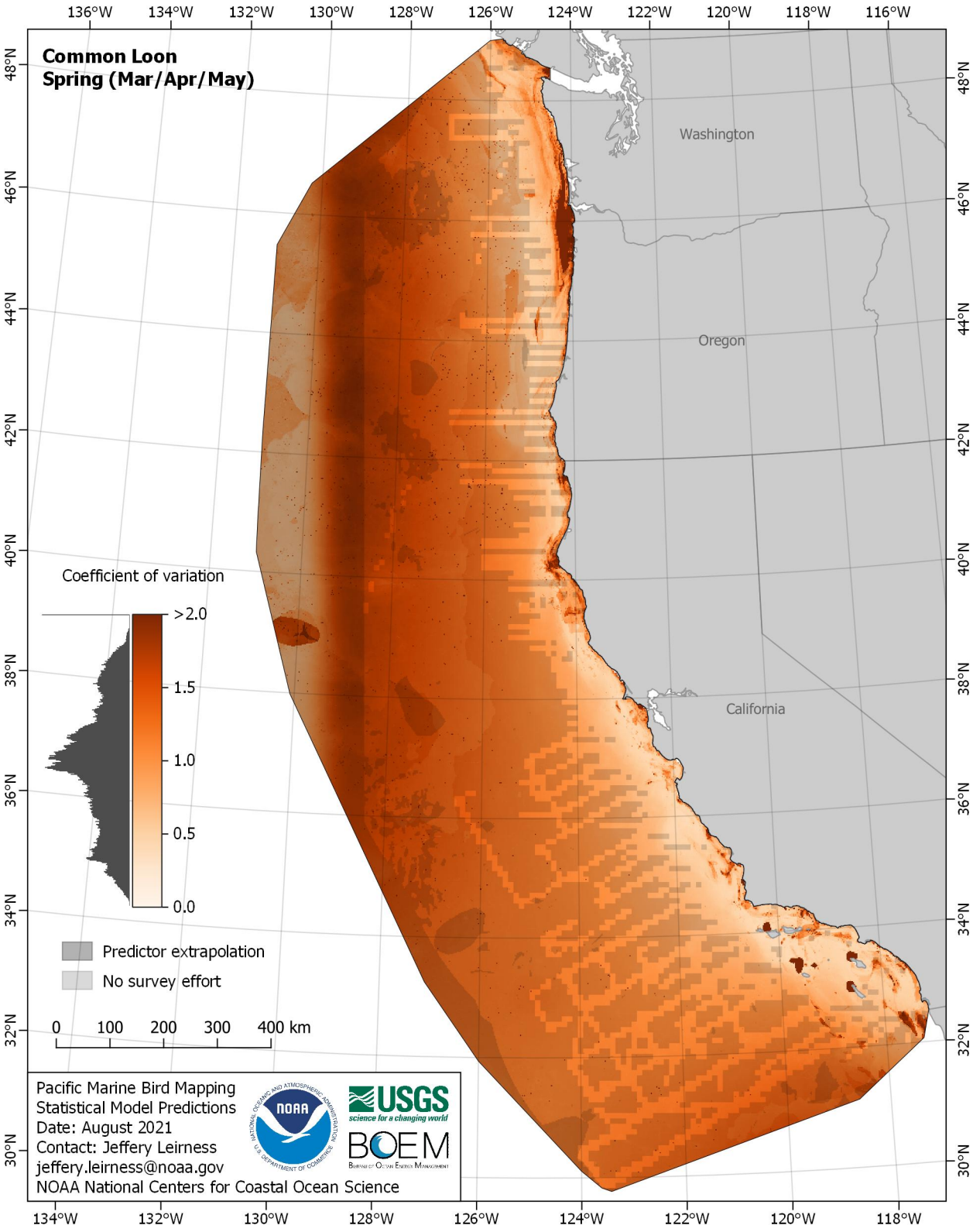

Figure E-156. Coefficient of variation for Common Loon (*Gavia immer*) in the spring season

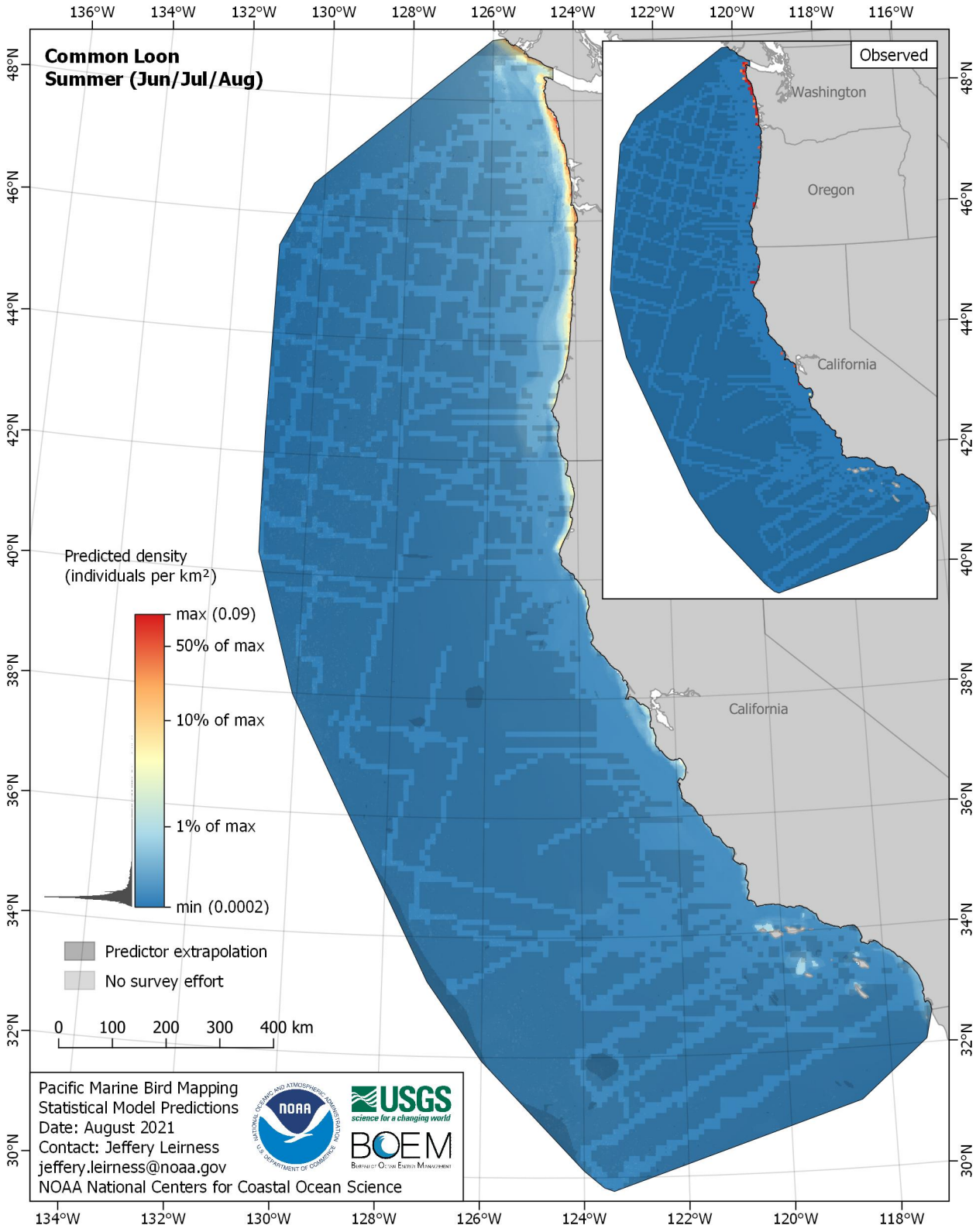

Figure E-157. Predicted density for Common Loon (*Gavia immer*) in the summer season

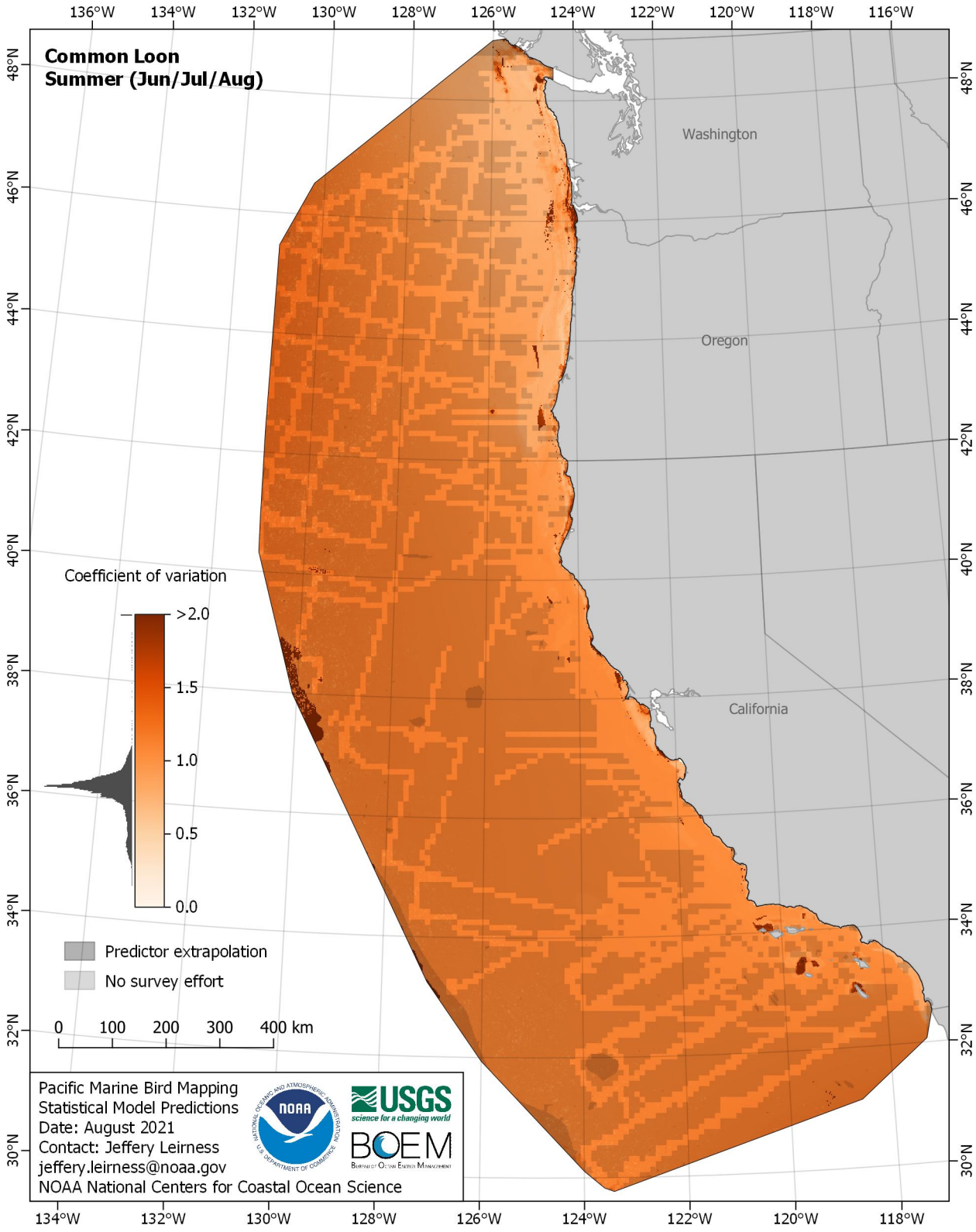

Figure E-158. Coefficient of variation for Common Loon (*Gavia immer*) in the summer season

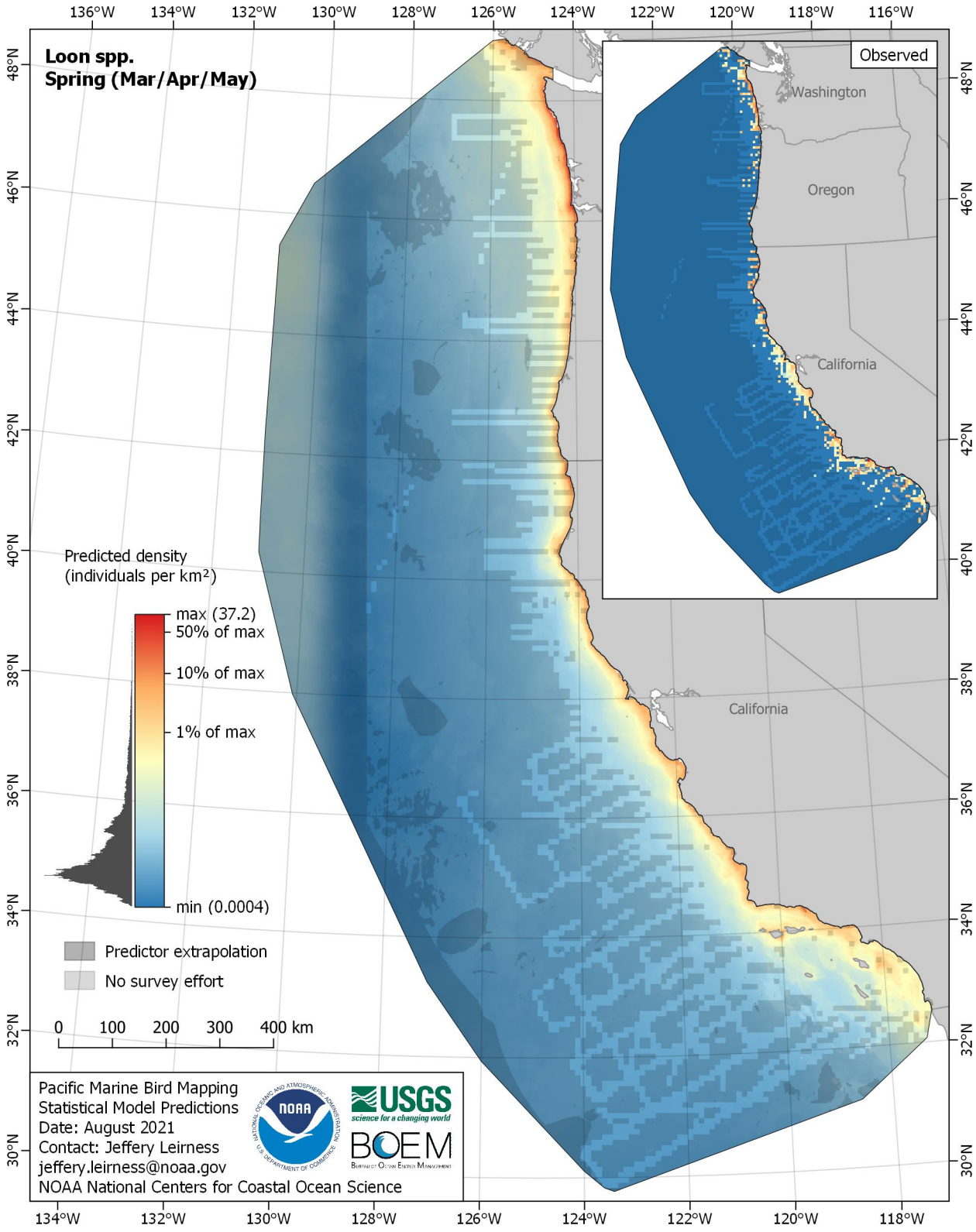

Figure E-159. Predicted density for Loon spp. (*Gavia spp.*) in the spring season

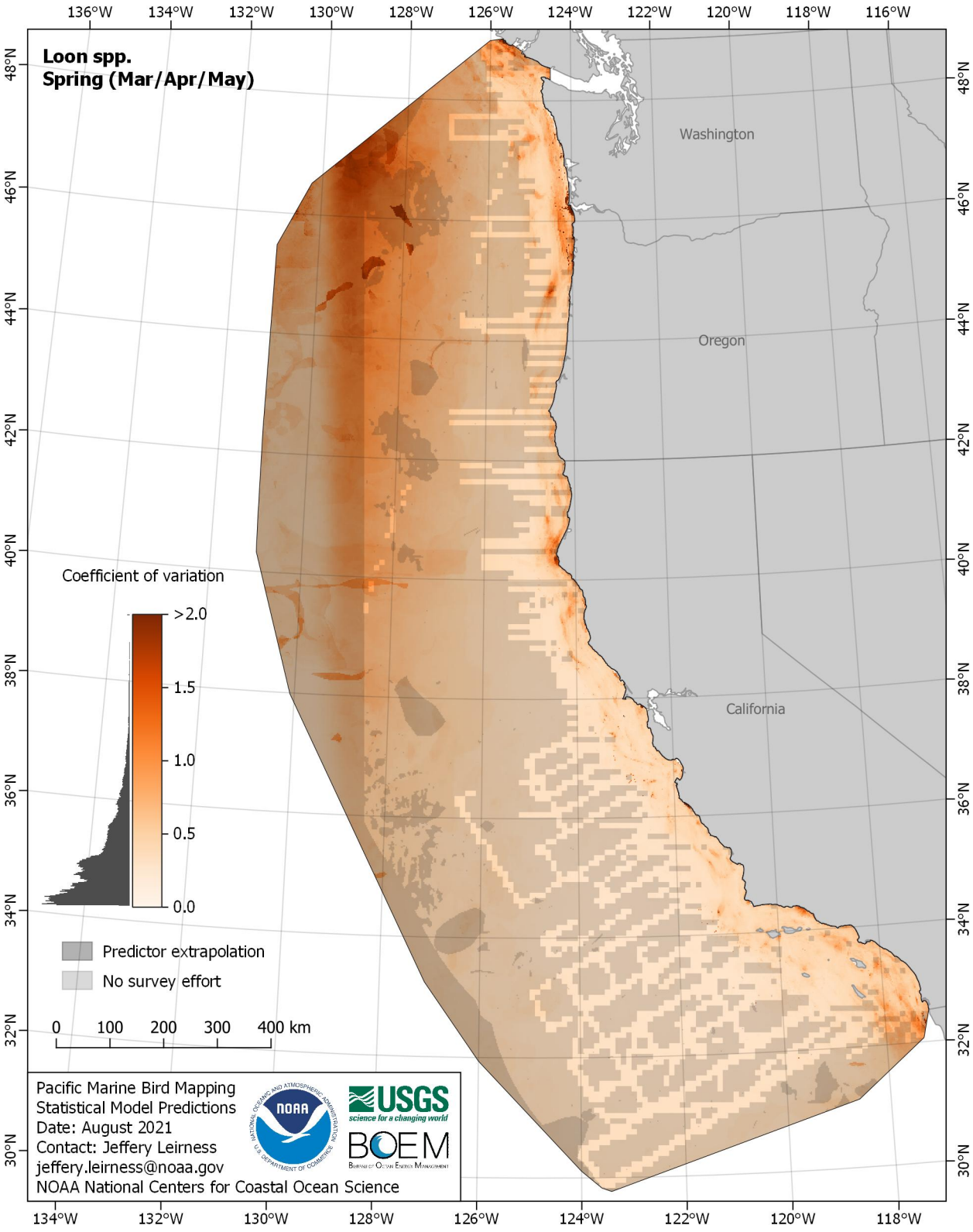

Figure E-160. Coefficient of variation for Loon spp. (*Gavia spp.*) in the spring season

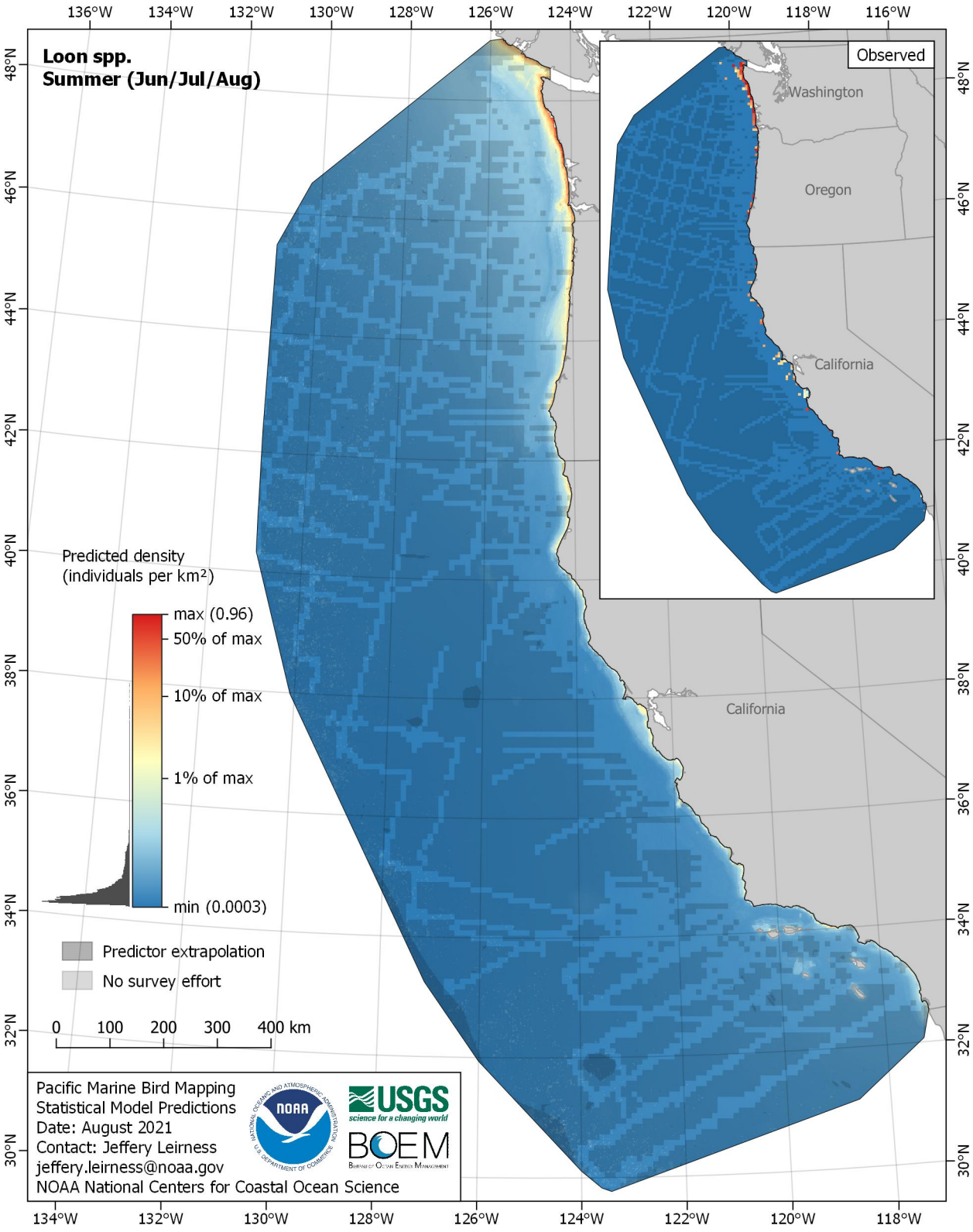

Figure E-161. Predicted density for Loon spp. (*Gavia spp.*) in the summer season

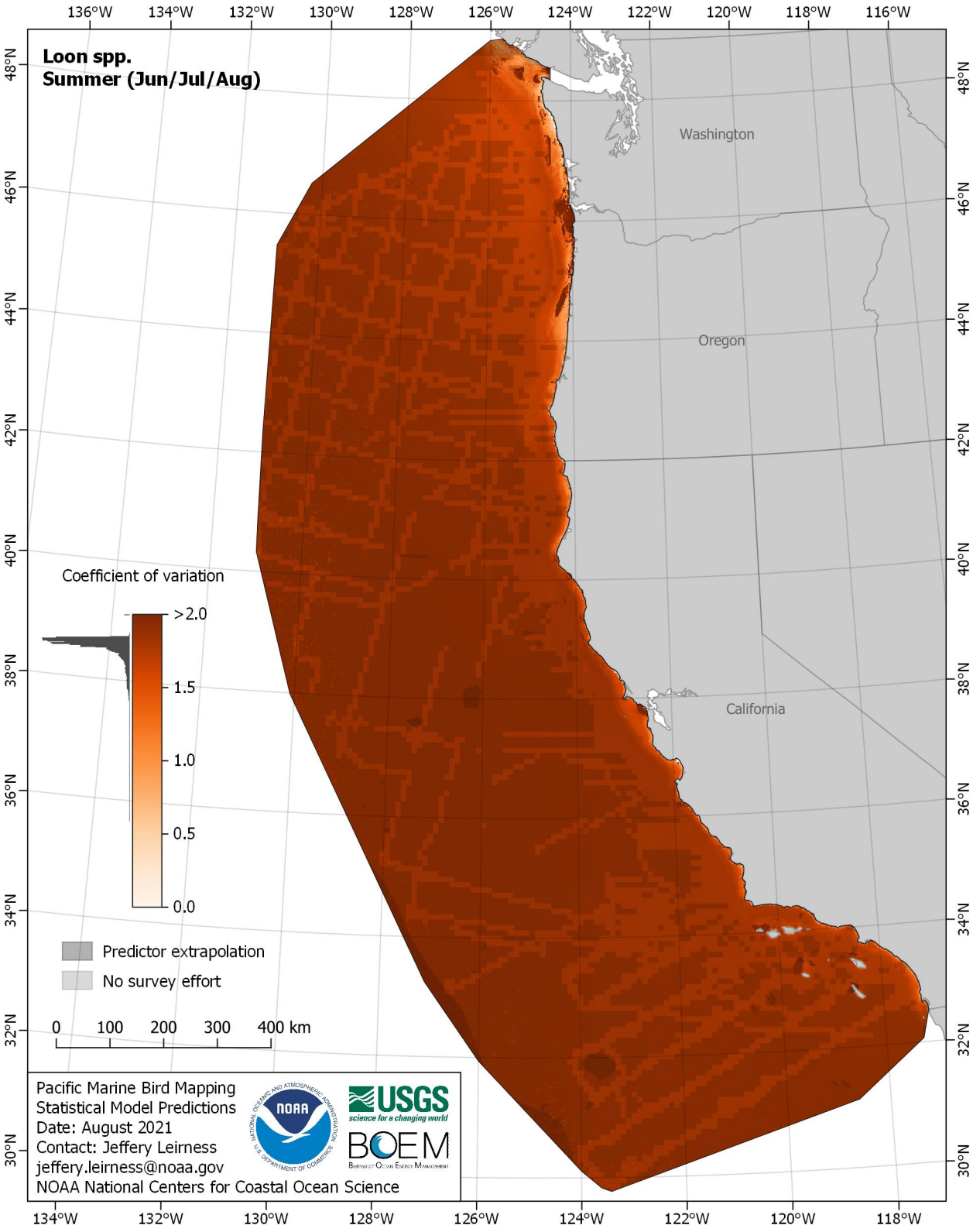

Figure E-162. Coefficient of variation for Loon spp. (*Gavia spp.*) in the summer season

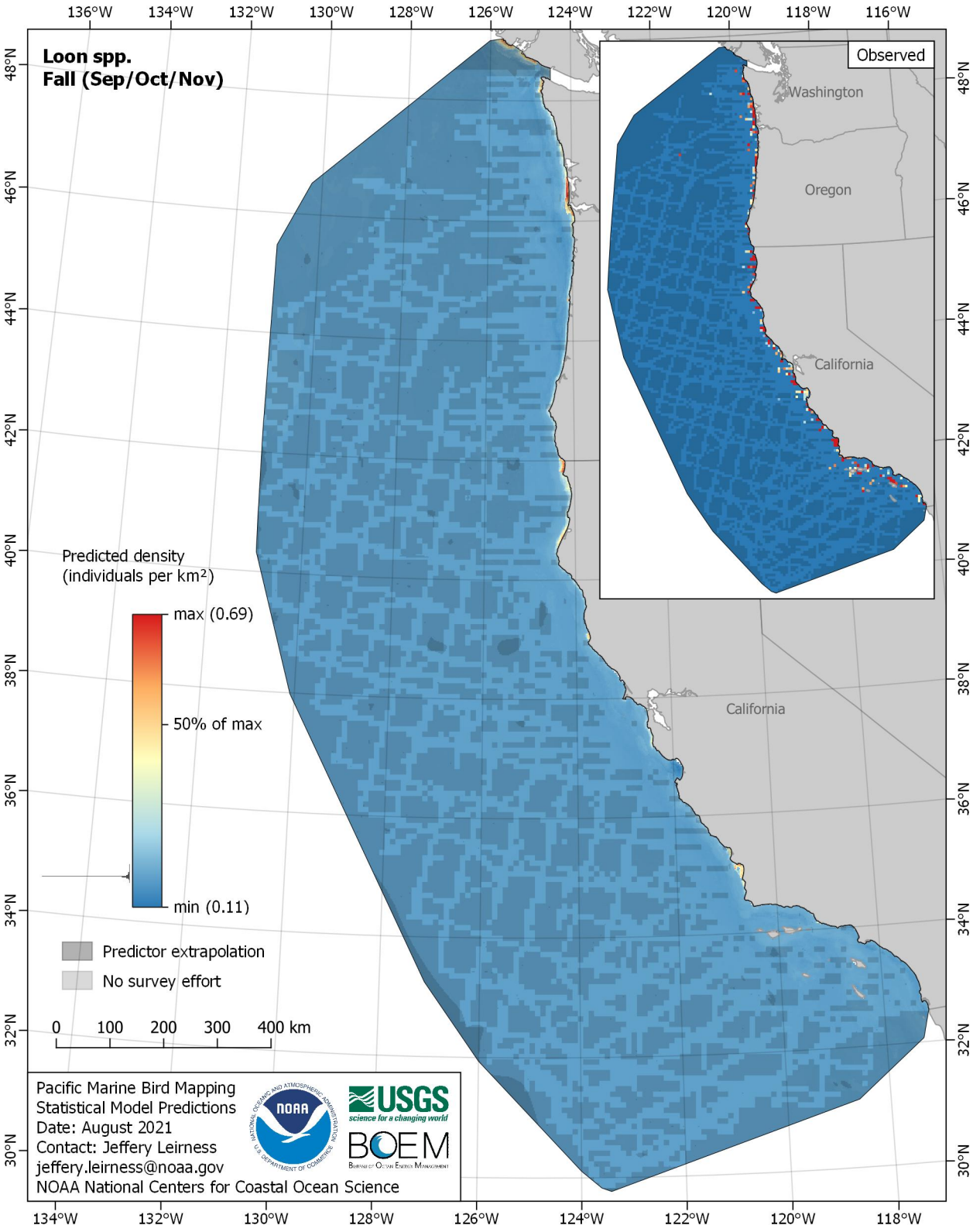

Figure E-163. Predicted density for Loon spp. (*Gavia spp.*) in the fall season

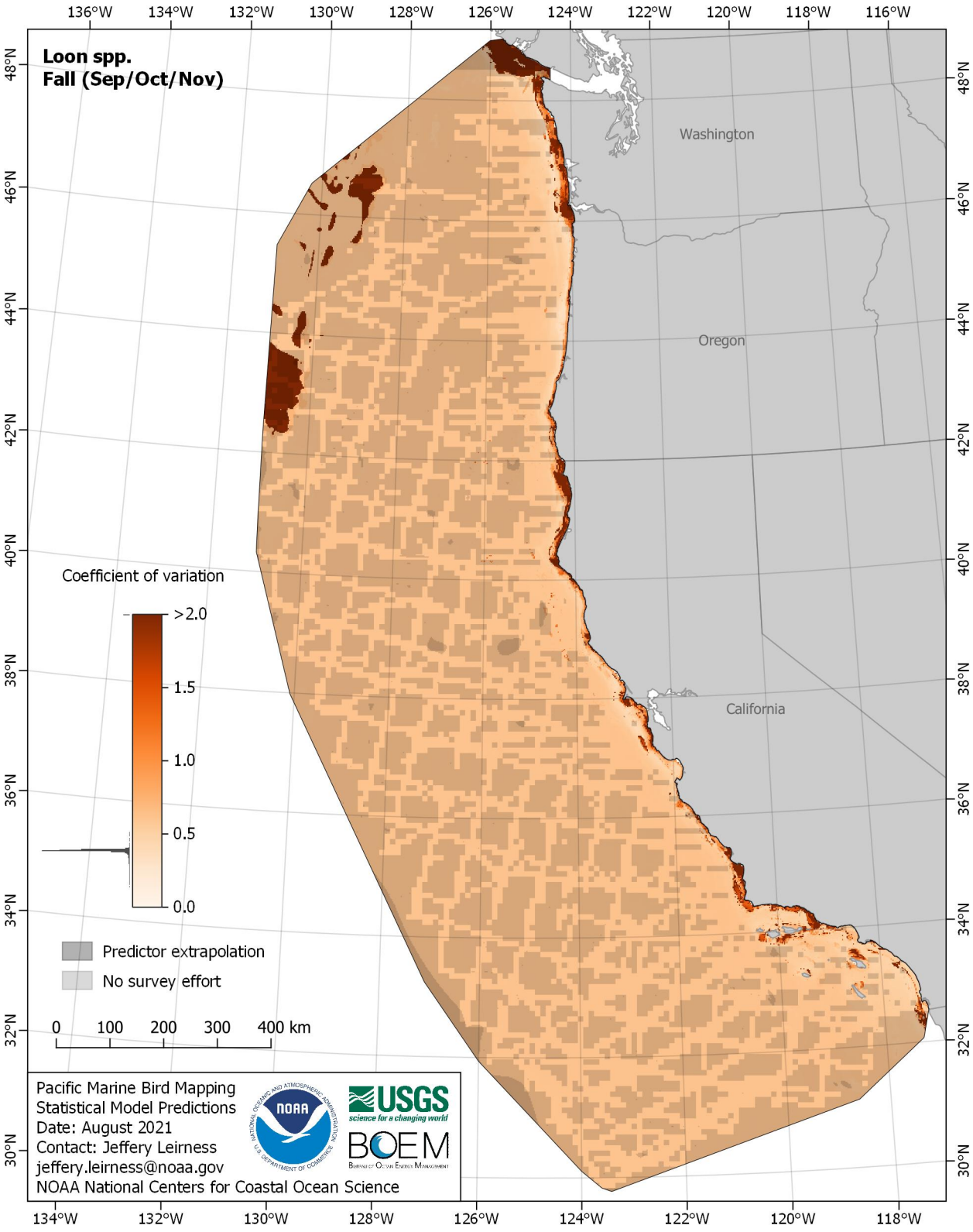

Figure E-164. Coefficient of variation for Loon spp. (*Gavia spp.*) in the fall season

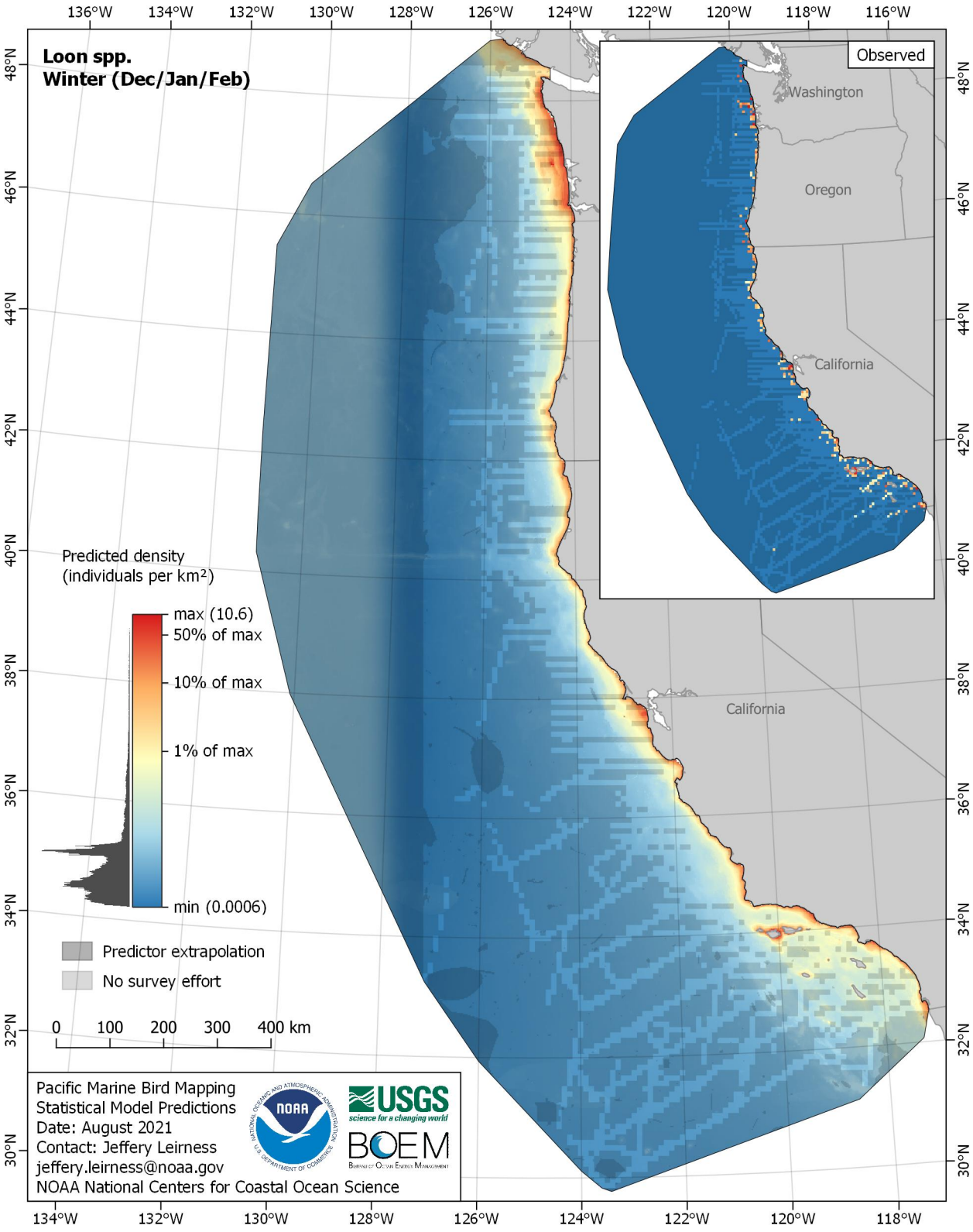

Figure E-165. Predicted density for Loon spp. (*Gavia spp.*) in the winter season

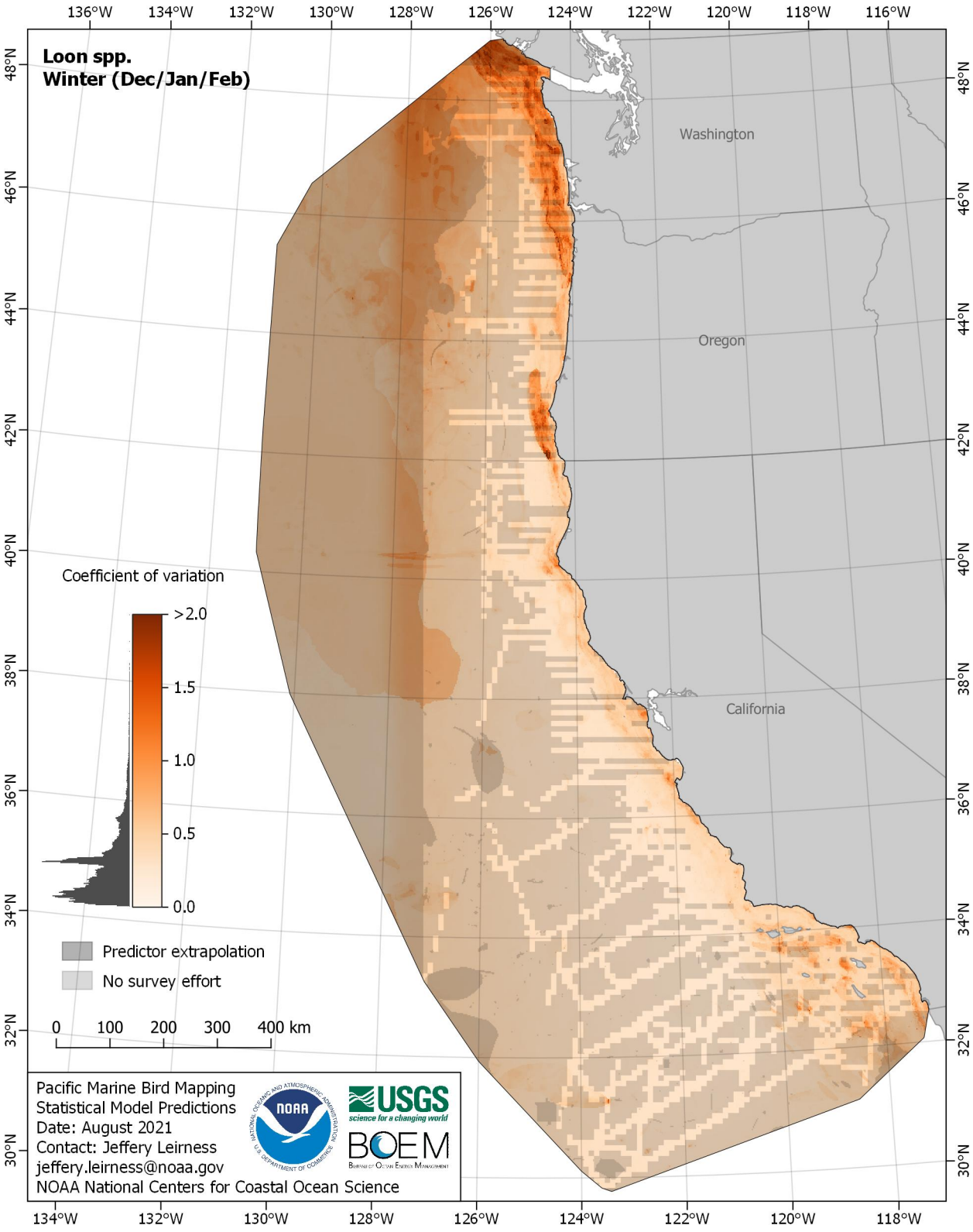

Figure E-166. Coefficient of variation for Loon spp. (*Gavia spp.*) in the winter season

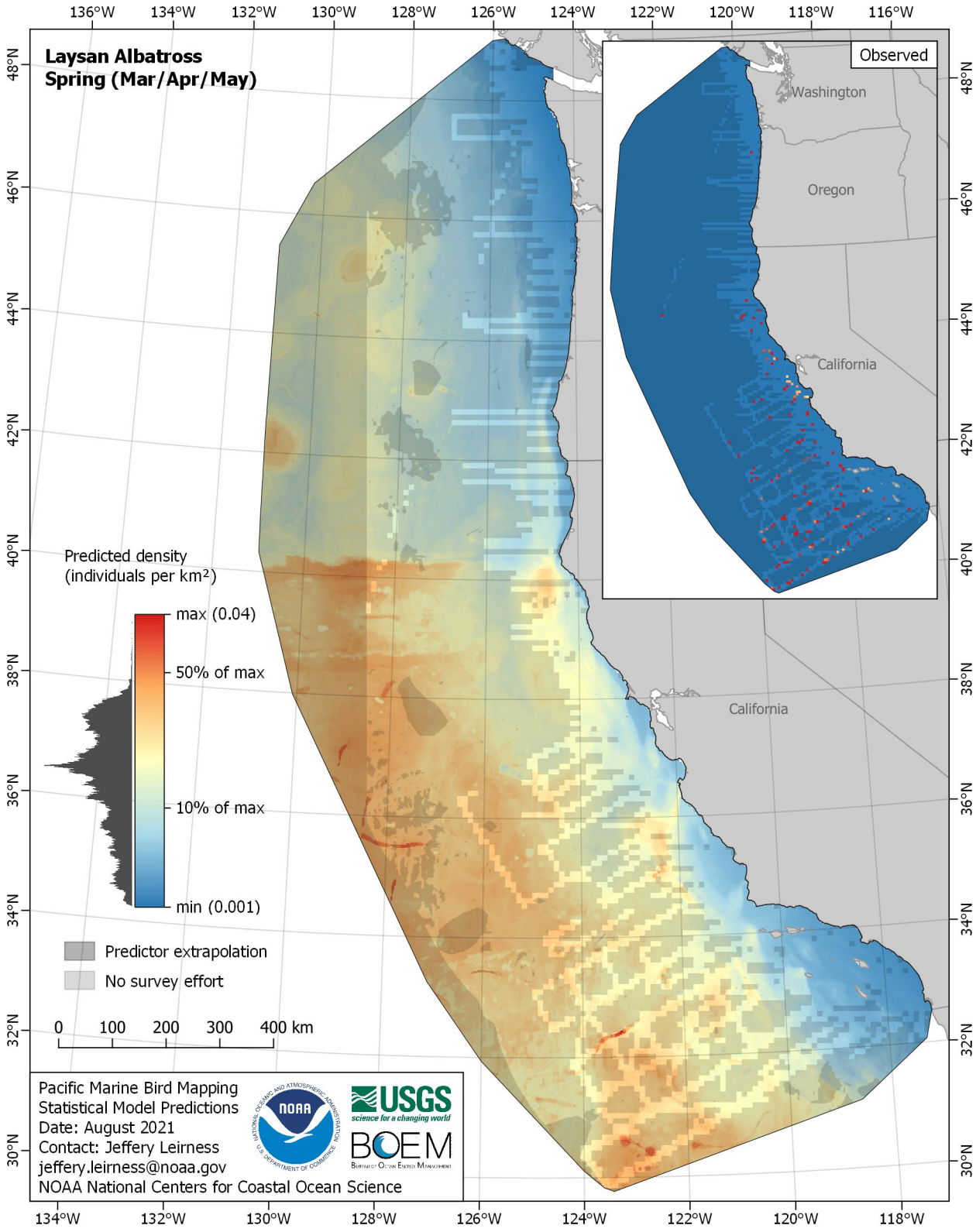

Figure E-167. Predicted density for Laysan Albatross (*Phoebastria immutabilis*) in the spring season

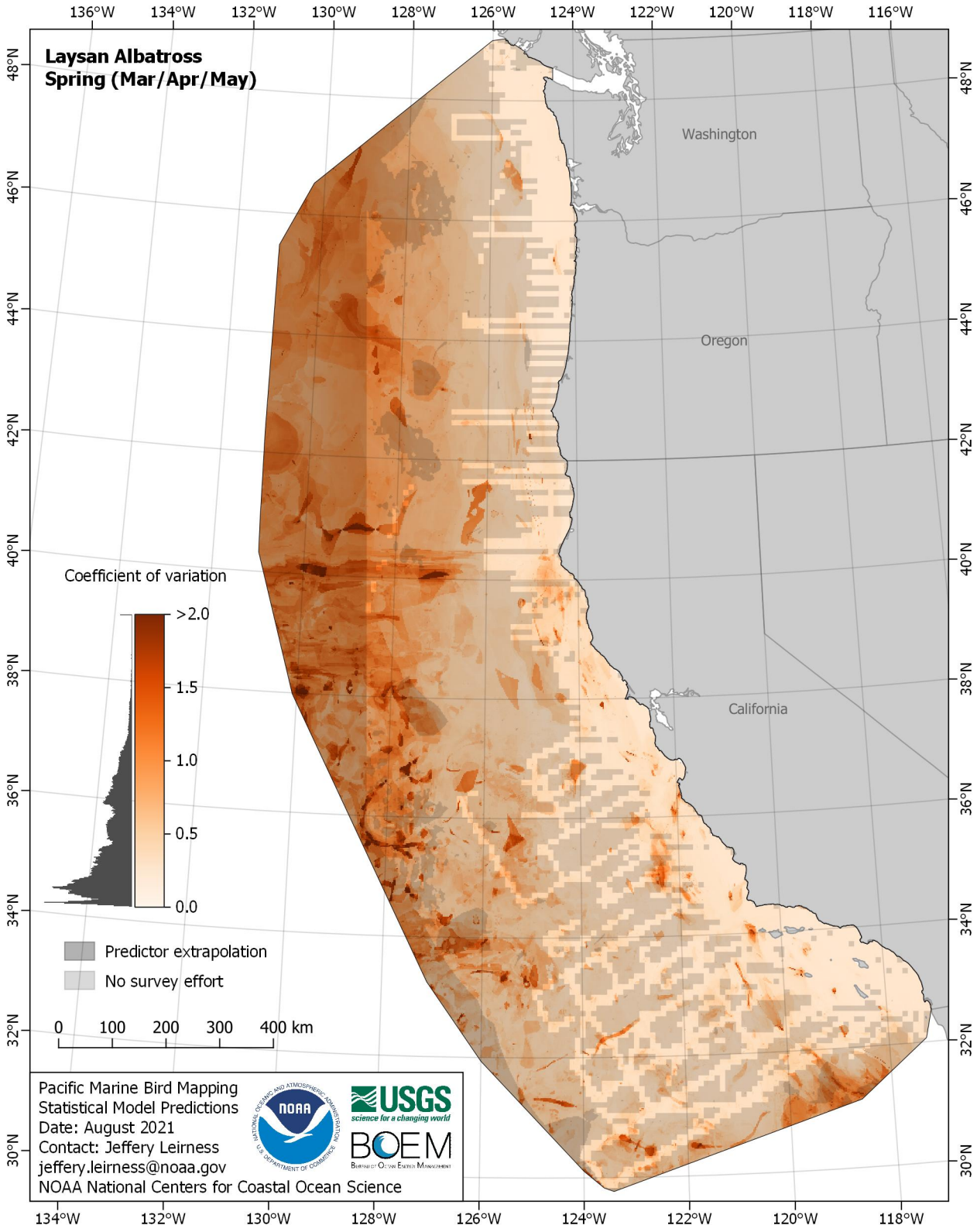

Figure E-168. Coefficient of variation for Laysan Albatross (*Phoebastria immutabilis*) in the spring season

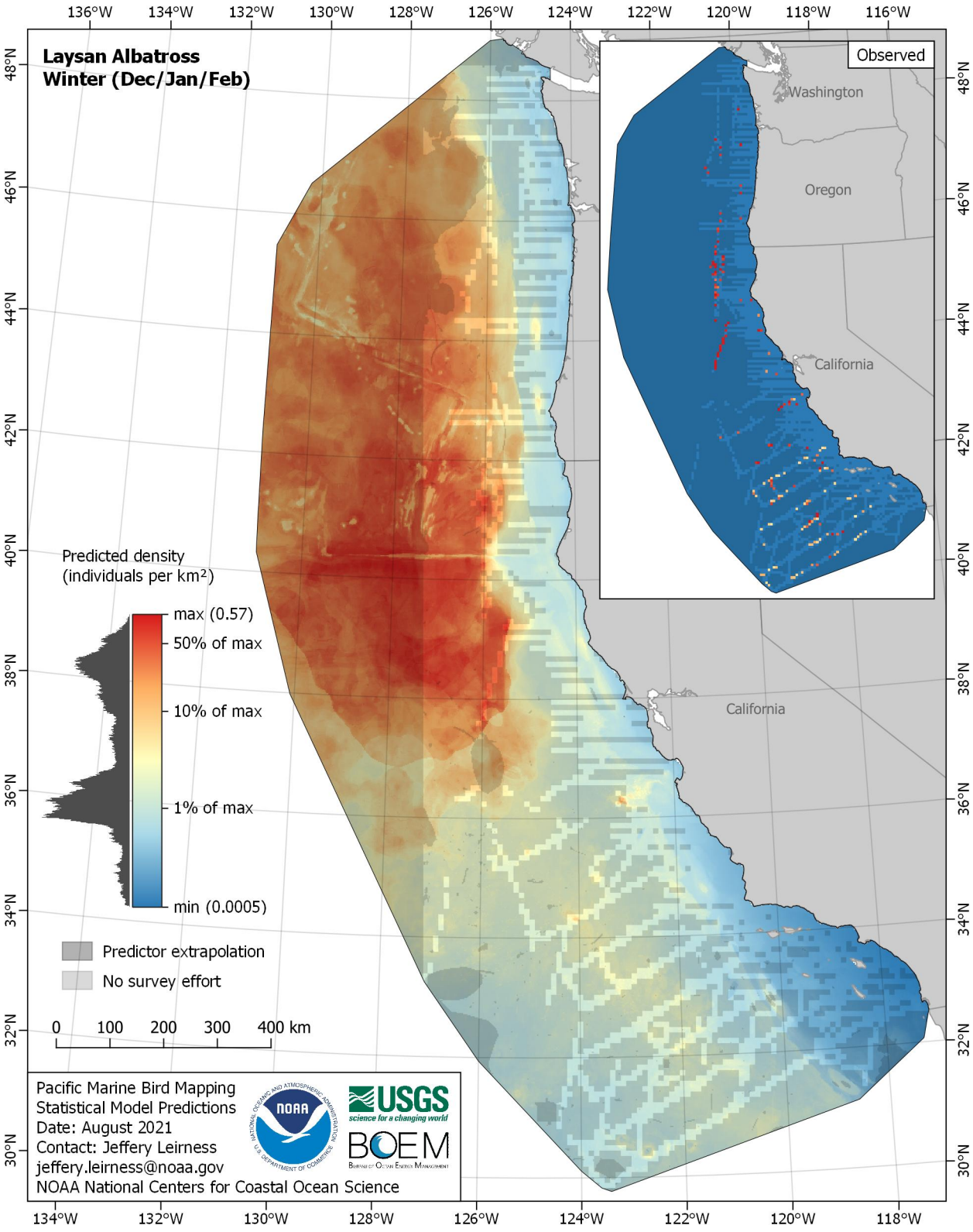

Figure E-169. Predicted density for Laysan Albatross (*Phoebastria immutabilis*) in the winter season

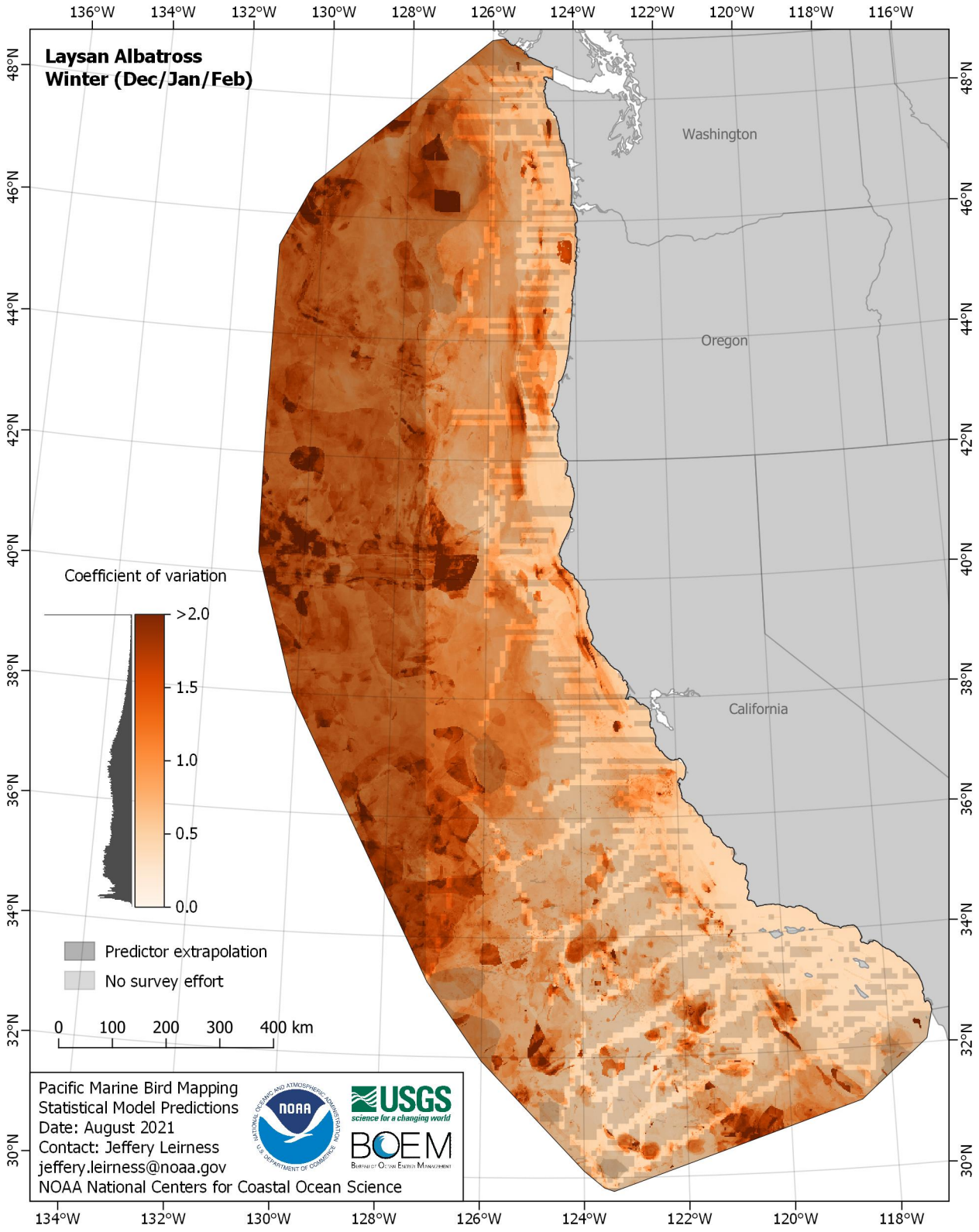

Figure E-170. Coefficient of variation for Laysan Albatross (*Phoebastria immutabilis*) in the winter season

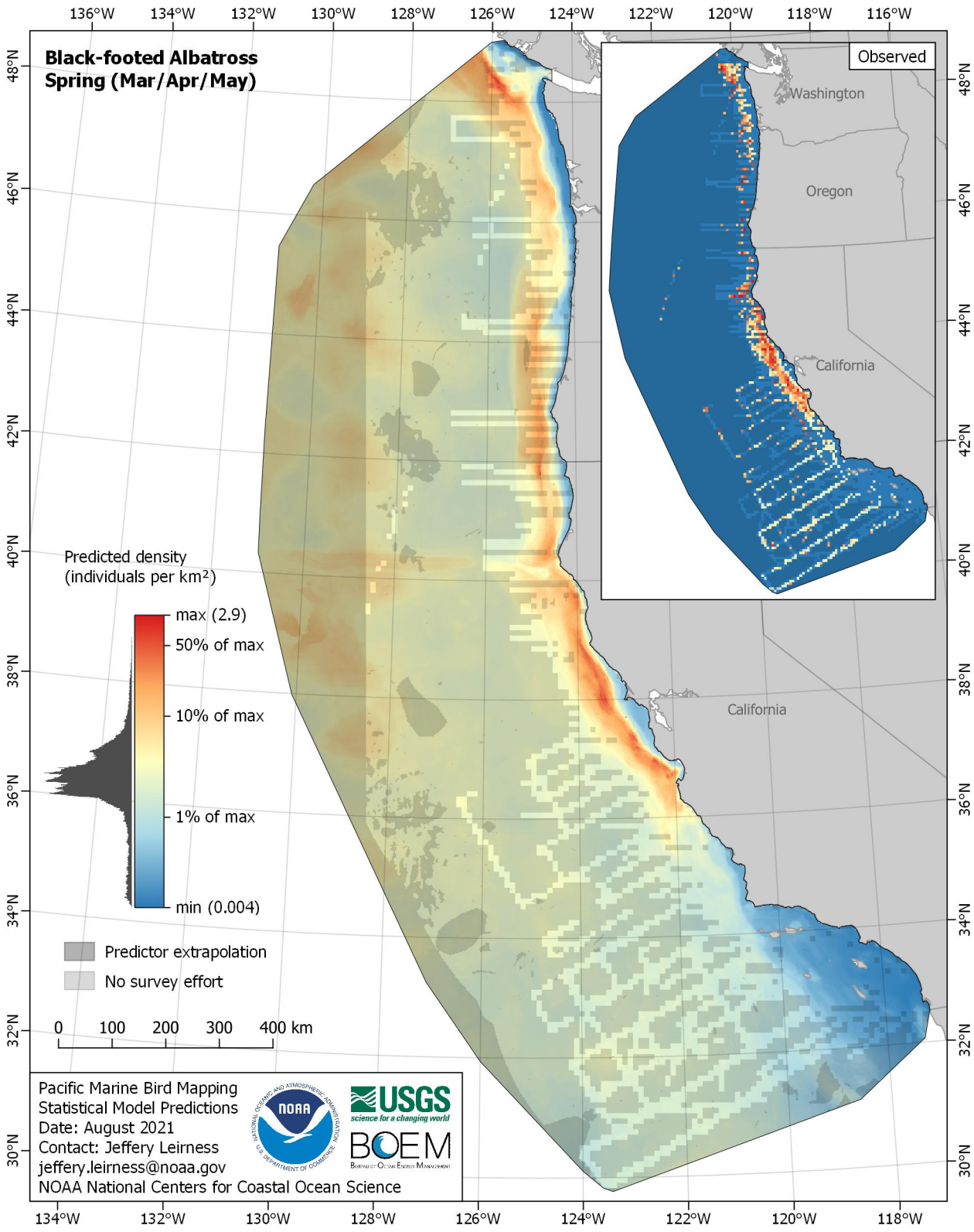

Figure E-171. Predicted density for Black-footed Albatross (*Phoebastria nigripes*) in the spring season

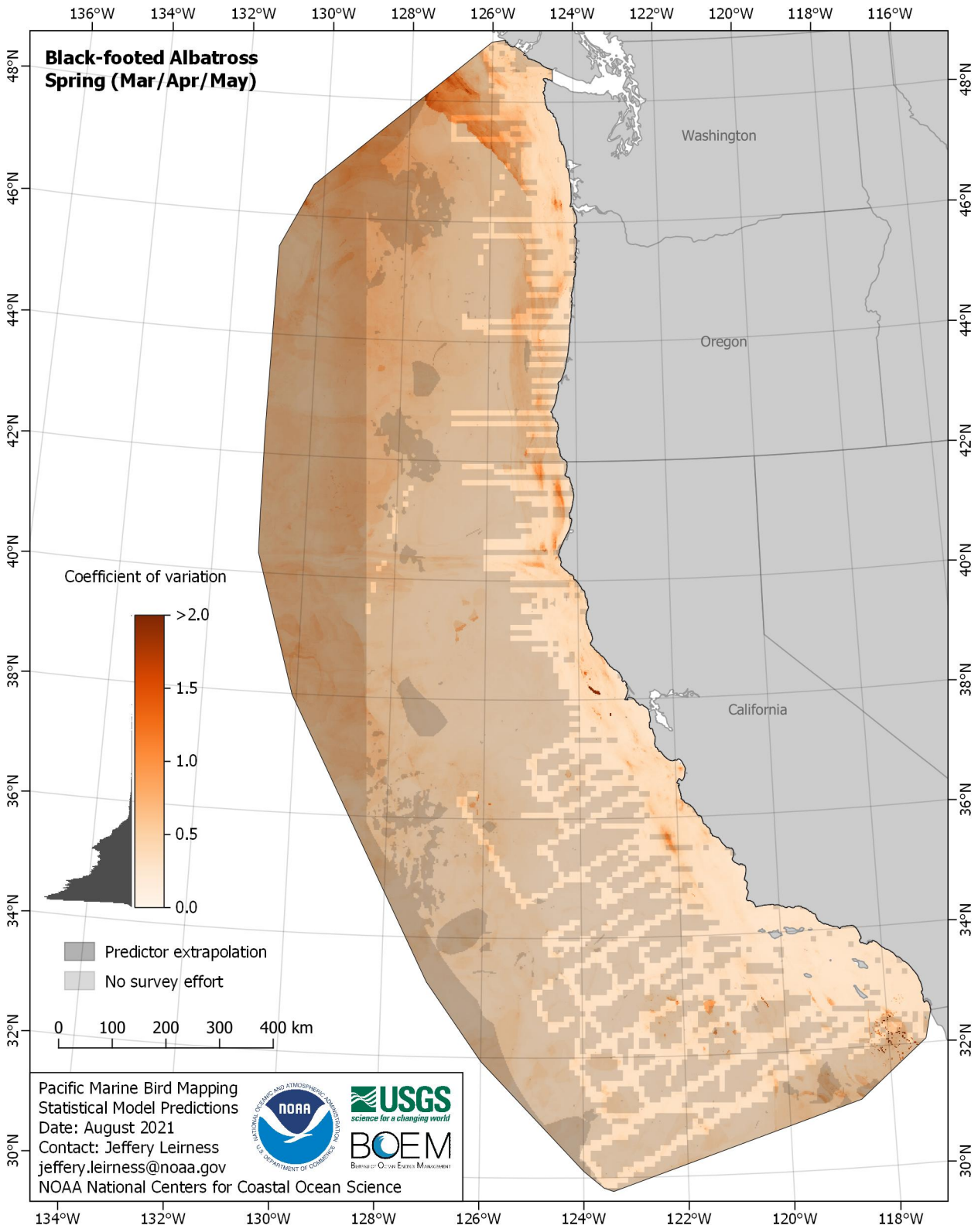

Figure E-172. Coefficient of variation for Black-footed Albatross (*Phoebastria nigripes*) in the spring season

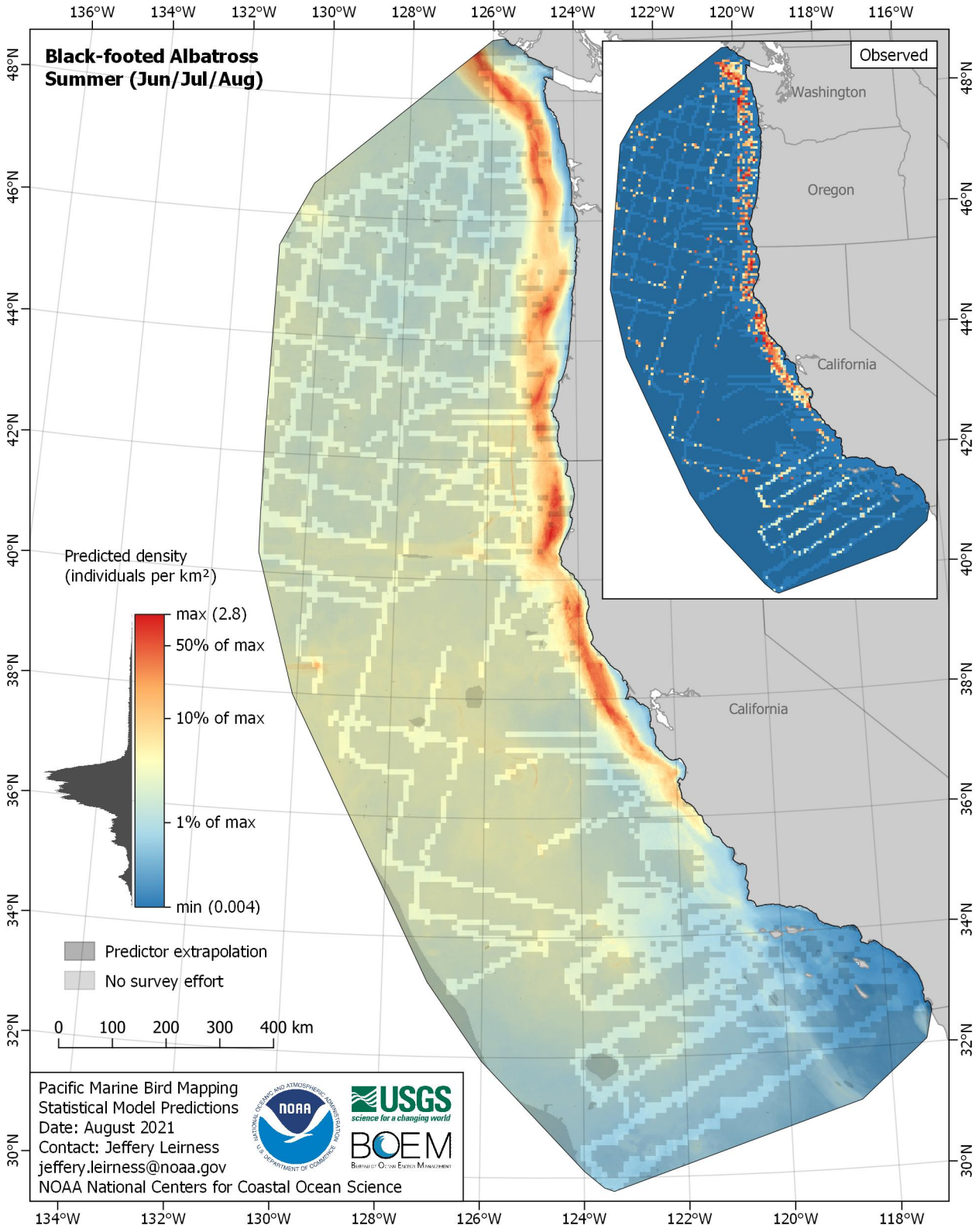

Figure E-173. Predicted density for Black-footed Albatross (*Phoebastria nigripes*) in the summer season

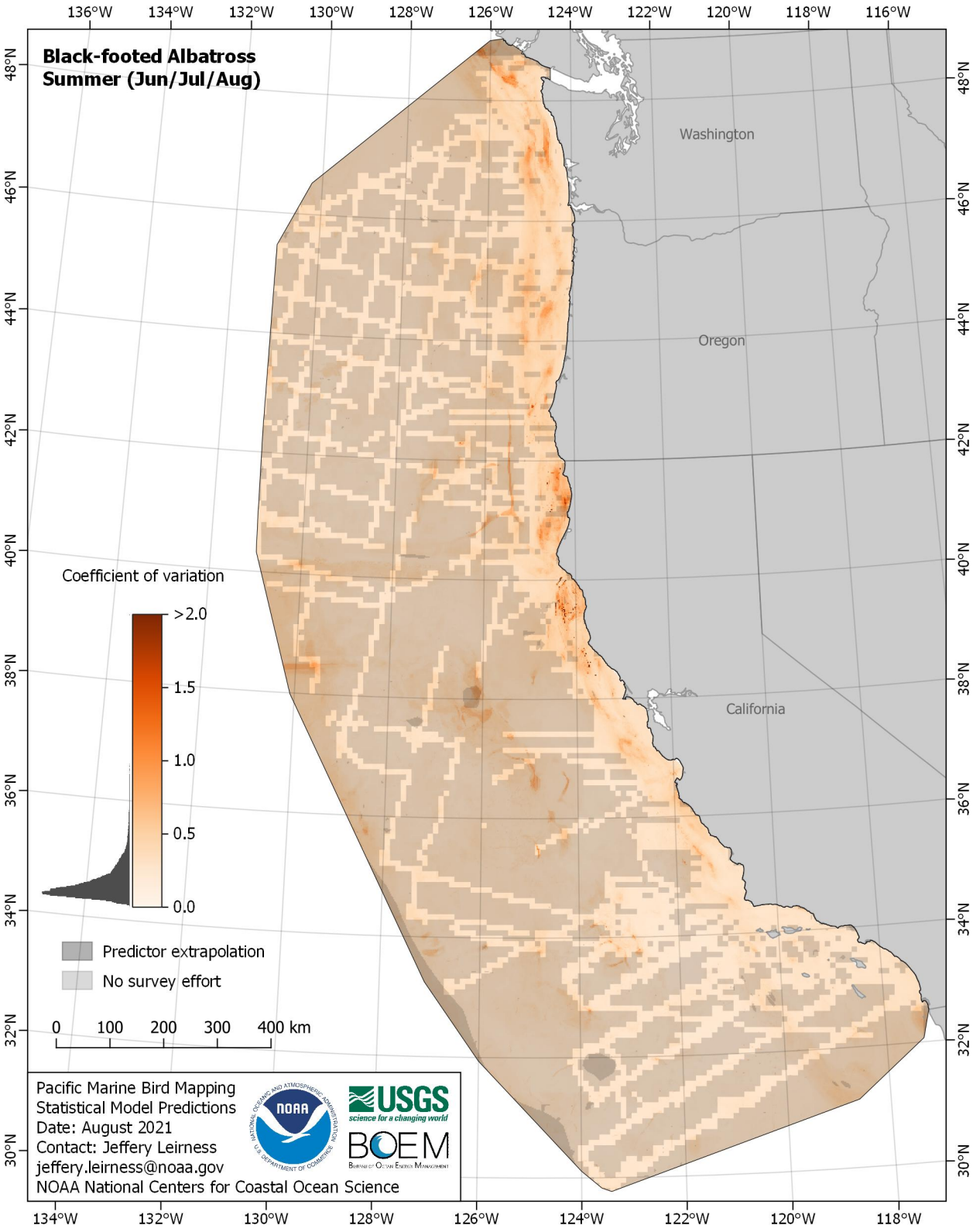

Figure E-174. Coefficient of variation for Black-footed Albatross (*Phoebastria nigripes*) in the summer season

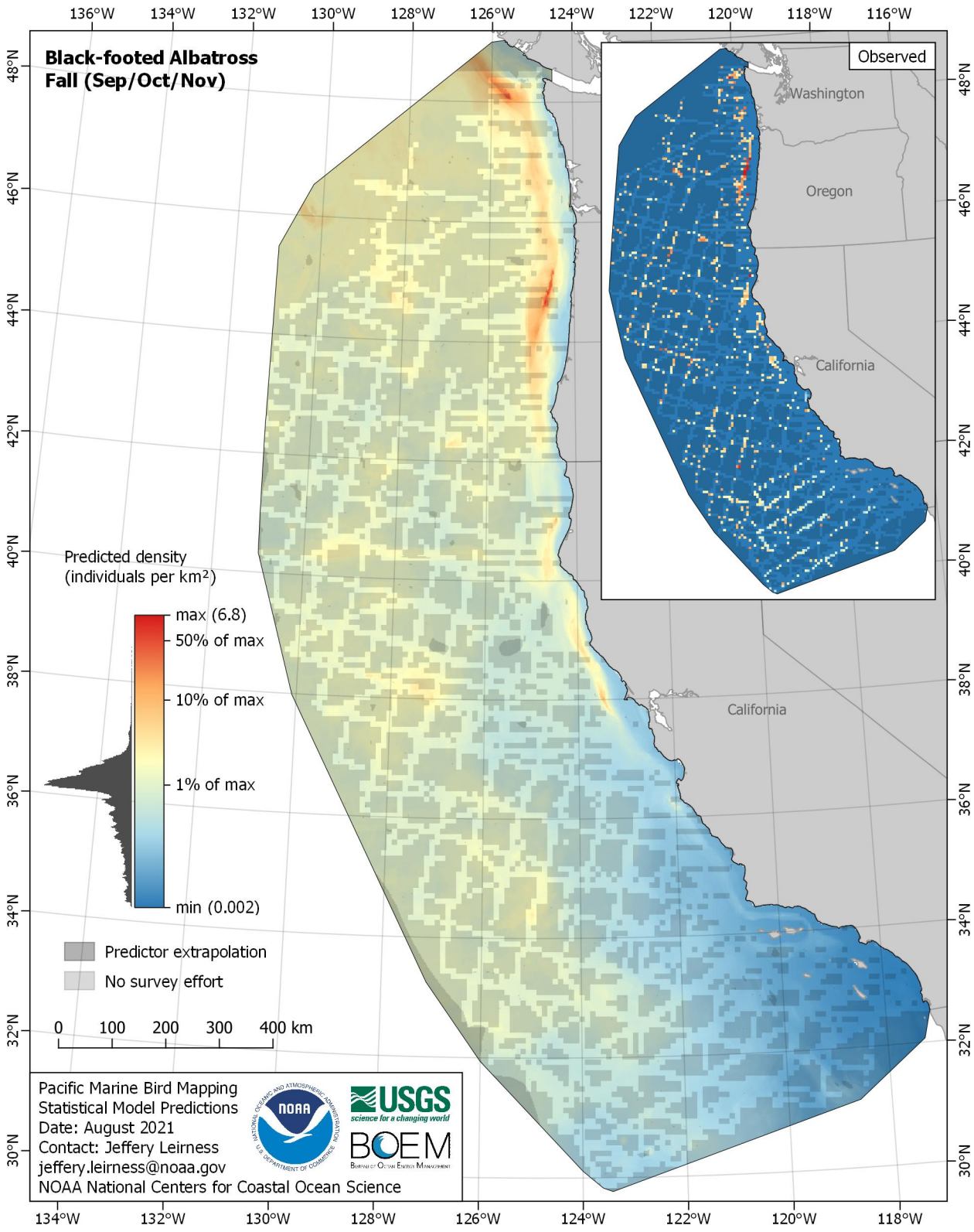

Figure E-175. Predicted density for Black-footed Albatross (*Phoebastria nigripes*) in the fall season

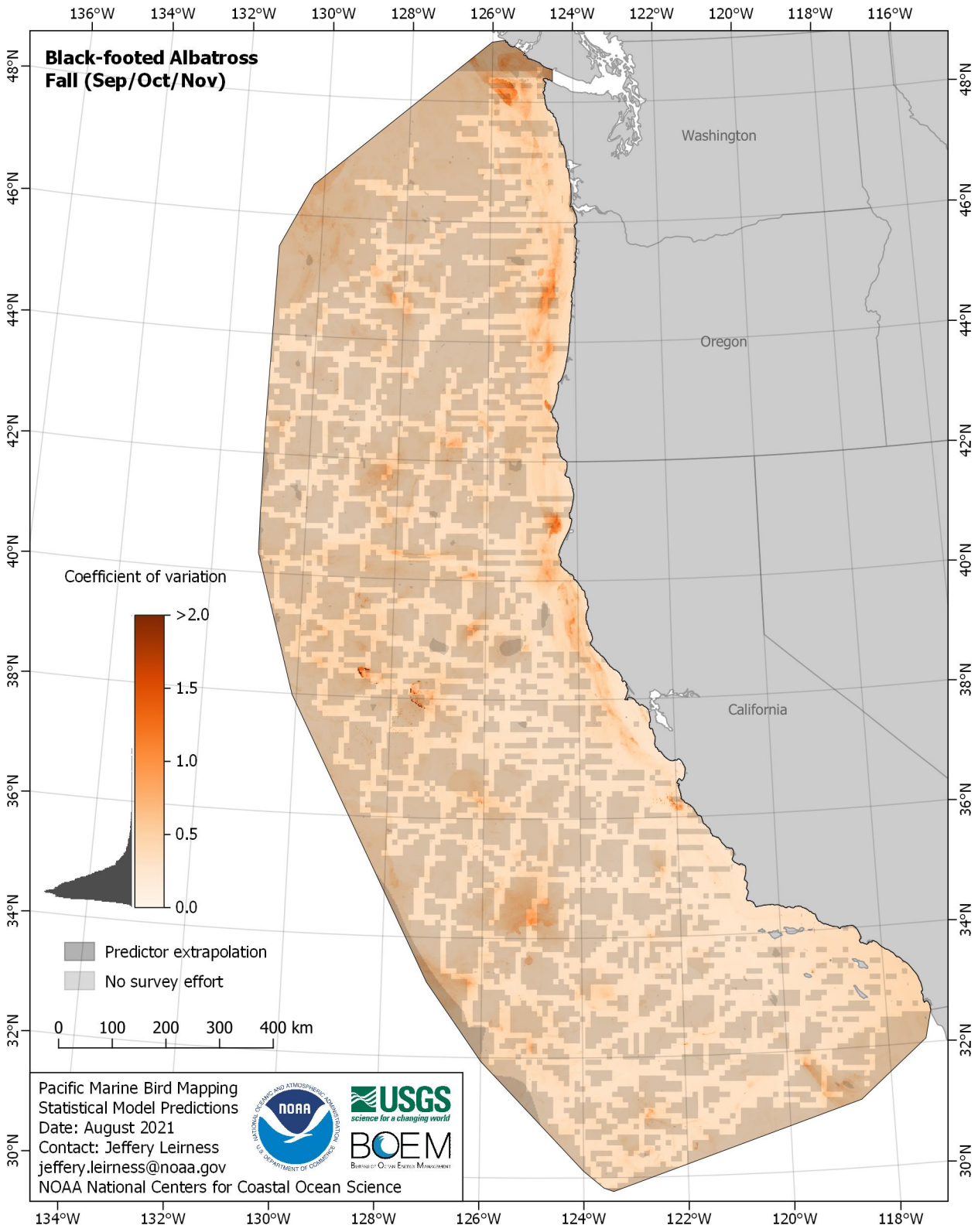

Figure E-176. Coefficient of variation for Black-footed Albatross (*Phoebastria nigripes*) in the fall season

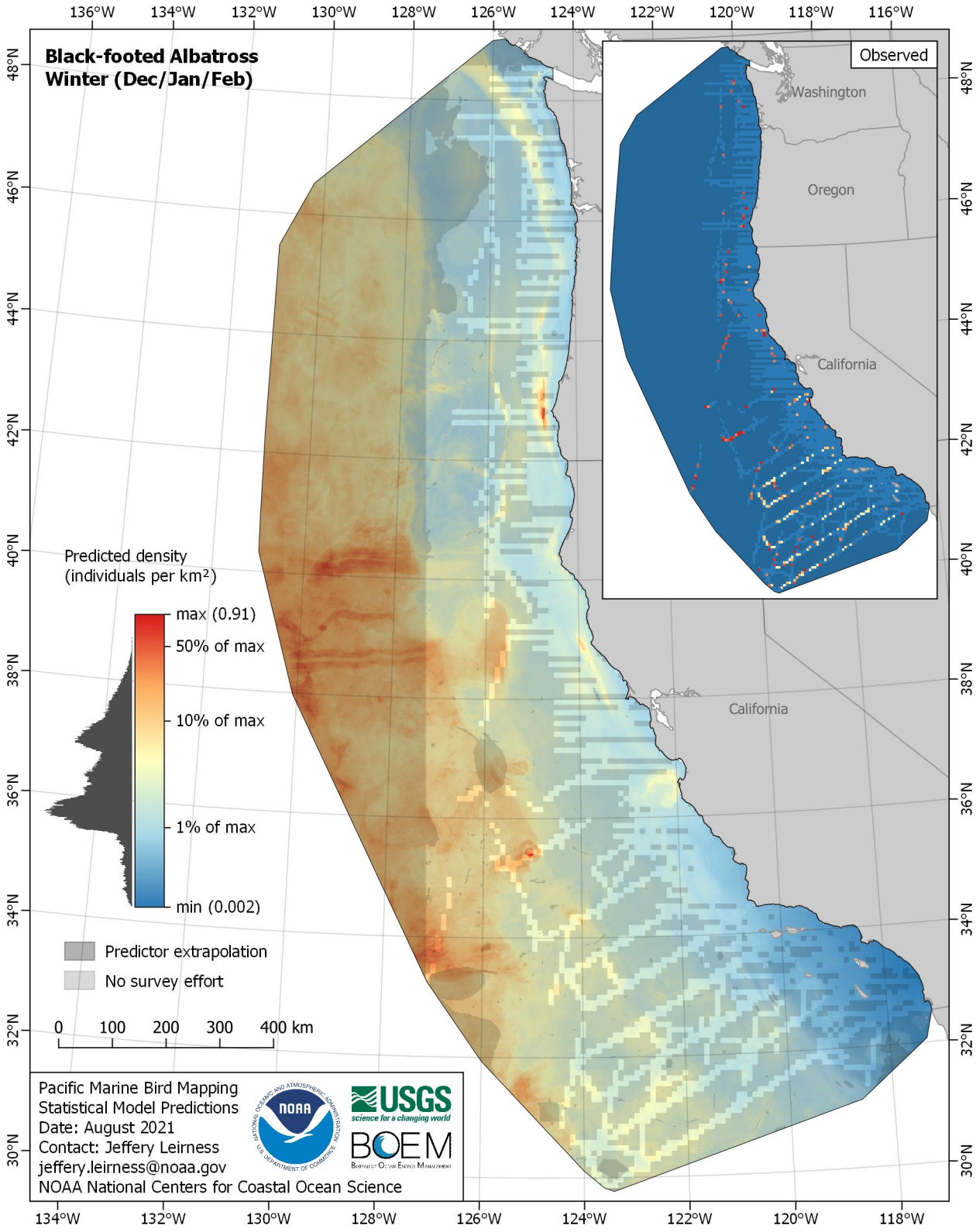

Figure E-177. Predicted density for Black-footed Albatross (*Phoebastria nigripes*) in the winter season

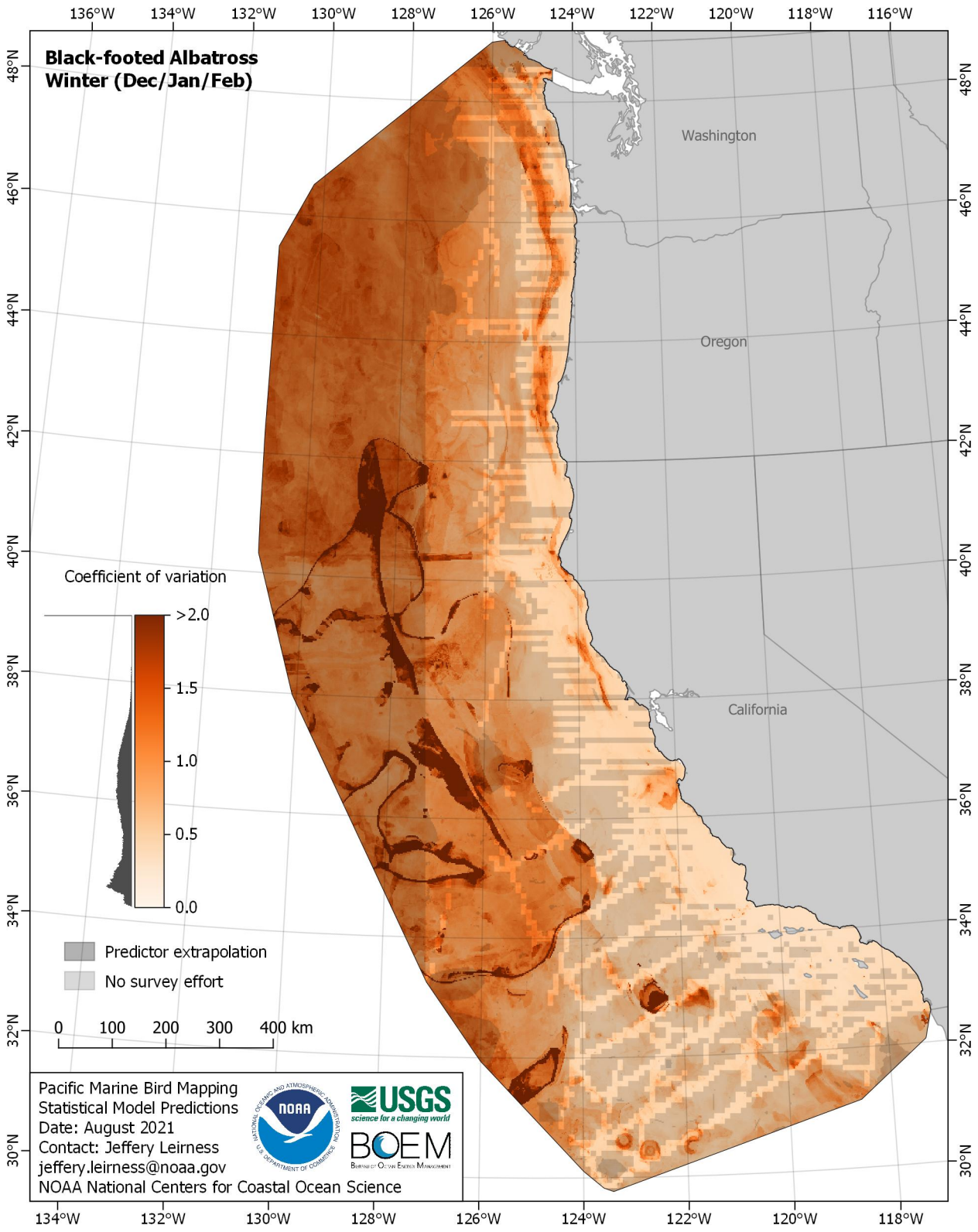

Figure E-178. Coefficient of variation for Black-footed Albatross (*Phoebastria nigripes*) in the winter season

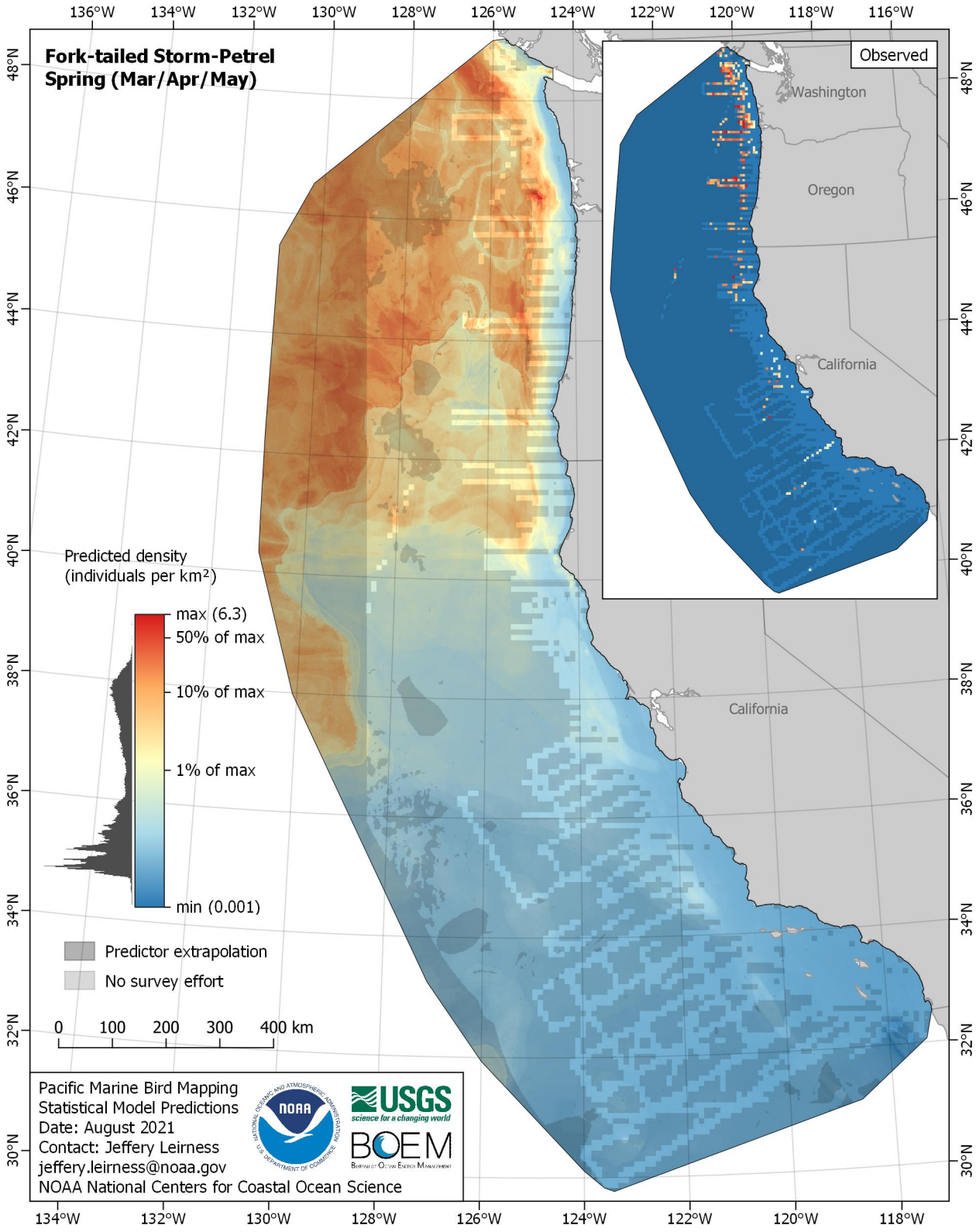

Figure E-179. Predicted density for Fork-tailed Storm-Petrel (*Hydrobates furcatus*) in the spring season

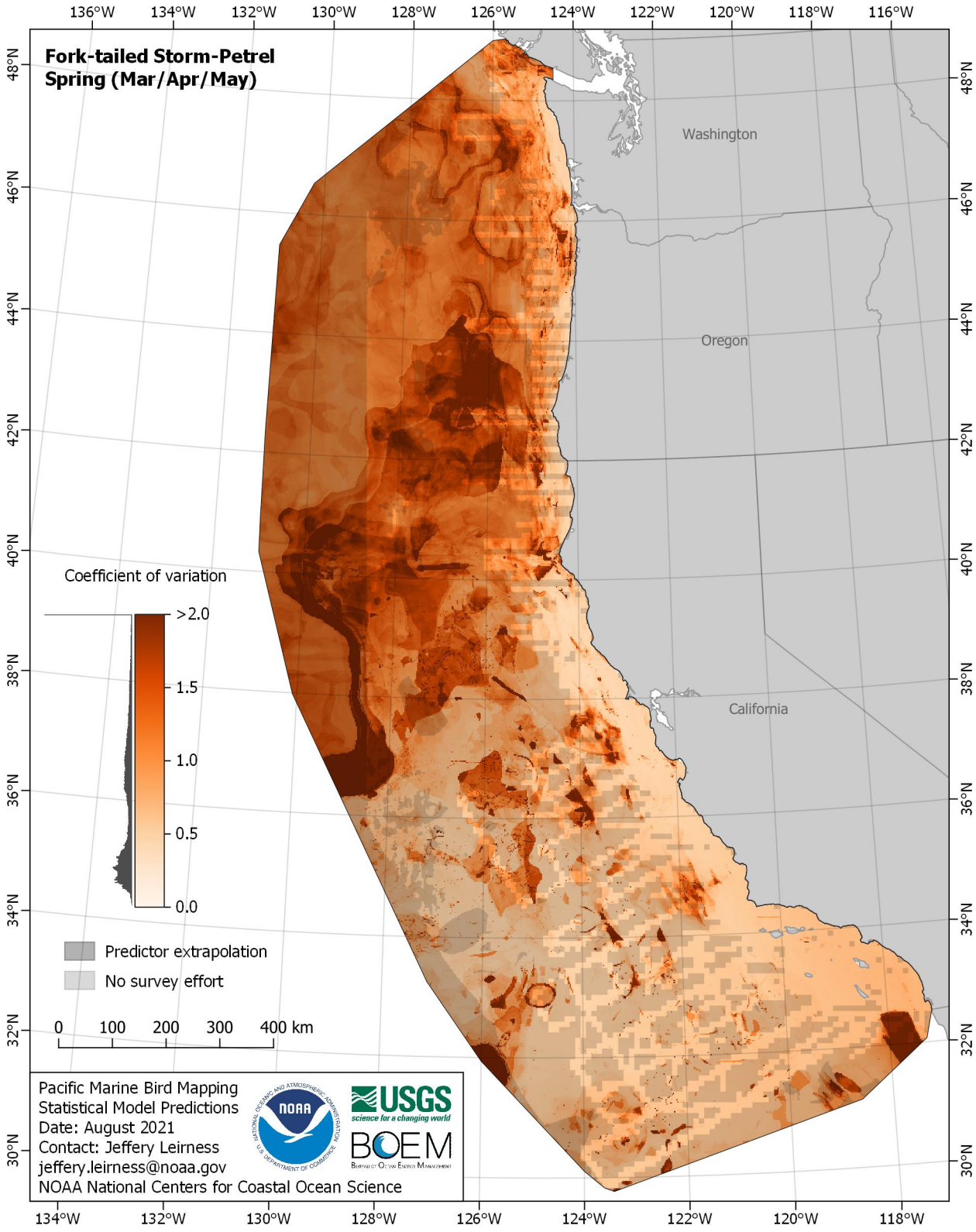

Figure E-180. Coefficient of variation for Fork-tailed Storm-Petrel (*Hydrobates furcatus*) in the spring season

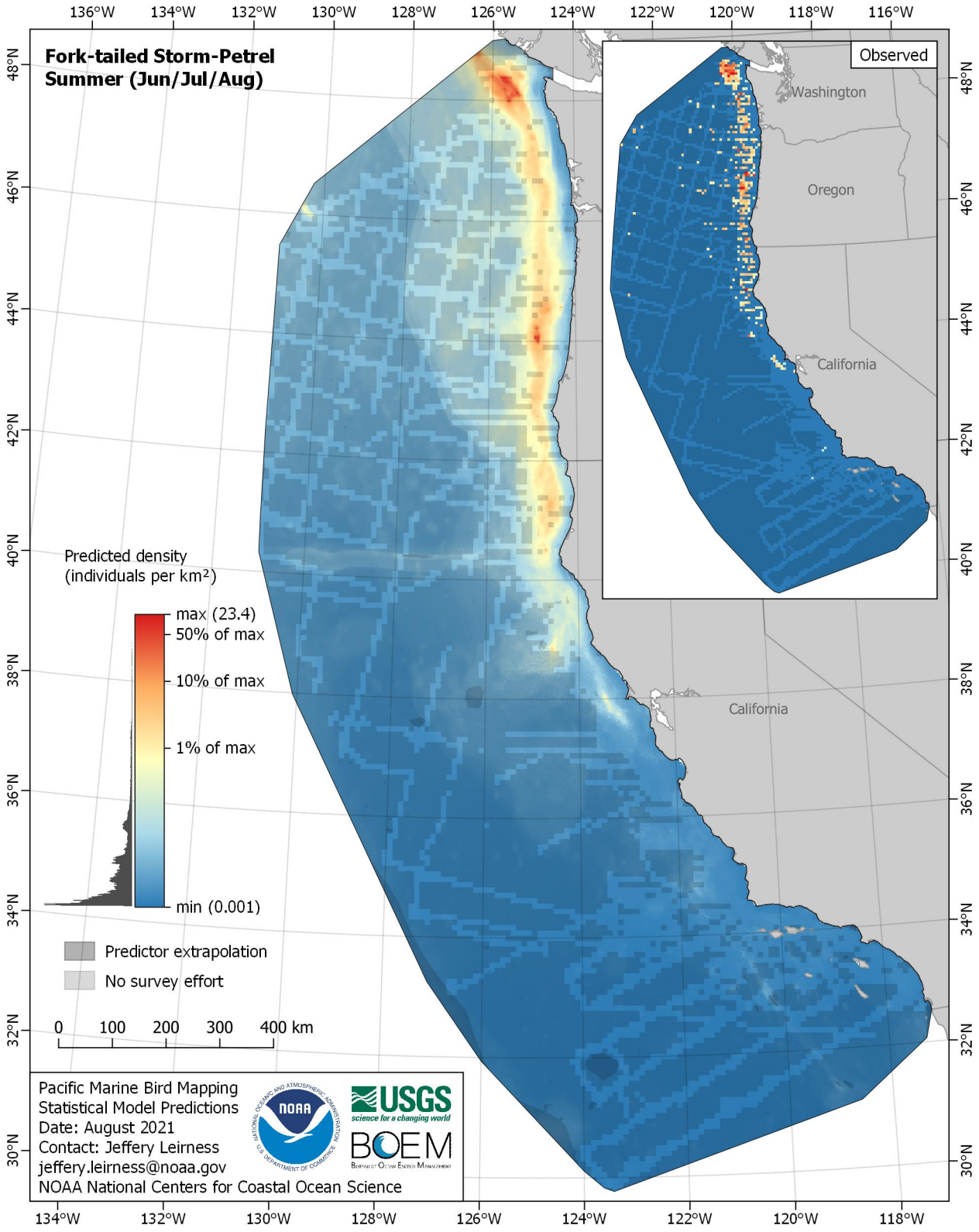

Figure E-181. Predicted density for Fork-tailed Storm-Petrel (*Hydrobates furcatus*) in the summer season

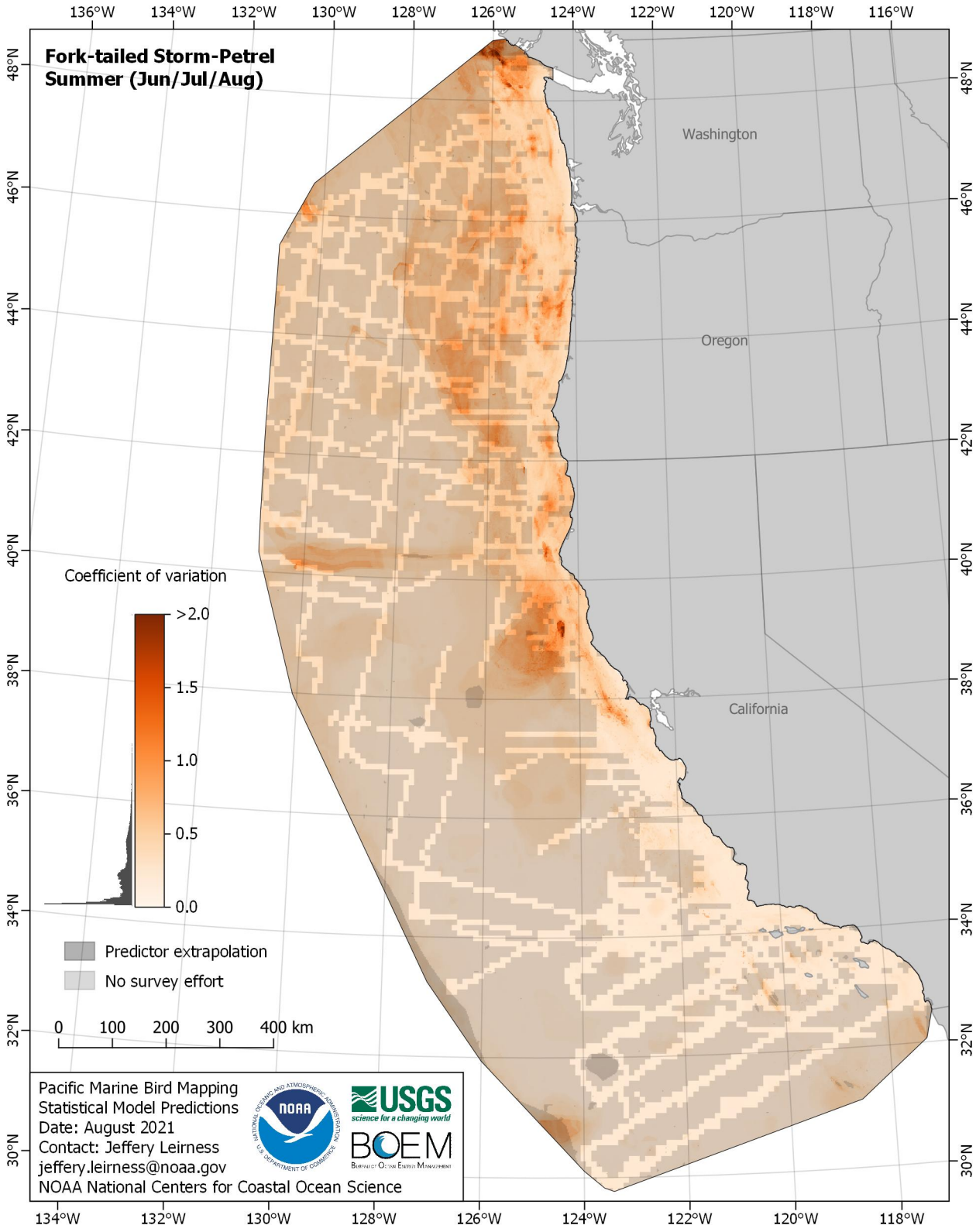

Figure E-182. Coefficient of variation for Fork-tailed Storm-Petrel (*Hydrobates furcatus*) in the summer season

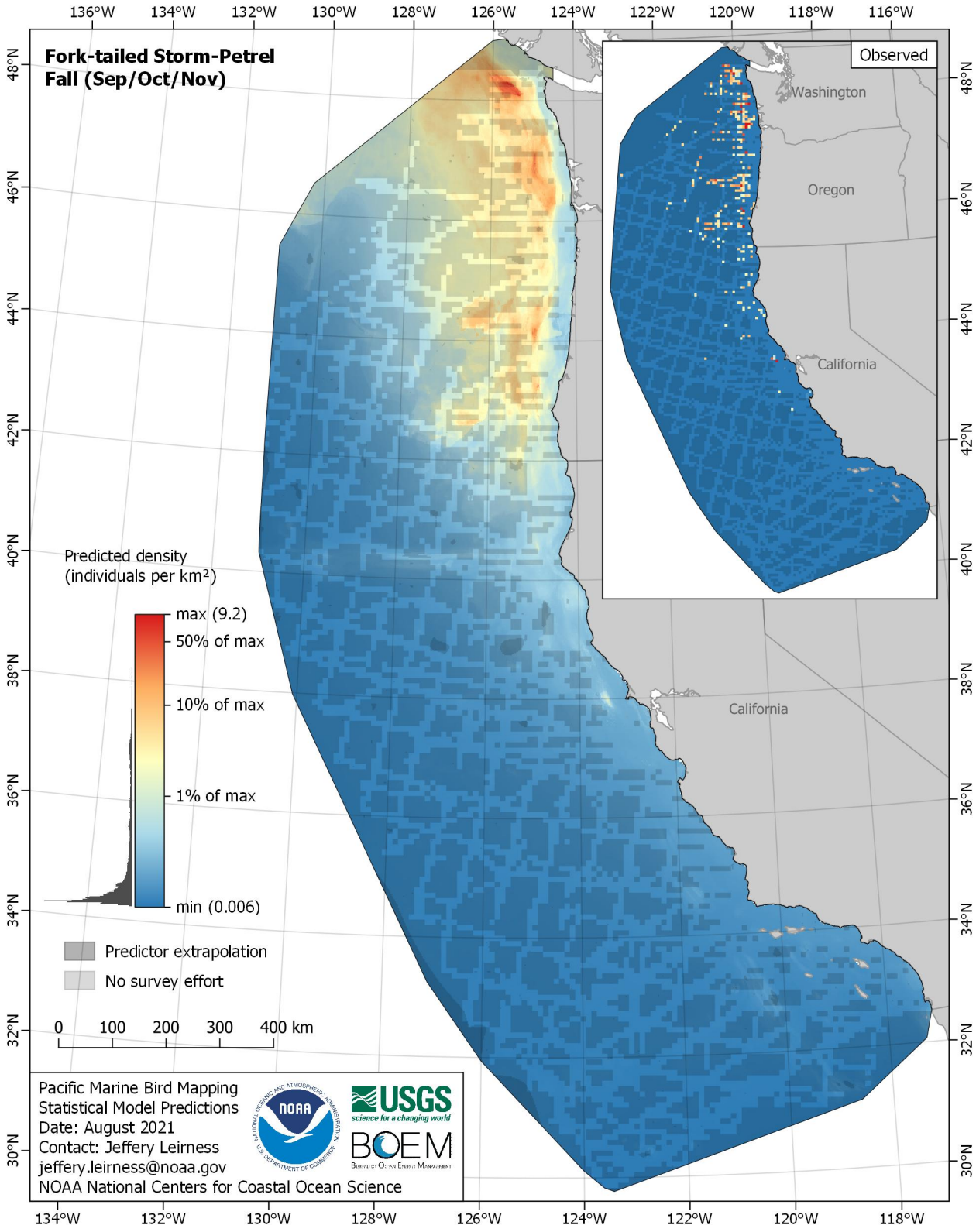

Figure E-183. Predicted density for Fork-tailed Storm-Petrel (*Hydrobates furcatus*) in the fall season

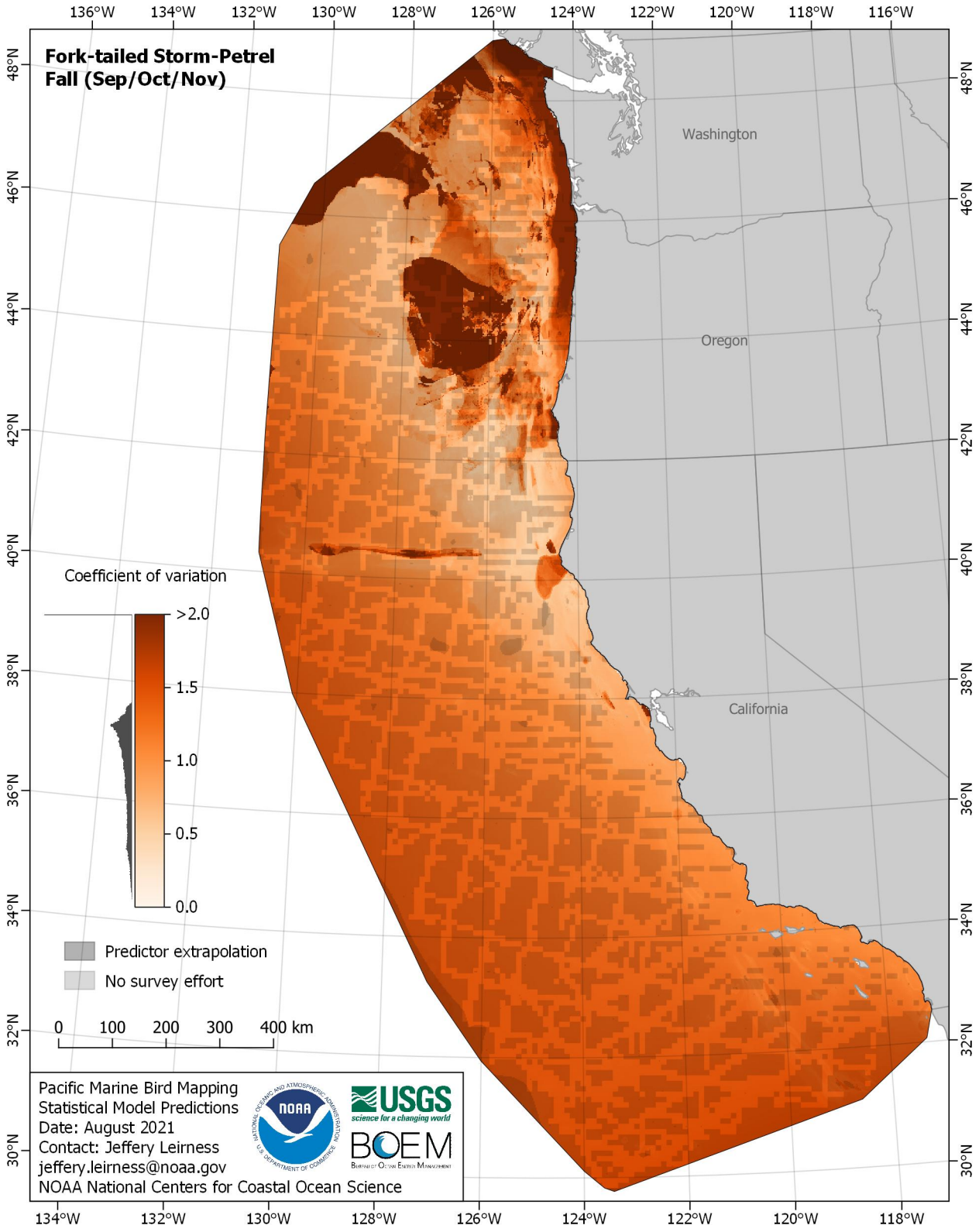

Figure E-184. Coefficient of variation for Fork-tailed Storm-Petrel (*Hydrobates furcatus*) in the fall season

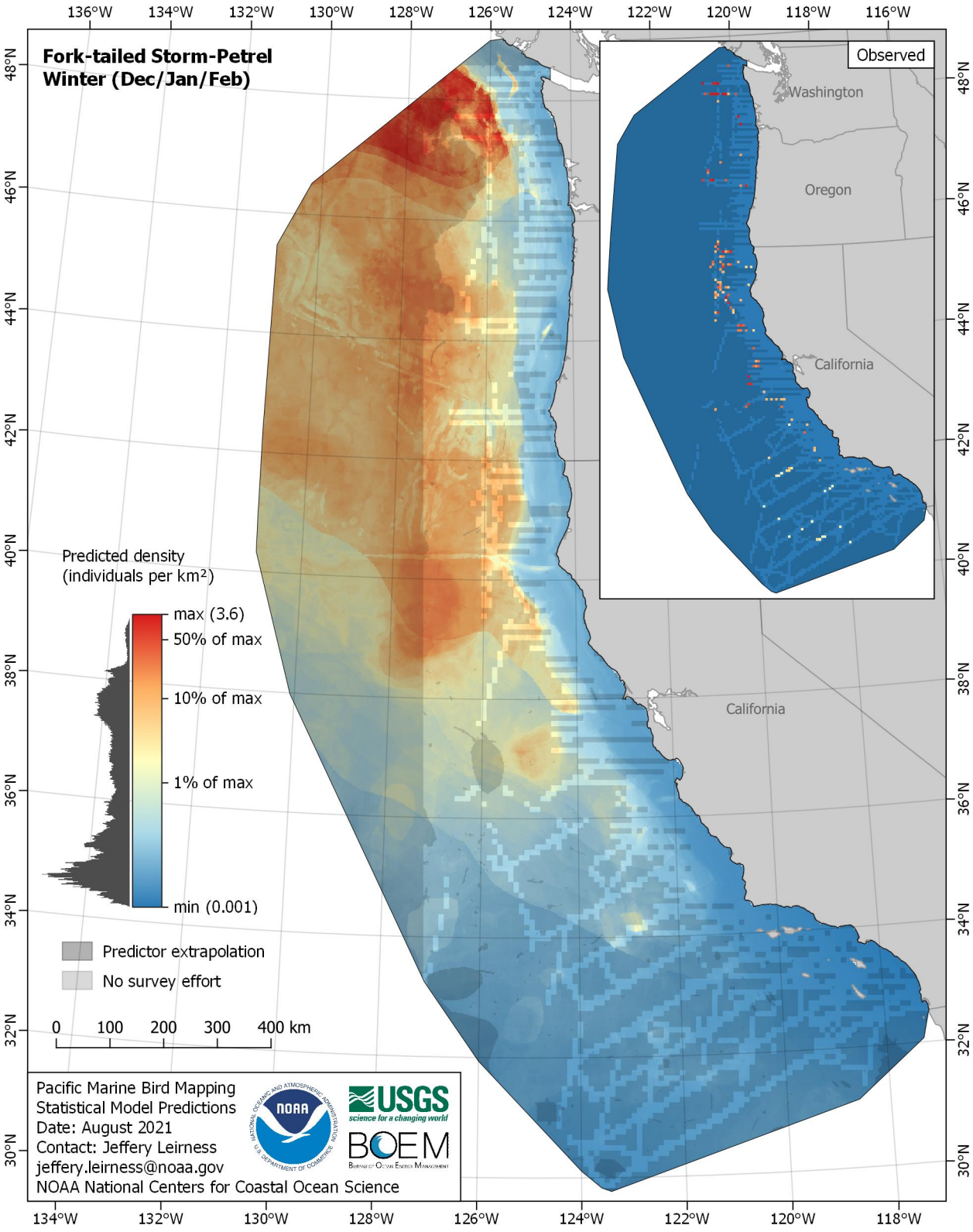

Figure E-185. Predicted density for Fork-tailed Storm-Petrel (*Hydrobates furcatus*) in the winter season

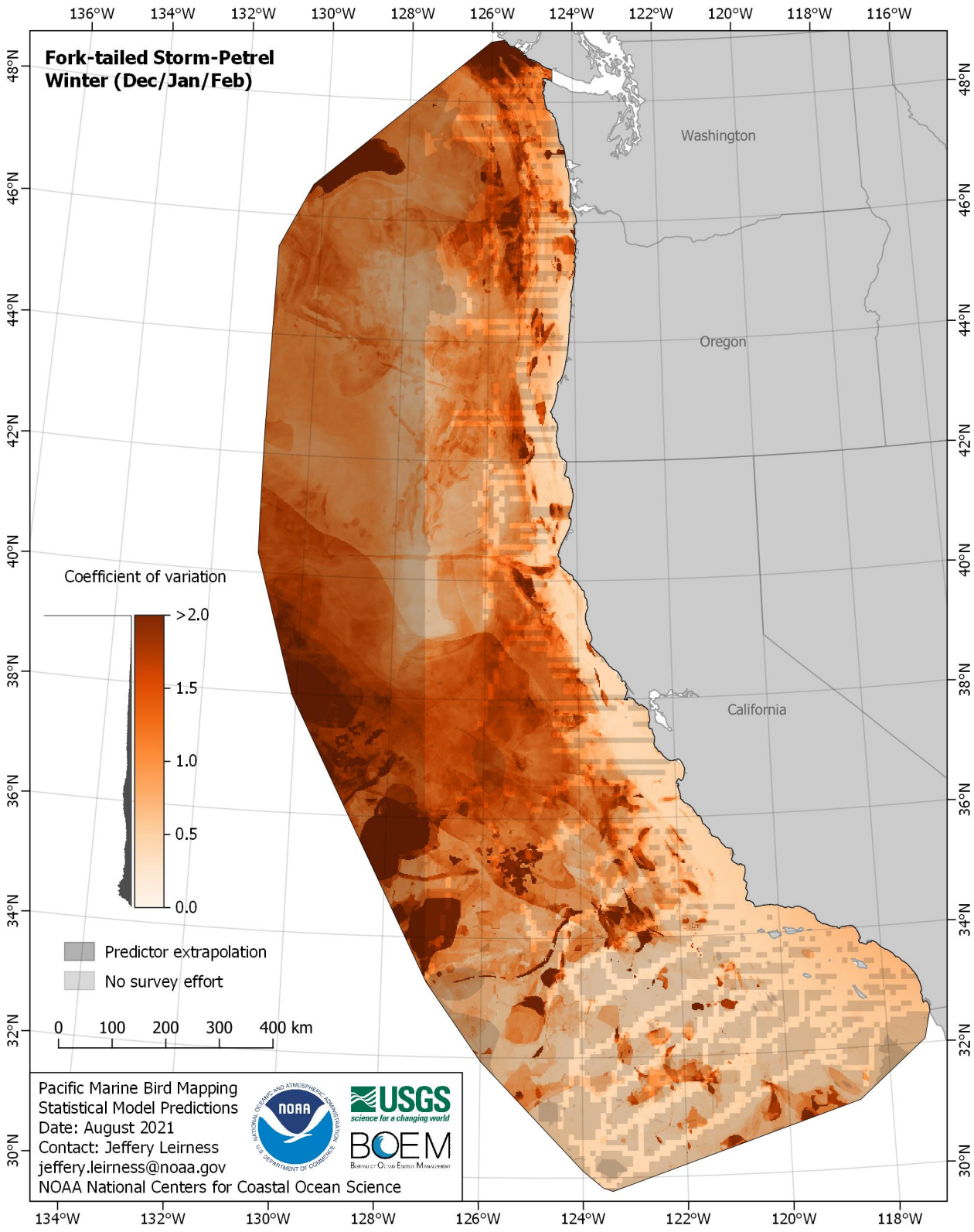

Figure E-186. Coefficient of variation for Fork-tailed Storm-Petrel (*Hydrobates furcatus*) in the winter season

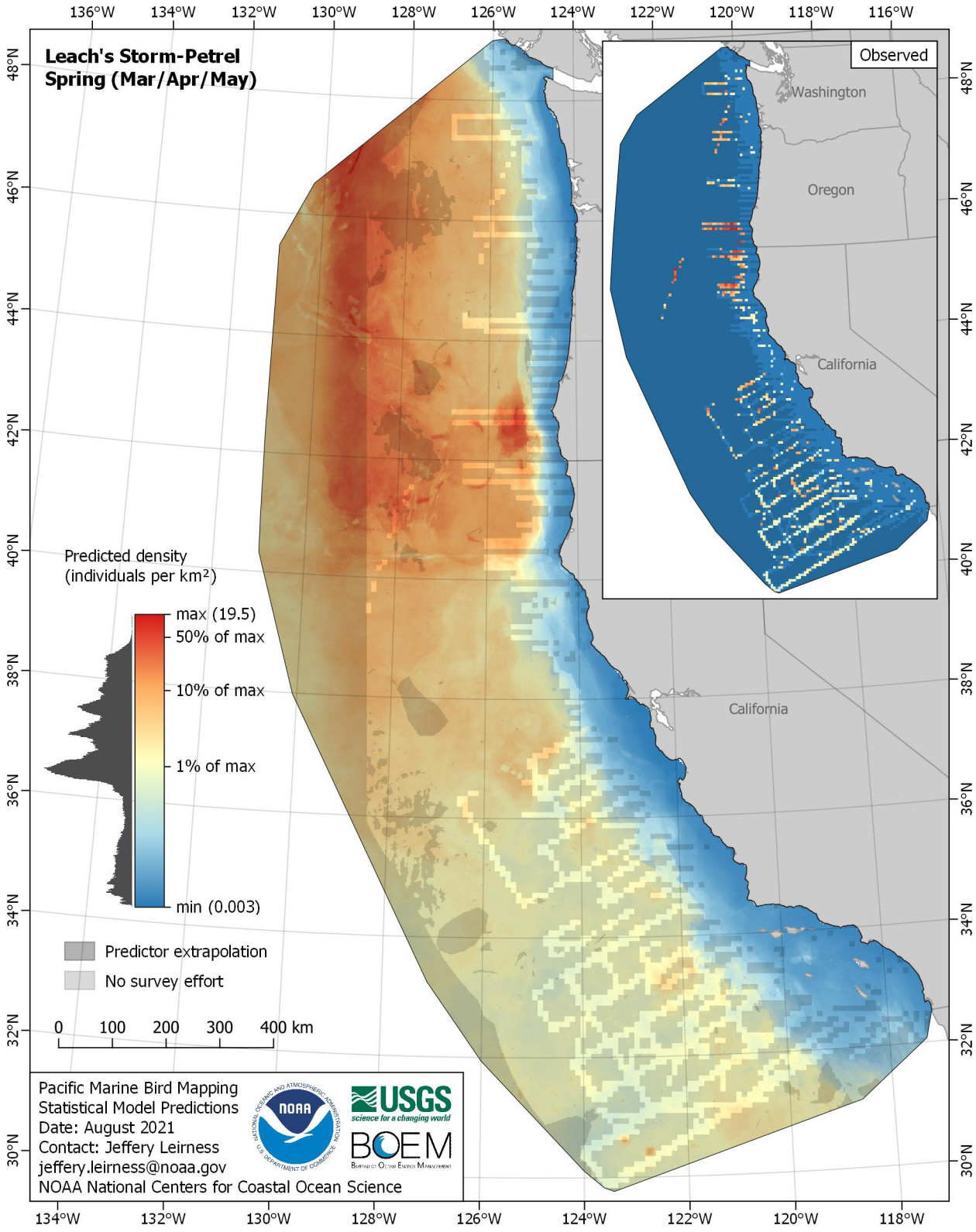

Figure E-187. Predicted density for Leach's Storm-Petrel (*Hydrobates leucorhous*) in the spring season

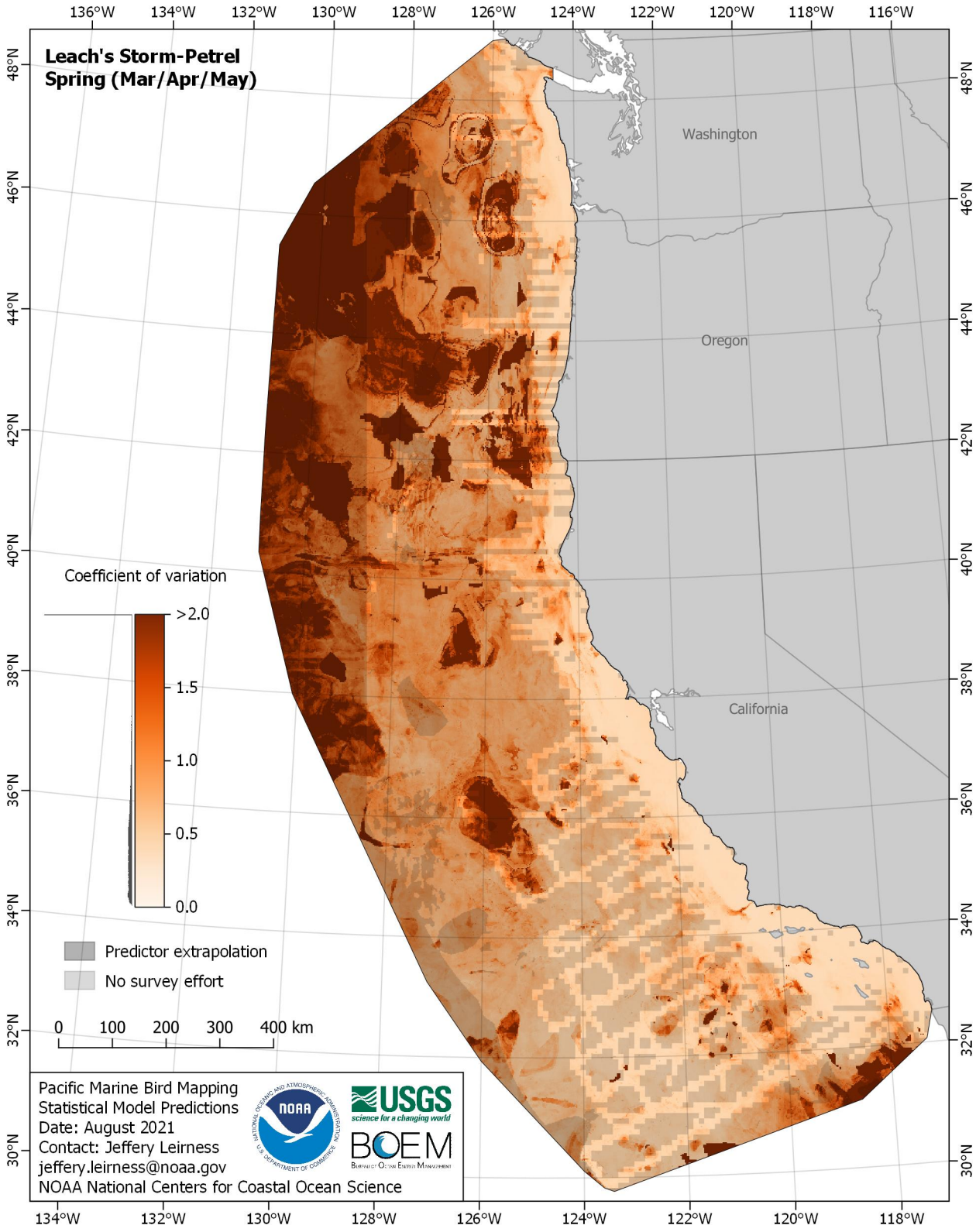

Figure E-188. Coefficient of variation for Leach's Storm-Petrel (*Hydrobates leucorhous*) in the spring season

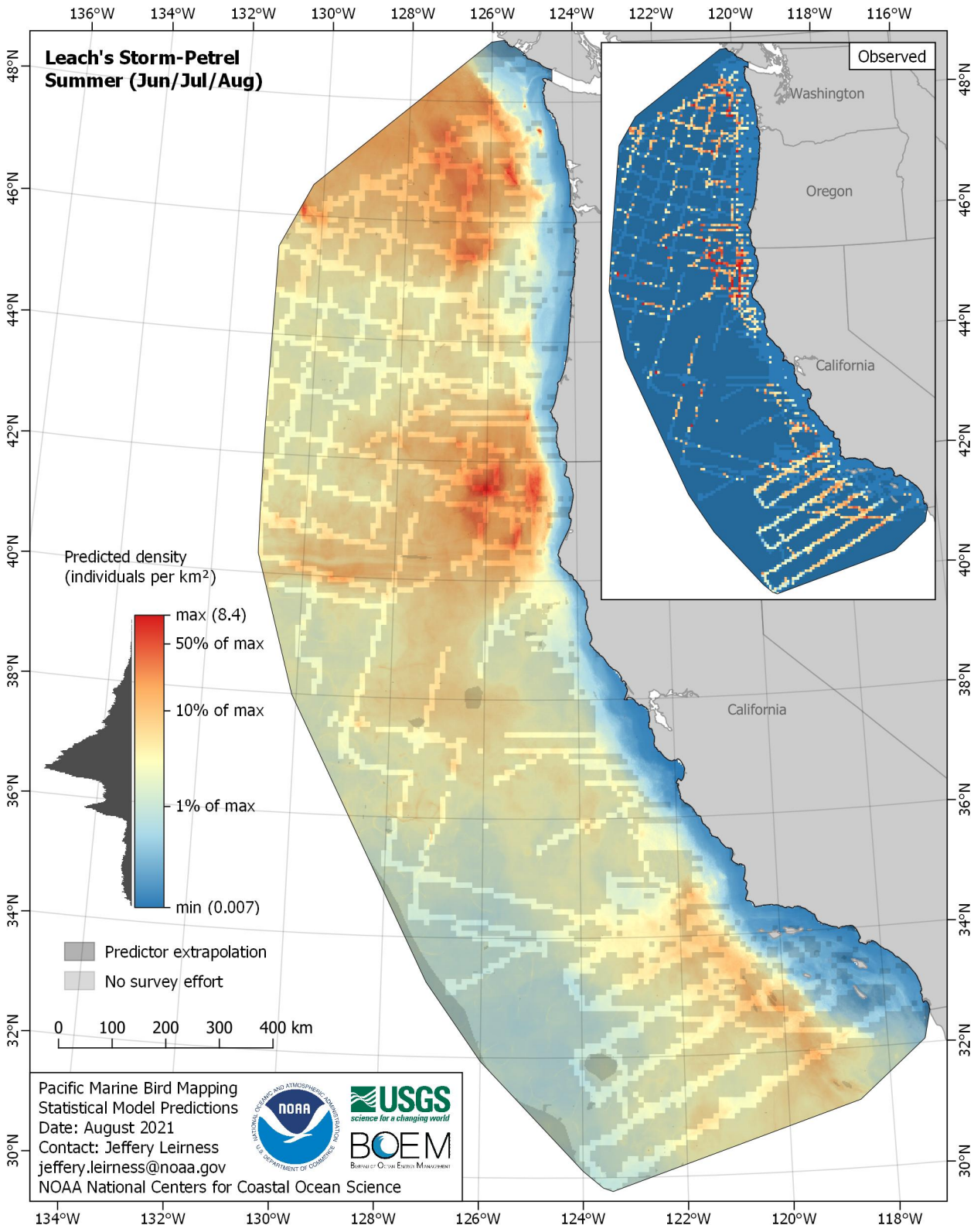

Figure E-189. Predicted density for Leach's Storm-Petrel (*Hydrobates leucorhous*) in the summer season

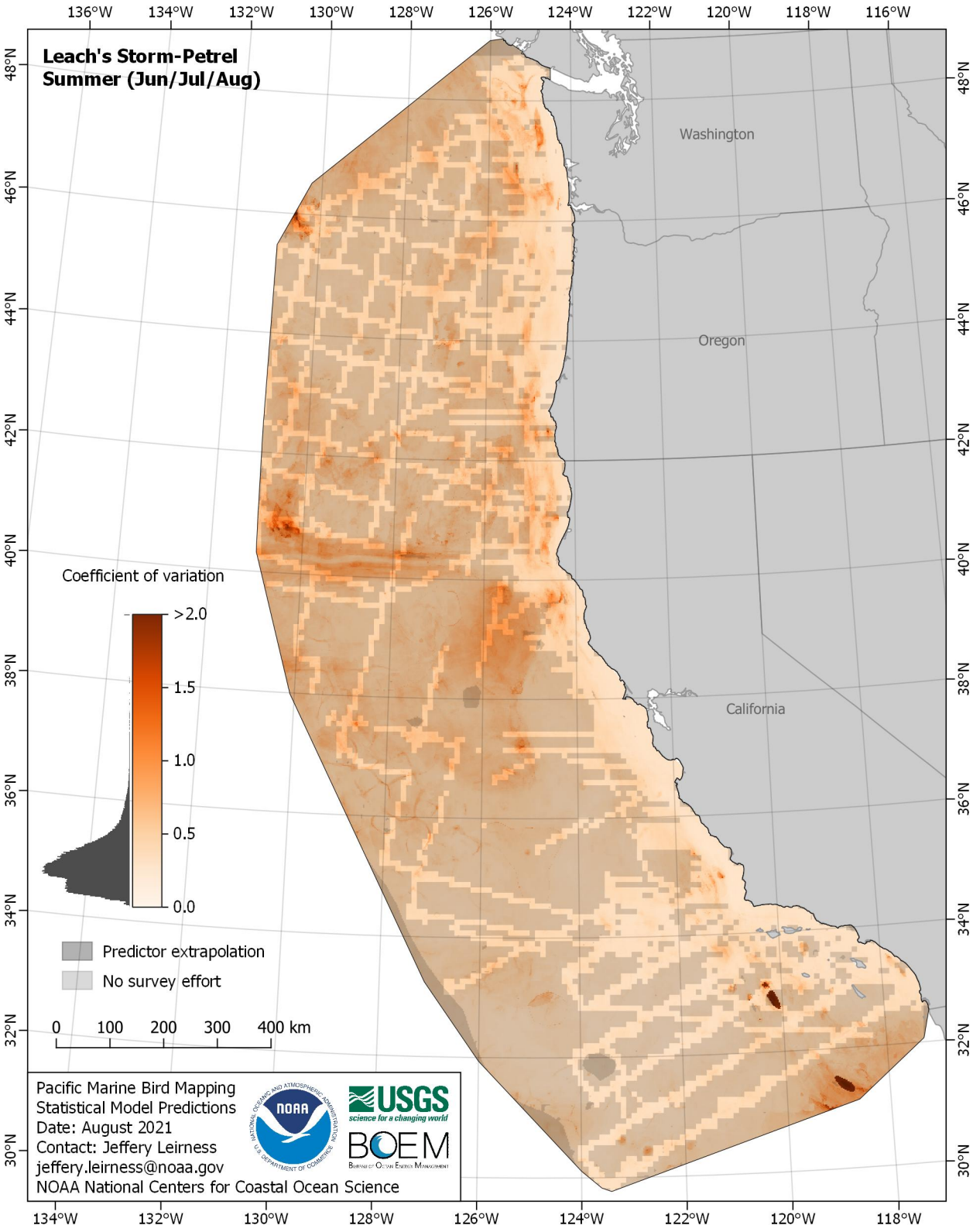

Figure E-190. Coefficient of variation for Leach's Storm-Petrel (*Hydrobates leucorhous*) in the summer season

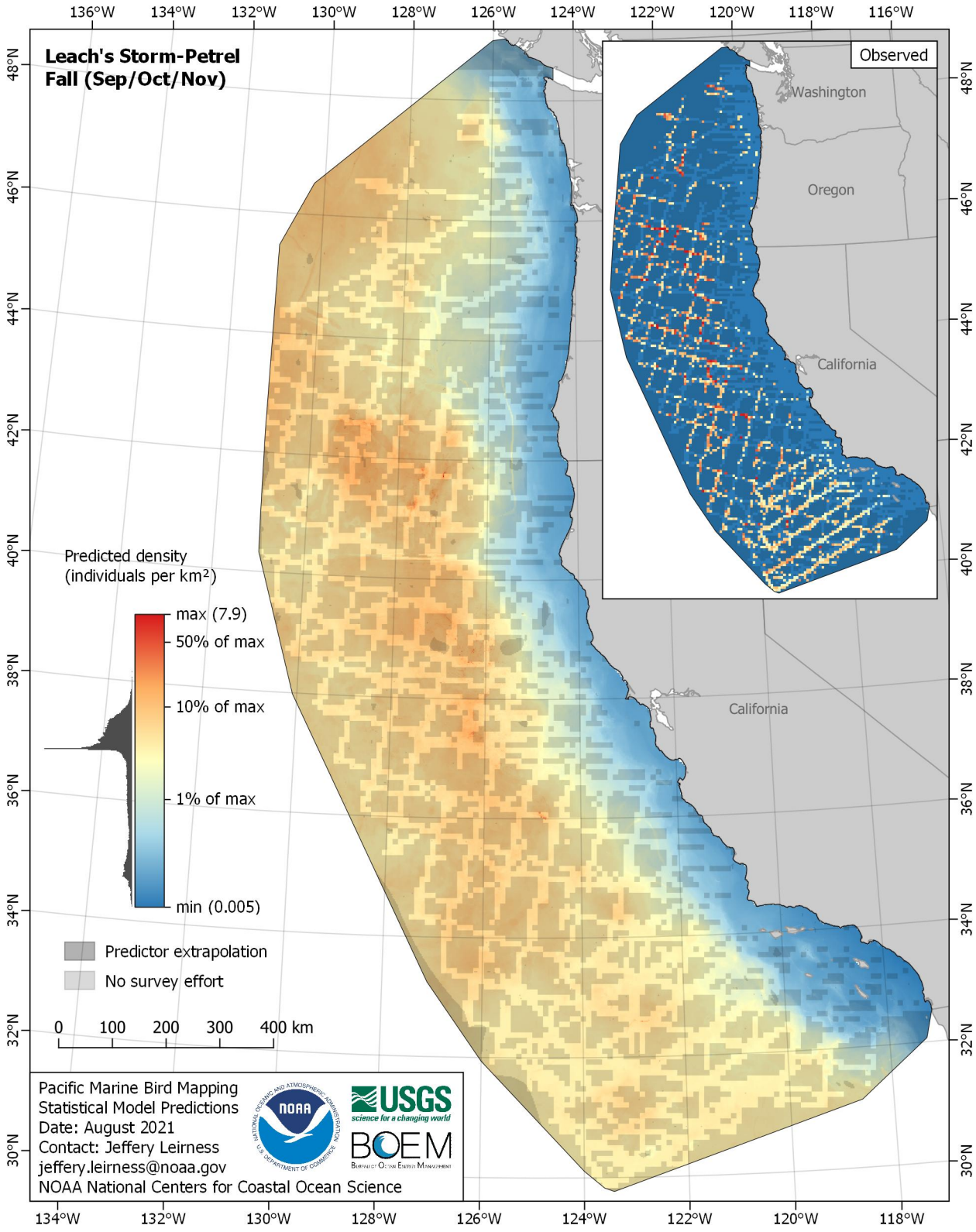

Figure E-191. Predicted density for Leach's Storm-Petrel (*Hydrobates leucorhous*) in the fall season

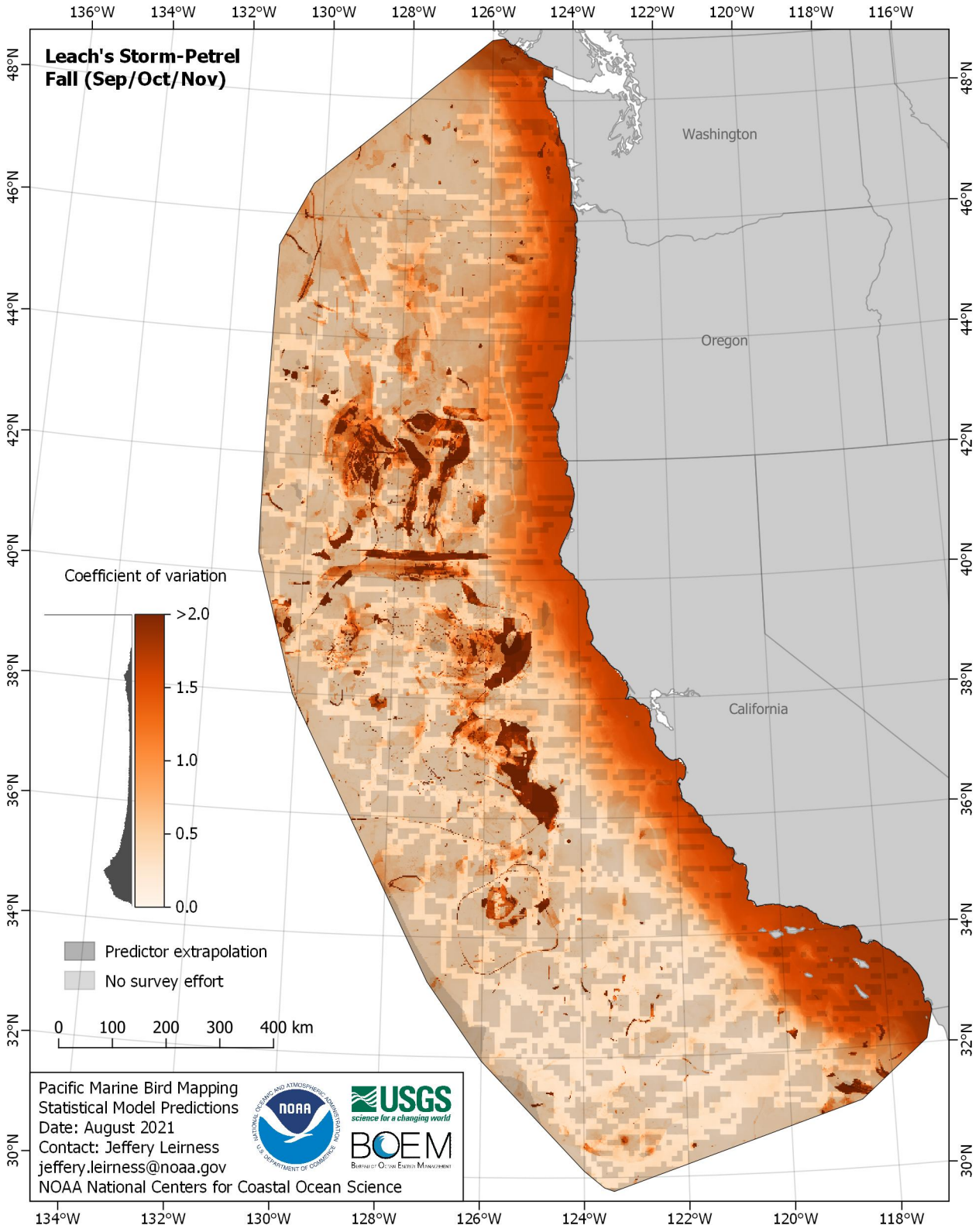

Figure E-192. Coefficient of variation for Leach's Storm-Petrel (Hydrobates leucorhous) in the fall season

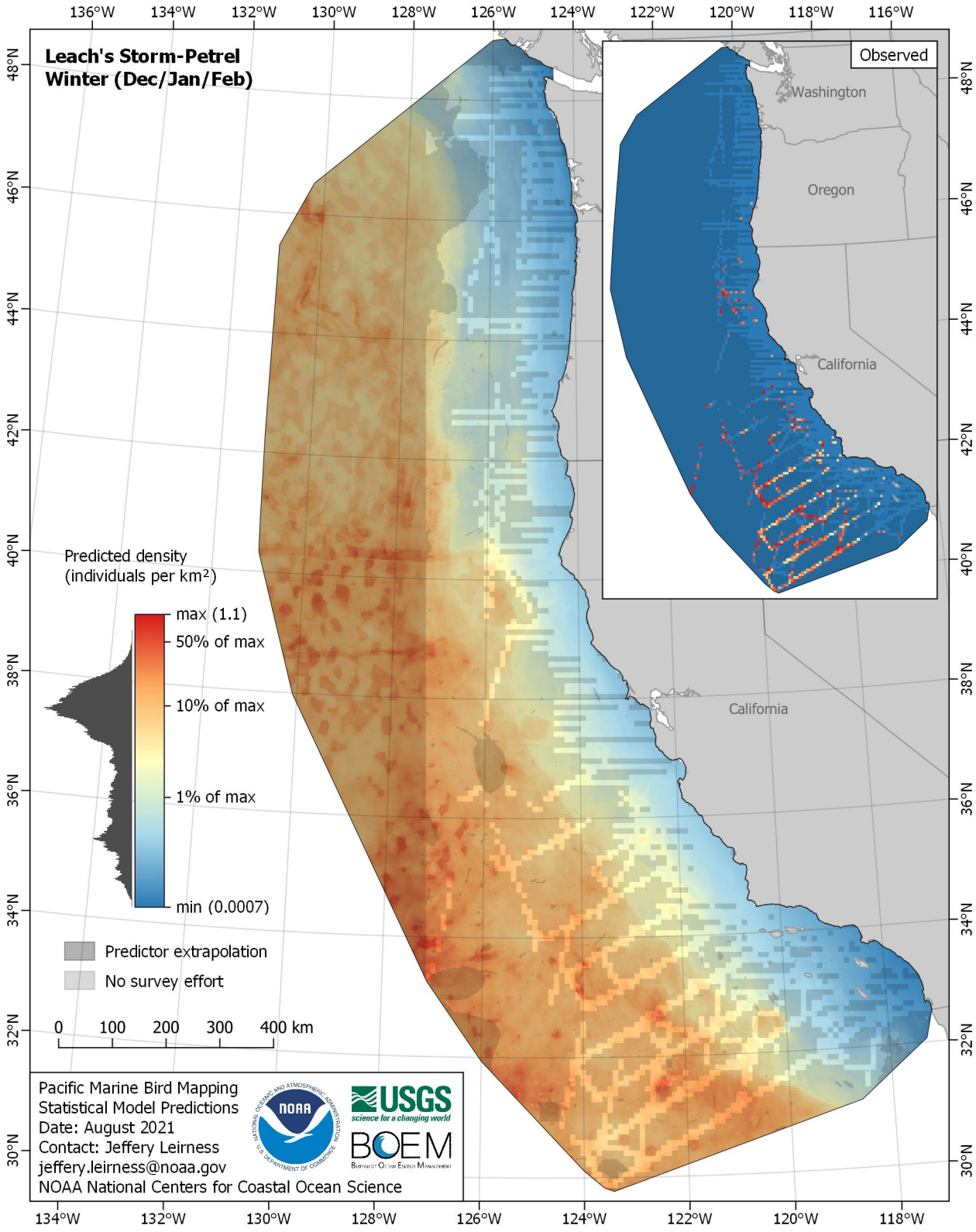

Figure E-193. Predicted density for Leach's Storm-Petrel (*Hydrobates leucorhous*) in the winter season

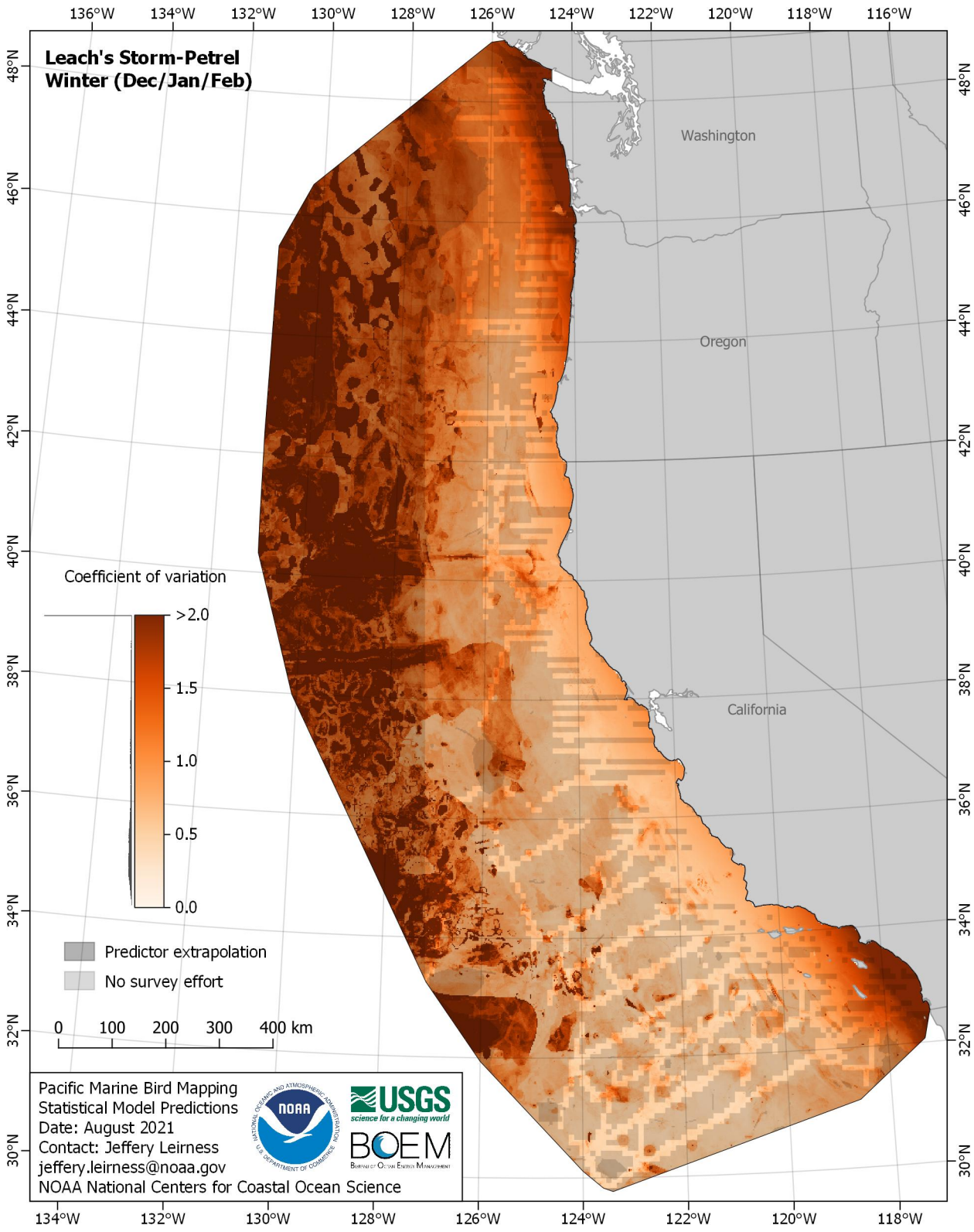

Figure E-194. Coefficient of variation for Leach's Storm-Petrel (*Hydrobates leucorhous*) in the winter season

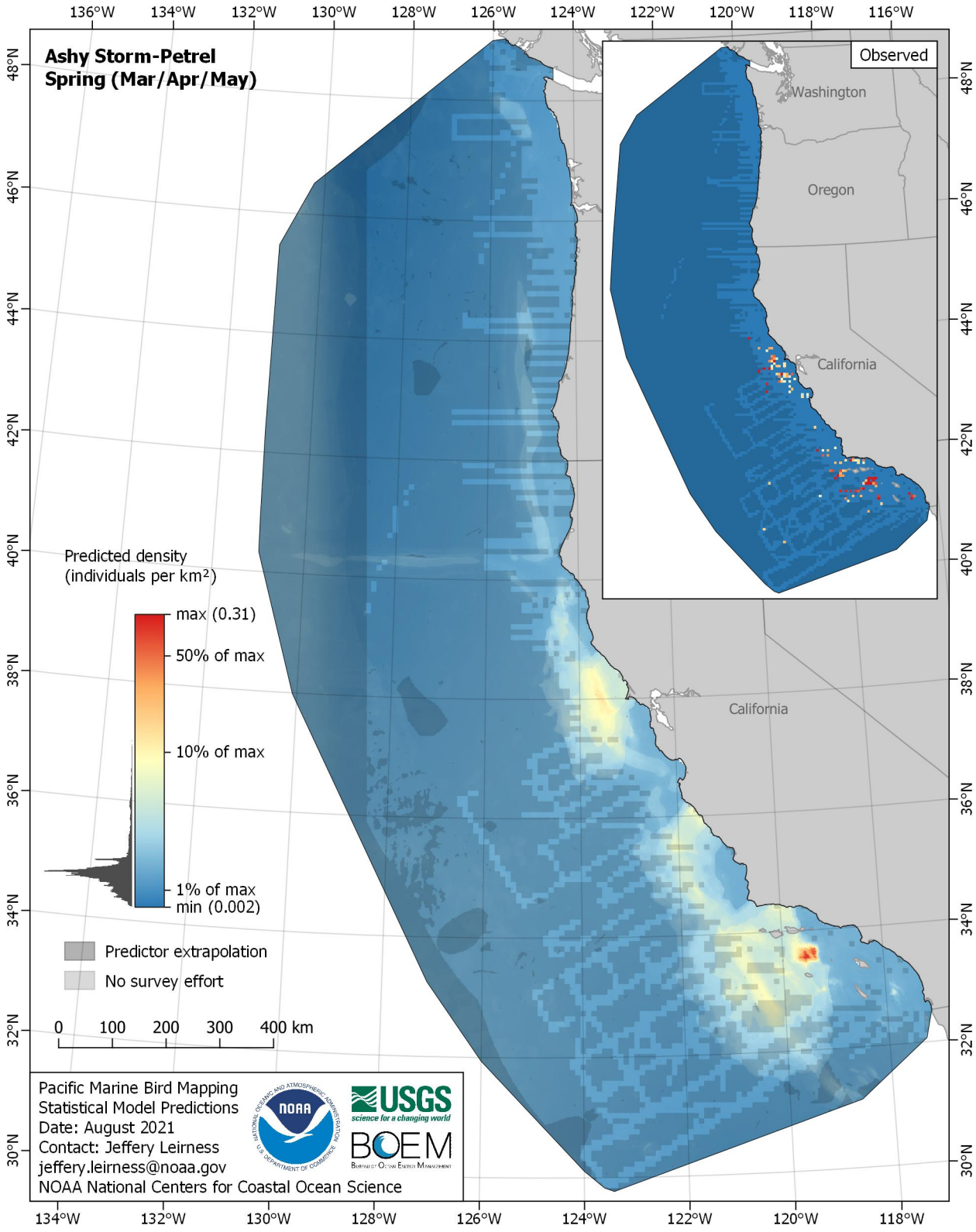

Figure E-195. Predicted density for Ashy Storm-Petrel (*Hydrobates homochroa*) in the spring season

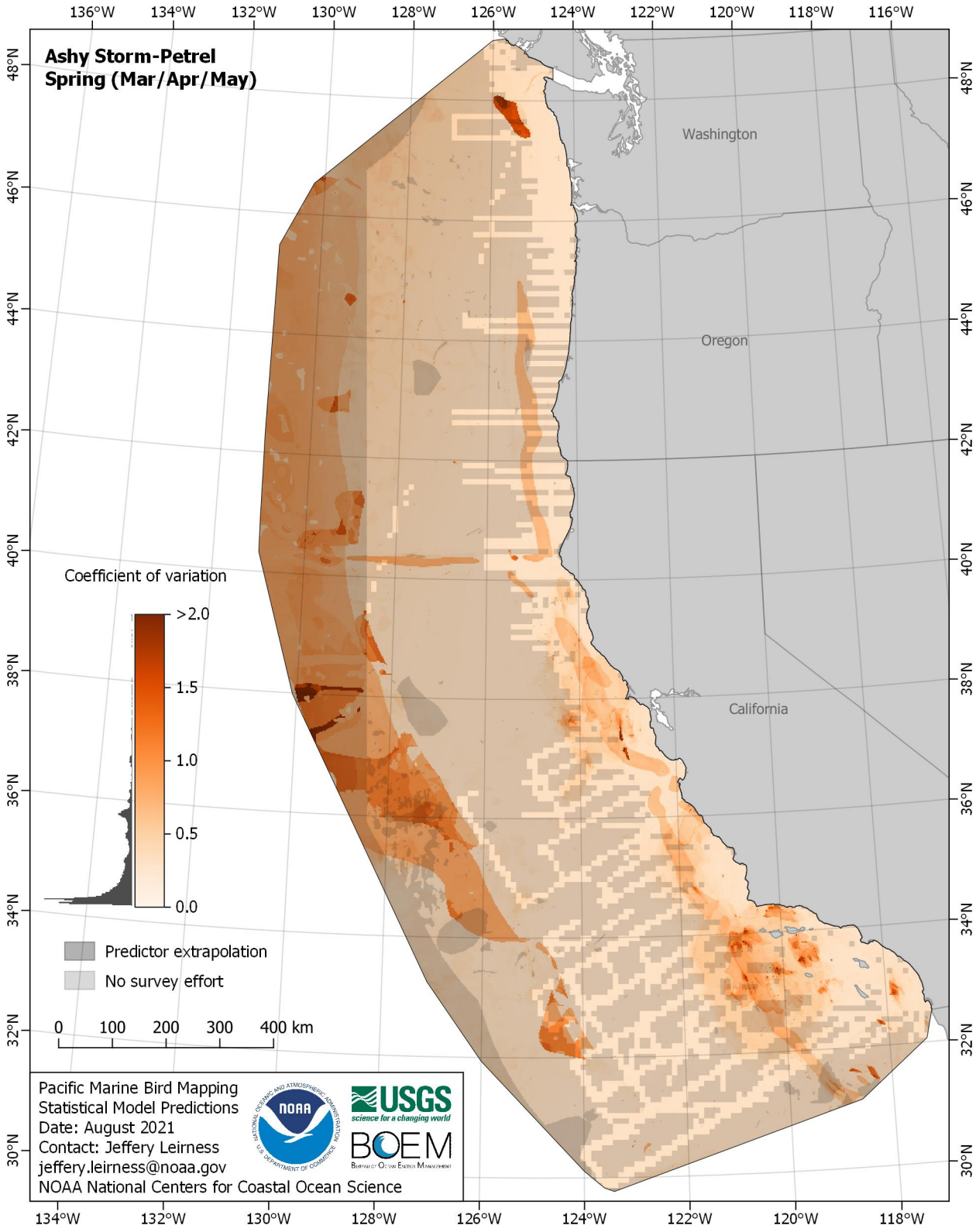

Figure E-196. Coefficient of variation for Ashy Storm-Petrel (*Hydrobates homochroa*) in the spring season

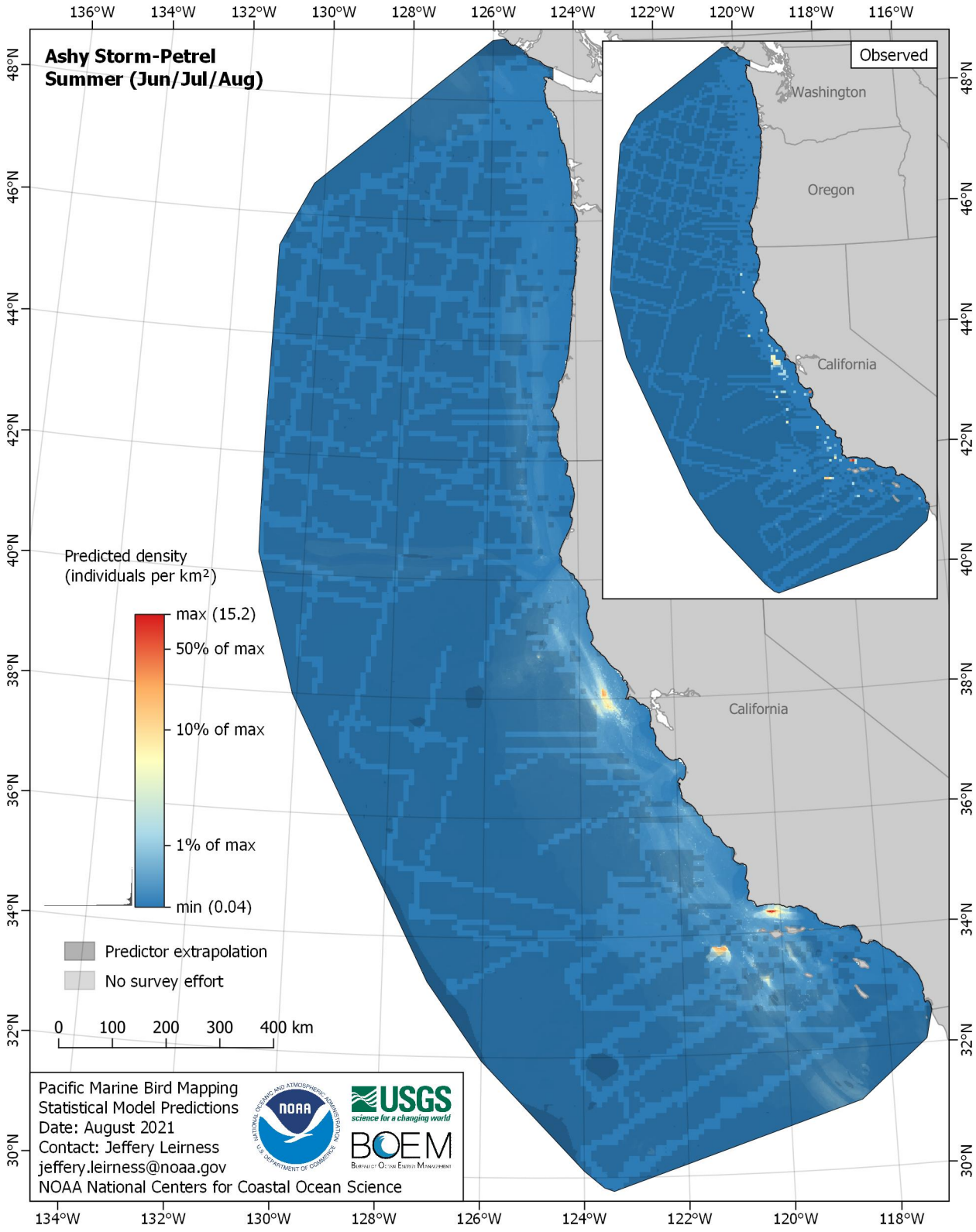

Figure E-197. Predicted density for Ashy Storm-Petrel (*Hydrobates homochroa*) in the summer season

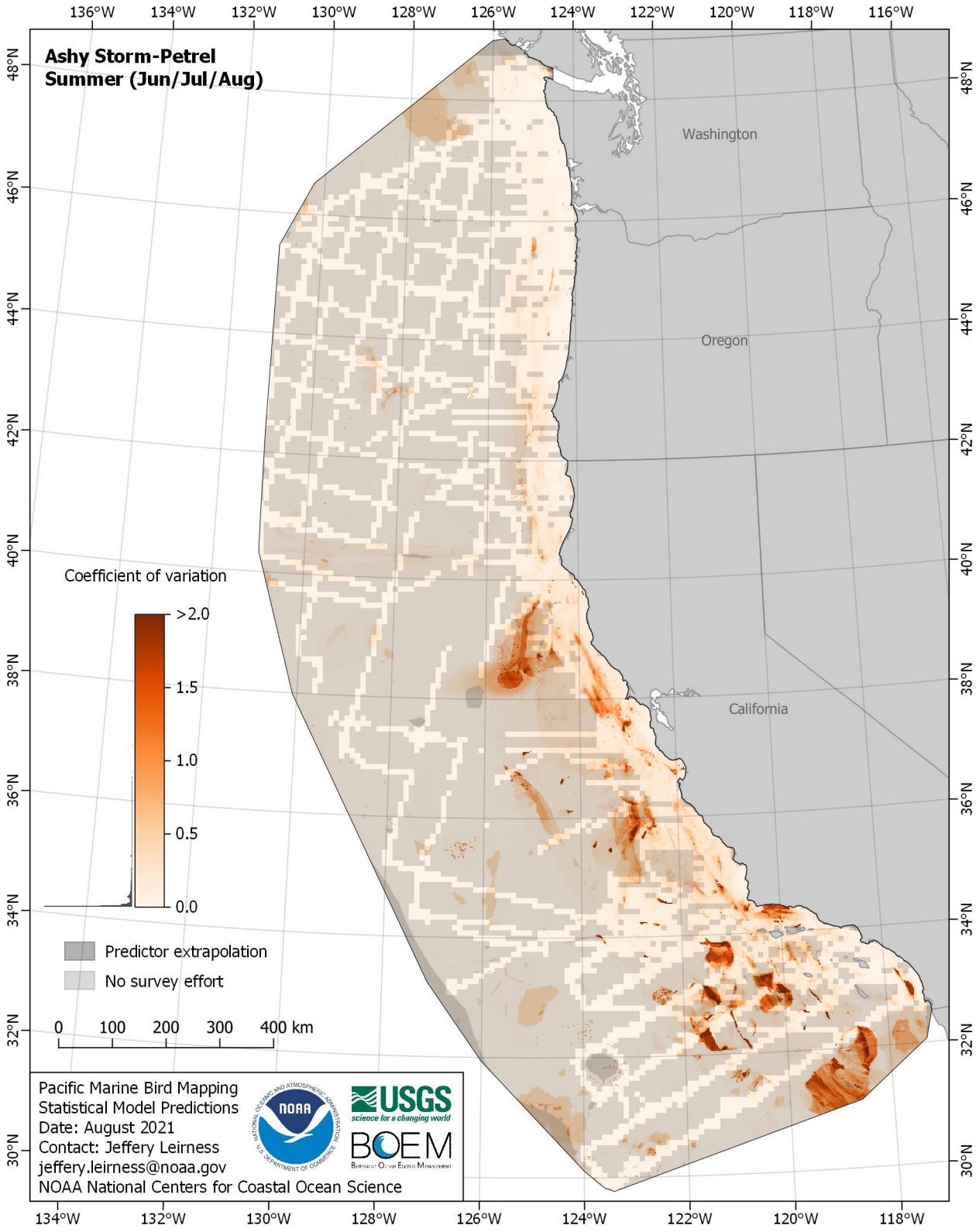

Figure E-198. Coefficient of variation for Ashy Storm-Petrel (*Hydrobates homochroa*) in the summer season

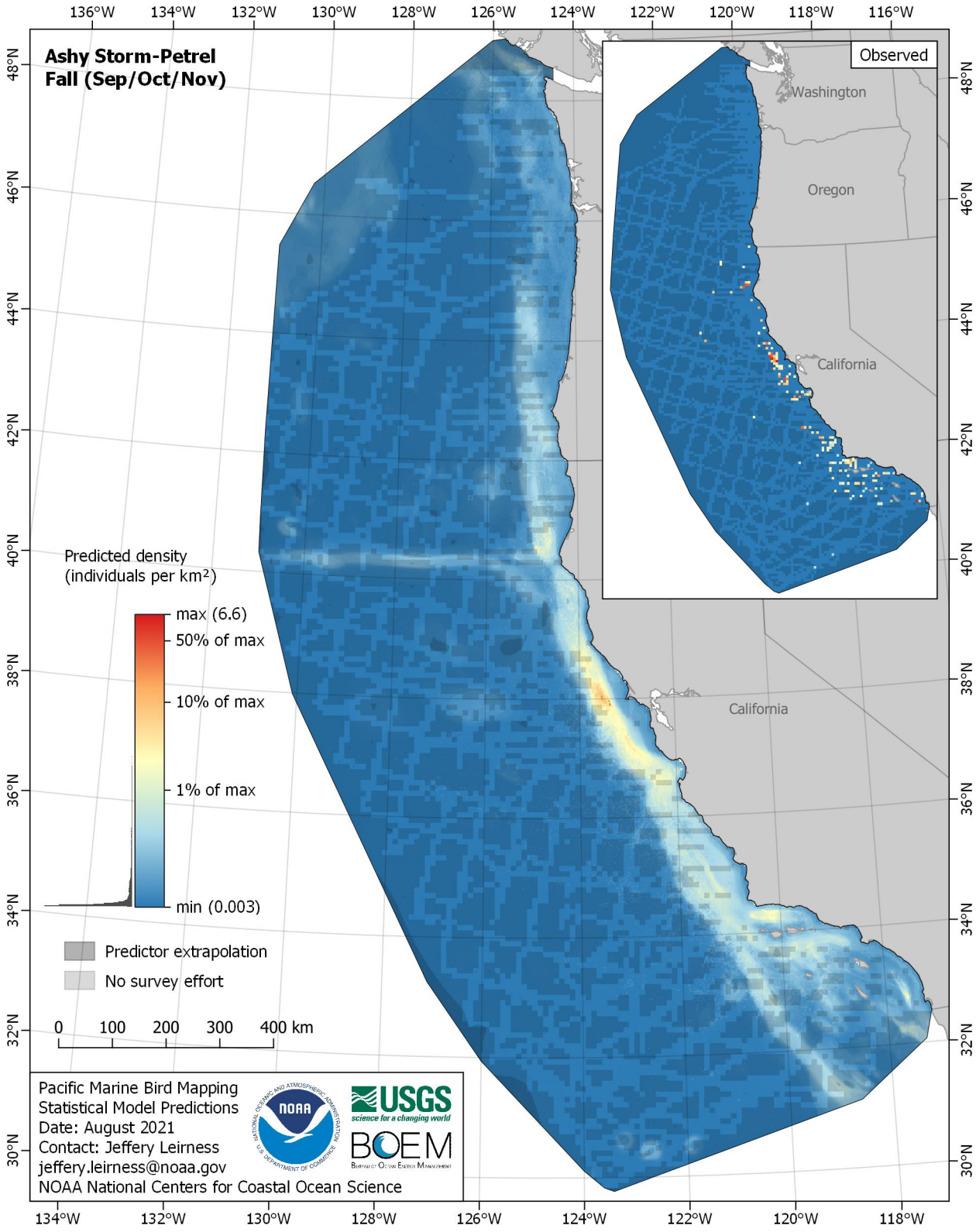

Figure E-199. Predicted density for Ashy Storm-Petrel (*Hydrobates homochroa*) in the fall season

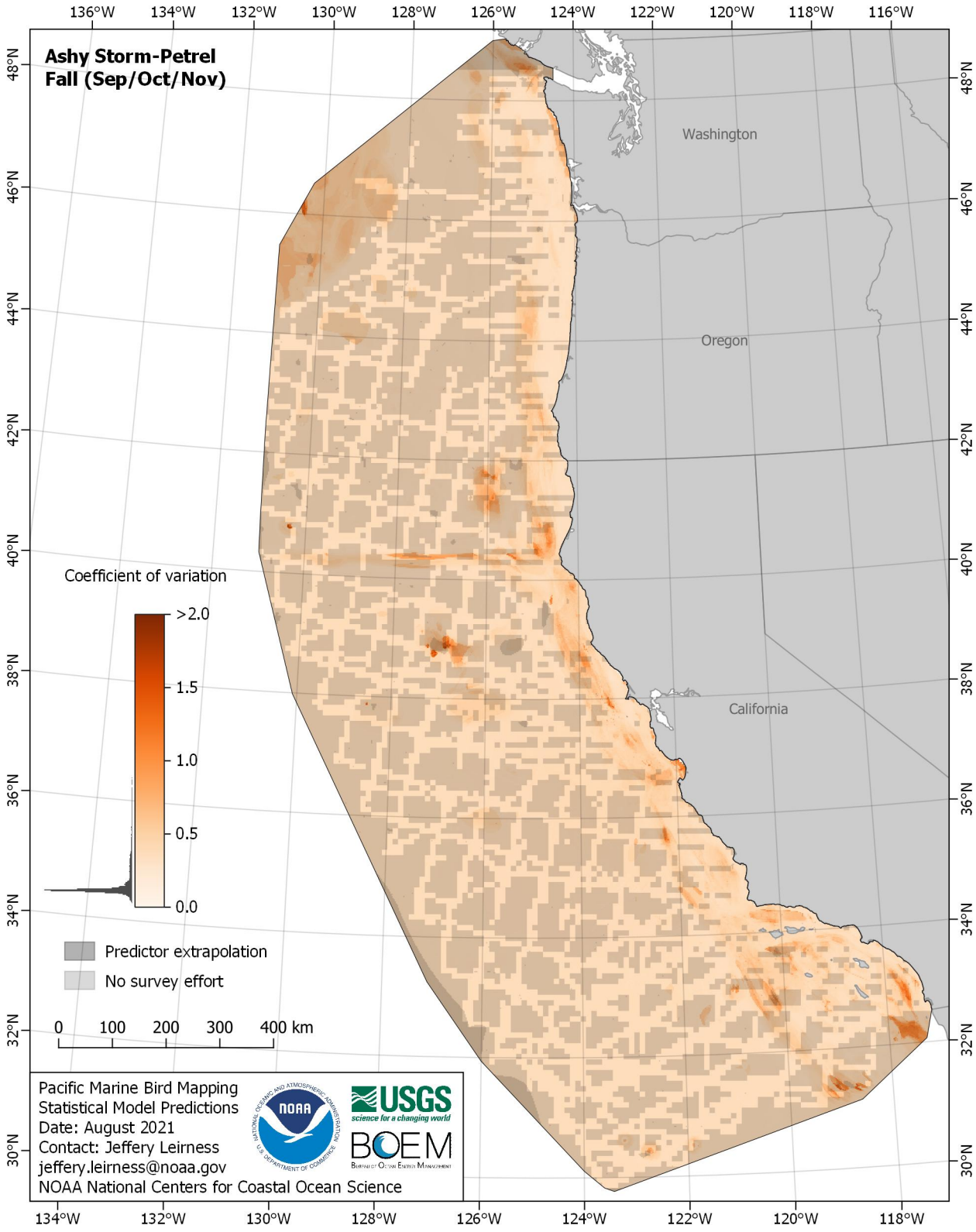

Figure E-200. Coefficient of variation for Ashy Storm-Petrel (*Hydrobates homochroa*) in the fall season

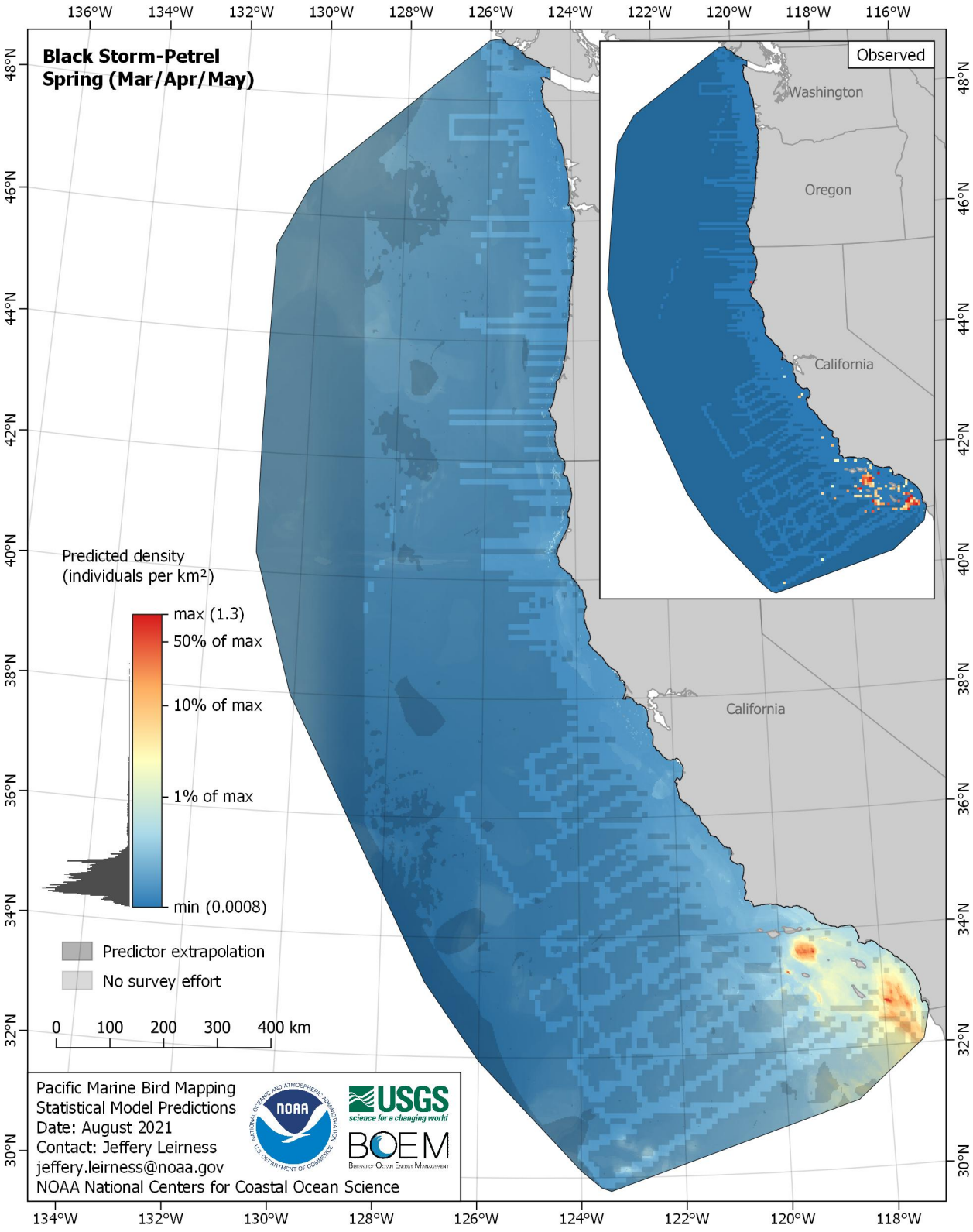

Figure E-201. Predicted density for Black Storm-Petrel (*Hydrobates melania*) in the spring season

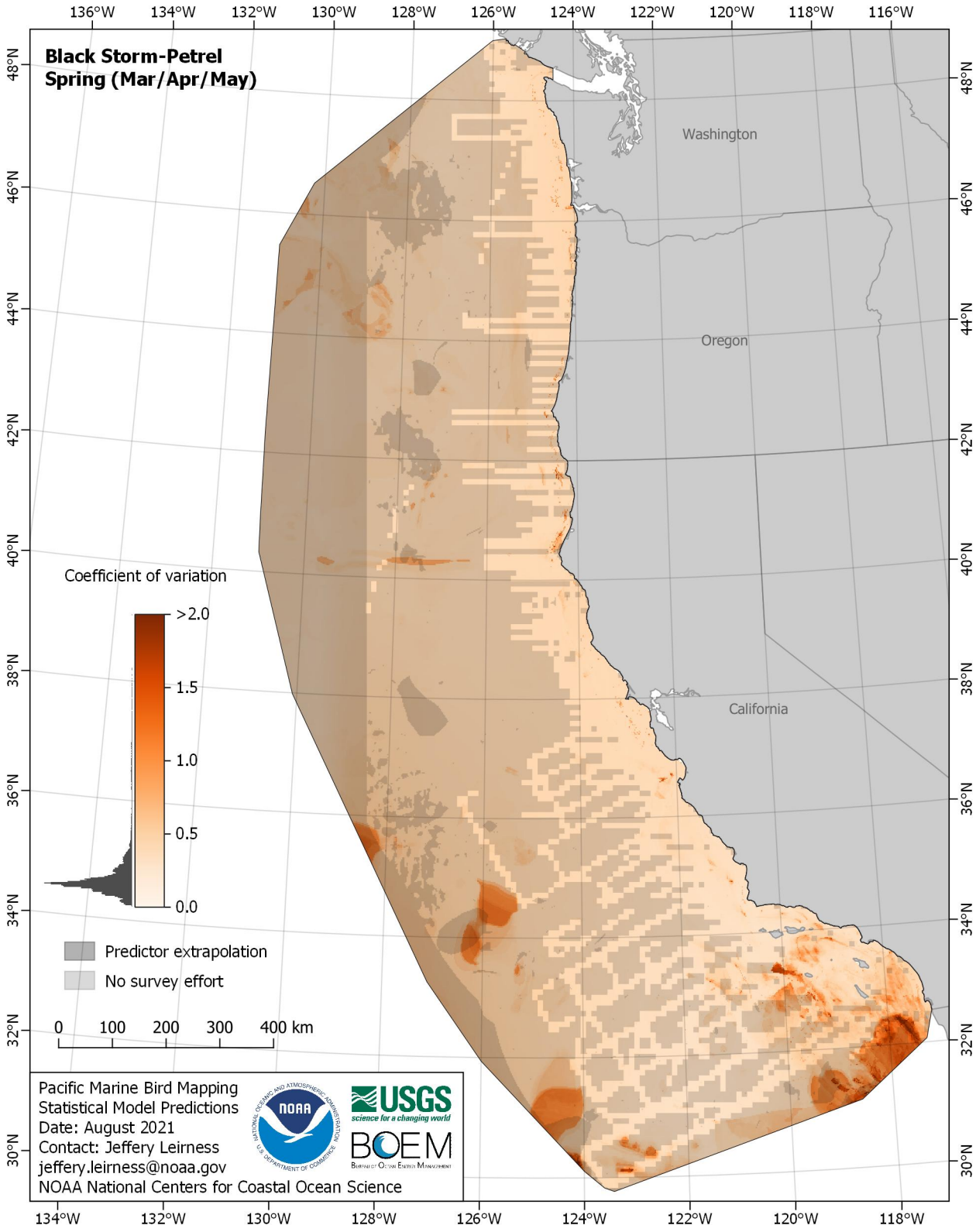

Figure E-202. Coefficient of variation for Black Storm-Petrel (*Hydrobates melania*) in the spring season

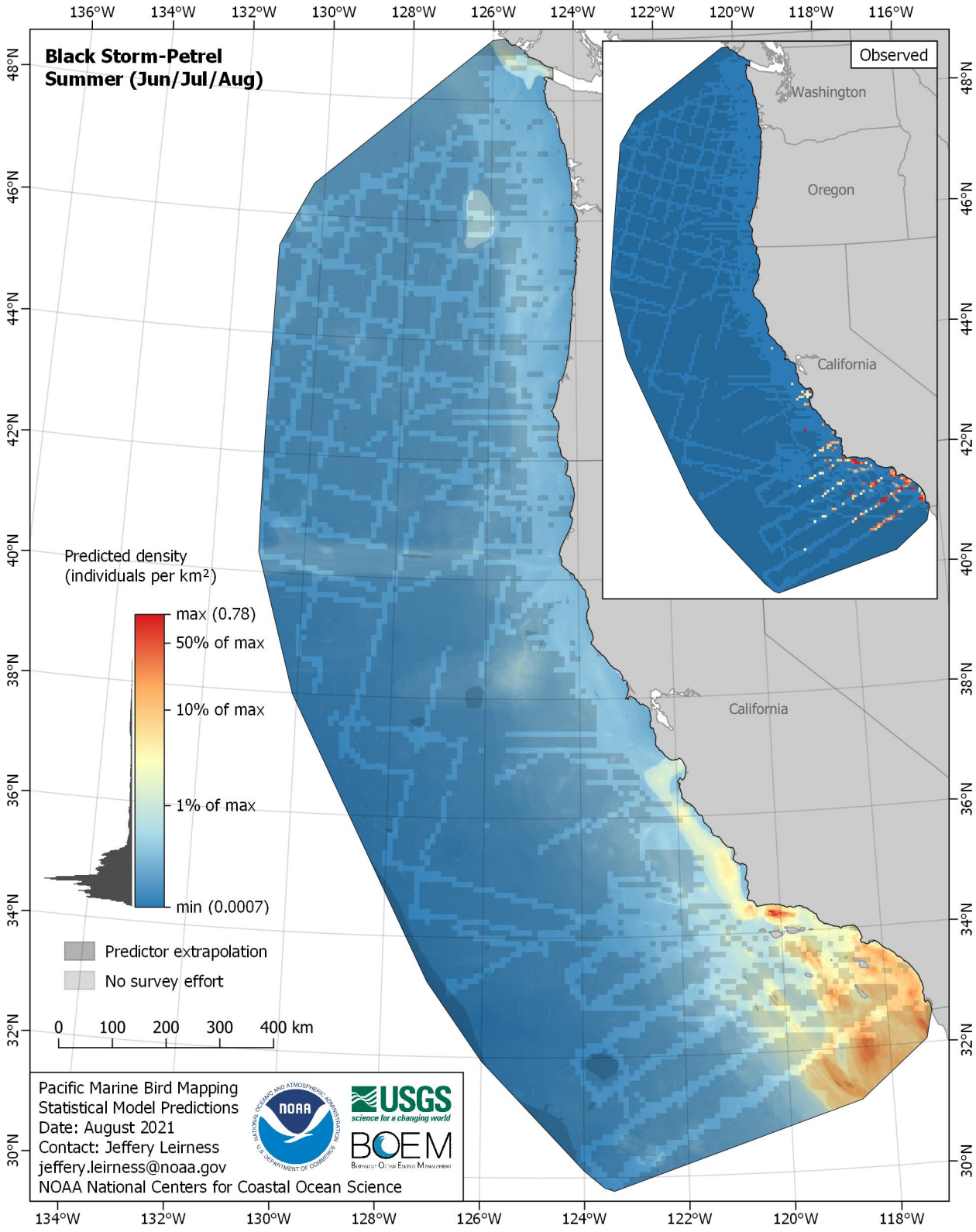

Figure E-203. Predicted density for Black Storm-Petrel (*Hydrobates melania*) in the summer season

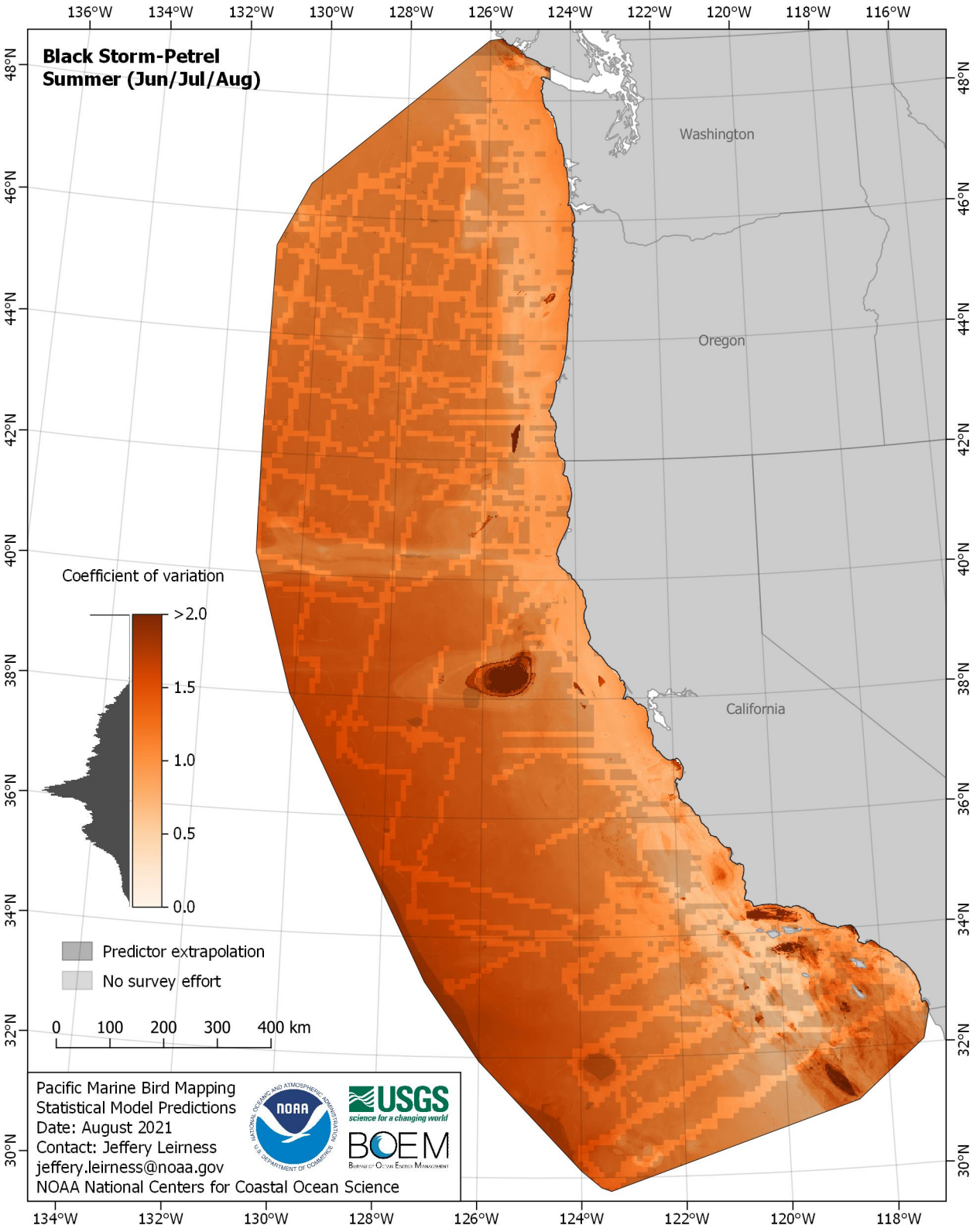

Figure E-204. Coefficient of variation for Black Storm-Petrel (*Hydrobates melania*) in the summer season

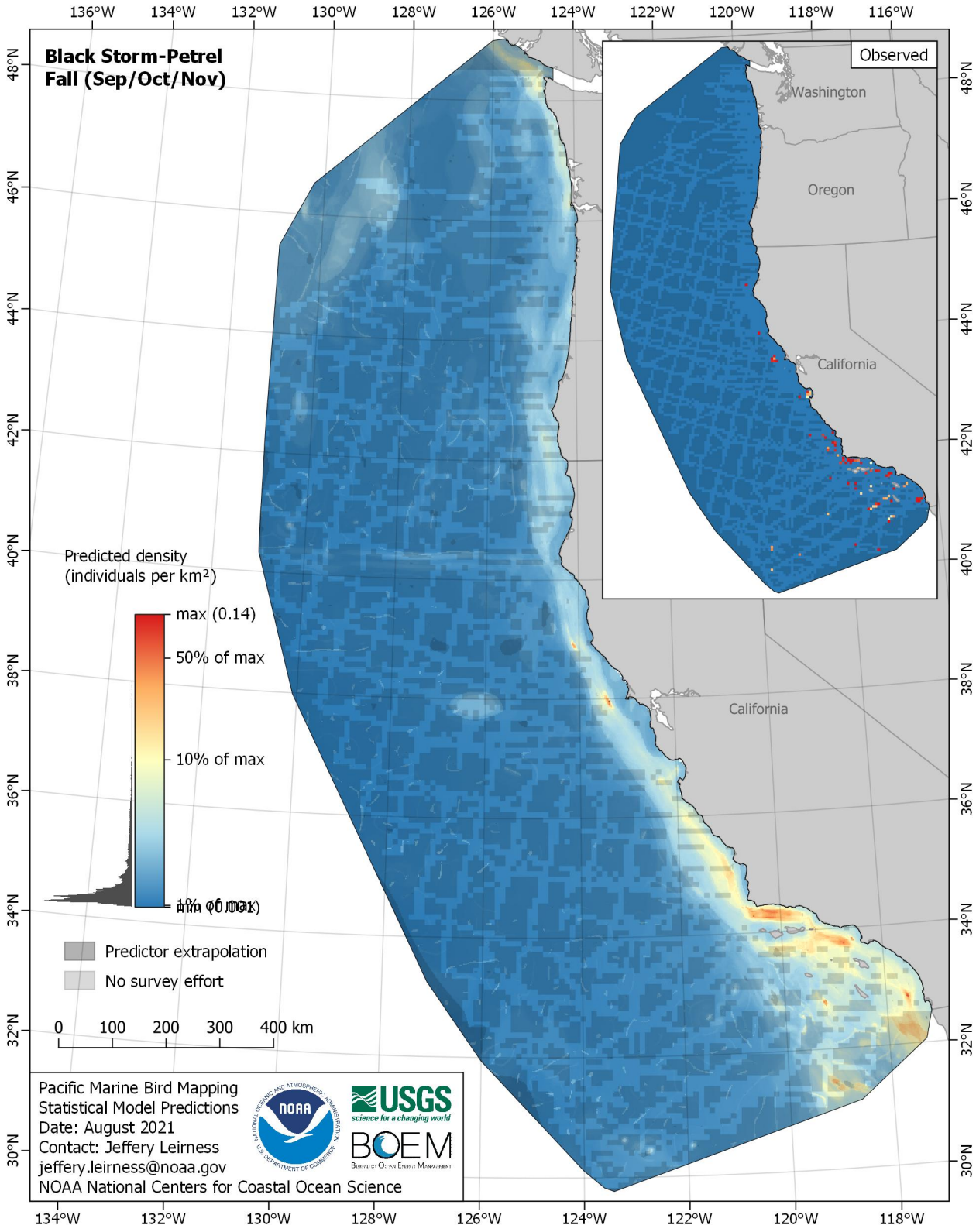

Figure E-205. Predicted density for Black Storm-Petrel (*Hydrobates melania*) in the fall season

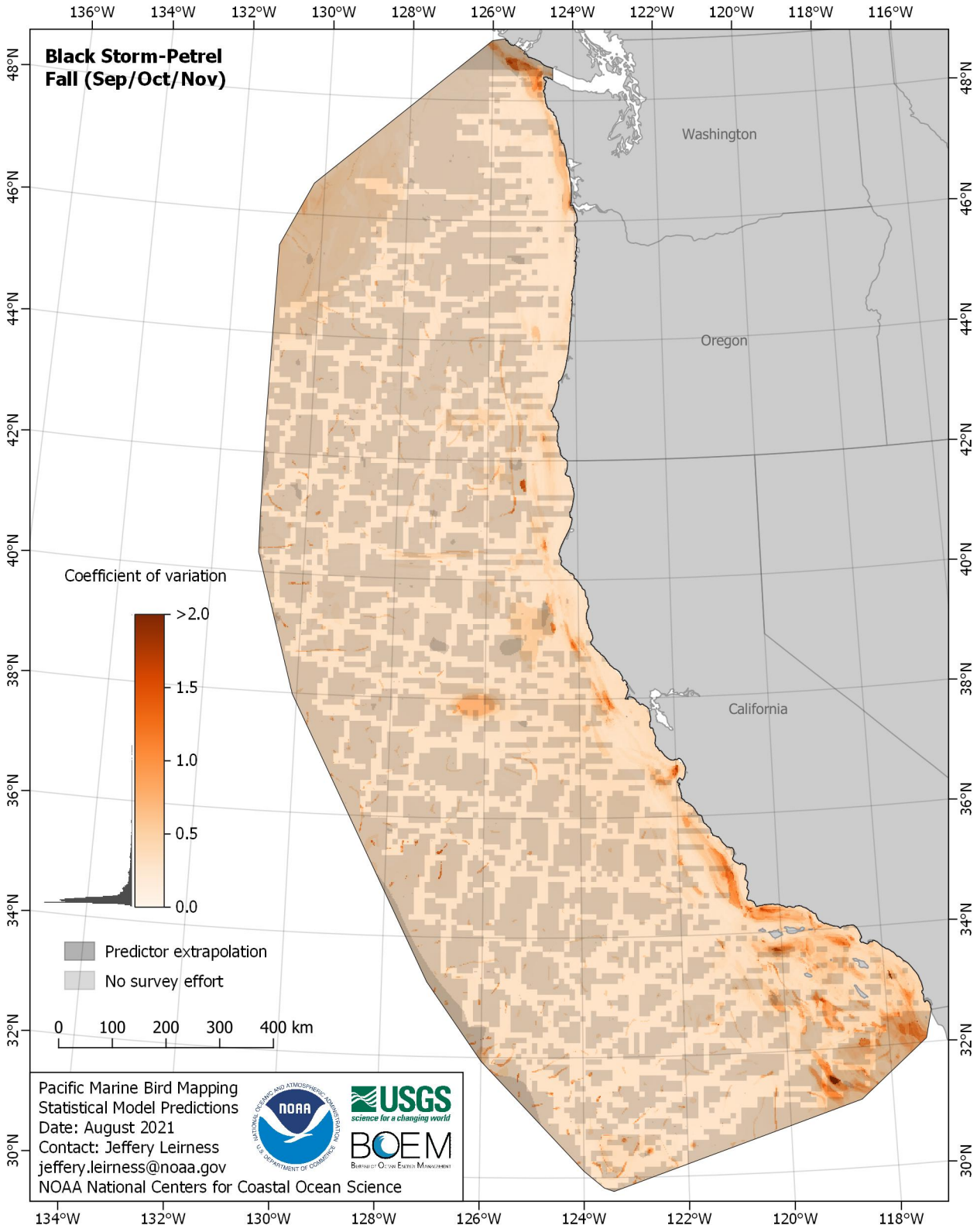

Figure E-206. Coefficient of variation for Black Storm-Petrel (*Hydrobates melania*) in the fall season

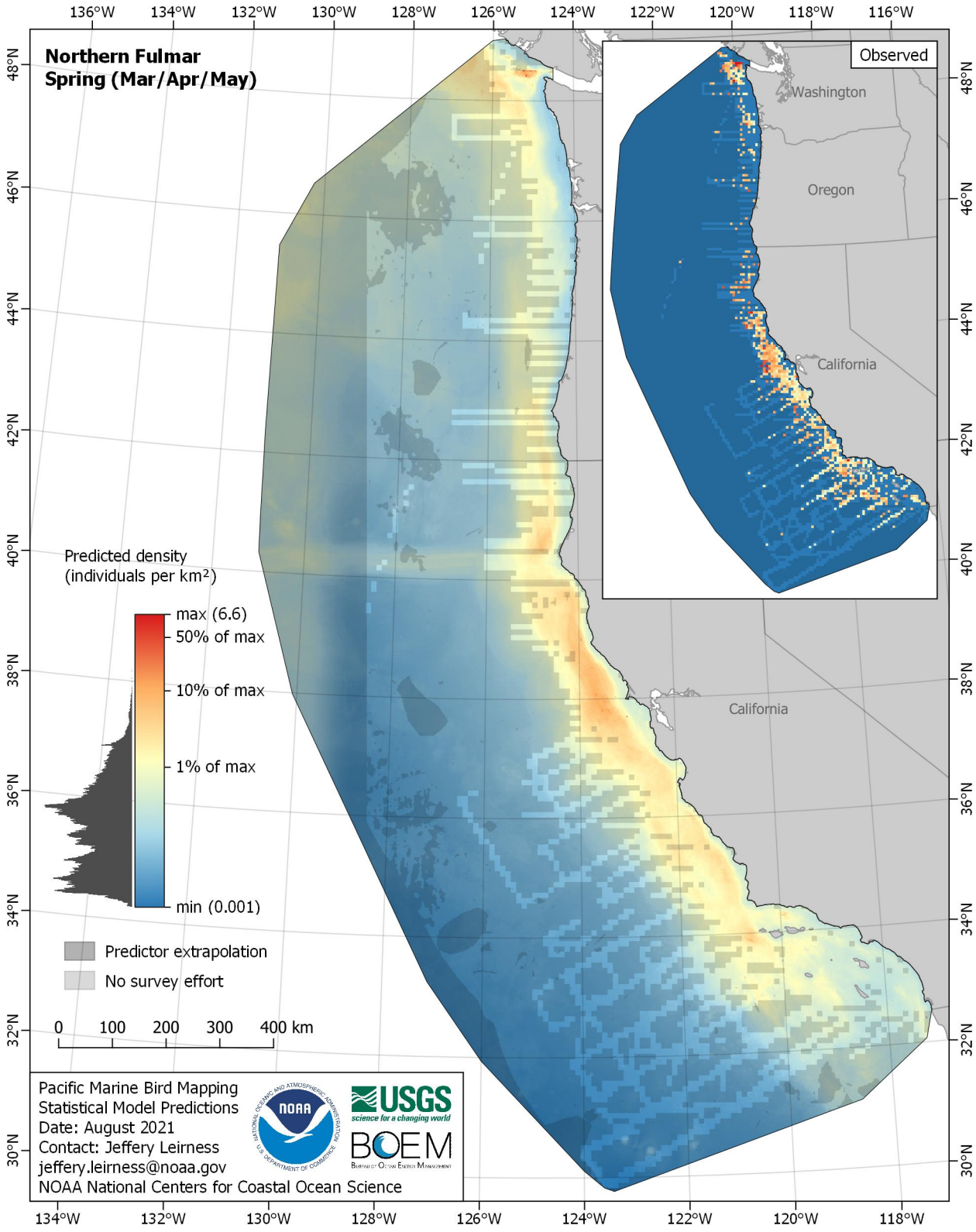

Figure E-207. Predicted density for Northern Fulmar (*Fulmarus glacialis*) in the spring season

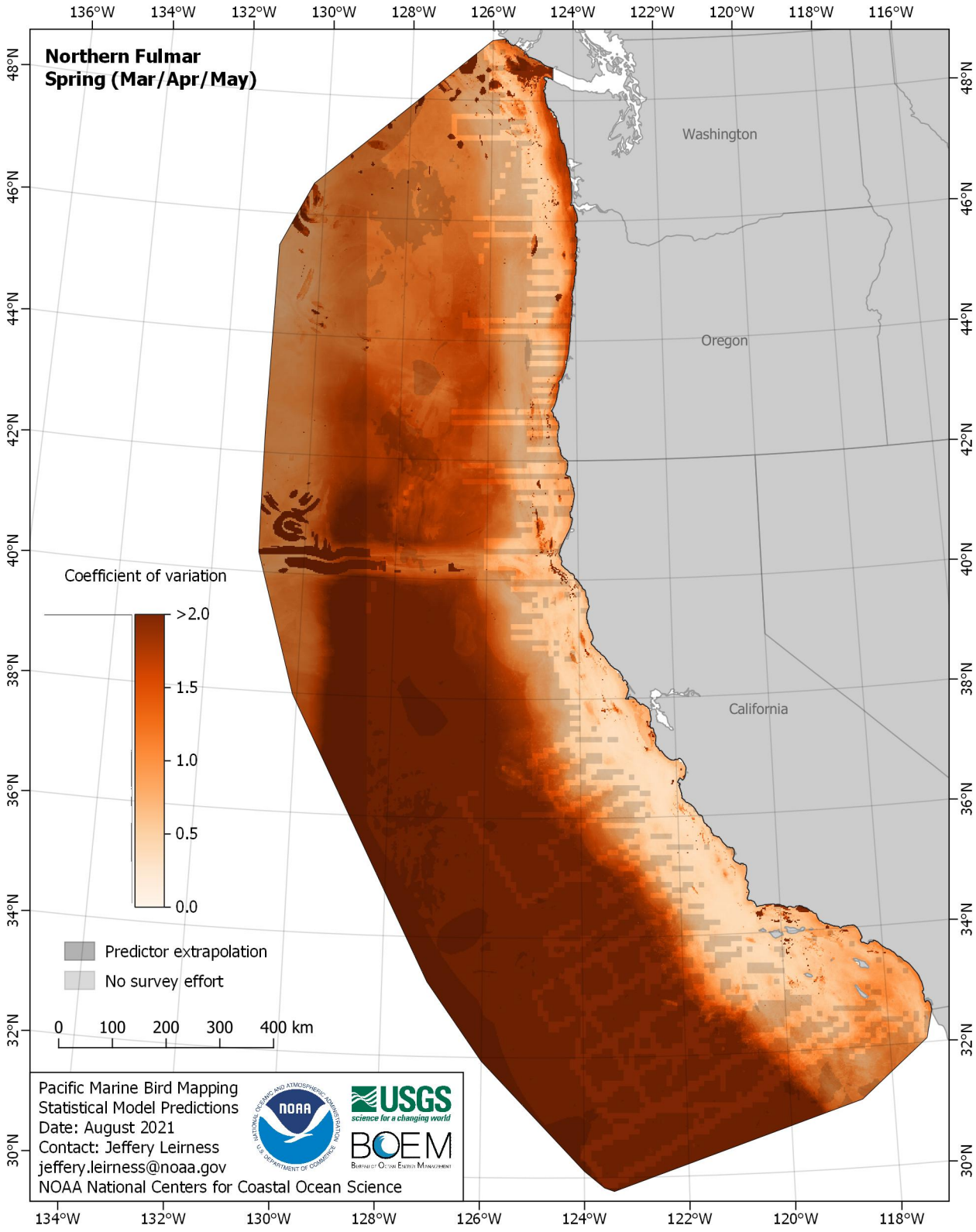

Figure E-208. Coefficient of variation for Northern Fulmar (*Fulmarus glacialis*) in the spring season

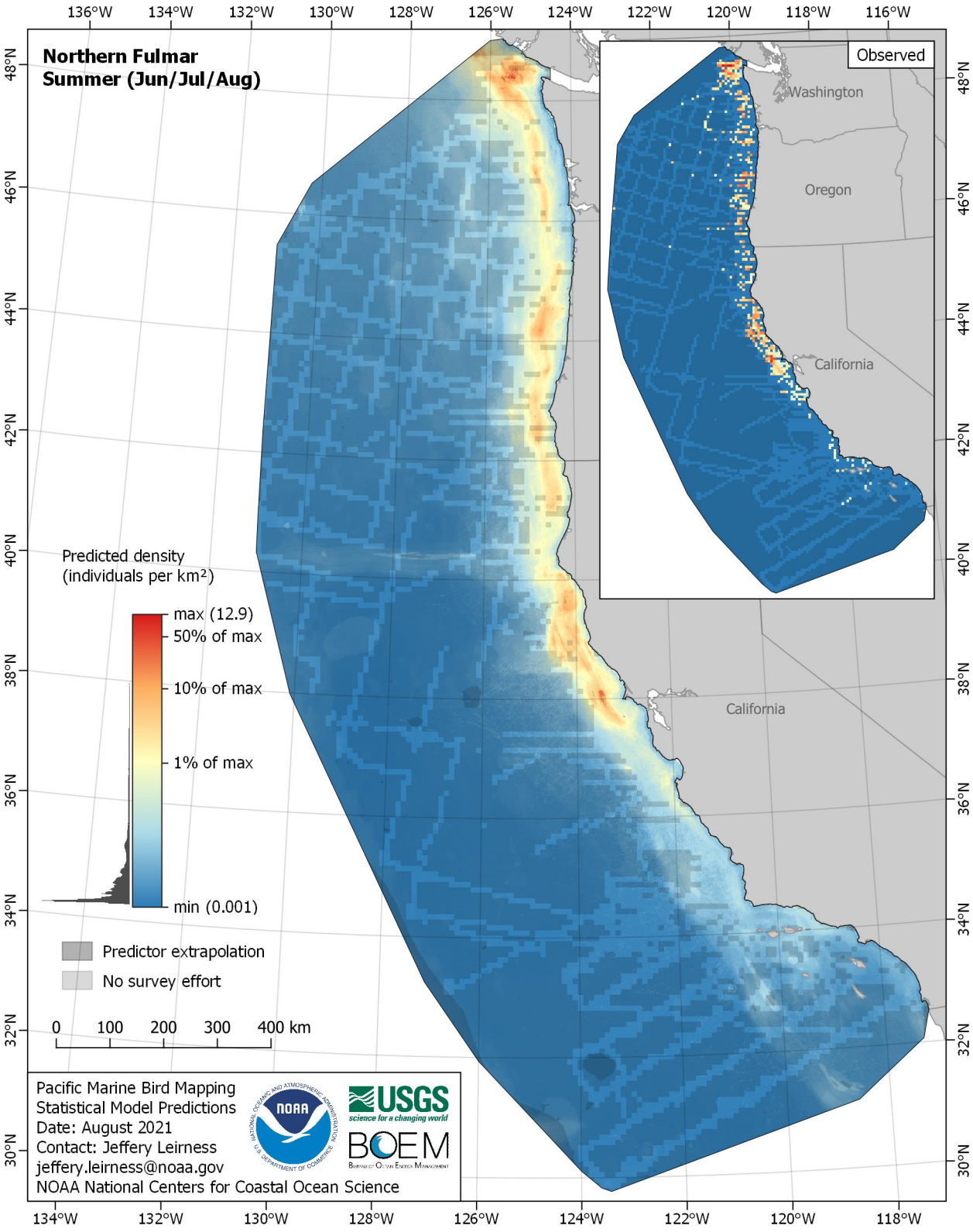

Figure E-209. Predicted density for Northern Fulmar (*Fulmarus glacialis*) in the summer season

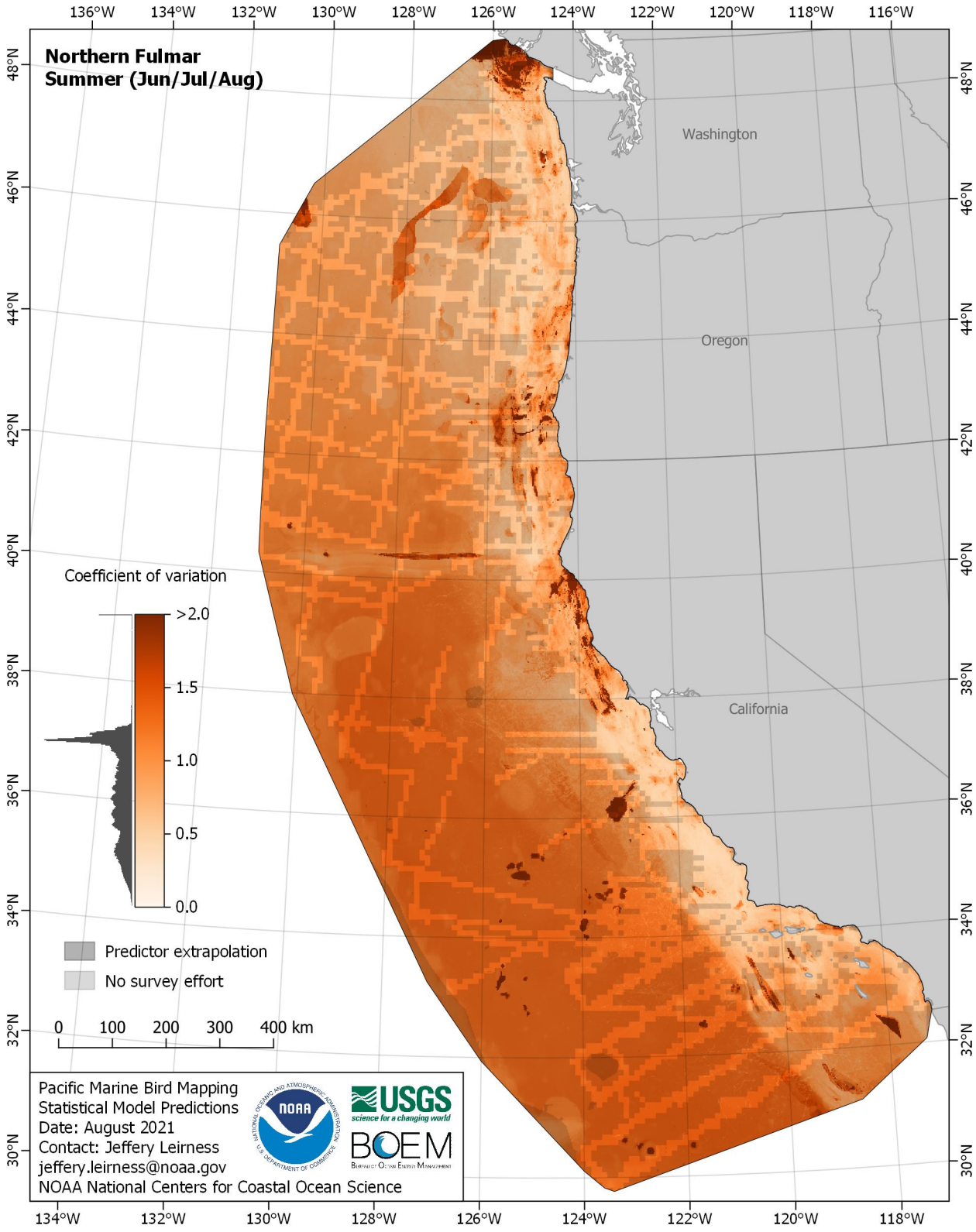

Figure E-210. Coefficient of variation for Northern Fulmar (*Fulmarus glacialis*) in the summer season

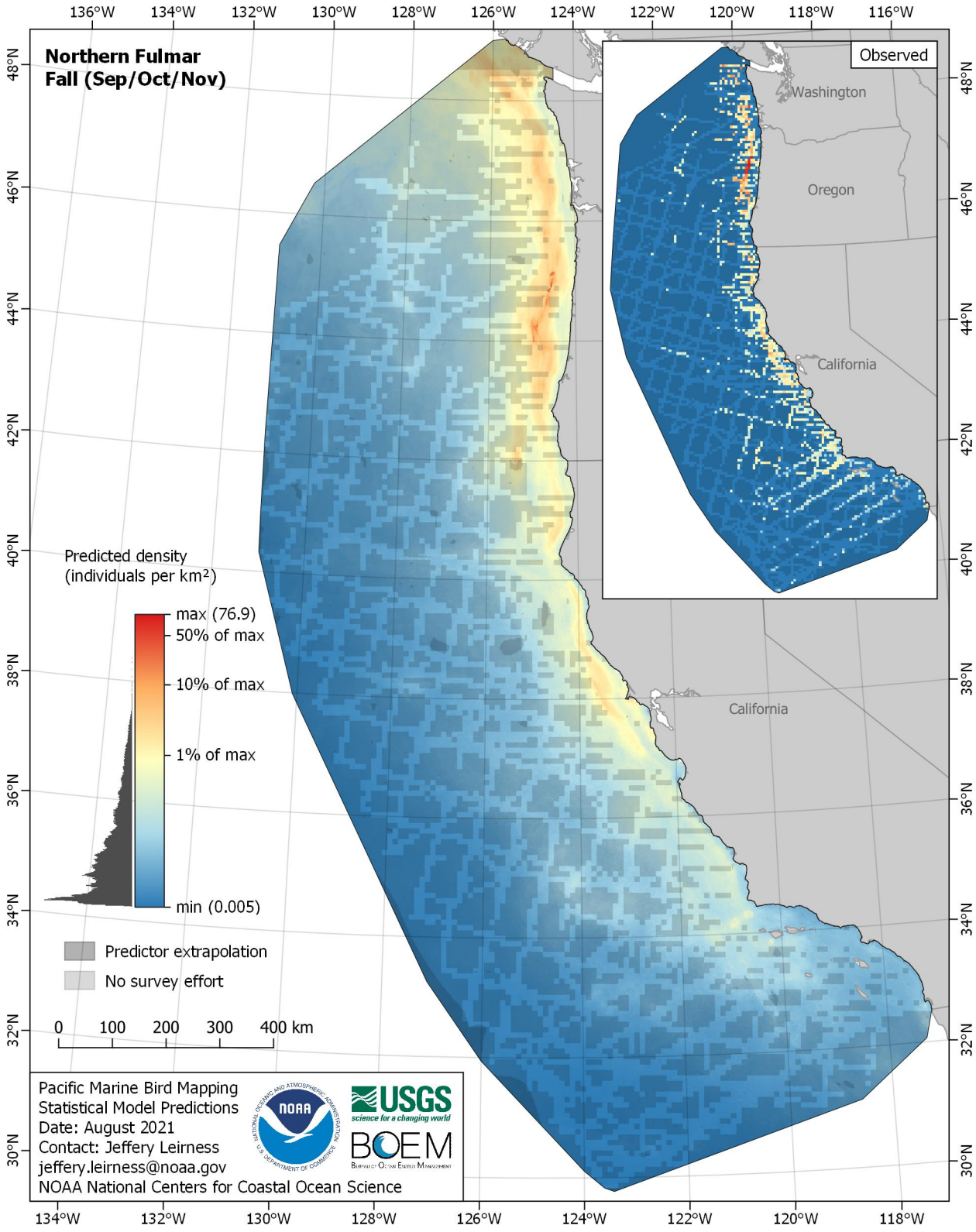

Figure E-211. Predicted density for Northern Fulmar (*Fulmarus glacialis*) in the fall season

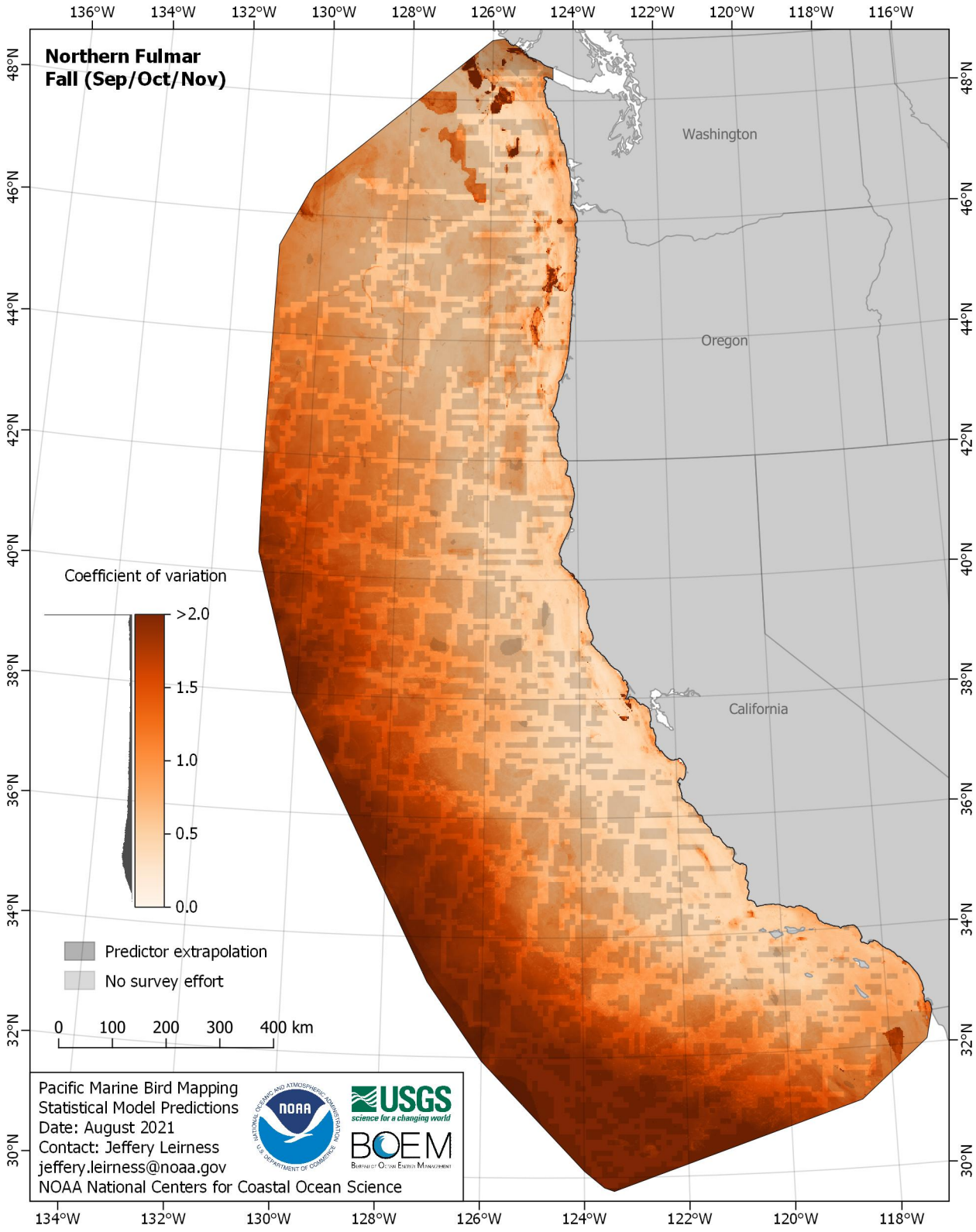

Figure E-212. Coefficient of variation for Northern Fulmar (*Fulmarus glacialis*) in the fall season

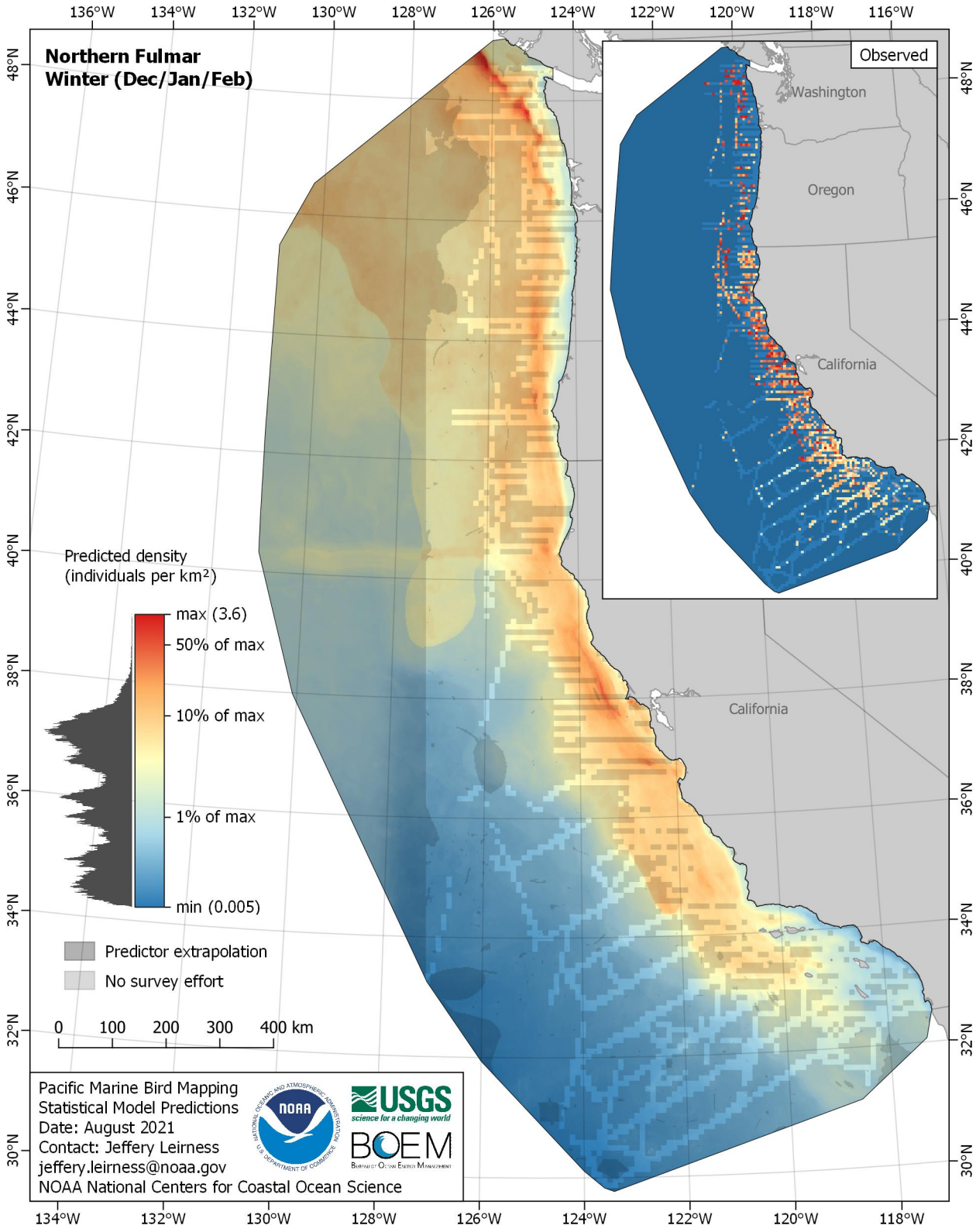

Figure E-213. Predicted density for Northern Fulmar (*Fulmarus glacialis*) in the winter season

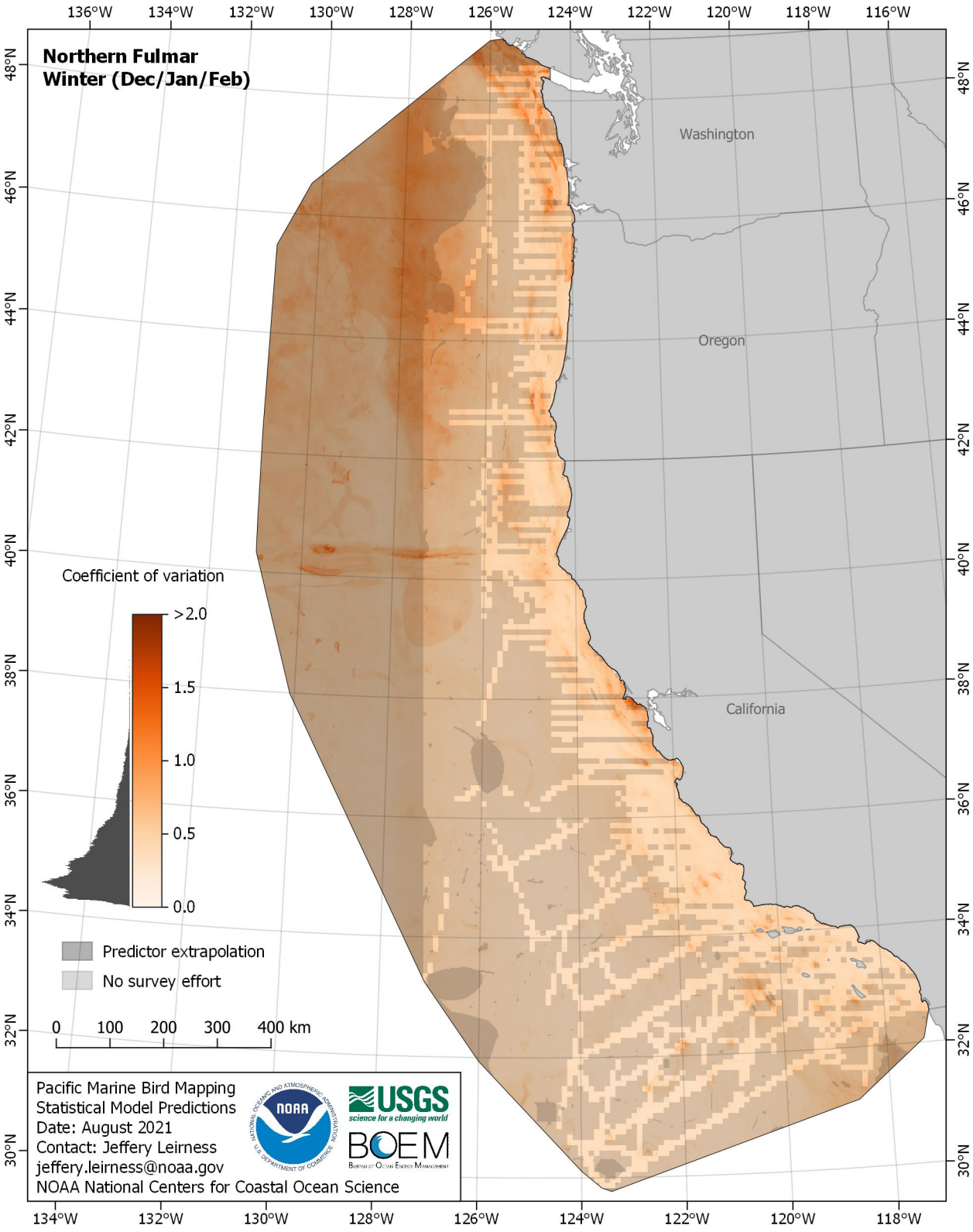

Figure E-214. Coefficient of variation for Northern Fulmar (*Fulmarus glacialis*) in the winter season

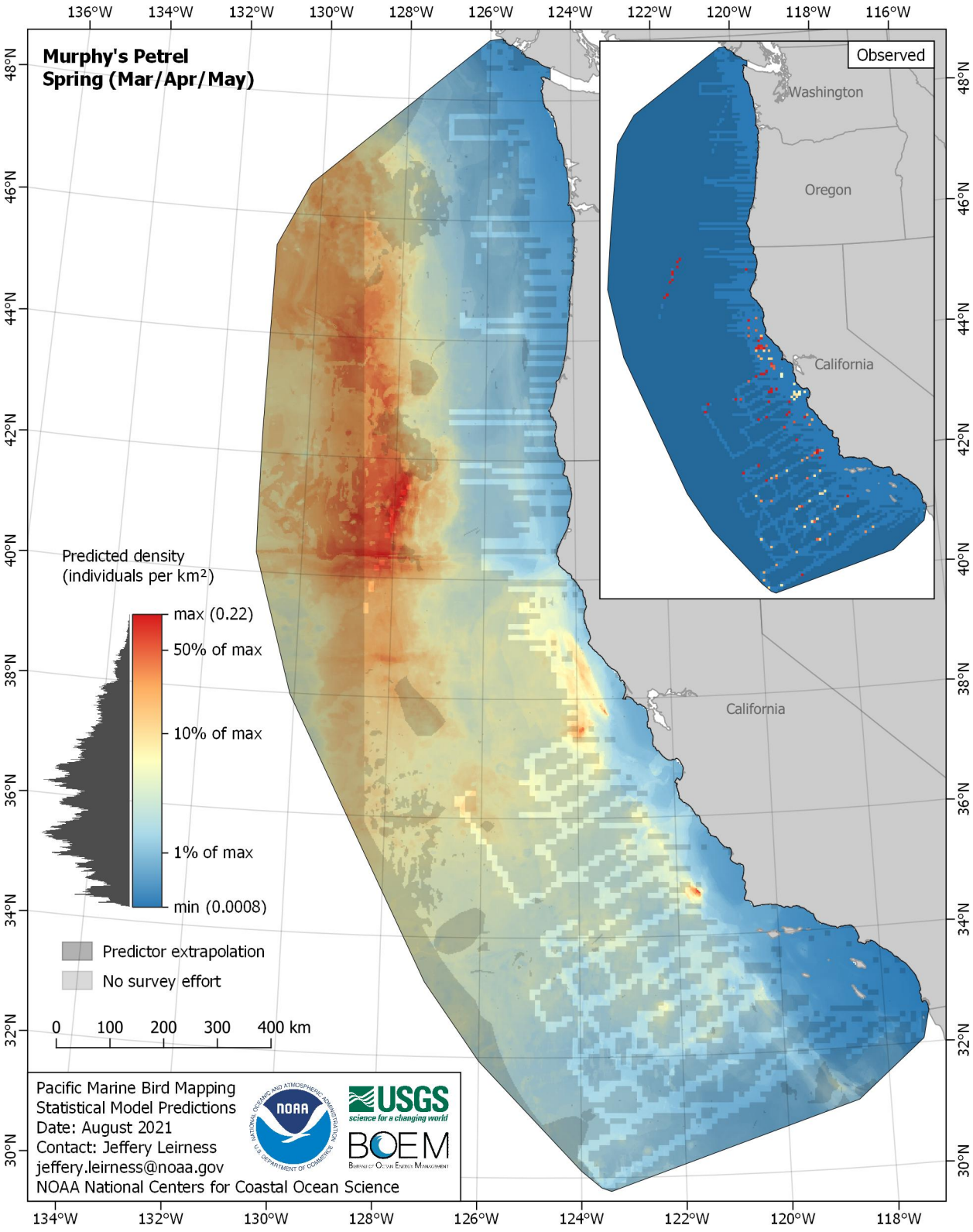

Figure E-215. Predicted density for Murphy's Petrel (*Pterodroma ultima*) in the spring season

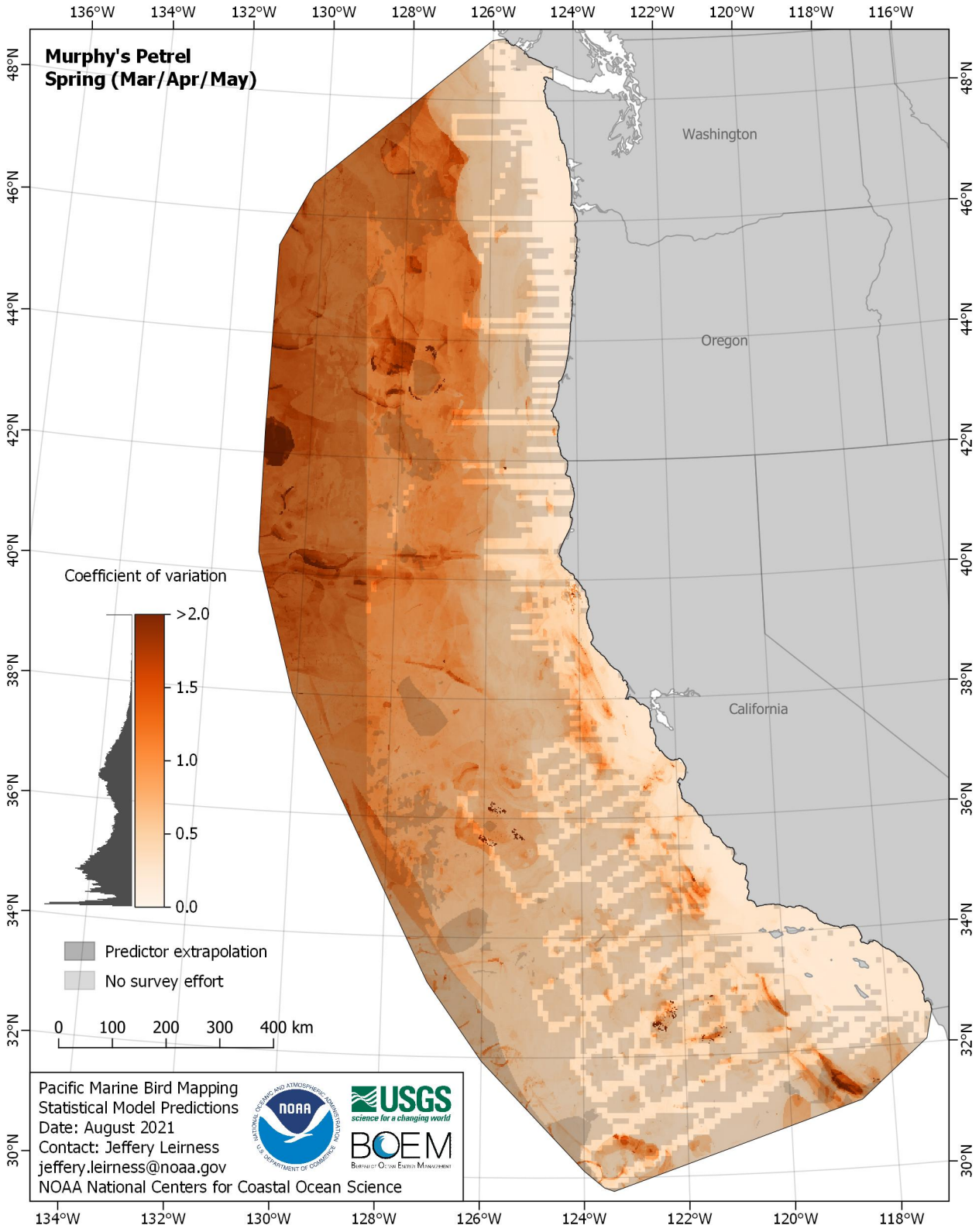

Figure E-216. Coefficient of variation for Murphy's Petrel (*Pterodroma ultima*) in the spring season

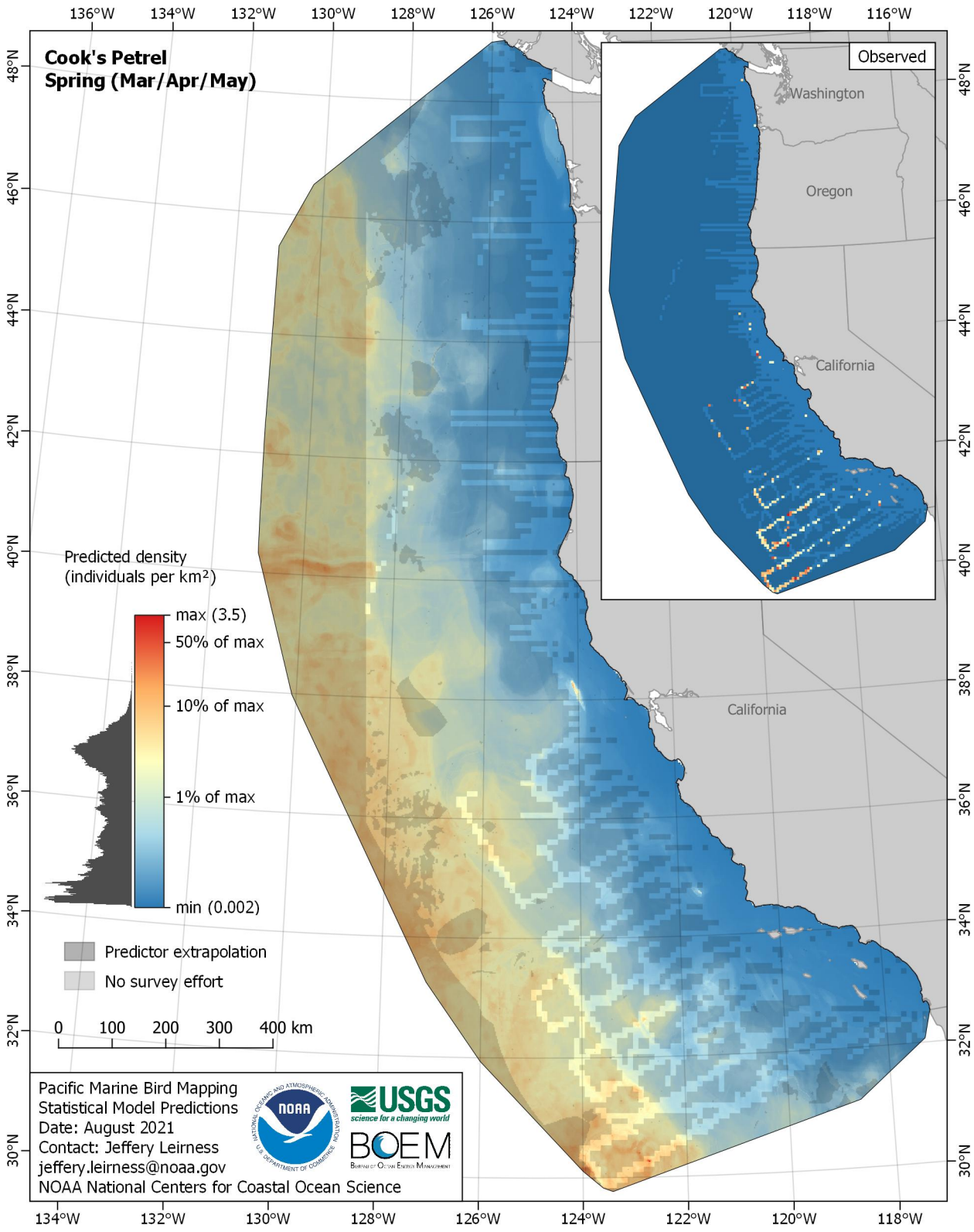

Figure E-217. Predicted density for Cook's Petrel (*Pterodroma cookii*) in the spring season

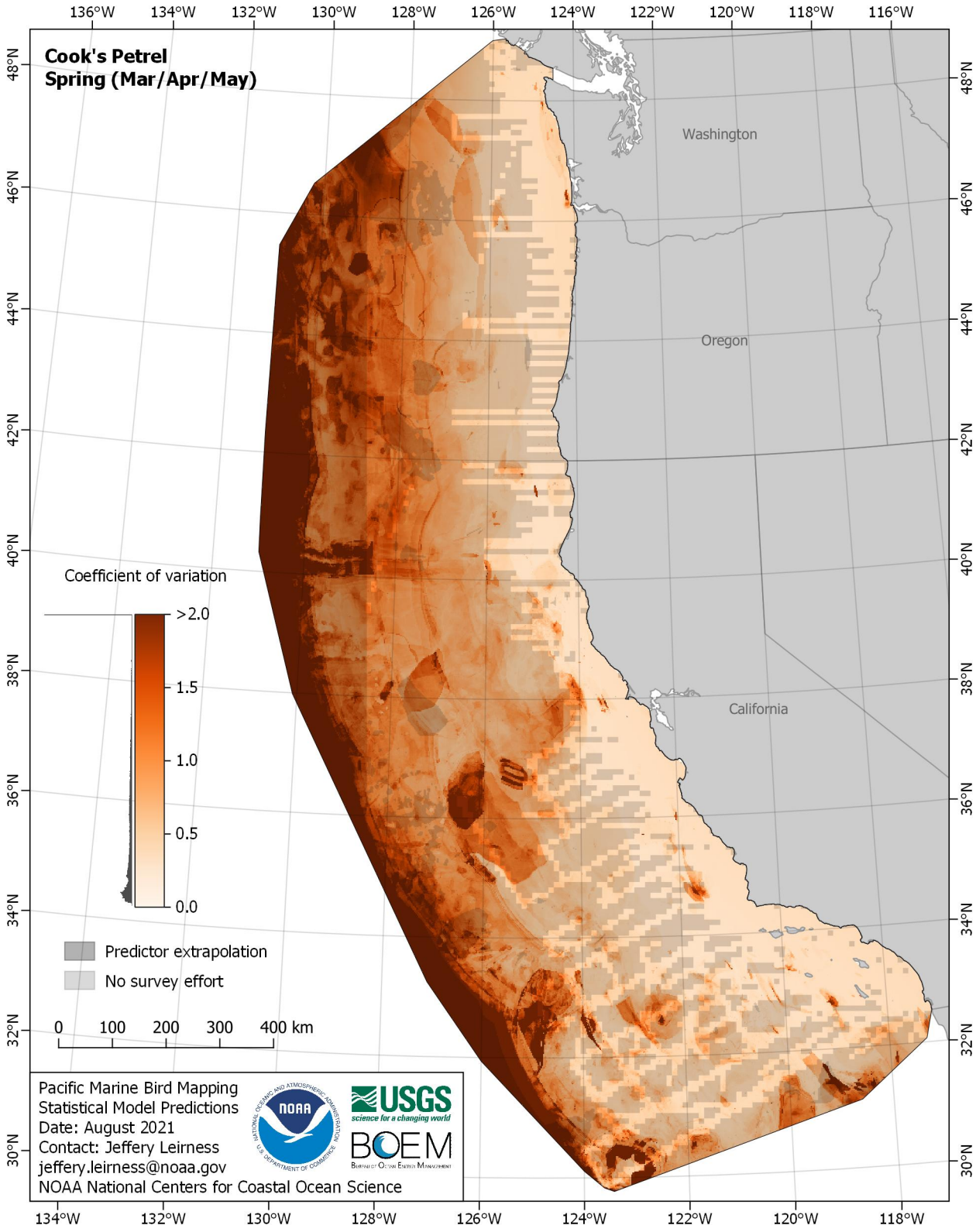

Figure E-218. Coefficient of variation for Cook's Petrel (*Pterodroma cookii*) in the spring season

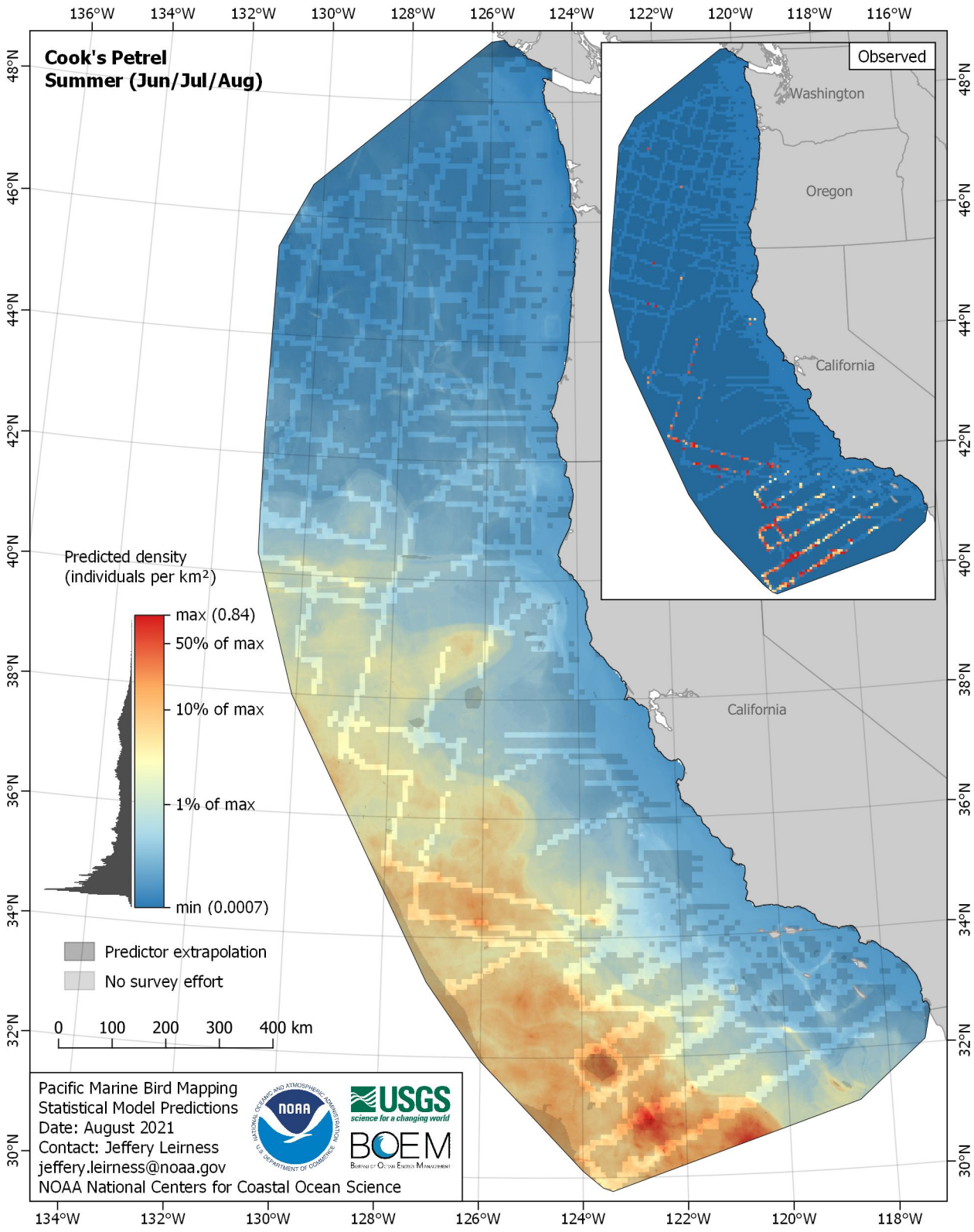

Figure E-219. Predicted density for Cook's Petrel (*Pterodroma cookii*) in the summer season

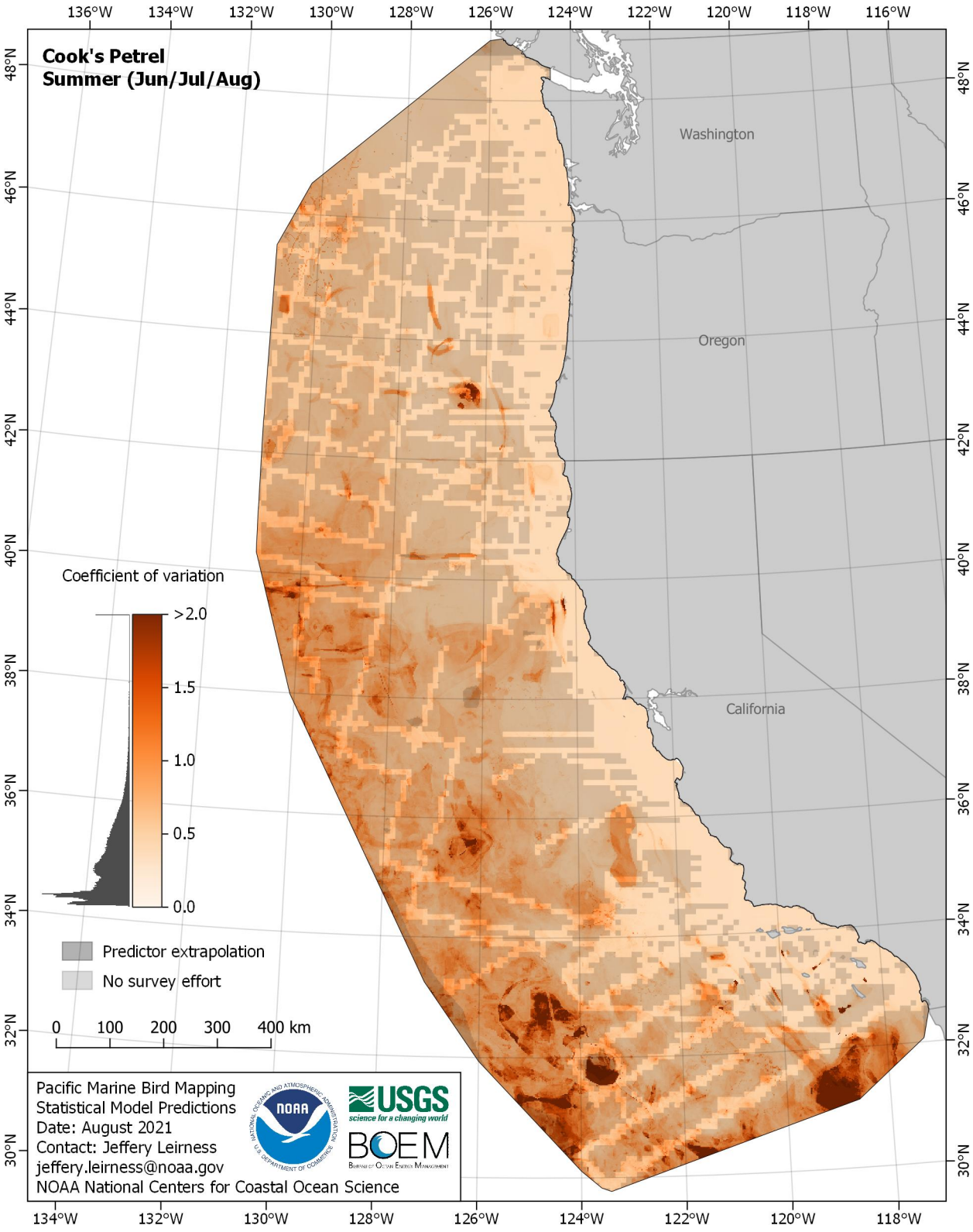

Figure E-220. Coefficient of variation for Cook's Petrel (*Pterodroma cookii*) in the summer season

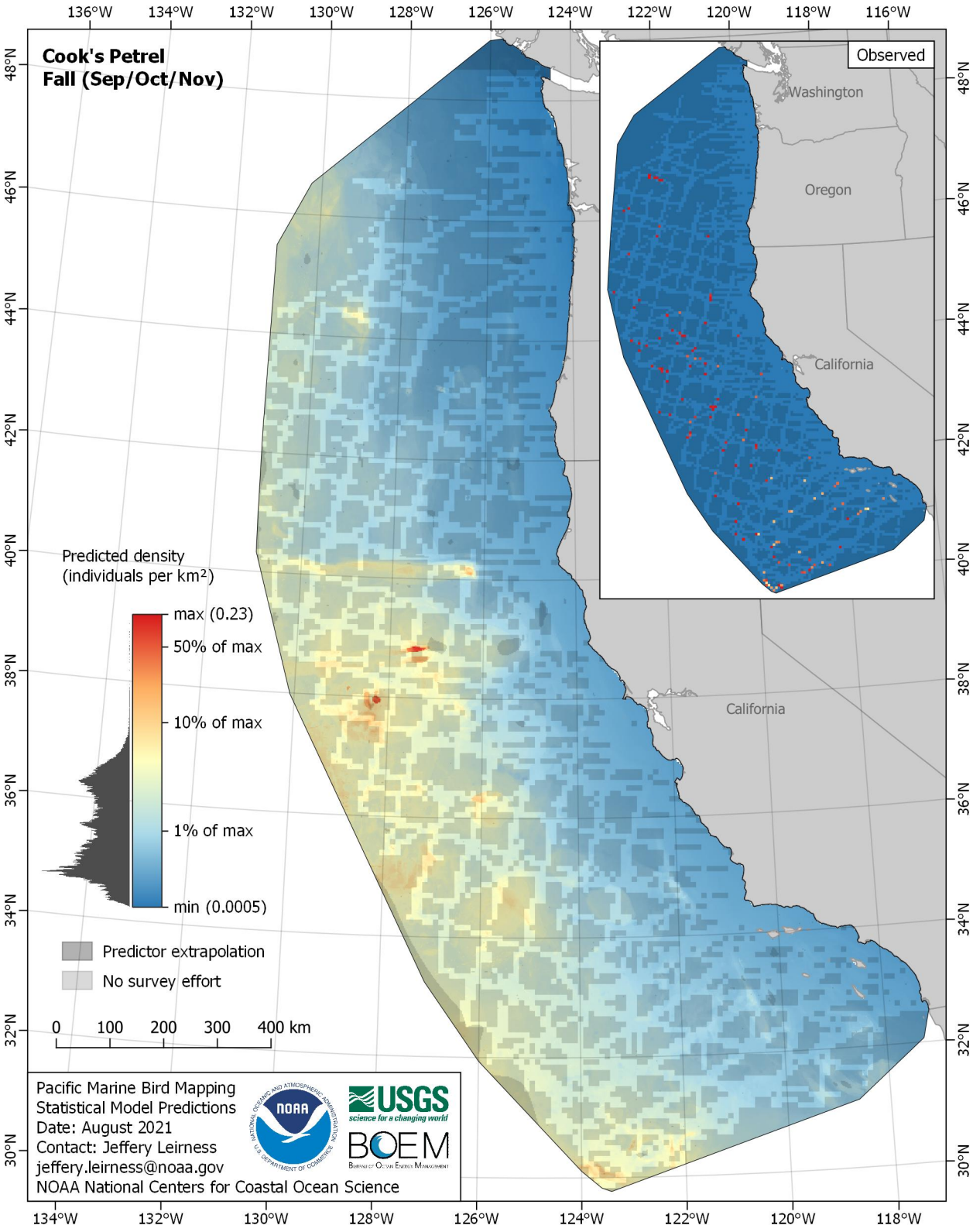

Figure E-221. Predicted density for Cook's Petrel (*Pterodroma cookii*) in the fall season

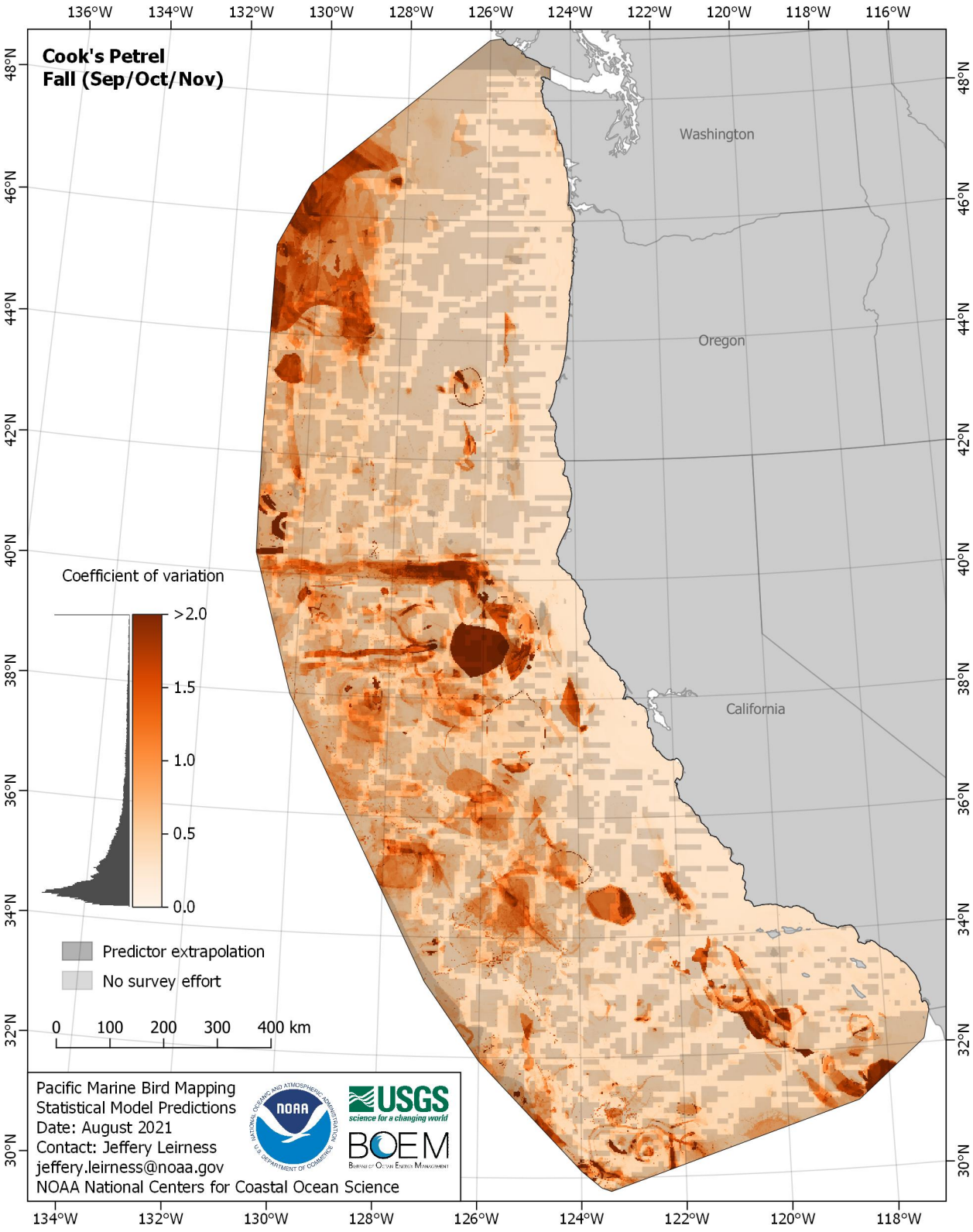

Figure E-222. Coefficient of variation for Cook's Petrel (*Pterodroma cookii*) in the fall season

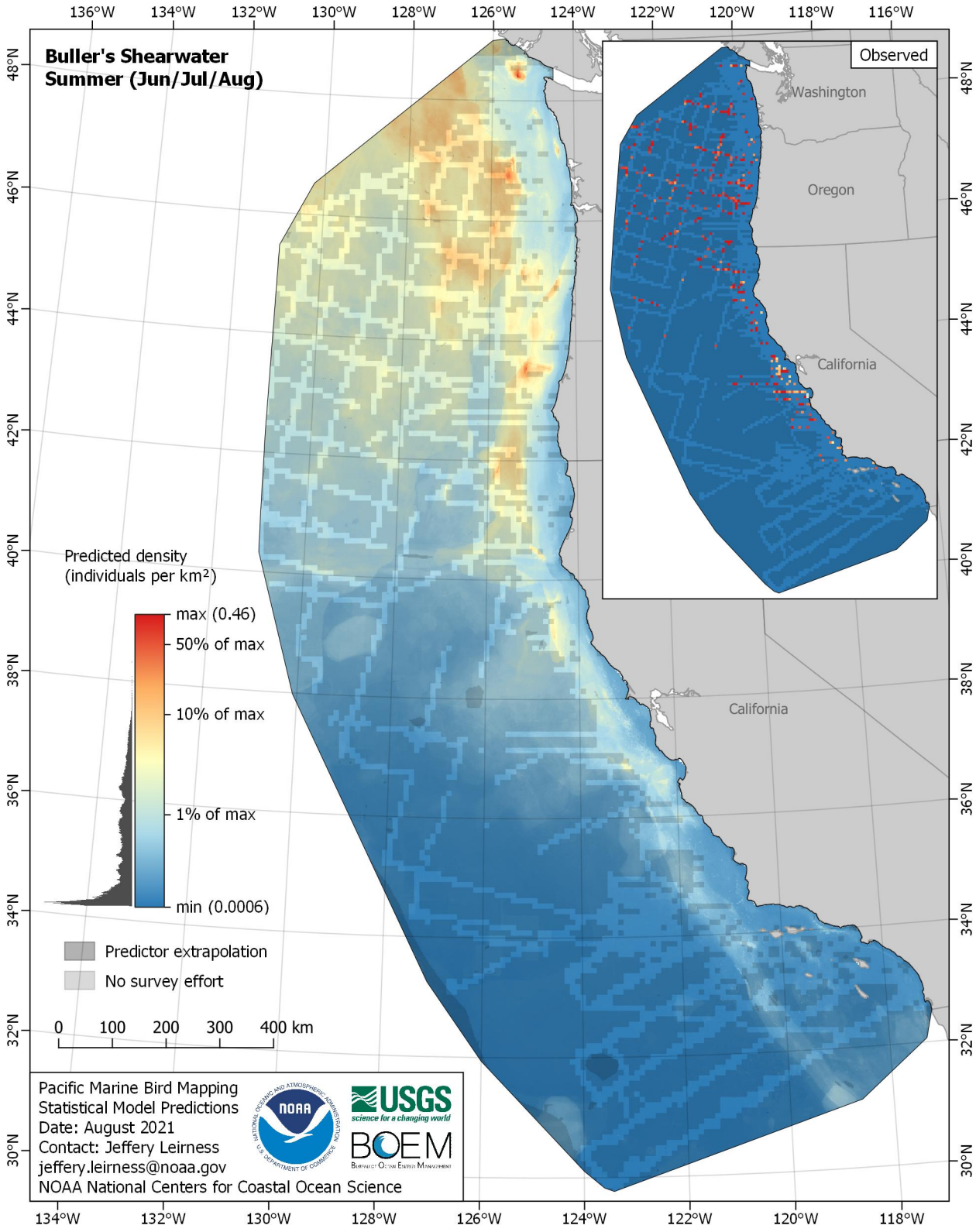

Figure E-223. Predicted density for Buller's Shearwater (*Ardenna bulleri*) in the summer season

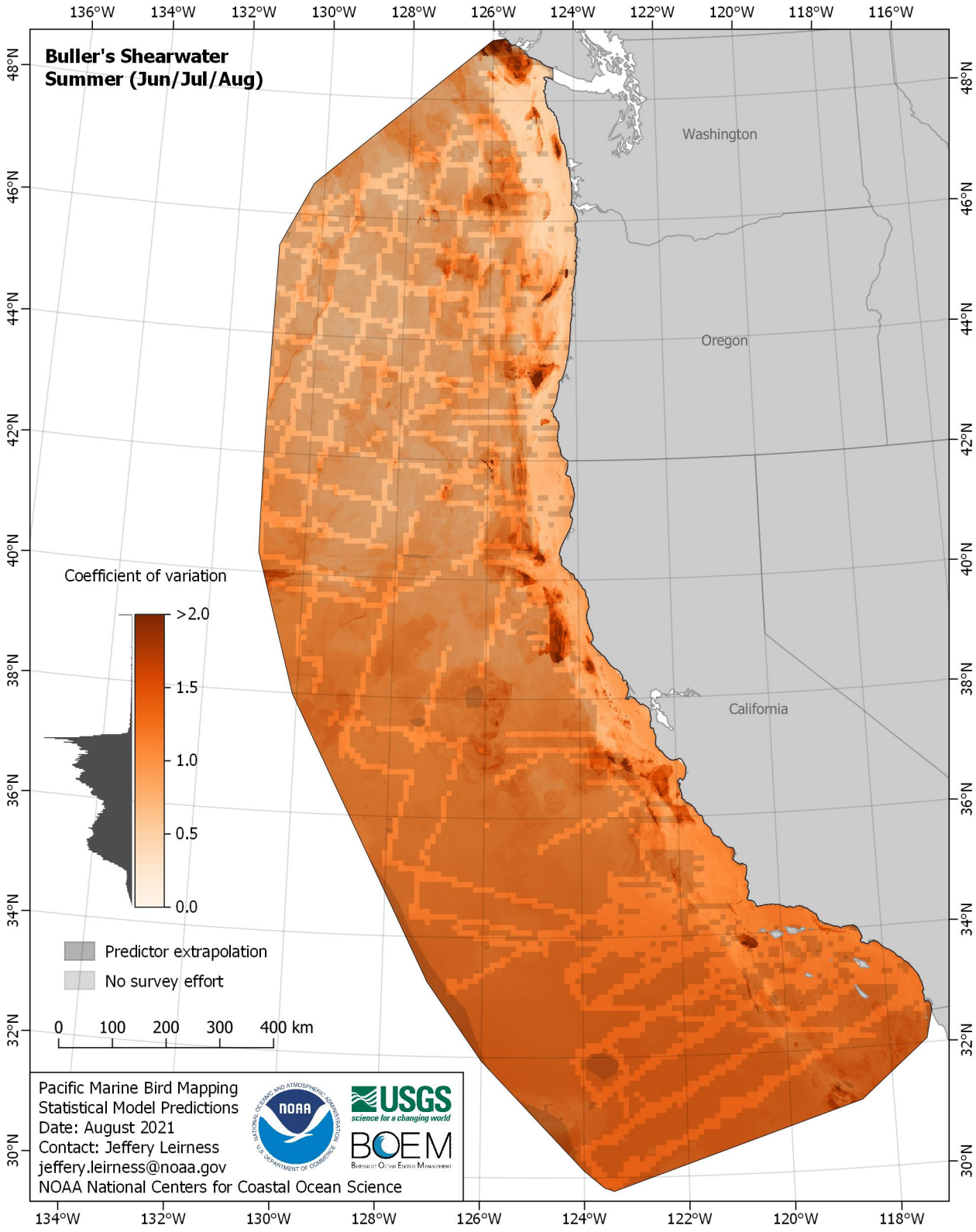

Figure E-224. Coefficient of variation for Buller's Shearwater (*Ardenna bulleri*) in the summer season

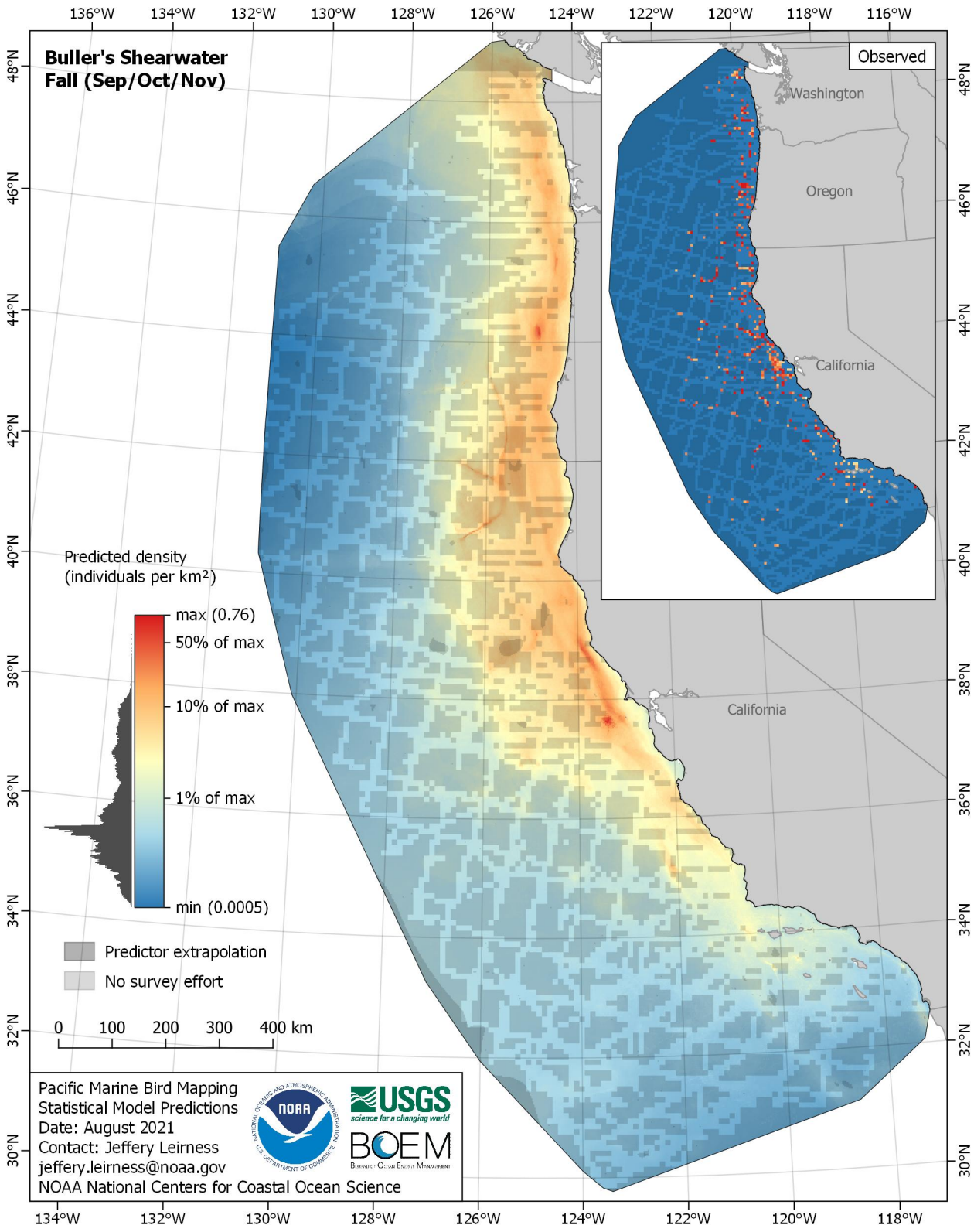

Figure E-225. Predicted density for Buller's Shearwater (*Ardenna bulleri*) in the fall season

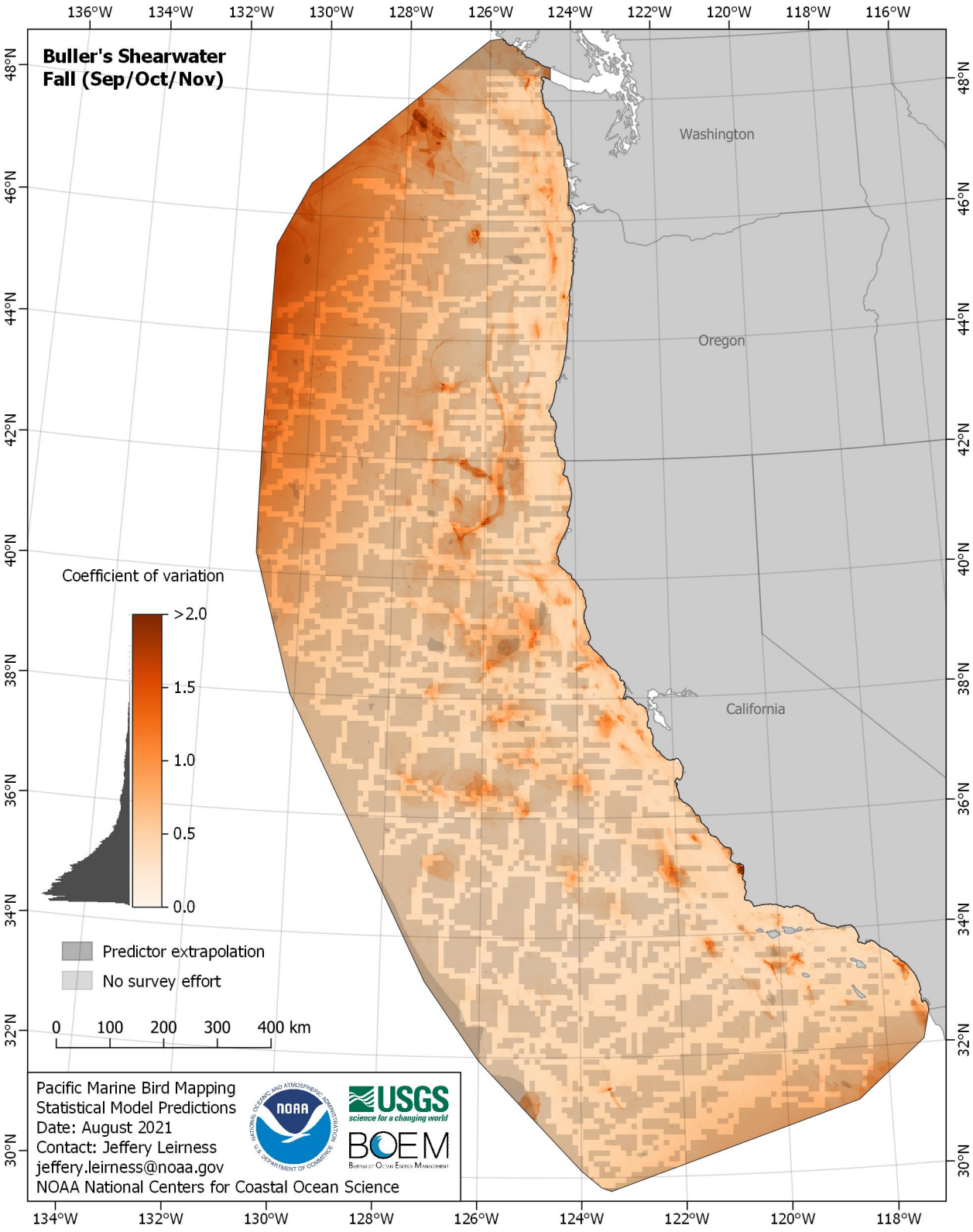

Figure E-226. Coefficient of variation for Buller's Shearwater (*Ardenna bulleri*) in the fall season

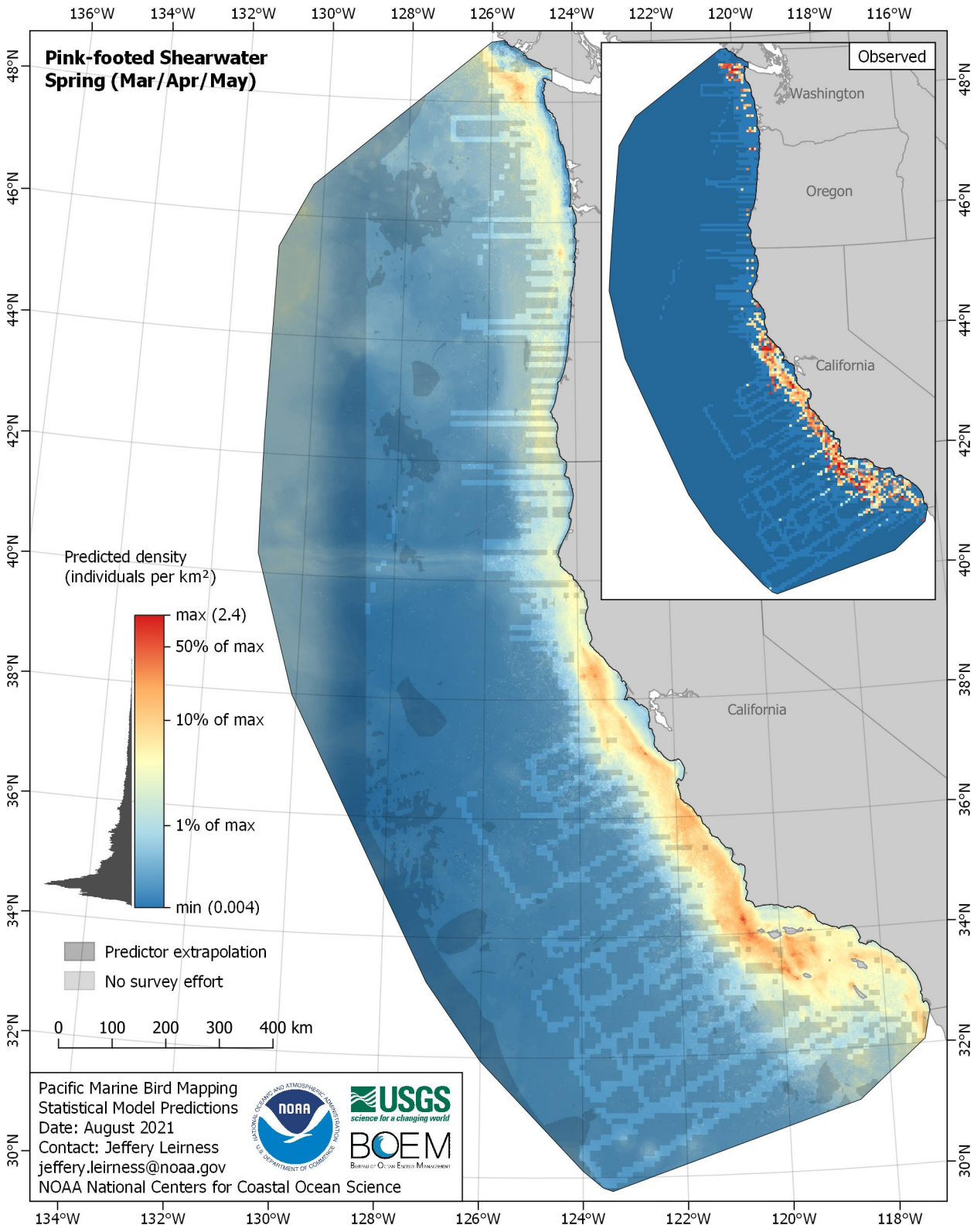

Figure E-227. Predicted density for Pink-footed Shearwater (*Ardenna creatopus*) in the spring season

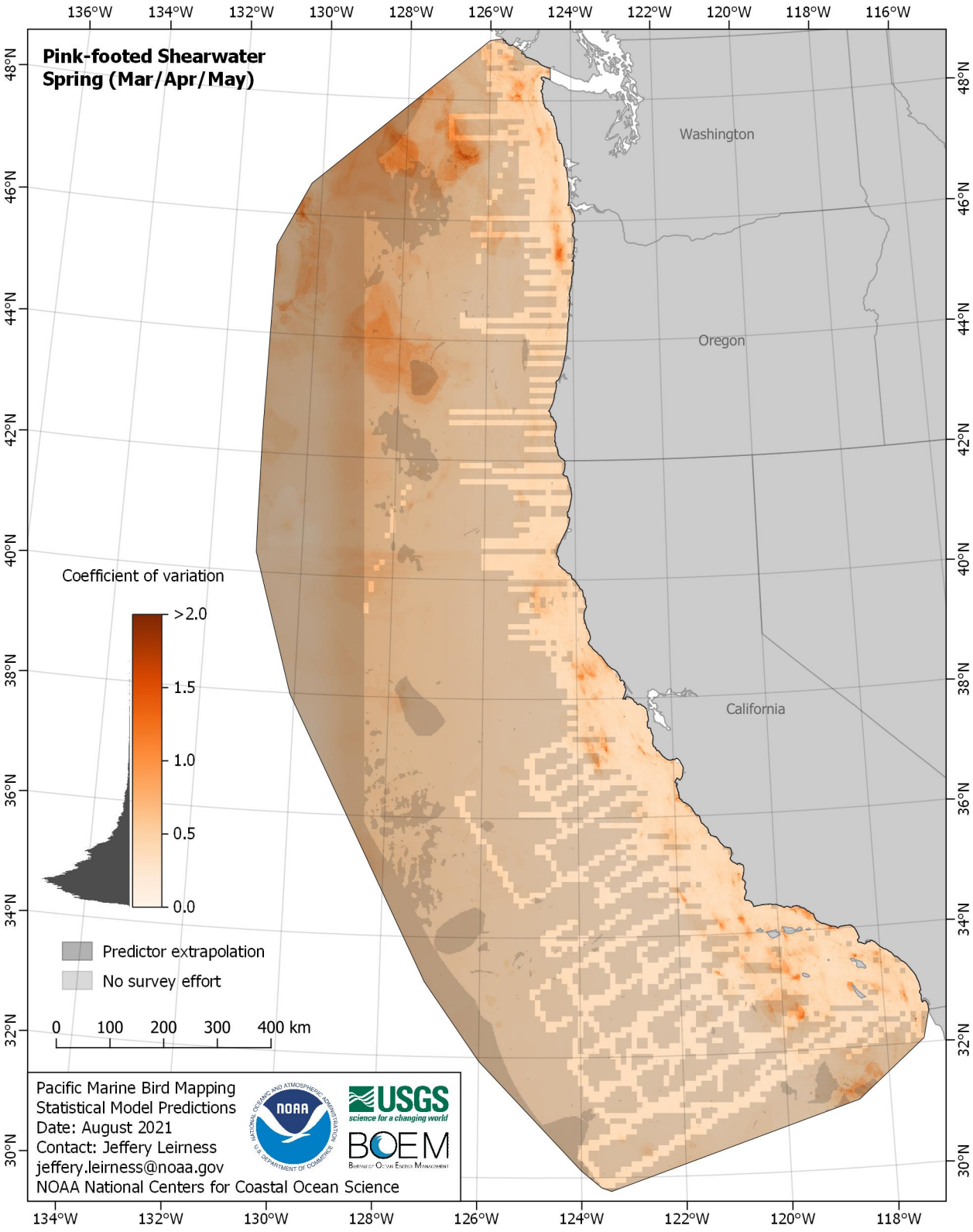

Figure E-228. Coefficient of variation for Pink-footed Shearwater (*Ardenna creatopus*) in the spring season

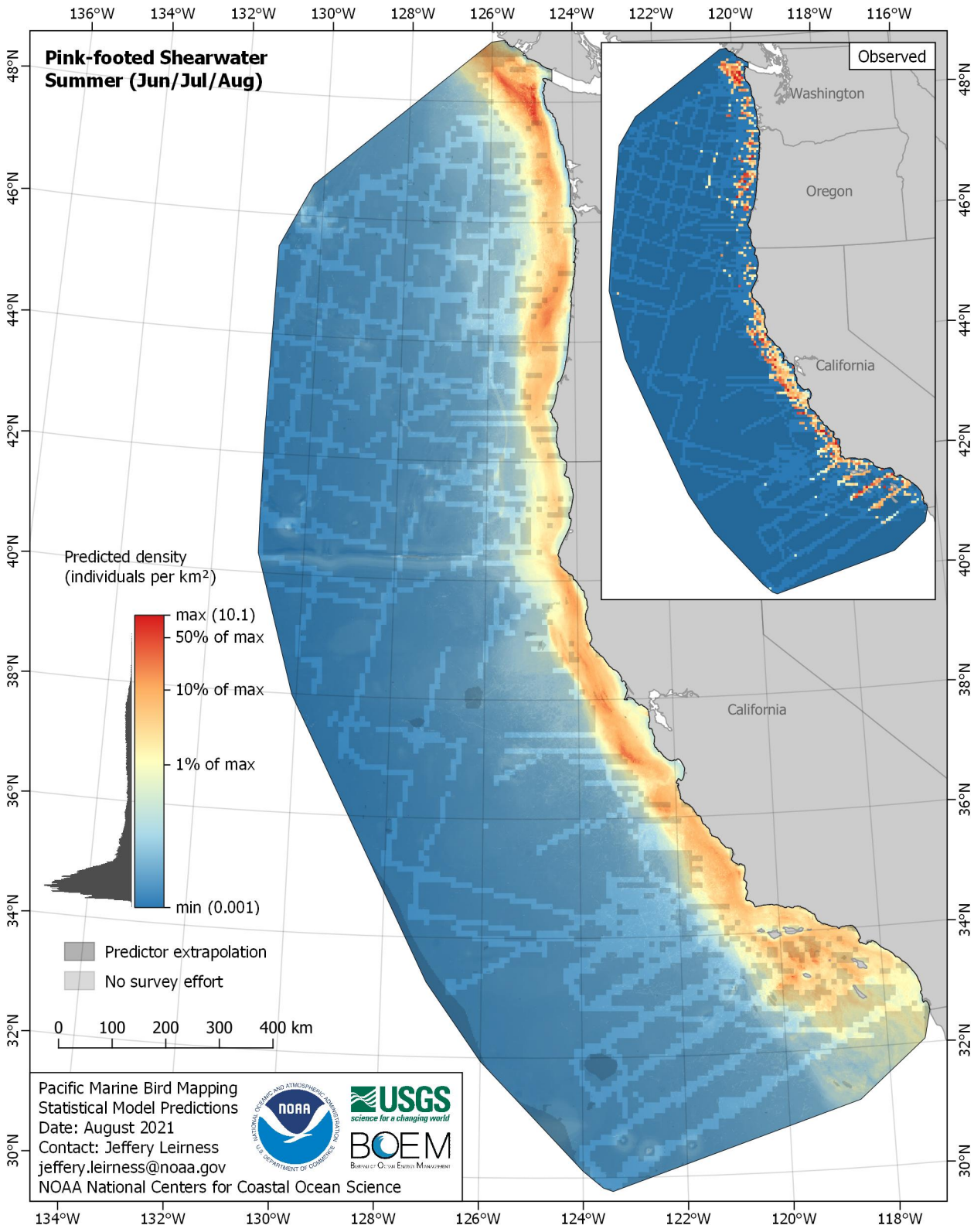

Figure E-229. Predicted density for Pink-footed Shearwater (*Ardenna creatopus*) in the summer season

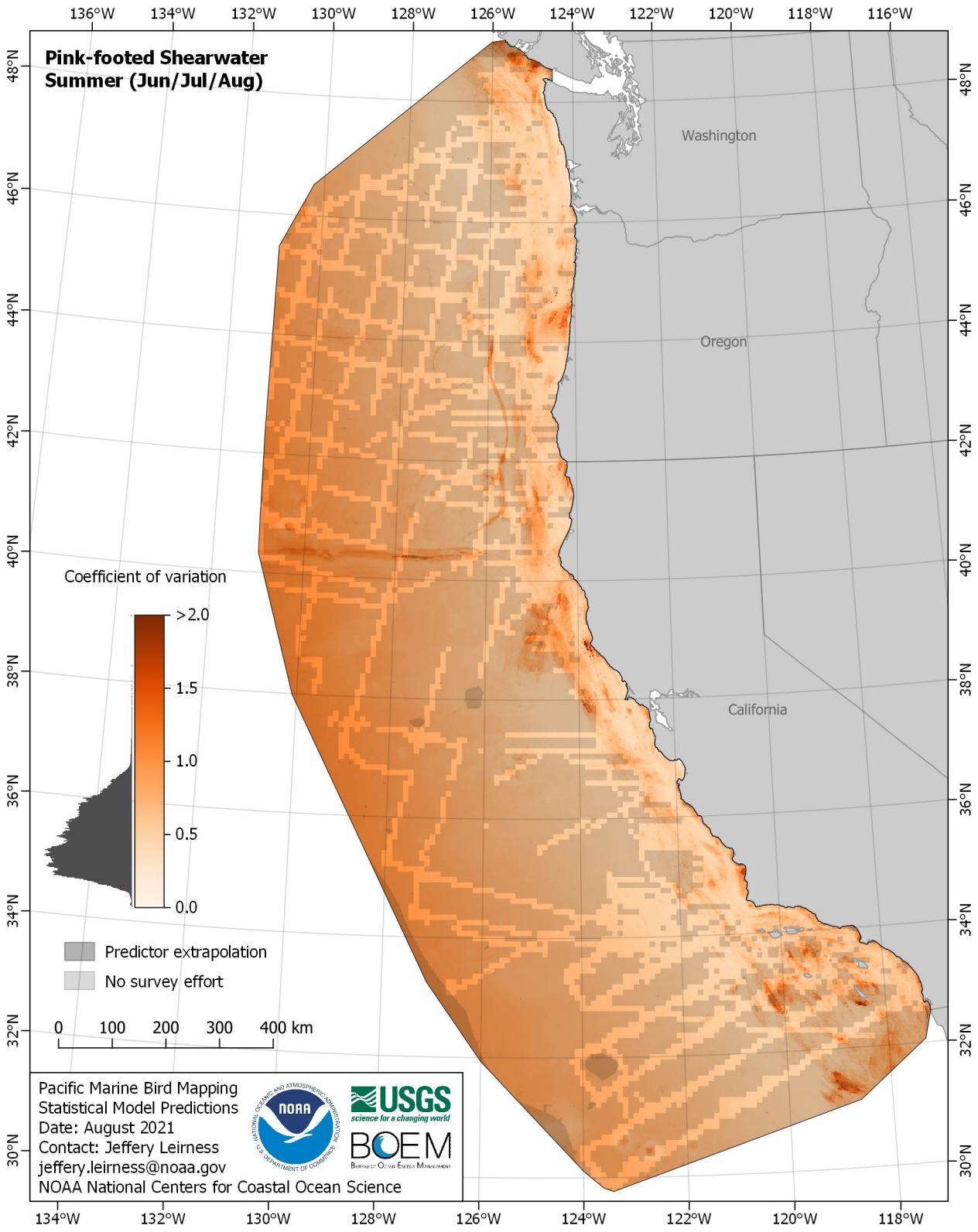

Figure E-230. Coefficient of variation for Pink-footed Shearwater (*Ardenna creatopus*) in the summer season

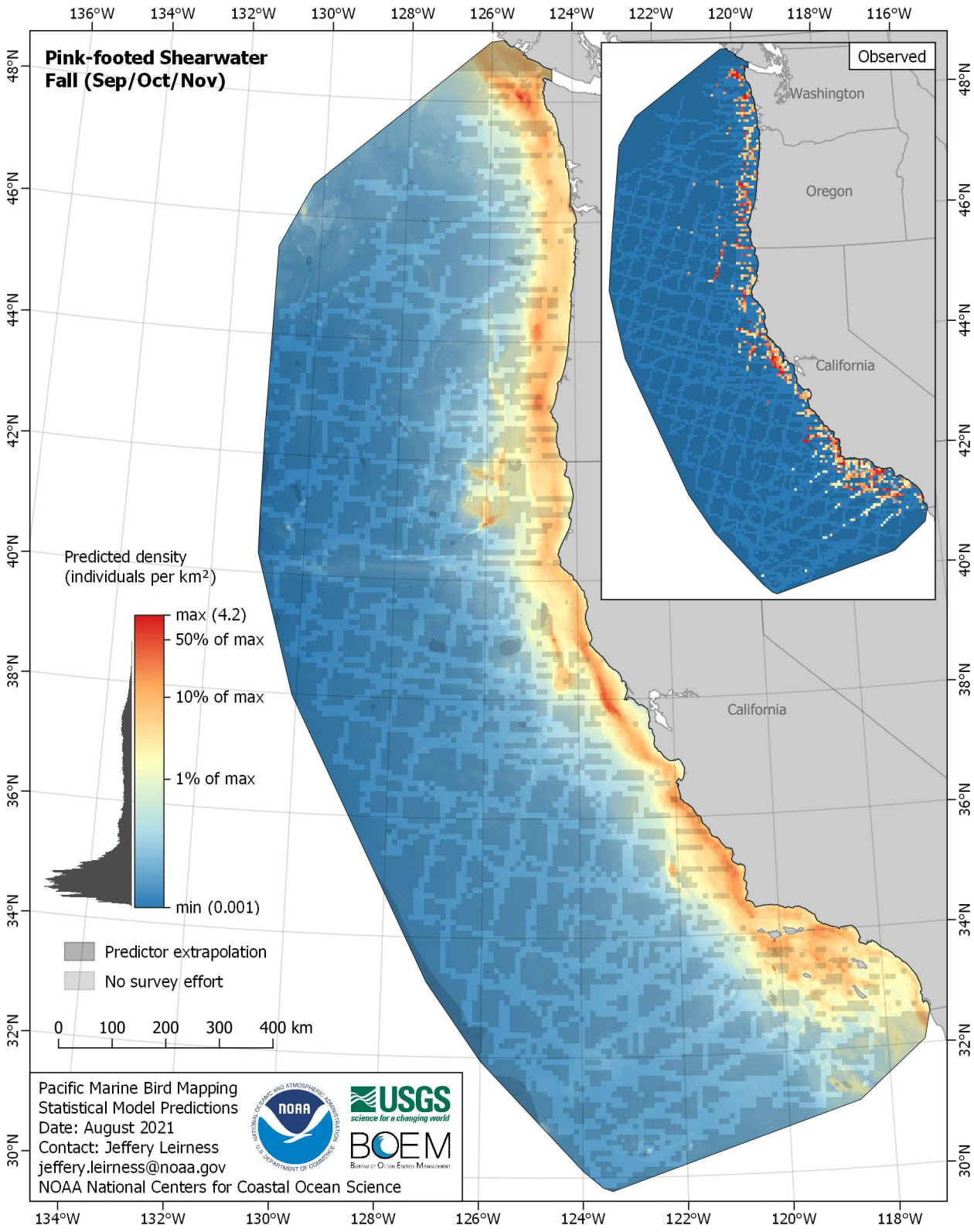

Figure E-231. Predicted density for Pink-footed Shearwater (*Ardenna creatopus*) in the fall season

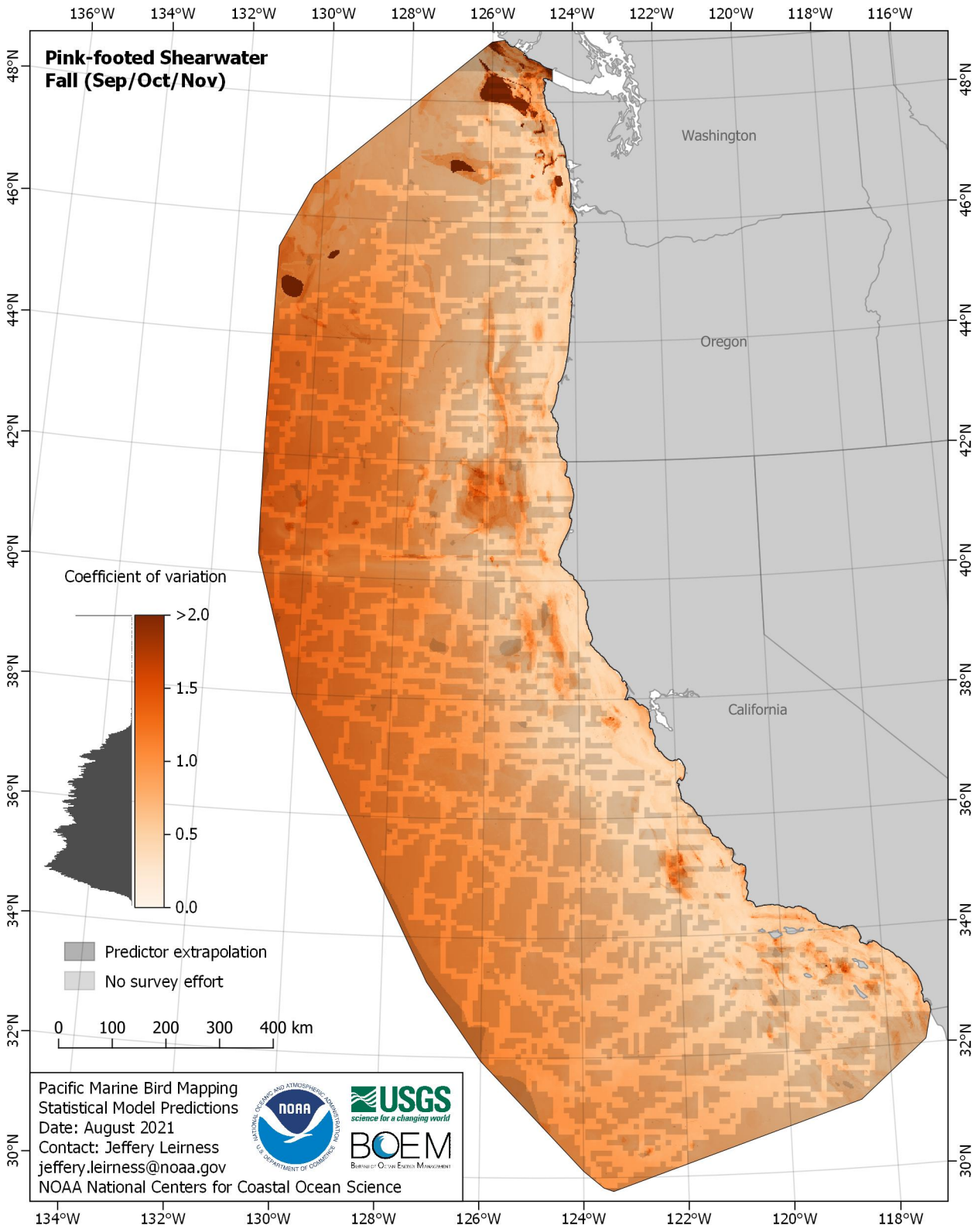

Figure E-232. Coefficient of variation for Pink-footed Shearwater (*Ardenna creatopus*) in the fall season

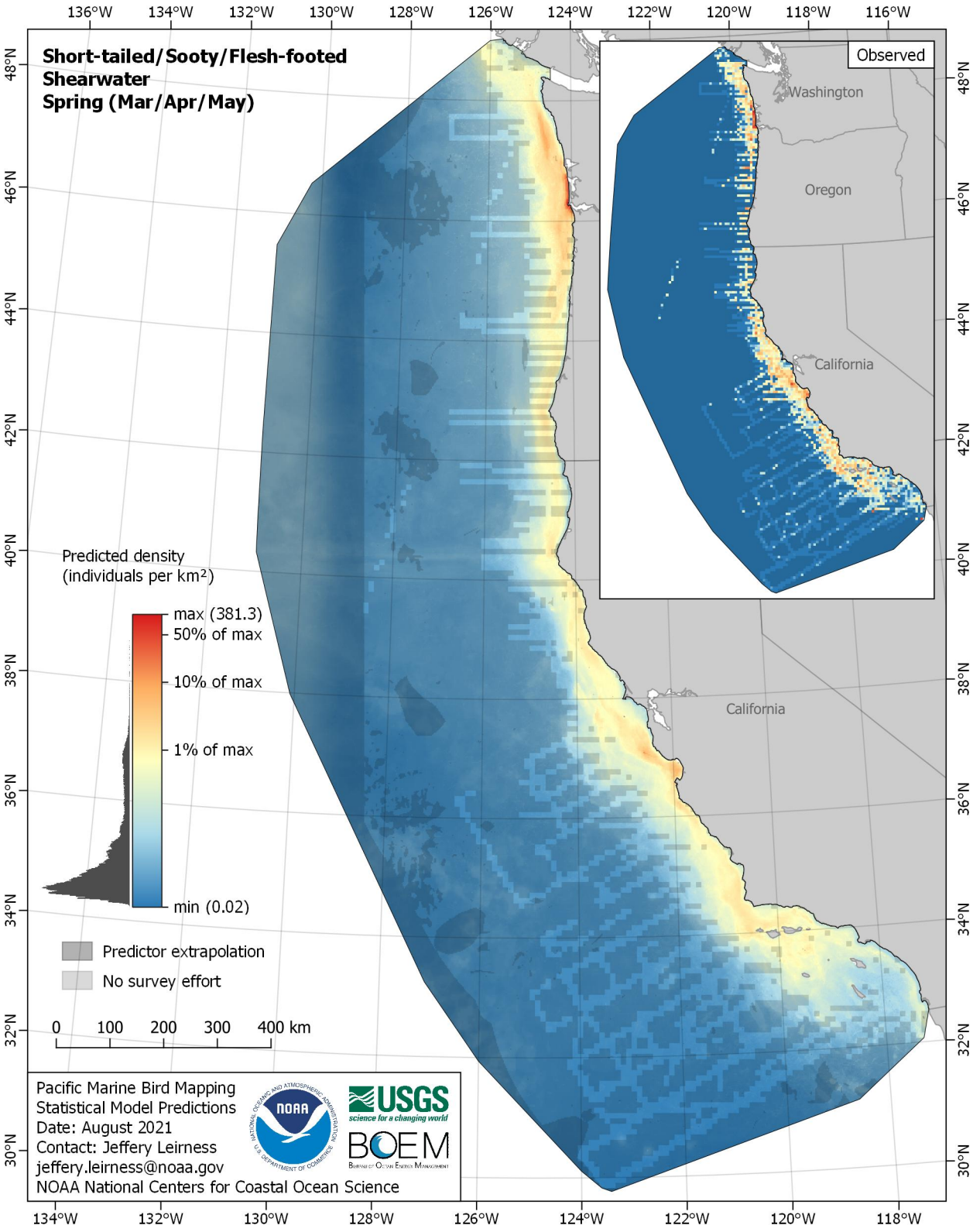

Figure E-233. Predicted density for Short-tailed/Sooty/Flesh-footed Shearwater (*Ardenna tenuirostris/grisea/carneipes*) in the spring season

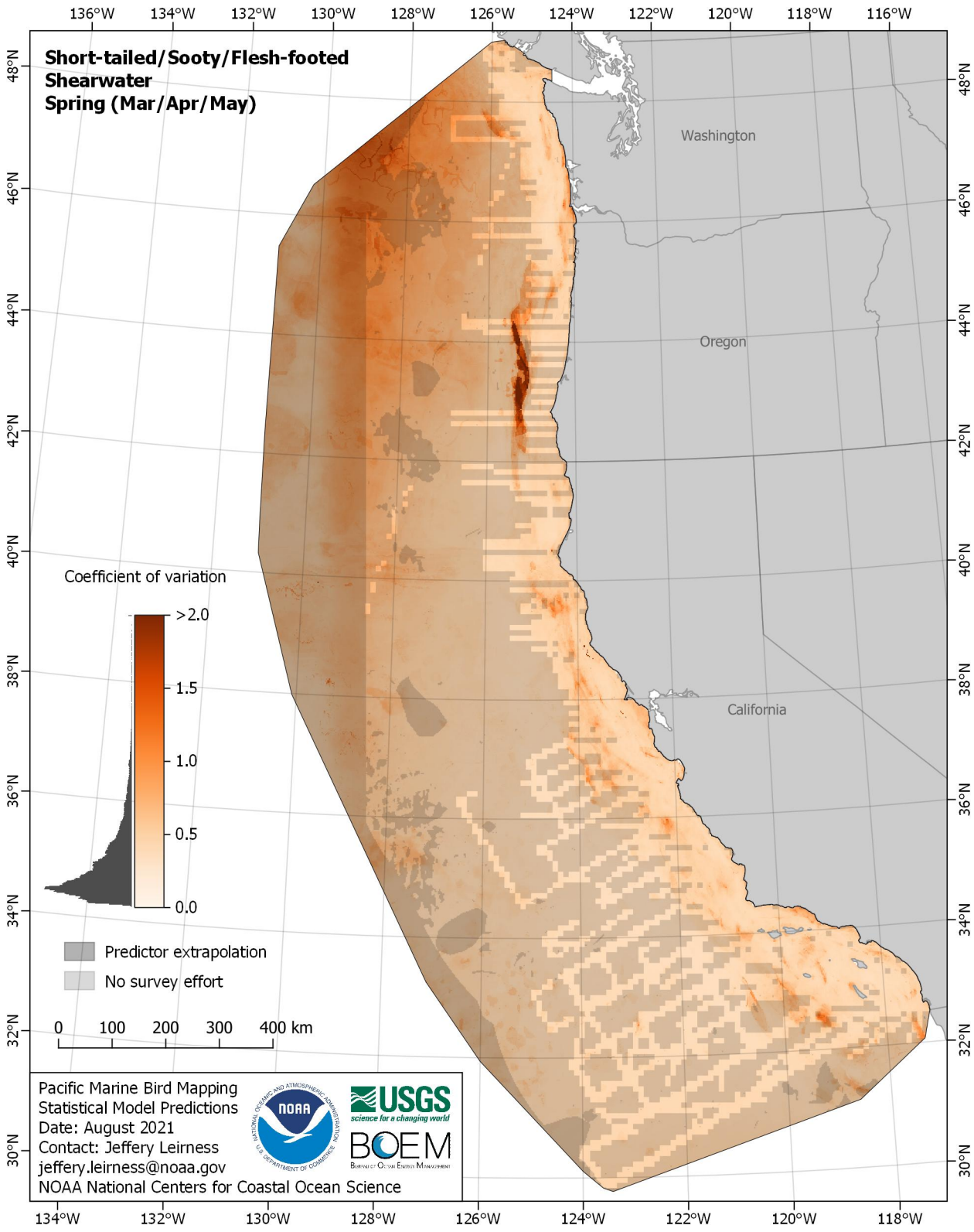

Figure E-234. Coefficient of variation for Short-tailed/Sooty/Flesh-footed Shearwater (*Ardenna tenuirostris/grisea/carneipes*) in the spring season

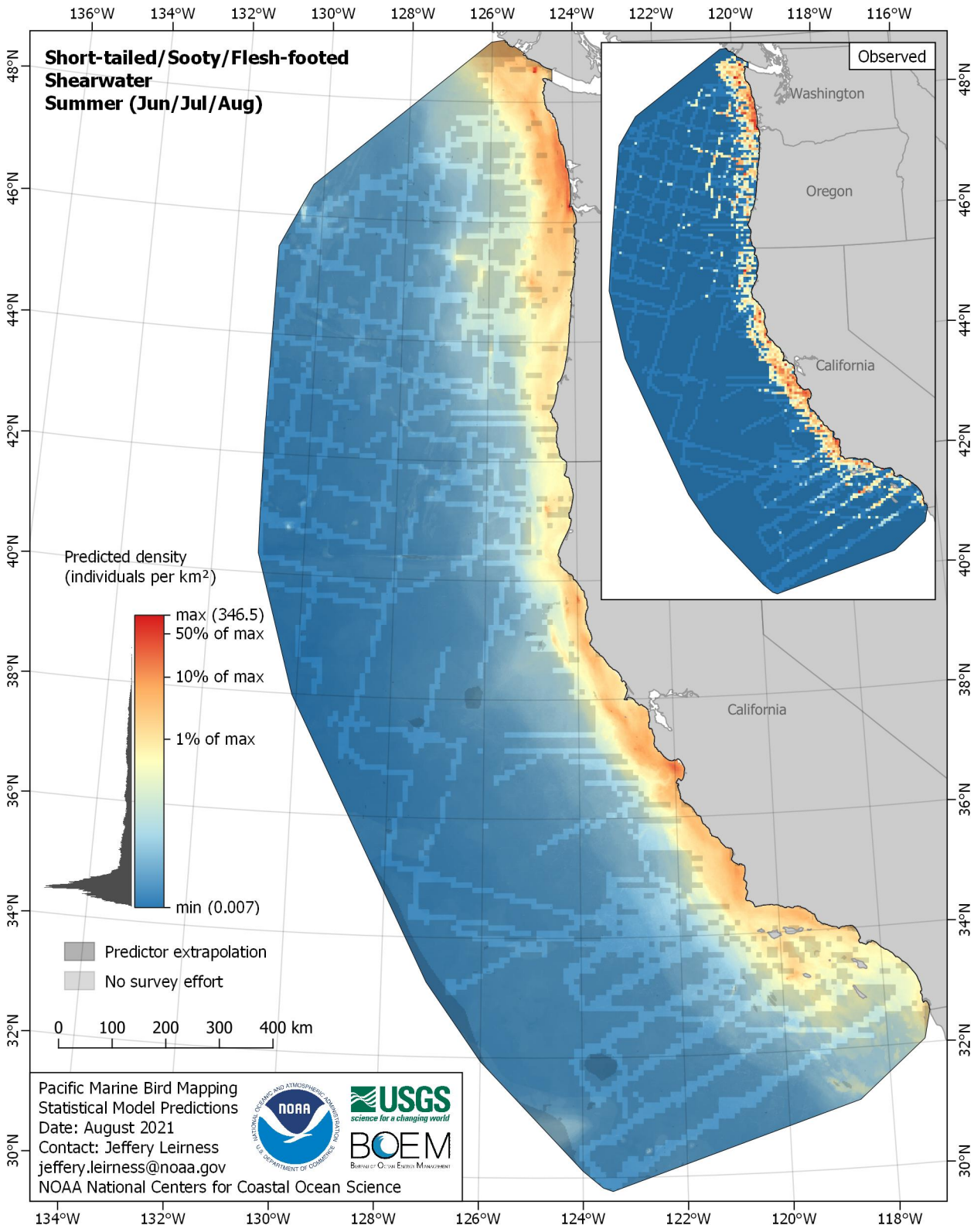

Figure E-235. Predicted density for Short-tailed/Sooty/Flesh-footed Shearwater (*Ardenna tenuirostris/grisea/carneipes*) in the summer season

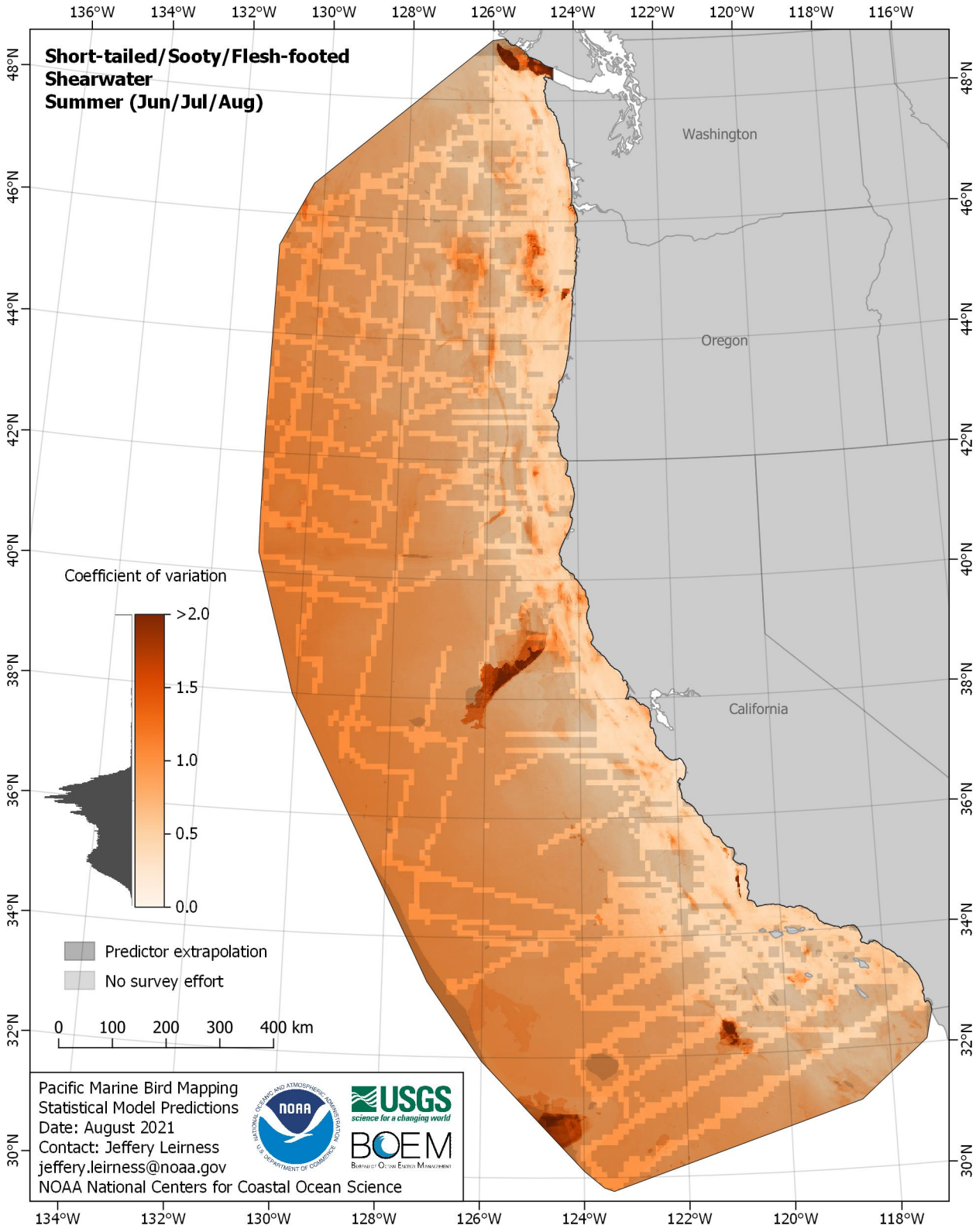

Figure E-236. Coefficient of variation for Short-tailed/Sooty/Flesh-footed Shearwater (*Ardenna tenuirostris/grisea/carneipes*) in the summer season

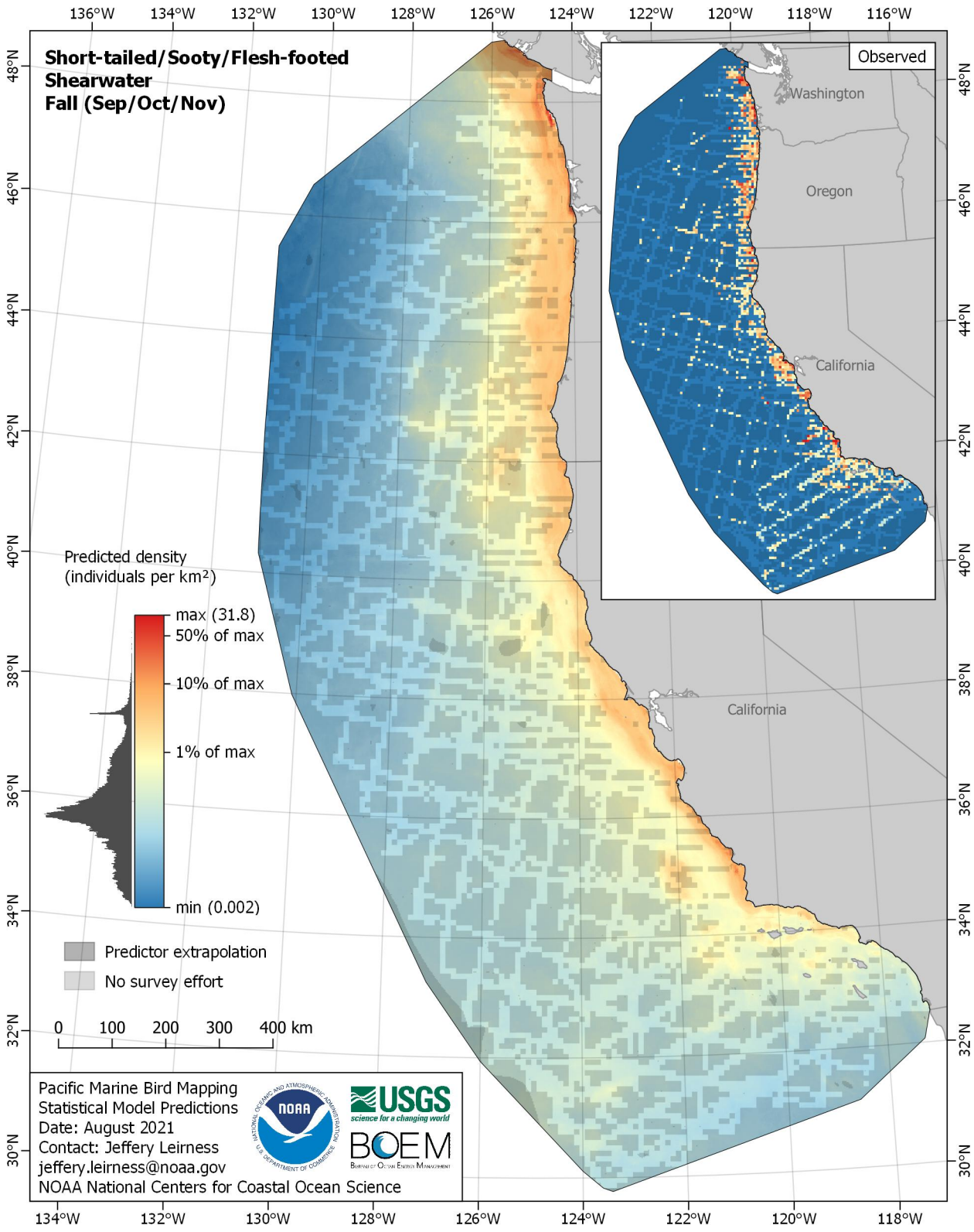

Figure E-237. Predicted density for Short-tailed/Sooty/Flesh-footed Shearwater (*Ardenna tenuirostris/grisea/carneipes*) in the fall season

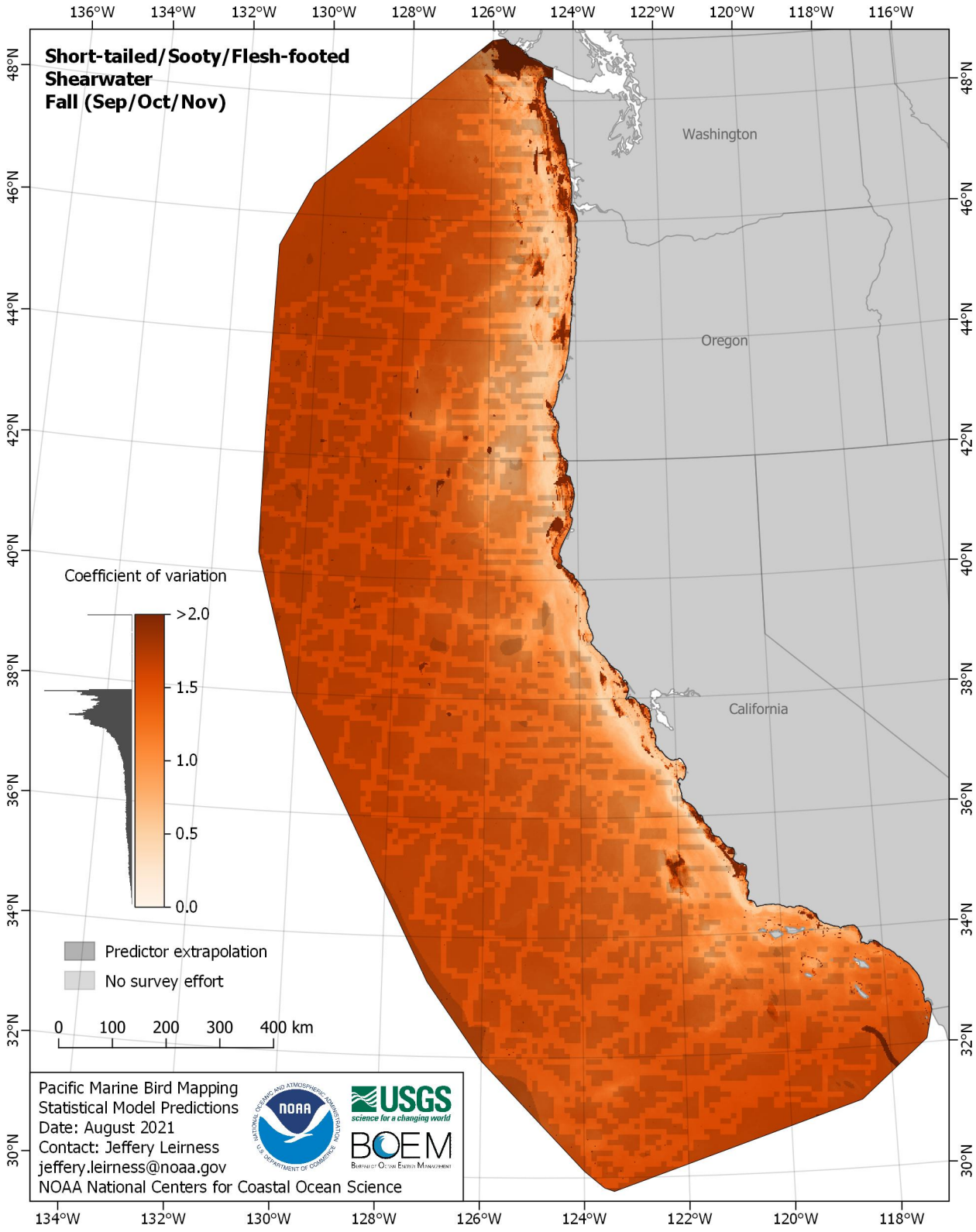

Figure E-238. Coefficient of variation for Short-tailed/Sooty/Flesh-footed Shearwater (*Ardenna tenuirostris/grisea/carneipes*) in the fall season

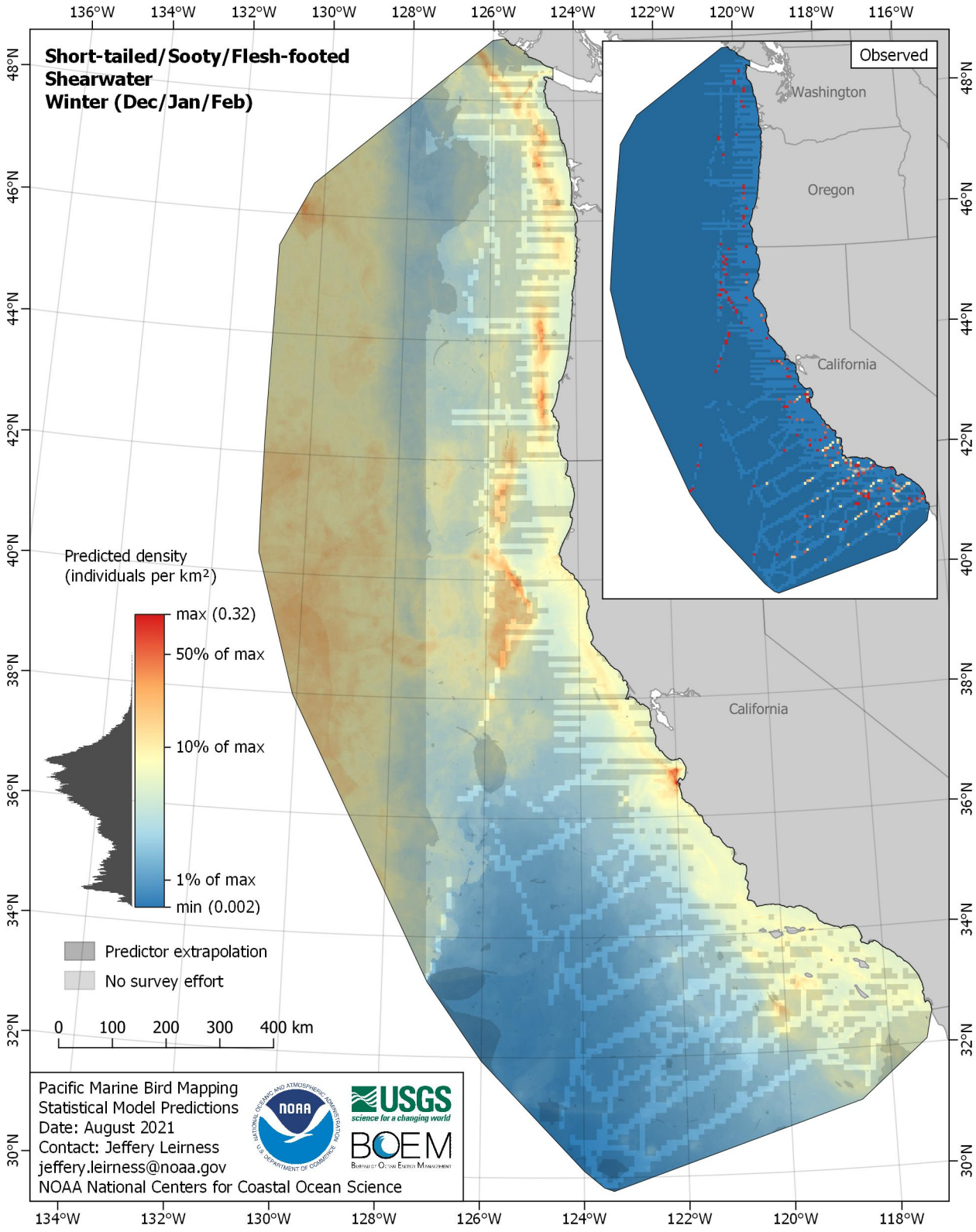

Figure E-239. Predicted density for Short-tailed/Sooty/Flesh-footed Shearwater (*Ardenna tenuirostris/grisea/carneipes*) in the winter season

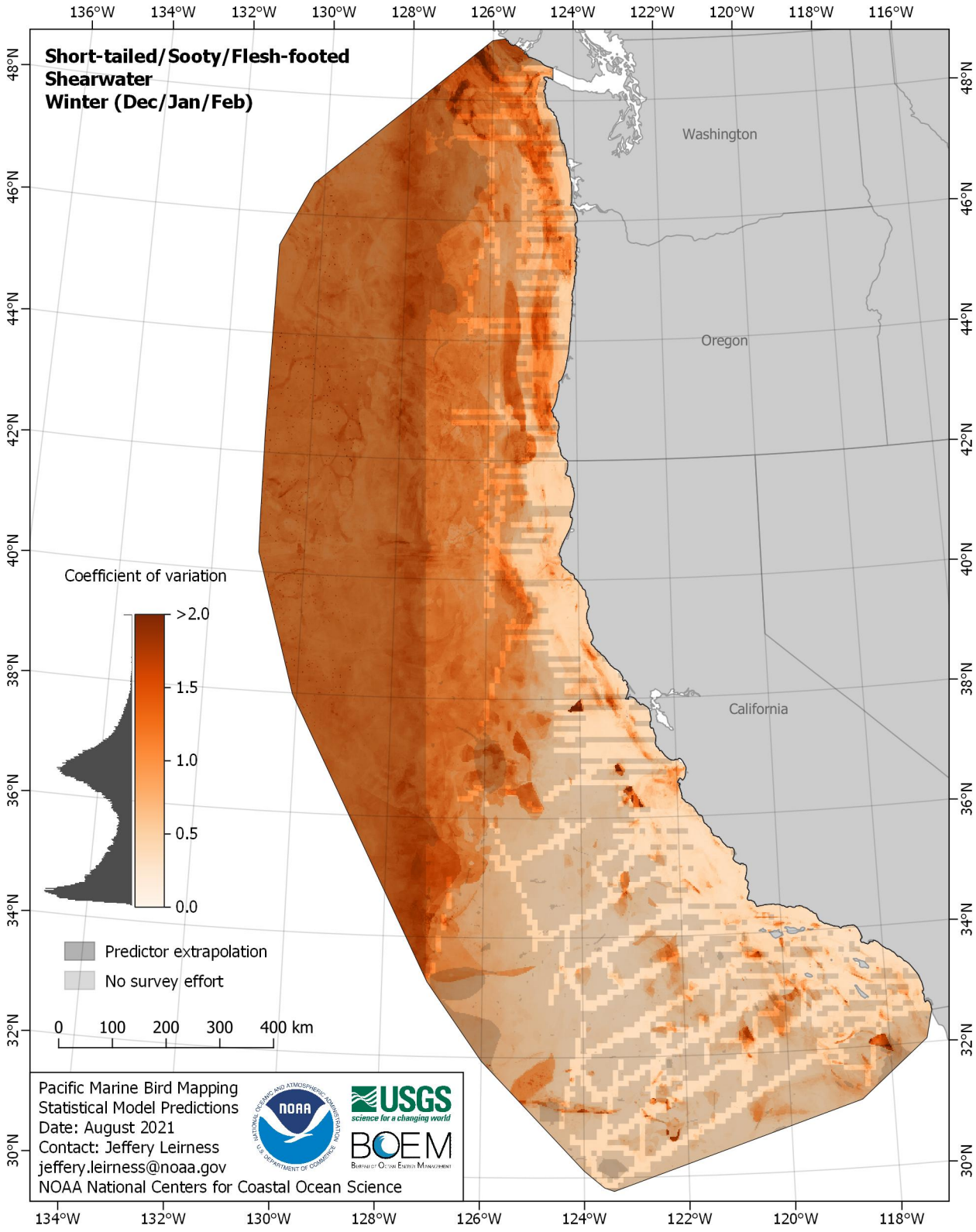

Figure E-240. Coefficient of variation for Short-tailed/Sooty/Flesh-footed Shearwater (*Ardenna tenuirostris/grisea/carneipes*) in the winter season

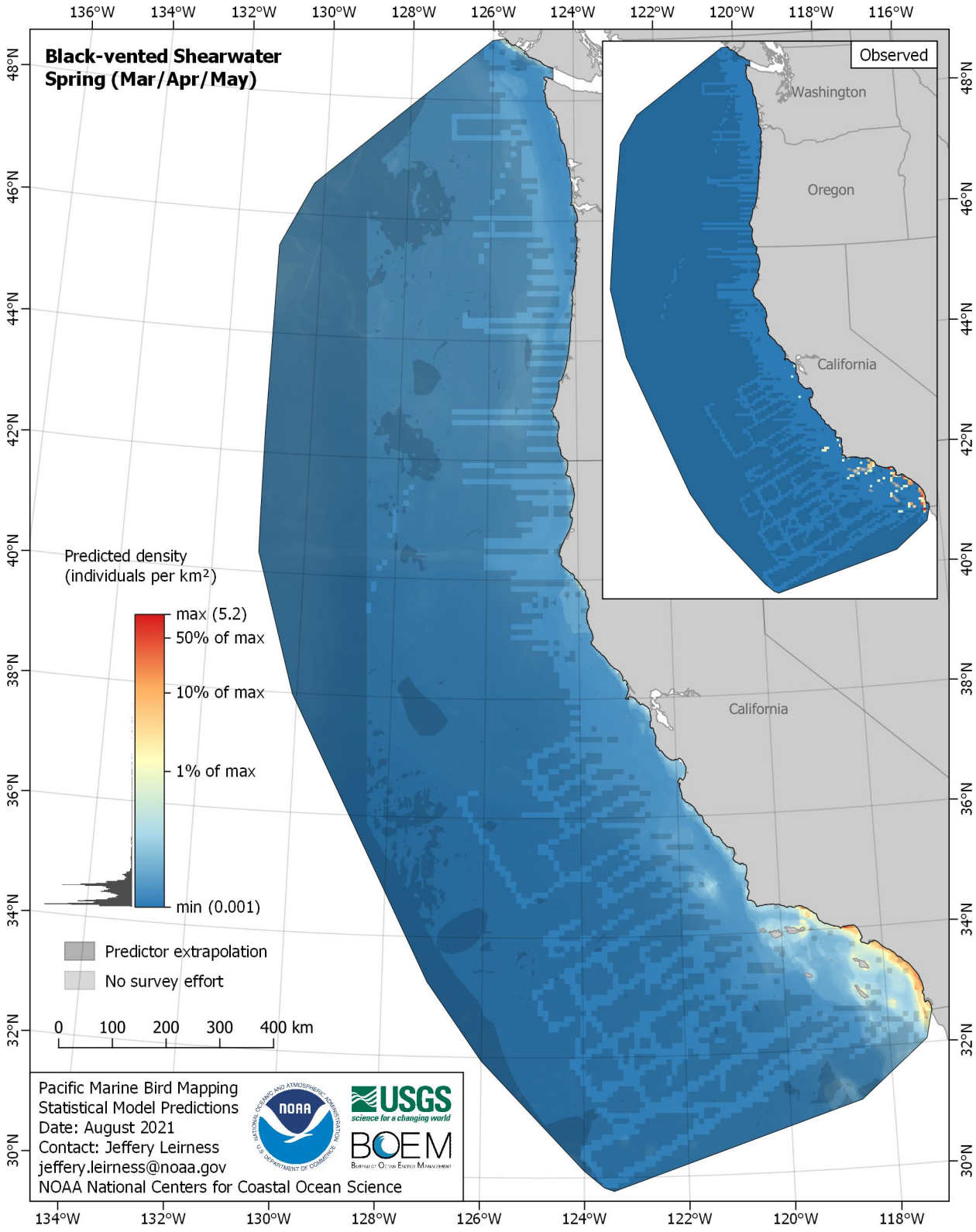

Figure E-241. Predicted density for Black-vented Shearwater (*Puffinus opisthomelas*) in the spring season

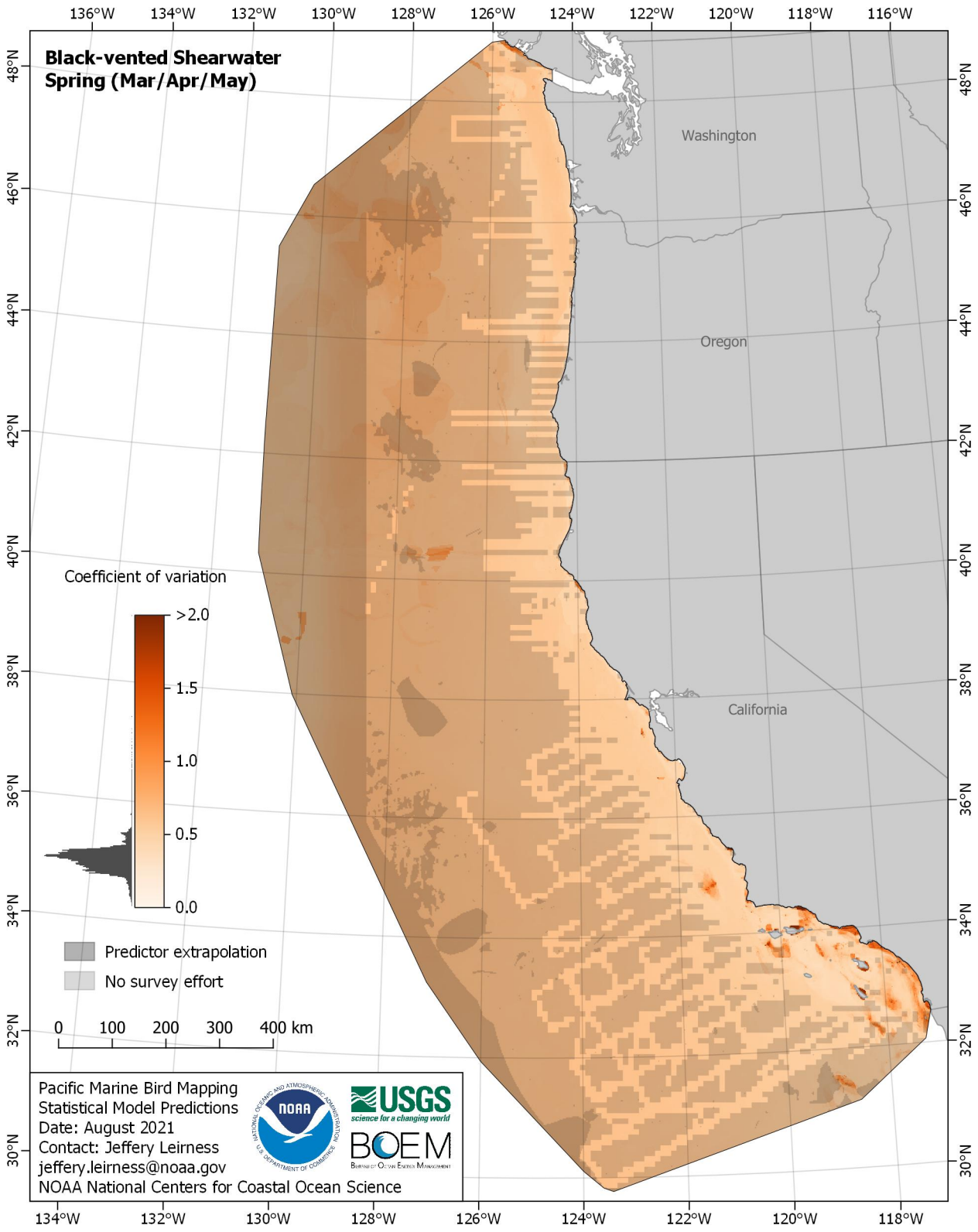

Figure E-242. Coefficient of variation for Black-vented Shearwater (*Puffinus opisthomelas*) in the spring season

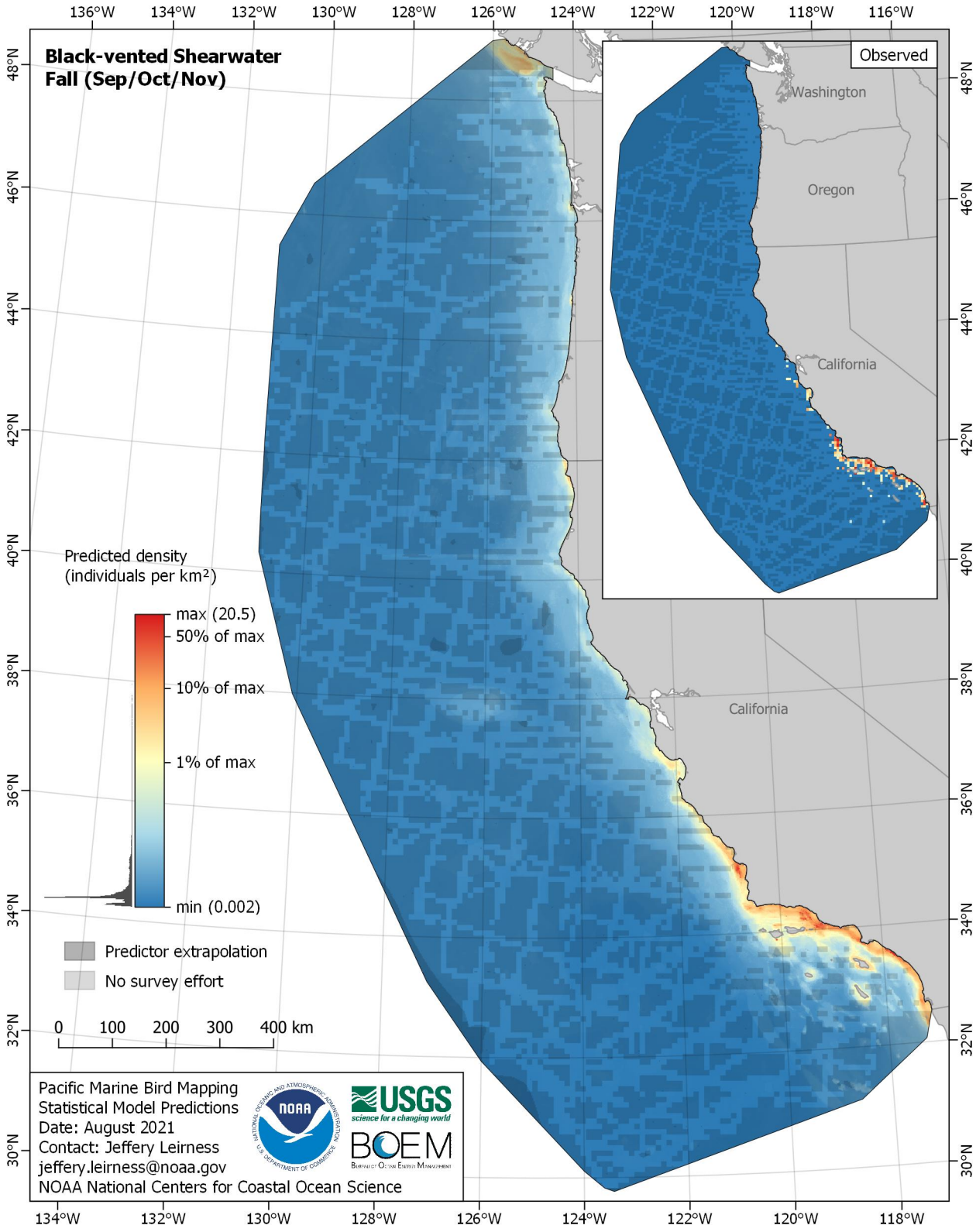

Figure E-243. Predicted density for Black-vented Shearwater (*Puffinus opisthomelas*) in the fall season

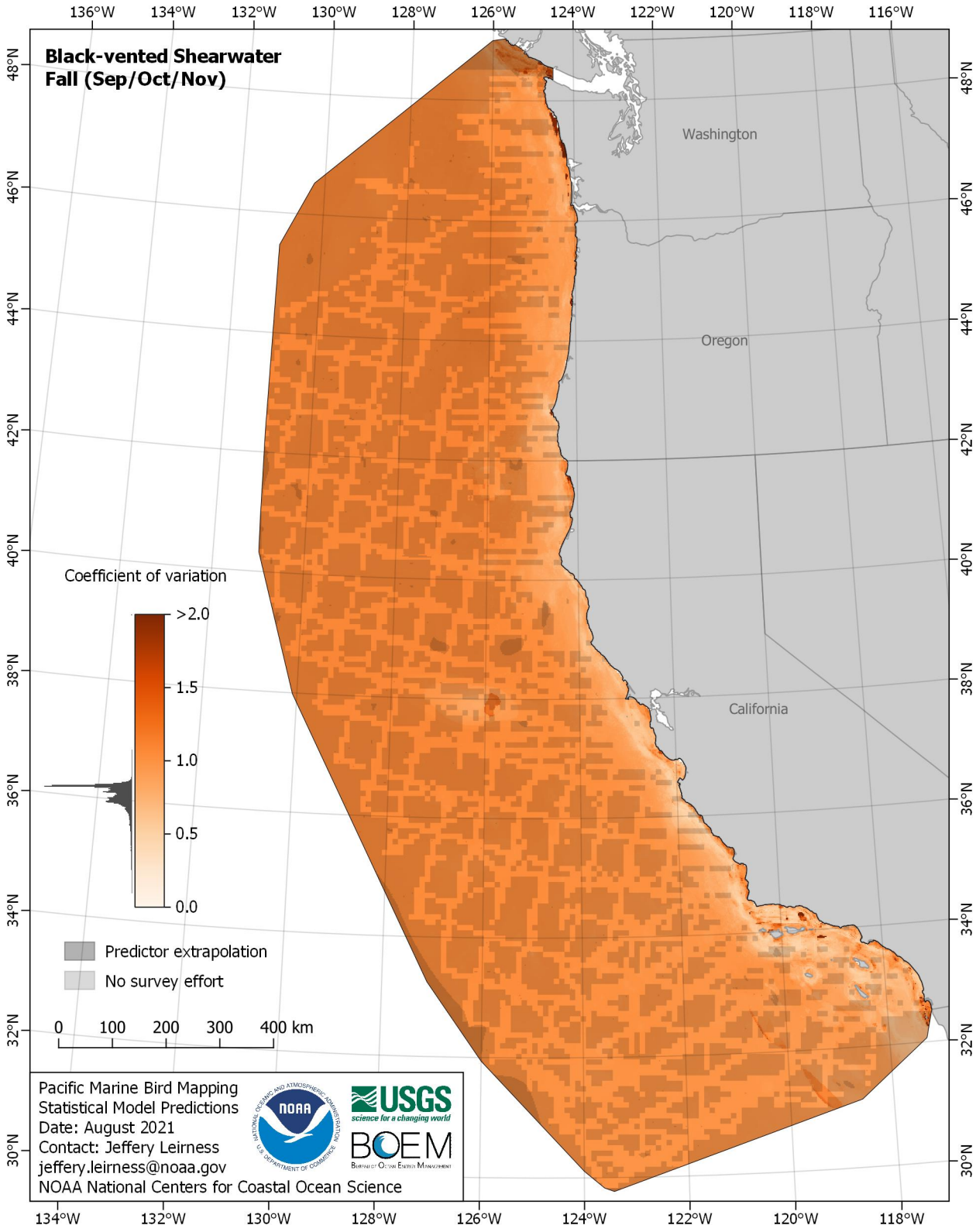

Figure E-244. Coefficient of variation for Black-vented Shearwater (*Puffinus opisthomelas*) in the fall season

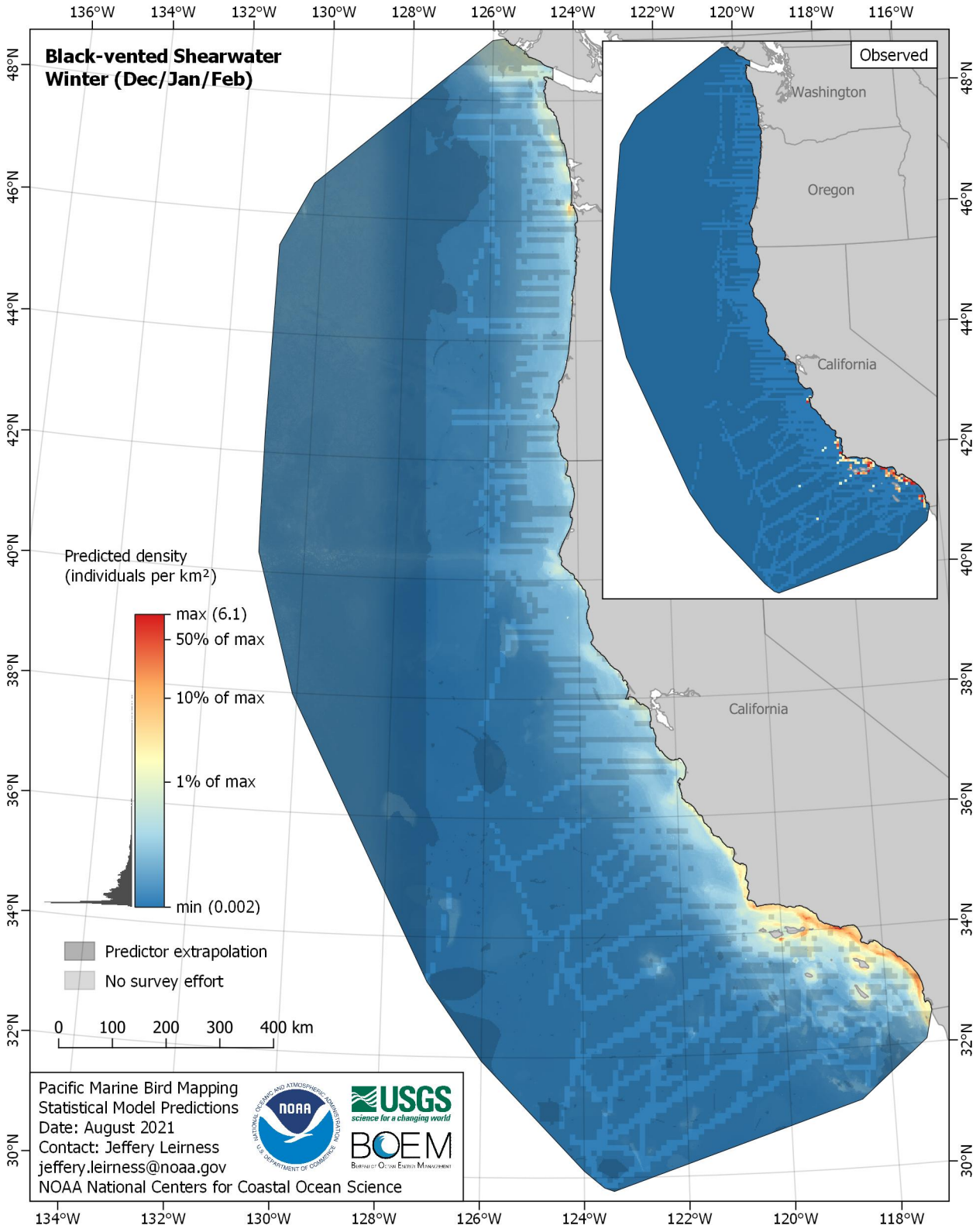

Figure E-245. Predicted density for Black-vented Shearwater (*Puffinus opisthomelas*) in the winter season

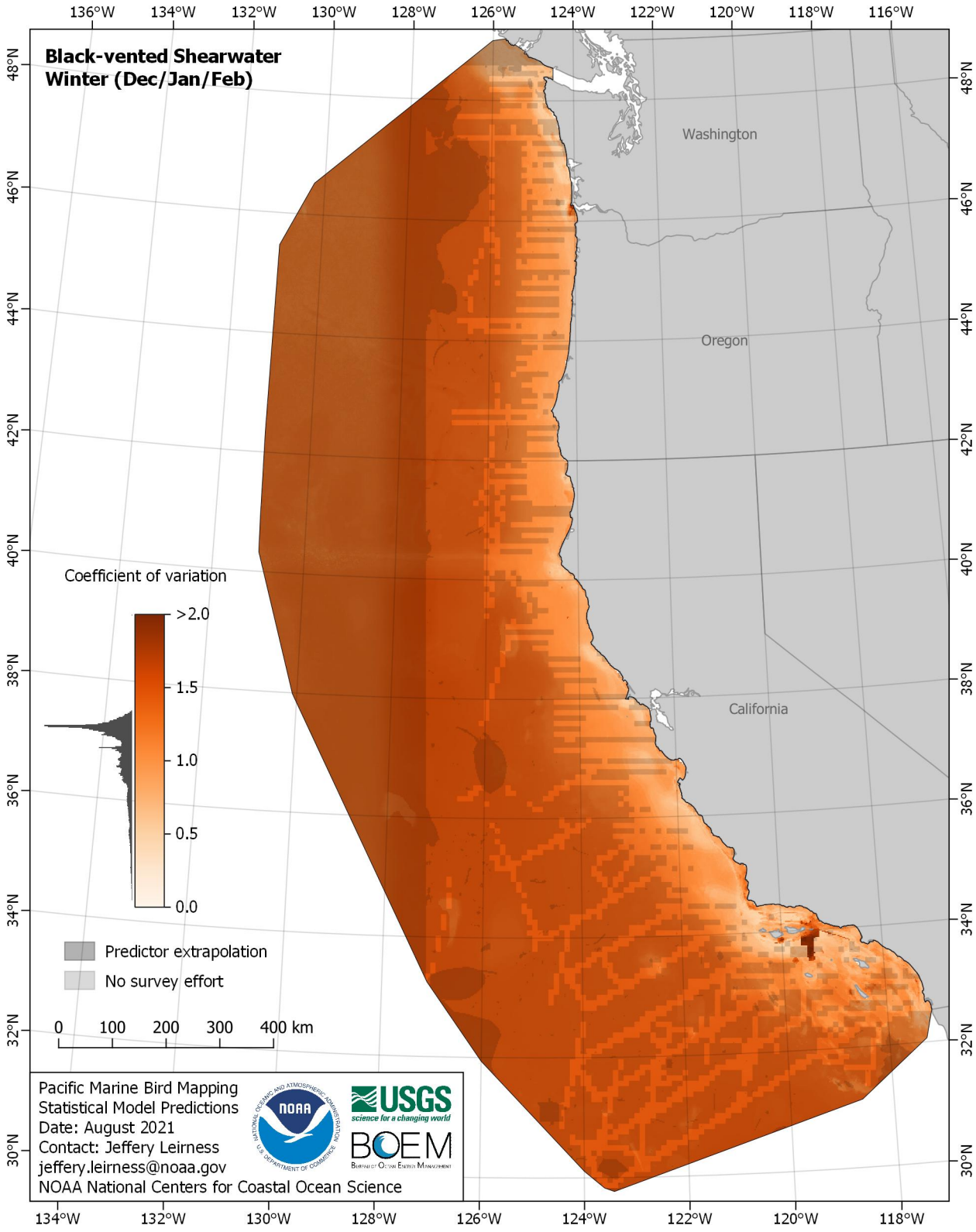

Figure E-246. Coefficient of variation for Black-vented Shearwater (*Puffinus opisthomelas*) in the winter season

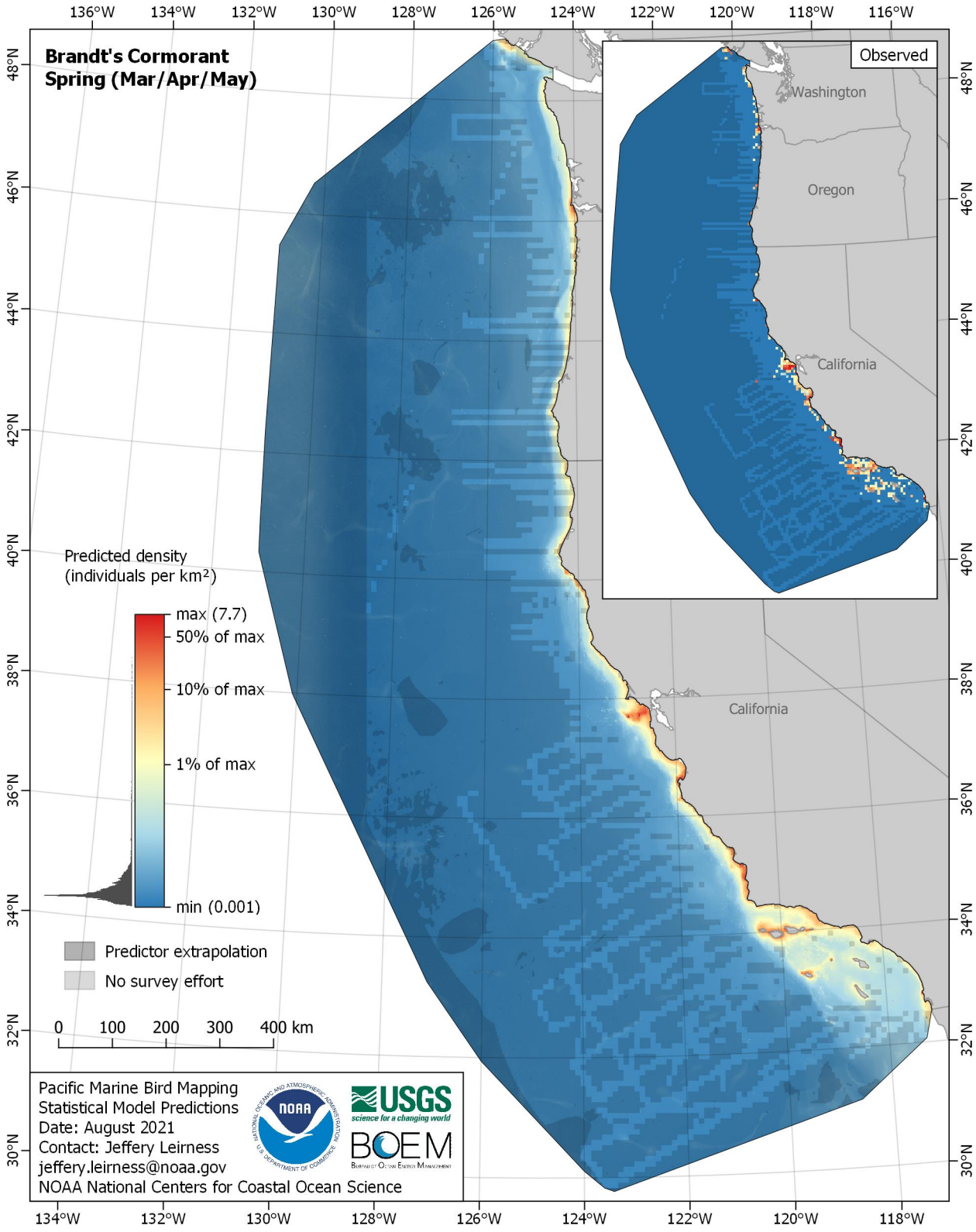

Figure E-247. Predicted density for Brandt's Cormorant (*Phalacrocorax penicillatus*) in the spring season

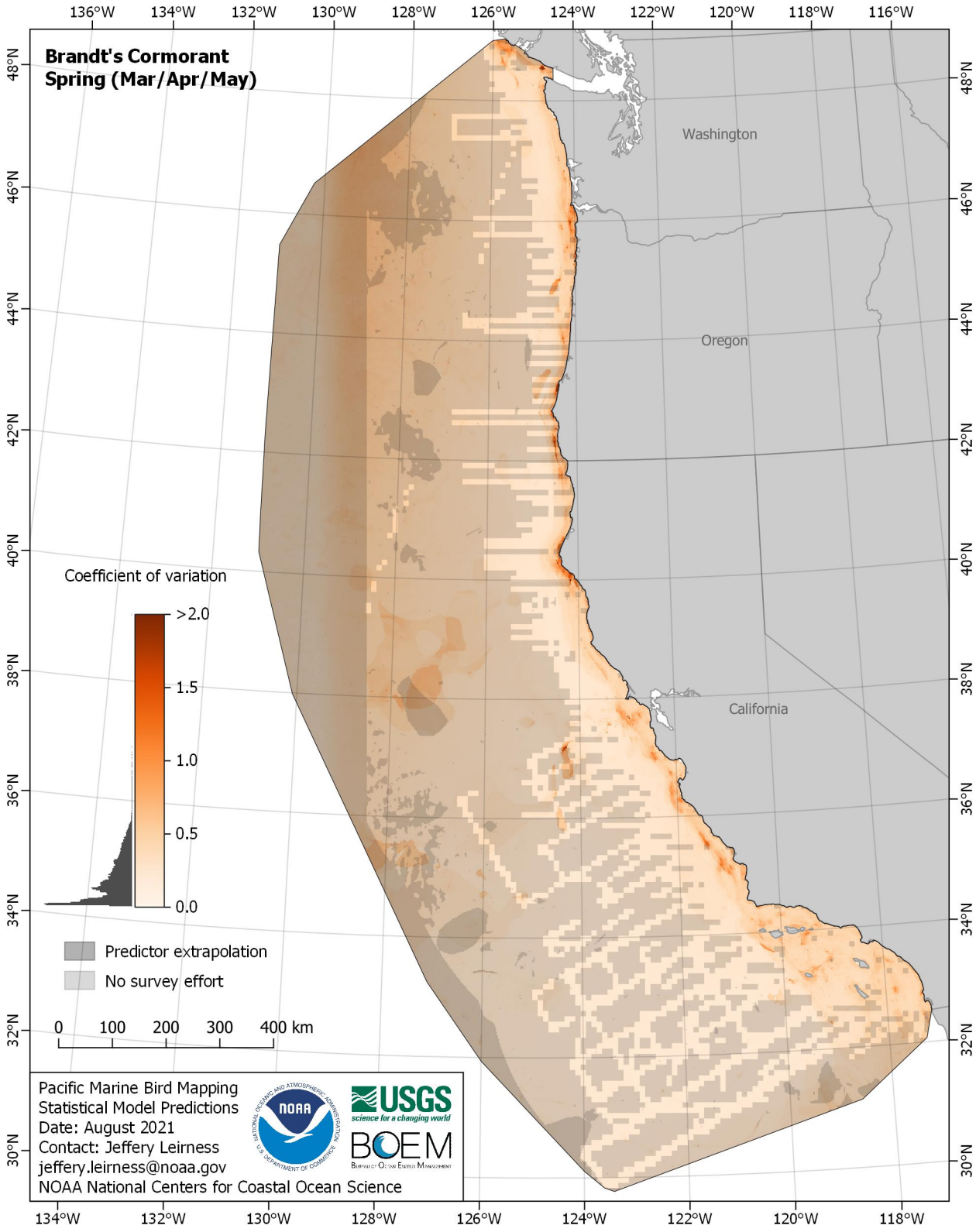

Figure E-248. Coefficient of variation for Brandt's Cormorant (*Phalacrocorax penicillatus*) in the spring season

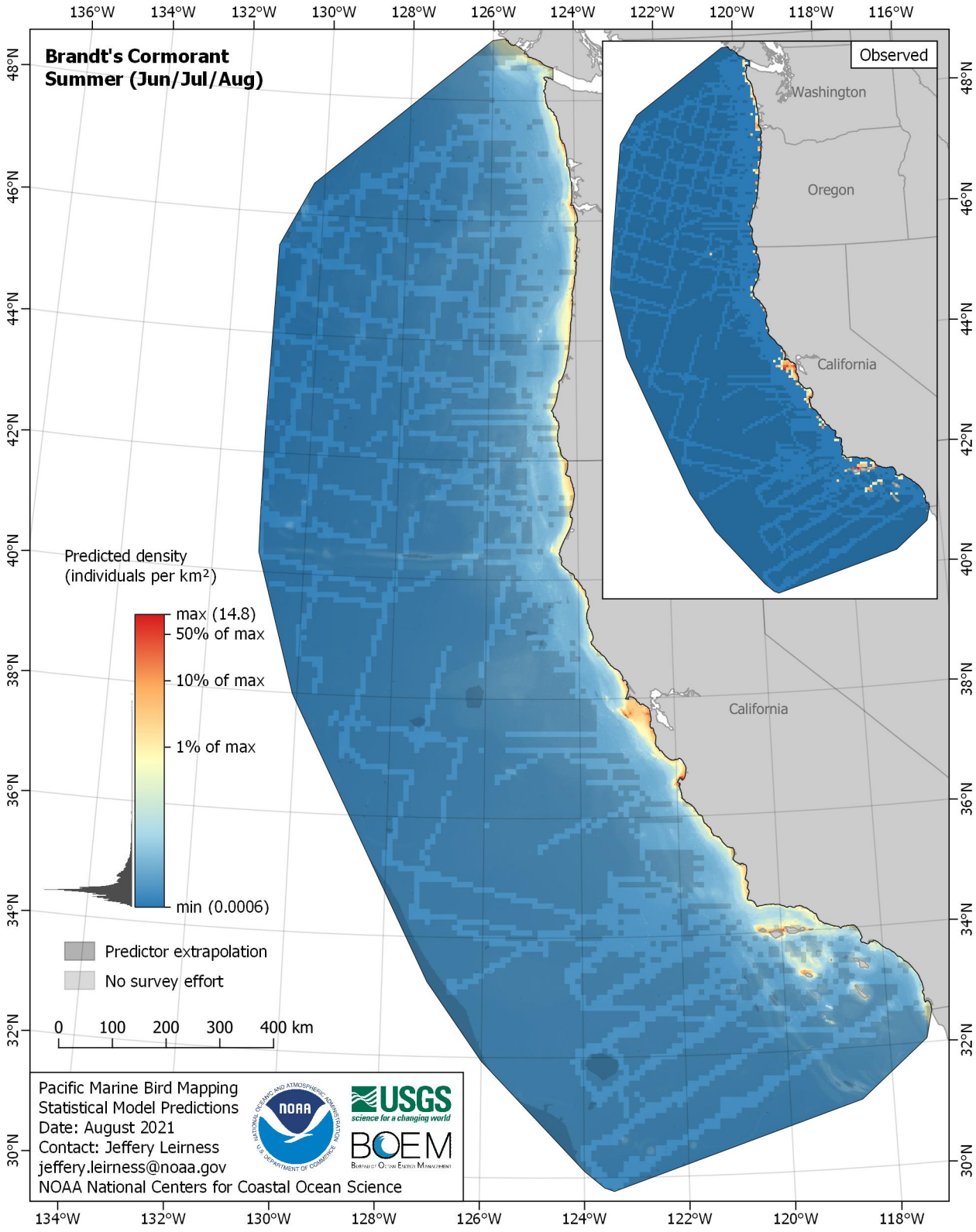

Figure E-249. Predicted density for Brandt's Cormorant (*Phalacrocorax penicillatus*) in the summer season

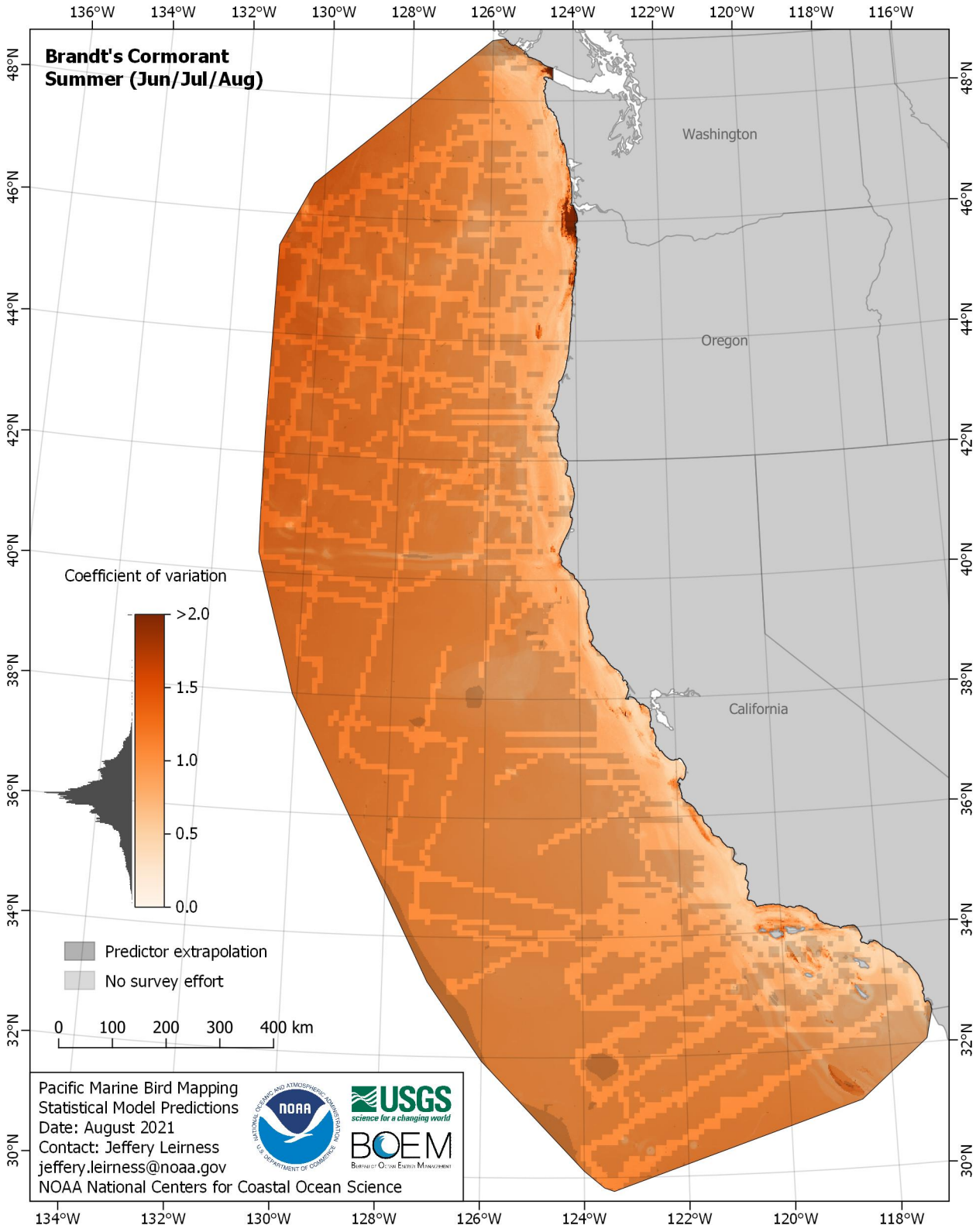

Figure E-250. Coefficient of variation for Brandt's Cormorant (*Phalacrocorax penicillatus*) in the summer season

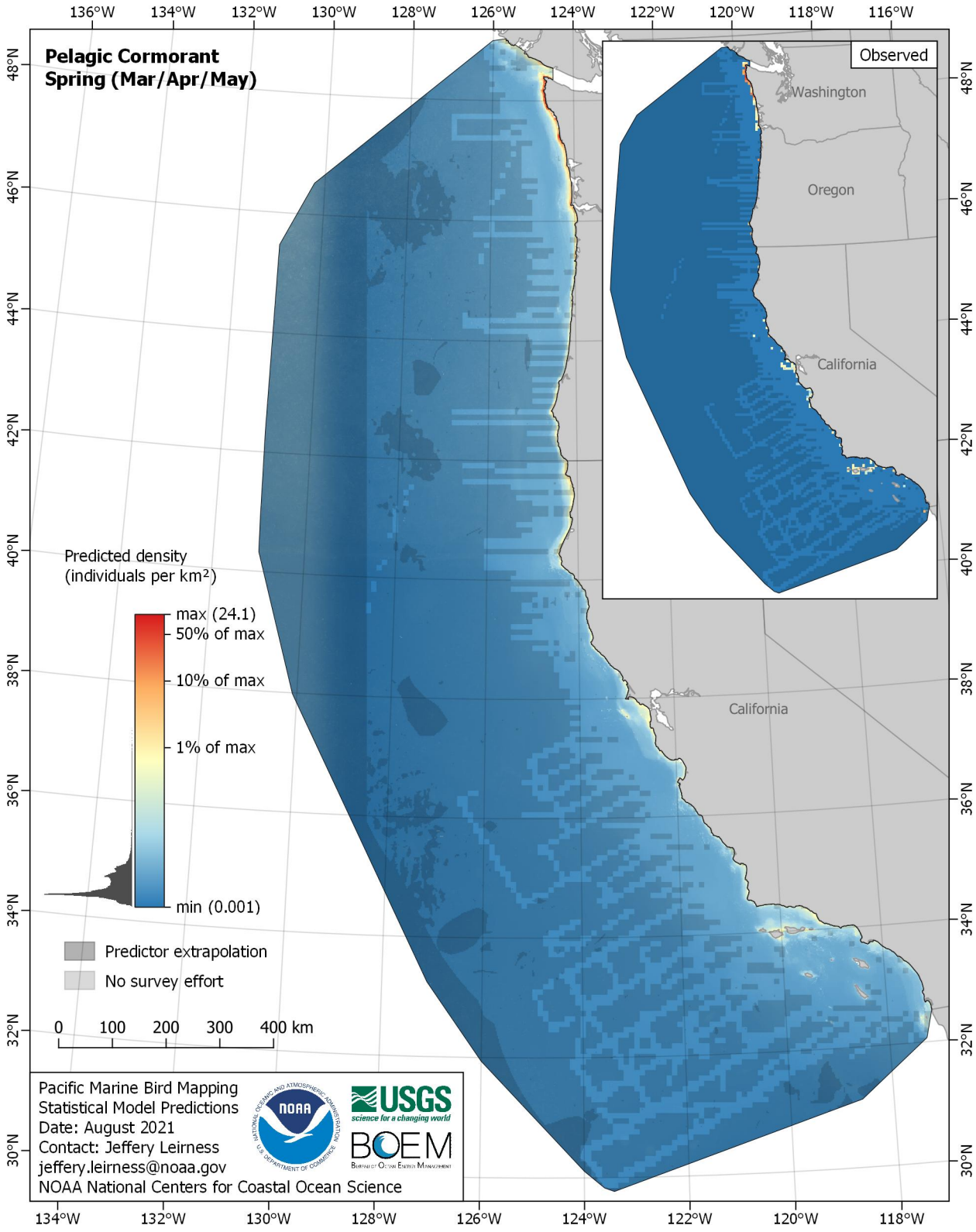

Figure E-251. Predicted density for Pelagic Cormorant (*Phalacrocorax pelagicus*) in the spring season

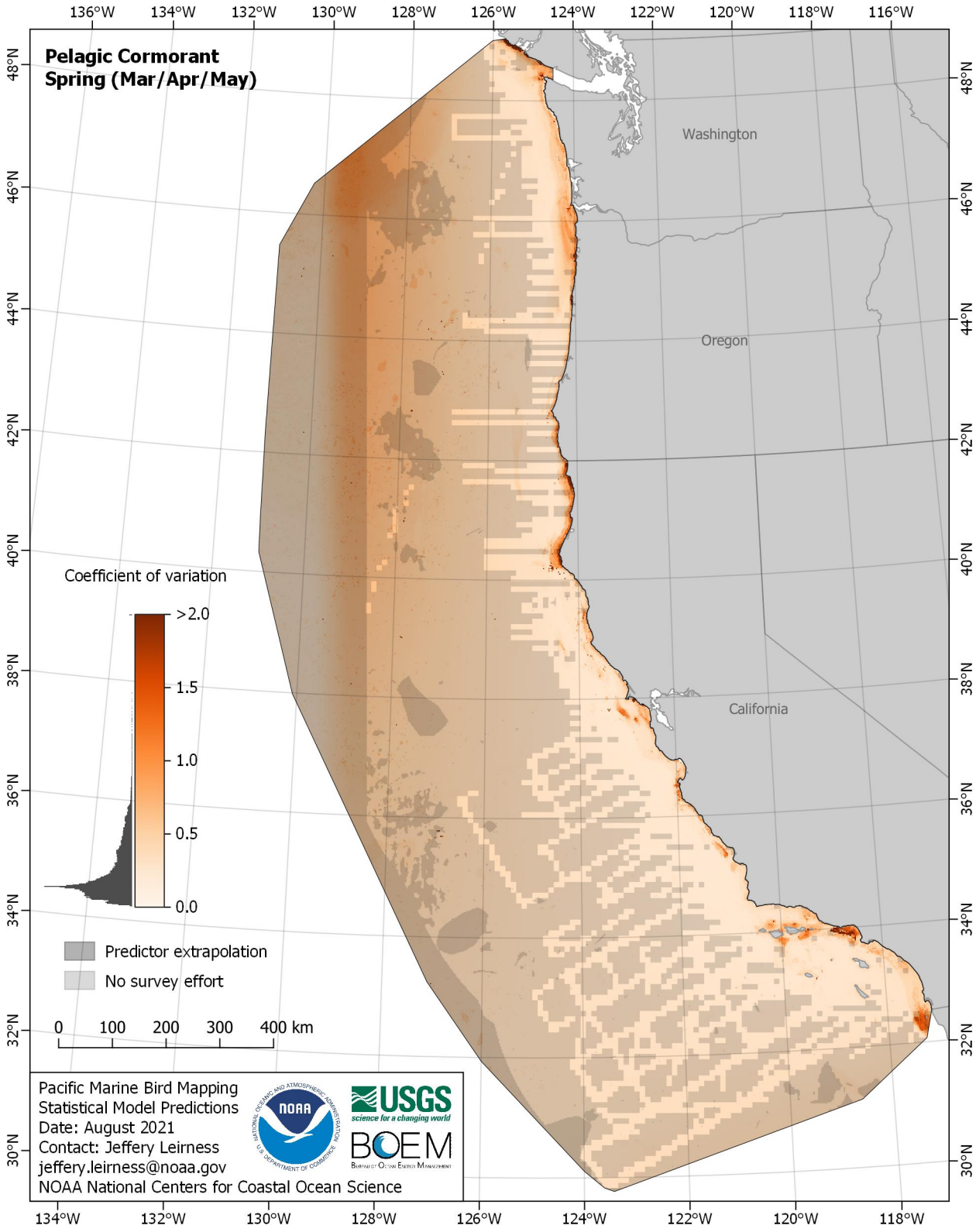

Figure E-252. Coefficient of variation for Pelagic Cormorant (*Phalacrocorax pelagicus*) in the spring season

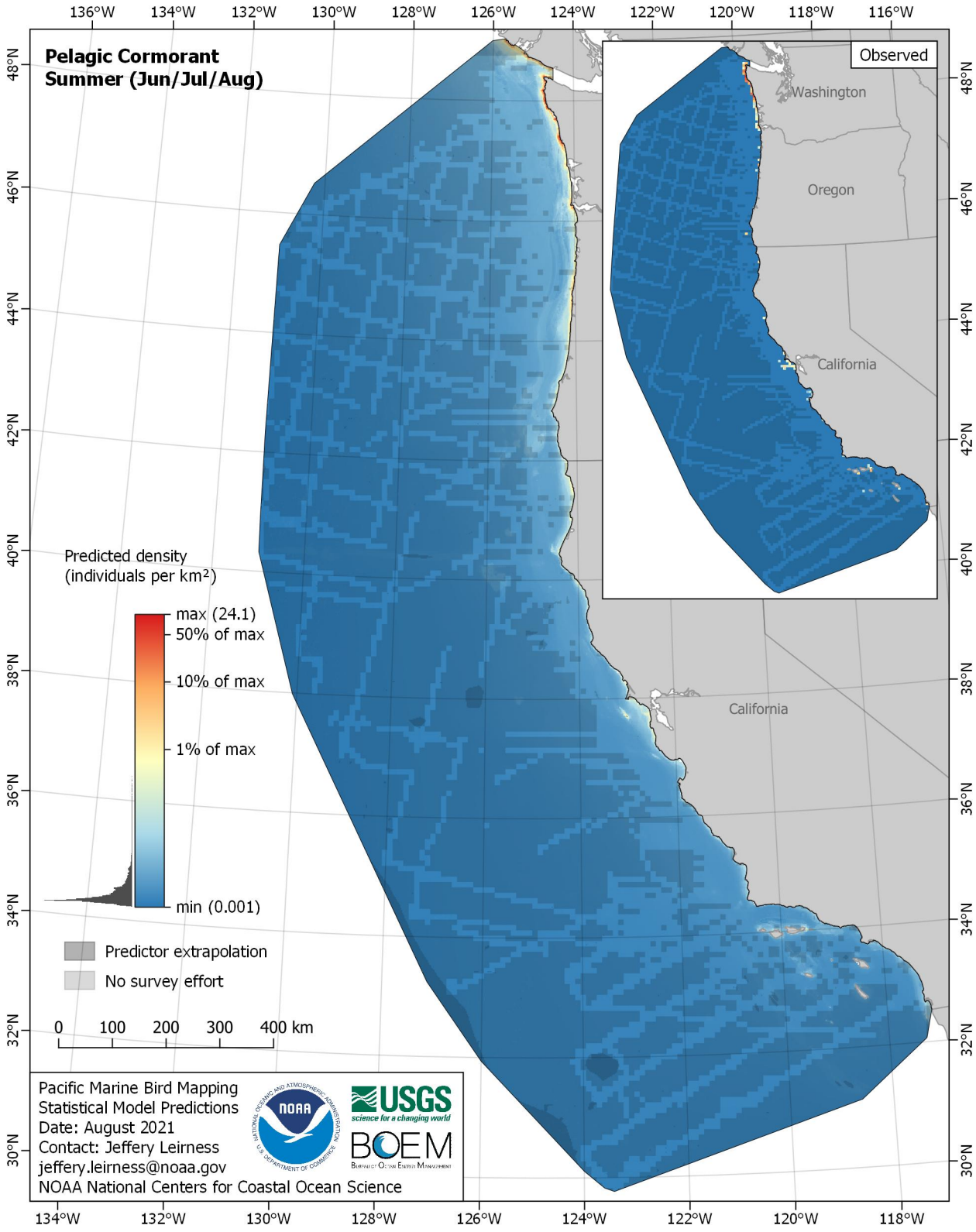

Figure E-253. Predicted density for Pelagic Cormorant (*Phalacrocorax pelagicus*) in the summer season

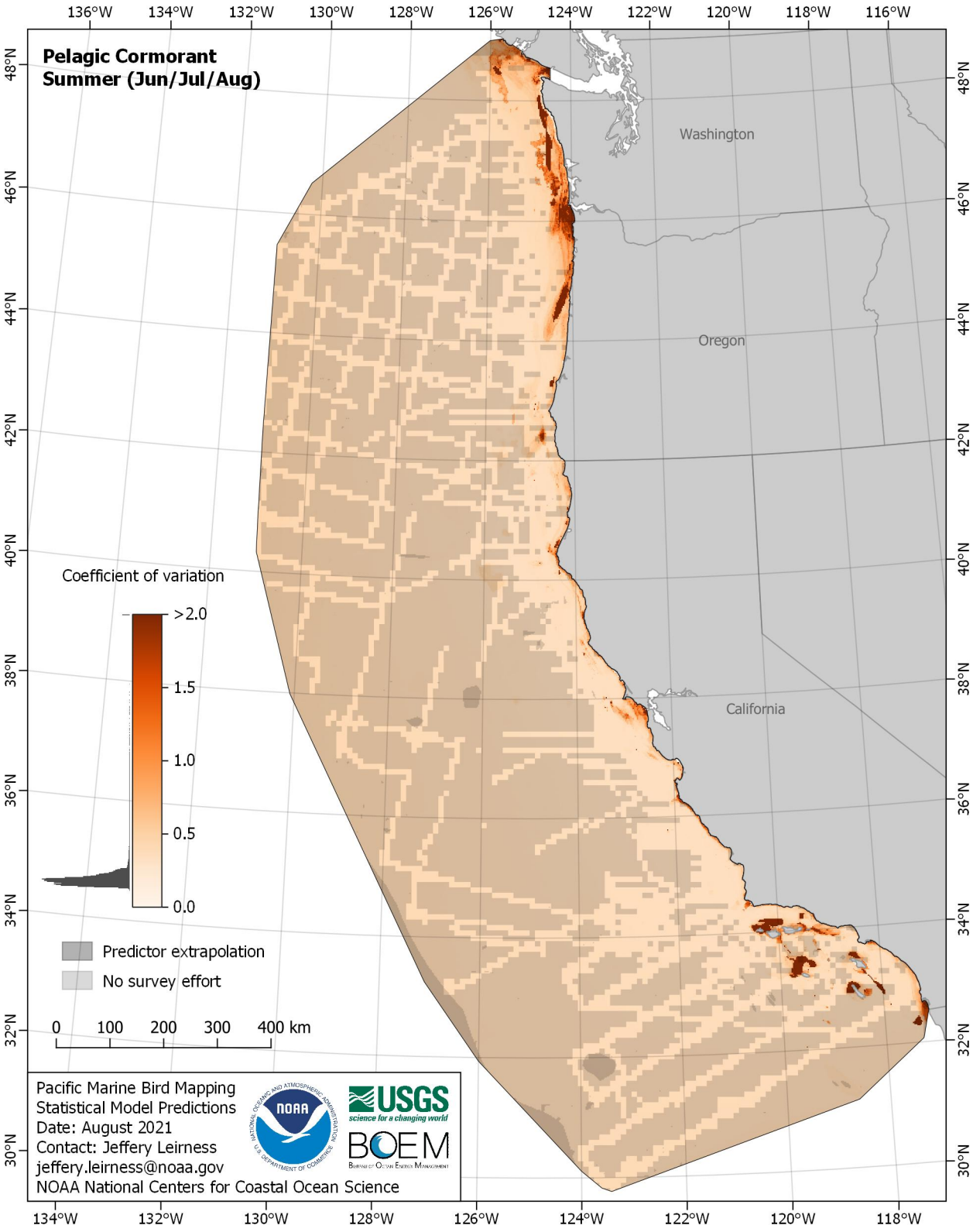

Figure E-254. Coefficient of variation for Pelagic Cormorant (*Phalacrocorax pelagicus*) in the summer season

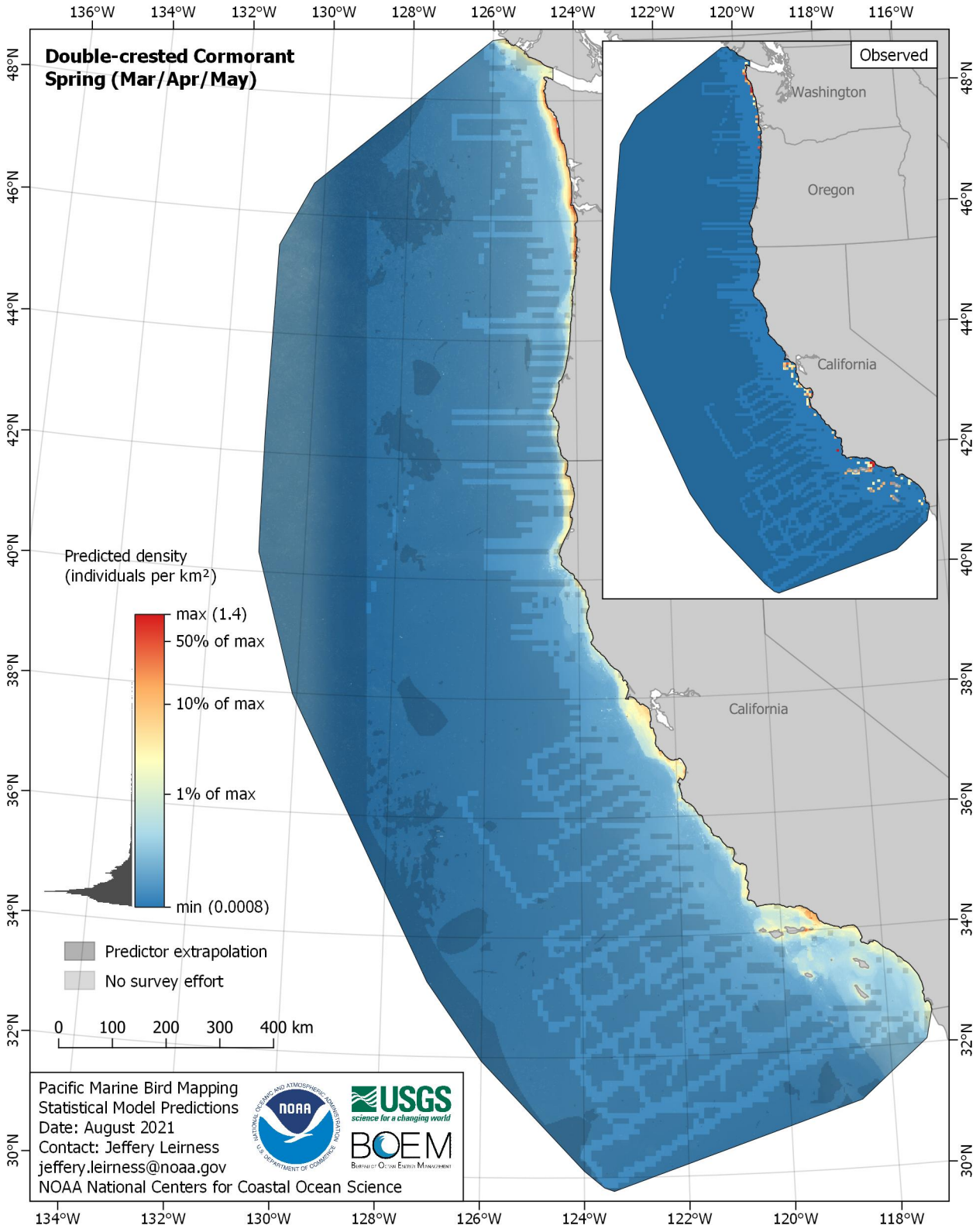

Figure E-255. Predicted density for Double-crested Cormorant (*Phalacrocorax auritus*) in the spring season

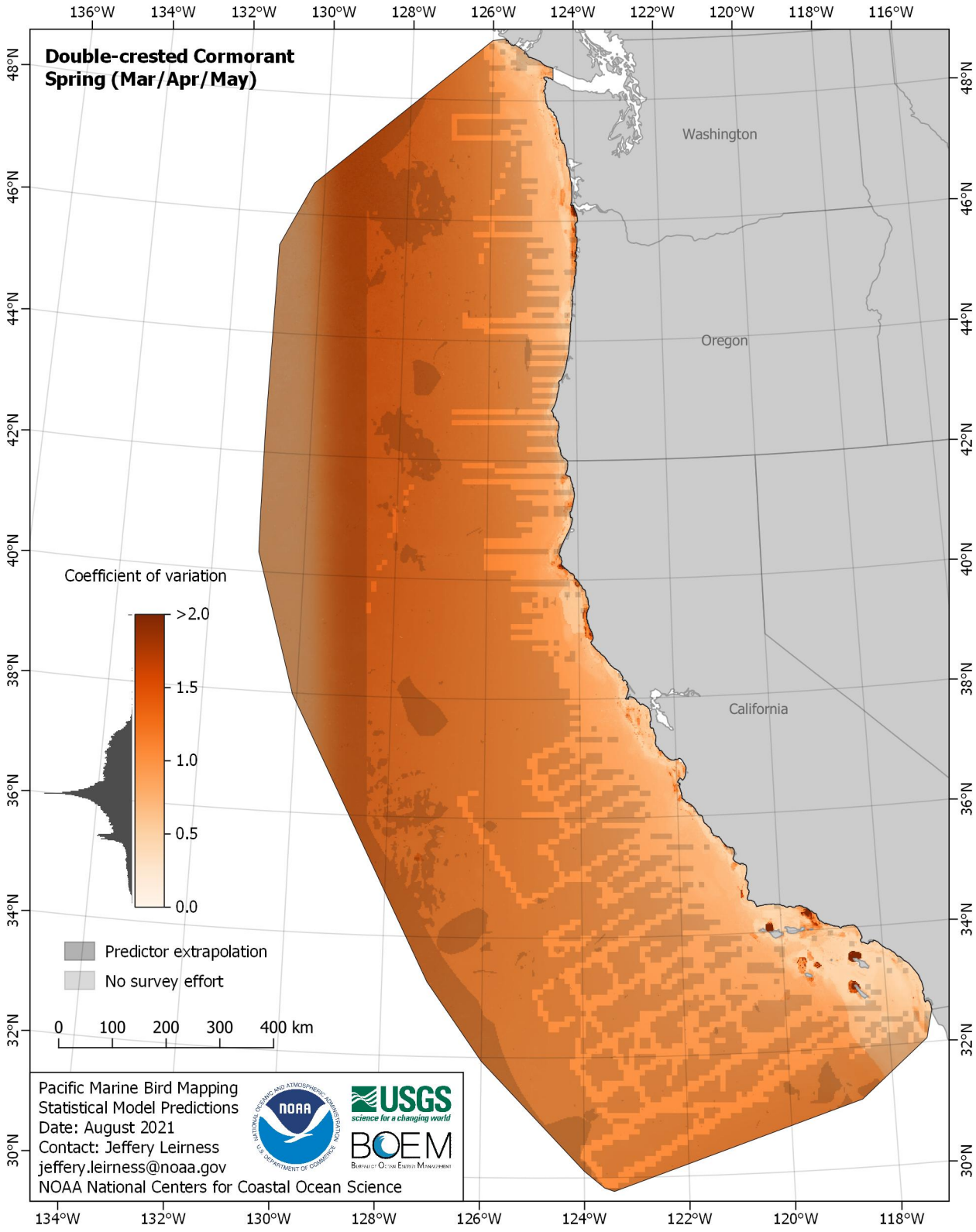

Figure E-256. Coefficient of variation for Double-crested Cormorant (*Phalacrocorax auritus*) in the spring season

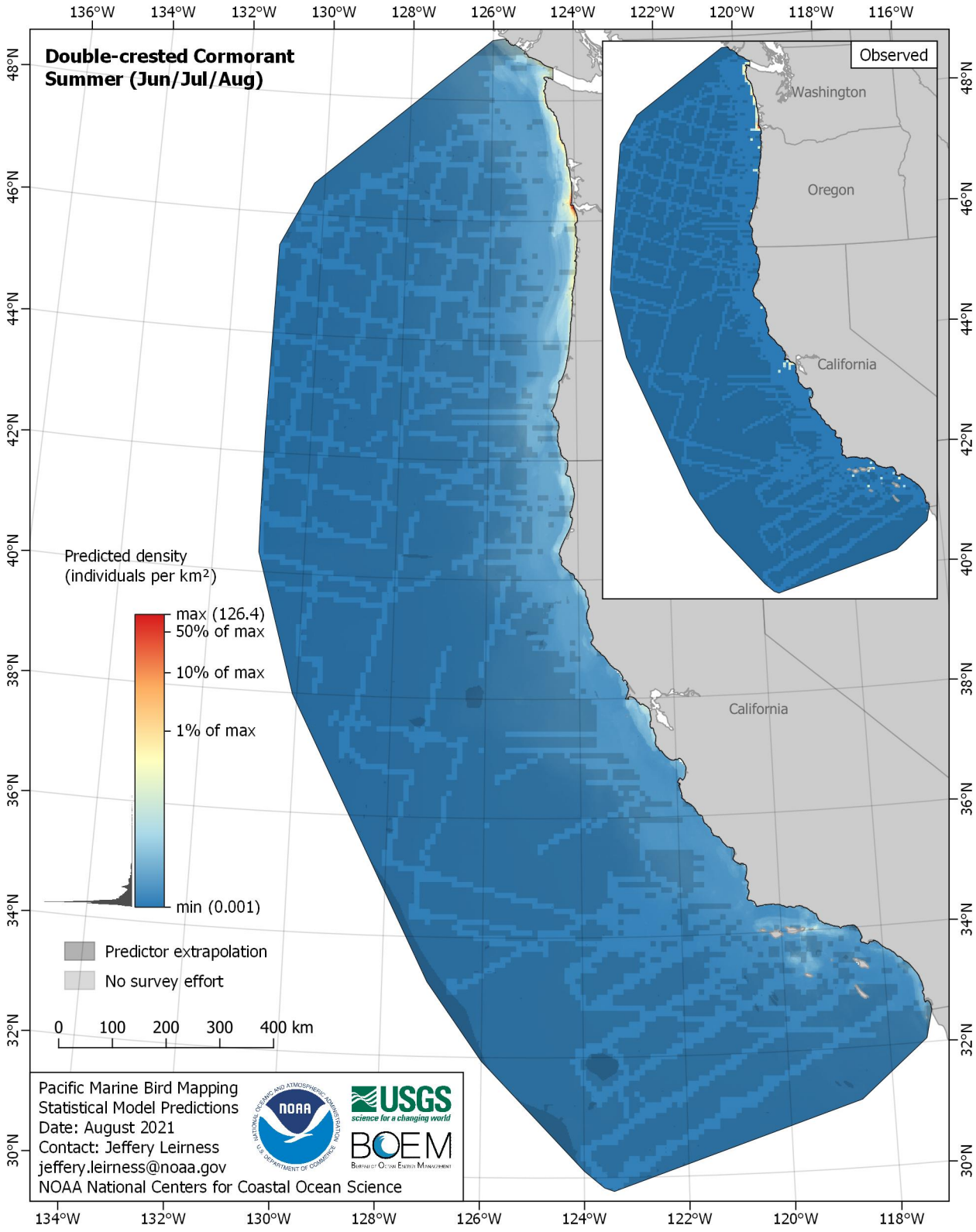

Figure E-257. Predicted density for Double-crested Cormorant (*Phalacrocorax auritus*) in the summer season

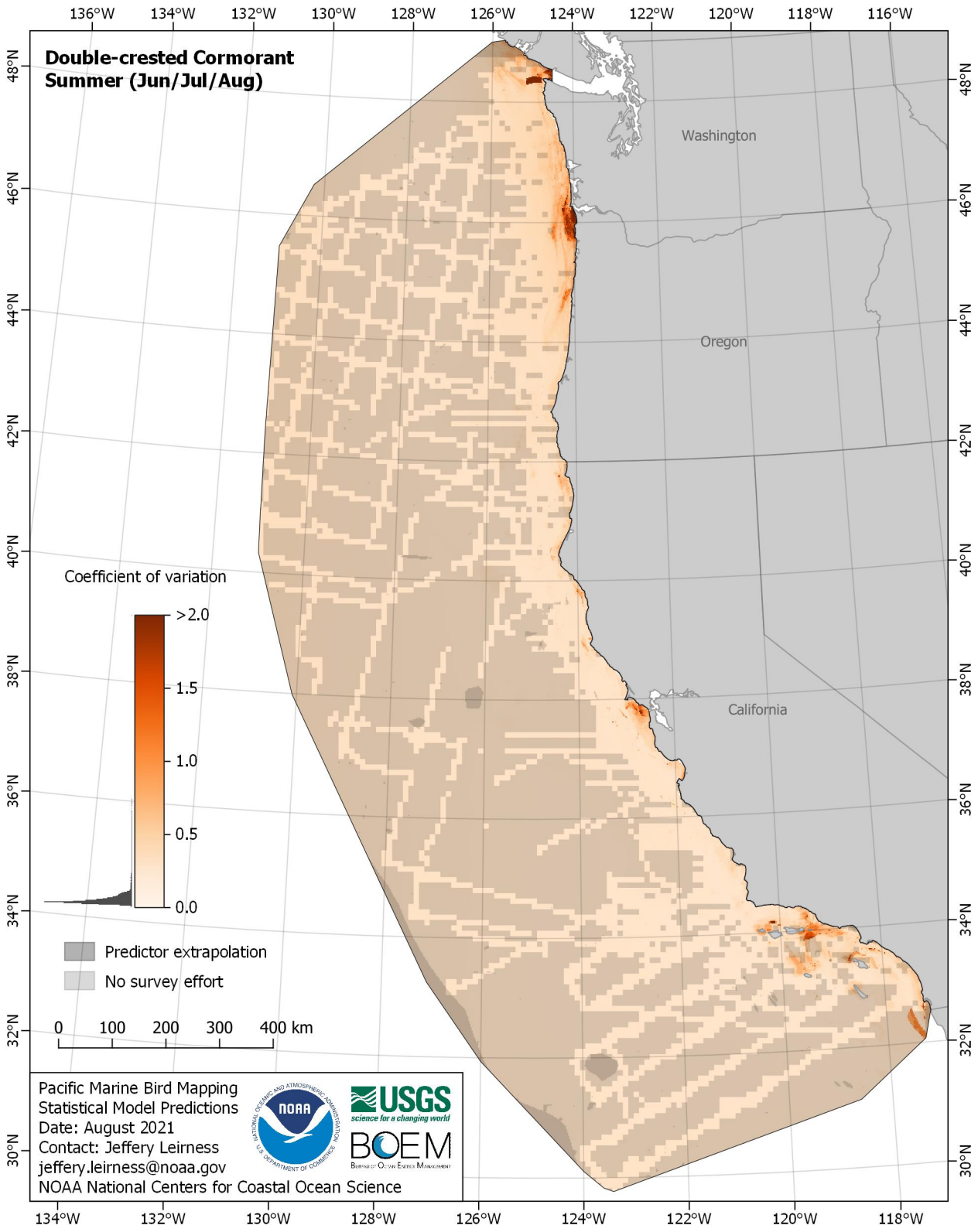

Figure E-258. Coefficient of variation for Double-crested Cormorant (*Phalacrocorax auritus*) in the summer season

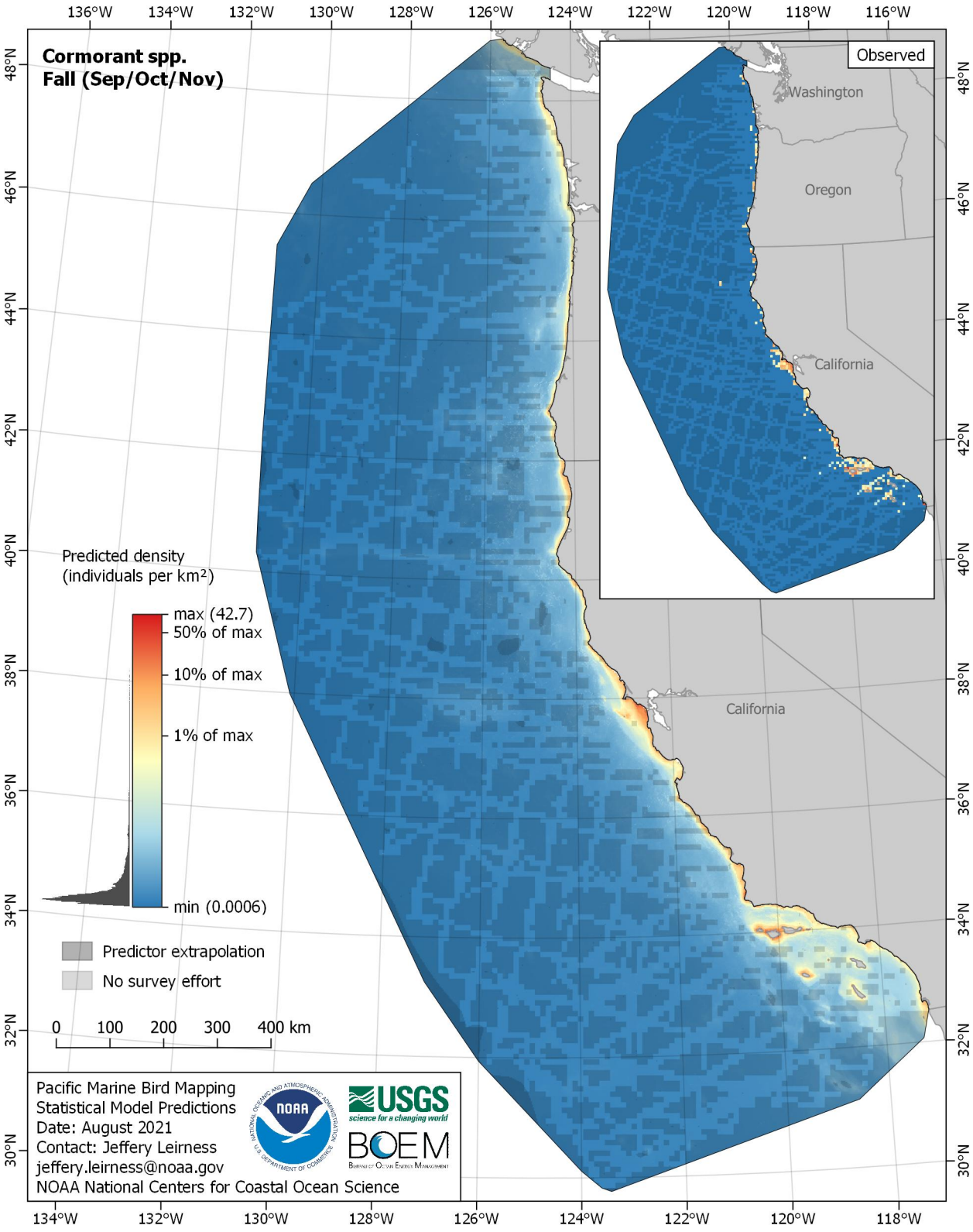

Figure E-259. Predicted density for Cormorant spp. (*Phalacrocorax spp.*) in the fall season

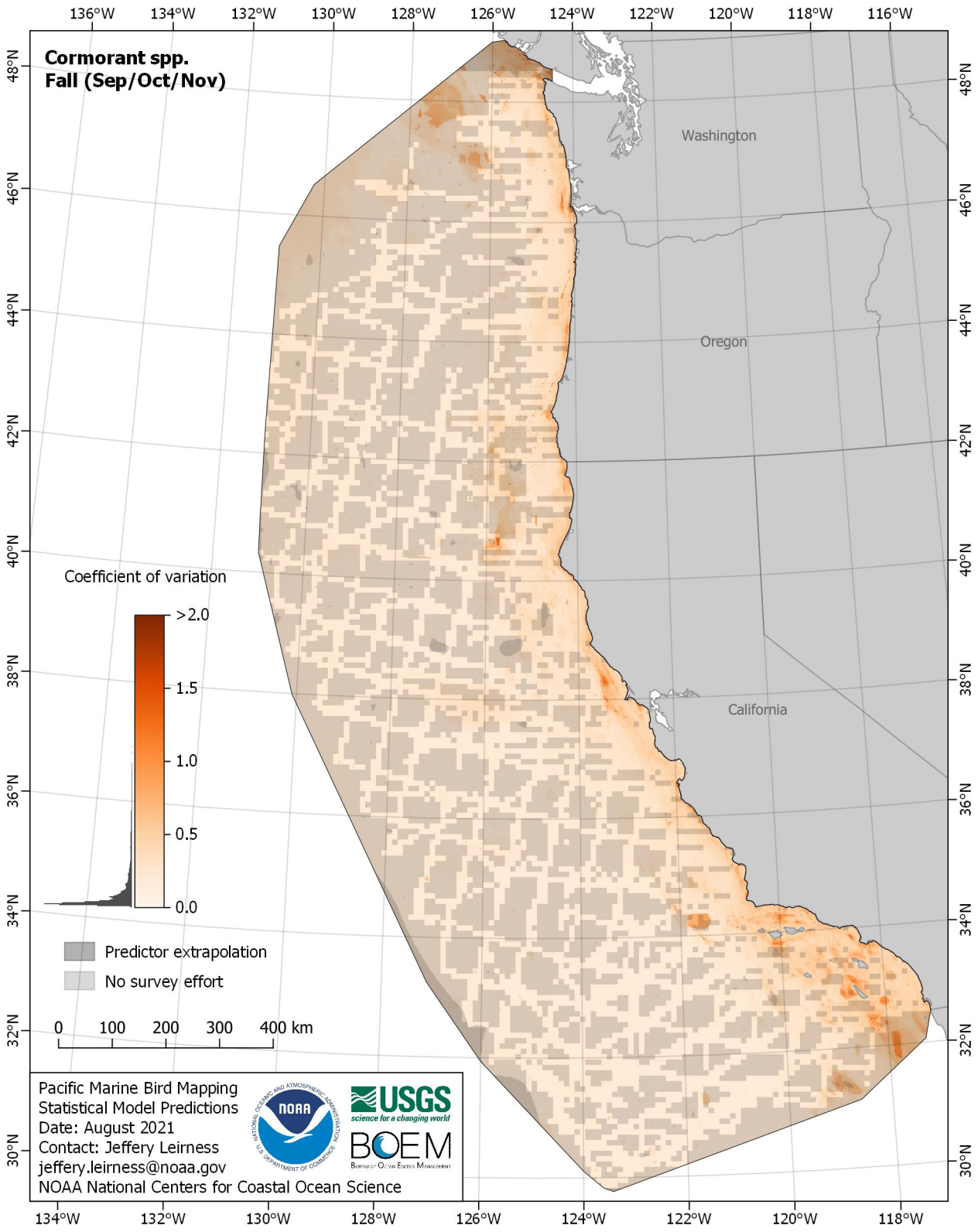

Figure E-260. Coefficient of variation for Cormorant spp. (*Phalacrocorax spp.*) in the fall season

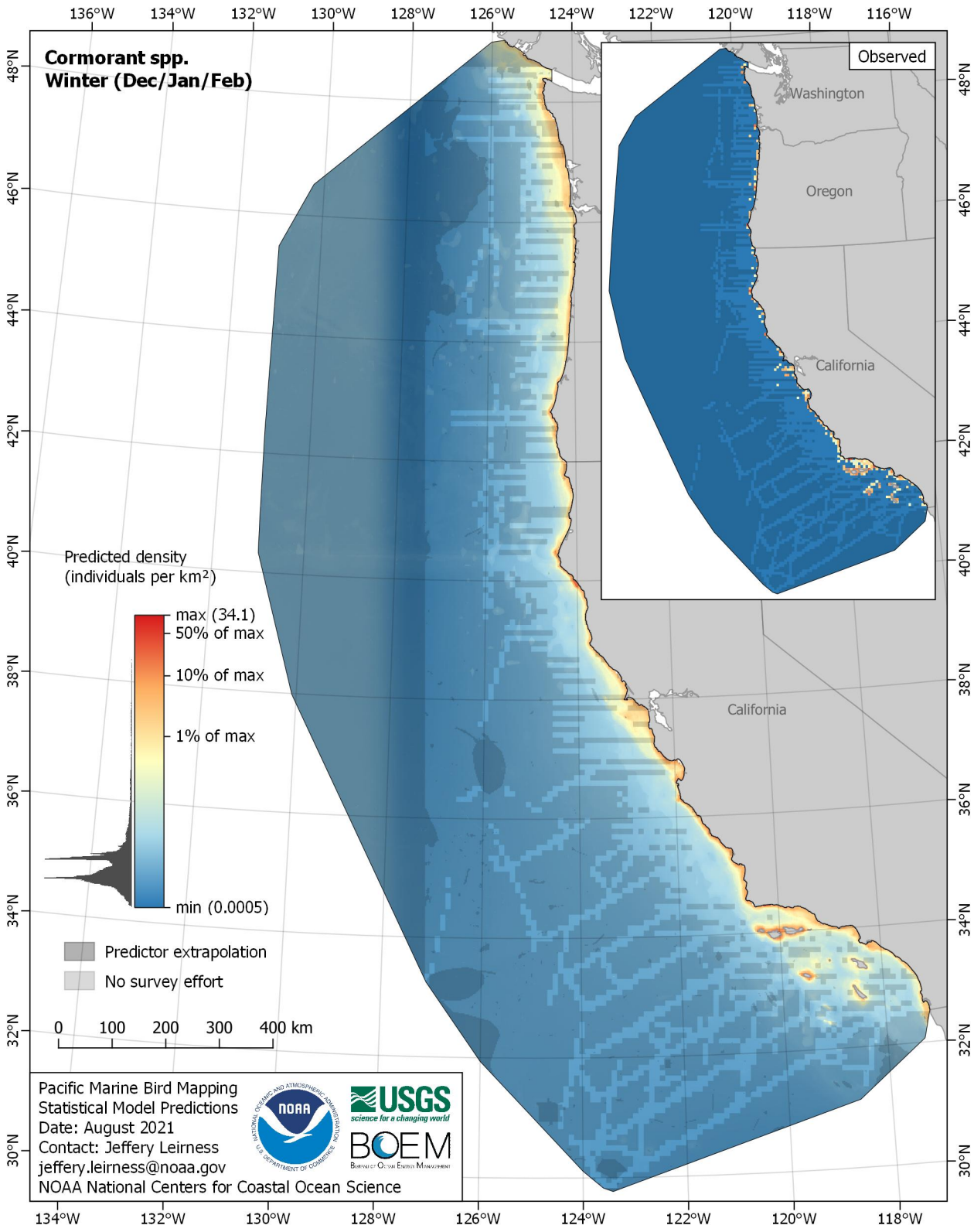

Figure E-261. Predicted density for Cormorant spp. (*Phalacrocorax spp.*) in the winter season

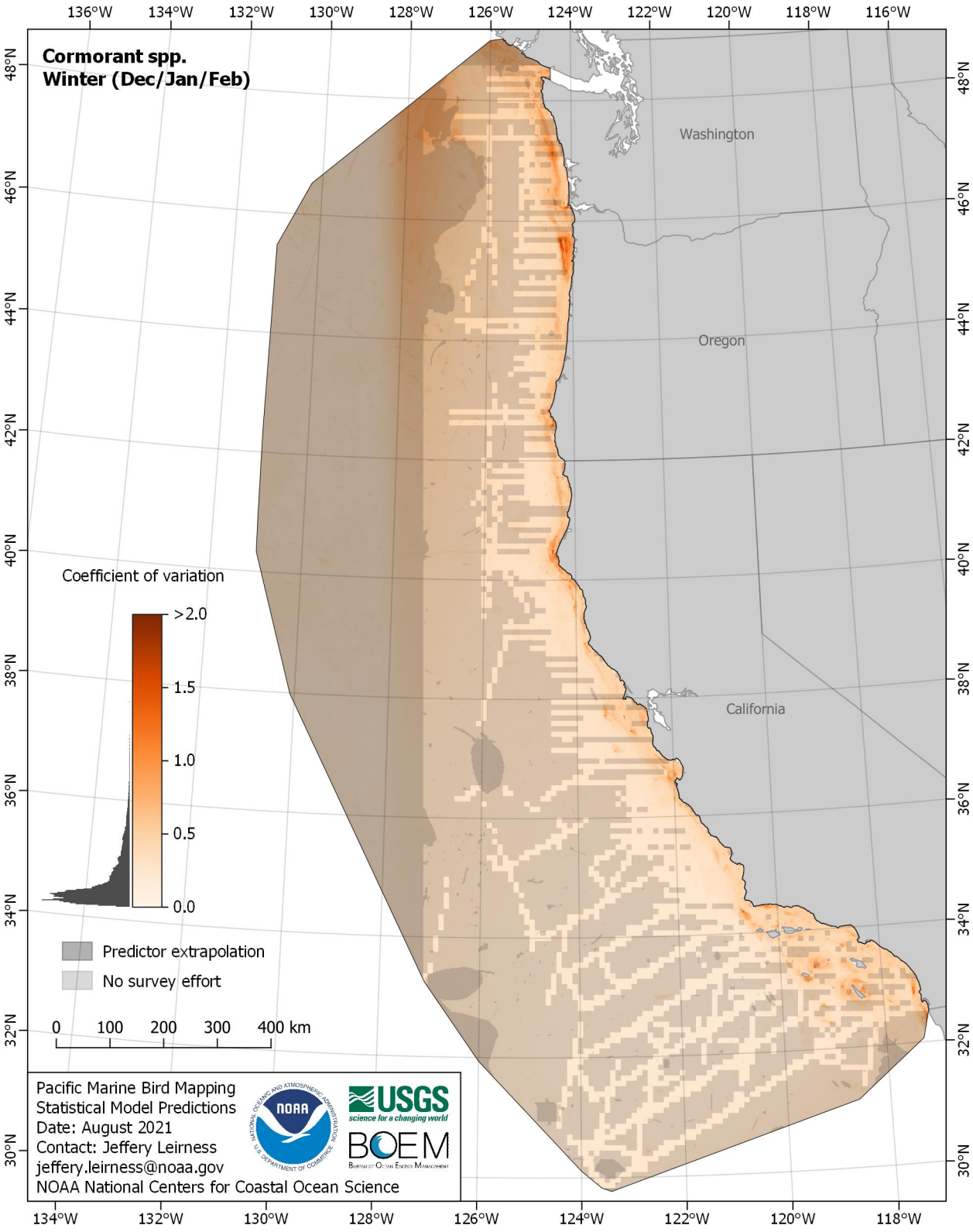

Figure E-262. Coefficient of variation for Cormorant spp. (*Phalacrocorax spp.*) in the winter season

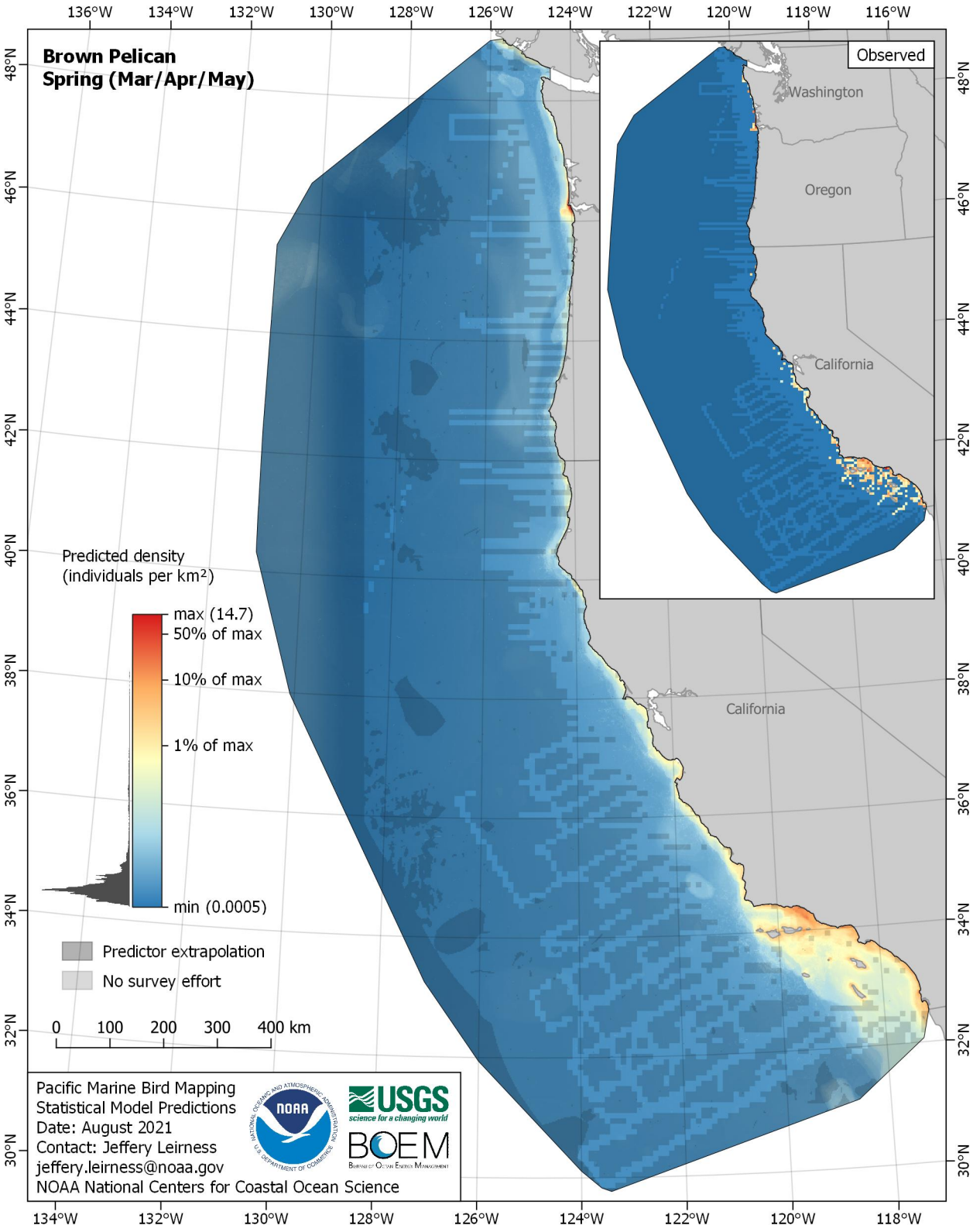

Figure E-263. Predicted density for Brown Pelican (*Pelecanus occidentalis*) in the spring season

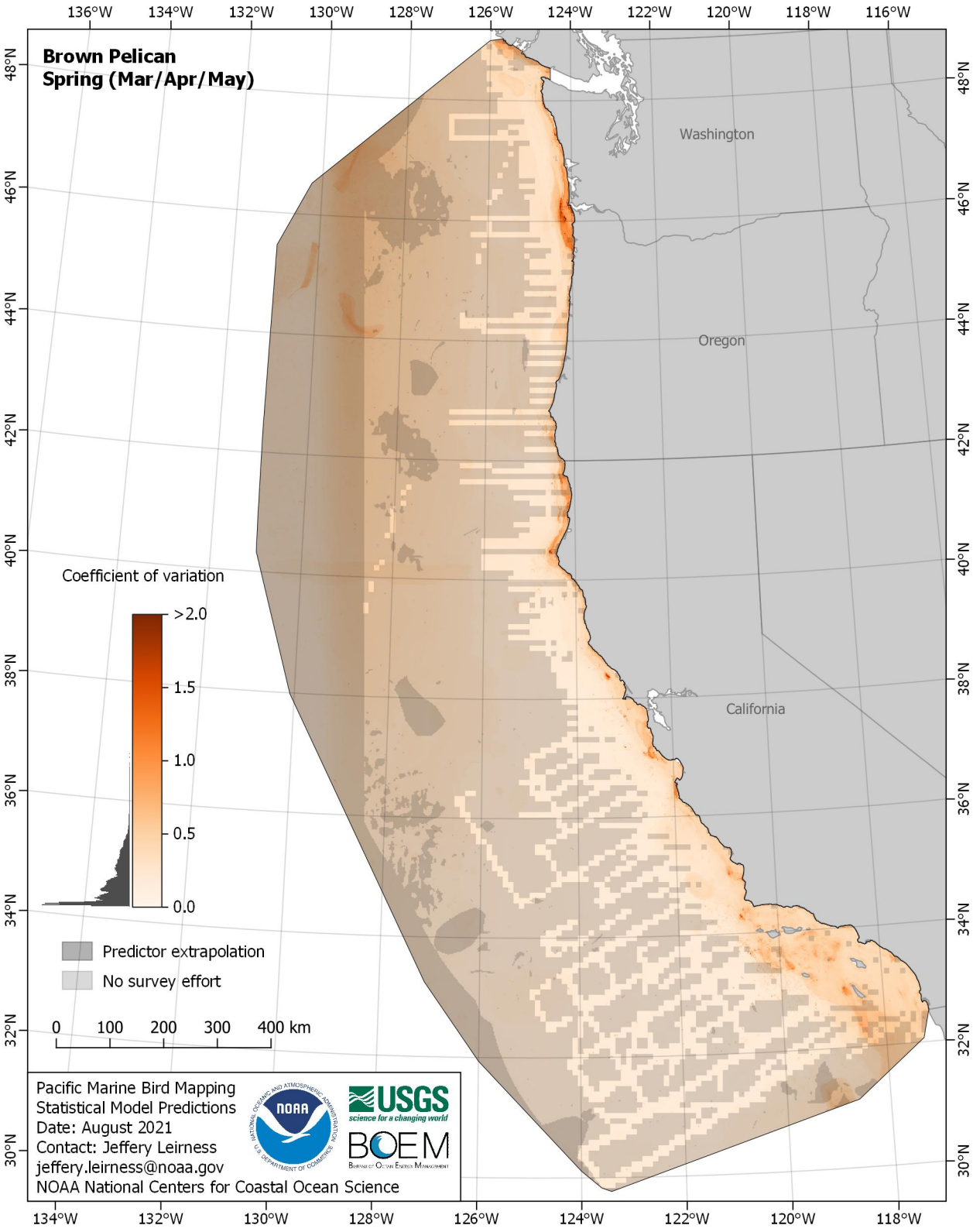

Figure E-264. Coefficient of variation for Brown Pelican (*Pelecanus occidentalis*) in the spring season

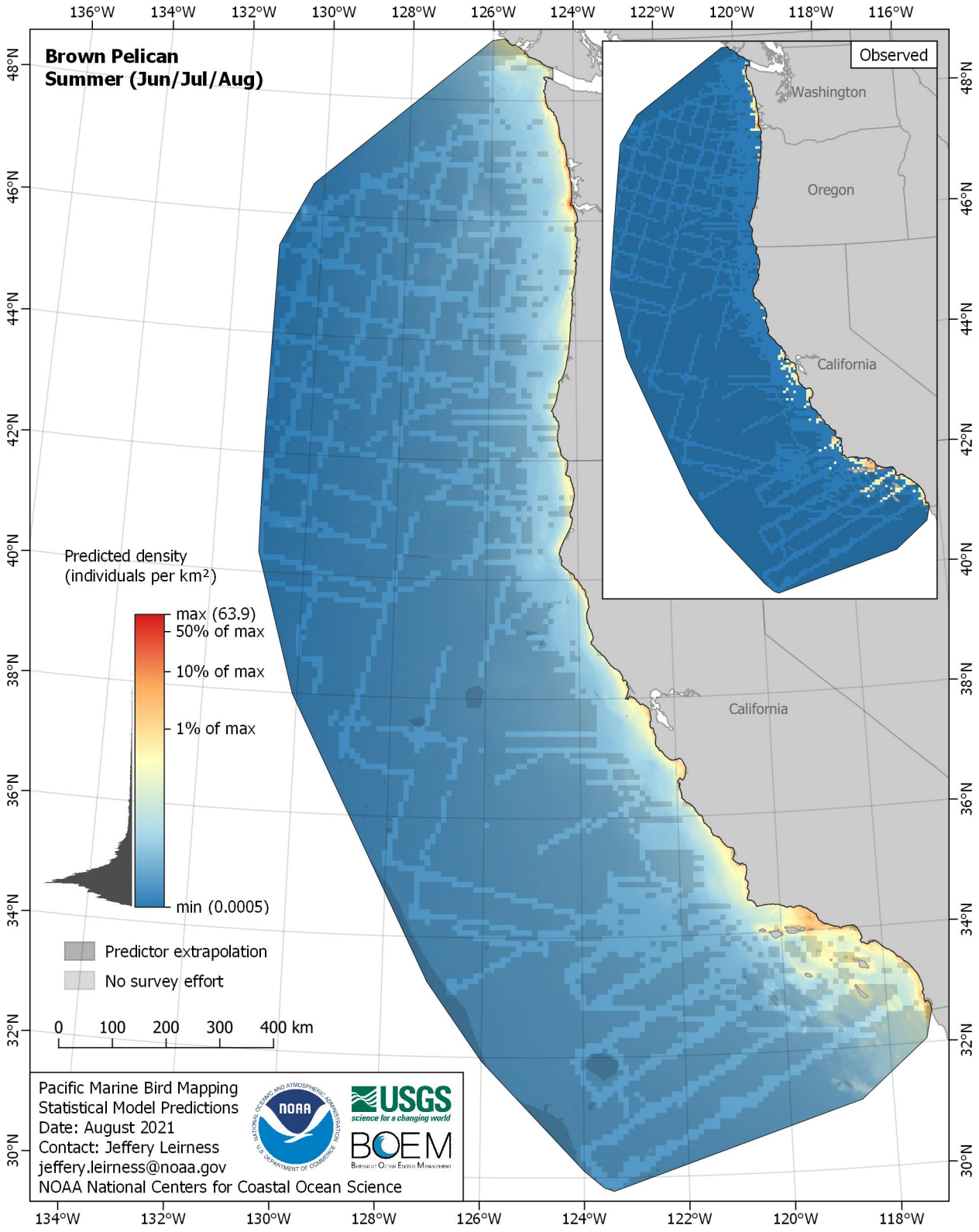

Figure E-265. Predicted density for Brown Pelican (*Pelecanus occidentalis*) in the summer season

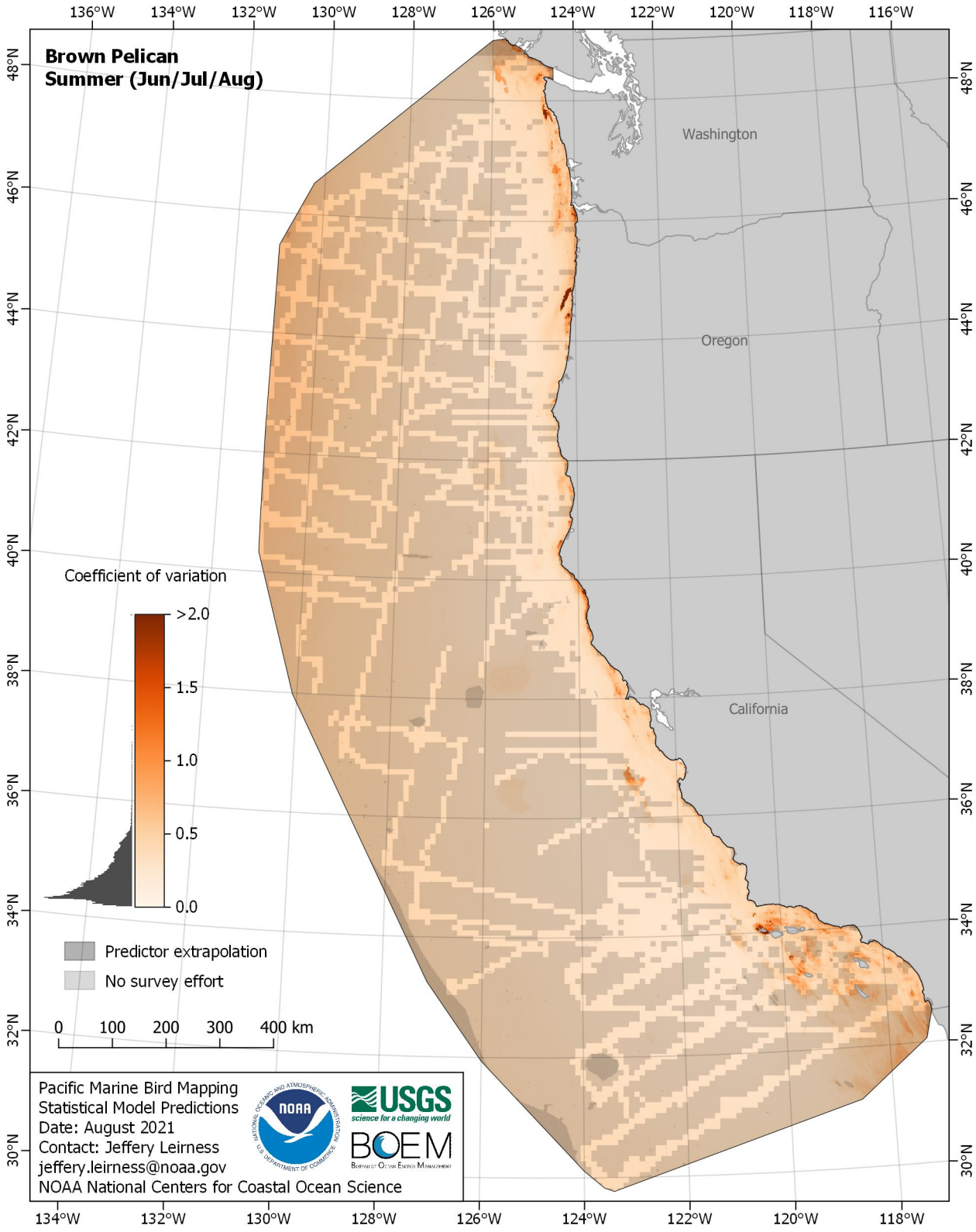

Figure E-266. Coefficient of variation for Brown Pelican (*Pelecanus occidentalis*) in the summer season

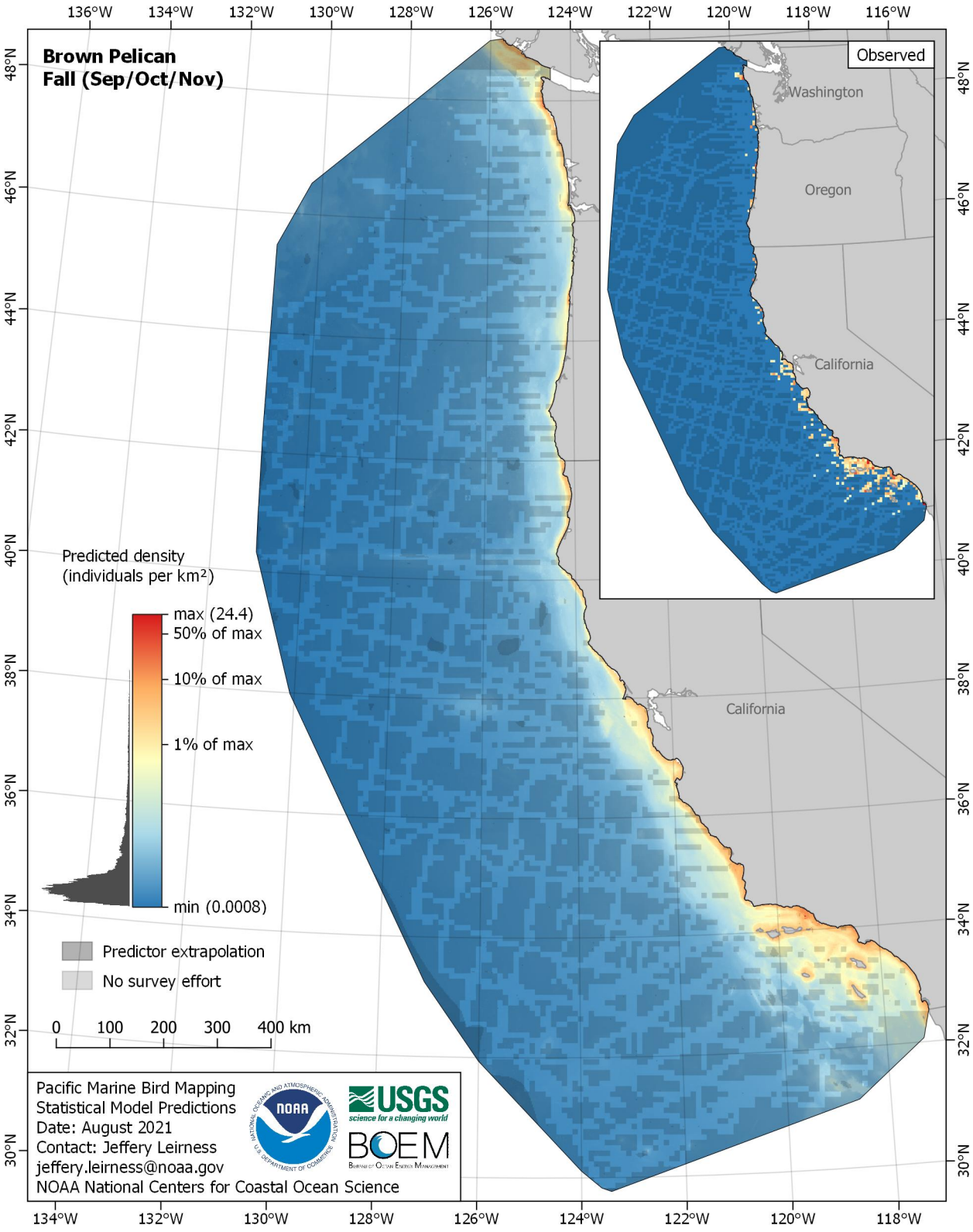

Figure E-267. Predicted density for Brown Pelican (*Pelecanus occidentalis*) in the fall season

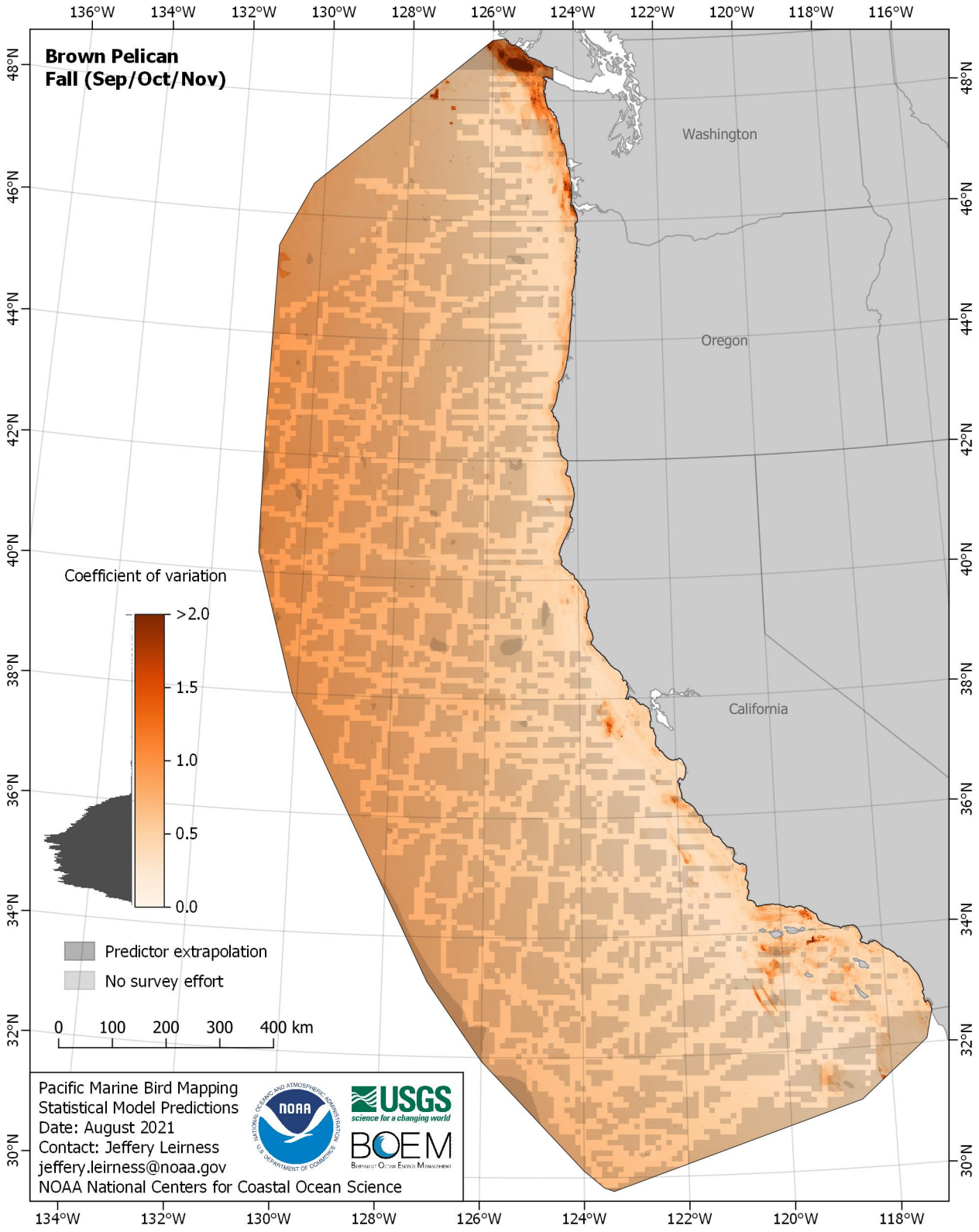

Figure E-268. Coefficient of variation for Brown Pelican (*Pelecanus occidentalis*) in the fall season

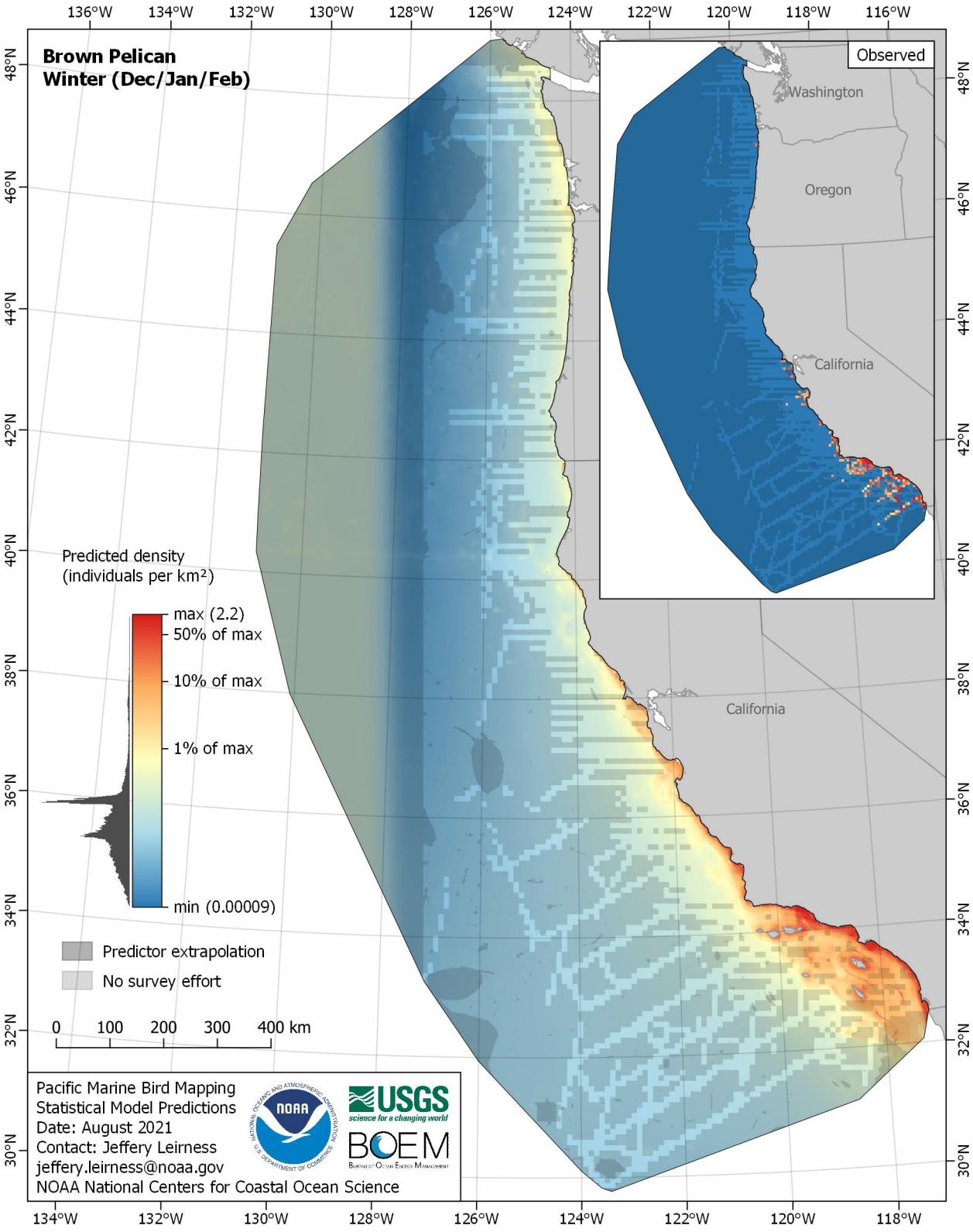

Figure E-269. Predicted density for Brown Pelican (*Pelecanus occidentalis*) in the winter season

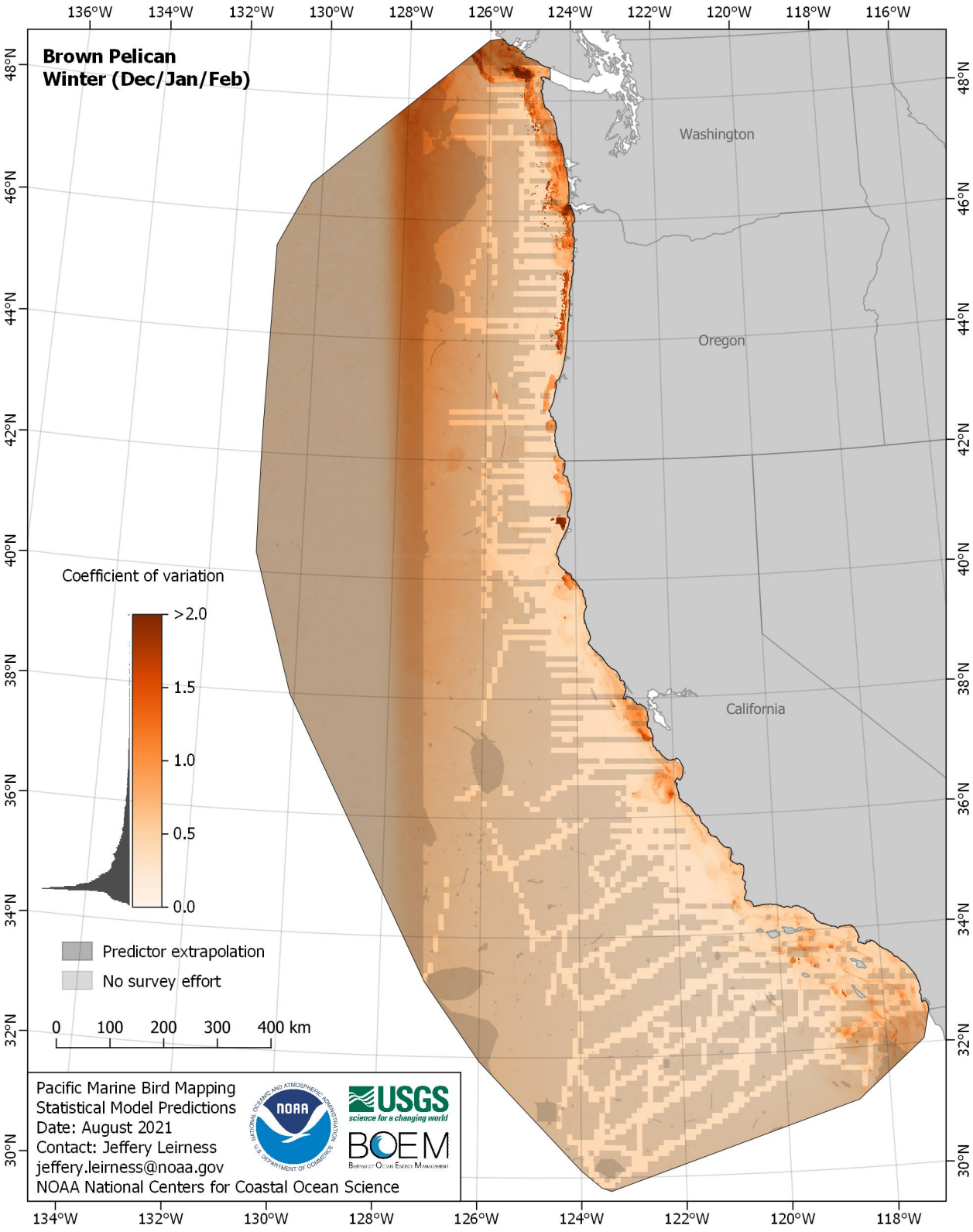

Figure E-270. Coefficient of variation for Brown Pelican (*Pelecanus occidentalis*) in the winter season

Appendix F: Predictor Variable Relative Importance Figures

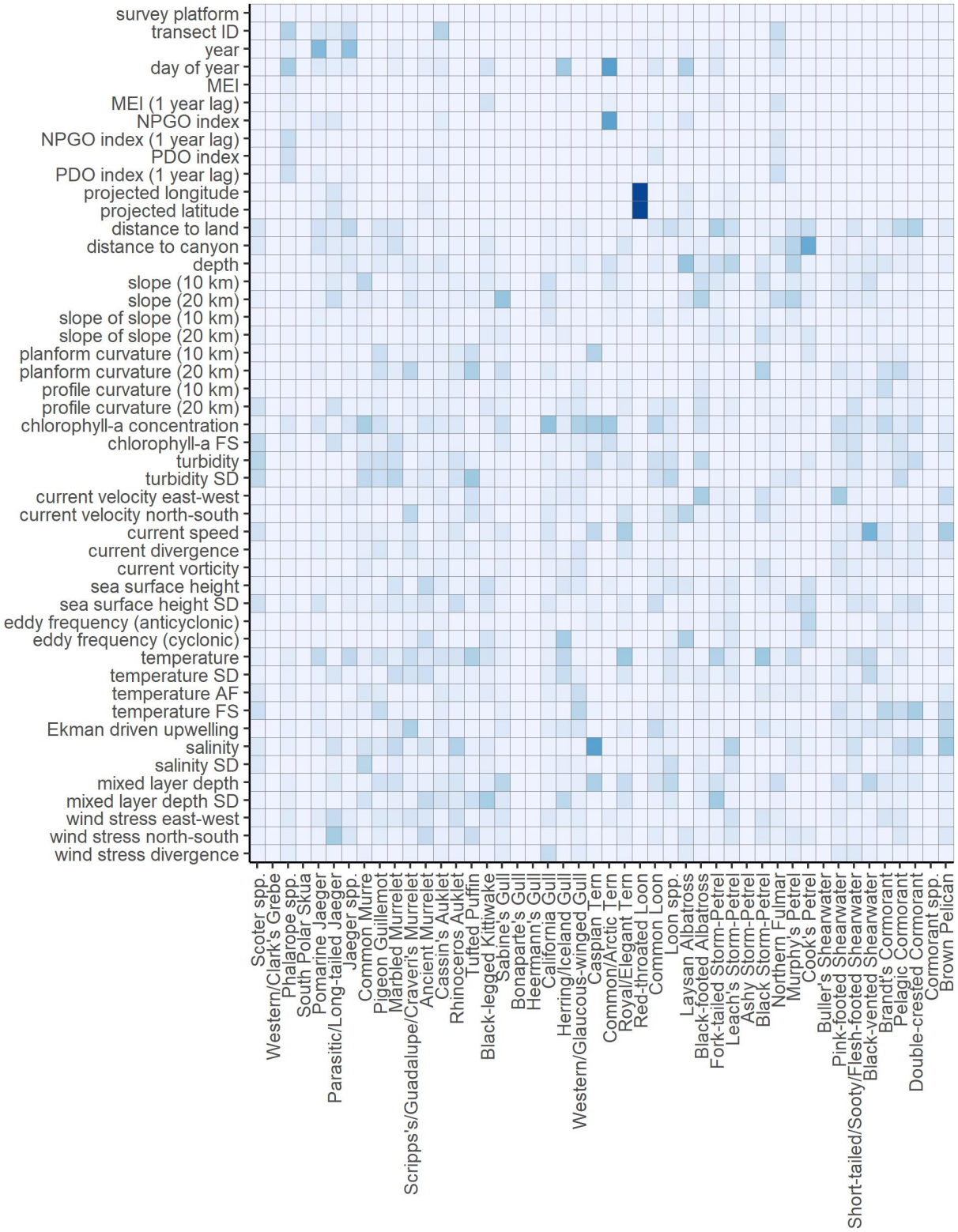

Figure F-1. Relative importance of predictor variables for the p component of the final selected model of each species/group during the spring season

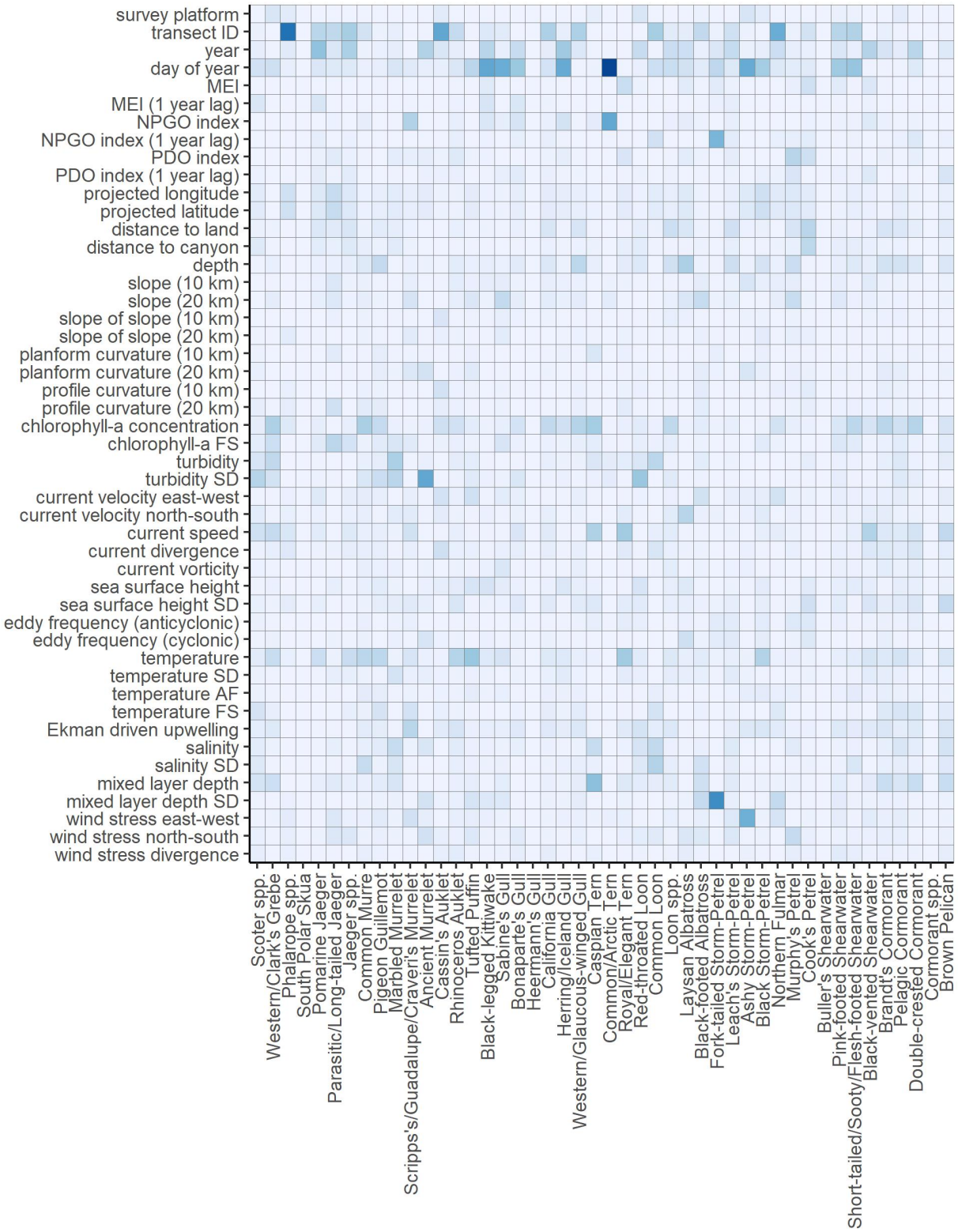

Figure F-2. Relative importance of predictor variables for the μ component of the final selected model of each species/group during the spring season

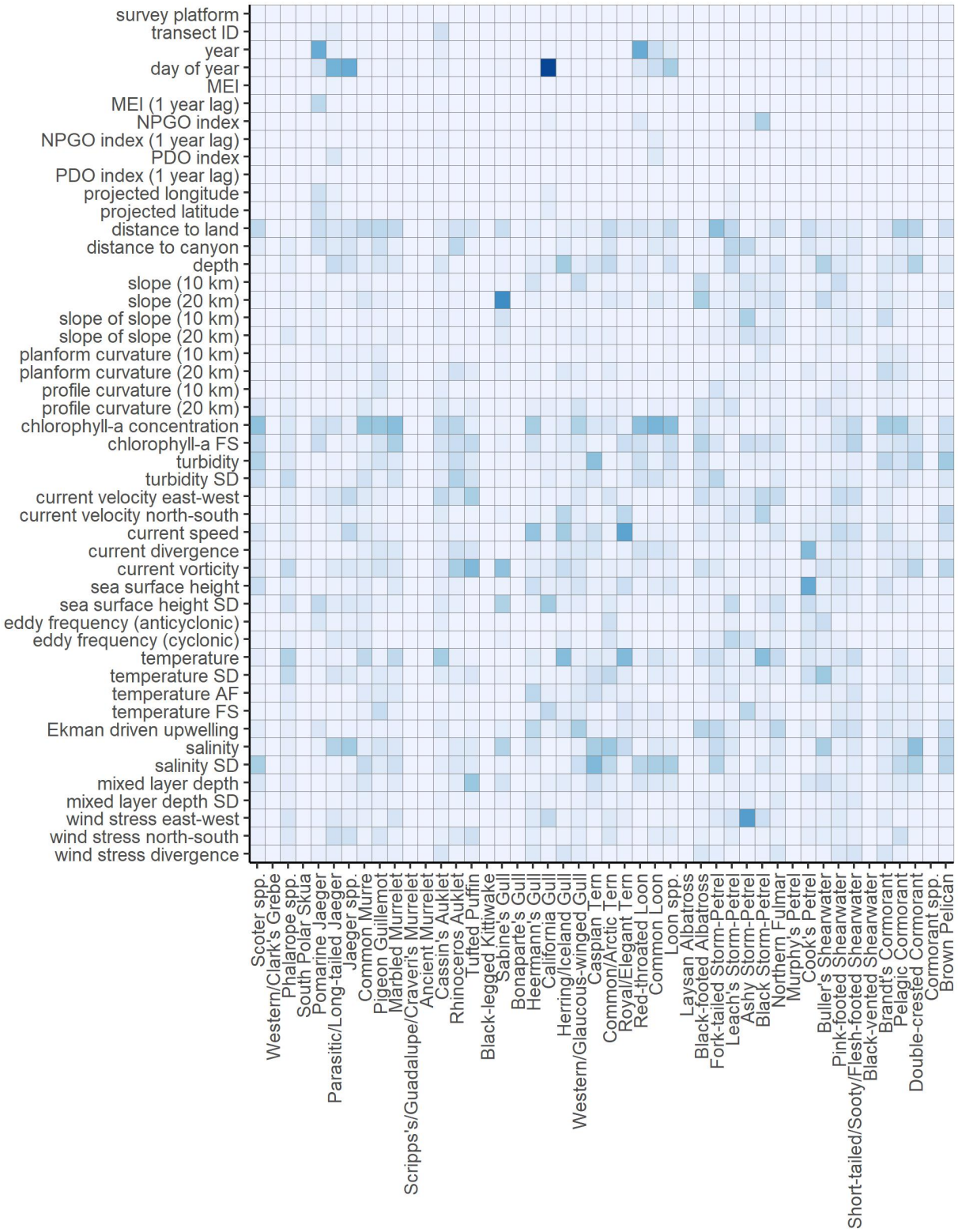

Figure F-3. Relative importance of predictor variables for the p component of the final selected model of each species/group during the summer season

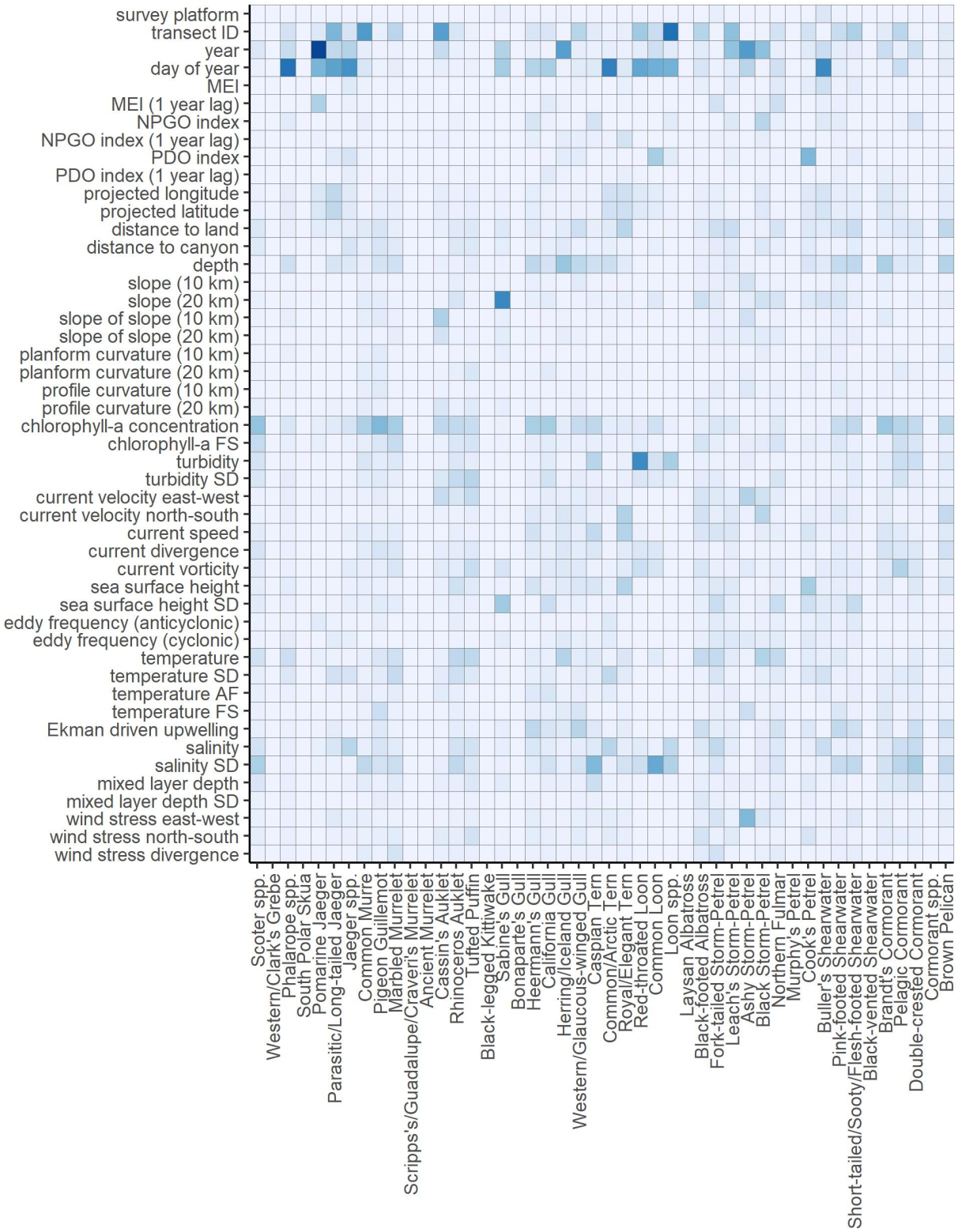

Figure F-4. Relative importance of predictor variables for the μ component of the final selected model of each species/group during the summer season

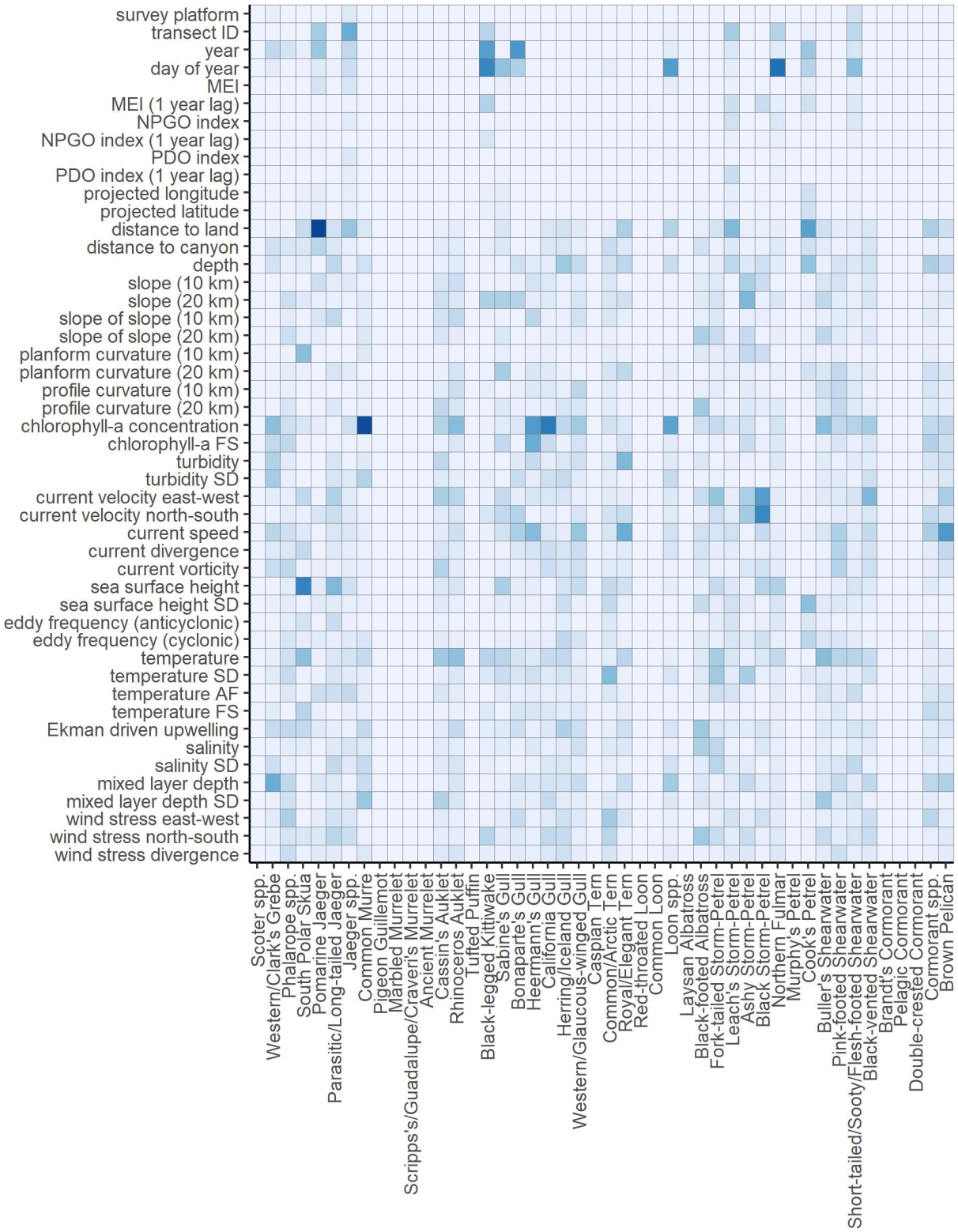

Figure F-5. Relative importance of predictor variables for the p component of the final selected model of each species/group during the fall season

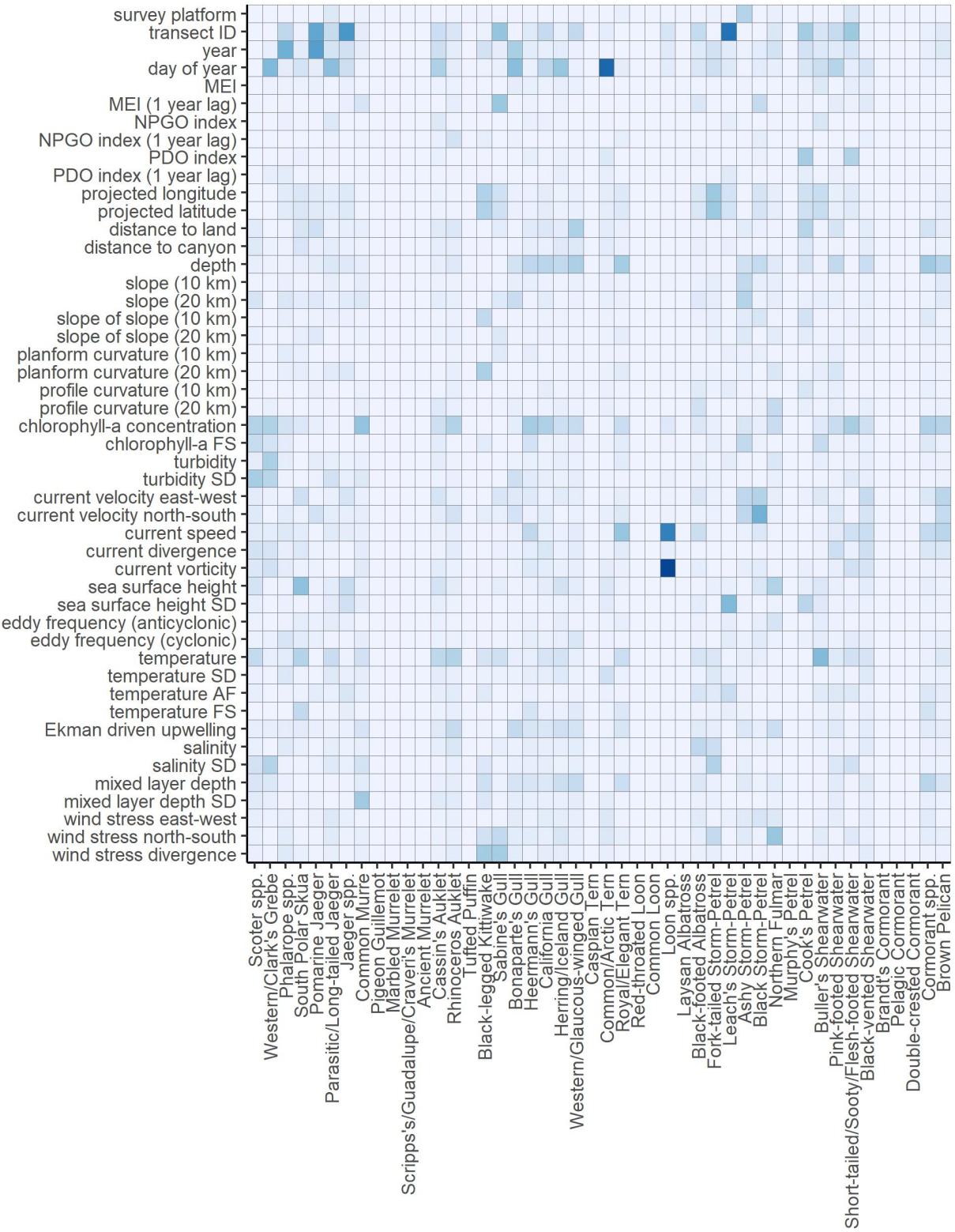

Figure F-6. Relative importance of predictor variables for the μ component of the final selected model of each species/group during the fall season

Figure F-7. Relative importance of predictor variables for the p component of the final selected model of each species/group during the winter season

Figure F-8. Relative importance of predictor variables for the μ component of the final selected model of each species/group during the winter season

Department of the Interior (DOI)

The Department of the Interior protects and manages the Nation's natural resources and cultural heritage; provides scientific and other information about those resources; and honors the Nation’s trust responsibilities or special commitments to American Indians, Alaska Natives, and affiliated island communities.

Bureau of Ocean Energy Management (BOEM)

The mission of the Bureau of Ocean Energy Management is to manage development of U.S. Outer Continental Shelf energy and mineral resources in an environmentally and economically responsible way.

BOEM Environmental Studies Program

The mission of the Environmental Studies Program is to provide the information needed to predict, assess, and manage impacts from offshore energy and marine mineral exploration, development, and production activities on human, marine, and coastal environments. The proposal, selection, research, review, collaboration, production, and dissemination of each of BOEM’s Environmental Studies follows the DOI Code of Scientific and Scholarly Conduct, in support of a culture of scientific and professional integrity, as set out in the DOI Departmental Manual (305 DM 3).